



BOOK OF ABSTRACTS



***9th BBBB International Conference
on Pharmaceutical Sciences***

Pharma Sciences of Tomorrow

Ljubljana, Slovenia, 15th-17th September, 2022

Impressum

9th BBBB International Conference on Pharmaceutical Sciences Pharma Sciences of Tomorrow: Book of Abstracts

Editors: Aleš Obreza, Rok Dreu, Alenka Zvonar Pobirk, Barbara Sterle Zorec

Reviewers: Mirjana Gašperlin, Janez Ilaš, et al.

Authors: Stanislav Gobec, Hatice Yeşim Karasulu et al.

Prepress design: Barbara Sterle Zorec, Alenka Zvonar Pobirk

Design: Sebastjan Jenko

Publisher: Slovensko farmacevtsko društvo in Univerza v Ljubljani, Fakulteta za farmacijo

URL address: The book of abstracts will be pdf format, available at:
<https://bbbb2022.sfd.si/programme/scientific-programme/>

Ljubljana, 2022

Kataložni zapis o publikaciji (CIP) pripravili v Narodni in univerzitetni knjižnici v Ljubljani

COBISS.SI-ID 120548355

ISBN 978-961-94230-4-2 (Slovensko farmacevtsko društvo, PDF)

Welcome letter

Dear colleagues,

We warmly welcome you to the 9th BBBB Conference in Ljubljana, where we have decided to continue the tradition of organizing international BBBB conferences after a break due to the Covid-19 pandemic. Unfortunately, the situation did not allow us to hold the meeting in 2021, when we celebrated three anniversaries, the 100th anniversary of the University of Ljubljana, the 70th anniversary of the Slovenian Pharmaceutical Society and the 60th anniversary of continuous pharmacy studies at the University of Ljubljana. The theme of this year's symposium is "Pharma sciences of tomorrow". The program consists of plenary and keynote lectures from different areas of pharmaceutical sciences, coming from all BBBB partners and broader scientific community. There will also be plenty of opportunity for younger researchers to present their results in the form of oral and poster presentations in an international environment. The conference will offer opportunities for exchange of scientific ideas between young and established scientists and professionals, as well as between people from academia, industry and regulatory authorities. At the conference, we invite you to also visit the capital of Slovenia, which was designated as the European Best Destination 2022 for 2022.

Conference Chair
Prof Dr Aleš Obreza

Chair of the Scientific Committee
Prof Dr Rok Dreu

General Secretary or the Conferece:
Assoc Prof Dr Alenka Zvonar Pobirk



CONTENT

Committees	7
Conference Floor Plane	9
Scientific Programme	11
Plenary Lectures	18
Keynote Lectures	25
Oral Presentations	59
Poster Presentations	140
Sponsors	296

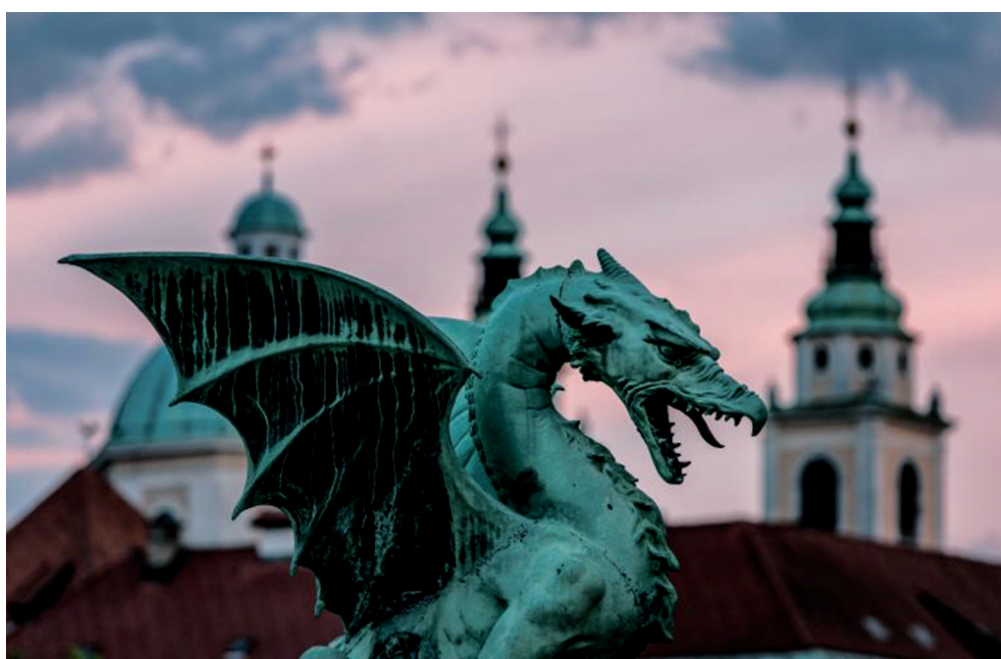
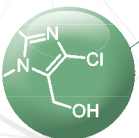


(Photo: Zmajski most / The Dragon bridge; Luka Esenko, Ljubljana Tourism photo library)



OUR KNOWLEDGE FOR YOUR HEALTH.

We contribute to effective treatment through our own development, innovative procedures and state-of-the-art products.



- 10% of total sales revenues invested in research and development
- Advanced pharmaceutical dosage forms and technologies
- Patent-protected innovations

www.krka.biz



Living a healthy life.

Lek d.d.



Recipients of the Novartis Awards for outstanding achievement in research and development (from left to right): Drago Kuzman, PhD, Nejc Golob MSc, Biljana Janković, PhD, Andrej Kocijan, PhD, and Rok Grahek, PhD

Our passion. Breakthrough innovations.

Teams of our scientists and experts are introducing pioneering approaches to the development and production of accessible therapies.

Novartis is the leading provider of medicines in Slovenia, where Lek, Novartis Pharma Services and Sandoz operate. State-of-the-art discoveries and production process excellence, facilitate our success in making the latest innovative and demanding generic medicines.

We are Novartis, and we are reimagining medicine.



 **NOVARTIS** | Reimagining Medicine

COMMITTEES

Scientific committee

- Rok Dreu (president), Slovenia
- Nevin Çelebi, Turkey
- Mirjana Gašperlin, Slovenia
- Stanislav Gobec, Slovenia
- Iztok Grabnar, Slovenia
- Judit Hohmann, Hungary
- Julijana Kristl, Slovenia
- Ivo Laidmäe, Estonia
- Jasmina Lovrić, Croatia
- Panos Macheras, Greece
- Janja Marc, Slovenia
- Irena Mlinarič Raščan, Slovenia
- Urve Paaver, Estonia
- Jelena Parojčić, Serbia
- Leena Peltonen, Finland
- Luka Peternel, Slovenia
- Jarkko Rautio, Finland
- Selma Şahin, Turkey
- Zvone Simončič, Slovenia
- Dieter Steinhilber, Germany
- Gabriele Stocco, Italy
- Tamás Tábi, Hungary
- Gordana Wozniak-Knopp, Austria

Organizing Committee

- Zrinka Abramovič
- Marko Anderluh
- Tomaž Bratkovič
- Nataša Karas Kuželički
- Petra Kocbek
- Janez Ilaš
- Odon Planinšek
- Robert Roškar
- Tomaž Vovk
- Barbara Sterle Zorec
- Natalija Škrbina Zajc
- Jurij Trontelj
- Anže Zidar

President of the Conference

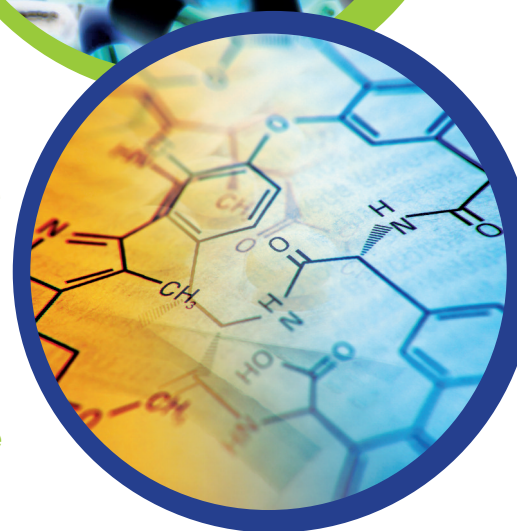
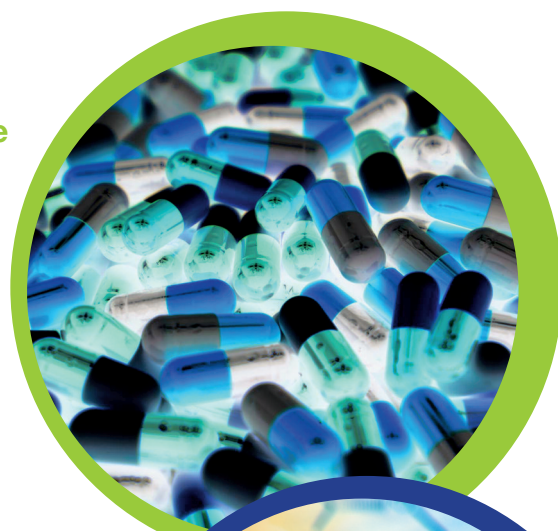
Aleš Obreza

General Secretary of the Conference

Alenka Zvonar Pobirk

Secretary of the Conference

Andrijana Tivadar



The BBBB International Conferences have been initiated under the auspices of the EUFEPS at the joint proposal of four founding associations: the Estonian Academic Society of Pharmacy and the Finnish Pharmaceutical Society (**B**altic), the Hungarian Society of Pharmaceutical Sciences (**B**alaton), the Slovenian Pharmaceutical Society (**B**led), the Turkish Pharmaceutical Technology Scientists' Association (**B**osphorus), and later the Finnish Pharmaceutical Society (Baltic). The founding board consisted of Prof Dominique Duchene (APGI, France), Prof Istvan Hermeecz (HSPS, Hungary), Prof Atilla Hincal (TÜFTAD, Turkey), Prof Hans Linden (EUFEPS), Prof Aleš Mrhar (SPS, Slovenia), Prof Christian R. Noe (EUFEPS) and Prof Peep Veski (EPS, Estonia). The aim of the BBBB conferences is to support young, promising scientists from these regions and to create a strong and stable background for an ongoing dialog between pharmacists and other scientists that goes beyond the traditional European links in the fields of Pharmaceutical Sciences, Research and Drug Development. The first BBBB conference was held in Siófok, Hungary, in 2005, followed by Tallinn-Tartu, Estonia (2007); Antalya, Turkey (2009); Bled, Slovenia (2011); Athens, Greece (2013); Helsinki, Finland (2015), Balatonfüred, Hungary (2017); and most recently Izmir, Turkey (2019).



Brinox is a company with almost forty years of experience offering complete turnkey solutions and equipment for the biopharmaceutical, pharmaceutical, and food industries.

The company's performance and growth are based on quality, innovation, flexibility and reliability.

Brinox guides the customer along the entire path from a complex process challenge to an optimal solution, tailor-made to meet the customer's needs. With the aim of producing first-rate products and systems, we carry out all the steps necessary for success, from research and development, process engineering, design, manufacturing, automation, testing and qualification, installation as well as all after-sales services.

Here at Brinox, our focus on customer satisfaction, adaptability, as well as our wealth of experience and innovative technical solutions, are the traits that attract and maintain our client base and lead the company to the realization of its vision – to stay the leading provider of unique technological process solutions for the biopharmaceutical and food industry in Europe by 2025.

Brinox d.o.o.

Sora 21 | SI-1215 Medvode | Slovenija
T: +386 1 361 97 30 | info@brinox.eu

Brinox Deutschland GmbH

Maria-und-Georg-Dietrich Str. 2 | 77652 Offenburg
Deutschland | T: +49 (0) 781 970 678 10 | info@brinox.de

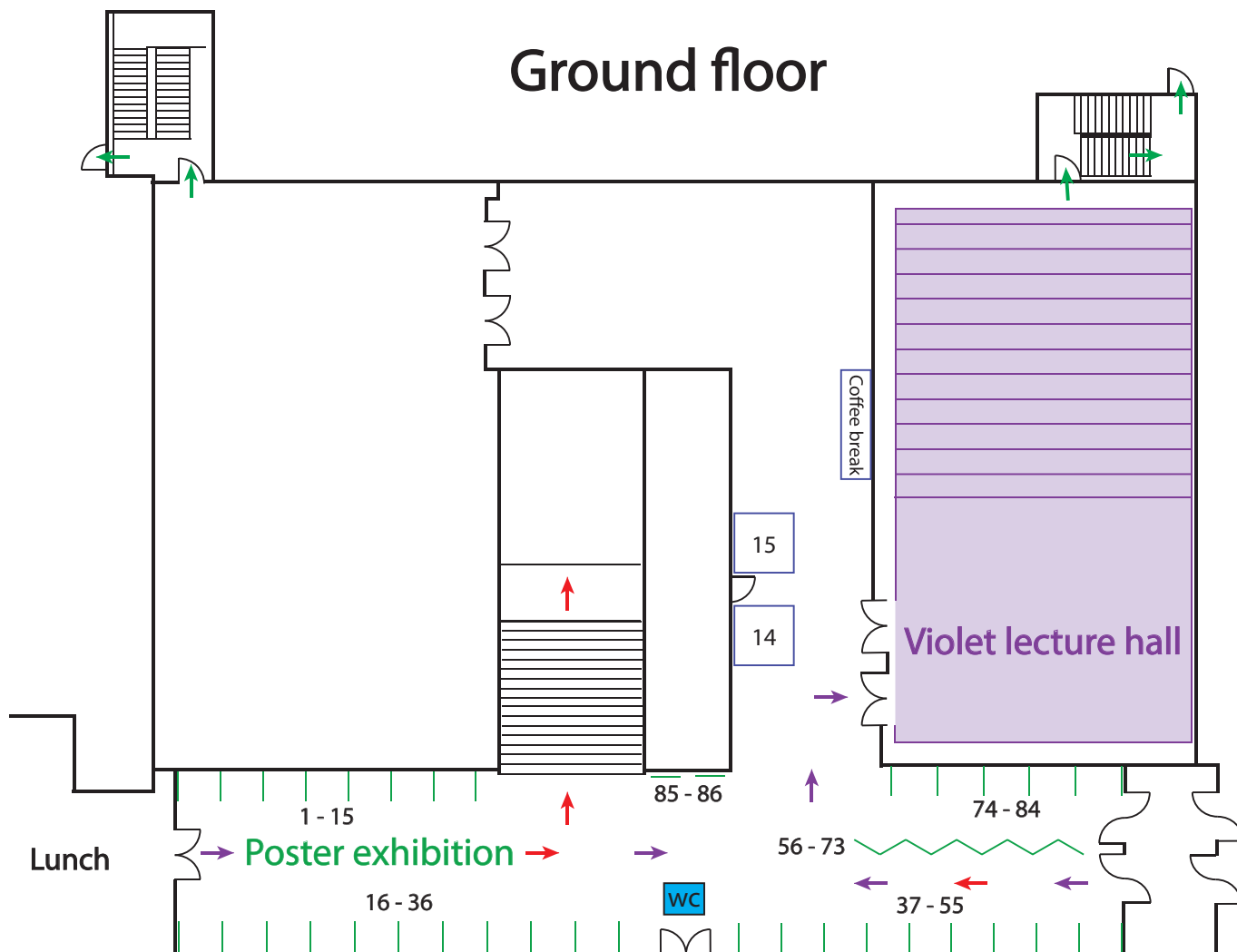
Brinox Innovations AG

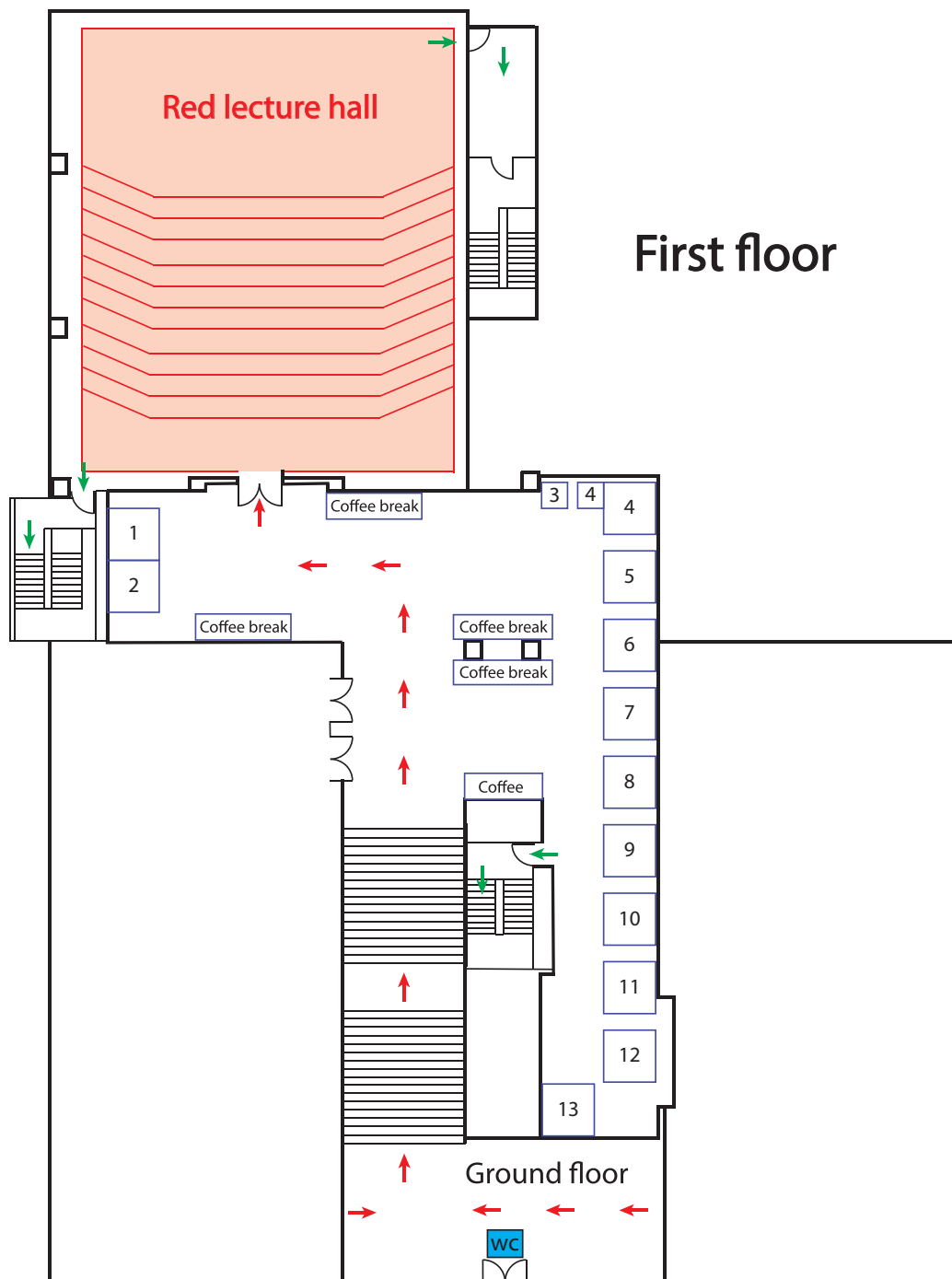
Poststrasse 14 | CH-6300 Zug | Switzerland
T: +41 41 727 81 50 | info@brinox-innovations.ch



Technology that delivers

CONFERENCE FLOOR PLAN





Exhibitors:

1. Krka	2. Lek/Novartis	3. Pfizer
4. Merck	5. Brinox	6. ASAHI KASEI
7. Harke Pharma	8. Melt Prep	9. Bioinicia
10. Munit	11. ABL&E Group / Teledyne Hanson	12. Chemass
13. Labtim	14. Simplivia	15. Mettler Toledo

DETAILED SCIENTIFIC PROGRAMME

9th BBBB International Conference on Pharmaceutical Sciences PHARMA SCIENCES OF TOMORROW



Thursday, September 15, 2022, MORNING SESSION		Red Lecture Hall
Chairpersons: Mirjana Gašperlin, Jelena Parojčić		
8.45–9.15	Conference Opening	
9.15–10.00	[PL1] Stanislav Gobec, University of Ljubljana, Faculty of Pharmacy, Slovenia Development and translation of lead compounds for the treatment of neurodegenerative diseases	
Session 1 - NEW TRENDS IN INDUSTRIAL PHARMACY		
Chairpersons: Mirjana Gašperlin, Jelena Parojčić		
10.10–10.40	[KL1] Hatice Yeşim Karasulu, Ege University, Turkey Scientific and regulatory approaches in formulation development with poorly soluble drugs	
10.40–11.10	[KL2] Biljana Janković, Lek, Sandoz & University of Ljubljana, Slovenia The power of data science in pharmaceutical industry	
11.10–11.45	Coffee Break & Poster session	
11.45–12.00	Leo Ohrem, Merck Continuous manufacturing in solid dose – how to leverage opportunities of this new technology	
12.00–12.15	[OP1] Klemen Kreft, University of Ljubljana, Slovenia Influence of the binder jetting process parameters and binder liquid composition on the relevant attributes of 3D printed tablets	
12.15–12.30	[OP2] Aljoša Gradišek, Krka, Slovenia Optimization of radial extrusion and pellet coating processes using PAT approaches	
12.30–12.45	[OP3] Gábor Vasvári, University of Debrecen, Hungary From batch technology to continuous manufacturing: formulation of gastroretentive dosage form based on melt foaming technique	
12.45–13.00	[OP4] Mila Kovačević, University of Ljubljana, Slovenia The influence of polymeric binder type and concentration on flow and dissolution properties of Syloid® 244FP-based SMEDDS granules	
13.00–13.15	[OP5] Mahwash Mukhtar, University of Szeged, Hungary Pulmonary dry powder for inhalation for targeted drug delivery to macrophages in tuberculosis	
13.15–14.15	Luncheon	
Thursday, September 15, 2022, MORNING SESSION		Violet Lecture Hall
Session 2 - NEW MOLECULES FOR TREATING NEURODEGENERATIVE DISEASES		
Chairpersons: Tamás Tábi, Stanko Gobec		
10.10–10.40	[KL3] István Szatmári, University of Szeged, Hungary Synthesis and transformations of kynurenic acid derivatives with potential neuroprotective activity	

Plenary lecture (PL), Keynote lecture (KL), Oral Presentations (OP)

10.40–11.10	[KL4] Urban Košak, University of Ljubljana, Slovenia Simple syntheses of synthons for potential anti-Alzheimer and antiviral drugs
11.10–11.45	Coffee Break & Poster session
11.45–12.15	[KL5] Aleš Obreza, University of Ljubljana, Slovenia Design, synthesis and biochemical evaluation of low-molecular-weight human neutrophil elastase inhibitors
12.15–12.30	[OP6] Damijan Knez, University of Ljubljana, Slovenia Fluorescent probes for detection of misfolded proteins in biological samples
12.30–12.45	[OP7] Urša Pečar Fonovič, University of Ljubljana, Slovenia Targeting cathepsin X in neurodegenerative diseases with novel triazole-benzodioxine inhibitors
12.45–13.00	[OP8] Anže Meden, University of Ljubljana, Slovenia Chalcogen carbamates as covalent cholinesterase inhibitors – surveying group 16 (VI) of the periodic table
13.00–13.15	[OP9] Selin Parmaksız, Hacettepe University, Turkey In vivo efficiency of a new liposomal adjuvant system based on porins
13.15–14.15	Luncheon

Thursday, September 15, 2022, AFTERNOON SESSION

Red Lecture Hall

Chairpersons: Petra Kocbek, Karin Kogermann

14.15–15.00	[PL2] Gerhard Winter, Ludwig Maximilian University of Munich, Germany 30 years in formulation of protein pharmaceuticals: What has been achieved – where do we stand today – what is next?
-------------	---

Session 3 - FORMULATION AND DELIVERY CHALLENGES OF SMALL MOLECULES AND BIOTECH DRUGS

Chairpersons: Petra Kocbek, Karin Kogermann

15.10–15.40	[KL6] Kairi Lorenz, University of Tartu, Estonia Electrospun antimicrobial peptides – novel approach for improved wound infection treatment
15.40–16.10	[KL7] Slavko Kralj, J. Stefan Institute, Slovenia Bioinspired anisotropic magnetic nanoparticles: design, synthesis and biomedical applications
15.10–16.45	Coffee break & Poster session
16.45–17.15	[KL8] Tapani Viitala, University of Helsinki & Åbo Akademi University, Finland Real-time label-free sensing platforms for nanoparticle and extracellular vesicle analysis
17.15–17.30	Peter Balogh, Merck The viscosity reduction platform enabling subcutaneous delivery
17.30–17.45	[OP10] Hayrettin Tonbul, Inonu University, Turkey In vivo evaluation of doxorubicin and elacridar co-loaded PLGA/silica hybrid nanoparticles against multidrug resistant breast cancer
17.45–18.00	[OP11] Nina K. Grilc, University of Ljubljana, Slovenia Nanofibers for local delivery of two bacillus strains with antibacterial activity

Plenary lecture (PL), Keynote lecture (KL), Oral Presentations (OP)

18.00–18.15	[OP12] Fabiola Guareschi, University of Parma, Italy Development of cyclosporine A – loaded micelles exhibiting a promising antiviral activity against SARS-CoV-2
18.15	Welcome reception

Thursday, September 15, 2022, AFTERNOON SESSION **Violet Lecture Hall**

Session 4 - NEW MOLECULES FOR TREATING BACTERIAL AND VIRAL INFECTIONS

Chairpersons: Anikó Borbás, Janez Ilaš

15.10–15.40	[KL9] Anikó Borbás, University of Debrecen, Hungary Semisynthetic glycopeptide antibiotics – one weapon against two deadly enemies
15.40–16.10	[KL10] Lucija Peterlin Mašič, University of Ljubljana, Slovenia Rational design of balanced dual-targeting antibacterial compounds with limited resistance
15.10–16.45	Coffee break & Poster session
16.45–17.15	[KL11] Marko Anderluh, University of Ljubljana, Slovenia Potent DNA gyrase inhibitors bind to their target through symmetrical bifurcated halogen bonding.
17.15–17.30	[OP13] Margherita Brindisi, University of Naples Federico II, Italy HDAC6 inhibition in cystic fibrosis: <i>in vivo</i> proof-of-concept study anti-inflammatory profile, effects on bacterial load, formulation and biodistribution studies
17.30–17.45	[OP14] Sveva Pelliccia, University of Naples Federico II, Italy New covalent reversible inhibitors of SARS-CoV-2 main protease
17.45–18.00	[OP15] Ivana Perković, University of Zagreb, Croatia Synthesis and biological evaluation of quinoline and anthranilic acid derivatives as potential quorum sensing inhibitors
18.00–18.15	[OP16] Peter Peršolja, University of Ljubljana, Slovenia Expanding the chemical space of n-phenylpyrrolamides as DNA gyrase B inhibitors
18.15	Welcome reception

Friday, September 16, 2022, MORNING SESSION **Red Lecture Hall**

Chairpersons: Ildikó Bácskay, Rok Dreu

9.00–9.45	[PL3] Daniel Markl, University of Strathclyde, United Kingdom Mechanistic Understanding of long-term performance of oral medicines
9.45–10.30	[PL4] Niklas Sandler, Nanoform, Finland (on-line presentation) Adoption of 3D printing technologies in pharmacies and hospital pharmacies

Session 5 - HOT-MELT PROCESSING AND PRINTING TECHNOLOGIES IN PHARMACEUTICAL MANUFACTURING

Chairpersons: Ildikó Bácskay, Rok Dreu

10.40–11.10	[KL12] Amrit Paudel, Graz University of Technology, Austria Long-acting drug delivery to female health via polymeric intravaginal ring: Innovative and rational principles underlying formulation design and hot-melt extrusion processing
11.10–11.45	Coffee Break & Poster session

Plenary lecture (PL), Keynote lecture (KL), Oral Presentations (OP)

11.45–12.15	[KL13] Gregor Lorbek, Krka, d.d., Slovenia Application of hot-melt technologies in designing formulations with poorly water-soluble active ingredient
12.15–12.30	[OP17] Ognjen Jakasanovski, Lek.d.d., Slovenia Rational development and process optimization of an amorphous solid dispersion generic drug product prepared by hot-melt extrusion (a case study)
12.30–12.45	[OP18] Serena Bertoni, University of Bologna, Italy Use of additives to control the polymorphism of solid lipid formulations: a simple way to face a complex problem
12.45–13.00	[OP19] Diren Sarisaltık Yaşın, Dicle University, Turkey Fabrication of 3DP colon-targeted tablets including fluticasone with enhanced solubility by γ-cyclodextrin
13.00–14.00	Luncheon

Friday, September 16, 2022, MORNING SESSION **Violet Lecture Hall**

Session 6 - EMERGING CONTAMINANTS IN ENVIRONMENTAL SAMPLES AND PHARMACEUTICAL PRODUCTS

Chairpersons: Robert Roškar, Jurij Trontelj

10.40–11.10	[KL14] Žiga Hodnik, Krka, d, d., Slovenia Mass spectrometry as a powerful tool for analysing degradation pathways: 1,4-benzodiazepine case study
11.10–11.45	Coffee Break & Poster session
11.45–12.15	[KL15] Mira Petrović, ICRA Catalan Institute for Water Research, Spain Pharmaceutical residues in the aquatic environment – Challenges and opportunities of using advanced analytical methods for their monitoring
12.15–12.30	[OP20] Andrej Grobin, University of Ljubljana, Slovenia A useful method for routine monitoring of endocrine disruptors in surface waters by SPE-LC-MS/MS
12.30–12.45	[OP21] Nejc Golob, Lek d.d., Slovenia Study of different sources of nitrosamine traces in pharmaceuticals by highly sensitive hyphenated mass spectrometry techniques
12.45–13.00	[OP22] Nika Osel, University of Ljubljana, Slovenia Selective determination of whey proteins by a chromatographic analytical approach
13.00–14.00	Luncheon

Friday, September 16, 2022, AFTERNOON SESSION **Red Lecture Hall**

Chairpersons: Odon Planinšek, Martin Brandl

14.00–14.45	[PL5] Sulev Reisberg, University of Tartu, Estonia Personalised medicine in Estonia – moving from research to practice
Session 7 - CREATING USER FRIENDLY ORAL DOSAGE FORMS	
Chairpersons: Odon Planinšek, Martin Brandl	
14.55–15.25	[KL16] Cansel Köse Özkan, University of Health Sciences, Turkey Personalized medicine: Drug development and usage

Plenary lecture (PL), Keynote lecture (KL), Oral Presentations (OP)

15.25–15.55	[KL17] István Antal, Semmelweis University, Hungary Microparticles and multi-unit systems for advanced drug delivery
15.55–16.55	Coffee break & Main Poster session (16.15–16.55)
16.55–17.10	[OP23] Krisztián Pamlényi, University of Szeged, Hungary Preparation of buccal films in Parkinson's disease
17.10–17.25	[OP24] Genada Sinani, Altinbas University, Turkey Design and evaluation of composite film formulations using quality by design for paediatric use
17.25–17.40	[OP25] Gülbeyaz Yıldız Türkyılmaz, Ege University, Turkey Development of a pediatric orally disintegrating tablet dosage form by masking the bitter taste of ornidazol with Eudragit E PO
17.40–17.55	[OP26] Katarina Bolko Seljak, University of Ljubljana, Slovenia Nanocellulose-based orodispersible films as a potential drug delivery system
17.55–18.10	[OP27] Pawel Balcerzak, Lubrizol Advanced Materials, Inc., USA Excipient's role in formulating user friendly oral dosage forms
18.10–18.25	[OP28] Ece Türkmen, Hacettepe University, Turkey A chitosan based bioadhesive gel for delivery of combined antimicrobials with enhanced activity in local treatment of skin infections in humans and animals
19.30	Conference Dinner

Friday, September 16, 2022, AFTERNOON SESSION

Violet Lecture Hall

**Session 8 - THERAPEUTIC DRUG MONITORING & PHARMACOGENOMICS
AS A TOOL TO IMPROVE DRUG EFFICIENCY AND SAFETY
IN PERSONALISED MEDICINE**

Chairpersons: Nataša Karas Kuželički, Tomaž Vovk

14.55–15.25	[KL18] Gabriele Stocco, University of Trieste, Italy Therapy personalization of anti-TNF drugs in pediatric patients with immune mediated diseases
15.25–15.55	[KL19] Dunja Urbančič, University of Ljubljana, Slovenia Pharmacogenomic and biological implications of thiopurine S-methyltransferase
15.55–16.55	Coffee break & Main Poster session (16.15–16.55)
16.55–17.20	[KL20] Eva Germovšek, Boehringer Ingelheim, Germany PK-PD modelling to optimise therapy and facilitate therapeutic drug monitoring of antimicrobials in neonates
17.20–17.45	[KL21] Jurij Aguiar Zdovc, University of Ljubljana, Slovenia Model-informed precision dosing of ustekinumab in Crohn's disease
17.45–18.10	[KL22] Eva del Amo Páez, University of Eastern Finland, Finland Crossing ocular barriers: pharmacokinetic models to support drug development in retinal diseases
18.10–18.25	[OP29] Alenka Šmid, University of Ljubljana, Slovenia Transcriptome analysis reveals involvement of thiopurine s-methyltransferase in oxidation-reduction processes
19.30	Conference Dinner

Plenary lecture (PL), Keynote lecture (KL), Oral Presentations (OP)

Saturday, September 17, 2022, MORNING SESSION **Red Lecture Hall**

Chairpersons: Julijana Kristl, Stane Srčič

9.00–9.45	[PL6] Helder Santos, University of Groningen, The Netherlands Microfluidics manufacturing of nanoparticle based formulations for pharmaceutical and biomedical applications
-----------	--

Session 9 - CONTEMPORARY CHALLENGES IN PHARMACEUTICS

Chairpersons: Julijana Kristl, Stane Srčič

10.00–10.30	[KL23] Panos Macheras, National and Kapodistrian University of Athens, Greece Physiologically based finite time pharmacokinetic (PBFTPk) models: the end of the beginning in oral drug absorption
10.30–10.45	[OP30] Martin Brandl, University of Southern Denmark, Denmark Microdialysis and nanofiltration allow to distinguish molecularly dissolved from colloid-associated drug concentrations during biomimetic dissolution testing of supersaturating formulations
10.45–11.00	[OP31] Gizem Tezel, Hacettepe University & Süleyman Demirel University, Turkey Memantine loaded PLGA nanoparticles for Alzheimer's disease
11.00–11.15	[OP32] Tamás Sovány, University of Szeged, Hungary An assessments of titanate nanotubes performance as protein carriers
11.15–11.30	[OP33] Anže Zidar, University of Ljubljana, Slovenia Immunomodulatory properties of simvastatin embedded in liposomes and electrospun nanofibers for wound healing
11.30–12.00	Coffee Break
12.00–12.15	[OP34] Jolanta Pyteraf, Jagiellonian University Medical College, Poland The effect of the structure – the evaluation of the disintegration and the dissolution processes of 3D printed orodispersible tablets
12.15–12.30	[OP35] Maja Bjelošević, University of Ljubljana, Slovenia Exploring the potential of new bulking agents for lyophilised biopharmaceutical formulations intended for subcutaneous administration
12.30–12.45	[OP36] Ágnes Rusznyák, University of Debrecen, Hungary Cyclodextrin polymer-based siRNA delivery systems
12.45–13.00	[OP37] Arle Kõrkjas, University of Tartu, Estonia Open liquid-surface ultrasound-enhanced electrospinning for generating multilayered nanofiber structures
13.00	Closing remarks

Saturday, September 17, 2022, MORNING SESSION **Violet Lecture Hall**

Session 10 - PEPTIDES AS THERAPEUTICS AND BIORECOGNITION ELEMENTS, M-RNA VACCINES

Chairpersons: Tomaž Bratkovič, Taavi Lehto

10.00–10.30	[KL24] Taavi Lehto, University of Tartu, Estonia Peptides-based drug delivery systems for RNA therapeutics
10.30–11.00	[KL25] Mojca Lunder, University of Ljubljana, Slovenia Short peptides and their role in research and immunotherapy of allergies

Plenary lecture (PL), Keynote lecture (KL), Oral Presentations (OP)

11.00–11.30	[KL26] Gordana Wozniak Knopp, University of Natural Resources and Life Sciences, Austria CD81 large extracellular loop as a novel alternative scaffold: laminin binding CD81 enhances specific uptake of extracellular vesicles
11.30–12.00	Coffee Break
12.00–12.15	Aleš Štrancar, BIA Separations, Slovenia Process related impurities in mRNA manufacturing
12.15–12.30	[OP38] Tomaž Bratkovič, University of Ljubljana, Slovenia Development of peptides as affinity ligands for human antibody purification
12.30–12.45	[OP39] Abida Zahirović, Jožef Stefan Institute, Slovenia Engineering IL-6-binding lactic acid bacteria for alleviation of inflammatory bowel disease
12.45–13.00	[OP40] Pasquale Russomanno, University of Naples Federico II, Italy Expression, purification, and NMR investigation of human KHSRP DNA binding protein using <i>E. coli</i> system
13.00	Closing remarks

**Saturday, September 17, 2022, MORNING SESSION
WORKSHOPS FOR YOUNG SCIENTISTS**

UL-FFA

10.30–12.30	Introduction to electrospinning / Introduction to flow cytometry Faculty of Pharmacy, University of Ljubljana, Aškerčeva cesta 7
13.00	Closing remarks

Plenary lecture (PL), Keynote lecture (KL), Oral Presentations (OP)



Plenary Lectures

PL2

30 YEARS IN FORMULATION OF PROTEIN PHARMACEUTICALS

What has been achieved- where do we stand today- what is next?

Gerhard Winter

¹ *Pharmaceutical Technology and Biopharmaceutics, Dept. Pharmacy, LMU München, Germany*

This lecture reviews the last, most relevant decades in protein formulation research.

Since recombinant protein drugs have entered the market in the early 1990ies this class of therapeutics has changed the scene of modern therapy dramatically. Since the turn of the century antibodies have outnumbered all other types of therapeutic proteins and the focus of formulation research efforts has focused in that direction.

The overarching goal of all formulation work has been and still is optimal storage stability at reasonable temperatures. Over the years, certain problems could be resolved, others came up new. For example, some of the first generation proteins were particularly low dose products and use of surfactants had focused on reducing losses due to surface adsorption. With high dose antibodies, such losses became mostly irrelevant, but surfactants remained necessary ingredients useful to minimize aggregation. Considered to be inert excipients first, they later became notorious to eventually degrade and contaminate formulations with their degradation products. With this background it has become necessary to also monitor their concentration in a formulation over time, adding significantly to the overall workload to qualify a marketable formulation.

Related to the issue of aggregate formation and particle contamination is the evolution of more sophisticated analytical methods to quantify and characterize such contaminations. The community still has to find the balance between high acclamations for new methods, allowing to measure submicron particle contaminations and the problem of the extremely small sample sizes and difficult interpretation of such data.

With the high dose antibody products other previously unknown complications evolved, the need to deal with high product viscosities, making fill and finish operations and application via injection needles quite problematic. It became clear, that only limited resolution of the problem can be achieved by classical formulation efforts, and a workaround via patch pumps, using higher volume or even the design of new protein molecules by protein engineering could help. The latter illustrates the most remarkable change that has happened in the last 30 years of protein galenics, i.e. the shift from starting formulation work late in the overall development process to a modern integrative development cycle, where stability, viscosity and other aspects are considered equally important as e.g. binding affinities when designing new antibodies. At that point, molecular modelling/MD simulations are part of the toolbox to optimize proteins and their formulation features.

Finally, the vision to select the most (long term) stable formulation from a few experiments, carried out in a few weeks or less, stimulated a lot of work in the past years. A combination of low volume-high sensitivity analytics, robotics, MD-simulations and better knowledge on aggregation pathways has brought us much closer, but we are not yet there. At least, for normal antibodies, platform approaches have replaced “from scratch” formulation programs quite successfully.

Now, new “formats” have received more interest and with viral vectors comprising physically spoken self-assembled protein envelopes a continuation of previous work with a bit higher complexity has become a recent challenge. Some of our own work in that field shall be presented to conclude the review circle.

PERSONALISED MEDICINE IN ESTONIA - MOVING FROM RESEARCH TO PRACTICE

Sulev Reisberg

Research fellow of health informatics Institute of Computer Science, University of Tartu

1. INTRODUCTION

Estonia is a global leader in the digitalisation of public services. Today, the central government and all municipalities provide services online through various e-government systems. Currently, Estonia is building a national IT infrastructure for bringing personalised medicine into common clinical practice. What have been the lessons learned so far?

2. METHODS

We outline the most important factors in Estonian policymaking and scientific works that have brought us to the current state of personalised medicine. We highlight the challenges that are still there to be solved.

3. RESULTS

When Estonia redeclared its independence in 1992 after the Soviet occupation, it had to build all organisations and processes from scratch. At the same time, the role of IT exploded globally, and Estonians were lucky to integrate IT into their processes from the start. In 2000, Estonia launched a national population-based biobank, which now covers 20% of the adult population and is one of the global research flagships on personalised medicine. After providing personal feedback for 3000 biobank participants in 2017 which included disease risks and pharmacogenetic information, it became clear that a special national IT infrastructure is needed for scaling personalised medicine services for the whole population. Since 2019, such a project has been ongoing. During this period, we have been facing several challenges.

4. DISCUSSION

Genetic data differs from other health data as it also reveals information about the others - how to deal with this? What is correct for most of the research cohort may be still incorrect for a single patient. Stricter regulations (for minimising risks) make personalised medicine more expensive - how to find an optimal

balance between cost, technical options, outcome, good healthcare service, data protection, legal and ethical aspects?

5. CONCLUSION

One can't optimise everything before putting first services into live - novel approaches require brave decisions to prevent losing time and human energy in an endless optimisation loop.

MICROFLUIDICS MANUFACTURING OF NANOPARTICLE BASED FORMULATIONS FOR PHARMACEUTICAL AND BIOMEDICAL APPLICATIONS

Hélder A. Santos^{1,2,3,4}

¹ Department of Biomedical Engineering,
University Medical Center Groningen / University of Groningen, 9713 AV Groningen, The Netherlands

² W.J. Kolff Institute for Biomedical Engineering and
Materials Science, University Medical Center Groningen / University of Groningen, 9713 AV Groningen, The Netherlands

³ Drug Research Program, Division of Pharmaceutical Chemistry and Technology, Faculty of Pharmacy,
University of Helsinki, FI-00014 Helsinki, Finland

⁴ Shanghai Key Laboratory for Prevention and Treatment of Bone and Joint Diseases, Shanghai
Institute of Traumatology and Orthopaedics, Ruijin Hospital, Shanghai Jiao Tong University
School of Medicine, 197 Ruijin Second Road, 200025 Shanghai, PR China

Drug carriers are gaining increased attention during recent years, due to their advantages. This includes increased drug stability, increased protection of drug against enzymatic metabolism, possibility of controlled drug release, high drug loading capacity, biocompatibility, less variability in release mechanisms and their kinetics, potential for increased permeability due to lipid and surfactant contents, and hence, enhanced bioavailability, and ligand mediated or passive targeting due to their small size through oral, parenteral, dermal, nasal, ocular, and pulmonary routes of administration.

Scale-up of nano/micro-particles fabrication process using batch techniques typically results in a reduction of control over the synthesis process, leading to wide particle size distributions and, in some cases, to uncontrolled particle aggregation. Current methods of particle synthesis rely largely on batch stirred homogenizers. However, major challenges persist in these systems with regard to process controllability and reproducibility, owing to the rapidity of the involved processes of mixing, nucleation, growth and agglomeration and their complex interactions when they take place concurrently.

Microfluidics has been defined as the manipulation of fluids in channels with dimension of tens of micrometer. Microfluidics has been extensively applied in the fabrication of materials with precisely controlled physicochemical features [1–16]. As a result of its excellent ability to manipulate nanoliters flows, microfluidics has emerged as an

alternative technique to the conventional methods for the preparation of nanoparticles. In comparison to the conventional methods, the particle preparation process is miniaturized in the microfluidic device, thereby leading to a reduction in the consumption of reagents. Furthermore, microfluidic approaches enable the continuous online synthesis of particles, which could reduce the batch-to-batch variations in the physicochemical properties of the obtained nanoparticles.

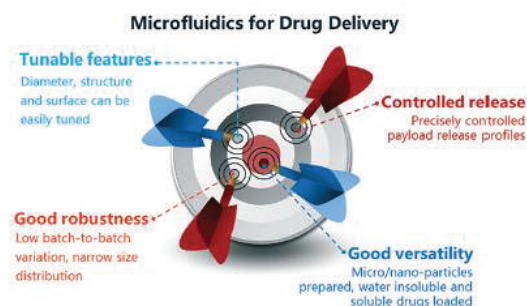


Figure 1. Figure legend. Please delete the square above and insert your figure in high resolution.

In this plenary talk, several examples on how different microparticles and nanoparticles can be prepared and scaled-up using microfluidics, as well as how they can be used to enhance the drug's targetability, intracellular drug delivery for both cancer chemo- and immune-therapy applications as well as other applications, will be highlighted and discussed.

Overall, our results suggest that microfluidics is a versatile technique to prepare advanced drug delivery systems for different pharmaceutical and biomedical applications

1. H. Zhang, W. Cui, X. Qu, H. Wu, L. Qu, X. Zhang, E. Mäkilä, J. Salonen, Y.-Q. Zhu, Z. Yang, D. Chen, H. A. Santos*, M. Hai*, D. A. Weitz*, *Proc. Natl. Acad. Sci. U.S.A.* 2019, 116, 7744.
2. Z. Liu*, Y. Li, W. Li, C. Xiao, D. Liu, C. Dong, M. Zhang, E. Mäkilä, M. Kemell, J. Salonen, J. T. Hirvonen, H. Zhang, D. Zhou, X. Deng, H. A. Santos*, *Adv. Mater.* 2018, 30, 1703393.
3. F. Fontana*, M.-A. Shahbazi, D. Liu, H. Zhang, E. Mäkilä, J. Salonen, J. T. Hirvonen, H. A. Santos*, *Adv. Mater.* 2017, 29, 1603239.
4. T. Yong, X. Zhang, N. Bie, H. Zhang, X. Zhang, F. Li, A. Hakeem, J. Hu, L. Gan, H. A. Santos*, X. Yang*, *Nature Commun.* 2019, 10, 3838.
5. M. Fuscillo, F. Fontana, S. Tähtinen, C. Capasso, S. Feola, B. Martins, J. Chiaro, K. Peltonen, L. Ylösmäki, E. Ylösmäki, F. Hamdan, O. K. Kari, J. Ndika, H. Alenius, A. Urtti, J. T. Hirvonen, H. A. Santos*, V. Cerullo*, *Nature Commun.* 2019, 10, 5747.
6. J. Zhang, Cheng Ji, Hongbo Zhang, Hui Shi, Fei Mao, Hui Qian, Wenrong Xu, Dongqing Wang, Jianming Pan, Xinjian Fang*, Hélder A. Santos*, Xu Zhang*, *Sci. Adv.* 2022, 8, eabj8207.
7. Z. Liu, W. Lian, Q. Long, R. Cheng, G. Torrieri, B. Zhang, A. Koivuniemi, M. Mahmoudzadeh, A. Bunker, H. Gao, H. He, Y. Chen, J. Hirvonen, R. Zhou, Q. Zhao*, X. Ye*, X. Deng*, H.A. Santos*, *Adv. Funct. Mater.* 2022.
8. Z. Wei, S.Wang, J. Hirvonen, H.A. Santos*, W. Li*, *Adv. Healthcare Mater.* 2022.
9. I. Arduino, Z. Liu, R.M. Iacobazzi, A.A. Lopodota, A. Lopalco, A. Cutrignelli, V. Laquintana, L. Porcelli, A. Azzariti, M. Franco, H.A. Santos*, N. Denora*, *Int. J. Pharm.* 2021, 610, 121246.
10. I. Arduino, Z. Liu, A. Rahikkala, P. Figueiredo, A. Correia, A. Cutrignelli, N. Denora*, H.A. Santos, *Acta Biomater.* 2021, 121, 566–578.
11. C. Costa, Z. Liu, S. Simões, A. Correia, A. Rahikkala, J. Seitsonen, J. Ruokolainen, A. Aguiar-Ricardo*, H.A. Santos, M. Luísa Corvo*, *Colloids Surf. B: Biointerfaces* 2021, 199, 111556.
12. C. Costa, Z. Liu, J.P. Martins, A. Correia, P. Figueiredo, A. Rahikkala, W. Li, J. Seitsonen, J. Ruokolainen, S.-P. Hirvonen, A. Aguiar-Ricardo, L. Corvo*, H.A. Santos*, *Biomater. Sci.* 2020, 8, 3270–3277.
13. S. Wang, S. Wannasarit, P. Figueiredo, J. Li, A. Correia, B. Xia, R. Wiwattanapatapee, J. Hirvonen, D. Liu, W. Li*, H. A. Santos*, *Mater. Horiz.* 2020, 7, 1573–1580.
14. P. Zhang, C. Du, T. Huang, S. Hu, Y. Bai, Cong Li, G. Feng, Y. Gao, Z. Li, B. Wang, J.T. Hirvonen, J. Fan, H.A. Santos*, D. Liu*, *Small* 2022, 18(15), 2200449.
15. P. Zhang, C. Li, T. Huang, Y. Bai, P. Quan, W. Li, Z. Zhang, F. Zhang, Z. Liu, B. Wan, A. Correia, J. Zhang, X. Wu, J.T. Hirvonen, H.A. Santos, J. Fan, T. Cai, D. Liu*, *Nano Lett.* 2021, 21(22), 9458–9467.
16. W. Li, J. Chen, S. Zhao, T. Huang, H. Ying, C. Trujillo, G. Molinaro, Z. Zhou, T. Jiang, W. Liu, L. Li, Y. Bai, P. Quan, Y. Ding, J. Hirvonen, G. Yin*, H.A. Santos*, J. Fan*, D. Liu*, *Nature Commun.* 2022, 13, 1262.

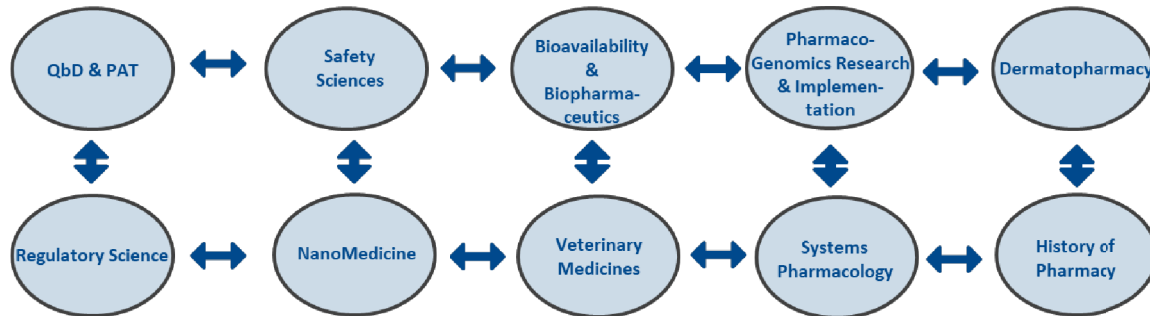
ACKNOWLEDGMENT

Sigrid Jusélius Foundation, the Academy of Finland (Grant No. 331151), China Scholarship Council and UMCG Research Funds.



EUFEPS was established on 21.09.1991 in Strasbourg as an independent scientific European body promoting the interests of the pharmaceutical sciences. EUFEPS is representing 15 societies from different countries with more than 15.000 pharmacists. The Mission of EUFEPS is to promote excellence in the pharmaceutical sciences and innovative drug research in Europe.

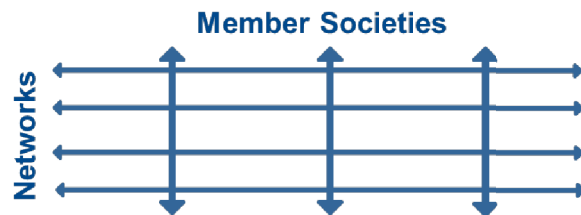
EUFEPS is a Matrix organization based on creating a platform for the productive interrelations and joint initiatives between member societies and individuals resulting EUFEPS Networks.



roles developing

- platforms for scientific exchange
- basis for research collaboration
- application for joint research grants
- collaborative education & training programs
- forum for strategy discussion and decision
- influence on science policy

towards a matrix organisation



Upcoming events:

5th GBHI Meeting

EUFEPS/AAPS GLOBAL Bio Equivalence HARMONISATION INITIATIVE

Amsterdam, The Netherlands |

September 28 -29, 2022

<https://gbhi.eufeps.org/>



Scan me

EUFEPS Annual Meeting 2023

International Meeting together with the Portuguese Pharmaceutical Society

Lisbon, Portugal | May 31 – June 2, 2023

<https://eufeps.org/eufeps-annual-meeting-conference-series.html>



Scan me

Contact us:

WEB: www.eufeps.org

Mail: secretariat@eufeps.org

Follow us:



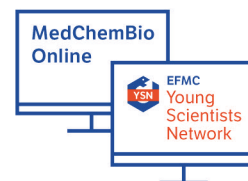
EFMC is an independent association founded in 1969, representing 29 societies from 25 European countries, and more than **9000 scientists**.
It's main objective is to **advance the science of medicinal chemistry and chemical biology**.

Upcoming Events

EFMC-YSN MedChemBioOnline

Webinars mixing science, soft-skills training & round table discussions

www.efmc.info/efmc-ysn-medchembioonline



EFMC-ISMC 2022

XXVII EFMC International Symposium on Medicinal Chemistry

Nice, France | September 4-8, 2022



EFMC-ISMC
International Symposium
on Medicinal Chemistry
Nice, France
September 4-8, 2022

EFMC-YMCS 2022

9th EFMC Young Medicinal Chemists' Symposium

Nice, France | September 8-9, 2022



EFMC-YMCS
Young Medicinal
Chemists' Symposium
Nice, France
September 8-9, 2022

Awards

- The Nauta Pharmacochimistry Award for Medicinal Chemistry and Chemical Biology
- The “UCB-Ehrlich Award for Excellence in Medicinal Chemistry”
- Prous Institute - Overton and Meyer Award for New Technologies in Drug Discovery

Visit www.efmc.info/awards for more information

Prizes

- EFMC Prizes for Young Medicinal Chemists in Industry & Academia

Visit www.efmc.info/prizes for more information

EFMC-YSN

The Young Scientists Network

Building a strong network at an early stage in your career is crucial!

The aim of the EFMC-YSN is to **inspire, connect** and **provide opportunities** to medicinal chemists and chemical biologists in their Early Career.

Visit www.efmc.info/ysn for more information

Keynote Lectures

SCIENTIFIC AND REGULATORY APPROACHES IN FORMULATION DEVELOPMENT WITH POORLY SOLUBLE DRUGS

H.Yesim KARASULU

Department of Pharmaceutical Technology, Faculty of Pharmacy, Ege University, Bornova Izmir, Turkiye

1. INTRODUCTION

In recent years, studies have attributed more than 40 percent of failures in new drug development to poor biopharmaceutical properties, particularly poor water solubility. Issues surrounding low solubility of the active ingredient, in particular can delay or completely hinder new drug development. New approaches in the formulation of water-insoluble drugs have provided significant benefits in reformulating many of the products currently on the market. More recently, it has been reported that 90 percent of new chemical substances in discovery and 75 percent for compounds under development show low solubility. For the poorly soluble and low bioavailability drugs, among the most promising approaches are developed lipid formulations. Lipid-based drug delivery systems (LBDDS) are one of the future-promising technologies designed to address such challenges [1,2]. A potential advantage of LBDDS is that the drug is administered to the gastrointestinal tract in solution and eliminates the need for dissolution. The drug remains in solution by digestion and occurs micellar dissolution caused by its own emulsification. The most important step in developing the formulation is to distinguish which excipient (s) and their proportions will resolve the drug dose. Lipid-based systems increase drug absorption from the gastrointestinal tract by accelerating the dissolution process, facilitating the formation of the dissolved phase by reducing the particle size to molecular levels, changing the drug intake, increasing the transportation of the drug to the systemic circulation through the intestinal lymphatic system by the enterocyte-based transport [3].

2. MATERIALS AND METHODS

2.1. Materials and Methods

This study includes development studies for many water-insoluble drugs for the oral administration, illustrated by formulation studies and regulations [4,5]. The purpose of these studies includes researchers and regulations in addressing formulation problems related to water-insoluble drugs [1-3]. Due to the essential influence of solubility on drug bioavailability, numerous strategies have been developed to improve the solubility, and consequently absorption and bioavailability of poorly water-soluble drugs [1-5].

3. RESULTS AND DISCUSSION

The formulation of drugs is carried out with the principal objective of enhancing their bioavailability. One of the most promising approaches is to also formulate as lipid-based formulations. Encapsulating or solubilizing the drug in lipid excipients can lead to increased solubilization and absorption, resulting in enhanced bioavailability drugs [1-3]. In this context, we would like to discuss the results of our recent work with these systems. Firstly, in our last study, different lipid-based drug delivery systems for valsartan were developed and then compared to a commercial tablet in vitro and in vivo. The new F2-SEDD formulation has been proposed as an ideal drug delivery system for valsartan with low solubility and bioavailability. As valsartan is a substance which solubility increases with increasing pH, the important thing is to increase its solubility at pH 1.2. At the end of the 24th hour at pH 1.2, the commercial formulation dissolved 63%, powder valsartan 9.4%, F2-SEDD 90.7%. Dissolution studies were also performed in fed and fasted media made with valsartan powder, F2-SEDD and commercial formulation (Fig. 1). The F2-SEDD formulation was released in gastric juice at a rate of 44.6%, while the commercial formulation was only released at a rate of 34.4%. This result indicates

that the F2-SEDD formulation may be more bioavailable than the commercial formulation due to the increased solubility of valsartan in an acidic environment. In vitro release results obtained with both the F2-SEDD formulation and the commercial formulation support the in vivo results. Under fasting (FaSSIF) and feding (FeSSIF) conditions, F2-SEDD and the commercial formulation show similar release rates in the intestinal fluid due to the high solubility of valsartan at pH 6.8 [4].

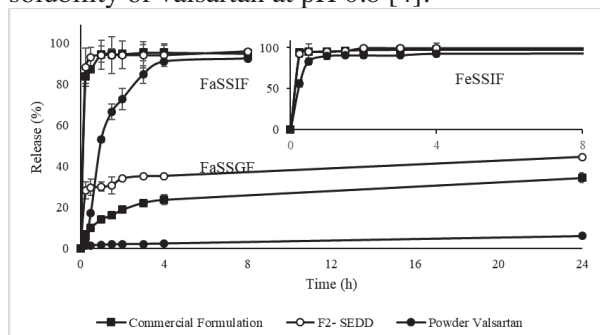


Figure 1. Dissolution graph of the valsartan formulation in different simulated fluids (FaSSGF, FaSSIF, FeSSIF)

Secondly, in our study, to improve oral bioavailability, new self-nanoemulsifying formulation (SNEDDS) of Rosuvastatin (RCa) was developed and characterized. RCa is a drug with low aqueous solubility and 20% oral bioavailability. The self-nanoemulsifying system was formulated with oil (Oleic acid), surfactant (Labrasol/Labrafil M 1944) and cosurfactant. According to the in vivo studies, RCa-SNEDDS has shown higher pharmacokinetic parameters than commercial RCa tablet. In addition, the RCa-SNEDDS unveiled safe pharmacodynamics effects for RCa in Yorkshire pig. Accordingly, the dosing amount for RCa may be reduced using SNEDDS formulation. Table 1 lists the pharmacokinetic parameters of RCa which were evaluated by a noncompartmental method using oral WinNonLin 5.3 program [5]. After RCa-SNEDDS administration, the $AUC_{0 \rightarrow 24}$ of RCa was significantly higher than the commercial RCa tablet ($P < 0.05$). In the case of oral administration, half-life of RCa in RCa-SNEDDS was significantly decreased (1.75-fold) when compared with commercial RCa tablet ($P < 0.05$).

Table 1. Pharmacokinetic parameters of SNEDDS - RCa and commercial tablet-RCa ($p < 0.05$)

Pharmacokinetic Parameters	RCa-SNEDDS	Commercial Tablet
$AUC_{0 \rightarrow 24}$ (h*ng/mL)	12867.9±5688.7	28.3±7.1
$AUC_{0 \rightarrow \infty}$ (h*ng/mL)	12883.9±5695.8	34.3±16.1
C_{max} (ng/mL)	30.3±14	4.7±1.4
T_{max} (ng/mL)	3±0.3	5.3±1.6

4. CONCLUSION

In this article, it was aimed to develop different lipid-based formulations containing poorly soluble drugs and to compare these formulations among themselves with in vitro such as legal regulations of these systems and in vivo characterization studies. Furthermore, by comparing the proposed formulation with the commercial formulation in terms of pharmacokinetics and pharmacodynamics, it offered higher possibility to propose a new lipid-based formulation. Consequently, in this study poorly soluble drug's new LBDDs may be suggested with increased oral bioavailability as an alternative to classical dosage forms.

5. REFERENCES

1. Kleberg, K. et al., Characterising the behaviour of poorly water soluble drugs in the intestine : application of biorelevant media for solubility, dissolution and transport studies. *Journal of Pharmacy and Pharmacology*, 2010.,2: 1656-1668.
2. Savla, R., et al., Review and analysis of FDA approved drugs using lipid-based formulations, *Drug Development and Industrial Pharmacy*, 2017. 43(11): 1743–1758.
3. Liu, R. (Ed), *Water - Insoluble Drug Formulation*, Second Edition, CRC Press, 2008.
4. Gulmezoglu, E., et al., Evaluation of valsartan's self-emulsifying drug delivery systems with in vitro lipolysis and in vivo and in vivo animal models, 8th BBBB International Conference on Pharmaceutical Sciences, 2019. P-53.
5. Karasulu, H.Y., et al., Enhancing Solubility and Bioavailability of Rosuvastatin into Self Nanoemulsifying Drug Delivery System, *Current Drug Delivery*, 2018. 15 (7), 1072-1082.

ACKNOWLEDGMENT

This study was supported by The Scientific and Technological Council of Turkey (TUBITAK Project No: 117S821; 112S637) and was also supported by Ege University Scientific Research Project (14/ECZ/005).

SIMPLE SYNTHESSES OF SYNTHONS FOR POTENTIAL ANTI-ALZHEIMER AND ANTIVIRAL DRUGS

Urban Košak¹, Stanislav Gobec¹

¹Faculty of pharmacy, University of Ljubljana, Slovenia

1. INTRODUCTION

There is a desperate need for new drugs for treating neurodegenerative diseases and viral infections. A simple way to develop new drugs is to synthesize analogues of approved drugs. This makes convenient methods for preparing key intermediates in the synthesis of these analogues highly desirable.

As part of our development of analogues of the anti-Alzheimer drug, donepezil, we needed orthogonally protected piperidines. Because procedures to prepare these compounds were not well documented outside of the patent literature, we developed a straightforward method to produce these building blocks in high overall yields (Fig. 1A) [1].

To develop analogues of the experimental anti-Alzheimer drug, phenserine, we needed 3- and 4-((phenylcarbamoyl)oxy)benzoic acids. The problem was that these compounds are not commercially available and procedures for their preparation have also not been reported yet. We solved this problem by developing a simple procedure to produce these acids in excellent overall yields (Fig. 1B) [2].

Aminocyclopentitols are structural motifs that are present in a number of pharmacologically important natural products and drugs including antiviral drug, peramivir. Because we identified a number of potential problems in the

previously described synthesis of the orthogonally protected aminocyclopentitols, we developed a more convenient way of making these important compounds [3].

2. RESULTS AND DISCUSSION

Orthogonally protected piperidines were prepared from commercially available nipecotamide, isonipecotamide, nipecotic acid and isonipecotic acid in 48-78% overall yields. Purification of the intermediates using this procedure is not necessary, and the final compounds were purified by simple flash column chromatography [1].

3- And 4-((phenylcarbamoyl)oxy)benzoic acids were prepared from commercially available 3- and 4-hydroxybenzoic acids in 76-90% overall yields. The main advantages of our method are the simplicity, as no purification of intermediates or final acids is required, and effectiveness [2].

Orthogonally protected aminocyclopentitols were prepared from commercially available D-(-)-ribose, L-(+)-ribose and D-(-)-lyxose in 11-22% overall yields. The absolute configurations of the synthesized final compounds were determined using NOESY spectroscopy [3].

KL4

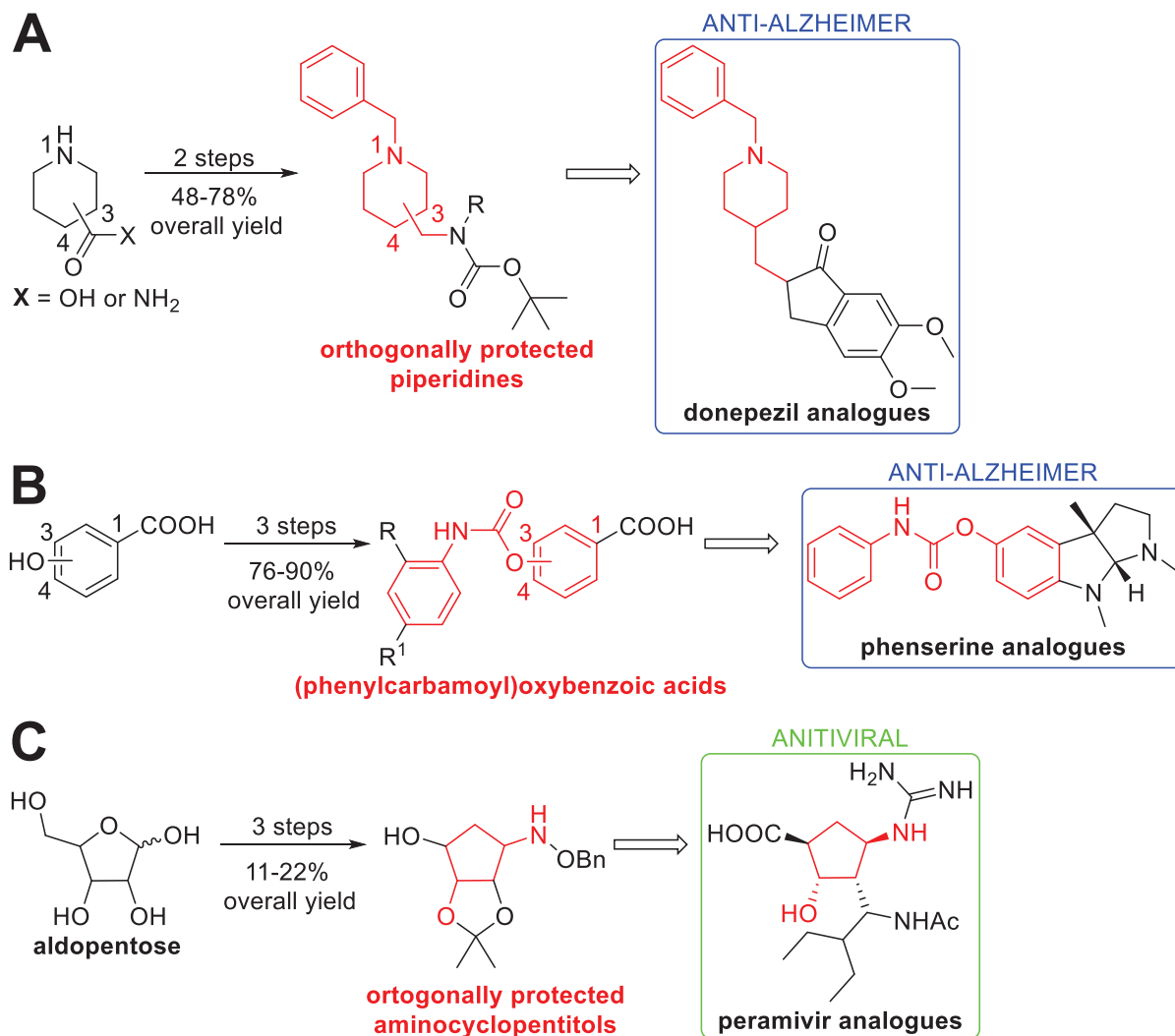


Figure 1. Simple syntheses to ease the development of new anti-Alzheimer drugs (A and B) and antiviral drugs (C).

KL4

3. CONCLUSION

We have developed convenient procedures for the synthesis of orthogonally protected piperidines, (phenylcarbamoyl)oxybenzoic acids and orthogonally protected aminocyclopentitols. These compounds are important building blocks which can ease the development of new anti-Alzheimer and antiviral drugs.

4. REFERENCES

1. Košak, U., et al., *Straightforward synthesis of orthogonally protected piperidin-3-ylmethanamine and piperidin-4-ylmethanamine derivatives*. Tetrahedron Letters, 2014. 55(12): 2037-2039.
2. Košak, U., et al., *A simple and effective synthesis of 3- and 4-((phenylcarbamoyl)oxy)benzoic acids*. Acta Chimica Slovenica, 2020. 67(3): 940-948.
3. Košak U., et al., *Convenient syntheses of orthogonally protected aminocyclopentitols from aldopentoses*. Tetrahedron Letters, 2015. 56(3): 529-531.

ACKNOWLEDGMENTS

We thank the Ministry of Higher Education, Science and Technology of the Republic of Slovenia, the Slovenian Research Agency ARRS (grant No. Z1-9195 and core funding P1-0208) and Lek Pharmaceuticals d.d. for financial support.

DESIGN, SYNTHESIS AND BIOCHEMICAL EVALUATION OF LOW-MOLECULAR-WEIGHT HUMAN NEUTROPHIL ELASTASE INHIBITORS

Aleš Obreza¹, Nina Porovne Černe¹, Sara Koščak¹, Špela Skala¹, Damjan Avsec¹, Maša Kandušer¹, Irena Mlinarič Raščan¹

¹ University of Ljubljana, Faculty of Pharmacy, Aškerčeva 7, 1000 Ljubljana, Slovenia

Correspondence: ales.obreza@ffa.uni-lj.si

1. INTRODUCTION

Serine proteases account for approximately one third of all known proteolytic enzymes. Their importance for organisms is shown by the fact that they are found in all kingdoms of living beings. In humans, they are involved in a variety of processes, such as blood clotting, intracellular signaling, apoptosis, immune response, and other processes. They are attractive targets in medicinal chemistry since the catalytic mechanisms of this class of enzymes have been extensively investigated over the past few decades and the three-dimensional structure of numerous enzymes has been published¹.

Human neutrophil elastase (HNE), a highly basic glycoprotein, is an important serine protease found in the azurophilic granules of the neutrophils. The potential substrates of an enzyme include almost all components of the extracellular matrix, as well as diverse proteins that include components of complement, immunoglobulins, clotting factors and cytokines.² It has been identified as a validated therapeutic target in several neurodegenerative and inflammatory diseases, its activity is upregulated in various cancer types. Many types of synthetic inhibitors have been reported in the literature and the inhibition of HNE has been reviewed.³

In the past years our research group has designed and synthesized a large number of serine protease inhibitors, which were screened for their activity against various enzymes. Compound **1** has been published recently and presented a useful lead compound in the design of new potent and selective derivatives.⁴

2. RESULTS AND DISCUSSION

The aim of current study was the synthesis of several related groups of *N*-benzylpiperazine-1-carbohydrazide derivatives, thereby optimizing the physicochemical and pharmacological properties of previously reported compounds. In particular, we tried to improve the potency and selectivity of compounds and increase their water solubility, which in turn may affect their bioavailability as well as facilitate the biochemical evaluation of the compounds *in vitro*.

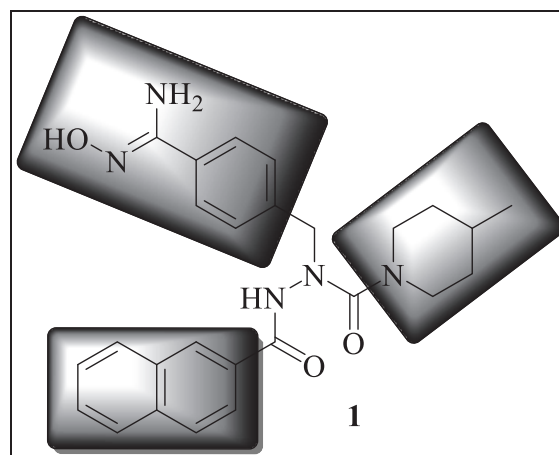


Figure 1. Structure of compound **1** with fragments that were replaced during the optimisation in the current study.

Compound **1** was optimized in three positions, marked in Figure 1. Instead of amidoxime we introduced nitrile, carboxylic, aminomethyl and amino groups at positions 3 and 4 of aromatic ring, piperidine in the side chain was replaced with other cyclic secondary amines, especially derivatives of piperazine. In the end we tried to

KL5

introduce more drug-like fragments instead of highly lipophilic and planar naphthalene ring. For this reason, we used sterically smaller, substituted benzene rings and alkyl groups of different length.

3. CONCLUSION

We prepared a medium-sized library of compounds that were *in vitro* biochemically evaluated against HNE, trypsin, chymotrypsin, cathepsin G and proteinase 3. The results show promising inhibition of HNE and selectivity against other enzymes of some derivatives, when tested in low micromolar concentrations.

4. REFERENCES

1. Di Cera, E. *Critical Review: Serine Proteases*. Life, 2009. 61(5): 510-515.
2. Korkmaz, B., et al. *Neutrophil elastase, proteinase 3, and cathepsin G as therapeutic targets in human diseases*. Pharmacological reviews 2010, 62(4): 726-759.
3. Groutas, WC., et al. *Neutrophil elastase inhibitors*. Expert opinion on therapeutic patents 2011, 21(3): 339-354.
4. Wang X, et al. *A Putative Serine Protease is Required to Initiate the RIPK3-MLKL—Mediated Necroptotic Death Pathway in Neutrophils*. Frontiers in pharmacology 2021, doi: 10.3389/fphar.2020.614928

ACKNOWLEDGMENT

The authors acknowledge the financial support from the Slovenian Research Agency.

ELECTROSPUN ANTIMICROBIAL PEPTIDES - NOVEL APPROACH FOR IMPROVED WOUND INFECTION TREATMENT

Kairi Lorenz¹, Celia Ramos^{1,2}, Marta Putrinš^{1,3}, Andres Meos¹, Tanel Tenson³, James Mason², Karin Kogermann¹

¹*Institute of Pharmacy, University of Tartu, Estonia, Country*

²*Institute of Pharmaceutical Science, King's College London, United Kingdom*

³*Institute of Technology, University of Tartu, Estonia*

1. INTRODUCTION

Non-healing wounds are a huge problem for society due to increased healthcare costs and significant burden to patients. It is known that biofilm formation is one of the main problems associated with chronic wounds. [1] That is why novel management strategies have been proposed such as topical antimicrobials in advanced wound dressings which can be used to eliminate the microbes. In addition, these advanced dressings can interact with the wound and support normal wound healing.

One of the methods that enables to produce such wound dressings is electrospinning (ES). [2] ES nanofiber mats, as wound matrices, can be functionalized using antimicrobial peptides (AMPs). [3] AMPs have many advantages compared to traditional antibiotics and topical AMP preparations are expected to have better treatment outcomes locally in the wound than systemic AMPs due to their antimicrobial, anti-inflammatory and/or immune modulating properties. [4]

The aim of the study was to understand the behaviour of AMPs during ES for preparing functionalised AMP-loaded wound matrices and characterise their physicochemical properties and antimicrobial efficacy relevant for the treatment of infected wounds. Hence, we formulated different AMP-loaded fiber matrices and investigated their antimicrobial properties in various antimicrobial assays.

2. MATERIALS AND METHOD

2.1. Materials

Different AMPs (Pleurocidin, its analogue D-Pleurocidin-KR, D-Pleurocidin and Temporin L) were purified and used (Cambridge Research Biomedicals, UK). For developing ES formulations, the selection of solvents and biodegradable high-quality polymers were

tested out. For efficacy studies, different pathogenic wound bacteria were used, such as *A. baumannii*, *P. aeruginosa*, *S. aureus*, *E. coli*.

2.2. ES fiber matrix development

Ten different peptide loaded ES matrices were created. Polymer solutions were made 24h prior ES. For matrix preparation an ESR200RD robotized ES system (NanoNC, Seoul, Republic of Korea) was used. Different ES methods and conditions were tested.

2.3. ES fiber matrix characterisation

Morphology of the ES matrices was investigated using scanning electron microscopy, SEM (Zeiss EVO 15 MA, Germany). Fiber diameter was measured in Image J (N=100).

Drug content and distribution across the matrix was analysed using high performance liquid chromatography (HPLC) (Shimadzu Europa GmbH, Germany). Three random 1 cm² or 4 cm² pieces were used for this.

Drug release was studied from the fiber matrix to a 5 mL buffer solution (1xPBS, pH 7.4) at 37 °C. Samples were collected at fixed timepoints and analysed by using HPLC.

Bacterial studies such as modified minimum inhibitory concentration (MIC) evaluation of ES matrices in liquid broth and on agar plate were carried out using pathogenic bacteria.

3. RESULTS AND DISCUSSION

3.1. Electrospinning (ES) and fiber morphology

Successful ES was performed with all ten different formulations in terms of stable and continuous ES process. SEM micrographs revealed smooth fibers with uniform diameter

KL6

confirming suitable ES formulations and conditions (Fig.1).

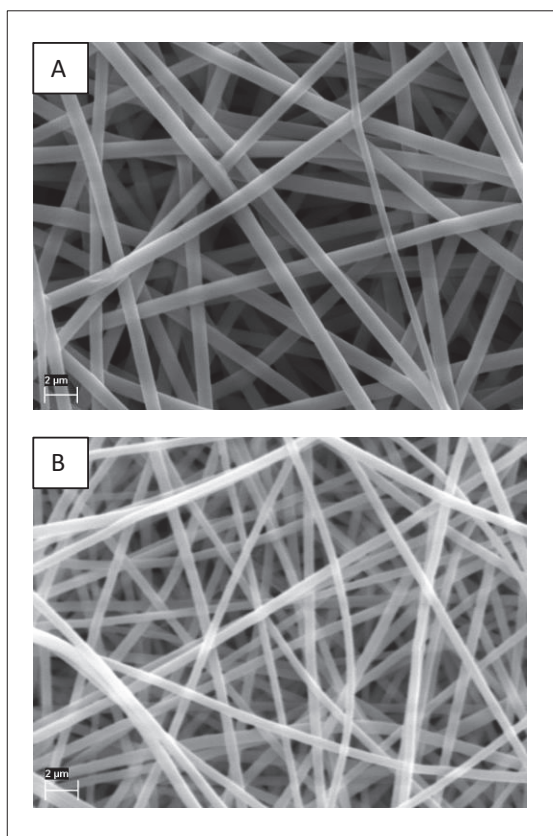


Figure 1. The morphology of AMP-loaded fiber matrices. SEM micrographs of two electrospun Pleurocidin-loaded fiber matrices, **A.** with a hydrophobic polymer, and **B.** with a hydrophilic polymer are shown as examples. Magnification 10 000x.

3.2. Peptide content in the fiber matrix and release into buffer solution

AMP content in fiber matrix varied largely between different formulations. Results showed that some solvents such as acetic acid degraded the peptide prior and during ES, whereas in other solvents the peptide was stable. Also, ES process affected the peptide stability, resulting in much higher peptide content when core-shell structured fibers were obtained. The release of AMP from the fibers was dependent on the chosen polymer. Our results showed that using hydrophobic polymers inhibited the drug release from the fiber matrix, but with hydrophilic polymer more than 50% of AMP was released into the buffer solution after 24 h.

3.3. Antimicrobial activity of peptide loaded fiber matrix

Traditional disc diffusion test on agar plate was unsuccessful for our formulations. On the other hand, formulations that successfully released the peptide from the matrix showed a drug loading dependent bacteriostatic or bactericidal effects in modified MIC test in liquid broth.

4. CONCLUSIONS

To conclude, our study showed that ES of antimicrobial peptides (AMP) can be affected by many parameters. It is of importance to find suitable solvents, polymers, and ES methods for the peptide to have a desired final fiber matrix with sufficient drug load and release from the fibers. Only then successful antimicrobial effects can be obtained. Further studies will investigate these matrices in our developed *in vitro* and *ex vivo* wound infection models.

5. REFERENCES

1. Lindholm C, Searle R. 2016. Wound management for the 21st century: combining effectiveness and efficiency. *Int Wound J* 13:5–15.
2. Preem L, Kogermann K. 2019. Electrospun Antimicrobial Wound Dressings: Novel Strategies to Fight Against Wound Infections, p. 1–41. *In* Recent Clinical Techniques, Results, and Research in Wounds. Springer, Cham.
3. Felgueiras HP, Amorim MTP. 2017. Functionalization of electrospun polymeric wound dressings with antimicrobial peptides. *Colloids Surfaces B Biointerfaces* 156:133–148.
4. Gera S, Kankuri E, Kogermann K. 2022. Antimicrobial peptides – Unleashing their therapeutic potential using nanotechnology. *Pharmacology & Therapeutics* 232, 107990

ACKNOWLEDGMENT

This work was funded by the Estonian Research Council grant PRG 1507. This presentation is supported by Doctoral School of Clinical Medicine, financed by the European Union Development Foundation (University of Tartu ASTRA Project PER ASPERA).

SEMISYNTHETIC GLYCOPEPTIDE ANTIBIOTICS - ONE WEAPON AGAINST TWO DEADLY ENEMIES

Anikó Borbás

Department of Pharmaceutical Chemistry, University of Debrecen, Egyetem tér 1, H-4032 Debrecen, Hungary

Antibiotic resistance is a very serious global healthcare issue, which we have to face every day. While Gram-negative bacteria are at the top of the list in causing severe, often incurable infections, antibiotic resistant Gram-positive bacteria also represent a major threat. Both MRSA and enterococci, namely *Enterococcus faecalis* and *E. faecium* are often resistant to traditional drugs such as vancomycin and other glycopeptide antibiotics. The COVID-19 pandemic has drawn attention to the limited scope of antiviral drugs, which, together with the increasing problem of antiviral drug resistance, also poses a serious global health threat.

Glycopeptides are a class of cell wall biosynthesis inhibitor antibiotics used to treat drug-resistant Gram-positive bacterial infections. In addition to the well-known antibacterial effect, glycopeptide antibiotics have exhibited potential for use against various enveloped viruses.

Over the past decade, our group has systematically studied modifications of glycopeptide antibiotics, vancomycin, teicoplanin, and ristocetin to produce compounds with high activity against glycopeptide resistant bacteria, and to design and prepare new derivatives that possess strong antiviral activity against deadly pathogens such as influenza viruses and SARS-CoV-2.

Among these derivatives, teicoplanin, ristocetin and vancomycin aglycones equipped with various lipophilic tags including natural apocarotenoids, or a dually lipophilic and hydrophobic perfluoroalkyl chain displayed either promising activity

against RNA viruses such as influenza and human coronaviruses 229E and SARS-CoV-2.¹⁻⁴ Moreover some of these derivatives also exerted high antibacterial effect against resistant Gram positive strains.⁵ Modification of the peptide core of teicoplanin with the superbasic guanidino-group resulted in high antibacterial effect against resistant enterococcus strains,⁶ while introduction of or multiple cationic aminoethyl moieties into the vancomycin aglycone led to synergistic activity against Gram-negative bacteria.

In this lecture, our recent results on synthesis, antibacterial and antiviral evaluations and SAR analysis of our semisynthetic glycopeptide derivatives will be presented.

REFERENCES:

1. Z. Szűcs, V. Kelemen, S. L. Thai, M. Csávás, E. Róth, G. Batta, A. Stevaert, E. Vanderlinden, L. Naesens, P. Herczegh, A. Borbás, Structure-activity relationship studies of lipophilic teicoplanin pseudoaglycon derivatives as new anti-influenza virus agents, *Eur. J. Med. Chem.* **2018**, *157*, 1017-1030.
2. Z. Szűcs, L. Naesens, A. Stevaert, E. Ostorházi, G. Batta, P. Herczegh, A. Borbás, Reprogramming of the antibacterial drug vancomycin results in potent antiviral agents devoid of antibacterial activity, *Pharmaceuticals*, **2020**, *13*, 139;
3. I. Bereczki, M. Csávás, Z. Szűcs, E. Róth, G. Batta, E. Ostorházi, L. Naesens, A. Borbás, P. Herczegh Synthesis of antiviral perfluoroalkyl derivatives of teicoplanin and vancomycin – *ChemMedChem* **2020**, *15*, 1661–1671.
4. I. Bereczki, H. Papp, ... P. Herczegh, A. Borbás, Natural apocarotenoids and their synthetic glycopeptide conjugates inhibit SARS-CoV-2 replication, *Pharmaceuticals*, **2021**, *14*, 1111
5. Z. Szűcs, E. Ostorházi, M. Kicsák, L. Nagy, A. Borbás, P. Herczegh, New semisynthetic teicoplanin derivatives have comparable in vitro

KL9

- activity to that of oritavancin against clinical isolates of VRE, *J. Antibiotics*, **2019**, *72*, 524-534.
6. Z. Szűcs, I. Bereczki, E. Róth, M. Márton, E. Ostorházi, G. Batta, L. Nagy, Z. Dombrádi, A. Borbás, P. Herczegh, N-Terminal guanidine derivatives of teicoplanin antibiotics strongly active against glycopeptide resistant *Enterococcus faecium*. *J. Antibiotics* **2020**, *73*, 603–614

RATIONAL DESIGN OF BALANCED DUAL-TARGETING ANTIBACTERIAL COMPOUNDS WITH LIMITED RESISTANCE

Lucija Peterlin Mašič¹, Martina Durcik¹, Tihomir Tomašič¹, Žan Toplak¹, Janez Ilaš¹, Petra Szili², Csaba Pal²

¹ University of Ljubljana, Faculty of Pharmacy, Aškerčeva 7, 1000 Ljubljana

² Synthetic and Systems Biology Unit, Biological Research Center, Szeged, Hungary

1. INTRODUCTION

There is an urgent need for new therapies and new antibiotics to treat deadly infections caused by so-called ESKAPE pathogens – bacteria that are often resistant to available antibiotics. Not only infections caused by these pathogens are difficult to treat, but discovering new therapies to overcome Gram-negative resistance is particularly challenging. The World Health Organization (WHO) classifies these pathogens as a critical threat because they are resistant to all or nearly all of the antibiotics available today. Over 95 percent of the antibiotics in development today are being researched by small companies and academia, not the big pharmaceutical companies that once dominated the field [1].

To ensure that the supply of new antibiotics keeps pace with these evolving pathogens, a robust pipeline of new antibiotics and innovative solutions is needed. One promising strategy to address this rapid evolution of resistance is the design of antimicrobial compounds that equipotently inhibit multiple bacterial targets. The rationale for this approach is that the development of resistance to multitargeting antibiotics would require the simultaneous occurrence of multiple specific mutations at all targets, which is extremely rare. Therefore, multitargeting antibiotics (MTA) should be less susceptible to resistance compared to monotargeting antibiotics. However, designing antibiotic compounds that equipotently inhibit two or more bacterial targets while exhibiting adequate antibacterial efficacy, safety, and physicochemical properties remains a challenge. Although a major focus of companies, only a handful of such antibiotics show balanced inhibition at multiple targets.

2. MATERIALS AND METHODS

2.1. Materials

Material and methods include hit-to-lead optimisation of new DNA gyrase B and topoisomerase IV (Fig. 1) inhibitors with integrated methodology to obtain high quality leads with antibacterial activity against methicillin-resistant (MRSA), vancomycin-intermediate (VISA) *Staphylococcus aureus* and *Acinetobacter baumannii* isolates that are less prone to resistance development. Integrated methodology includes structure-based drug design, organic synthesis, PADMET profiling, antibacterial testing and *in vivo* antibacterial efficacy testing [2, 3].

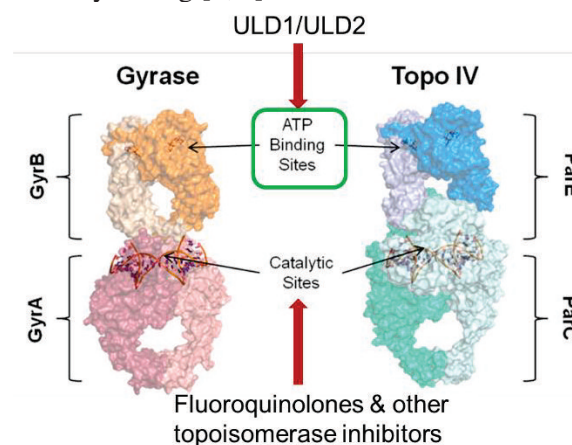


Figure 1. Targeted proteins: ATP-binding sites of DNA gyrase B and topoisomerase IV (ParE).

3. RESULTS AND DISCUSSION

3.1. Design of ULD1 and ULD2 compounds

ULD1 and ULD2 compounds were designed using structure-based design based on several cocrystal structures [2].

KL10

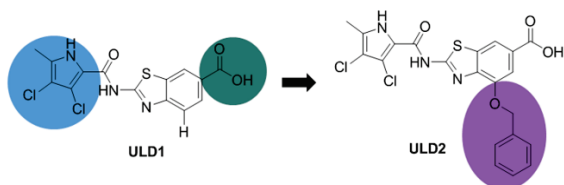


Figure 2. Structures of ULD1 and ULD2.

3.2. Balanced dual enzyme inhibition

Fig. 3 presents low nanomolar balanced dual inhibitions of ULD1 and ULD2 on DNA gyrase B and topoisomerase IV from several bacterial species [2].

Enzyme	Novobiocin IC ₅₀ (nM)	ULD2 IC ₅₀ (nM)	ULD1 IC ₅₀ (nM)
<i>A. baumannii</i> DNA gyr	16.0	19	16.9
<i>A. baumannii</i> topo IV	4040	64	n.d.
<i>P. aeruginosa</i> DNA gyr	22.8	9.4	1.2
<i>P. aeruginosa</i> topo IV	4960	235	n.d.
<i>S. aureus</i> DNA gyr	1.7	0.78	3.3
<i>S. aureus</i> topo IV	2000	2.0	9.3

Figure 3. Dual inhibition of compounds ULD1 and ULD 2.

3.3. Antibacterial potencies of ULD1 and ULD2

Antibacterial potencies against Gram-negative and Gram-positive bacteria are presented in the Fig. 4 [2].

Species (Resistance)	Strain	ULD-01 MIC (µg/mL)	ULD-02 MIC (µg/mL)
<i>Staphylococcus aureus</i>	ATCC 29213	1	0.5
<i>Staphylococcus aureus</i>	ATCC 33594	0.5	0.125
<i>Staphylococcus aureus</i> , MRSA, VISA, Quinolone ^R	ATCC 700699	0.5	≤0.03125
<i>Staphylococcus aureus</i> , USA400, MRSA	NRS123	0.5	0.125
<i>Staphylococcus aureus</i> , LZD-NS, MRSA, Quinolone ^R	NRS271	1	0.25
<i>Staphylococcus aureus</i> , MRSA, Van ^R , Quinolone ^R	ECL 2963646	0.125	≤0.03125
<i>Staphylococcus aureus</i> , MRSA, VISA, Quinolone ^R , Mup ^R	CDC/AR-BANK 0218	1	0.125
<i>Staphylococcus aureus</i> , USA800, MRSA, Quinolone ^R	NRS22	2	0.5
<i>Staphylococcus epidermidis</i> , MRSE	ATCC 51625	0.0625	≤0.03125
<i>Enterococcus faecalis</i>	ATCC 29212	0.125	≤0.03125
<i>Enterococcus faecalis</i> , VanB	ATCC 51575	0.0625	≤0.03125
<i>Enterococcus faecium</i>	ATCC 19434	2	0.5
<i>Enterococcus faecium</i> , VanA, Quinolone ^R	BAA-2320	0.25	≤0.03125
<i>Enterococcus faecium</i> , VanB, Quinolone ^R	CCUG 56858	2	0.25
<i>Streptococcus pneumoniae</i>	ATCC 49619	0.25	0.25
<i>Streptococcus pneumoniae</i> , MDR	ATCC 51916	0.5	0.25
<i>Streptococcus pneumoniae</i> , MDR	ATCC 700673	0.5	0.25
<i>Streptococcus pyogenes</i>	ATCC 14289	0.25	0.25
<i>Neisseria gonorrhoeae</i>	ATCC 700825	≤0.03125	≤0.03125
<i>Neisseria gonorrhoeae</i> , MDR, WHO-L, Quinolone ^R	CCUG 57598	≤0.03125	≤0.03125
<i>Haemophilus influenzae</i>	ATCC 49247	≤0.03125	0.125
<i>Haemophilus influenzae</i>	ATCC 35056	0.125	1
<i>Helicobacter pylori</i>	ATCC 43504	4	4
<i>Clostridium difficile</i> , toxigenic, ribotype 078	BAA-1875	≤0.03125	≤0.03125
<i>Acinetobacter baumannii</i>	ATCC 17978	4	2
<i>Pseudomonas aeruginosa</i>	ATCC 27863	8	4
<i>Klebsiella pneumoniae</i>	ATCC 10031	1	4
<i>Escherichia coli</i>	ATCC 25922	4	32

Figure 4. Antibacterial potencies of ULD1 and ULD2.

3.4. Antibacterial activities against 95 *S. aureus* MRSA and vancomycin-resistant isolates *in vitro*

100% of the strains were inhibited at 1 µg/mL concentration of ULD1 and ULD2 (Fig. 5) [2].

3.5. Efficacy of ULD1 (iv) in a neutropenic mouse infection of *Staphylococcus aureus* VISA ATCC 700699

The antibacterial activity of ULD1 was comparable to that of linezolid, a widely used

clinical antibiotic against systemic MRSA infections, but resistance against this drug is emerging rapidly [2].

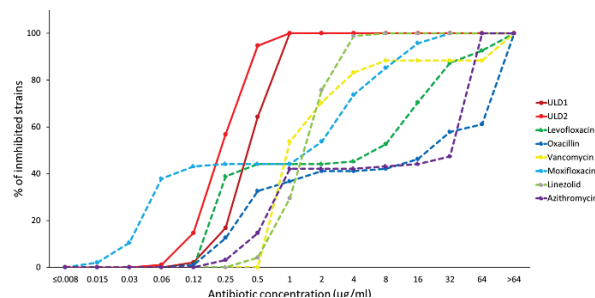


Figure 5. Antibacterial activities of ULD1 and ULD2 against a panel of 95 *S. aureus* clinical isolates.

4. CONCLUSION

We have discovered new multitargeting antibacterial compounds, namely ULD1 and ULD2, which belong to a new chemical class. They inhibit almost equipotent in the low nanomolar range bacterial DNA gyrase and topoisomerase complexes IV from *S. aureus*, *A. baumannii* and *E. coli* and interact with several evolutionarily conserved amino acids in the ATP binding pockets of their target proteins. Resistance mutations to these compounds are rare, have limited effects on compound sensitivity, and significantly reduce bacterial growth. Based on their antibacterial potency and lack of toxicity demonstrated in mice in the VISA infection model, these compounds could lead to new therapies against multidrug-resistant bacterial infections.

5. REFERENCES

1. Brown, ED et al. *Nature*, 2016, 529, 336.
2. NYERGES, A. TOMAŠIČ, T., DURCIK, M. ET AL., *PLOS BIOL* 18(10): E3000819.
3. TOMAŠIČ, T, ZIDAR, N, DURCIK, M, ILAŠ, Janez, ZEGA, A, DURANTE CRUZ, C, TAMMELA, P, PÁL, C, NYERGES, Á, KIKELJ, D, PETERLIN-MAŠIČ, L. *New class of DNA gyrase and/or topoisomerase IV inhibitors with activity against gram-positive and gram-negative bacteria : Patent application publication US 2021/0323957 A1, 2021-10-21.*

ACKNOWLEDGMENT

This research was funded by Slovenian Research Agency (ARRS) grant numbers J1-9192, N1-0098, P1-0245, J1-3030 and IMI ENABLE project: European Gram-negative Antibacterial Engine.

APPLICATION OF HOT-MELT TECHNOLOGIES IN DESIGNING FORMULATIONS WITH POORLY WATER-SOLUBLE ACTIVE INGREDIENTS

Gregor Lorbek¹, Klemen Korasa¹

¹ *Krka, d. d., Novo mesto, Slovenia*

1. INTRODUCTION

The pharmaceutical industry encounters many challenges, e.g. poor active ingredient solubility, rising manufacturing costs, tightening environmental policies and extensive patent protection. Newer approaches, such as hot-melt granulation, extrusion or coating are becoming recognized for their speed, cost-effectiveness and small environmental footprint. Their versatility can be used to increase active ingredient solubility and bioavailability, taste masking, and for modifying or controlling active ingredient release. For instance, the dissolution rate of poorly water-soluble active ingredients can be significantly improved with melt granulation by using hydrophilic binders that improve wettability through intimate contact with the active ingredient [1]. Also, hot-melt extrusion has become a method of choice for improving dissolution rate through amorphous solid dispersions, where a systematic developmental approach of polymer screening, multivariate statistics and Quality-by-Design is highly recommended [2]. Nevertheless, several potential disadvantages should be considered, e.g. stability of thermolabile active ingredients due to high processing temperatures or potential recrystallization of amorphous solid dispersions. To a certain extent we still lack knowledge about predictability and modelling of these processes. We intend to show possible applications of hot-melt granulation and extrusion technologies used in development and production of formulations containing poorly water-soluble active ingredients.

2. MATERIALS AND METHODS

2.1. Materials

We used hot-melt granulation to prepare a film-coated tablet containing a poorly water-soluble active ingredient, a low-melting point hydrophilic binder poloxamer 188 (BASF, USA), and other suitable commercially available excipients. Hot-melt extrusion process was investigated with polymers polyvinyl alcohol (PVA) (Merck, Germany), copovidone (Ashland, USA), and Soluplus® (BASF, USA). Extrudates of solid dispersions were then formulated into film-coated tablets with other excipients.

2.2. Hot-melt granulation in a high-shear mixer

GEA Collette Gral 10 high-shear mixer (GEA, Germany) was used for hot-melt granulation. Temperature of the heated jacket ranged between 70–80 °C, and end-point granulate temperature between 58–68 °C. A 3² full factorial design of experiments (Design Expert v12, Stat-Ease, USA) was employed to assess the influence of the two temperatures on assay and content uniformity.

2.3. Hot-melt extrusion with twin-screw extruder

Coperion ZSK MI18 twin-screw extruder (Coperion, Germany) was used for hot-melt extrusion. Barrel temperature in the range between 190–230 °C, feed rate from 10–30 g/min, different active ingredient particle sizes and various active ingredient-to-polymer ratios were assessed for their effects on physicochemical properties of solid dispersions.

3. RESULTS AND DISCUSSION

KL13

3.1. Optimization of hot-melt granulation process

According to literature, solubility of a model poorly water-soluble active ingredient can be increased by a hydrophilization process in a fluid-bed granulator. Our approach was to use hot-melt in-situ granulation using hydrophilic binders [1] that led to a low-cost water-free formulation with desired active ingredient solubility. The assay and content uniformity challenges were investigated by varying temperatures of the heated jacket and end-point granulate temperatures using a 3² full factorial experimental design. Shorter granulation times resulted in lower assay, and longer times in higher assay, whereas no effect was observed on content uniformity, which remained high [Fig. 1]. This was solved with particle size reduction of poloxamer 188, since more nucleation points for granule growth were introduced to the granulation mixture this way, shifting from bimodal to more uniform particle size distribution of the granulate, which reduced the relative standard deviation of content three-fold.

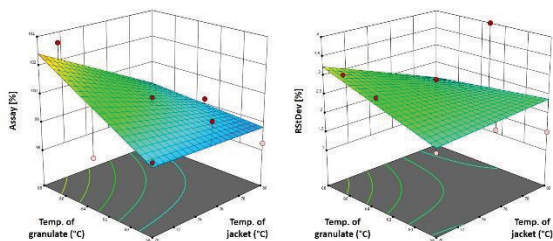


Figure 1. Contour plots of the heated jacket and end-point granulate temperature showing higher assay at longer processing times (i.e. at lower jacket and higher end-point granulate temperatures), and lower assay at shorter processing times (i.e. higher jacket and lower end-point granulate temperatures). No significant effect on content uniformity was observed.

3.2. Designing a hot-melt extrusion formulation

In the second example, hot-melt extrusion was applied to design a solid dosage form containing poorly water-soluble active ingredient. An initial screening of high-degradation temperature polymers copovidone, Soluplus®, and PVA by DSC showed good mixing of high-melting point active ingredient only with copovidone. Nevertheless, we were able to

produce amorphous solid dispersions with all three polymers at a small scale. Soluplus® was later discarded because the dissolution rate was too low compared with the other two polymers. PVA formed a very hard extrudate that was difficult to reduce to finer particles by milling, which led to problems with content uniformity. In the next phase, we therefore optimized the process only with copovidone in order to achieve continuous production of physically stable amorphous solid dispersion with no detectable crystalline drug particles that could trigger recrystallization. The extrusion temperature, active ingredient-to-polymer ratio, dwell time that was controlled by feed rate, and drug particle size had an important effect on the level of residual crystallinity in the amorphous solid dispersion. By determining optimal values of these critical processing parameters, we were able to produce physically stable, completely amorphous solid dispersion on the pilot scale with the desired dissolution rate.

4. CONCLUSION

We were able to produce physically stable formulations with improved active ingredient solubility, the desired dissolution rate, and good technological processability by employing hot-melt granulation and extrusion techniques. During the development, we obtained good understanding of the processes that will hopefully further advance the use of hot-melt technologies in the pharmaceutical industry.

5. REFERENCES

1. Kukec S., Dreu R., Vrbanec T., Srčić S. and Vrečer F., *Characterization of agglomerated carvedilol by hot-melt process in a fluid bed and high shear granulator*. International Journal of Pharmaceutics, 2012. 430(1-2): 74-85.
2. Simões M.F., Pinto R. M. A., Simões S., *Hot-melt extrusion in the pharmaceutical industry: toward filing a new drug application*. Drug Discovery Today, 2019. 24(9):1749-1768.

ACKNOWLEDGMENT

This research was supported by Krka, d. d., Novo mesto.

MASS SPECTROMETRY AS A POWERFUL TOOL FOR ANALYSING DEGRADATION PATHWAYS: 1,4-BENZODIAZEPINE CASE STUDY

Žiga Hodnik¹, Jure Bezenšek², Aleš Judež¹

¹ Pharmaceutical R&D, Analytics Development, Krka, d. d., Slovenia

² API R&D, Chemistry, Krka, d. d., Slovenia

1. INTRODUCTION

Control of active pharmaceutical ingredient (API) degradation products is essential for safety of pharmaceutical products. Therefore, understanding API degradation pathways works as the basis for analytical and pharmaceutical formulation scientists when they are developing new products or improving product life cycles [1].

High-resolution mass spectrometry coupled with high- or ultra-performance liquid chromatography (LC-HRMS) is one of the most established techniques for analysing the structure of degradation products, since it does not require their isolation, which is demanding due to their low presence in pharmaceutical products [1]. On the other hand, inductively coupled plasma mass spectrometry (ICP-MS) represents one of the most powerful tools for detection and quantification of elemental impurities in pharmaceutical products due to ICP-MS detection limits in ppm or sub-ppm ranges [2].

Herein, we present a less common degradation pathway of 1,4-benzodiazepine depressant in parenteral solutions, which was discovered using aforesaid techniques. 1,4-Benzodiazepines, which act as enhancers of inhibitory neurotransmitter GABA, most often degrade to aminobenzophenone impurity in an acidic aqueous medium, while we discovered a metal catalysed redirection of degradation pathway into phenylquinoline-2-one impurity (Fig. 1).

2. RESULTS AND DISCUSSION

While performing routine high-performance liquid chromatography (HPLC), we detected an unusual trend in the content of related substances of 1,4-benzodiazepine in one of the development batches of parenteral formulation.

According to our experience and reference data [3], aminobenzophenone, is a predominant degradation product in 1,4-benzodiazepine parenteral products, while the aforesaid batch showed a significant degradation to a so far unknown impurity in our development formulation.

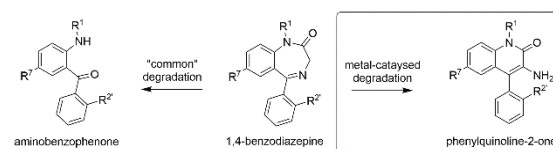


Figure 1. Common, acid-catalysed degradation pathway of 1,4-benzodiazepine versus metal-catalysed degradation pathway.

We therefore performed a LC-HRMS analysis of the batch sample. After overcoming different ionization behaviour of the degradation product compared to the parent API, the analysis revealed the same exact mass, together with comparable MS/MS spectrum. Furthermore, hydrogen-deuterium exchange experiment revealed the presence of two additional exchangeable hydrogen atoms in the degradation product, which indicated possible phenylquinoline-2-one structure. The LC-HRMS results were later confirmed using a suitable reference substance.

A statistical analysis of manufacturing process and routine analyses data for all development batches was performed. The statistical analysis did not detect any trends or outliers. While pH and temperature, as most common factors for directing degradation pathways in parenteral formulations, did not stand out, we decided to perform an ICP-MS analysis of elemental impurities.

ICP-MS revealed only a minor difference in a single metal ion content in the outlier batch compared to other development batches. Even though the difference was present in the very

KL14

low-ppm range, we performed additional ICP-MS analyses, which revealed that glass ampoules were a source of the low-ppm range content of pathway-directing metal.

Finally, the spiking of a suitable metal salt in the otherwise stable batch of parenteral solution confirmed its pathway-directing impact.

3. CONCLUSION

To summarize, the capacity of the state-of-the-art LC-HRMS instruments to provide for a detailed insight into chemical structures of API degradation products together with ICP-MS high sensitivity for the presence of trace elemental impurities is a powerful tool for an analytical chemist involved in the development of pharmaceutical products.

Despite the negligible presence of contaminants in low-ppm range, such contaminants can act as powerful catalysts, which significantly affect

the stability of pharmaceutical products. The rigorous control of contaminants in pharmaceutical industry therefore represents an important element for the quality and safety of pharmaceutical products.

4. REFERENCES

1. Baertschi, S W et al., *Pharmaceutical Stress Testing: Predicting Drug Degradation*. Informa Healthcare, 2011. 2nd Edition.
2. Barin, S J et al., *Determination of Elemental Impurities in Pharmaceutical Products and Related Matrices by ICP-Based Methods: a Review*. *Analytical and Bioanalytical Chemistry*, 2016. 408(17): 4547-4566.
3. Loftsson, T et al., *1,4-Benzodiazepines: Chemical Stability and Cyclodextrin Solubilisation*. *Journal of Drug Delivery Science and Technology*, 2021. 66: 102936.

Cansel KOSE OZKAN

Gulhane Faculty of Pharmacy, Department of Pharmaceutical Technology, University of Health Sciences, Ankara, TURKIYE

1. INTRODUCTION

Personalized medicine, also called precision medicine in some studies, is a medical model that divides people into different groups by tailoring medical decisions, practices, interventions and/or products to each patient according to the predicted response or risk of disease [1]. The terms personalized medicine, precision medicine, layered medicine, and P4 medicine are often used interchangeably to describe this concept, although the terms are sometimes used separately to indicate specific points [2]. This concept is summarized as therapy in the right patient, with the right drug, at the right dose.

The main goal of the design and development process is to create a product that can be used safely and effectively by the patient group. From a pharmaceutical industry perspective, ICH Q8 guidance leads to the definition of a Quality Targeted Product Profile (QTPP) for a particular drug product and patient population. It is recognized that designing drugs suitable for paediatrics, adults and elderly patients will result in multiple presentations that can lead to smaller production batch sizes. Dosage flexibility, easy-to-swallow formulations and more accessible packaging are all factors to consider. Dose flexibility can be achieved with a variety of dosage forms such as oral liquids, mini-tablets, or multiple particles [3]

Pharmaceutical compounding is one of the applications of personalised medicine. Though not always utilizing genetic data, the specialized manufacturing of a medication with a range of qualities (e.g. dose, ingredient selection, route of administration, etc.) are selected and crafted for an individual patient is accepted as an area of personalised medicine.

Pharmaceutical compounding offers a variety of benefits, like gives a prescriber the option to

select the specific administration form that a patient needs.

The effective delivery of tailored medications created through pharmacy compounding to the body's illness locations is one ongoing study field. For instance, by combining real-time imaging and examining the pharmacodynamics of the drug delivery, researchers are attempting to create nanocarriers that can precisely target the specific location.

Although alternative routes such as mucosa, skin, and lung have become popular in recent years taking advantage of advances in drug delivery technology, cost is significant and many oral formulations can be produced at lower costs, allowing for a wide variety of alternatives.

The oral route remains the most important pillar of drug dosing methods due to cost, convenience, and patient compliance.

The likelihood of patient non-adherence increases with the complexity of the drug regimen and is of particular concern in patients with complex health conditions combined with multiple drug experience from various indications. Complex dosing regimens often benefit from oral user-friendly dosage forms due to their reduced side effects and simplified regimens in studies of the treatment of patients.

Good taste sensation and taste masking techniques in patients who refuse or cannot swallow tablets, such as paediatric and geriatric patients, may change the drug perception, especially in paediatric patients, such as the resistance of the bitter pill. Products that disintegrate rapidly in the mouth dissolve in the mouth within seconds and in such cases may increase the clinical effect of the drug due to pre-gastric absorption in the mouth, pharynx, and oesophagus, avoiding first pass hepatic metabolism. the drug can significantly increase compared to conventional tablets.

KL16

In some indications, such as migraine, the faster onset of action associated with orally disintegrating drug forms may increase patient satisfaction and adherence to treatment. While advanced formulations may be more expensive than conventional dosage forms, user-friendly dosage forms often have more favourable pharmacological profiles and therefore have the potential to reduce overall treatment cost by reducing the burden on healthcare.

Another aspect that is critical for certain patient populations is the need to take multiple medications, especially for the elderly who are battling multiple diseases. The development of fixed-dose combination products may result in fewer prescriptions and a better cost-benefit ratio than prescribing drugs individually.

The most important challenges to be overcome in the development of oral user-friendly formulations are physiologically impaired swallowing function in specific patient groups, the widespread need for taste masking in oral solutions or orodispersible tablets, the need to develop more analytical technologies, with the addition of more excipients to make a more user-friendly product, which techniques are more complex and more interactive thereby increasing the possibility of much more formulation instability. Minimum dosing frequency is particularly important in the case of adherence, and there have been numerous studies investigating the role the dosing schedule can play in medication adherence. There are significant physiological and metabolic differences between children and adults in the design of paediatric drugs, and there are significant differences in drug dose, especially in cases where chronic disease is evident. Understanding the properties and requirements of an active ingredient in terms of formulation is critical to proper product design and performance. Before an API formulated into a dosage form, its chemical and physical properties need to be characterized. Certain physicochemical properties may make oral administration of a substance impossible; this is generally accurate for proteins. The required solubility also requires specific formulation approaches [4,5].

2. CONCLUSION

In conclusion, patient comfort is a decisive factor in drug compliance and better outcomes. The benefit of a drug can be achieved primarily by designing and developing appropriate formulation options tailored to the needs of specific groups of patients. Oral delivery systems save costs because they can be produced in large quantities within short production times while maintaining consistent quality. It should be noted that the healthcare system benefits financially from user-friendly dosage forms. However, much more research is needed to balance both patient dosage preferences and the needs of the caregiver, prescriber, and payer.

3. REFERENCES

1. Academy of Medical Sciences. Stratified, personalised or P4 medicine: a new direction for placing the patient at the centre of healthcare and health education. 2015.
2. Movafagh, A. Personalised medicine in modern era. *Asian Pacific Journal of Cancer Biology*, 2016, 1.(2): 31-32.
3. Page, S, et al., An industrial perspective on the design and development of medicines for older patients. *Int J Pharm.* 2016 Oct 30;512(2):352-354.
4. Thomas, F. Making the Ideal Dosage Form. *Pharmaceutical Technology, Supp.: APIs, Excipients, and Manufacturing*, 2020. 4: 17-18.
5. Tovey, G. D. (ed.). *Pharmaceutical Formulation: The Science and Technology of Dosage Forms*. Royal Society of Chemistry, 2018.

PHARMACOGENOMIC AND BIOLOGICAL IMPLICATIONS OF THIOPURINE S-METHYLTRANSFERASE

Dunja Urbančič¹, Alenka Šmid¹, Anita Kotar², Janez Plavec², Nataša Karas Kuželički¹, Irena Mlinarič-Raščan¹

¹ Faculty of Pharmacy, University of Ljubljana, Slovenia

² Slovenian NMR Centre, National Institute of Chemistry, Slovenia

1. INTRODUCTION

Despite major therapeutic advances in the field of biologic agents, small molecules remain an important therapeutic pillar in many diseases. Among them, thiopurines - cytostatics and immunosuppressants - are a regularly prescribed agents for the treatment of childhood leukemia and certain autoimmune diseases. One of the most important factors affecting their efficacy and toxicity is the activity of an enzyme thiopurine S-methyltransferase (TPMT). Genetic polymorphisms in its gene, metabolic factors that stabilize TPMT, or drug interactions associated with thiopurine treatment often lead to interindividual differences in response to thiopurines. Our studies thus aim to identify novel genetic determinants of response to thiopurines and to define molecular mechanisms of drug interactions during thiopurine therapy. Since the biological role of TPMT is still unclear, we further try to understand its endogenous function and its involvement in physiological processes.

2. TPMT AS FARMACOGENOMIC BIOMARKER

Individuals differ with respect to their TPMT activity. TPMT activity depends mainly on genetic variants, with *TPMT*3C* and *TPMT*3A* being the most common, coding for lower enzyme activity [1]. However, in the search for new pharmacogenomic markers, we realised that the exact DNA sequence in the *TPMT* promoter, which contains a variable number of tandem repeats (VNTR), is also important. The ABnC motifs are in complete linkage disequilibrium with the *TPMT*3C* and *TPMT*3A* genetic polymorphisms (Fig. 1) [2]. Since *TPMT*3* alleles are clinically established in thiopurine dosage adjustment, ABnC motifs

represent a useful indirect pharmacogenomic marker for future thiopurine treatment.

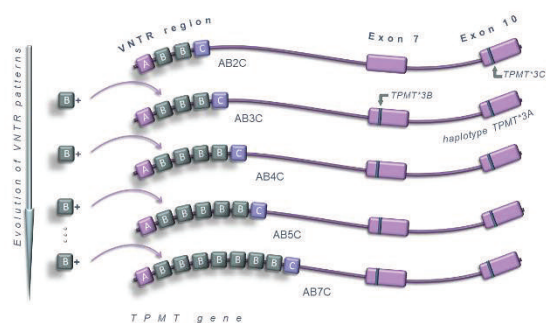


Figure 1. The evolution of motifs ABnC in VNTR region of *TPMT* and their linkage with *TPMT*3* genetic polymorphisms [2].

3. INFLUENCE OF DRUGS AND CO-FACTOR ON TPMT ACTIVITY

In addition to genetic variants, other factors, such as the cofactor S-adenosylmethionine (SAM), substrates, and inhibitory drugs, may modulate TPMT activity and thus influence the outcomes of thiopurine therapy. The role of SAM in stabilising the TPMT structure and consequently maintaining its activity is well documented [3]. On the other hand, the mechanisms of interaction between thiopurines and other drugs that are often administered concomitantly with them remain to be elucidated. In this context, we specifically focused on the interaction of TPMT with sulfasalazine, a derivative of 5-aminosalicylic acid, which is used as a first-line treatment for inflammatory bowel disease. By measuring the fluorescence change of tryptophan residues in human recombinant TPMT, we confirmed the binding of sulfasalazine to TPMT, and by

KL19

measuring TPMT activity, we determined mixed inhibition of the enzyme.

4. THE BIOLOGY OF TPMT

Despite the importance of TPMT in clinical practice, it appears that decreased TPMT activity does not cause changes in the development and function of the (human) body. In the absence of thiopurine exposure, individuals with inactive TPMT are phenotypically indistinguishable from individuals whose TPMT has normal activity. A number of orthologous TPMT proteins are known. The relatively high homology between TPMT sequences from biological species that are very distant in evolutionary development indicates that TPMT has been present for a long time and suggests the importance of the enzyme in the survival of individual species. In humans, the TPMT enzyme is expressed in most tissues and organs, most abundantly in the thyroid gland, followed by the kidneys, various parts of the intestine, and the liver.

5. INVOLVEMENT OF TPMT IN SELENIUM METABOLISM

Since certain selenium-containing organic compounds have chemical properties similar to those of thiopurines, we have investigated the role of this enzyme in selenium metabolism. Using STD NMR spectroscopy and tryptophan fluorescence measurements, we demonstrated the binding of an organic selenium compound, selenocysteine (Sec), to human recombinant TPMT. The incubation of Sec with TPMT and SAM, resulted in a formation of a methylated product, Se-methylselenocysteine, revealing Sec to be the first known biological compound to act as a substrate for TPMT [4].

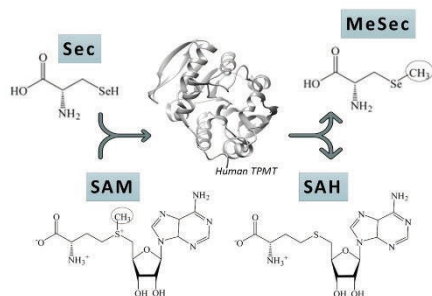


Figure 2. Selenocysteine methylation reaction catalysed by TPMT [4].

To investigate the biological relevance of this finding, we performed experiments using different *in vitro* systems: lymphoblastoid cell

lines (LCLs) from individuals with different TPMT genotypes, TPMT knock-out Hap1 cells, and TPMT-transfected cells. When we evaluated the sensitivity of the cells to selenium compounds, we found that cells with high TPMT activity were less sensitive to selenium compounds than cells with low or undetectable TPMT activity.

6. CONCLUSION

Our studies focus on deciphering TPMT from pharmacological and biochemical perspectives. Expanding the spectrum of genetic markers for susceptibility to thiopurines may contribute to future improvements in thiopurine treatment outcomes. The demonstration of methylation of selenium compounds by TPMT was a good starting point for further elucidation of the role of TPMT in pathological processes through selenium metabolism.

7. REFERENCES

1. Tamm, R., et al., *Polymorphic Variation in TPMT Is the Principal Determinant of TPMT Phenotype: A Meta-Analysis of Three Genome-Wide Association Studies*. Clinical pharmacology and therapeutics, 2017. 10 (5): 684-695.
2. Urbancic, D., et al., *Novel motif of variable number of tandem repeats in TPMT promoter region and evolutionary association of variable number of tandem repeats with TPMT*3 alleles*. Pharmacogenomics, 2018. 19 (17): 1311-1322.
3. Karas Kuzelicki N., et al., *From pharmacogenetics to pharmacometabolomics: SAM modulates TPMT activity*. Pharmacogenomics. 2014. 15(11): 1437-1449.
4. Urbancic, D., et al. *Methylation of selenocysteine catalysed by thiopurine S-methyltransferase*. Biochimica et Biophysica Acta - General Subjects, 2019. 1863(1): 182-190.

ACKNOWLEDGMENT

This work was supported by Slovenian Research Agency [P1-0208], and by the Ministry of Education, Science, and Sport (MIZŠ) and the European Regional Development Fund OP20.05187 RI-SI-EATRIS.

MODEL-INFORMED PRECISION DOSING OF USTEKINUMAB IN CROHN'S DISEASE

Jurij Aguiar Zdovc¹, Jurij Hanžel^{2,3}, Erwin Dreesen^{4,5}, Debby Thomas⁴, Barbara Ostanek¹, Tomaž Vovk¹, David Drobne^{2,3}, Iztok Grabnar¹

¹ University of Ljubljana, Faculty of Pharmacy, Ljubljana, Slovenia

² Department of Gastroenterology, University Medical Centre Ljubljana, Ljubljana, Slovenia

³ University of Ljubljana, Medical Faculty, Ljubljana, Slovenia

⁴ Department of Pharmaceutical and Pharmacological Sciences, KU Leuven, Leuven, Belgium

⁵ Department of Bioengineering and Therapeutic Sciences, University of California San Francisco, San Francisco, California, USA

1. INTRODUCTION

Crohn's disease (CD) is a chronic relapsing-remitting inflammatory bowel disease. The decreased fecal calprotectin (FC) concentration indicates a decreased biochemical disease activity [1, 2]. Ustekinumab is a monoclonal antibody used in moderate-to-severe CD [3], but there is an unmet need for the optimization of the standard treatment based on the reported proportions of patients achieving remission [4–11]. However, the optimal dosing strategy and the identification of patients with a benefit from dose optimization remain unresolved dilemmas in clinical practice. To compare the efficacy of several clinically relevant treatment regimens of ustekinumab in CD, we developed a population pharmacokinetic-pharmacodynamic (PK-PD) model of ustekinumab and FC.

2. MATERIALS AND METHODS

We performed a prospective, observational, single-center cohort clinical study including 57 CD patients, aged 18 years or older who started treatment with ustekinumab between October 2017 and June 2019. All patients received a standard ustekinumab treatment and were followed for 32 weeks after the first dose. We prospectively measured unbound serum ustekinumab concentration and FC concentration, as well as recorded other patients' characteristics, clinical data and biochemical markers. Polymorphisms in *IL12B* (rs3212227, rs3213094, rs6887695), *FCGR2A* (rs1801274), and *FCGR3A* (rs396991) were genotyped. Target mediated drug disposition (TMDD) model and its approximations were

fitted to the unbound serum concentrations [12, 13]. Stepwise covariate modeling was used for covariate testing and sequential PD modeling was performed to describe the relationship between ustekinumab, latent target and FC. A population of 10000 virtual patients and the final PK-PD model were used for simulation of various treatment regimens. To compare the efficacy, the proportion of patients achieving biochemical remission (FC < 100 mg/kg) at weeks 8, 16, 24 and 32 was calculated.

3. RESULTS AND DISCUSSION

Ustekinumab exposure, as well as the probability for biochemical remission, increased with increasing serum albumin, decreasing fat-free mass, decreasing C-reactive protein, previous non-exposure to biologics and *FCGR3A*-158 V/V variant. Model-based simulation demonstrated that proportions of patients in remission at week 32 receiving standard treatment, treatment with initial induction and subsequent maintenance dosing every 4 weeks or treatment with induction dosing every 8 weeks were 41.9%, 52.2% and 56.0%, respectively.

4. CONCLUSION

Our model could be used to guide future attempts to stratify treatment with ustekinumab in CD.

5. REFERENCES

1. Ng SC, Shi HY, Hamidi N, et al (2017) Worldwide incidence and prevalence of inflammatory bowel disease in the 21st century: a systematic review of population-

KL21

- based studies. *Lancet* 390:2769–2778.
2. Peyrin-Biroulet L, Sandborn W, Sands BE, et al (2015) Selecting Therapeutic Targets in Inflammatory Bowel Disease (STRIDE): Determining Therapeutic Goals for Treat-to-Target. *Am J Gastroenterol* 110:1324–1338.
 3. Feagan BG, Sandborn WJ, Gasink C, et al (2016) Ustekinumab as Induction and Maintenance Therapy for Crohn's Disease. *N Engl J Med* 375:1946–1960.
 4. Iborra M, Beltrán B, Fernández-Clotet A, et al (2019) Real-world short-term effectiveness of ustekinumab in 305 patients with Crohn's disease: results from the ENEIDA registry. *Aliment Pharmacol Ther* 50:278–288.
 5. Biemans VBC, van der Meulen - de Jong AE, van der Woude CJ, et al (2019) Ustekinumab for Crohn's Disease: Results of the ICC Registry, a Nationwide Prospective Observational Cohort Study. *J Crohn's Colitis* jjz119.
 6. Battat R, Kopylov U, Bessissow T, et al (2017) Association Between Ustekinumab Trough Concentrations and Clinical, Biomarker, and Endoscopic Outcomes in Patients With Crohn's Disease. *Clin Gastroenterol Hepatol* 15:1427-1434.e2.
 7. Ma C, Fedorak RN, Kaplan GG, et al (2017) Clinical, endoscopic and radiographic outcomes with ustekinumab in medically-refractory Crohn's disease: real world experience from a multicentre cohort. *Aliment Pharmacol Ther* 45:1232–1243.
 8. Verstockt B, Dreesen E, Noman M, et al (2019) Ustekinumab Exposure-outcome Analysis in Crohn's Disease Only in Part Explains Limited Endoscopic Remission Rates. *J Crohn's Colitis* 1–9.
 9. Hanžel J, Zdovc J, Kurent T, et al (2021) Peak Concentrations of Ustekinumab After Intravenous Induction Therapy Identify Patients With Crohn's Disease Likely to Achieve Endoscopic and Biochemical Remission. *Clin Gastroenterol Hepatol* 19:111-118.e10.
 10. Zdovc JA, Hanžel J, Kurent T, et al (2021) Ustekinumab dosing individualization in crohn's disease guided by a population pharmacokinetic–Pharmacodynamic model. *Pharmaceutics* 13:1–16.
 11. Wang Z, Verstockt B, Sabino J, et al (2021) Population pharmacokinetic-pharmacodynamic model-based exploration of alternative ustekinumab dosage regimens for patients with Crohn's disease. *Br J Clin Pharmacol* 1–13.
 12. Gibiansky L, Gibiansky E (2009) Target-mediated drug disposition model: approximations, identifiability of model parameters and applications to the population pharmacokinetic–pharmacodynamic modeling of biologics. *Expert Opin Drug Metab Toxicol* 5:803–812.
 13. Ternant D, Monjanel H, Venel Y, et al (2019) Nonlinear pharmacokinetics of rituximab in non-Hodgkin lymphomas: A pilot study. *Br J Clin Pharmacol* 85:2002–2010.

CROSSING OCULAR BARRIERS: PHARMACOKINETIC MODELS TO SUPPORT DRUG DEVELOPMENT IN RETINAL DISEASES

Eva Maria del Amo¹

¹ *University of Eastern Finland, School of Pharmacy, Biopharmaceutics, Yliopistonranta 1, 70210 Kuopio, Finland*

1. INTRODUCTION

The eye is an amazing and complex organ that allows us to interact with the surrounding world. Ocular protective mechanisms, flows, and barriers limit the access of therapeutics drugs into the eye, and the drug delivery to the posterior segment (i.e. retina) is especially difficult. The route of administration that can ensure retinal drug delivery is the intravitreal injection (Fig. 1), and the pharmacokinetics is described in this presentation. A comprehensive quantitative pharmacokinetic data and analysis of low- and high-molecular-weight (MW) drugs are presented, with the key pharmacokinetic parameters, the contributing mechanisms, and the link to the ocular physiology. Pharmacokinetic models to predict ocular drug concentration profiles are presented, which are extremely useful when designing new formulations or deciding new dosing regimens.

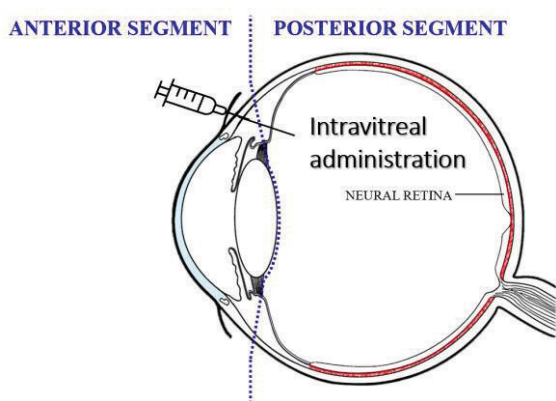


Fig. 1. Intravitreal injection to treat diseases of the posterior segment of the eye.

2. MATERIALS AND METHODS

In vivo, *in silico*, and literature data and related methods were utilized:

- *In vivo* pharmacokinetics studies in humans (from literature) and rabbits (from literature or

in-house using LC-MS analytical method) after intravitreal injection (1-4).

- *In silico* calculation of molecular descriptors of low-MW drugs with *ACDlabs software* (v 12, *Advanced Chemistry Development, Inc., Canada*), regression Quantitative Structure-Property Relationships (QSPR) modeling with *Simca+v.10.5 Umetrics, Umeå, Sweden* and pharmacokinetics analysis using compartmental & non-compartmental analysis with *Phoenix WinNonlin (build 8.3.1, Certara L.P.)* and simulations with *Stella professional, Modelling & Simulation software (v1.5.1, isee systems, Inc., USA)* (1-5).

3. RESULTS AND DISCUSSION

- Comprehensive data collections and the intravitreal primary pharmacokinetic parameters for low- and high-MW drugs were obtained (1-3):

- 1) Volume of distribution ($V_{ss,ivt}$) of the investigated drugs was fairly similar,

- 2) Clearance (CL_{ivt}) had broad variance, and predictive CL_{ivt} QSPR model was built for low-MW drugs where $\log D_{7.4}$ and hydrogen bonding were the key descriptors.

In general, metabolism do not impact clearance, and the relevant routes are the posterior and anterior routes (for low- and high-MW drugs, respectively).

- Human and rabbit intravitreal pharmacokinetic correlate well. The scaling factors generated allows reliable translation from rabbit-to-human (4).

- *In silico* tools integrating the CL_{ivt} QSPR model and $V_{ss,ivt}$ typical values in pharmacokinetic simulation models allow reliable calculations of drug ocular concentration profiles. Intravitreal delivery systems can be incorporated into the

KL22

simulations to estimate dose-requirement as a function of the constant release of the system, or the dosing interval. This provides the appropriate framework of various scenarios in designing drug delivery systems (2-5).

4. CONCLUSION

The generated knowledge and pharmacokinetic models can be relevant tools to advance ophthalmic drug development and guide the design of drug delivery systems to treat retinal diseases.

5. REFERENCES

1. del Amo EM, et al. *Ocular metabolism and distribution of drugs in the rabbit eye: quantitative assessment after intracameral and intravitreal administrations*, Int J Pharm 2022, 613: 121361. doi.org/10.1016/j.ijpharm.2021.121361
2. del Amo EM, et al. *Intravitreal clearance and volume of distribution of compounds in rabbits: In silico prediction and pharmacokinetic simulations for drug development*. Eur J Pharm Biopharm. 2015; 95: 215-26. doi.org/10.1016/j.ejpb.2015.01.003
3. del Amo EM, et al. *Pharmacokinetic aspects of retinal drug delivery*. Prog Retinal Eye Res. 2017;57:134-85. doi.org/10.1016/j.preteyeres.2016.12.001
4. del Amo EM et al. *Rabbit as an animal model for intravitreal pharmacokinetics: Clinical predictability and quality of the published data*. Exp Eye Res. 2015;137: 111-24. doi.org/10.1016/j.exer.2015.05.003
5. Subrizi A, del Amo EM et al. *Design principles of ocular drug delivery systems: importance of drug payload, release rate, and material properties*. Drug Discov Today. 2019; 24:1446-1457. doi.org/10.1016/j.drudis.2019.02.001

ACKNOWLEDGMENTS

All the co-authors and the corresponding funding sources of the cited publications.

PHYSIOLOGICALLY BASED FINITE TIME PHARMACOKINETIC (PBFTP) MODELS: THE END OF THE BEGINNING IN ORAL DRUG ABSORPTION

Panos Macheras¹, Athanasios Tsekouras²

¹ Department of Pharmacy, National and Kapodistrian University of Athens, Greece

² Department of Chemistry, National and Kapodistrian University of Athens, Greece

1. INTRODUCTION

Drugs administered orally are absorbed in the blood while they are in the gastrointestinal (GI) tract. This fact poses a time limit in the drug absorption duration. This observation is not appreciated in most pharmacokinetic models. The Finite Absorption Time (FAT) concept [1] poses constraints, leads to modifications in data analyses and can, eventually, rewrite sampling schemes and regulatory requirements.

2. MATERIALS AND METHODS

2.1. Materials

Starting material used in this work was derived from published pharmacokinetic data.

2.2. Methods

The presence of drugs in the GI tract and, consequently, their absorption is limited by the duration of gastrointestinal transit times. Given the sink conditions arising due to the high flow rate in the vena cava [2], zero-order kinetics sufficiently describes the absorption process. Different input rates may operate at various parts of the GI tract for finite duration in each part [1,3,4]. The absorption sequences can be described by appropriate sets of differential equations depending on whether one or two compartments need to be taken into account [4]. We coined the term Physiologically Based Finite Time Pharmacokinetic (PBFTP) models for the models derived. These have been solved analytically allowing their use both for simulations and fits to experimental pharmacokinetic data. For simulations a diverse set of conditions are tried to explore a variety of situations. Fits have been performed using

standard optimization with least squares methods, while monitoring parameter uncertainties and correlations to establish the validity of the models [4]. The quality of each fit for a given set of data determined which model was the most relevant for the data revealing basic physical characteristics of the absorption and disposition process of the corresponding formulation.

3. RESULTS AND DISCUSSION

3.1. Models and equations

The PBFTP models implemented involved 1, 2 or 3 consecutive input stages of finite duration in one- or two-compartment systems [4]. In the latter case expressions needed to be derived for the peripheral compartment, although actual concentrations cannot be monitored there.

3.2. Simulations

Concentration-time curves were generated using the model equations developed in [4]. Figure 1 shows a set of simulated data. In all cases, the simulated data resemble real life data.

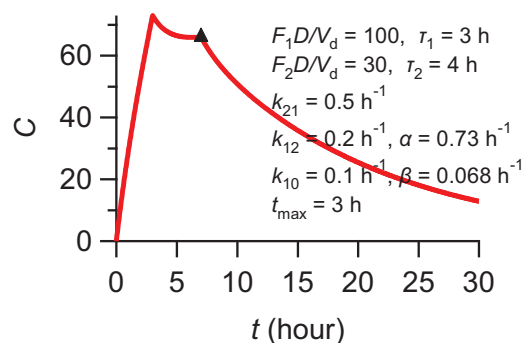


Figure 1. Simulated drug concentration in the blood in a two-compartment model with two successive constant (zero-order) absorption stages. The black

triangle marks the end of all absorption processes [4].

3.3. Data fits

A large number of pharmacokinetic data were analysed using the PBFTP models. In all cases, nice fitting results were obtained; the drug input rates were estimated along with the duration, τ , of each absorption stage. Representative examples are shown in Figure 2.

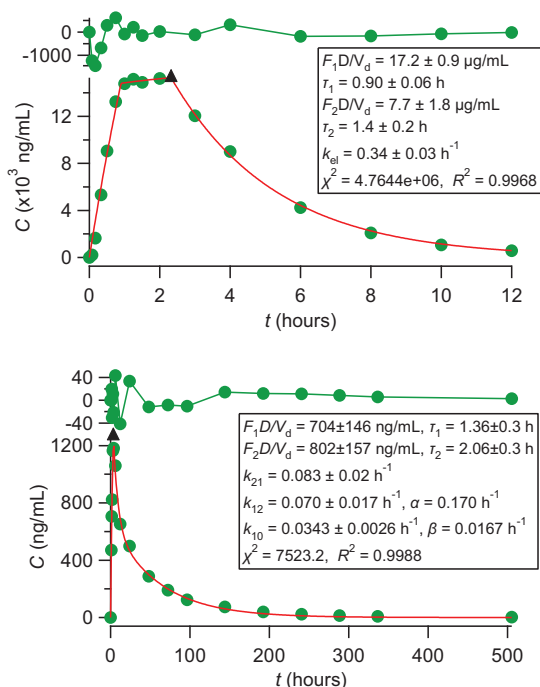


Figure 2. Ibuprofen (top panel) and niraparib (bottom panel) pharmacokinetic data were used to obtain optimum parameter values (shown in the inset) that correspond to a one- or two-compartment model, respectively, with two stages of constant absorption rate (each of duration τ_1 and τ_2).

4. CONCLUSION

The finite absorption time (FAT) of drugs is a physiologically sound concept and the relevant estimate for τ derived from the analysis of oral data using an immediate release formulation is a characteristic drug property. The application of PBFTP models to the analysis of oral drug absorption data will enhance our understanding of oral drug absorption phenomena.

5. REFERENCES

1. Macheras, P., et al. Revising Pharmacokinetics of Oral Drug Absorption: I Models Based on Biopharmaceutical/Physiological and Finite

Absorption Time Concepts. *Pharmaceutical Research*, 2020. 37: 187
<https://doi.org/10.1007/s11095-020-02894-w>
 (cover page of the issue). Erratum. *Pharmaceutical Research*, 2020. 37: 206
<https://doi.org/10.1007/s11095-020-02935-4>

2. Iranpour, P., et al. Altered Doppler flow patterns in cirrhosis patients: an overview. *Ultrasonography*, 2016. 35: 3–12.
<https://doi.org/10.14366/usg.15020>.
3. Chrysafidis, P., et al. Revising Pharmacokinetics of Oral Drug Absorption: II Bioavailability-Bioequivalence Considerations. *Pharmaceutical Research*, 2021. 38: 1345–1356
[10.1007/s11095-021-03078-w](https://doi.org/10.1007/s11095-021-03078-w)
4. Chrysafidis, P., et al. Re-writing oral pharmacokinetics using physiologically based finite time pharmacokinetic (PBFTP) models. *Pharmaceutical Research*, 2022. 39: 691-701.
<https://doi.org/10.1007/s11095-022-03230-0>.

PEPTIDE-MEDIATED DELIVERY OF RNA THERAPEUTICS

Taavi Lehto^{1,2,3}*1 Institute of Technology, University of Tartu, Estonia**2 Department of Pharmacy, University of Tartu, Estonia**3 Department of Laboratory Medicine, Karolinska Institutet, Sweden***1. INTRODUCTION**

RNA Therapeutics, such as short oligonucleotides, modified mRNA or CRISPR/Cas9 gene editing modalities, hold enormous therapeutic potential for the treatment of human disease¹. Due to their high specificity, any gene or gene product can be targeted with these technologies, meaning that theoretically any disease is amenable for treatment. However, these biomacromolecules typically display poor bioavailability in vivo due to inefficient uptake into tissues and cells. Therefore, a wide variety of delivery vectors have been devised and developed over the years either of biological nature, such as viruses and extracellular vesicles, or synthetic, e.g. lipid nanoparticles (LNPs) or cell-penetrating peptides (CPPs, peptides)². In particular CPPs is an interesting class of delivery vectors since they are rapidly taken up in entire cell populations and are able to transport various cargos ranging from impermeable small molecules to large plasmid DNA to their target cells³.

2. RESULTS

We have previously developed a series of fatty acid modified CPP-based delivery vectors called PepFect peptides^{4,5}. These peptides demonstrated high delivery capacity for a variety of nucleic acid-based molecules both cell culture modes in vitro and also in local and systemic delivery in vivo. Based on our previous experience, we have recently developed a novel peptide platform, called hPep peptides, with improved activity/safety profile and highly universality for the delivery of various novel classes of RNA therapeutics⁶. hPep peptides are designed to adopt α -helical

conformation and are further orthogonally modified with short hydrocarbon/lipidic modifications. We have recently shown that we can deliver short oligonucleotide in nanoparticles with hPep peptides in vitro and in vivo⁶. Our recent studies have further demonstrated that hPep peptides display excellent delivery capacity for the transporting chemically modified mRNAs both in vitro and in vivo settings. In contrast to existing leading non-viral delivery modalities, ie LNPs, our peptides primarily localize to lungs and spleen and to lesser extent to liver in mice. Furthermore, we have also extended hPep peptides for the delivery of CRISPR/Cas9 RNP and demonstrate their potential for gene editing application in the cell culture models.

3. CONCLUSION

Taken together, hPep peptides comprise excellent potential for the delivery of various RNA Therapeutics and has the potential to challenge the lipid-mediated delivery vectors for extra-hepatic delivery and translation of new RNA therapeutics in the future.

4. REFERENCES

1. Crooke, S. T. *et al. Cell Metab.* **27**, 714–739 (2018).
2. Bost, J. P. *et al. ACS Nano* **15**, 13993–14021 (2021).
3. Lehto, T., *et al. Adv. Drug Deliv. Rev.* **106**, 172–182 (2016).
4. Lehto, T. *et al. Mol. Ther.* **19**, 1457–1467 (2011).
5. Andaloussi, S. E. *et al. Nucleic Acids Res* **39**, 3972–87 (2011).
6. Bazaz, S. *et al. Biomedicines* **9**, 1046 (2021).

SHORT PEPTIDES AND THEIR ROLE IN RESEARCH AND IMMUNOTHERAPY OF ALLERGIES

Mojca Lunder¹, Abida Zahirović², Ana Koren³, Jerneja Debeljak³, Peter Korošec³

¹ Department of Pharmaceutical Biology, Faculty of Pharmacy, University of Ljubljana, Slovenia

² Department of Biotechnology, Jožef Stefan Institute, Slovenia

³ University Clinic Golnik, Golnik, Slovenia

1. INTRODUCTION

Allergic diseases are affecting up to 20-30% of the world population. Allergen-specific immunotherapy emerged as an effective treatment for some allergic conditions, in particular stinging insect hypersensitivity [1]. It typically involves subcutaneous administration of gradually increasing quantities of allergen extracts until immunotolerance is induced. However, this approach is not available for all allergies (e.g. peanuts), it requires repetitive administrations over 3-5 years and it is often associated with adverse events [2]. Novel therapeutic strategies with reduced side effects and decreased treatment time are thus required. Identification of IgE epitope-like peptides enables research of immunodominant epitopes of relevant allergens and their role in allergy occurrence as well as enables development of next-generation allergy vaccines containing solely the necessary epitope-like peptides or epitope mimetics (mimotopes), thus eliminating undesirable side effects induced by irrelevant determinants. We have focused on epitope-based immunotherapeutics for life-threatening allergies, such as allergies to insect venoms and food allergies, particularly peanut allergy.

2. MATERIALS AND METHODS

Peptide mimotopes of selected major allergens were obtained by screening biological peptide libraries (PhD-12, PhD-7 and PhD-C7C; New England Biolabs) against anti-allergen antibodies (Indoor Biotechnologies). For allergen Ves v 5 phage display was combined with next generation sequencing (MiSeq, Illumina) and bioinformatics processing of the obtained sequences (PuLSE software). Binding characteristics of peptides were evaluated by

immunodetection methods (ELISA or Peptide Microarrays; JPT Peptide Technologies). Synthetic epitope-like peptides were purchased from commercial providers. Reactivity of peptides with patients' IgE was tested by immunodetection methods (western and dot blot). Computational mapping (PepSurf algorithm) of allergen 3D structure was performed to identify location of dominant epitopes. Selected peptides were coupled to an immunogenic carrier. Minor coat protein pIII from M13 bacteriophage was used for mimotopes of Api m 1 and *L. lactis*, for mimotopes of Ara h 2. Allergenicity of mimotopes was tested by *ex vivo* activation of basophils from allergic patients. Marker of basophil activation and degranulation CD63 was monitored by flow cytometry. Peptides displayed on carrier were also tested for their ability to influence allergen specific T cells of allergic patients, by measuring cytokine response (Cytometric Bead Array; BD Biosciences) on FACSCalibur flow cytometer (BD Biosciences). Sera from allergic patients were obtained at University Clinic Golnik.

3. RESULTS AND DISCUSSION

We have focused on Ara h 2 (major peanut allergen), Api m1 (major bee venom allergen) and Ves v 5 (major wasp allergen). By screening phage libraries displaying linear or cyclic peptides of various lengths against anti-allergen antibodies we obtained sequences binding to these paratopes and thereby mimicking epitopes on allergens. Sequences of peptides in combination with computer algorithms enabled mapping and identification of dominant epitopes on the selected allergens.

3.1. Ara h 2

KL25

Selected peptides were aligned to the first part of the loop between helices 2 and 3 containing amino acid residues DPYSPSQD. Due to the flexibility of the loop only the first part is visible in the crystal structure. Within the loop the motif DPYSP(S) is repeated three times and it has been shown previously that this loop region contains important epitopes. Synthetic peptides showed decreased basophil activation compared to Ara h 2 or peanut extract. The mimotope with the highest sequence similarity with Ara h 2 showed some activation of basophils suggesting its allergenic activity is partially preserved. After stimulation with Ara h 2 higher production of cytokines specific for type 2 T cell response was observed. Peptides fused to carrier (either on *L. lactis* or fused to *L. lactis* anchoring protein) yielded significantly lower concentrations of cytokines compared to the allergen. Except production of IFN- γ was higher, particularly with one IgE like peptide which may suggest shifting the T cell immune response to non-allergic type 1. Additionally, the peptides markedly reduced allergenic activity of Ara h 2 and were able to prevent degranulation of patients' effector cells [4].

3.2. Api m 1

Peptide sequences were arranged into two groups according to the consensus motifs. Conformational mapping overlapped with primary sequence alignment, indicating that the regions 17-24 and 119-124 represent the epitopes of Api m 1. Both defined epitopes are located on the solvent-exposed loops protruding from the allergen surface and do not include glycosyl moiety. Corresponding peptide mimotopes showed no allergenic activity in basophil activation test. In contrast to bee venom and Api m 1, which stimulated predominantly type 2 cytokine response, mimotopes induced only T cell secretion of type 1 cytokines, suggesting a shift from TH2 to TH1 immune response [5].

3.3. Ves v 5

From screening phage libraries followed by NGS we obtained three groups of peptide motifs and align them to three major epitopes of Ves v 5. Using peptide microarrays variations of the three peptide motifs were profiled using allergic patients and control sera. The profiling revealed peptides with strongest binding to IgE from wasp venom allergic patients.

4. CONCLUSION

Identification of Api m 1 and Ves v 5 IgE epitopes is a very important step for better understanding of pathogenesis of bee or wasp sting anaphylaxis and can improve diagnosis and prognosis of Hymenoptera venom allergy. Furthermore, their respective mimotopes represent novel candidates for development of more precise and safer Hymenoptera venom immunotherapy. We have identified Ara h 2 IgE epitope-like peptides that successfully prevent binding of causative allergen, and thereby prevent degranulation and secretion of allergic inflammation mediators from effector cells. Such peptides represent new preventive treatment option in accidental exposures to allergens or intentional exposures during immunotherapy. Our efforts are focused towards further optimization of these peptides for therapeutic use.

5. REFERENCES

1. James, C., et al., *Allergen immunotherapy: an updated review of safety*. Current Opinion in Allergy and Clinical Immunology. 2017. 17(1):55-59.
2. Zahirović, A., et al., *Bee Venom Immunotherapy: Current Status and Future Directions*. Clinical Reviews in Allergy and Immunology. 2020. 58, 326–341.
3. Lunder, M., et al., *IgE epitope-like peptides and uses thereof*. Publication number US 2021/0115097 A1. Alexandria, VA: US Patent and Trademark Office, 2021.
4. Zahirović A, et.al., *Identification of bee venom Api m 1 IgE epitopes and characterization of corresponding mimotopes*. The Journal of allergy and clinical immunology. 2019. 143(2):791-794.e5.

ACKNOWLEDGMENT

We would like thank former lab members Peter Molek, PhD and Jernej Luzar, PhD for help with screening phage libraries. This work was supported by the Slovenian Research Agency (program P4-0127).

CD81 LARGE EXTRACELLULAR LOOP AS A NOVEL ALTERNATIVE SCAFFOLD: LAMININ BINDING CD81 ENHANCES SPECIFIC UPTAKE OF EXTRACELLULAR VESICLES

Gordana Wozniak Knopp^{1,2}, Stefan Vogt^{1,3}, Gerhard Stadlmayr^{1,2}, Katharina Stadlbauer², Madhusudhan Reddy Bobbili^{1,4}, Jørgen Kjems⁵, Florian Rüker¹, Johannes Grillari^{1,4}

¹ Institute of Molecular Biotechnology, Department of Biotechnology, University of Natural Resources and Life Sciences (BOKU), Vienna, Austria

² Christian Doppler Laboratory for Innovative Immunotherapeutics, Department of Biotechnology, University of Natural Resources and Life Sciences (BOKU), Vienna, Austria

³ acib GmbH (Austrian Centre of Industrial Biotechnology), Austria

⁴ Ludwig Boltzmann Institute for Experimental and Clinical Traumatology in the AUVA Research Center, Austria

⁵ Centre for Cellular Signal Patterns (CellPat), Interdisciplinary Nanoscience Centre (iNANO), Department of Molecular Biology and Genetics, Aarhus University, Denmark

1. INTRODUCTION

In recent years, extracellular vesicles (EVs) have entered the limelight as multifaceted drug delivery vehicles [1]. These about 100 nm large membrane enveloped structures are important cell-to-cell messengers, as their contents, composed of a cocktail of proteins, miRNAs and other non-coding RNAs, originating from the producing cell, can efficiently be transferred to a recipient cell upon fusion with its cellular membrane. EVs mediate intercellular communication and thus sustain homeostasis in tissues and organs, as well as further support processes such as regeneration after injury and limitation of tumorigenesis and malignant transformation. On the other hand, targeted delivery of EVs has long been recognized as a feature that could crucially improve their biological effect. Directed delivery was enhanced when their surface has been modified to enable the specific recognition of the target cells. For this purpose, we have modified the innately overrepresented EV surface protein CD81, which is at the same time regarded as their hallmark surface marker, into an antigen-recognition scaffold. This protein is a member of the tetraspanin family with four transmembrane segments (TM1–4) linked by a small intracellular loop, a small extracellular loop (SEL) and a large extracellular loop (LEL). Previously, we have designed highly stabilized mutants of CD81 LEL via introduction of *de novo* disulfide bonds [2], and 2 were chosen for randomization to produce libraries of potential

binding molecules recognizing an antigen of choice. The selection platforms using LEL as an independent folding unit were constructed using yeast display as a validated method of molecular evolution *in vitro*. The chosen antigen was human placental laminin, important in muscular and neural regeneration processes.

2. MATERIALS AND METHODS

2.1. Molecular design

Solvent-exposed residues of CD81 LEL were identified that could upon randomization form a novel antigen binding site of about 600 Å² in size (Fig. 1). The first scaffold molecule was a CD81 LEL mutant with two novel disulfide bonds with the midpoint of thermal transition (T_M) of 109.4°C, 43°C above that of the wild-type CD81 LEL. The second library design was based on the CD81 LEL mutant with the ability to reversibly refold when heated up to 110 °C, unlike the wild-type CD81 LEL.

2.2. Yeast display and binder validation

Yeast display libraries with about 10⁹ members were processed with MACS and FACS-based antigen selection until visible enrichment. Unique binders were displayed on the surface of mammalian cells to confirm specific antigen binding.

2.3. EV preparation and characterization

EVs were isolated from the supernatant of HeLa cells stably expressing CD81-eGFP variants using ultracentrifugation. Nanoparticle

KL26

tracking analysis, Western blotting and transmission electron microscopy (TEM) were used for particle characterization. Specificity of laminin binding was determined with a competition experiment.

2.4. Uptake of targeting EVs

Two laminin-secreting cell lines, Huh-7 and NCI-N87 were exposed to recombinant EV preparations and flow cytometry was used to measure the uptake levels of eGFP-positive EVs.

2.5. Transfer of cel-miR-39 by targeting EVs

Huh-7 cell line was treated with EVs loaded with cel-miR-39 and the levels of transfer were determined after RNA isolation, cDNA synthesis and qPCR in real time.

3. RESULTS AND DISCUSSION

3.1. Isolation of laminin binders

Laminin-binding clones were enriched after 3-4 selection rounds and 9 unique sequences were identified.

3.2. Recombinant EVs

Recombinant EVs were prepared at a high yield with the median size between 100 and 125 nm. At least 25-60% of the particles were eGFP-fluorescent. EV marker proteins syntenin, Alix and TSG101 were shown to be enriched while calnexin, as a non-EV protein, was absent. TEM analysis confirmed the presence of the typical cup-shaped structures.

3.3. Laminin-binding EVs mediate enhanced cellular uptake

The enhanced laminin-binding EV internalization was observed in both in Huh-7 and NCI-N87 cells with up to 8-fold increase in fluorescence compared to wild-type EVs. Remarkably, cel-miR-39 was detected in recipient Huh-7 cells, which was found to be significantly increased in Huh-7 cells exposed to laminin-binding variant EVs compared to wild-type CD81 EVs.

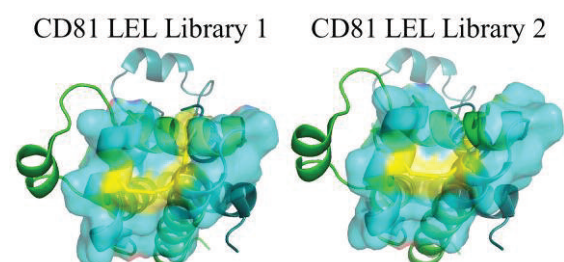


Figure 1. Models of CD81 library designs (PDB: 1G8Q) with novel disulphide bonds in yellow and the randomized residues surfaced in cyan.

4. CONCLUSION

We have established a novel selectable antigen binding platform based on the CD81 LEL scaffold [3]. The recombinant laminin-binding EVs shown a higher level of internalization into laminin-secreting cells. This method can rapidly deliver EV binding to any antigen of choice, simply by “clicking” recombinant LEL onto the full-length CD81.

5. REFERENCES

1. Yamamoto, T., et al., *Latest advances in extracellular vesicles: from bench to bedside.* Science and Technology of Advanced Materials, 2019. 20(1): 746-757.
2. Vogt, S., et al., *Stabilization of the CD81 large extracellular loop with De Novo disulfide bonds improves its amenability for peptide grafting.* Pharmaceutics, 2018. 10(3):138-151.
3. Vogt S, et al., *An engineered CD81-based combinatorial library for selecting recombinant binders to cell surface proteins: Laminin binding CD81 enhances cellular uptake of extracellular vesicles.* Journal of Extracellular Vesicles, 2021. 10(11): e12139.

ACKNOWLEDGMENT

This project has been supported by the Austrian FFG-COMET-Funding Program and Evercyte GmbH. SV was a fellow of the international PhD programme “BioToP” (FWF grant W1224). This project was also supported by EQ-BOKU VIBT GmbH and the BOKU Core Facilities for *Biomolecular and Cellular Analysis and Multiscale Imaging*



Capping Issues?

Edge chipping?

Compactability challenge?

We offer a problem **solver**

Microcrystalline cellulose

Ceolus KG-1000/KG-802

Ceolus UF-702/UF-711

Oral Presentations

CONTINUOUS MANUFACTURING IN SOLID DOSE - HOW TO LEVERAGE OPPORTUNITIES OF THIS NEW TECHNOLOGY

Leo Ohrem

¹*Merck*

There is a constant pressure from both authorities to develop robust and safe drugs as well from the industry to reduce cost. Continuous manufacturing can be a solution.

The presentation shows up the specific challenges of this new technology and how to tackle these by the choice of excipients.

THE VISCOSITY REDUCTION PLATFORM ENABLING SUBCUTANEOUS DELIVERY

Peter Balogh

¹*Merck*

Subcutaneous administration can improve patient convenience and reduce healthcare costs by avoiding the need for hospitalization.

Yet in some cases, high protein concentrations make formulations far more viscous, prohibiting this route of administration.

The presentation will introduce an excipient platform that makes it possible to combine excipients in a ways that can reduce protein viscosity.

PROCESS RELATED IMPURITIES IN MRNA MANUFACTURING

Kristina S Nemec, Urh Cernigoj, Jana Vidic, Andreja G Livk, Blaz Goricar, Klemen Bozic, Anze Martincic Celjar, Nina Mencin, Tomas Kostelec, Rok Sekirnik, Pete Gagnon, Ales Strancar

¹*BIA Separations*

The recently demonstrated efficacy of mRNA-based Covid-19 vaccines has shown promise of this therapeutic format, but also highlighted the need for higher efficiency of mRNA production to meet enormous needs for global vaccine supply.

Typical mRNA production process involves three key steps: 1) plasmid DNA production, linearization and purification, 2) in-vitro transcription reaction and 3) mRNA purification.

Here we present a chromatographic toolbox and mRNA IVT synthesis for integrated mRNA production from pDNA to mRNA purification, including in-process analytics to address key process related impurities.

INFLUENCE OF THE BINDER JETTING PROCESS PARAMETERS AND BINDER LIQUID COMPOSITION ON THE RELEVANT ATTRIBUTES OF 3D PRINTED TABLETS

Klemen Kreft¹, Zoran Lavric¹, Tijana Stanic², Petra Perhavec², Rok Dreu¹

¹ Faculty of Pharmacy, University of Ljubljana, Askerceva Cesta 7, 1000 Ljubljana, Slovenia

² Lek Pharmaceuticals d.d., a Sandoz Company, Verovskova Ulica 57, 1000 Ljubljana, Slovenia

1. INTRODUCTION

In the last decade, 3D printing has received a considerable interest from the pharmaceutical research community, primarily due to its ability to prepare personalized medication on demand. One of the most advanced and promising 3D printing technologies for pharmaceutical purposes is binder jetting. It is a layer-by-layer manufacturing process, where the powder blend is deposited in a fine layer. The particles are then bound together by a binding liquid. This process repeats in layers several times to achieve the final tablet form [1]. Binder jetted tablets are porous in nature and therefore exhibit instant disintegration, which is advantageous for high-risk patient groups who have trouble with swallowing. The lack of any compression force yields a fragile tablet structure, resulting in troublesome handling and transportation. To address this issue, several formulation approaches have already been reported [1,2]. However, not enough effort is devoted to understanding the printing process itself. In this study, key printing parameters with the influence on the relevant properties of tablets were identified, while the binding liquid composition was also examined.

2. MATERIALS AND METHODS

2.1 Materials

Active pharmaceutical ingredient ketoprofen was sourced internally from Lek d.d. stock. Fillers Pharmatose® 125M (lactose monohydrate) was sourced from DFE Pharma (Goch, Germany) and Pearlitol® 100 SD (mannitol) from Roquette Frères (Lestrem, France). Solid binder Plasdone® K-25

(polyvinyl pyrrolidone grade K 25) was sourced from Ashland (Wilmington, Delaware, USA). Glidant Syloid® 244 FP (silica) was sourced from Grace GmbH (Worms, Germany). The final powder blend was composed of 20.0 % ketoprofen, 34.75 % Pharmatose® 125M, 34.75 % Pearlitol® 100 SD, 10.0 % Plasdone® K-25 and 0.5 % Syloid® 244 FP. Binding liquids were ethanol-water mixtures in 10, 20 and 30 % m/m concentration.

2.2. 3D printing

A custom-developed pharmaceutical 3D printer Picojet D220 (Spectra Laboratories, Ljubljana, Slovenia), functioning as a standard binder jetting device, was used for sample preparation. Tablets with 15 mm diameter and 5 mm height were designed and the information was transferred to the printer. 40 tablets were prepared per each experiment batch. When the printing process was finished, tablets were dried in a convective drying chamber (Kambic, Semic, Slovenia) at 60 °C for 150 minutes to LOD values below 2 %.

2.3. Design of experiments

A screening and optimization DoE study was performed with use of software Modde 12.01 (Sartorius, Göttingen, Germany) and utilization of 20 m/m % ethanol-water binding fluid. 18 experiments were executed to evaluate the influence of 5 process parameters on properties of 3D printed tablets. In addition, 9 experiments were carried out at three tablet strength levels to assess the impact of the binding liquid composition on the final properties of tablets.

OP1

2.4. Analysis of tablets

Printed tablet samples were analysed for hardness, friability, disintegration time, mass, mass uniformity and dimensions according to the European Pharmacopoeia procedures and with use of internally validated equipment.

3. RESULTS AND DISCUSSION

3.1. Influence of process parameters on tablet properties

Since binder jetted tablets can be troublesome to handle, it is crucial to optimize the process parameters to achieve the best mechanical properties. 5 printing parameters were analysed in the screening phase. Doser speed, spreader speed and printhead speed are related to the manner and speed of powder and liquid deposition, while layer height (thickness of each layer) and saturation parameter (number of active nozzles) are connected to the amount of material in each layer. Well-fitting models ($R^2=0.65-0.89$) with good predictability (Q^2 values are close to R^2) were obtained for all responses with exception of mass RSD and tablet height models (Fig. 1).

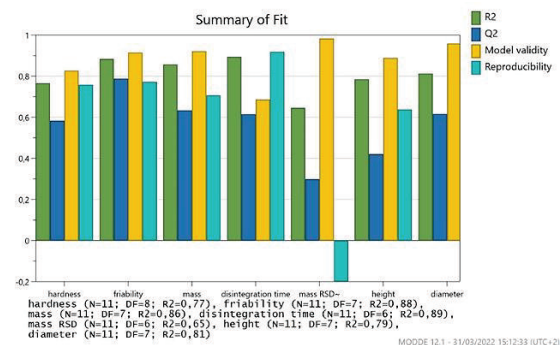


Fig 1. Summary of fit plot for the screening phase of the DoE study

Coefficient plots from screening phase showed, that the doser speed, spreader speed and printhead speed did not have any major influence on tablet properties. This demonstrates that the printing process is very robust. On the other hand, layer height and saturation parameters both proved a significant influence. The higher the saturation and the lower the layer height, the better the mechanical properties of printed tablets. Tablet hardness, friability and disintegration time can be

changed by the factor of two when adjusting both printing parameters accordingly.

3.2. Influence of binding liquid on tablet properties

Binding fluid composition could also affect tablet properties. Three strength levels of tablets (best, medium, worst) were prepared by setting layer height and saturation accordingly. Within each strength level, tablets were prepared with 10, 20 and 30 % ethanol-water mixture. The amount of ethanol in binding liquid did not influence the properties of tablets to the same degree as process parameters (Fig. 2). We could argue that the potential difference in capillary effect of employed binding liquids was of lesser importance in comparison to standard wet granulation as during binder jetting procedure powder layer height is thin and controlled.

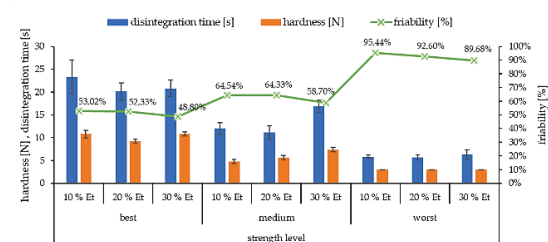


Fig 2. Impact of ink composition on hardness, friability and disintegration time at three strength levels.

4. CONCLUSION

An in-depth study of the binder jetting 3D printing process revealed that the settings of the layer height and saturation are significant for final properties of tablets. Binding fluid composition affects the properties to a lesser extent.

5. REFERENCES

1. Chang, S.Y., et al., *Binder-Jet 3D Printing of Indomethacin-Laden Pharmaceutical Dosage Forms*. Journal of Pharmaceutical Sciences, 2020. 109: 3054–3063
2. van den Heuvel, K.A., et al., *Evaluation of Lactose Based 3D Powder Bed Printed Pharmaceutical Drug Product Tablets*. Powder Technology, 2021. 390: 97–102.

OPTIMIZATION OF RADIAL EXTRUSION AND PELLET COATING PROCESSES USING PAT APPROACHES

Aljoša Gradišek¹, Gregor Ratek¹, Franc Vrečer^{1,2}, Klemen Korasa¹

¹ *Krka d. d., Novo mesto, Slovenia*

² *University of Ljubljana, Faculty of Pharmacy, Ljubljana, Slovenia*

1. INTRODUCTION

In 2002, FDA launched a new initiative to implement risk-based modern approaches in pharmaceutical development, manufacturing and quality assurance. One of the key technological approaches within this initiative is process analytical technology (PAT). FDA describes PAT as a system for designing, analyzing and controlling manufacturing through timely measurements of critical quality and performance attributes of raw and in-process materials and processes, with the goal of ensuring final product quality. [1] Statistical PAT tools include design of experiment (DoE), that is a systematic approach to understanding and predicting end product properties. Another branch of PAT tools are process analyzers among which NIR spectroscopy is one of the most promising approaches for real to near-real time process monitoring. Use of PAT tools are especially important in case of challenging technological operations, such as radial extrusion and functional film coating, which were thoroughly evaluated in the present study. [2]

2. MATERIALS AND METHODS

2.1. Materials

Neutral pellets were manufactured using microcrystalline cellulose (MCC; Vivapur® 102; JRS Pharma, Germany) and polyvinylpyrrolidone (PVP; Kollidon® K-30; BASF; Germany). Suspension for film coating was prepared using polymer hydroxypropylmethylcellulose (HPMC; Pharmacoat® 606; Shin-Etsu; Japan) and talc (Imerys talc; Italy). Sodium salt of tartrazine (Sigma Aldrich, USA) was added to determine film-coating quantity using UV-VIS spectroscopy.

2.2. Preparation of neutral pellets

Wetted mass for extrusion was prepared by high shear granulation (HSM; Gea UltimaGral™ 25; GEA; Germany) of MCC type 102 with PVP.

The mass was extruded using (Gea NICA™ IPS25; GEA; Germany) radial extruder. Extrudates were dried in fluid bed dryer (GEA MP-1 S; GEA; Germany) and milled (Frewitt Hammerwitt 3; Frewitt; Switzerland) to produce pellets with median diameter 810 μm. Parameters of radial extrusion, extrusion speed, screen size and water content in wetted mass, were optimized using DoE.

2.3. Pellet coating

Pellets were coated in bottom spray fluid bed coater (GEA MP-1 S; GEA; Germany) to target weight gain of 20% of the starting pellet weight. During coating of the first three batches, pellets were periodically sampled at predefined points calculated from coating suspension consumption ranging from 4% to 28% weight gain. UV-VIS spectra were taken to measure the content of tartrazine and to calculate the actual coating quantity at each of the sampling points. Antaris Target analyser (ThermoFischer scientific, USA) FT-NIR probe was used to measure the spectra of previously mentioned samples at a spectral range of 5560-7400 cm⁻¹. Partial least squares regression (PLS) model for the prediction of film-coating quantity was created using Unscrambler version 11 (AspenTech; USA). NIR spectral data was used as independent variable and film-coating quantity as dependent variable. Ability to predict the film-coating quantity was tested by coating a batch where pellets were periodically sampled and NIR spectra were recorded at-line to determine the process end point. The final product was compared to previous batches by SEM measurements of coating thickness and by coating suspension consumption, assuming similar process yield.

3. RESULTS AND DISCUSSION

3.1. Radial extrusion optimization with DoE

A response surface design with two quantitative factors, quantity of granulation liquid and extrusion speed at three levels, and categorical variable extrusion screen size at two levels, was created and 13 experiments were performed with the goal to maximize the sphericity and minimize the width of particle size distribution and friability of pellets. The desired properties (Fig. 1) were achieved using extrusion screen with dimensions 0.8×0.7 mm that gave us extrudates with higher sphericity and narrower particle size distribution, compared to 0.5×0.5 mm screen. Higher water quantity and 110% of total dry mass used for preparation of extrusion mixture gave extrudates with lower friability, especially in combination with a larger extrusion screen. Extrusion speed had no significant effect on the evaluated attributes. Multiple batches were produced at defined process parameters to produce enough pellets for film-coating trials.

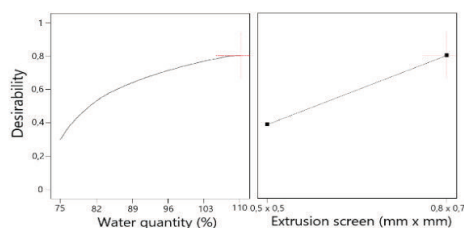


Figure 1. Process parameter optimization graph

3.2. Coating thickness prediction using the NIR probe

A PLS model for coating quantity prediction was calibrated, based on differences in the intensity of film-coating component NIR bands. A narrow sharp band of talc at wave number around 7180 cm^{-1} contributed the most spectral variability. First principal component of the model explained 99.9% of the variability. R^2 of the calibrated PLS model was 0.999, slope of the linear regression line was 0.999, and root mean standard error (RMSE) was 1.23%. That showed good correlation between predicted and reference values throughout the whole model, which was later used to predict coating quantity of independent test batch, where film coating was stopped at the estimated coating quantity of 98.5% of our target value. From coating suspension consumption, theoretical film-coating quantity of 100.2% of the target value was calculated. By plotting individual predicted values throughout the coating process against the theoretical quantity calculated from coating

suspension consumption (Fig. 2), relatively low RMSE of prediction (4.21%) and high R^2 (0.991) was observed.

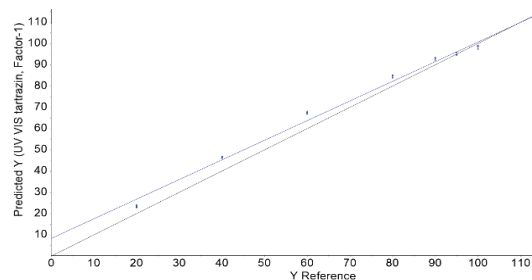


Figure 2. Coating quantity prediction graph

Film-coating thickness of the test batch was measured using SEM and compared to samples from model calibration batches. The test batch coating thickness was not statistically different from samples with 100 and 105% of the target value and was thicker compared to the sample with 90% of the target value.

4. CONCLUSION

In the present study, DoE was applied successfully to optimize critical process parameters for consistent production of pellets. The PLS model for coating quantity prediction was calibrated using NIR spectral data as independent variable and coating quantity as dependent variable. The model enabled accurate film coating quantity prediction in near real time, especially around our target film-coating quantity. Additional improvements like larger sample size for model calibration and inclusion of more test batches would increase reliability of the prediction. In the future, use of in-line NIR probe that allows real-time coating quantity monitoring needs to be evaluated.

5. REFERENCES

1. FDA. Guidance for Industry PAT — A Framework for Innovative Pharmaceutical Development, Manufacturing, and Quality Assurance, 2004.
2. Korasa K., Vrečer F., Overview of PAT process analysers applicable in monitoring of film coating unit operations for manufacturing of solid oral dosage forms. *European Journal of Pharmaceutical Sciences*, 2018, Volume 111

ACKNOWLEDGMENT

This research has been supported by Krka, d. d., Novo mesto.

FROM BATCH TECHNOLOGY TO CONTINUOUS MANUFACTURING: FORMULATION OF GASTRORETENTIVE DOSAGE FORM BASED ON MELT FOAMING TECHNIQUE

Gábor Vasvári¹, Ádám Haimhoffer^{1,2}, Ildikó Bácskay^{1,2} Ferenc Fenyvesi¹

¹ Department of Pharmaceutical Technology, University of Debrecen, Hungary

² Institute of Healthcare Industry, University of Debrecen, Hungary

1. INTRODUCTION

Variabilities of the digestive system challenges innovations in the development of drug delivery systems. Motility and pH differences of GI juices affects the oral bioavailability of small molecules. Up to date, oral targeted delivery platforms can be considered the most effective tools to increase the absorption rate of drugs with poor solubility or permeability. Gastric retention offers site-specific prolonged release of active ingredients in the stomach. Low density compositions can avoid the passage to the duodenum by floating on the gastric content. To produce such floating systems, several technologies can be considered including hot melt extrusion, gas generating compositions or HBS capsules. Extrusion is a continuous process, but in most cases, high temperature or pressure is needed to reshape the solids, floating lag time exists for gas generating tablets and HBS capsules are susceptible to the churning movements.

Foamed molten dispersions are in the focus of our research since 2018. At the very beginning we have created an in-house apparatus for foaming batches of molten lipid dispersions, later the concept was revised, redesigned and upgraded into a novel, lab-scale apparatus for continuous production, the QUICKfoamcell Lab®.

2. MATERIALS AND METHODS

2.1. Materials

PEG 4000 and stearic acid, type 50 (SA) was used to create the foamed matrices. Metronidazol (MNZ) was used for the batch technology, BaSO₄ was the X-ray contrast agent for the *in vivo* imaging study while verapamil hydrochloride (VER) was used for the continuous production of *in vivo* pharmacokinetic study. These materials were Ph Eur.

grade and purchased from Molar Chemicals, while others were from Sigma-Aldrich.

2.2. Device setups and foaming

The batch apparatus was built from polypropylene tube, the jacketed vessel (60mL) was closed with a valve (d:10mm) at the bottom. Molten dispersions of MNZ were foamed with air at atmospheric pressure with a whisker agitator (Fig. 1A). QUICKfoamcell Lab® is presented on Fig. 1B. Briefly, the molten dispersion is pumped from a melt container to the foam cell (30 mL) where a roto-stator homogenizing tool (IKA®, S25 N 10G) disperses the injected air to create hot foam. Finally, the hot foam can be dosed with a pinch valve.

2.3. Dissolution and mathematical analysis

900 mL of hydrochloric acid media, pH: 1.2 without pepsin was used for dissolution tests (Erweka DT800, rotating paddle method, 75 rpm and 37°C) API release was detected by UV/VIS spectrophotometry. Dissolution data was fitted to zero-order, first-order, and Korsmeyer–Peppas models.

2.4. *In vivo* studies

For the *in vivo* CT Imaging, 16-week-old, male Fischer-344 rats (n=3; 250–300g, Animalab Ltd.) were used. CT scans were acquired after 30 and 120 mins. The pharmacokinetic study (approval number: HB/06-ÉLB/1657-4/2019) included six female Beagle dogs, verapamil solution and verapamil molten foams were administered orally, PK parameters were compared, gastric retention was checked by gastroscopy.

OP3

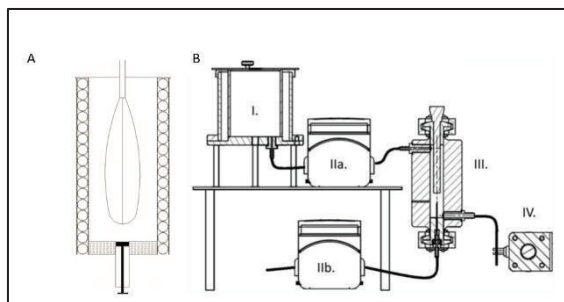


Figure 1. Batch apparatus (A) and the QUICKfoamcell Lab® (B).

3. RESULTS AND DISCUSSION

3.1. Density of the foams

In case of the batch apparatus, 53°C was selected for foaming temperature. Dispersion containing 30 m/m% MNZ was successfully foamed when 5 or 10% SA was added to the melt, densities decreased to 0.82 and 0.93 g/mL, respectively.

Process optimization was done with the QUICKfoamcell Lab® using a Box–Behnken experimental design. Injected gas volume (mL), rate (mL/s) and tool speed (rpm) were varied, while foaming cell temperature was 56°C in all runs. It was found that 14 500 rpm is enough to decrease density below 1 g/mL, while the optimal range for gas volume was 2.5–3.25 mL with the injection rates of 0.25–0.35 mL/s. Production speed was also calculated, resulting 300–500 capsules/h (capsule size 00). Capsules filled with melt foams containing 15 m/m% VER and 12.5% SA were prepared for the PK study with the average density of 0.75 g/mL.

3.2. Dissolution properties

MNZ foams containing 5 or 10 % SA released their content after 5 and 10 hours, following first-order drug release model. VER capsules with 10, 12.5 or 15% SA released 85.3%, 79.4% and 77.4% of its content in 10 hours. Data analysis revealed first-order drug release. In all experiments, the PEG-SA based foamed matrices released their API content due to the erosion of matrix, no swelling was observed.

3.3. In vivo studies

BaSO₄ loaded foams were administered orally to rats, CT scans proved the ability of the foam to remain in the stomach for at least 2 hours to satisfy the desired needs of such formulations.

Plasma VER levels of the PK study are presented in Fig. 2. Beside the blood sample analysis, gastroscopies were also performed on

the animals. VER capsules were present after 2 hours, while empty stomachs were observed after 4 hours.

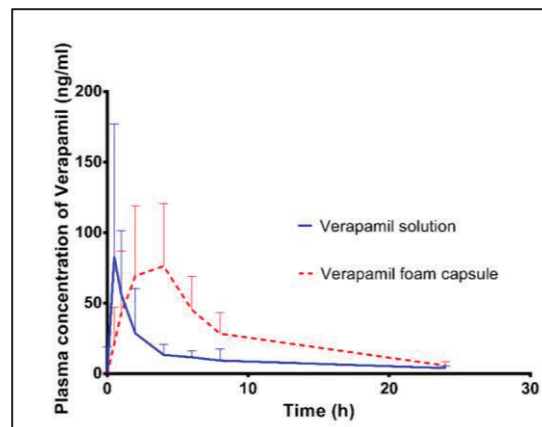


Figure 2. Mean plasma levels of VER solution (50mg/dose) and VER foamed capsules (120mg/dose).

4. CONCLUSION

Melt foam techniques was designed and realized in batch technology, then transferred to continuous manufacturing. Molten dispersions were successfully foamed, closed spheroid cells were present, 90% of them are smaller than 100 microns. PEG and SA based matrix provided prolonged release for 10 hours, via matrix erosion. CT scans and gastroscopy proved the retention of the matrices in rat and canine stomachs. Compared to the VER oral solution, a relative bioavailability of 99.3% was reached.

5. REFERENCES

1. G, V., et al., *Development and Characterisation of Gastroretentive Solid Dosage Form Based on Melt Foaming*. AAPS PharmSciTech, 2019. 20(290): 1-11.
2. Á, H., et al., *Process Optimization for the Continuous Production of a Gastroretentive Dosage Form Based on Melt Foaming*. AAPS PharmSciTech, 2021. 22(187): 1-9.
3. Á, H., et al., *In Vitro and In Vivo Studies of a Verapamil-Containing Gastroretentive Solid Foam Capsule*. Pharmaceutics, 2022. 14(350): 1-18.

ACKNOWLEDGMENT

Project no. TKP2021-EGA-18 has been implemented with the support provided from the National Research, Development and Innovation Fund of Hungary, financed under the TKP2021-EGA funding scheme.

OP4

THE INFLUENCE OF POLYMERIC BINDER TYPE AND CONCENTRATION ON FLOW AND DISSOLUTION PROPERTIES OF SYLOID® 244FP-BASED SMEDDS GRANULES

Mila Kovačević¹, Ilija German Ilić¹, Alenka Zvonar Pobirk¹

¹University of Ljubljana, Faculty of Pharmacy, Department of Pharmaceutical Technology, Slovenia

1. INTRODUCTION

Mesoporous carriers, such as Syloid® 244FP, are known for their high liquid load capacity and ability to maintain characteristics of dry powders when loaded with liquid lipid-based dispersions [1]. Therefore, they are a convenient choice for solidification of self-microemulsifying drug delivery systems (SMEDDS) that are designed to improve the solubility of poorly water-soluble drugs [2]. The loading of mesoporous carriers with SMEDDS, frequently results in sticky powders with poor flow properties, which are inappropriate for further processing [1]. Thus, the aim of this study was to investigate the influence of different polymeric binders and their concentrations used in granulation dispersions for SMEDDS solidifications on the quality attributes of granules, with particular focus on flow and dissolution properties.

2. MATERIALS AND METHODS

2.1. Materials

Carvedilol (CTX Life Sciences LTD, India) was used as a model drug.

Liquid SMEDDS was composed of mixture of Capmul® MCM EP/NF (mono-diglyceride of medium chain fatty acids, Arbitec Corporation, USA), refined castor oil (Ph. Eur. Grade, Caesar & Loretz GmbH, Germany), Kollisolv® PEG E 400 (Sigma-Aldrich, USA) and Kolliphor® RH 40 (polyoxyl 40 hydrogenated castor oil, Sigma-Aldrich, USA).

Syloid® 244 FP (Grace GmbH & Co. KG, Germany) was used as mesoporous carrier for SMEDDS solidification. Different binder types and concentrations were used in granulation dispersion: vinylpyrrolidone-(co)polymers (PVP/VA 64, PVP K30 or K90) and

hypromellose (Pharmacoat® 603, Pharmacoat® 615 or Methocel® K100 LV).

2.2. Preparation of SMEDDS granules by wet granulation

SMEDDS granules were prepared manually by wet granulation method, followed by tray drying. Granulation dispersion containing microemulsion with SMEDDS/water ratio of 70/30 and binding polymer (povidone or hypromellose) in concentration range 0.00-7.45 % w/w, was added to mesoporous Syloid® 244FP. Granules with high and low binder concentration (1.85 and 7.45 %) were prepared using laboratory high-shear granulator as well, to study the influence of method preparation on granule characteristics.

2.3. Characterisation of SMEDDS granules

Produced granules were evaluated for particle size and size distribution, flow properties, self-microemulsifying properties and *in vitro* carvedilol release profile.

3. RESULTS AND DISCUSSION

3.1. The influence of polymer type on SMEDDS granules characteristics

All povidone-based granules showed median diameter 600–800 µm and passable flow properties (according to Carr index criteria in Ph. Eur.). Neither concentration nor type of binder had a major influence on these properties. On the other hand, hypromellose-based granules were smaller (d_{50} value 300–600 µm), exhibiting better flowability, in comparison to other polymer. Still, the flow time of all produced granules was 5.0-7.2 s/100

OP4

g, which is considered well enough for further tableting.

Regarding *in vitro* dissolution testing, SMEDDS loaded granules with low molecular weight PVP K30 exhibited the fastest drug release, in contrast to ones with high molecular weight PVP K90, thus increasing molecular weight showing a negative influence on release profile (Fig. 1). The same trend could be observed when hypromellose was used as binder, as from SMEDDS granules with low molecular weight Pharmacoat® 603, 74 % of carvedilol was released in 5 minutes, in comparison to 58 % for medium molecular weight Pharmacoat® 615 and 41 % for granules with high molecular weight Methocel® K100 LV (Fig. 1).

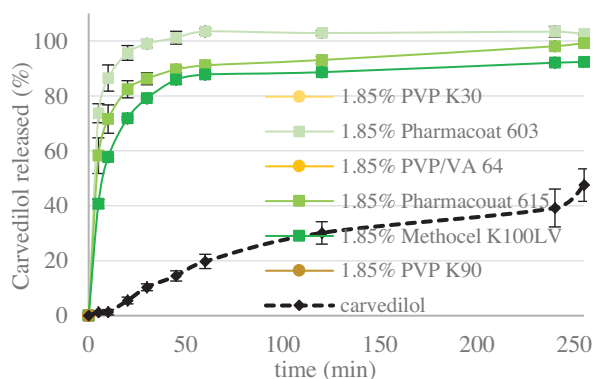


Figure 1. *In vitro* carvedilol dissolution profiles (medium with pH 6.8) of SMEDDS granules prepared using 1.85% of different binders in granulation dispersion.

3.2. The influence of polymer concentration on SMEDDS granules characteristics

When hypromellose was used as binder in granulation dispersion, the difference in flowability was noticed regarding concentration. Hence, SMEDDS granules with lower polymer amount were classified as good, in comparison to fair flow properties of particles with 7.45% of polymer (according to the same Carr index criteria).

Concerning *in vitro* carvedilol properties, SMEDDS granules with higher binder amount showed slightly faster carvedilol release, in

comparison to ones with lower polymer amount, as shown in Fig. 2.

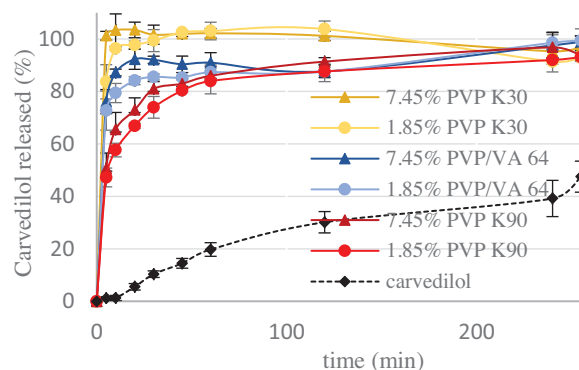


Figure 2. *In vitro* carvedilol dissolution profile (medium with pH 6.8) of SMEDDS granules with high and low binder concentration (1.85 and 7.45%) in granulation dispersion.

3.3. The influence of granulation method on SMEDDS granules characteristics

The rate of carvedilol release was affected by granulation method, as the release was faster from all manually prepared SMEDDS granules. Contrary to this, the extent of released drug, wasn't influenced by preparation method, as the drug was completely released until the end of testing period in both cases.

4. CONCLUSION

By incorporation of polymeric binders into the granulation dispersion it was possible to produce Syloid® 244FP-based free-flowing granules, with preserved self-microemulsifying properties, responsible for improved *in vitro* carvedilol release. Incorporation of higher molecular weight polymers resulted in slower *in vitro* carvedilol release profile, while higher binder concentration was related to faster drug release.

5. REFERENCES

1. Mandić J. et al. Overview of solidification techniques for self-emulsifying drug delivery systems from industrial perspective. *Int. J. Pharm.* 2017 533(2): 335–45.
2. Pouton CW. et al. Lipid formulations for oral administration of drugs: non-emulsifying, self-emulsifying and 'self-microemulsifying' drug delivery systems. *Eur J Pharm Sci.* 2000 11: 93

PULMONARY DRY POWDER FOR INHALATION FOR TARGETED DRUG DELIVERY TO MACROPHAGES IN TUBERCULOSIS

Mahwash Mukhtar¹, Noemi Csaba^{2,3}, Sandra Robla^{2,3}, Rubén Varela-Calviño⁴, Árpád Farkas⁵, Rita Ambrus¹

¹ *Institute of Pharmaceutical Technology and Regulatory Affairs, Faculty of Pharmacy, University of Szeged, Szeged, Hungary*

² *Department of Pharmacology, Pharmacy and Pharmaceutical Technology, University of Santiago de Compostela, Santiago de Compostela, Spain*

³ *Center for Research in Molecular Medicine and Chronic Diseases, University of Santiago de Compostela, Santiago de Compostela, Spain*

⁴ *Department of Biochemistry & Molecular Biology, School of Pharmacy University of Santiago de Compostela, Santiago de Compostela, Spain*

⁵ *Center for Energy Research, Hungarian Academy of Sciences, Budapest, Hungary*

1. INTRODUCTION

The marketed oral therapies fail to deliver the anti-tubercular agent directly to the lungs. The conventional drug delivery systems are ineffective in the treatment of tuberculosis (TB) due to the off-site drug release, inadequate drug concentration at the targeted site and therefore cause systemic toxicity. As the causative agent *Mycobacterium tuberculosis* resides in the alveolar macrophages, therefore targeted nanotechnology-based dry powder for inhalation was fabricated to deliver the anti-tubercular isoniazid (INH) in the deeper lung tissues.

2. MATERIALS AND METHODS

2.1. Materials

Isoniazid, Hyaluronic acid (HA), Chitosan (CS) 75–85 % deacetylated, Mannosylated chitosan (MC).

2.2. Method to obtain nanopowder

An ionic gelation method was used to develop the nanosuspension. Briefly, the developed polymer, MC was dissolved in 0.05 M glacial acetic acid. The aqueous solution of HA was added dropwise to the MC solution along with the cross-linker, sodium tripolyphosphate with continuous stirring. Later, INH solution in methanol was added to the above mixture to yield the drug-loaded nanoparticles which were

freeze-dried to obtain INH-MC/HA nanopowder [1]. All the studies were compared with the INH-CS/HA nanopowder, synthesized in a similar way using chitosan instead of MC.

2.3. *In vitro* aerodynamic profile

Andersen cascade impactor (ACI) (Copley Scientific Limited, UK), was used to determine the aerodynamic characteristics of the nanopowder. Nanopowder filled into the HPMC capsules was delivered to the ACI using Breezhaler[®] device. The particles deposited on each plate were dissolved in (2:1) methanol:water and emitted dose (ED) was spectrophotometrically analyzed. The flow rate was set to 60 L/minute during an experiment. Mass median aerodynamic diameter (MMAD) and fine particle fraction (FPF < 3 μ m) were analyzed using KaleidaGraph software [2].

2.4. Studies on macrophages

The cytotoxicity of nanopowders was evaluated using an MTS assay on the primary macrophages. The macrophage phenotypic analysis was performed after incubation of nanoparticles with macrophages and staining with antibodies (CD83-APC and CD80-PE) [3].

Also, 2,3-Indoleamine dioxygenase (IDO) assay was performed to evaluate the tolerogenic effect of nanoparticles on macrophages [4].

3. RESULTS AND DISCUSSION

3.1. *In vitro* aerodynamic profile

FPF < 3 μm was found to be promising which presents the drug deposition in the lower areas of the lungs, particularly in the alveolar region. MMAD was within the acceptable range for inhalation (Table 1).

Table 1. Particle characteristics of the nanopowder

Parameters	INH-CS/HA nanopowder	INH-MC/HA nanopowder
Particle size (nm)	3.42 ± 6.5	302 ± 3.2
MMAD (μm)	2.46 ± 0.09	1.679 ± 0.1
FPF < 3 μm (%)	50.90 ± 0.07	62 ± 0.09
ED (%)	75 ± 0.88	87.70 ± 0.21

3.2. Studies on macrophages

The % cell viability was evidently but not primarily dependent on the increase in the concentrations of the samples (Fig. 1). All the samples presented a viability of more than 70 %.

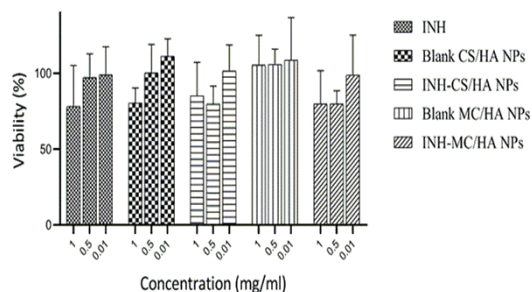


Figure 1. Effect of nanoformulations on the viability of a primary culture of macrophages after 24 h incubation.

The expression of T-lymphocyte costimulatory molecules (CD83 and CD80), the indicators of pro-inflammatory activated phenotype in macrophages, was evaluated by the incubation of NPs with macrophages for 2 h. The expression was higher for the MC/HA nanoformulations (Fig. 2a). No tolerogenic activity was observed by the nanoparticles. This shows that the T-cell immune response was not suppressed, characteristic of the pro-inflammatory response, which is essential to the treatment of TB (Fig. 2b).

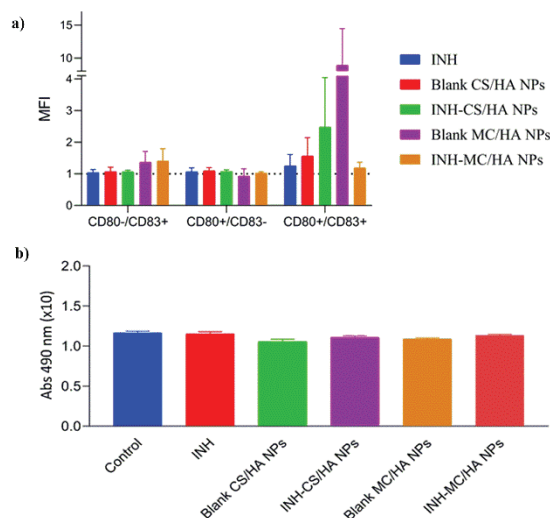


Figure 2. % Quantification of the expression of macrophage maturation markers, CD80 and CD83 (a), IDO activity in macrophages cell culture (b)

4. CONCLUSION

The developed nanopowder for inhalation was found to be promising in terms of the aerodynamic deposition profile and cellular studies. This approach can be optimistic in targeting macrophages in TB by exploiting the biocompatible polymers.

5. REFERENCES

- Mukhtar, M., et al., *Freeze-dried vs spray-dried nanoplex DPIs based on chitosan and its derivatives conjugated with hyaluronic acid for tuberculosis: In vitro aerodynamic and in silico deposition profiles*. European Polymer Journal, 2021. 160: 110775.
- Mukhtar, M., et al., *Aerodynamic properties and in silico deposition of isoniazid loaded chitosan/thiolated chitosan and hyaluronic acid hybrid nanoplex DPIs as a potential TB treatment*. International Journal of Biological Macromolecules, 2020. 165: 3007-3019.
- Robla, S., et al., *A chitosan-based nanosystem as pneumococcal vaccine delivery platform*. Drug Delivery and Translational Research, 2021. 11(2): 581-597.
- Crecente-Campo, J., et al. *Design of polymeric nanocapsules to improve their lympho-targeting capacity*. Nanomedicine, 2019. 14(23): 3013-3033.

ACKNOWLEDGMENT

TKP2021-EGA funding scheme (Hungary).

FLUORESCENT PROBES FOR DETECTION OF MISFOLDED PROTEINS IN BIOLOGICAL SAMPLES

Damijan Knez¹, Luka Rejc², Lana Blinc³, Matic Rogan², Bruno Aleksander Martek², Ross Jansen van Vuuren², Jerneja Kladnik², Anže Meden¹, Gabriela Molina-Aguirre⁴, Balazs Pinter⁴, Maja Bresjanac³, Stanislav Gobec¹, Janez Košmrlj²

¹ University of Ljubljana, Faculty of Pharmacy, Department of Medicinal Chemistry, Slovenia

² University of Ljubljana, Faculty of Chemistry and Chemical Technology, Department of Organic Chemistry, Slovenia

³ University of Ljubljana, Faculty of Medicine, Institute of Pathophysiology, Slovenia

⁴ Department of Chemistry and Biochemistry, University of Texas at El Paso, Texas, USA

1. INTRODUCTION

Amyloid β ($A\beta$) has long been considered a major contributor to the pathology of Alzheimer's Disease (AD). Recent therapeutic efforts with aducanumab, an antibody developed to remove $A\beta$ from the brain, have demonstrated that this concept deserves reevaluation. Timely diagnosis of AD is challenging because of the lack of reliable detection methods [1]. Accurate information with predictive diagnostic value currently relies on positron emission tomography (PET) imaging of cerebral deposition of $A\beta$ and CSF markers ($A\beta$, tau, and phosphorylated tau). These analyses have gained acceptance and are included in the diagnosis of AD; however, they remain relatively inaccessible or invasive. To overcome this, new platforms and immunoassays have been developed in recent years to measure $A\beta$ in the periphery, since $A\beta$ is elevated in early prepathological stages [2]. In addition, fluorescent probes that selectively stain $A\beta$ deposits in brain samples have also been developed and could also be used to detect $A\beta$ species in blood samples. *Ex vivo* quantification of misfolded proteins in blood would be a minimally invasive method for diagnosing AD and also for tracking disease progression. The development of diagnostic tools should consider the specificity of detection and sensitivity to detect AD biomarkers at femtomolar concentrations in blood.

We focused on the design, synthesis, and evaluation of fluorescent molecular probes to detect AD biomarkers, i.e., $A\beta$ and tau protein, by fluorescence spectroscopy in blood and brain tissue from AD patients.

2. MATERIALS AND METHODS

2.1. Design and synthesis of probes

Fluorescent probes were synthesized following established procedures for the synthesis of (F)DDNP analogues [3, 4].

2.2. Spectral properties of the probes

The spectral properties, i.e., absorption and emission spectra, quantum yields in different solvents (e.g. methanol, acetonitrile, dichloromethane) were determined as described previously [3].

2.3. *In vitro* binding experiments

$A\beta_{1-42}$ fibrils were prepared in 10 mM HCl at 37 °C, preformed tau-441 fibrils were acquired from rPeptide LLC. *In vitro* binding properties of probes in the presence of $A\beta$ and tau-441 fibrils, non-aggregated $A\beta$, and BSA were determined on 96- or 384-well microplates in 150 mM HEPES buffer solution (pH = 7.4, 150 mM NaCl) using Biotek Synergy H4 and Tecan Spark microplate readers. *K_d* values were determined as described previously [5].

2.4. Binding to misfolded protein in human brain samples

Human brain sections from AD patient and healthy controls were stained with selected probes [3], and examined under a fluorescence confocal microscope.

3. RESULTS AND DISCUSSION

3.1. Synthesis of probes and DFT studies

The fluorescent probes were designed to contain three building blocks: a) core framework with π -system, i.e., linker, b) electron donor group, and c) electron acceptor

OP6

groups. Such structure enables the push-pull effect, which is often reflected in the fluorescence properties. The optical properties showed a clear influence of the core linker on the measured fluorescence emission maxima and quantum yields. DFT simulations revealed a charge-transfer excited singlet state responsible for the solvent/environment-dependent fluorescence of the probes. In addition, it was generally observed that these probes twist in the excited state with donor-acceptor groups nearly perpendicular to each other.

3.2. *In vitro* binding properties

Binding of probes to the A β ₁₋₄₂ fibrils was accompanied by changes in fluorescence emission, which was followed to determine K_d values (Table 1). The spectral changes in the presence of monomeric A β ₁₋₄₂ indicated that the probes bound only to fibrils. The spectra in the presence of BSA indicated the degree of nonspecific binding, which was lower compared with A β ₁₋₄₂ fibril binding. Two selected probes and ThT were subjected to further assays, i.e., binding to tau441 fibrils and experiments on human plasma. In plasma samples spiked with A β ₁₋₄₂ fibrils, an increase in probe's fluorescence emission was observed, indicating that the probes were able to detect fibrils in a complex matrix.

Table 1. Spectral properties and binding affinities of probes towards A β ₁₋₄₂ fibrils.

Cpd	A β ₁₋₄₂ fibrils		
	$\lambda_{em,max}$ [nm]	Fold increase of emission	K_d [μ M]
<u>1</u>	595	328 \pm 32	0.88 \pm 0.22
<u>2</u>	560	200 \pm 2	0.36 \pm 0.10
ThT	485	17 \pm 4	30.6 \pm 5.0

3.3. Fluorescence and Confocal Microscopy

Selected probes bound to and distinguished between different types of AD-specific misfolded protein aggregates in human brain samples as demonstrated by ultraviolet and confocal microscopy images (Fig. 1).

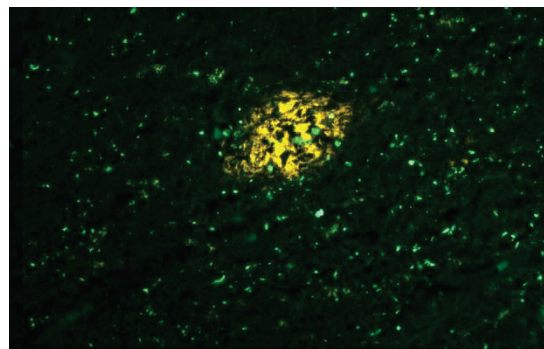


Figure 1. Amyloid plaque (orange, granular) and neurofibrillary tangles (turquoise, filamentous), stained with probe 1.

4. CONCLUSION

We have developed probes that differentially stain amyloid plaques and neurofibrillary tangles in human brain samples. The question of whether the probes are capable of detecting A β species in blood samples from patients with AD will be the subject of further investigation.

5. REFERENCES

1. Villemagne, VL., et al., *Imaging tau and amyloid- β proteinopathies in Alzheimer disease and other conditions*. Nature Reviews Neurology, 2018. 14(4): 225-236.
2. Chong, JR., et al., *Blood-based high sensitivity measurements of beta-amyloid and phosphorylated tau as biomarkers of Alzheimer's disease: a focused review on recent advances*. Journal of Neurology, Neurosurgery and Psychiatry, 2021. 92(11): 1231-1241.
3. Rejc, L., et al., *Design, Syntheses, and in Vitro Evaluation of New Fluorine-18 Radiolabeled Tau-Labeling Molecular Probes*. Journal of Medicinal Chemistry, 2017. 60(21): 8741-8757.
4. Petrič, A., et al., *Dicyanovinylphthalenes for neuroimaging of amyloids and relationships of electronic structures and geometries to binding affinities*. The Proceedings of the National Academy of Sciences, 2012. 109(41): 16492-16497.
5. Espargaró, A., et al., *On the Binding of Congo Red to Amyloid Fibrils*. Angewandte Chemie International Edition, 2020. 59(21): 8104-8107.

ACKNOWLEDGMENT

Financial support from Slovenian Research Agency ARRS is acknowledged (P1-0208, P1-0230, P3-0171 and J1-3018).

TARGETING CATHEPSIN X IN NEURODEGENERATIVE DISEASES WITH NOVEL TRIAZOLE-BENZODIOXINE INHIBITORS

Urša Pečar Fonovič¹, Damijan Knez², Ana Mitrovič¹, Anja Pišlar¹, Martina Hrast², Nace Zidar², Jure Stojan³, Matic Proj², Simon Žakelj⁴, Jurij Trontelj⁴, Bojan Doljak¹, Boris Brus², Tanja Jakoš¹, Stanko Gobec², Janko Kos¹

¹ Department of Pharmaceutical Biology, Faculty of Pharmacy, University of Ljubljana, Slovenia

² Department of Pharmaceutical Chemistry, Faculty of Pharmacy, University of Ljubljana, Slovenia

³ Institute of Biochemistry, Medical Faculty, University of Ljubljana, Slovenia

⁴ Department of Biopharmaceutics and Pharmacokinetics, Faculty of Pharmacy, University of Ljubljana, Slovenia

1. INTRODUCTION

Cathepsin X is a cysteine cathepsin with carboxymonopeptidase activity. It is expressed mainly in immune and neuronal cells and physiologically implicated in cell proliferation, migration, adhesion, etc. When up-regulated, like in cancer and neurodegenerative disorders, it is involved in diverse pathological processes where it acts through cleavage of its distinct substrates [1]. In neuronal cells cathepsin X abolishes the neurotrophic activity of γ -enolase by cleaving its C-terminus, and is involved in the generation of plasmin. Therefore, cathepsin X regulates neuronal differentiation and neurite outgrowth and moreover it regulates neuronal survival and apoptosis.

Activity of cathepsin X is poorly controlled by endogenous cysteine peptidase inhibitors [3], and is thus a promising target for the development of new therapeutic agents. Inhibitor AMS-36 which was designed based on the general clan CA cysteine protease inhibitor E-64 with epoxysuccinyl covalent warhead [4], showed only limited selectivity towards cathepsin X, cross-reactivity with cathepsin B being the most problematic [5].

2. MATERIALS AND METHODS

2.1 Relative inhibition of cathepsins

579 compounds from the *in-house* library, and subsequent 20 analogues of hit compounds were screened for the inhibition of cathepsin X at 50 μ M concentration using Abz-FEK(Dnp)-OH substrate at 37 °C. For compounds inhibiting cathepsin X by more than 50%, K_i was determined, and their inhibitory potencies toward cathepsins B, L, S and H were

determined using enzyme specific substrates. Reversibility of binding was determined by the washout experiment, and by step-wise dilution experiment.

2.2 Cell assays

After determining cytotoxicity with MTS assay, the impact of selected compounds on migration was tested in prostate cancer PC-3 cell model and on neurite outgrowth in pheochromocytoma PC-12 cell model. Real-time cell migration assay was performed on a RTCA DP Instrument, xCELLigence System (ACEA Biosciences) and measured continuously for 72 hours. Neurite outgrowth was measured with Neurite Outgrowth Staining Kit 48 hours after cell exposure to the compound. Cell F-actin content was determined with fluorescence microscopy using phalloidin-TRITC.

2.3. Synthesis

A concise series of analogues was synthesized by varying the benzodioxine and triazole moieties. The central ketomethylenethio linker was also modified to gain deeper insight into SARs.

3. RESULTS AND DISCUSSION

3.1 Triazole-benzodioxine compounds inhibit cathepsin X reversibly

Following the initial screening and the assays of the “analogues by catalogue” compounds, K_i values in low μ M concentration were determined for the five most potent inhibitors. All hit compounds selectively and reversibly inhibited cathepsin X, and 1-(2,3-dihydro benzo[*b*][1,4]dioxin-6-yl)-2-((4-isopropyl-4*H*-1,2,4-triazole-3-yl)thio)ethan-1-one, compound Z9, was identified as the most potent inhibitor of the series.

OP7

3.2 Compound Z9 up-regulated neurite outgrowth in PC-12 cells and inhibited migration of cancer cells

New inhibitors were not cytotoxic at 10 μ M concentration. Three of the inhibitors inhibited PC-3 migration, Z9 by more than 30%. Five assayed inhibitors up-regulated neurite outgrowth as measured with the kit, Z9 for 85%. Neurite outgrowth was shown also through the up-regulation of actin polymerisation after cathepsin X inhibition (Fig.1).

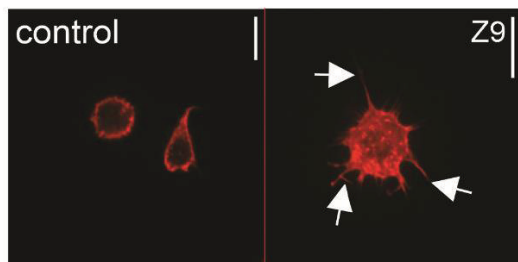


Figure 1. After 2-hour inhibition of cathepsin X by compound Z9, up-regulation of neurite outgrowth is shown by visualisation of actin polymerisation in PC-12 cells.

3.3 Structure activity relationships (SARs)

52 analogues of Z9 were synthesized to explore SAR, which ultimately point to the importance of the central linker for cathepsin X inhibition. Variations of the triazole heterocycle had no significant effect on inhibitory potencies, whereas inhibition was diminished when the benzodioxine moiety was replaced with substituted phenyls. Five compounds were analysed in more detail, and showed reversible binding and selective inhibition of cathepsin X. Their inhibitory activities were in the same concentration range as that of Z9.

4. CONCLUSION

Based on an *in-house* screening of a compound library, reversible triazole-based cathepsin X inhibitors were developed. K_i values were in the low micromolar range, inhibitors showed high selectivity for cathepsin X, and performed well in cell-based assays.

5. REFERENCES

1. Kos, J., et al., *Intracellular signaling by cathepsin X: Molecular mechanisms and diagnostic and therapeutic opportunities in cancer*. *Seminars in Cancer Biology*, 2015. 31: 76-83.
2. Pišlar, A., et al., *Cysteine Cathepsins in Neurological Disorders*. *Molecular Neurobiology*, 2014. 49: 1017-1030.
3. Pečar Fonovič, U., et al., *The Carboxypeptidase Activity of Cathepsin X is Not Controlled by Endogenous Inhibitors*. *Acta Chimica Slovenica*, 2019. 66(1): 58-61.
4. Sadaghiani, A.M., et al., *Design, synthesis, and evaluation of in vivo potency and selectivity of epoxysuccinyl-based inhibitors of papain-family cysteine proteases*. *Chemistry & biology*, 2007. 14(5): 499-511.
5. Pečar Fonovič, U., et al., *Identification and characterization of the novel reversible and selective cathepsin X inhibitors*. *Scientific Reports*, 2017. 7: 11459.

ACKNOWLEDGMENT

This study was supported by the Slovenian Research Agency (Research Programs P1-0208 and P4-0127, and Research project J4-8227).

CHALCOGEN CARBAMATES AS COVALENT CHOLINESTERASE INHIBITORS – SURVEYING GROUP 16 (VI) OF THE PERIODIC TABLE

Anže Meden¹, Damijan Knez¹, Xavier Brazzolotto², Fabrice Modeste², Milica Denic², Stanislav Gobec¹

¹ Department of Pharmaceutical Chemistry, University of Ljubljana, Faculty of Pharmacy, Aškerčeva 7, Ljubljana, Slovenia.

² Département de Toxicologie et Risques Chimiques, Institut de Recherche Biomédicale des Armées, Brétigny sur Orge, France.

1. INTRODUCTION

Aryl carbamate alkaloids, such as physostigmine, were not only the first discovered cholinesterase inhibitors, but also the first covalent, pseudo-irreversible cholinesterase inhibitors (ChEIs).[1] The ChEIs found their use in medicine (Alzheimer's disease, myasthenia gravis, glaucoma, etc.), pest control, and, unfortunately, also as chemical weapons. The rates of carbamylation and decarbamylation are governed by both steric and electronic factors.[2] Review of the literature has shown that besides the *O*-aryl carbamate ChEIs, the chemical space of different carbamates remains largely unexplored.

The group 16 (VIA) elements of the periodic table are also called chalcogens ("ore formers"). The periodicity effects upon descending within a group in the periodic table of elements, e.g., the decrease in the hydrides' *pK*_a-s, the increase in the atomic radii, and the decrease in electronegativities, have been well studied within the field of inorganic chemistry but are quite neglected in medicinal chemistry.

2. MATERIALS AND METHODS

2.1. Synthesis

The leaving groups were synthesized by halogen-lithium exchange and quenching with electrophile from 7-bromoindole, the dimethylcarbamoyl group was introduced with *N,N*-dimethylcarbamoyl chloride and the rest of the molecule attached *via* Mannich reaction with formaldehyde and 2-cycloheptyl-*N*-

methylethan-1-amine. The compounds were analyzed to confirm identity and purity.

2.2. *In vitro* characterization, crystallization, and LC-MS proof of carbamylation

The inhibitory potencies of the compounds against the ChEs were determined using the method of Ellman, and for time-dependency measurements, the pre-incubation time was varied (1 min, 5 min, 15 min, and 30 min). The crystallization also followed a reported procedure.[3]

In LC-MS experiments, recombinant human BChE (approx. 5 μ M) was incubated with 50 μ M compound for 5 min, then 2 μ L of the mixture were injected on a bioZenTM 3.6 μ m Intact XB-C8 LC column 100 \times 2.1 mm (Phenomenex) on an Agilent 1290 Infinity UHPLC coupled to an Agilent iFunnel Q-TOF 6550 HRMS, and eluted with MQ water/0.1% HCOOH – acetonitrile/0.1% HCOOH (linear gradient). Data were treated using OpenChrom (v 1.4) and extracted spectra were deconvoluted with UniDec software (v 5.0.1).

3. RESULTS AND DISCUSSION

To elucidate the factors that determine the carbamate leaving group prerequisites for covalent inhibition, we prepared a variety of dimethylcarbamates (Figure 1) based on a previously reported, reversible, butyrylcholinesterase-selective inhibitor scaffold.[3] The covalent mechanism of binding was tentatively determined by IC₅₀ time-dependency and kinetic experiments. For selected dimethyl *O*-aryl carbamates, the carbamylation of butyrylcholinesterase's

OP8

Ser198 was also unambiguously confirmed by mass spectrometry (71 ± 1 Da mass increase due to the dimethylcarbamoyl moiety and protonated His438), and crystallization (carbamoylated catalytic Ser198 was observed in the crystal structure). Regarding different leaving group chemotypes, oxime and enol ether carbamates functioned as covalent ChEIs, whereas aliphatic alcohol and trifluoroethanol carbamates did not.

To evaluate the periodicity effects within the chalcogens, we synthesized and evaluated thio-, seleno- and telluro-analogues of the *O*-aryl carbamate. The compounds indeed functioned as covalent inhibitors, but their potency was decreased compared to their oxygen predecessor. To evaluate the steric requirements, smaller fragments featuring the same warhead motif were also tested, and to evaluate the electronic effects, QM/MM modelling was undertaken.

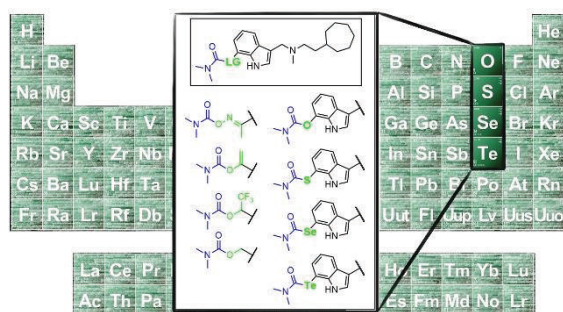


Figure 1. Examples of compounds synthesized and evaluated. The blue-coloured carbamate moiety is transferred to the catalytic serine in the enzyme active site. The green-coloured moiety functions as the leaving group (LG), while the black-coloured portion of the molecule is responsible for recognition and confers selectivity for butyrylcholinesterase. The four non-radioactive chalcogens are highlighted within the periodic table of elements.

4. CONCLUSION

To the best of our knowledge, despite the simplicity of the idea, this is the first time that all non-radioactive chalcogen carbamates, i.e., *O*-, *S*-, *Se*-, and *Te*-aryl carbamates, were prepared and reported as cholinesterase inhibitors.

5. REFERENCES

1. Scheindlin, S., Episodes in the Story of Physostigmine. *Molecular Interventions*, **2010**, *10* (1): 4.
2. Groner, E., et al., The Kinetics of Inhibition of Human Acetylcholinesterase and Butyrylcholinesterase by Two Series of Novel Carbamates. *Molecular Pharmacology*, **2007**, *71* (6): 1610–1617.
3. Meden, A., et al., From Tryptophan-Based Amides to Tertiary Amines: Optimization of a Butyrylcholinesterase Inhibitor Series. *European Journal of Medicinal Chemistry*, **2022**, *234*: 114248.

ACKNOWLEDGMENT

This research was funded by the Slovenian Research Agency (ARRS), Research Core Funding N° P1-0208 and a young researcher grant to A.M. X.B., F.N. and J.D. were supported by the French Ministry of Armed Forces (Direction Generale de l'Armement and Service de Sante des Armees, NBC-5-C-4210). Authors would like to thank the SOLEIL synchrotron for long-term beamtime access (20181022 IBS BAG).

IN VIVO EFFICIENCY OF A NEW LIPOSOMAL ADJUVANT SYSTEM BASED ON PORINS

Selin Parmaksız¹, Ece Türkmen¹, Aykut Özkul², Vanessa Rivero-Arredondo³, Louis Ontiveros-Padilla³, Maryam T. Hussein⁴, Neil Liam Andrew Forbes⁴, Constantino López-Macías³, Yvonne Perrie⁴, Sevda Şenel^{1*}

¹Department of Pharmaceutical Technology, Faculty of Pharmacy, Hacettepe University, Turkey

² Department of Virology, Faculty of Veterinary Medicine, Ankara University, Turkey

³ Medical Research Unit on Immunochemistry, Specialties Hospital, National Medical Centre "Siglo XXI", Mexican Social Security Institute (IMSS), Mexico City, Mexico

⁴ Strathclyde Institute of Pharmacy and Biomedical Sciences, University of Strathclyde, United Kingdom

*Correspondence: ssenel@hacettepe.edu.tr

1. INTRODUCTION

Liposomes have been shown to exert immunostimulatory effects besides being used as a delivery system for vaccines [1]. The size, charge, bilayer rigidity and composition of liposomes allow for tailored antigen delivery and have an impact on stimulation of immune response [1-3]. On the other hand, *Salmonella Typhi* (*S. Typhi*) porins have been shown to exert adjuvant effect on antibody responses to several antigens [4]. In this study, we have combined neutral and cationic liposomes with porins and evaluated immune response against a model antigen, OVA in immunized BALB/c mice.

MATERIALS AND METHODS

a. Preparation of liposomal formulations

Liposomes were prepared by the film-hydration method [3]. Lipids were obtained from Avanti Lipis, USA. DSPC (distearoyl-sn-glycero-3-phosphocholine), Cholesterol and TDB (1,2-trehalose 6,6-dibehenate) were used for neutral liposomes and DDA (dimethyl-dioctadecyl ammonium) and TDB were used for cationic liposomes. 1 mg/mL endotoxin-free ovalbumin (Invivogen, France) and 0,2 mg/mL porins (purified from *S. Typhi* 9,12, Vi: d ATCC 9993) [4] were added to the lipid film.

b. Immunisation

36 female, 6 to 10 weeks old BALB/c mice were divided into twelve groups (n=3) (Table 1). Mice were immunized intraperitoneally on days 0 and 15. Saline solution was used as a control. The administration volume was 100 µl. All animal care and experimental protocols were approved by animal experimentations local ethics board (protocol no: 2015/75-14).

C. Determination of humoral immune response

On 0, 8, 12 and 30 days the animals were bled via the submandibular route. IgM and IgG levels were determined by ELISA at 492 nm.

RESULTS AND DISCUSSION

The properties of the liposomal adjuvant system and the adjuvanted formulations are given Table 1.

Table 1. Animal study groups

	Groups	Particle Size (nm)	Zeta Potential (mV)
1	Saline solution	-	-
2	Porins	-	-20,83±0,55
3	OVA	-	-24,36±1,16
4	Porins+OVA	-	-22,75±0,59
5	Neutral Liposome	524,0 ± 20,4	-6,05±0,81
6	Porins+ Neutral Liposome	466,5 ± 28,9	-9,96±0,74
7	OVA+ Neutral Liposome	662,8 ± 14,5	-5,49±0,29
8	Porins+ OVA+ Neutral Liposome	481,7 ± 5,8	-8,62±2,28
9	Cationic Liposome	407,7 ± 3,9	39,73±0,85
10	Porins+ Cationic Liposome	423,1 ± 7,8	19,13±2,09
11	OVA+ Cationic Liposome	310,8 ± 96,2	16,77±1,10
12	Porins+ OVA+ Cationic Liposome	383,5 ± 72,5	14,67±1,31

IgM levels: Our results showed that the combination of porins with cationic or neutral liposomes induced higher anti-porins and anti-OVA IgM antibody levels compared to that porins, OVA, porins+OVA and empty liposomes on Day 8 (p <0.001) (Fig. 1). Cationic liposomal adjuvant induced higher anti-porins IgM than neutral liposomal adjuvants, whereas with OVA, anti-OVA IgM levels were higher with neutral liposomal systems after first immunization. After booster,

OP9

IgM levels were found to be similar with cationic and neutral liposomal adjuvants and these levels were slightly higher than that of porins, OVA, porins+OVA and empty liposomes on Day 30 ($p>0.5$).

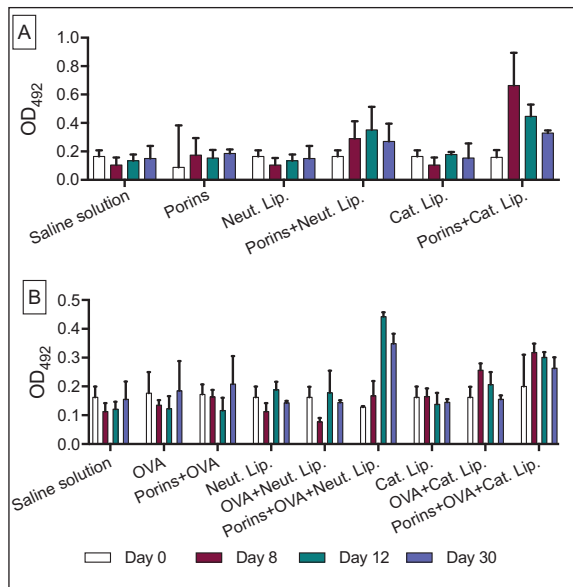


Figure 1. Anti-porins (A) and anti-OVA (B) IgM responses (n=3)

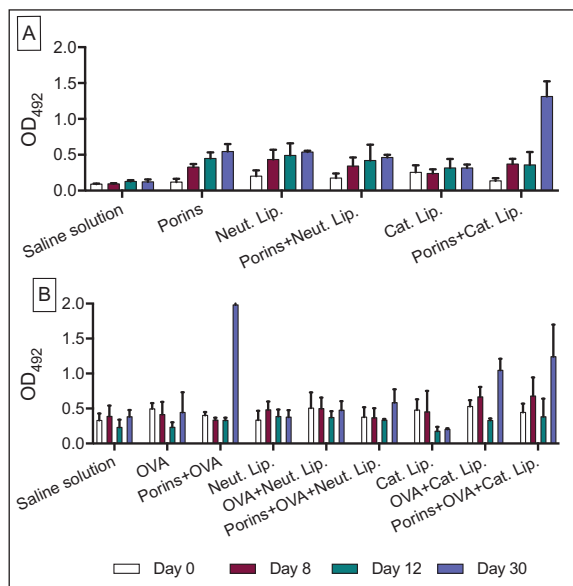


Figure 2. Anti-porins (A) and anti-OVA (B) IgG responses (n=3)

IgG levels: A significant increase in IgG levels was observed with the combination of porins with cationic liposomes after booster when compared to that obtained with the porins alone and the combination of porins with neutral liposomes ($p<0.0001$). Anti-OVA IgG levels were induced with cationic liposomal systems higher than with neutral liposomal systems

($p<0.001$). IgG levels were not induced with any groups after the first immunization. After booster, IgG level with porins+OVA without adjuvant was observed to increase significantly when compared to adjuvanted groups ($p<0.0001$).

4. CONCLUSION

We have showed that our adjuvant system prepared by combination of porins with liposomes resulted in significantly increased immune responses. The charge of the liposomal system (neutral and cationic) was found to have a significant impact on the immune responses. It was observed that neutral liposomal adjuvant systems were able to stimulate only the early-stage IgM immune response, whereas cationic liposomal systems stimulated both the early-stage IgM and the long-term IgG immune responses. Cationic liposomal adjuvant system based on combination of liposomes and *S. Typhi* porins are suggested as a promising adjuvant/delivery system that exerts long-lasting immune responses

5. REFERENCES

- [1] Perrie, Y., et al. *Advanced Drug Delivery*, 2015; 99:85-96.
- [2] Carstens, M. G., et al. *Vaccine*, 2011;29(29-30):4761-70.
- [3] Henriksen-Lacey, M., et al. *J. Control. Rel.*, 2010;145(2):102-8.
- [4] Pérez-Toledo M., et al. *Frontiers in Immunology*. 2017; 9(8):230.

ACKNOWLEDGMENT

This project was supported by TÜBİTAK-Turkey (SBAG-215S995) and UK GCRF Networks in Vaccines Research and Development which was co-funded by the MRC and BBSRC, through BactiVac-Network project BVNCP3-21.

All authors have equal contributions.

IN VIVO EVALUATION OF DOXORUBICIN AND ELACRIDAR CO-LOADED PLGA/SILICA HYBRID NANOPARTICLES AGAINST MULTIDRUG RESISTANT BREAST CANCER

Hayrettin Tonbul¹, Adem Şahin², Süleyman Can Öztürk³, Gözde Ultav⁴, Güneş Esendağlı⁵, Yılmaz Çapan⁶

¹*Department of Pharmaceutical Technology, Faculty of Pharmacy, Inonu University, Turkey*

²*Department of Pharmacy Service, Vocational School of Health Services, Bilecik Seyh Edebali University, Turkey*

³*Laboratory Animals Research and Application Centre (HUDHAM), Hacettepe University, Turkey*

⁴*Department of Pharmaceutical Biotechnology, Faculty of Pharmacy, Inonu University, Turkey*

⁵*Department of Basic Oncology, Hacettepe University Cancer Institute, Turkey*

⁶*Department of Pharmaceutical Technology, Faculty of Pharmacy, Lokman Hekim University, Turkey*

1. INTRODUCTION

Although doxorubicin (Dox) is very effective in several cancer treatment, being a P-glycoprotein (P-gp) substrate limits its effectiveness. The multidrug resistance (MDR) observed in many cancers is frequently associated with overexpression of P-gp and some other membrane transporters. Various approaches have been developed to overcome the growing resistance to these drugs including Dox. One of them is the co-delivery of Dox with a P-gp inhibitor substance such as elacridar (Elc). Elc is a third generation P-gp inhibitor that has been one of the most studied inhibitors because of the BCRP (breast cancer resistant protein) and P-gp inhibition ability [1]. Another promising approach about overcoming MDR resistance is developing a nanoparticulate drug delivery system. Mesoporous silica nanoparticles (MSN) have attracted high interest for use as drug delivery system due to possibility to obtain very small size, high storage capacity and excellent colloidal stability. PLGA nanoparticles (NPs) is one of the most investigated nanoparticles due to their several advantages including excellent biocompatibility, biodegradability, FDA and EMA approval, possibility to controlled release and surface modification. Furthermore, combining these two type nanoparticles in a single entity and obtain hybrid nanoparticles (HyNPs) hold big potential in the treatment of several diseases including cancer [2].

In this study, folic acid modified Dox loaded MSN were prepared and these nanoparticles were co-loaded with Elc to pegylated PLGA nanoparticles to obtain hybrid nanoparticles. Effectiveness of developed drug delivery system were evaluated with mouse tumor-

bearing models that obtained with Dox resistant EMT6/AR1 breast cancer cell line.

2. MATERIALS AND METHODS

2.1. Materials

All chemicals were obtained from Sigma Aldrich (MO, USA). All cell culture consumables obtained from Lonza (Basel, Switzerland). All other used reagents were analytical or reagent grade.

2.2. Preparation and Characterization of PLGA/Silica HyNPs

To produce HyNPs, first of all folic acid (FA) conjugated Dox loaded MSNs were obtained with previously optimized method [2]. After that, elacridar and MSNs were loaded to PLGA-PEG NPs with double emulsion method. For this, 50 mg PLGA-PEG, 7,5 mg MSN and Elc were dispersed in 1 ml dichloromethane (DCM). 200 µL distilled water added to the mixture and sonicated for 1 min. After that obtained emulsion system were sonicated another 1 min after adding 4 mL %1 PVA solution. Finally, obtained system poured to 20 mL 0.3 % PVA solution and mixed overnight to evaporate the DCM. Obtained nanoparticles centrifuged and washed several times. Both MSN and HyNPs average particle size and PDI were measured with Horiba Nanopartica SZ-100v2 and TEM analysis (FEI Tecnai BioTwin)

2.3. In vivo experiments with tumor-bearing mice

In vitro evaluation of HyNPs were previously shown and cell culture results show that obtained system readily uptake and show highly cytotoxic effect on ZR-75-1, T-47 and EMT6/AR1 cell lines [2]. For in vivo studies, female Balb/C mice were used and breast

OP10

cancer tumor model were developed with Dox resistant EMT6/AR1 cell line. Mice were divided to 8 groups as **I.** PBS, **II.** blank HyNPs, **III.** Dox solution, **IV.** Caelyx® (marketed liposomal dox formulation), **V.** Dox+Elc solution **VI.** Caelyx+Elc solution, **VII.** Only Dox loaded HyNP formulation (HyNP-) **VIII.** Dox and Elc loaded HyNP formulation (HyNP+). Formulations were applied to mice at 0, 4, 8, 12, 16 and 20th days as IV with 5 mg/kg Dox and 5,18 mg/kg Elc concentration. Formulation effect on tumor growth were evaluated. Moreover, in vivo biodistribution studies were conducted using animal imaging device (Vilber Newton 7.0, France).

3. RESULTS AND DISCUSSION

3.1. Characterization of PLGA/Silica HyNPs

DLS results show that average particle size of FA conjugated MSNs and HyNPs were found 61.3 ± 5.9 and 248.1 ± 11.8 , respectively which is correlated with TEM results (Figure 1)

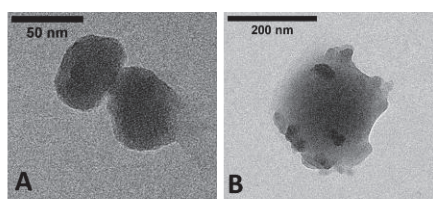


Figure 1. TEM image of MSN (A) and HyNP (B).

3.2. In vivo experiments with tumor-bearing mice

After 24 hours from injection of Indocyanine green (ICG, dye) solution and ICG loaded HyNP+, accumulation of dye in the organs shown in Figure 1.

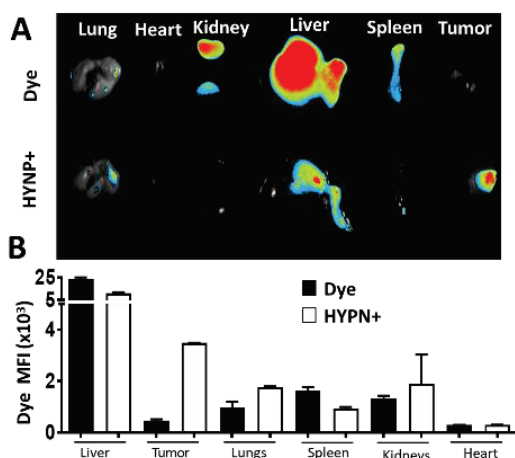


Figure 1. Biodistribution of ICG (dye) solution and ICG loaded HyNP+ formulation **A.** Real image **B.** MFI value after 24h from IV injection to mice.

Results show that accumulation of dye in liver significantly decrease in HyNP+ formulation where there is no dye in tumor in dye solution group.

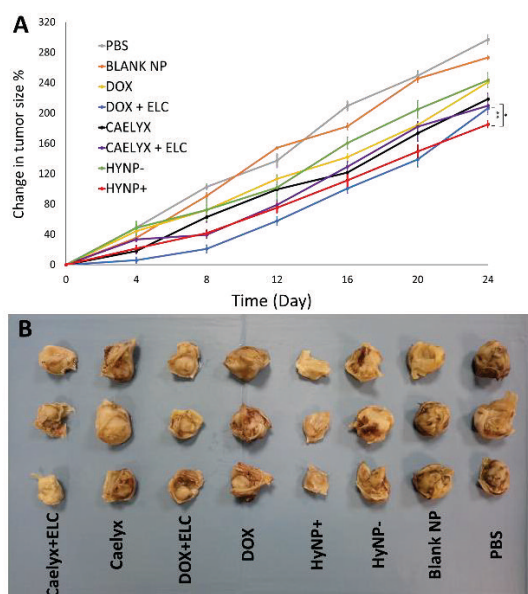


Figure 2. **A.** Change in tumor size in mice during 24 days. **B.** Real image of tumors in mice after sacrifice in 24th day.

After 24 days, elacridar founded groups showed lesser tumor growth among the all groups, where HyNP+ formulation showed least tumor growth.

4. CONCLUSION

Results show that unique hybrid nanoparticle formulation that combine MSN and PLGA nanoparticles hold big potential in MDR resistant breast cancer treatment.

5. REFERENCES

1. Tonbul H., et al. Combination drug delivery with actively-targeted PLGA nanoparticles to overcome multidrug resistance in breast cancer. *Journal of Drug Delivery Science and Technology*, 2019, 101380.
2. Tonbul, H., Development of doxorubicin and elacridar loaded PLGA/silica hybrid nanoparticles and evaluation of activity against breast cancer, Hacettepe University Graduate School of Health Science PhD Thesis, 2019.

ACKNOWLEDGMENT

This work was supported by The Scientific and Technological Research Council of Turkey (TUBITAK), Project Number: 216S999 and Research Fund of the Inonu University, Turkey Project Number: TCD-2021-2229.

NANOFIBERS FOR LOCAL DELIVERY OF TWO *BACILLUS* STRAINS WITH ANTIBACTERIAL ACTIVITY

Nina K. Grilc, Tomaž Rijavec², Anže Zidar¹, Aleš Lapanje², Petra Kocbek¹, Julijana Kristl¹, Špela Zupančič¹

¹ Department of Pharmaceutical Technology, Faculty of Pharmacy, University of Ljubljana, Ljubljana, Slovenia

² Department of Environmental Sciences, Jožef Stefan Institute, Ljubljana, Slovenia

1. INTRODUCTION

Dysbiotic biofilm-related infectious diseases hinder the efficacy of conventional treatment with antibiotics and contribute to the spread of antibiotic resistance (1). Probiotics represent a promising alternative strategy for the treatment of dysbiosis-related diseases. Live therapeutic bacterial strains used as probiotics should be well-characterised and exhibit antibacterial potential (2), while the products containing appropriate strains must retain their viability and enable their precise local administration and release at the target site which can be achieved with bioadhesive nanofibers (3).

The aim of this study was the incorporation of two genetically characterised *Bacillus* strains into bioadhesive nanofibers intended for periodontitis treatment. The nanofibers were designed to retain the viability of probiotics and provide their controlled release. The probiotic potential of the biomaterial was evaluated based on their antibacterial properties.

2. MATERIALS AND METHODS

2.1. Materials

Polyethylene oxide (PEO) 900 kDa and 2 MDa, Nutrient broth and MnSO₄·H₂O were from Sigma-Aldrich. Sodium alginate (MW 138 kDa) Protanal LF 10/60 was from FMC BioPolymer and select agar from Invitrogen.

2.2. Culturing, sporulation of bacteria and their incorporation into nanofibers

Both studied bacterial strains (*Bacillus* strains 27.3.Z and 25.2.M, isolated from healthy oral microbiota) were sporulated by culturing in manganese-supplemented media (nutrient broth). Incorporation of spores of individual strains or their combination into nanofibers was carried out by electrospinning of the spore-

containing 4% (w/v) polymeric dispersions of PEO and ALG to yield the nanofibrous mats with different ALG content (0, 40 and 80 %).

2.3. Nanofiber characterisation

Fabrication of nanofibers and incorporation of spores into their structure was studied by scanning electron microscopy (SEM). The preservation of bacterial viability was evaluated based on the colony forming unit (CFU) counts in the serially diluted dispersion of dispersed nanofibers (compared to the theoretical loading of the starting spore dispersion).

Spore-loaded nanofibrous samples were placed into phosphate buffer (pH 6.8) and spore release from nanofibers was studied based on the CFU counts in serially diluted aliquots taken from the medium at different time points.

2.4. Characterisation of the studied probiotic potential of bacterial strains

The studied strains were genotypically characterised. Their antibacterial activity was evaluated by studies of growth kinetics of select periodontopathogens in the medium containing metabolites of the studied probiotics.

3. RESULTS AND DISCUSSION

3.1. Nanofiber characterisation

Successful incorporation of spores into all three nanofiber formulations was revealed by SEM which also revealed the fabrication of smooth non-beaded fibers (Fig. 1). Spore loadings in the nanofibers were also confirmed by CFU concentration in the dispersed nanofibers which revealed the preservation of viability during the electrospinning process as well as six months storage, achieving the loading of more than 7 log(CFU/mg). This indicates that pre-electrospinning sporulation of both strains is an appropriate strategy for viability preservation

OP11

compared to the fabrication of nanofibers containing bacteria in their vegetative state.

The release of spores from the bulk nanofibrous product was studied in order to elucidate the potential of the different formulations to provide prolonged release of the bacterial strains to the targeted epithelium with dysbiotic biofilm. Both studied strains exhibited comparable release kinetics from nanofibers with the same composition (Fig. 2).

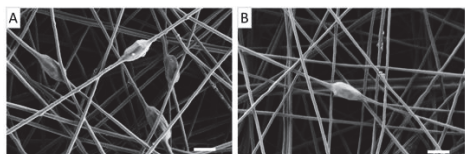


Figure 1. Spore-loaded nanofibers: (a) 40 % ALG + 27.3.Z bacteria, (b) 80 % ALG + 25.2.M bacteria.

Following the initial burst release in the first hour, the remaining spores were gradually released over the next three to eight hours for PEO and PEO/ALG nanofibers, respectively. The burst release is attributed to rapid dissolution of hydrophilic polymers resulting in the dispersion of nanofibers from the surface and outer layers of the nanofibrous mat. The later prolonged release can be attributed to the entrapment of spores in the swollen matrix of the inner layers of the nanofibrous mat as PEO and ALG are known to swell (4), likely closing the interfiber pores. Thus, spore release is limited by polymer erosion. The kinetics of spore release from nanofibers was dependant on PEO/ALG ratio with higher ALG content prolonging the spore release. The release of spores from nanofibers can therefore be controlled with the ratio of the two polymers, whereas the use of ALG provides the feature of bioadhesion (3), desired to prolong nanofiber retention at the targeted oral cavity surfaces.

3.2. Probiotic potential of the studied bacterial strains

The probiotic potential of both studied bacterial strains (27.3.Z and 25.2.M) was evaluated by genotypic characterisation and genomic sequencing, revealing that the strains did not match completely in the genes coding for antibiotics, corroborating the rationale for their

concurrent use. Antibacterial action of the investigated strains against selected periodontopathogens (*Aggregatibacter actinomycetem-comitans*, *Fusobacterium nucleatum*, *Porphyromonas gingivalis*) was also confirmed experimentally.

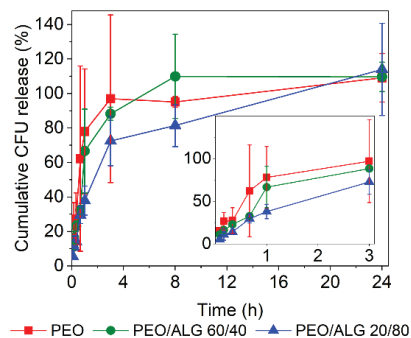


Figure 2. Release of spores 27.3.Z from nanofibers. The smaller figure shows spore release in the first 3 hours in more detail.

4. CONCLUSION

The developed spore-loaded nanofibers are a promising approach for periodontitis treatment and are capable of delivering high loadings of viable bacteria in a controlled manner. The use of well-characterised strains represents a foundation for the development of a complex biomaterial with desired probiotic properties, such as antibacterial efficacy against relevant pathogens. Meanwhile, the combination of the strains aims toward a higher complexity of the locally delivered microbial community.

5. REFERENCES

1. Del Pozo, J.L., *Biofilm-related disease*. Expert Review Anti-infective Therapy, 2018. 1:51-65.
2. Gupta, G., *Probiotics and Periodontal health*. Journal of Medicine and Life, 2011. 14(4):387-94.
3. Brako, F., et al. *Making nanofibres of mucoadhesive polymer blends for vaginal therapies*. European Polymer Journal, 2015. Vol. 70:186-196.
4. Christe, S.M., *Sodium Alginate with PEG/PEO Blends as a Floating Drug Delivery Carrier – In vitro Evaluation*. Advanced Pharmaceutical Bulletin, 2016. 6(3):435–442.

ACKNOWLEDGMENT

This work was supported by the Slovenian Research Agency [Programme J1-9194], European Commission, SurfBio project [grant no. 952379].

DEVELOPMENT OF CYCLOSPORINE A-LOADED MICELLES EXHIBITING A PROMISING ANTIVIRAL ACTIVITY AGAINST SARS-COV-2

Fabiola Guareschi¹, S. Pescina¹, F. Buttini¹, M. Brandolini², V. Sambri^{2,3}, E. Del Favero⁴, L. Cantù⁴, C. Ricci⁴, F. Sonvico¹

¹ Department of Food and Drug, University of Parma, Parma, Italy

² Unit of Microbiology, The Great Romagna Hub Laboratory, 47522 Pievesestina, Italy

³ Department of Experimental, Diagnostic and Specialty Medicine—DIMES, Alma Mater Studiorum—University of Bologna, 40138 Bologna, Italy

⁴ Department of Medical Chemistry, Biochemistry and Biotechnology, University of Milan, Milan, Italy

1. INTRODUCTION

The immunosuppressive peptide drug Cyclosporine A (CSA) has been shown to have an inhibitory activity against the viral replication of several coronaviruses, but its efficacy against SARS-CoV-2 has been hypothesized but not demonstrated [1–3].

CSA-loaded vitamin E polyethylene glycol succinate (TPGS) micelles were developed for intranasal administration and were evaluated for their potential antiviral activity against SARS-CoV-2 *in vitro*.

2. MATERIALS AND METHODS

2.1. Materials

Cyclosporine A was from Metapharmaceutical (Barcelona, Spain); vitamin E polyethylene glycol succinate was from Recordati S.p.A (Milan, Italy); sodium chloride was from VWR International (Leuven, Belgium); acetonitrile and trifluoroacetic acid were of analytical grade.

2.2. Preparation and characterization of the blank and CSA-loaded micelles

CSA-loaded micelles (0.1, 0.25 and 0.5 mg/mL) were prepared by directly adding CSA to the blank formulation prepared by dissolving TPGS in a NaCl 9 g/L solution [4]. The micelles were characterized at time 0 and after 1 month stored at 25°C for particle size, PDI and Zeta potential by Dynamic Light Scattering (DLS) and for CSA encapsulation efficiency (EE%) by HPLC. The molecular structure of the micelles and their interaction with mucus were further

analyzed by Small Angle X-ray Scattering (SAXS, ID02 high-brilliance beamline, ESRF, Grenoble, France).

2.3. *In vitro* activity of the micelles against SARS-CoV-2

The *in vitro* tests were performed on Vero E6 cells. The cytotoxicity of the micelles was tested by treating the cells for 2 hours, then they were washed with PBS and maintained in (Minimum Essential Medium) MEM with 2% Fetal Bovine Serum (FBS) for 72 hours. Six different concentrations of CSA were tested: 64 μM, 32 μM, 16 μM, 8 μM, 4 μM and 2 μM [1]. Seven protocols have been followed to understand at what level of the viral replication cycle the micelles acted: **A.** Pre-treatment, **B.** Treatment contextual to the infection, **C2.** Treatment 2 hours after the infection, **C6.** Treatment 6 hours after the infection, **D.** Pre-treatment associated to a Treatment 2 hours after the infection, **E.** 3 post-treatments; **F.** Pre-treatments associated to 3 post-treatments. Viral concentrations of 0.005 m.o.i and 0.0005 m.o.i were chosen, and the Omicron BA.1 was selected as viral variant.

3. RESULTS AND DISCUSSION

3.1. Characterization and stability study of the blank and CSA-loaded micelles

All the micelles showed stable particle size never exceeding 15 nm, narrow PDI and null surface charge, suitable for avoiding the binding to mucin glycoproteins [5], thus favouring mucopenetration. The SAXS analysis highlighted the tendency of micelles to assume a more spherical shape with increasing CSA

OP12

encapsulation, and a high rate of mucodiffusion. The CSA EE% was in all the cases higher than 95%, with a slight reduction after a month at 25°C.

3.2. *In vitro* antiviral activity of the micelles against SARS-CoV-2

The toxicological study pointed out a reduction of the cytotoxicity with increasing loading of CSA in the micelles. The 0.5 mg/mL CSA-loaded micelles indeed exhibited a cytotoxicity only at the highest concentration of CSA (64 μ M) used, while the 0.1 mg/mL CSA-loaded ones were already toxic at 16 μ M. These results highlighted that TPGS, as a surfactant, exhibits an intrinsic cytotoxicity.

As shown in Table 1, both the 0.5 and the 0.25 mg/mL CSA-loaded micelles exhibited the highest antiviral activity at the lowest CSA concentration (2 μ M) tested, and they turned out to be more active when used following the protocol E and F, respectively. The 0.1 mg/mL micelles showed the highest antiviral activity when a CSA concentration of 8 μ M and protocol F were used.

micelles a potential strategy for both the prevention and the treatment of the COVID-19 disease.

5. REFERENCES

- 1 De Wilde, A.H. et al., *Cyclosporin A inhibits the replication of diverse coronaviruses*, Journal of General Virology, 2011. Vol. 92(11): 2542–2548
- 2 Ma-Lauer, Y. et al., *Influences of cyclosporin A and non-immunosuppressive derivatives on cellular cyclophilins and viral nucleocapsid protein during human coronavirus 229E replication*, Antiviral Research, 2020. Vol. 173: 104620.
- 3 Pfefferle, S. et al., *The SARS-Coronavirus-host interactome: Identification of cyclophilins as target for pan-Coronavirus inhibitors*, PLoS Pathogens, 2011. Vol. 7(10): e1002331.
- 4 Pescina, S. et al., *Preliminary investigation on simvastatin-loaded polymeric micelles in view of the treatment of the back of the eye*, Pharmaceutics, 2021. Vol. 13(6): 855.
- 5 Araújo, F. et al., *Chemical modification of drug molecules as strategy to reduce interactions with mucus*, Advanced Drug Delivery Reviews, 2018. Vol. 124: 98–106.

Table 1. Antiviral activity of the CSA-loaded micelles against SARS-CoV-2.

	0.5 mg/mL micelles (2 μ M CSA) 3 post-treatments		0.25 mg/mL micelles (2 μ M CSA) pre-treatments associated to 3 post-treatments.		0.1 mg/mL micelles (8 μ M CSA) pre-treatments associated to 3 post-treatments.	
<i>Viral concentration</i>	0.005 m.o.i	0.0005 m.o.i	0.005 m.o.i	0.0005 m.o.i	0.005 m.o.i	0.0005 m.o.i
<i>Antiviral activity</i>	117%	136%	122%	155%	115%	122%

4. CONCLUSION

The very low particle size, high CSA encapsulation efficiency and great long-term stability make the developed TPGS micelles a promising peptide-drug delivery system.

Moreover, the promising results obtained by testing the antiviral activity make the developed

ACKNOWLEDGMENT

We thank Sara Nicoli and Davide D'Angelo (University of Parma, Food and Drug Department) for the support provided during the development of the CSA-loaded drug delivery systems prepared for this study, and for sharing with us their knowledge regarding the potential antiviral action of CSA.

OP13

HDAC6 INHIBITION IN CYSTIC FIBROSIS: IN VIVO PROOF-OF-CONCEPT STUDY ANTI-INFLAMMATORY PROFILE, EFFECTS ON BACTERIAL LOAD, FORMULATION AND BIODISTRIBUTION STUDIES.

Margherita Brindisi¹, **Simona Barone**¹, **Emilia Cassese**¹, **Alice Rossi**², **Nunzio Del Gaudio**³, **Alvaro Feliz Morel**⁴, **Gessica Filocamo**⁴, **Camilla Montesano**⁵, **Alessandra Bragonzi**², **Lucia Altucci**³, **Vincenzo Summa**¹

¹University of Naples Federico II, Dept. of Pharmacy, Via D. Montesano 49, 80131 Naples, Italy;

²Infections and Cystic Fibrosis Unit, San Raffaele Scientific Institute, Via Olgettina 58, 20132 Milan, Italy;

³University of Campania Luigi Vanvitelli, Dept. of Precision Medicine, Via de Crecchio, 80138 Naples, Italy;

⁴Exiris s.r.l., Via di Castel Romano, 100, 00128 Castel Romano, Italy

⁵Sapienza University of Rome, Dept. of Chemistry, Piazzale Aldo Moro 5, 00185 Rome, Italy.

1. INTRODUCTION

Compelling new support has been provided for histone deacetylase isoform 6 (HDAC6) as a common thread in the generation of the dysregulated proinflammatory phenotype in cystic fibrosis (CF). HDAC6 also plays a crucial role in bacterial clearance or killing as a direct consequence of its effects on CF immune responses. Inhibiting HDAC6 functions thus eventually represents an innovative and effective strategy to tackle multiple aspects of CF-associated lung disease.[1] In this study, we provided the first *in vivo* PoC of the efficacy of a selective HDAC6 inhibitor in contrasting the CF-associated proinflammatory phenotype and effectively reducing bacterial load in treated animals.

2. MATERIALS AND METHODS

2.1 Methods

C57BL6/NCrl male (8-10 weeks old) purchased by Charles River were anesthetized by an i.p. injection of 2.5% Avertin (0.015 ml/g body weight) and infected by intratracheal (i.t.) injection of 4.51×10^5 *P. aeruginosa* MDR-RP73 clinical strain embedded in agar beads.[8,9] To evaluate the efficacy of F2F-2020187-00X mice were treated soon after the infection, by aerosol administration using Penn Century device with different doses (5 mg/kg, 10 mg/kg and 20 mg/kg or with vehicle (PBS+4%DMSO)). Mice were treated daily for 3 or 7 days. Mice were sacrificed at two different time point: after 3 days and after 7 days.

After 3- or 7-days post infection mice were monitored weight loss and sacrificed with an overdose of Avertin. BALF was collected and lung was aseptically excised to evaluate bacterial burden and inflammatory response in the lung homogenate and bronco-alveolar lavage fluid (BALF).

3. RESULTS AND DISCUSSION

3.1. Results and Discussion Sub-headings

We embarked a careful compound selection by performing a thorough analysis of scientific literature and relevant patents in the field. We thus identified compound **1** as the most suitable candidate to be engaged in *in vivo* PoC studies based on its high HDAC6 inhibitory potency and relevant selectivity over other HDAC isoforms (Fig. 1). We re-profiled compound **1** in house on its HDAC1/6 potency and its ability in selectively increasing levels of acetylated tubulin in HeLa and A549 cells. We also evaluated solubility of **1** in the vehicle selected for the planned aerosol administration. Gratifyingly, compound **1** demonstrated no toxicity in mouse and was able to dose-dependently reduce the total cell counts and neutrophils in bronchoalveolar lavage fluid (BALF), when locally administered (5, 10 and 20 mg/kg) in a mouse model of chronic *Pseudomonas aeruginosa* (PA) infection using a Penn-Century MicroSprayer® Aerosoliser. We also performed a cytokines/chemokines profiling by Bioplex assay, which highlighted relevant changes in the levels of interleukins (eg. IL-1a, IL-1b, IL-6) and other inflammatory markers, thus confirming the potential of **1** in

OP13

effectively reverting the pro-inflammatory phenotype. Moreover, we proved that **1** is able to reduce bacterial load in the same model at the three tested doses, as determined by the reduction of colony-forming units (Fig. 1).

Quantitative determination of **1** in plasma samples collected from treated mice showed that the compound is not distributed in the body even after a 7-day treatment, thus supporting the safe profile of **1** in our administration settings.

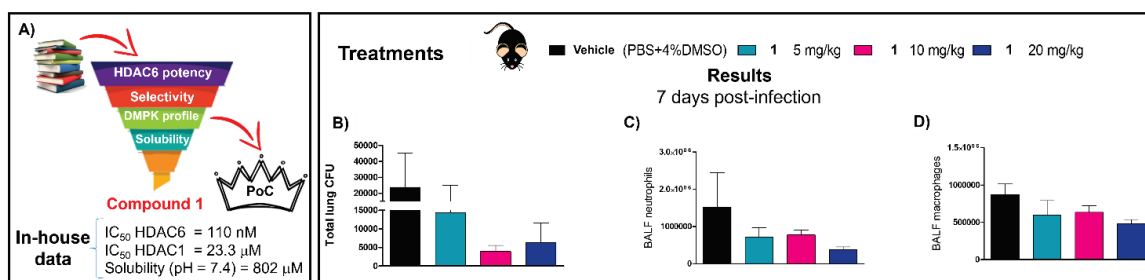


Figure 1. (A) General workflow for proof-of-concept (PoC) compound identification; efficacy of selected compound **1** on (A) bacterial load and (B,C) inflammatory cell count in a murine model of *Pseudomonas Aeruginosa* chronic infection.

4. CONCLUSION

Our study is of particular significance since it demonstrates for the first time the utility of selective HDAC6 inhibitors as innovative therapeutic option for CF, using a relevant *in vivo* model. Our data pave the way to the development of novel HDAC6 inhibitors specifically tailored for chronic administration in CF patients, thus improving the CF-associated inflammatory phenotype and promoting an effective immune response against infections.

5. REFERENCES

[1] Barone, S.; Cassese, E.; Alfano, A. I.; Brindisi, M.; Summa, V. *J. Med. Chem.* **2022**, 3080–3097.

ACKNOWLEDGMENT

The Authors kindly acknowledge Fondazione Fibrosi Cistica (FFC Grant 20-2020) for financial support.

NEW COVALENT REVERSIBLE INHIBITORS OF SARS-CoV-2 MAIN PROTEASE

Sveva Pelliccia¹, Paola Storici², Elisa Costanzi², Enzo Tramontano³, Angela Corona³, Carmen Cerchia¹, Vincenzo Summa¹

¹Department of Pharmacy, University of Naples, Federico II via D. Montesano 49, Napoli, 80131, Italy

²Protein Facility, Elettra Sincrotrone Trieste S.C.p.A., SS 14 - Km 163, 5 in AREA Science Park, Trieste, 34149, Italy

³Department of Life and Environmental Sciences, University of Cagliari, Monserrato, 09042, Italy

1. INTRODUCTION

In 2019, SARS-CoV-2 caused worldwide the current outbreak named COVID-19. Despite multiple countermeasures implemented and approved DNA, RNA and protein subunits vaccines an additional step forward has been made thanks to approved drugs targeting the CoV RdRp (e.g. Remdesivir i.v., Molnupiravir p.o.) and the CoV 3CL Protease (Nirmatrelvir) although they suffer of modest efficacy or suboptimal PK properties. It is an urgent global need to identify new direct-acting antiviral drugs (DAAs) against this pathogen and new emerging viruses, in order to prevent the progression to severe disease or new pandemic. In particular, the main protease (M^{pro}) of SARS-CoV-2 is a cysteine protease playing the essential role in viral replication, thus being identified as a solid target for the development of effective antiviral drugs [1]. The most favored P2–P1–P1' sequence is Leu-Gln-Ser (or Ala and Gly instead of Ser), and the exclusive cleavage of polypeptides by M^{pro} after a glutamine (Gln) residue, that no known human protease displays, allows the identification of novel selective drugs.

2. MATERIALS AND METHODS

2.1. Materials

A series of dipeptides exploring the P1' region through the use of α -ketoamide moiety as “warhead” which unlike the aldehyde can be derivatized using different alkyl/aryl groups, preserving the reported 5-membered ring derivative of glutamine (γ -lactam) in P1 that enhanced the inhibition up to 10- fold. For the

synthesis, enantiomerically pure starting materials were employed.

2.2. Method

The knowledge of both catalytic mechanism and substrate specificity of the M^{pro} triggered the idea to exploit multicomponent reactions (MCRs) as a fast and versatile synthetic tool toward novel M^{pro} inhibitors. Accordingly, the Passerini reaction-amine deprotection-acyl migration (PADAM) oxidation route, was employed for the development of novel small peptidomimetic compounds with a ketoamide warhead behaving as covalent reversible inhibitors (Figure 1) [2].

3. RESULTS AND DISCUSSION

3.1. Results and Discussion

The peptidomimetics prepared were evaluated in SARS-CoV-2 M^{pro} biochemical and antiviral cell-based assays, showing IC₅₀ and EC₅₀ in nanomolar/low micromolar range. Furthermore, X-ray co-crystal structures of protease–inhibitor complexes were determined as a part of this study, revealing the molecular determinants of the interaction with the M^{pro}.

OP14

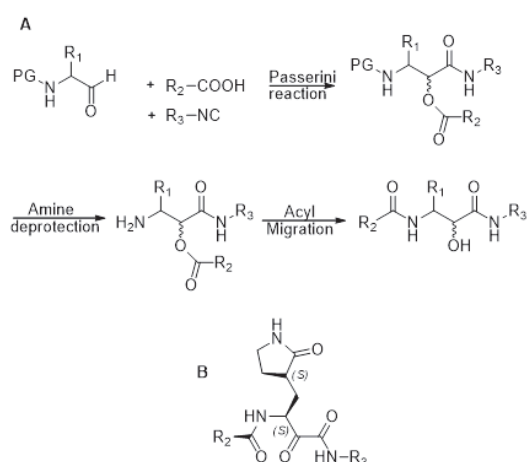


Figure 1. A. The PADAM strategy for the α -hydroxy- β -amino amides. B. General structure of our synthesized α -ketoamides.

4. CONCLUSION

The knowledge of both catalytic mechanism and the substrate specificity of the M^{pro} combined with the possibility to exploit the milestone Multicomponent reactions (MCRs), using the PADAM oxidation route, has led us in the synthesis of novel covalent reversible inhibitors. SARS-CoV-2 M^{pro} biochemical and antiviral cell-based assays, showed IC₅₀ and EC₅₀ in nanomolar / low micromolar range. Two crystal structures of protease-inhibitor complexes were determined as part of this study, revealing the molecular determinants of the interaction with the M^{pro} and providing key hints for further optimization.

5. REFERENCES

- [1] Cannalire, R.; Tramontano, E.; Summa, V. A Focus on Severe Acute Respiratory Syndrome (SARS) Coronavirus (SARS-CoVs) 1 and 2. Book Series: Methods and Principles in Medicinal Chemistry Chapter 18, New Drug Development for Known and Emerging Viruses, First Edition. Wiley **2022**.
- [2] Banfi, L.; Guanti, G.; Riva, R. Passerini multicomponent reaction of protected α -aminoaldehydes as a tool for combinatorial synthesis of enzyme inhibitors. *Chem. Commun.*, **2000**, 985–986.

ACKNOWLEDGEMENTS

PON R&I 2014-2020-Asse IV- REACT-EU “Green technologies” is gratefully acknowledged.

SYNTHESIS AND BIOLOGICAL EVALUATION OF QUINOLINE AND ANTHRANILIC ACID DERIVATIVES AS POTENTIAL QUORUM SENSING INHIBITORS

Ivana Perković¹, Tanja Poljak², Maja Beus³, Kirsi Savijoki⁴, Pekka Varmanen⁴, Anja Kučević¹, Ivan Džajić¹

¹ University of Zagreb, Faculty of Pharmacy and Biochemistry, Croatia

² Selvita Ltd., Croatia

³ Institute for Medical Research and Occupational Health, Croatia

⁴ Department of Food and Nutrition, Faculty of Agriculture and Forestry, University of Helsinki, Finland

1. INTRODUCTION

Quorum sensing (QS) is a mechanism of bacterial cell-to-cell communication and gene expression co-ordination; an important strategy performed by bacteria to enhance its virulence and promote host damage [1]. Thus, inhibition of QS is widely investigated as a novel approach to combat bacteria which would act by blocking their ability to cause disease and is considered as an alternative approach to conventional antibacterial therapy [2]. In the present study, we report the synthesis of novel compounds composed of two distinctive structural motifs, anthranilic acid and 4-amino-7-chloroquinoline derivatives linked with oxadiazole or semicarbazide. The compounds were screened for their anti-QS and antibacterial activity using gram-negative *Chromobacterium violaceum* as the reporter strain.

2. MATERIALS AND METHODS

2.1. Synthesis of novel compounds

A series of oxadiazole linked compounds composed of anthranilic acid and 7-chloroquinoline moieties were synthesized together with their precursors. The 4-amino-7-chloroquinoline part of the molecule varied in the length of the alkyl chain on the 4-aminoquinoline group (2 or 4 carbon atoms) and anthranilic acid was substituted at various positions of the phenyl ring with halogen atoms (F, Cl or Br). The compounds were obtained by using standard synthetic procedures.

2.2. Anti-QS and bactericidal activity screening

The *Chromobacterium violaceum* ATCC31532 (ATCC; Wesel, Germany) was used as the indicator reporter strain to screen the title

compounds for anti-QS and bactericidal activities as described in previous report [2].

3. RESULTS AND DISCUSSION

3.1. Results and Discussion – Chemistry

The synthesis of title compounds was divided in two parts. First, the building blocks for the final reaction step were obtained. The quinoline building blocks bearing terminal amino group were prepared in the reaction of 4,7-chloroquinoline and ethylenediamine or 1,4-diaminobutane. The anthranilic acid building blocks were obtained in multiple reaction steps, first, from the carboxylic acid, corresponding hydrazide was obtained, which was then converted to the corresponding 3-*H*-1,3,4-oxadiazole-2-ones in a reaction with CDI. In the reaction of two building blocks the corresponding 1,4-disubstituted semicarbazides were obtained (Fig. 1), which in the presence of triphenylphosphine and carbon tetrachloride formed 1,3,4-oxadiazoles (Fig. 2).

3.2. Results and Discussion – Anti-QS and bactericidal activity

The 1,3,4-oxadiazole and semicarbazide derivatives were screened for their anti QS and bactericidal activity. Quercetin (Q) was used as the positive control for QS and azithromycin as the positive control for bactericidal activity (cell viability). Inhibitory activity was tested at 400 μ M concentrations and for the most potent compounds at 100 μ M and 40 μ M as well. Six out of total of twelve tested compounds inhibited the violacein production in *C. violaceum* to the same extent as Q. However, two compounds exerted also a strong bactericidal effect on the reporter. Dose-concentration-response analyses with the most promising compounds indicated that each compound with concentrations at 400 and 100

OP15

μM reduced the violacein production by more than 50 % compared to the control cells with DMSO, while the viability of the reporter under the same conditions was marginally affected.

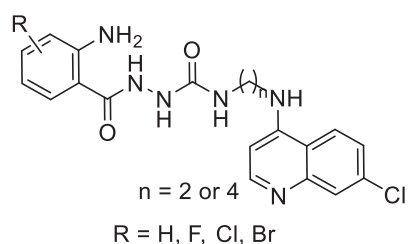


Figure 1. Semicarbazide derivatives

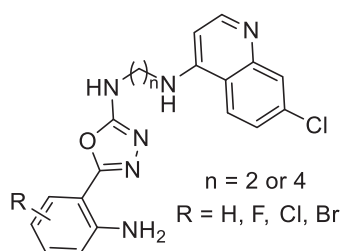


Figure 2. 1,3,4-oxadiazole derivatives.

4. CONCLUSION

We have successfully prepared and characterized a series of 9 novel 1,3,4-oxadiazole derivatives with short/long alkyl chain 4-amino-7-chloroquinoline and anthranilic acid moieties and evaluated their potential as OS inhibitors together with their semicarbazide precursors (three compounds). The most active compounds come from the series of short chain 1,3,4-oxadiazoles.

5. REFERENCES

1. Ilangovan, A., et al., *Structural Basis for Native Agonist and Synthetic Inhibitor Recognition by the Pseudomonas aeruginosa Quorum Sensing Regulator PqsR (MvfR)*. PLOS Pathogens, 2013. 9:e1003508.
2. Beus, M., et al., *Chloroquine fumardiamides as novel quorum sensing inhibitors*. Bioorganic and Medicinal Chemistry Letters, 2020. 30(16): 127336.

ACKNOWLEDGMENT

The authors acknowledge the financial support by University of Zagreb (support for 2021) and Tampere Tuberculosis Foundation (support for 2020-21).

EXPANDING THE CHEMICAL SPACE OF *N*-PHENYLPYRROLAMIDES AS DNA GYRASE B INHIBITORSPeter Peršolja¹, Martina Piga¹, Tihomir Tomašič¹, Janez Ilaš¹, Lucija Peterlin Mašič¹, Anamarija Zega¹, Danijel Kikelj¹, Nace Zidar¹¹ University of Ljubljana, Faculty of Pharmacy, Aškerčeva 7, 1000 Ljubljana, Slovenia

Correspondence: nace.zidar@ffa.uni-lj.si

1. INTRODUCTION

The growing threat of antibacterial resistance is intensifying the need for antibiotics with novel modes of action [1]. Fluoroquinolones are effectively used for the treatment of infections by inhibiting the bacterial topoisomerase subunits GyrA and ParC, but they also suffer from the ever-expanding antibiotic resistance and certain toxicity drawbacks. However, inhibition of GyrB and ParE subunits provides a viable alternative, as demonstrated by novobiocin [2].

DNA gyrase and topoisomerase IV are enzymes essential for the replication of the DNA double helix in bacteria [3]. Both are constructed as heterotetrametric complexes consisting of two subunits responsible for the cleavage and transport of DNA (DNA gyrase, 2x GyrA; topoisomerase IV, 2x ParC) and two subunits responsible for the hydrolysis of ATP (DNA gyrase, 2x GyrB; topoisomerase IV, 2x ParE) [1, 3].

Since novobiocin was withdrawn from the market, no other GyrB inhibitor managed to reach clinical use. Since then, several other compounds have been discovered that can utilise this unexploited mechanism of action [1-4]. Due to discouraging physicochemical properties, pharmacokinetic issues, and high attrition rates in antibiotic R&D, no other candidate has yet reached the market [1].

Effective antibacterials against the “ESKAPE” pathogens are urgently needed. Recently, substantial research has been taking place in both industry and academia. The amount of

generated knowledge gives hope that a candidate might reach clinical use in the near future [2].

2. MATERIALS AND METHODS

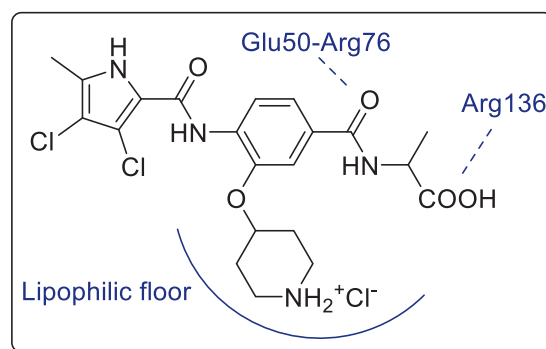
2.1. Materials

The research was conducted at the Department of Pharmaceutical Chemistry, Faculty of Pharmacy, University of Ljubljana. All chemicals and solvents used were acquired from reputable sources.

2.2. Methods

We focused on further expanding the knowledge of *N*-phenylpyrrolamides and their activity as DNA gyrase B inhibitors. *N*-Phenylpyrrolamides primarily exhibit high affinity for the GyrB subunit, while they also often display good inhibitory values towards the ParE subunit [4].

In this work, we aimed to advance the development of an in-vitro effective antibacterial agent against “ESKAPE” pathogens. To achieve this goal, we planned to further explore the influence of different key groups on the inhibitory properties of our compounds.



OP16

Figure 1. Representative *N*-phenylpyrrolamide inhibitor of DNA gyrase B with indicated substrate-enzyme interactions

As depicted in **Figure 1**, we aimed to optimize the interactions with the eastern part of the molecule by introducing groups capable of forming ionic or hydrogen bonds with the positively charged Arg136 residue and/or cation- π interactions with the Glu50-Arg76 salt bridge. When targeting the lipophilic floor, our goal was to enhance the hydrophobic and H-bond interactions, while improving the physicochemical properties of our compounds.

The final compounds were fully characterized using ^1H and ^{13}C NMR, HRMS, IR spectroscopy, melting point analysis, and their purity was confirmed to be above 95% by HPLC. Finally, they were evaluated for their inhibitory properties against DNA gyrase B from *E. coli* in the DNA supercoiling assay.

3. RESULTS AND DISCUSSION

Our synthetic work focused on the generation of a library of analogues bearing diverse side groups at the *ortho* position in respect to the amido-substituted central benzene ring (**Figure 2**, R^1). The focus was on maximizing the interactions with the lipophilic floor of the enzyme via the introduction of bulkier substituents.

Additionally, we aimed to construct analogues with diverse carboxylic acid bioisosters to optimise the interactions with the positively charged roof of the enzyme's active site (**Figure 2**, R^2).

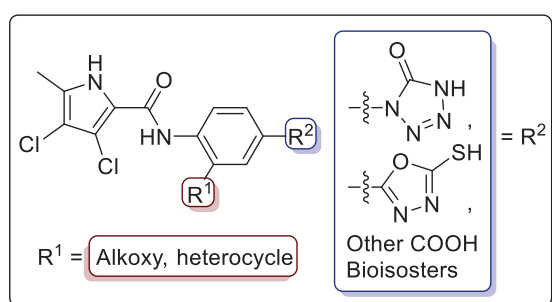


Figure 2. General structure of proposed new inhibitors

4. CONCLUSION

The synthesised compounds were tested for their inhibitory activity against DNA gyrase B. Additionally, the most potent compounds were tested against a range of Gram-positive and Gram-negative bacteria, many of which belong to the “ESKAPE” pathogens panel.

5. REFERENCES

- [1] Zidar, N., et al., New *N*-phenyl-4,5-dibromopyrrolamides as DNA gyrase B inhibitors. *MedChemComm*, 2019. 10: 1007-1017.
- [2] Durcik, M., et al., ATP-competitive DNA gyrase and topoisomerase IV inhibitors as antibacterial agents. *Expert opinion on therapeutic patients*, 2019. 29(3): 171-180.
- [3] Zidar, N., et al., New *N*-phenyl-4,5-dibromopyrrolamides and *N*-Phenylindolamides as ATPase inhibitors of DNA gyrase. *European Journal of Medicinal Chemistry*, 2016. 117: 197-211.
- [4] Benedetto, D. T., et al. An optimised series of substituted *N*-phenylpyrrolamides as DNA gyrase B inhibitors. *European Journal of Medicinal Chemistry*, 2019. 167: 269-290.

ACKNOWLEDGMENT

The authors acknowledge the financial support from the Slovenian Research Agency, Projects J1-3031 and J1-3021.

Rational development and process optimization of an amorphous solid dispersion generic drug product prepared by hot-melt extrusion (a case study)

Ognen Jakasanovski¹, Katja Berginc¹, Vid Puž¹, Žiga Jeraj¹, Ivana Gazić Smilović¹, Petra Perhavec¹, Katarina Zajc Kreft¹, Polonca Kralj¹, Biljana Janković¹

¹ Sandoz Development Center, Lek Pharmaceuticals d.d., Slovenia

1. INTRODUCTION

A significant number of drug substances in development are poorly water soluble and have low bioavailability (BCS II and IV). Hot-melt extrusion (HME) is a promising technology that enables enhanced solubility and bioavailability of drug substance through drug amorphization that does not require the use of organic solvents. An immediate release film coated tablet generic product with poorly soluble (BCS IV) drug substance based on a solid dispersion with copovidone was prepared using hot-melt extrusion process. Since generic product bioequivalence testing involved steady-state clinical study on patients, *in vitro* drug release methods with sufficient discriminatory power and bio-relevance are important for the assurance of bioequivalence.

2. MATERIALS AND METHODS

2.1. Hot-melt extrusion design of experiments

A Design of Experiments (DoE) was performed to study the influence of extrusion process parameters (barrel temperature, feed rate, screw speed) on drug release (full factorial 2³, interaction model). Experiments were performed on Leistritz ZSE 18 HP-PH hot-melt extruder.

2.2. Drug release methods

- Non-sink dissolution (Dissolution in small volume): Apparatus 2, 150 rpm, 100 mL SGF/FeSSIF pH 5.0
- Microflux dissolution
- QC release method

2.3. Characterization techniques

Hot stage polarized light microscopy (HS-PLM) and differential scanning calorimetry (DSC) were used for detection of residual crystallinity in extrudates.

2.4. *In vivo* dog PK study

To determine the bioequivalence of the generic drug product and the originator product, a PK study was performed. 90% confidence limits for the geometric means ratio of C_{max} and AUC₀₋₄₈ parameters were determined. Generic drug product test sample was prepared according to HME parameters stated in Table 1.

Table 1. HME process parameters used in preparation of test sample for *in vivo* study on dogs

Parameter	Barrel temp. (zone 1)	Barrel temp. (zone 2)	Barrel temp. (zone 3)	Barrel temp. (zone 4-8)	Screw speed (rpm)	Feed rate (kg/h)
Test sample for dog PK study	25	70	150	215	250	3.0

3. RESULTS AND DISCUSSION

3.1. Hot-melt extrusion design of Experiments

DoE model with suitable fit was obtained for influence of HME process on non-sink drug release rate, for time points in which precipitation was observed (after 60 minutes). Only barrel temperature had significant influence on the drug release rate, with higher barrel temperatures assuring higher average drug release (Figure 1).

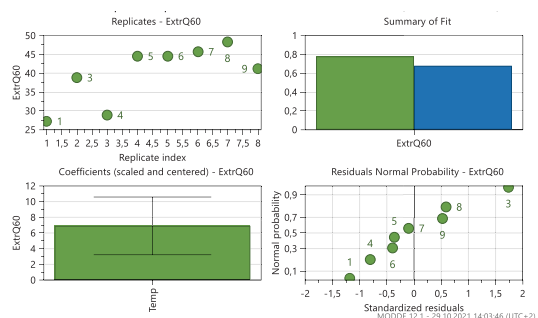


Figure 1. DoE model overview for influence of extrusion barrel temperature (*Temp*) on drug release after 60 minutes (non-sink dissolution method).

Based on further experiments (Table 2), influence of feed rate on drug release in non-sink dissolution test was additionally observed. Sample with lowest feed rate (Sample 6)

OP17

assured highest amount of drug released at the end of the test, likely due to the increase of material residence time (prolonged exposure to high temperature inside the hot-melt extruder).

Table 2. Influence of hot-melt extrusion process parameters on drug release in non-sink dissolution test (samples S1-S9).

Parameter	S1	S2	S3	S4	S5	S6	S7	S8	S9
% diss. at 160 min.	61.0	62.6	65.4	69.2	83.7	94.5	88.7	87.5	77.2
Temp. zone 3 (°C)	130	130	130	160	160	170	130	130	170
Temp. zone 4 (°C)	150	150	150	220	220	220	150	150	220
Temp. zone 5-8 (°C)	220	220	220	220	220	220	220	220	220
Screw speed (rpm)	200	300	400	300	400	200	200	200	300
Feed rate (kg/h)	3.0	3.0	3.0	4.5	4.5	2.0	3.0	3.0	4.5

3.2. Precipitation in non-sink dissolution

Hot-stage microscopy and DSC characterization confirmed that no residual crystalline drug substance is present in the extrudate samples which exhibited precipitation, indicating that precipitation is likely caused by other incoming drug substance properties. Drug substance quality was shown to affect the degree of precipitation, as incoming drug substance from same supplier with the same polymorphic form obtained from lab-scale and full-scale synthesis process had different extent of precipitation.

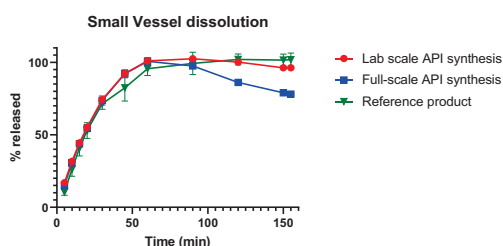


Figure 2. Non-sink dissolution of samples prepared using lab-scale and full-scale drug substance, as well as reference product.

3.2. In vivo study on dogs

Despite precipitation of test sample observed on *in vitro* experiments (non-sink dissolution, donor compartment of microflux studies), there was no impact of precipitation on bioequivalence observed on *in vivo* dog PK study (PK parameters for generic product and reference were comparable). This finding was also confirmed with results in the receiver

compartment of the microflux system (Figure 3, Figure 4).

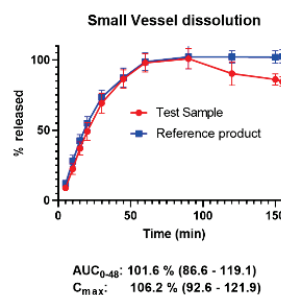


Figure 3. Non-sink dissolution of test sample and reference product used in dog PK study. Geometric means ratios of C_{max} and AUC_{0-48} parameters are stated above.

Microflux Dissolution

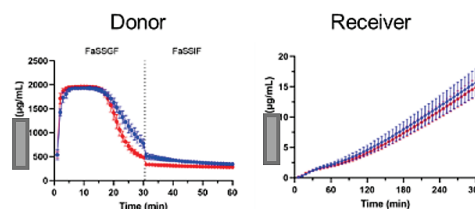


Figure 4. Summary of microflux dissolution results for donor and receiver compartment for test sample (blue) and reference product (red).

4. CONCLUSION

Based on DoE and additional experiments, it was concluded that extrusion barrel temperature had strongest influence on the extent of drug precipitation in non-sink media. An effect of feed rate on precipitation was also observed. Although the dog study test sample exhibited precipitation in non-sink dissolution it was found to be bioequivalent to the reference product, suggesting that non-sink dissolution method is over discriminatory.

The gained knowledge from the *in vitro* methods, as well as the *in vivo* dog PK study serve as a valuable guidance for the hot-melt extrusion process optimization for bioequivalence study.

5. REFERENCES

/

ACKNOWLEDGMENT

The authors would like to thank associates from Novartis Technical Research & Development and Faculty of Pharmacy, University of Copenhagen.

USE OF ADDITIVES TO CONTROL THE POLYMORPHISM OF SOLID LIPID FORMULATIONS: A SIMPLE WAY TO FACE A COMPLEX PROBLEM

Serena Bertoni¹, Elena Simone², Nadia Passerini¹, Beatrice Albertini¹

¹ Department of Pharmacy and Biotechnology, University of Bologna, Italy

² Department of Applied Science and Technology (DISAT), Politecnico di Torino, Italy.

1. INTRODUCTION

Solid lipid formulations have recently received interest due to their ability to modulate drug release, as well their intrinsic safety and sustainability. Despite their advantages, challenges within the production and storage of solid lipid-based products exist, due to their complex solid state behavior. Solid triacylglycerides (TAGs), the most common class of natural, edible lipids, have the ability to form different crystal structures (polymorphism). TAGs polymorphism is based around three main forms, which are defined according to the different subcell structure: hexagonal (α -form), orthorhombic (β' -form) and triclinic (β -form), from the less stable to the most stable structure, respectively [1]. Upon cooling during melting-based manufacturing processes, TAGs generally crystallize in the metastable α -form. Polymorphic transformations into more stable structures then happen during downstream processes and/or storage, affecting the release profile and the overall performance of the formulation [2]. At present, little attention has been given to the effect of additives on the crystallization of lipid systems during melting-based manufacturing processes.

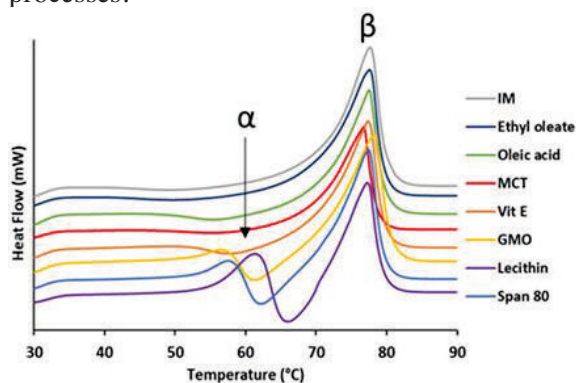


Figure 1. DSC analysis of MPs with 5% w/w of LL after 7 days from production (heat flow endo up).

We have recently shown that polymorphic transitions of tristearin can be modified by

addition of 10% w/w of liquid lipids (LL) [3]. This study aims to investigate the effect of a wide variety of additives with different chemical composition and amount on the crystallization and polymorphism of tristearin. The ultimate goal is to obtain a stable formulation in terms of polymorphic transitions, able to achieve a controlled release of hydrophilic drugs with unaltered dissolution profiles during storage.

2. MATERIALS AND METHODS

2.1. Materials

Different oral-approved additives were added to tristearin (Dynasan®118) at different amounts. Additives included fatty acids: oleic, lauric, myristic, palmitic and stearic acids; fatty acid esters, such as isopropyl myristate (IM) and ethyl oleate (EO); sorbitan esters (Span®); other LL: medium chain triglycerides (MCT), vitamin E acetate (Vit E), glyceryl monooleate (GMO), soya lecithin.

2.2. Methods

As example of melting-based process, we employed spray congealing, a simple solvent-free process based on the atomization of the molten lipid with obtaining of solid spherical microparticles (MPs). The effect of the additives on the crystallization, polymorphism, phase transition behavior and crystal structure of tristearin was studied by DSC, X-ray diffraction analysis (PXRD), polarized light microscopy (PLM) and scanning electron microscopy (SEM). In order to estimate the kinetics of polymorphic transformations characteristic of each additive/tristearin mixture, selected samples were analysed at the Austrian SAXS beamline at Elettra-Sincrotrone Trieste. Finally, the most promising MPs formulation were loaded with a model hydrophilic drug (caffeine) at 30% w/w and *in vitro* release tests in different media (water, FaSSGF, FaSSIF) were performed.

3. RESULTS AND DISCUSSION

3.1. Effect of additives on tristearin crystallization and polymorphism

Differently from solid additives, liquid additives promoted the transition of tristearin from the α -form to the stable β -form with a kinetic varying from few minutes to months, depending both on the additive structure and its amount (Fig. 1). The polymorphic transformation was monitored by synchrotron SAXS/WAXS studies and the results confirmed that liquid additives, specifically IM and EO, were the most effective in accelerating the transformation. Isothermal crystallization studies suggested that LL mostly caused the polymorphic transformation via solid state, i.e. after completion of α -crystallization, as the initial fast α -crystallization was followed by a second exothermic event attributed to the evolution into the β -form.

3.2. Effect of additives on tristearin structure

PLM studies showed that the most “active” LL in favouring $\alpha \rightarrow \beta$ transition were included in the β -tristearin crystal lattice favoring the compaction and maximizing interactions, leading to a more compact crystalline network. Differently, the other liquid additives determined a heterogeneous microstructure with larger spherulites. PLM, DSC and PXRD studies suggested that solid fatty acids have partial miscibility with tristearin and crystallize separately forming two different solid phases.

3.3. Effect of additives on drug release

The presence of LL strongly enhanced the drug release with respect to pure tristearin in the β form. The release profiles of MPs with 5% of LL increased passing from water to the fluid simulating the fasted gastric conditions (FaSSGF) and further enhanced in fasted state intestinal environment (FaSSIF). Notably, MPs determined a gradual and sustained release over 5 hours in both *biorelevant media*, as shown in Fig. 2. MPs collected after release studies in water and in FaSSGF, analysed by SEM, showed mostly intact particles with spherical shape, while partially fragmented MPs with eroded surface were observed after the test in FaSSIF. This may indicate that, beside a diffusion mechanism, which is common to all media, the lipid degradation/digestion become important in the intestinal environment.

4. CONCLUSION

The use of small amount of lipid additives is an interesting approach to achieve TAGs crystallization in the β -form. In particular, addition of 5% w/w of IM, EO, oleic acid and MCT allowed the complete conversion of the formulation into the stable polymorphic form within 1 week from production, concurrently with a controlled release of hydrophilic drugs in media simulating fasted state gastric and intestinal conditions. From the industrial viewpoint, this approach might be advantageous as any polymorphic change will be accelerated, hence enabling the production of stable lipid formulations.

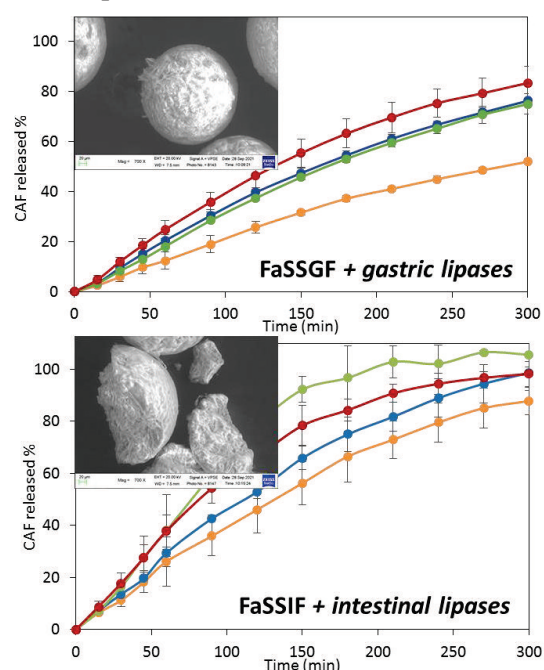


Figure 2. In vitro release profiles of CAF from MPs with 5% of selected LL in FaSSGF and FaSSIF and SEM images of MPs with EO (yellow curves) collected after the test.

5. REFERENCES

1. Chapman, D. *The Polymorphism of Glycerides*. Chemical Reviews, 1962. 62: 433–456.
2. Lopes, D. G., et al., *Microphase separation in solid lipid dosage forms as the cause of drug release instability*. International Journal of Pharmaceutics, 2017. 517: 403–412.
3. Bertoni, S., et al., *Liquid lipids act as polymorphic modifiers of tristearin-based formulations produced by melting technologies*. Pharmaceutics, 2021. 13(7):1089.

FABRICATION OF 3DP COLON-TARGETED TABLETS INCLUDING FLUTICASONE WITH ENHANCED SOLUBILITY BY γ -CYCLODEXTRIN

Diren Sarisaltik-Yasin¹, Cennet Duran¹, Sevgi Takka²

¹*Department of Pharmaceutical Technology, Dicle University, Turkey*

²*Department of Pharmaceutical Technology, Gazi University, Turkey*

1. INTRODUCTION

Orally colon-targeted drug delivery systems have recently gained importance in reducing side effects of corticosteroids used in the local treatment of colonic diseases such as inflammatory bowel diseases (IBD). However, there are limitations such as lower fluid volumes, and longer transit times in colon-targeting of corticosteroids which may cause inter/intra-individual variability. This makes it difficult to adjust the dose. These problems can be solved with personalized 3DP tablets specifically designed for the course of the disease (1).

Fluticasone propionate (FLT) is a second-generation corticosteroid with lower side effects and more potent local effects compared with the first generations. However, the very low solubility of FLT poses a major challenge in formulation development.

The aim of this study is to develop colon-targeted tablets of FLT to improve its solubility with γ -cyclodextrin using the FDM 3DP.

2. MATERIALS AND METHODS

2.1. Materials

FLT is supplied by Ontario Chemicals. Citric acid monohydrate (CAMH), magnesium stearate (MgS), and talc (Tc) were donated by Drogosan. Eudragit S100 (ES100), Ethocel (EC), γ -cyclodextrin (GCD), Gelucire (Gl), and triacetin (TA) were gifted from Evonik, Dupont, Barentz, Gattefosse, and BASF, respectively.

2.2. Extruding the Filaments

ES100 was plasticized with 50% of TA. The plasticized ES100 and other excipients (Table 1) were mixed and the formulations and

extruded at 125°C and 70 rpm in a single-screw extruder (Noztec Pro HME, UK).

Table 1. The formulation components

Components (%)	F1	F2	F3	F4
ES100*	64	64	64	64
GCD	-	7,5	7,5	7,5
FLT	5	5	3,75	2,5
Talc	10	2,5	3,75	5
CAMH	7	7	7	7
Gl	4	4	4	4
EC	3	3	3	3
MgS	7	7	7	7

2.3. 3D Printing of Tablets

The filaments were printed by an FDM 3D Printer (Craftbot 3, Hungary). The printing parameters were set as follows: nozzle temperature: 165°C; build plate temperature: 70°C; extrusion speed: 30 mm/s, travelling speed: 120 mm/s, layer height: 0,2 mm; the number of shells: 4, shell thickness: 0.8 mm; infill density: 50%, infill pattern: parallel line.

2.4. Characterization of Filaments and 3D Tablets

Diameters were measured by a caliper. Mechanical properties of filaments were examined by Texture Analyzer (Stable Micro Systems, TA.XTPlus). Morphological properties of filaments and tablets were determined by SEM (FEI Quanta 250 FEG, The Netherlands).

2.5. In Vitro Dissolution Studies

Dissolution tests were carried out in buffer media of pH 1,2 for 2 hours, pH 6,8 for 4 hours, and pH 7,4 for 18 hours, respectively, by using the USP apparatus-2 (Pharmatest, Germany). Drug release studies were performed in dissolution media with and without SLS (2%).

OP19

The dissolution profiles were evaluated by similarity factor (f_2).

3. RESULTS AND DISCUSSION

3.1. The Printability of Filaments

The formulations were successfully extruded to produce filaments and the filaments were printed without failing (F1-F4) (Fig 1). The diameters of the filaments were within the acceptable limits as 1.70-1.80 mm. The surfaces of the filaments were smooth and non-sticky. The mechanical properties of the filaments were suitable for 3DP. The structural integrity and homogeneity of the tablets were demonstrated by SEM.



Figure 1. Three Dimensional Printing (3DP) Tablets

3.2. In Vitro Dissolution Studies

The dissolution profiles (Fig. 2) of the two formulations with (F2) and without GCD (F1) were similar ($f_2 > 50$). The GCD-dependent solubility improvement was not observed in the dissolution media containing SLS %2 since FLT was completely released from both F1 and F2. Therefore, the dissolution tests for F1 and F2 were repeated in the dissolution medium without SLS. Thereby, the ratio of dissolved FLT increased tenfold within 24 h (from 0.48% to 4.9%).

3.3. Dose Proportionality in Formulations

The dose proportionality was investigated in two different ways (2). In the first, the loading percentage of FLT in the formulations was altered by keeping the tablet weights constant (200 mg). In this method, 5 mg, 7.5 mg and 10 mg doses of FLT were loaded to the formulations F3, F4 and F2, respectively. The f_2 factors revealed that there was no significant difference in the dissolution profiles of F2, F3, and F4 tablets of the same size and weight (200 mg) ($f_2 > 50$).

In the second method, doses were adjusted by printing tablets in different sizes and weights (200 mg, 300 mg, and 400 mg) by using the F4 filament. Due to the dissolution rate decrease with an increasing tablet size and weight, dose proportionality was not observed in this method. This may be related to the smaller surface area/mass ratio of larger tablets.

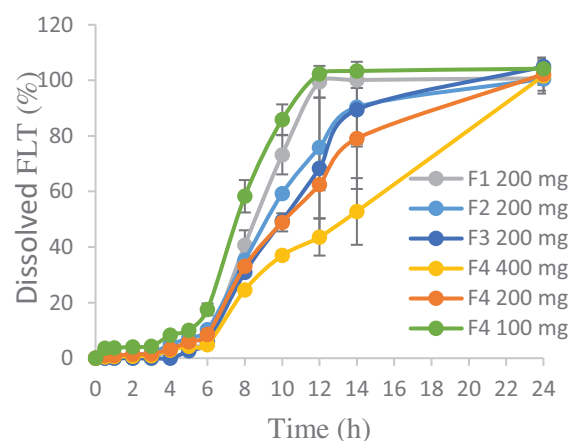


Figure 2. In vitro Release Profiles of FLT-loaded 3D Tablets

4. CONCLUSION

In conclusion, FDM-3DP was successfully utilized to fabricate colon-targeted 3D tablets of FLT with enhanced solubility for the personalized therapy of IBD. Additionally, the dimensions and weight of the tablets have been shown to be crucial in tailoring the dose.

5. REFERENCES

1. Charbe N.B., et al., Application of three-dimensional printing for colon targeted drug delivery systems, *International Journal of Pharmaceutical Investigation*, 2017. 7(2): 47-59.
2. Buyukgoz, G.G., et al., Exploring tablet design options for tailoring drug release and dose via fused deposition modeling (FDM) 3D printing. *International Journal of Pharmaceutics*, 2020. 591(11987): 1-13.

ACKNOWLEDGMENT

This study was supported by a grant of TUBITAK (SBAG-219S197).

A USEFUL METHOD FOR ROUTINE MONITORING OF ENDOCRINE DISRUPTORS IN SURFACE WATERS BY SPE-LC-MS/MS

Andrej Grobin¹, Robert Roškar¹, Jurij Trontelj¹

¹*Department of biopharmaceutics and pharmacokinetics, University of Ljubljana, Faculty of Pharmacy, Slovenia*

1. INTRODUCTION

Endocrine disruptors (EDs) are one of the most important environmental contaminants with natural and synthetic steroid hormones being among the most active endocrine disrupting compounds, while bisphenols also exhibit strong endocrine effects [1]. These effects are important in terms of decreasing aquatic wildlife populations, and their biodiversity, and may also pose a risk for negative effects on human fertility rates which are a serious modern public health issue [2]. Various EDs are highly effective and can present serious risks even at very low amounts while being present in the environment simultaneously [3]. Therefore, it is necessary to study the environmental presence of a broad selection of substances which can cause combined effects in organisms with suitable sensitivity. Our aim was therefore the development and validation of a method suitable for monitoring EDs from the aforementioned groups of substances in surface waters with suitable quantitation limits and simple sample preparation.

2. MATERIALS AND METHODS

2.1 Materials

Analytical standards of estrone (E1), estradiol (E2), estriol (E3), chlormadinone acetate, cyproterone, dienogest, drospirenone, ethinyl estradiol (EE2), gestodene, norethindrone, norgestrel, tibolone (Carbosynth), testosterone (Fluka), progesterone (Pion UK), BPAP, BPE, BPF (TCI Europe), BPB (Fluorochem), corticosterone, BPA, BPAF, BPC, BPG, BPS and BPZ (Sigma-Aldrich) were used.

2.2. LC-MS/MS Analysis

Chromatographic separation was performed using an Agilent Infinity 1290 system with a Kinetex Biphenyl column at 45 °C. 0.2 mM ammonium fluoride in MQ water and methanol were used as a mobile phase in a gradient method. The Agilent 6460 Triple Quadrupole was used for MS/MS analysis. Two chromatographic and MS/MS methods were used, one for the analysis of analytes in their non-derivatized form, and another for their derivatized form, where applicable.

2.3. Sample Preparation

Strata X Polymeric reversed phase 60 mg / 3 mL SPE cartridges were used for extraction. 200 mL of unfiltered surface water samples were loaded onto the cartridges, achieving a concentration factor of 1000. Aliquots of each sample were derivatized with dansyl chloride, while the rest of the sample was used for non-derivatized sample analysis.

2.4. Sample Collection

1 litre of sample was collected at a standardized depth of 1 meter in precleaned sampling bottles. For method validation purposes, several samples with different matrices were selected (a lake sample, river samples, a stream, and a channel sample).

3. RESULTS AND DISCUSSION

3.1. Method Sensitivity Optimization

By using simple sample preparation, the sensitivity was adequate for analytes ionizing in positive mode and inadequate for those ionizing in negative mode. Therefore, all the analytes ionizing in negative mode were successfully derivatized with a simple procedure using dansyl chloride, improving ionization by a

OP20

factor of 2.3 to 453 (Fig. 1). Thus, limit of quantitation (LOQ) values lower than ng/L were achieved for most analytes.

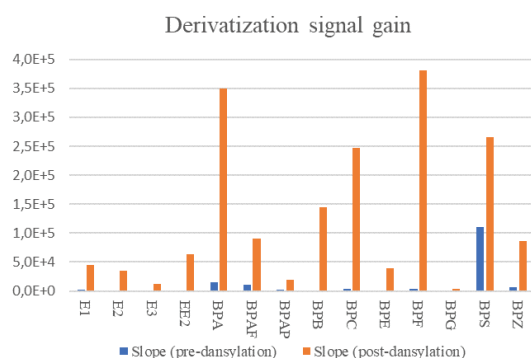


Figure 1. Derivatization signal gain by comparing signals pre- and post-derivatization of all analytes eligible for derivatization.

3.2. Method Validation

The developed method was fully validated in terms of selectivity, linearity, limits of quantitation, accuracy, precision, extraction efficiency, matrix effect, and stability. The achieved LOQ values in the range below 1 ng/L were determined as the lowest calibrators with suitable accuracy, precision, signal to noise, and signal to blank. The method has a wide linear range, achieves great repeatability and is accurate. To further underline the accuracy of the method, a standard addition principle was used on samples from three significantly different surface water matrices. The results confirmed the method's accuracy without the need to routinely fortify samples.

3.3. Method Application

The method was applied to a selection of surface water samples to determine the occurrence of EDs and their concentration levels in the environment. The samples were collected from the upper course of the Sava River and its tributaries. A representative chromatogram is presented in Fig. 2. E1, E3, progesterone, EE2, drospirenone, BPA, BPF and BPS were the most commonly found analytes in concentrations up to 670 ng/L.

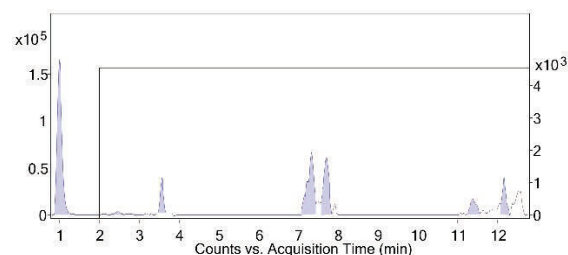


Figure 2. A combined MRM chromatogram of a river sample for non-derivatized analytes. The time segment from 2 minutes onwards is magnified on a smaller scale (right Y-axis) for better visibility.

4. CONCLUSION

The developed methodology was based on a simple SPE extraction, and two LC-MS/MS methods, and was extensively validated. The environmentally relevant LOQs were experimentally confirmed in samples with concentrations lower than 1 ng/L. This was achieved with a simple dansyl chloride derivatization which improved signals for all derivatized analytes with the least amount of sample manipulation necessary utilizing a mid-ranged LC-MS/MS system. The method therefore provides a reliable tool for the routine monitoring of important endocrine disruptors to provide relevant information on their presence in the environment.

5. REFERENCES

- 1 Delfosse V., et al., *Structural and mechanistic insights into bisphenols action provide guidelines for risk assessment and discovery of bisphenol A substitutes*. Proceedings of the National Academy of Sciences, 2012. 109 (37): 14930–14935.
- 2 Gunnarsson L., et al., *Pharmacology beyond the patient – The environmental risks of human drugs*. Environment International, 2019. 129: 320–332.
- 3 Dravvik E., et al., *Statement on advancing the assessment of chemical mixtures and their risks for human health and the environment*. Environment International, 2020. 134: 105267.

ACKNOWLEDGMENT

This research was financially supported by the Slovenian Research Agency (ARRS) [P1-0189].

STUDY OF DIFFERENT SOURCES OF NITROSAMINE TRACES IN PHARMACEUTICALS BY HIGHLY SENSITIVE HYPHENATED MASS SPECTROMETRY TECHNIQUES

Nejc Golob^{1,2}, Rok Grahek¹, Robert Rožkar²

¹*Lek Pharmaceuticals d.d., Sandoz Development Center Slovenia, Ljubljana, Slovenia*

²*University of Ljubljana, Faculty of Pharmacy, Ljubljana, Slovenia*

1. INTRODUCTION

Nitrosamines have been identified as mutagenic components that may be present in foods, cosmetics and in water for many years [1]. They became the focus of pharmaceutical regulatory authorities when *N*-nitrosodimethylamine (NDMA) was first detected in sartan medicines, in 2018. Later other nitrosamines were identified as contaminants, linked to the usage of certain solvents, reagents and catalysts which are either secondary amines or secondary amine precursors which can react with nitrosating agents ultimately yielding nitrosamines. Most lately, drug substances that are secondary amines, have been recognized as a risk for *N*-nitrosylation [2]. The significance of these findings and the regulatory requirements have been addressed by European Medicines Agency (EMA), the U.S. Food and Drug Administration (FDA) as well as other regulatory authorities [1]. Since the acceptable daily intake limits for nitrosamines are extremely low (ng per day range), the trace analysis of these compounds requires analytical methods with highly sensitive instruments. Therefore most of the methods which were published use hyphenated mass spectrometry techniques (gas chromatography-mass spectrometry and liquid chromatography-mass spectrometry). During our work we observed a case wherein *N*-nitrosamines at very low levels were detected in the finished dosage form but could not be found in the bulk drug product [1]. Findings of the investigation emphasized nitrocellulose (NC) blister material as a nitrosating agent for secondary amines, present in printing inks, yielding *N*-nitrosamines. These were shown to evaporate from a lidding foil and contaminate drug product in an adjacent blister cavity.

2. MATERIALS AND METHODS

2.1. Materials

2.1.1. Standards/reagents

Standards of nitrosamines NDMA, NDEA and NDMA-d6 were used for quantitation. Tetrahydrofuran (THF) and dichloromethane (DCM) were used as extraction solvents. Diethylamine (DEA) was used for experiments on nitrosamine formation in a lidding foil.

2.1.2. Drug products

Commercial 20 mg FCTs were plate-sealed in blister packs during SPME (solid-phase microextraction) sampling of nitrosamine vapours.

2.1.3. Blister material/printing ink

Lidding foil without print with polyester (PES) primer, lidding foil without print with NC primer and printing ink Verde color were used for experiments on nitrosamine formation in a lidding foil. NC lidding foils were used for plate and roller sealing, during SPME sampling of nitrosamine vapours.

2.2. GC-MS/MS method

GC-MS/MS method for nitrosamine analysis was an optimized FDA method [3]. For the SPME method, 50/30 μm DVB/Carboxen/PDMS fiber was used.

2.3. Sample preparation

Powdered tablets were extracted with DCM. Lidding foils were shredded and extracted with THF. Printing ink/DEA was added onto the lidding foil which was after 20 min shredded and extracted with THF. Empty blister cavities were extracted with THF. SPME sampling of nitrosamines vapours was performed on two types of blistering equipment, operating with plate sealing and roller sealing technology.

3. RESULTS AND DISCUSSION

OP21

3.1. Formation of nitrosamines in a lidding foil with addition of printing ink or DEA

Printing ink Verde color as a source of secondary amines (present as non-intentionally added substances (NIAS)) was added onto both lidding foils. On subsequent re-analysis, there was a significant increase in nitrosamines content, with NDEA being predominant, in a lidding foil containing NC. Higher NDEA increased levels in comparison with NDMA levels were expected because printing ink that was used for the experiment contained higher amounts of DEA than dimethylamine (DMA). Additionally, DEA was added onto both lidding foils. A significant increase in NDEA content was detected in a lidding foil containing NC, whereas no NDEA formation was observed in a lidding foil without NC. These experiments confirmed that NC as a primer in lidding foil acts as a nitrosating agent for secondary amines present in the printing ink, resulting in nitrosamine formation in a lidding foil.

3.2. SPME sampling of nitrosamine vapours at blistering equipment

Since nitrosamines NDMA and NDEA have relatively low boiling points, the possibility of their evaporation from lidding foil and subsequent contamination of drug product in blister cavities with their vapours was considered. This assumption was supported by the information that elevated temperatures > 200 °C are used during the blistering/sealing process. Several SPME fibers were exposed near the blistering equipment (plate sealing/roller sealing) and nitrosamines adsorbed during the blistering of drug products. In both cases lidding foils containing NC and nitrosamines were used for blistering of drug products. Results confirmed traces of NDMA and NDEA during blistering operation in vicinity of both types of equipment, with significantly higher amounts detected in the case of plate sealing technology. The highest values were detected closest to the sealing region. These results indicated that less NDMA and NDEA vapours were produced during blistering with roller sealing equipment, although lidding foils used for the experiment contained approximately the same amounts of nitrosamines in both cases, and moreover, higher sealing temperature was used during roller sealing. This could be partially explained by the fact that during plate sealing a larger area of lidding foil was exposed to high temperature

in the same time, and that total air flow and air movement through the equipment were restricted when compared to roller sealing. In addition, drug product (20 mg FDF) blistered with plate sealing equipment was analyzed and contamination confirmed. Moreover, NDMA and NDEA traces were also confirmed in cavities of empty blisters that were plate-sealed, in contrast to the ones that were roller-sealed. This is in line with the observation that more nitrosamine vapours were produced during plate sealing.

Table 1. Results of GC-MS/MS analysis of 20 mg FDF and blister cavities, sealed using plate sealing and roller sealing technology (SPME experiment).

Sample	NDMA (ng per tablet /cavity)	NDEA (ng per tablet /cavity)
20 mg FDF (plate sealing)	< 1.0 (0.8)*	< 1.0 (0.5)*
Blister cavity (plate sealing)	< 1.0 (0.2)*	< 1.0 (0.2)*
Blister cavity (roller sealing)	< LOD (0.2)	< LOD (0.2)

*estimated values below LOQ

4. CONCLUSION

Results of this investigation provided an insight into an additional source of *N*-nitrosamine contamination of drug products, which may lead to trace quantities of *N*-nitrosamines in the finished dosage form. Switching to NC-free blister material should be considered to avoid potential *N*-nitrosamine traces in finished dosage forms.

5. REFERENCES

1. Golob, N., et. al., *Nitrocellulose blister material as a source of N-nitrosamine contamination of pharmaceutical drug products*. International Journal of Pharmaceutics, 2022. 618(121687).
2. EMA, *Q&A for MAHs/applicants on the CHMP Opinion for the Article 5(3) of Regulation (EC) No 726/2004 referral on nitrosamine impurities in human medicinal products*. 2022. Available on: https://www.ema.europa.eu/en/documents/referral/nitrosamines-emea-h-a53-1490-questions-answers-marketing-authorisation-holders/applicants-chmp-opinion-article-53-regulation-ec-no-726/2004-referral-nitrosamine-impurities-human-medicinal-products_en.pdf. Accessed July 2022.
3. FDA, *Combined Direct Injection NDMA, NDEA, NEIPA, NDIPA and NDBA Impurity Assay by GC-MS/MS*. 2019. Available on: <https://www.fda.gov/media/123409/download>. Accessed July 2022.

SELECTIVE DETERMINATION OF WHEY PROTEINS BY A CHROMATOGRAPHIC ANALYTICAL APPROACH

Nika Osel¹, Timeja Planinšek Parfant¹, Albin Kristl¹, Robert Roškar¹

¹Department of Biopharmacy and Pharmacokinetics, University of Ljubljana, Faculty of Pharmacy, Slovenia

1. INTRODUCTION

Whey has been considered a waste material for many years. However, due to its rich composition, mainly due to its protein content, it is gaining in importance [1]. The evaluation of the isolation and purification processes of individual whey proteins (WPs) from whey, the development of formulations with selected WPs, and the evaluation of their stability require the development of appropriate analytical support which presents a special challenge due to the structural complexity of proteins [2]. Moreover, the concentration range of WPs in whey is relatively wide and individual WPs exist in multiple genetic variants or isoforms. The development of analytical methods is further complicated by the complex and variable composition of whey-based samples [1,3]. Therefore, the main purpose of our work was to develop a chromatographic analytical approach that would allow a selective evaluation of WPs in various samples. The most common WPs and WPs with positive effects on human health were included in the study.

2. MATERIALS AND METHODS

2.1. Reagents and chemicals

Reference standards of lactoferrin (Lf), α -lactalbumin (α -LA), β -lactoglobulin (β -LG), bovine serum albumin (BSA), IgG, and lactoperoxidase (LPO) were obtained from Sigma-Aldrich. HPLC-grade acetonitrile was purchased from Honeywell. All mobile phases and sample solutions were prepared using the Milli-Q water obtained through a Milli-Q A10 Advantage water purification system. All other chemicals used were of analytical grade.

2.2. Methods

We were focused on the development of complementary chromatographic methods. Various ion-exchange (IEX), size-exclusion (SEC), and reversed-phase (RP) chromatographic columns obtained from six manufacturers were tested (Agilent, Vydac, Phenomenex, Sigma-Aldrich, BIA Separations, and Waters). An Agilent 1100/1200 HPLC system, equipped with a diode array detector (DAD) was used. The chromatographic analytical approach was further extended by two-dimensional liquid chromatography (2D-LC; Waters).

3. RESULTS AND DISCUSSION

It was observed that LPO can be selectively determined in the presence of other WPs at a different wavelength by using a DAD. LPO has a heme moiety in its structure and therefore absorbs at 405 nm (Fig. 1).

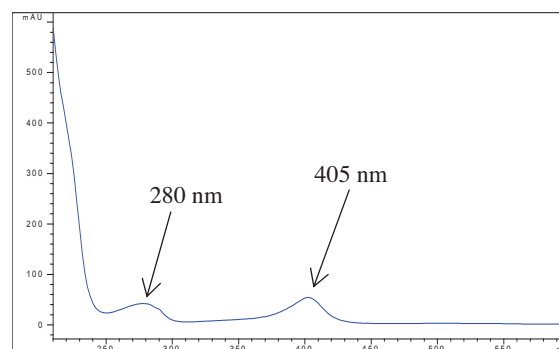


Figure 1. Absorption spectrum of LPO.

WPs differ in their isoelectric point (pI) values. Therefore, an IEX method using a weak cation exchange 0.1 mL column CiMAC (BIA Separations) was developed. WPs were eluted by a salt gradient at a pH of 7.0. The IEX method allows selective determination of Lf and LPO in the presence of more acidic WPs (e.g. β -LG, IgG, α -LA) (Fig. 2).

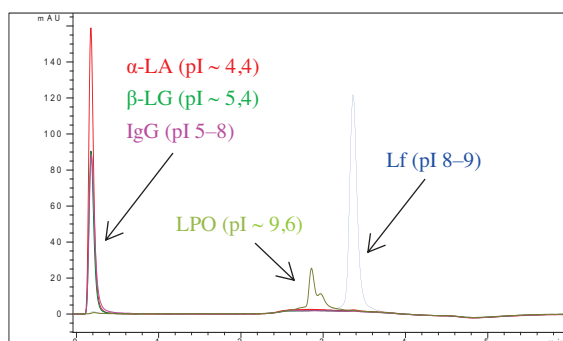


Figure 2. Selective determination of Lf and LPO by IEX.

The developed SEC method can be used in stability studies for the evaluation of the aggregation and fragmentation behaviour of individual WPs [4]. However, not all WPs can be separated using the SEC method since some of them (LPO, Lf, BSA) have a similar molecular weight (Fig. 3). Therefore, due to its poor selectivity, this method is unsuitable for the analysis of complex samples containing WPs.

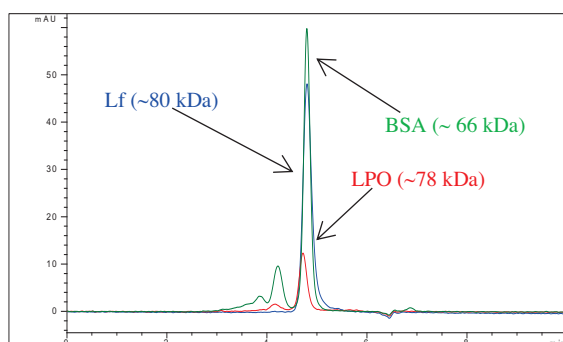


Figure 3. Size-exclusion chromatograms of Lf, BSA, and LPO.

The most challenging was the development of the RP-HPLC method as the separation (Lf and BSA) or the appropriate chromatographic peak shape (IgG) of selected analytes was difficult to achieve. The optimized RP-HPLC methods were used for the evaluation of the selected WPs in relatively simple samples (Fig. 4). For more complex samples, a 2D-LC method which was based on a combination of SEC and RP-HPLC methods was developed. The 2D-LC method enabled the separation of all selected WPs. However, it is less appropriate for routine use since it is a relatively sophisticated technique.

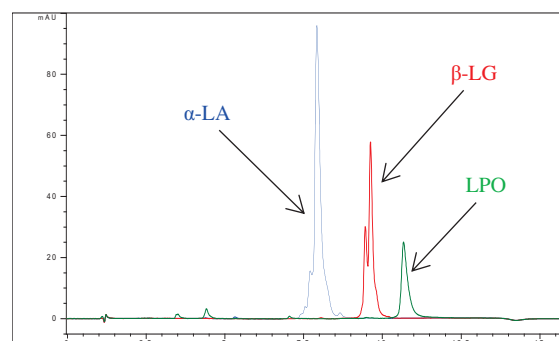


Figure 4. RP-HPLC chromatograms of β -LG, α -LA, and LPO.

4. CONCLUSION

The development of an appropriate analytical methodology is necessary for the evaluation of WPs in complex samples. A combination of various chromatographic methods coupled with different detectors allows the selective evaluation of WPs in various samples. In the future, the analytical approach will be extended with mass spectroscopy, which will allow a more reliable and selective evaluation of WPs in complex samples.

5. REFERENCES

1. Smithers G.W., *Whey-ing up the options – Yesterday, today and tomorrow*. International Dairy Journal, 2015. 48: 2–14.
2. ICH Q5C, 1995.
3. Guo M., et al., *Chemistry of Whey Proteins*. Whey Protein Production, Chemistry, Functionality, and Applications (1st edition), 2019.
4. Osel N., et al., *Stability-Indicating Analytical Approach for Stability Evaluation of Lactoferrin*. Pharmaceutics, 2021. 13(7): 1065 (2021).

ACKNOWLEDGEMENT

This research was co-funded by Slovenian Research Agency, grant number [P1 0189] and by Support of Research and development projects (TRL 3–6): LAKTIKA.

PREPARATION OF BUCCAL FILMS IN PARKINSON'S DISEASE

Krisztián Pamlényi¹, Géza Regdon Jr.¹, Dániel Nemes², Ildikó Bácskay², Katalin Kristó¹

¹ Institute of Pharmaceutical Technology and Regulatory Affairs, University of Szeged, Eötvös u. 6., H-6720 Szeged, Hungary

² Department of Pharmaceutical Technology, University of Debrecen, Nagyerdei krt. 98., H-4032 Debrecen, Hungary

1. INTRODUCTION

Parkinson's disease (PD) is the second most common movement disorder. It affects 2-3% of the population over the age of 65 years [1]. PD is caused by the death of dopaminergic neurons in the substantia nigra area of the human brain [2]. Enzymatic and non-enzymatic oxidation of dopamine generates reactive oxygen species, which induces apoptotic cell death in dopamine neurons.

Current treatment of PD focuses on replacing the dopamine level from an external source (Levodopa-L-DOPA) or on applying a dopamine agonist API, which can stimulate the dopamine receptors in the central nervous system.

In Parkinson's disease, the advantages of buccal films include that the patients do not have to swallow the dosage form, so they can be used in the case of swallowing problems, which is a common symptom in this disease.

In this project, we applied pramipexole dihydrochloride (PR) as an active agent in the polymer film system, which can also be used on the buccal mucosa to improve the success of current Parkinson's therapy with PR compound.

2. MATERIALS AND METHODS

2.1. Materials

Sodium alginate (SA) (Biochemica GmbH, Germany) (10,000 – 600,000 g/mol) and HPMC (Metolose[®] 2208, Shin Etsu Chemical Co., Ltd., Japan) were used as film forming agents in the polymer film. Glycerol (GLY) 85% (w/w%) was added to the film as a plasticizer (Ph. Eur.8.). Pramipexol dihydrochloride (PR) (Ph. Eur. 8.) was the API, which was a gift from KRKA, d.d., (Novo Mesto, Slovenia).

2.2. Preparation of buccal films

The films were prepared at room temperature with the solvent casting method. As the first step of preparation, SA was dissolved in distilled water and mixed at room temperature. PR was incorporated in the polymer solution. As the third step, HPMC was added to the solution with mixing. In the fourth step, GLY was added to the solution. Mixing was stopped and it was placed in an ultrasonic cleaning unit (Elmasonic S 30 H, Germany) for 30 minutes to help the air bubbles disappear from the solution. The solution was cast on a glass surface in Petri dishes, then it was dried at room temperature (24.4±0.5 °C). **Table 1** shows the different compositions of the prepared polymer films.

Table 1. Composition of prepared PR films

Sample	SA (w/w %)	HPMC (w/w %)	GLY (w/w %)	PR (0.7 mg)
1	1	2	1	+
2	1	2	2	+
3	1	2	3	+
4	1.5	1.5	1	+
5	1.5	1.5	2	+
6	1.5	1.5	3	+
7	2	1	1	+
8	2	1	2	+
9	2	1	3	+

2.3. Mechanical properties of films

The thickness of the polymer films was measured with a screw micrometre (Mitutoyo Co. Ltd, Japan), sensibility was 0.001 mm [3]. Tensile strength was measured with a texture analyser developed in our department, with a needle-like probe. [3].

OP23

Mucoadhesion was measured with the same texture analyser with a rod-like probe and different settings [3].

2.5. Dissolution test

Films with a size of 4 cm² were measured in the dissolution test. The dissolution test was performed in a 100 mL glass lab beaker, 50 mL of phosphate buffer (pH=6.8) was used as dissolution medium, its temperature was 37 °C. Aliquots of 5 mL were analyzed with UV-spectrophotometry at $\lambda=262$ nm wavelength.

2.6. Cytotoxicity test

Biocompatibility was studied by flow cytometry. TR-146 buccal mucosa cells were treated in a 1 million cell/mL concentration with 1 mL of PR solution (PR films dissolved in HBSS). After 30 minutes of incubation, the cells were stained with propidium iodide. Non-cellular events were excluded and the ratio of stained and non-stained cells was calculated.

3. RESULTS AND DISCUSSION

3.1. Mechanical properties of films

The thickness of the films can be increased by the amount of SA, so the concentration of SA can influence the thickness of the films. It can be concluded the GLY can increase film thickness. Films with a higher GLY concentration have higher breaking hardness values. SA can increase the breaking hardness of the films. Every composition has great and adequate mucoadhesive properties. The in vitro mucoadhesion force of all samples is larger than 15 N.

3.2. Dissolution test

As it can be seen in **Figure 1**, all the amount of the API can dissolve from each composition in the first 20 minutes. The dissolution of the API is faster from the films which contain a low GLY concentration.

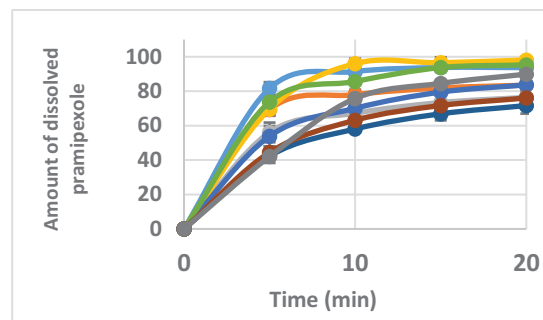


Figure 1. Dissolution of pramipexole from the different polymer films in 20 minutes

3.3. Cytotoxicity test

It can be said that most formulations had cell viability higher than 87%. Buccal film Sample 8 had the lowest impact on cell viability as 87.1% of the treated cells survived.

4. CONCLUSION

It can be concluded that we can formulate buccal films with PR. The films have adequate thickness, flexibility, breaking hardness, and mucoadhesivity is also appropriate for use on the buccal mucosa. All films can release 100 % API in less than 20 minutes from the films fit for the purpose.

5. REFERENCES

1. Poewe, W., et al., *Parkinson Disease*. Nature Reviews Disease Primers, 2017. 3: 1-21
2. Naoi, M., et al., *Cell death of dopamine neurons in aging and Parkinson's disease*. Mechanisms of Ageing and Development, 1997. 111 (2-3): 175-88
3. Pamlényi, K., et al., *Formulation and Optimization of Sodium Alginate Polymer Film as a Buccal Mucoadhesive Drug Delivery System Containing Cetirizine Dihydrochloride*. Pharmaceutics, 2021. 13 (5) 619-37

ACKNOWLEDGMENT

The authors thank Krka, d. d., Novo Mesto, Slovenia for supplying pramipexole dihydrochloride. This research work was supported by the ÚNKP-21-3 New National Excellence Program of the Ministry for Innovation and Technology from the Source of the National Research, Development and Innovation Fund.

DESIGN AND EVALUATION OF COMPOSITE FILM FORMULATIONS USING QUALITY BY DESIGN FOR PAEDIATRIC USE

Genada Sinani¹, Mohammed Kalayi¹, Buket Aksu¹

¹ Department of Pharmaceutical Technology, Altinbas University, Türkiye

1. INTRODUCTION

Lidocaine is widely used to treat different painful conditions like oral ulcers, teething, or gingivitis in children. However, it is stated in various reports that the use of oral viscous lidocaine solution in infants and young children can result in serious side effects, including heart and brain problems, due to overdose or when the drug is accidentally swallowed [1]. Thus, there is a need to develop paediatric-friendly oral formulation for anaesthetic drugs. The use of buccal films for lidocaine delivery could provide a safe and easy way for treating mouth disorders in children [2]. Herein, composite film formulations containing hydroxypropyl methylcellulose and sodium alginate as polymers were developed and optimized by QbD approach to ensure their use as potential paediatric dosage forms.

2. MATERIALS AND METHODS

2.1. Materials

Hydroxypropyl methylcellulose (HPMC) (Ashland, Germany), sodium alginate (SA) (Sigma Aldrich, Switzerland), lidocaine hydrochloride (Doğa İlaç, Istanbul, Türkiye), glycerol (Tekkim Kimya, Bursa, Türkiye). All other chemicals were of analytical grade.

2.2. Preparation of polymeric films

The polymeric films were prepared by solvent casting method, as described earlier with modifications [3]. Different amounts of HPMC and SA polymers at different ratios were added in distilled water to make a total polymer concentration of 2-3% (w/v%) and stirred overnight to allow the formation of a homogeneous solution. Further, glycerol used as plasticizer was added at concentrations varying 40-60% (w/v% polymer weight) and stirred for 2 h. The formulation was stored overnight in refrigerator to remove the air bubbles and cast on glass petri dishes. The films

were allowed to dry at 45 °C for 48 h. After drying, the films were carefully peeled off and stored wrapped in an aluminium foil in a desiccator until further use in characterization studies.

2.3. Formulation development and optimization of films using QbD approach

The main purpose of applying QbD approach for the development and optimization of polymeric film formulations was to investigate the optimum amounts of polymers and glycerol to be used in the formulation of composite films with ideal mechanical characteristics. Thus, amount of HPMC (X1), SA (X2) and glycerol (X3) were selected as independent variables, while tensile strength (Y1) and percentage elongation (Y2) that are indicative of mechanical properties of polymeric films were selected as dependent variables. QbD approach for the optimization of the film formulations was performed by using MODDE Pro version 12.1 software. Different 30 film formulations were investigated in triplicate using Texture Analyzer (TA.XT.Plus C Stable Micro Systems, UK).

2.3. Characterisation of optimum composite film formulations

Following development and optimisation studies drug loaded formulations were prepared as described earlier and the effect of drug loading on mechanical characteristics of films was further investigated. In addition, optimum composite film formulations were characterised in terms of weight uniformity and thickness, folding endurance, pH, drug uniformity and drug release profile.

3. RESULTS AND DISCUSSION

3.1. Formulation development and optimisation.

Considering that the formulation composition is closely related with mechanical properties such

OP24

as tensile strength and percentage elongation of films, their evaluation is important to ensure appropriate production, handling, and use of polymeric films. In this study, the design space (Figure 1.) was determined to investigate and assure the development of drug formulation with desired quality. As expected, the careful selection of the amount and type of polymer as well as the amount of plasticizer is necessary to ensure the formation of uniform films with good mechanical properties. It was observed that increasing the amount of HPMC in formulation resulted in formation of films showing increased tensile strength, whereas increasing the amount of glycerol generally resulted in decreased tensile strength. It was observed that blending of the polymers improved the mechanical properties compared to films prepared using only one polymer.

further studies. It might also help to increase the availability of high-quality medicines designed for children.

5. REFERENCES

1. Curtis, L.A., et al., *Are one or two dangerous? Lidocaine and topical anesthetic exposures in children*. The Journal of emergency medicine, (2009). 37(1), 32-39.
2. Kottke, D., et al., *Development and evaluation of mucoadhesive buccal dosage forms of lidocaine hydrochloride by ex-vivo permeation studies*. International Journal of Pharmaceutics, (2020). 581, 119293.
3. Morales, J.O., & McConville, J.T., *Manufacture and characterization of mucoadhesive buccal films*. European Journal of Pharmaceutics and Biopharmaceutics, (2011). 77(2), 187-199.

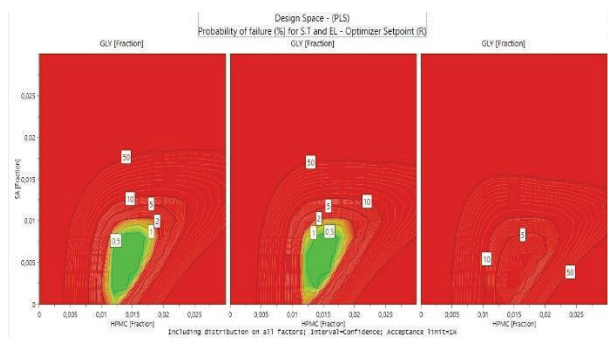


Figure 1. Design space graph of optimal parameters for tensile strength and percentage elongation at break

3.2. Evaluation of characteristics of optimised composite film formulations

To evaluate the suitability of optimised composite films formulations to be used for lidocaine delivery in paediatric patients further characterisation studies were performed. Films showing thickness of approximately 0.1 mm, good physical appearance, weight and drug uniformity were prepared. The pH values measured for the films showed that they were compatible with the buccal mucosa. Prolonged drug release was observed depending on formulation characteristics.

4. CONCLUSION

The optimised composite polymeric film formulations developed in this study using QbD approach for buccal administration films might be promising to be used as effective and safe patient-friendly formulations in children after

DEVELOPMENT OF A PEDIATRIC ORALLY DISINTEGRATING TABLET DOSAGE FORM BY MASKING THE BITTER TASTE OF ORNIDAZOL WITH EUDRAGIT E PO

Gülbeyaz YILDIZ TÜRKYILMAZ¹, Çağlar AKGÜNLÜ², Ozan ÜNSALAN³, Mehmet Ali EGE², Çisem ALTUNAYAR ÜNSALAN⁴, Hatice Yeşim KARASULU²

¹ Department of Biopharmaceutics and Pharmacokinetics, Faculty of Pharmacy, Ege University, Izmir, Turkey

² Department of Pharmaceutical Technology, Faculty of Pharmacy, Ege University, Izmir, Turkey

³ Department of Physics, Faculty of Science, Ege University, Izmir, Turkey

⁴ Central Research Testing and Analysis Laboratory Research and Application Center, Ege University, Izmir, Turkey

1. INTRODUCTION

Ornidazole (ORN) is an antiprotozoal with a sharp bitter taste [1] and an important drug in antibacterial therapy against anaerobic bacteria. Pediatric use is limited to the iv dosage form only that can only be administered to the hospitalized patient. Therefore, it is not possible to continue treatment at home and the antibiotic must be changed. In this study, the development of a dosage form suitable for pediatrics is the mainly goal in terms of ensuring the sustainability of the treatment. One of the dosage forms applicable to pediatrics is the orally disintegrating tablet (ODT) form. The problem here is the bitter taste of the active ingredient. The secondary main aim of the study is to mask this bitter taste. One of the bitter taste masking techniques is coating the active ingredient by spray drying. The bitter-tasting active substance should not be released or dispersed from the coated material that will disperse in the mouth. For this purpose, Eudragit EPO (E-EPO) polymer, which is slightly soluble in saliva pH, was chosen as the coating.

During the study, in vitro taste masking test was performed with the digital taste transmitter prototype [2]. After appropriate masking, the ODT formulation was prepared from the coated active substance. Since the dose is administered per kg, notched tablets were compressed considering ease of dosage. Developed ODTs were evaluated with in vitro quality control tests determined by pharmacopeias and guidelines.

2. MATERIALS AND METHODS

2.1. Materials

ORN, E-EPO supplied by Deva İlaç. All other materials are pharm grade, all consumables used in the analysis are in HPLC grade. Ornisid® Fort 500 mg film-coated tablet (Abdi

İbrahim) was used as the reference drug.

2.2. Coating with spray dryer

For the coating study, many experiments were carried out by changing the pump speed from the spray dryer conditions to 20% or 40% and changing the ORN:E-EPO ratio to 1:0.5-4 and ethanol (EtOH) as a solvent to 50 or 60 in the feed solution content. The optimum spray drying condition that masked the bitter taste was determined and production was carried out under these conditions. Quantification, flowability, bulk angle, density, Carr's index, moisture determination, particle size measurement and raman analysis were performed. The amount of ORN was determined according to the pharmacopoeia method [3].

2.3 Development of ODT formulation

The coated powder, which was taken to contain 125 mg of ORN, together with different ratios of super dispersant, filler and lubricants were mixed in a cubic mixer and the formulation suitable for compressing was determined. Notched tablets were printed with a 1 cm diameter seal using the direct compression method. Quantification of the final product was made using the validated method. Thickness-diameter, hardness, brittleness, dispersion determination, content uniformity, wetting time and water absorption capacity and dissolution test were performed. A comparative in vitro dissolution study and similarity test with the market preparation was performed.

The stability of the formulation was followed for 3 months at 25 °C ± 2; RH 60% ± 5 and 40 °C ± 5; RH 75% ± 5.

3. RESULTS AND DISCUSSION

3.1. Coating with spray dryer

The taste scale of the formulations performed with spray drying under the conditions in Table 1 were measured (Figure 1). According to the Raman spectra, when the polymer ratio was higher, taste masking was higher. It was decided to produce in F3 conditions, where the bitter taste is the least and the yield is high.

3.2. Development of ODT formulation

The formulation suitable for production was determined as F3E according to Hausner ratio (HR) and compressibility limit (CI).

F3E was found suitable relative to EP/TF with a disintegration time of 80 seconds [4]. Wetting time and water absorption capacity were found to be better with values of 30.5 ± 2 seconds and $75.1 \pm 1.1\%$, respectively, compared to similar ODT forms performed with E-EPO [1]. All other characterization test results were evaluated according to the pharmacopoeia and found to be appropriate.

Dissolution studies were performed at pH 1.2, 4.5 and 6.8 (both salivary and intestinal media). As a result of the comparative dissolution study with the Ornidazole®, f_2 values were below 50 in all results except pH 6.8, showing that the formulation was not similar.

It was observed that its stability continued for 3 months in long and accelerated stability environments.

As a result, the taste of ORN was masked in a single operation compared to other taste masking methods with E-EPO and an ODT dosage form suitable for pediatric use was developed [1,5].

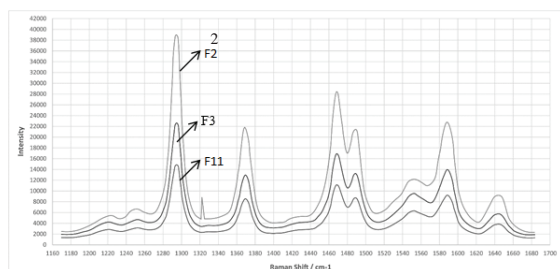


Figure 1. Raman spectra of coated powders such as F2, F3, F11 formulations

Table 1. Spray drying trials and results

	F1	F2	F3	F3.1	F4	F11
ORN (g)	1	1	1	1	1	1
E-EPO (g)	1	2	3	3	4	0.5

	F1	F2	F3	F3.1	F4	F11
SA (g)	-	-	-	-	-	1
Method						
EtOH %	50	60	60	60	60	60
Inlet / outlet (°C)	120 / 40	120 / 51	120 / 56	120 / 68	120 / 58	120 / 68
PR (%)	40	40	40	20	40	40
Result						
Yield (%)	68	56	72	59	55	65
Taste	More bitter	Bitter	Less bitter	Bitter	Bitter	Sour bitter

SA=Sitric acid; PR=Pump rate

Table 2. HRs and CIs of F3 formulation and powder mixtures prepared from F3 formulation

	F3	F3A	F3B	F3C	F3D	F3E
ORN (mg)	125	125	125	125	125	125
E- EPO (mg)	375	375	375	375	375	375
Lubricant ¹ (mg)	-	1	1	2	2	9
Super dispersant ² (mg)	-	-	-	2	2	5
Filler ³ (mg)	-	-	-	-	80	86
HR	1,85	1,5	1,6	1,6	1,42	1,3
CI (%)	46	50	33	40	29	25

¹Magnesium stearat; ²Collidon® CL-F; ³Avicel pH-102

4. CONCLUSION

In this study, successful results were obtained in terms of taste masking by coating ornidazole, which has a sharp bitter taste, with Eudragit E PO at a ratio of 1:3. The proposed ODT formulation has the potential to close both an economic and therapeutic gap in the pharmaceutical market with in vivo tests.

5. REFERENCES

- Shishu, Kamalpreet, Kapoor, V. R. Development of taste masked oral formulation of ornidazole. *Indian J Pharm Sci*, 2010. 72(2):211-5
- Turkish Patent and Trademark Office Application No: 2021/018046
- Ornidazole Monograph in EP 2019
- European Pharmacopoeia (EP) 2019
- Chivate A, Sargar V, Nalawade P, Tawde V. Formulation and development of oral dry suspension using taste masked Ornidazole particles prepared using Kollicoat(®) Smartseal 30 D. *Drug Dev Ind Pharm*. 2013 Jul;39(7):1091-7.

NANOCELLULOSE-BASED ORODISPERSIBLE FILMS AS A POTENTIAL DRUG DELIVERY SYSTEM

Katarina Bolko Seljak, Mirjana Gašperlin, Mirjam Gosenca Matjaž

Department of Pharmaceutical Technology, Faculty of Pharmacy, University of Ljubljana, Slovenia

1. INTRODUCTION

The use of nanocellulose, a fully sustainable and biodegradable polymer, in drug delivery has been gaining attraction. In particular, nanocrystalline cellulose (NCC) can be inexpensively isolated from renewable cellulosic biomass. Depending on the input cellulosic material and hydrolysis conditions, the geometrical dimensions of the isolated NCC can vary greatly. Nevertheless, its biocompatibility, biodegradability and low cytotoxicity are broadening its possibility of use in biomedical applications [1].

In drug delivery research, the focus has been shifting from traditional dosage forms towards those offering more tailor-made options. Among these, oral drug delivery films are gaining interest due to faster rate of drug absorption, improved bioavailability and better compliance among patients facing swallowing deficiencies, such as children and elders. Moreover, their potential for delivering proteins and peptides has been attracting further attention [2].

In this research, we present the use of NCC as a novel reinforcing material in orodispersible films (ODF), while still allowing for unhindered disintegration.

2. MATERIALS AND METHODS

2.1. Materials

Nanocrystalline cellulose from wood pulp-gNCC (Nano-crystalcell, Slovenia) and pNCC (Celluforce, Canada), sodium alginate Protanal LF 10/60 (FMC Biopolymer), pectine (Sigma Aldrich) were used in the present study.

2.2. Methods

Hydrogels of 1 % NCC with 2 % of alginate (alg) were prepared. Alternatively, 0,6 % of NCC was blended with 1,2 % of pectin (pec). 3 % of glycerol was added to all hydrogels. Variations with addition of 0,14 % of Ca²⁺ were

also prepared. Afterwards, hydrogels were evenly distributed across glass plates using ZUA applicator, dried at 60°C to form films and cut into even pieces.

Rheological properties were measured with Physica MCR301 rheometer (Anton Paar). Mechanical properties of 10 cm long films were measured with Instron 5567 compression and tensile tester at 100 mm/min speed.

3. RESULTS AND DISCUSSION

Since NCC properties can vary depending on the source and manufacturing procedures, films were developed using NCC from two different manufacturers – gNCC was supplied in the form of water gel, while pNCC was presented as spray-dried powder.

While all hydrogels exhibited behaviour of non-newtonian liquids prior to solvent casting (data not shown), alg-pNCC sample displayed the highest viscosity at 12.05 Pa·s. Overall, pNCC allowed for formulations with higher viscosities compared to gNCC formulations, although the longer polymer chains are attributed to the latter (Table 1).

Table 1. NCC properties according to manufacturer's specifications.

NCC	Crystallinity	Fibre width	Fibre length
gNCC	90,3 %	10- 15 nm	150 -300 nm
pNCC	88 %	7,5 nm	150 nm

Frequency sweeps confirmed weaker gel structure of gNCC samples compared to pNCC, as storage modulus (G') and loss modulus (G'') values crossed (Fig. 1). At lower radious frequencies, the G' of pNCC was 24 x the G'' value compared to 3 x for gNCC.

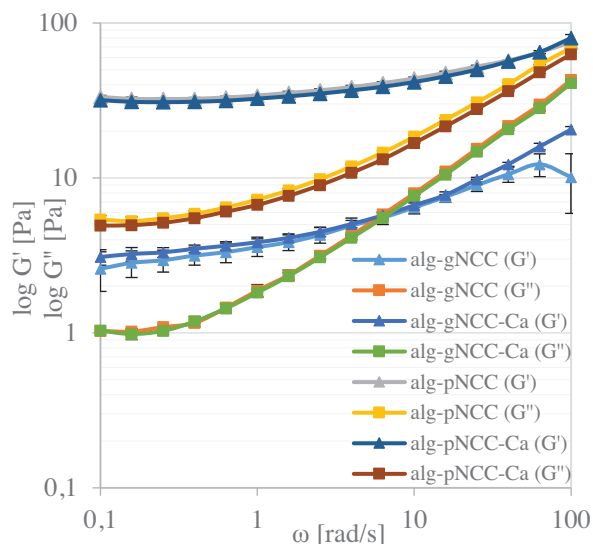


Figure 1. Frequency sweep test of alg-NCC films.

Adequate mechanical properties enable handling and application of ODFs. All developed ODF exhibited excellent elongation at break (Table 2). pNCC films, in particular alg-pNCC were the most elastic ($E \sim 3,65$ Mpa). Moreover, tensile strength of all films was in the range of 2 MPa or higher.

Table 2. Mechanical properties of prepared films: Tensile strength (TS), Young modulus (E), Elongation at break (emax).

ODF SAMPLE	TS [MPa]	E [MPa]	emax [%]
alg-gNCC	2.601 ± 0,44	0.557 ± 0.21	97,9 ± 11.1
alg-gNCC-Ca	2.051 ± 0.56	0.711 ± 0.47	50.7 ± 13.8
alg-pNCC	5.902 ± 1,11	3.653 ± 1.25	90.3 ± 10.2
alg-pNCC-Ca	1.727 ± 1,38	1.634 ± 0.99	38.4 ± 14.3
pek-gNCC	3.029 ± 0.48	0.499 ± 0.12	31.97 ± 5.25
pek-gNCC-Ca	3.643 ± 0.72	0.532 ± 0.12	26.63 ± 4.13
pek-pNCC	2.688 ± 0.44	0.461 ± 0.27	31.97 ± 6.02
pek-pNCC-Ca	4.269 ± 0.98	0.618 ± 0.09	42.84 ± 6.80

When ODFs came in contact with water, alginate and pectine containing films behaved similarly (data not shown). Regardless of the choice of natural polymer in ODFs, the use of gNCC over pNCC resulted in shorter disintegration time when in contact with water (example in Fig. 2), which is of importance for potential drug delivery applications.

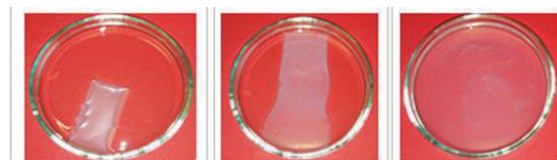


Figure 2. Disintegration behaviour of alg-gNCC film in contact with water (at 0, 2 min and 20 min from left to right).

The addition of Ca^{2+} ions did not attribute to rheological and mechanical properties of ODFs in a meaningful way; it did however prolong their disintegration time due to formation of egg box structure (data not shown).

While longer polymer chain lengths usually attribute to higher viscosities and stronger hydrogels, this was not the case for the investigated NCCs. Overall, rheological properties of hydrogels prior to solvent casting were better predictors of mechanical properties of resulting ODFs and their disintegration behaviour.

4. CONCLUSION

The ability of NCC from renewable cellulose sources to form multi-polymeric ODF films with adequate rheological and mechanical properties was demonstrated.

Nanocellulose-based ODF therefore present a novel step towards improved sustainability in drug delivery while catering to specific demographic populations. Future research should explore potential of nanocellulose-based ODFs for carrying and delivering active pharmaceutical ingredients.

5. REFERENCES

1. Pachau LS. *A Mini Review on Plant-based Nanocellulose: Production, Sources, Modifications and Its Potential in Drug Delivery Applications*. Mini Reviews in Medical Chemistry. 2015;15(7):543-52.
2. He M, et al. *Recent advances of oral film as platform for drug delivery*. International Journal of Pharmaceutics. 2021 Jul 15;604:120759.

ACKNOWLEDGMENT

The research was financially supported by the Slovenian Research Agency (research core funding number P1-0189).

EXCIPIENTS ROLE IN FORMULATING USER FRIENDLY ORAL DOSAGE FORMS

Pawel Balcerzak¹, Liliana Miinea², Elena Draganoiu³

¹Lubrizol Advanced Materials, Inc., Belgium;

²Lubrizol Advanced Materials, Inc., USA

³Lubrizol Canada Limited, Canada

1. INTRODUCTION

Designing user friendly oral dosage forms implies use of effective formulation techniques and versatile excipients to allow for desired therapeutic effect and patient compliance.

Carbopol[®] polymers (carbomers) are crosslinked polyacrylic acid polymers proven to be highly effective in controlling drug release at low usage levels.¹ Furthermore, there are reported studies regarding their mucoadhesive properties.² Our work has been focused on using Carbopol[®] polymers to design user friendly oral dosage forms.

Metformin HCl remains the first line of treatment of type 2 diabetes. Due to increased frequency of dysphagia in diabetes patients, it is necessary to formulate stable compositions with higher drug loading (500/1000 mg) and reduced tablet size. Regulatory agencies have issued guidance regarding control of potential carcinogenic nitrosamine impurities in drug products that has resulted in global recalls, metformin HCl being one of the most affected. Work has been conducted to develop small size, high dose metformin HCl extended release (ER) tablet compliant formulations.

Cold and cough oral liquid formulations can benefit from a mucoadhesive excipient that would enable the formulation to coat the mucous membrane, providing soothing benefits in addition to potential improved retention and absorption. We have evaluated cold and cough formulations with mucoadhesive polymers in comparison with commercial formula.

2. MATERIALS AND METHODS

2.1. Materials

Metformin HCl; acetaminophen (APAP); dextromethorphan (DXTR); Carbopol[®] 971P NF and 71G NF polymers; hypromellose

K100M; magnesium hydroxide; anhydrous colloidal silica; magnesium stearate.

2.2. Methods

Metformin HCl formulation development

Metformin HCl formulations (500/1000 mg), were developed by aqueous high shear wet granulation using intra-granular and extra-granular ingredients listed in Table 1. The formulations were tested for physical parameters, dissolution profile, assay and impurities. Dissolution was carried as per USP Test 4. Stability studies were conducted as per ICH guidelines at accelerated (ACC) conditions (40°C/75% RH).

Nitrosamine impurities analysis was performed.

Table 1. Ingredients in Metformin HCl ER tablets

Intra-granular	Extra-granular
Metformin HCl	Magnesium hydroxide
Hypromellose K100M	Hypromellose K100M
Carbopol [®] 971P NF polymer	Carbopol [®] 971P NF polymer
Carbopol [®] 971P NF polymer	Carbopol [®] 71G NF polymer
Magnesium hydroxide	Anhydrous colloidal silica
	Magnesium stearate

Cold and cough formulation development

Mucoadhesive liquid formulations were prepared by dissolving acetaminophen, dextromethorphan and sweetener in deionized water followed by mixing with an aqueous dispersion of Carbopol[®] polymer. The inclusion level of Carbopol[®] polymer in the formulation was varied (0 - 1%). The mucoadhesive properties of the formulations were tested using a device adapted from in-vitro oesophageal retention model (IVOR).³

3. RESULTS AND DISCUSSION

3.1. Metformin HCl ER tablets

The 500 mg and 1000 mg strength tablets were successfully formulated at small sizes (achieving 20-30% size reduction compared to commercial formulations of the respective strengths). Smaller tablet size enables more tablets per batch, resulting in increased productivity and cost savings (analytical testing, inventory, packaging and storage). The tablets complied to the USP monograph and were stable under accelerated conditions when packed in HDPE bottles (Fig. 1, Table 2).

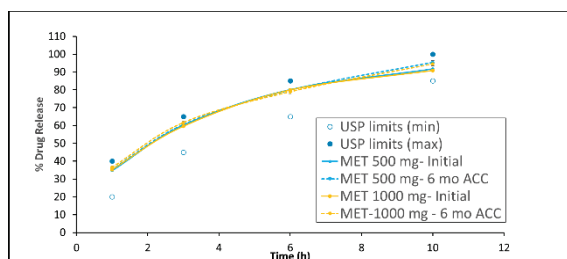


Figure 1. Metformin HCl ER tablets dissolution in pH 6.8 phosphate buffer (initial and six month accelerated conditions - 6 M ACC)

Table 2. Metformin HCl ER tablets - six month accelerated conditions (6 M ACC) stability

Test	USP specs	Metformin 500 mg	Metformin 1000 mg
Assay (%)	90-100	99.9	97.1
Single max impurity (%)	0.1	0.04	0.06
Total impurity (%)	0.6	0.10	0.16

Selected tablet formulations were tested at an FDA approved testing laboratory as per US FDA guidelines and were found to be compliant for all eight nitrosamine impurities.⁴

3.2. Cold and cough formulation

In our study it was demonstrated that the presence of Carbopol® polymer prolonged the retention of the formulation on the substrate simulating oral mucosa (artificial membrane hydrated in a mucin solution; Fig. 2). Additionally, increasing the polymer concentration resulted in longer retention. These results correlate well with similar findings on using Carbopol® polymer to formulate other liquid, semi-solid and film dosage forms.⁵

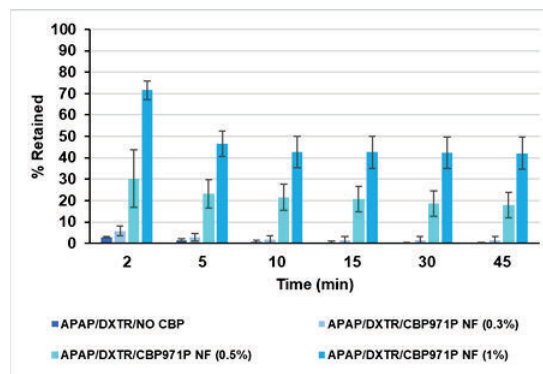


Figure 2. Impact of Carbopol® 971P NF polymer (CBP971P NF) on mucoadhesion of oral liquids

4. CONCLUSION

Small size, high dose stable metformin HCl ER tablet formulations were successfully developed using Carbopol® polymers. The tablets complied to Nitrosamines (NDMA) impurities as per US FDA guidance.

Cough and cold mucoadhesive liquid formulations were designed to ensure prolonged contact with mucosal membranes, providing patient compliance and product differentiation. Carbopol® polymers have been used as key excipient to formulate smaller extended-release tablets and liquid product for mucosal delivery, proving to be versatile excipients to design user friendly drug products.

5. REFERENCES

1. Lubrizol Bulletin 01 *Polymers for Pharmaceutical Applications* Lubrizol Pharmaceutical Excipient Resource Hub
2. Draganoiu, E., *Properties of mucoadhesive polymers and their use in tablets and other dosage forms*. Tablets and Capsules, 2016. 14 (5) 17-23.
3. Young, S. A., et al., *A novel in-vitro apparatus for evaluating the mucoadhesion of liquid and semi-solid formulations*. Journal of Pharmacy and Pharmacology, 1998. 50(Supplement): 167.
4. US FDA Guidance “Control of Nitrosamine Impurities in Human Drugs” <https://www.fda.gov/regulatory-information/search-fda-guidance-documents/control-nitrosamine-impurities-human-drugs>
5. Lubrizol *Mucoadhesive Polymers in Pharmaceutical Formulations* <https://www.lubrizol.com/-/media/Lubrizol/Health/Literature/Mucoadhesive-Polymers-in-Pharmaceutical-Formulations.pdf>

A CHITOSAN BASED BIOADHESIVE GEL FOR DELIVERY OF COMBINED ANTIMICROBIALS WITH ENHANCED ACTIVITY IN LOCAL TREATMENT OF SKIN INFECTIONS IN HUMANS AND ANIMALS

Ece Türkmen¹, Selin Parmaksız¹, Şeyma Nigiz², Meral Sağıroğlu², Sevda Şenel¹

¹ Department of Pharmaceutical Technology,

² Department of Pharmaceutical Microbiology,
Hacettepe University, Faculty of Pharmacy, Turkey

Correspondence: ssenel@hacettepe.edu.tr

1. INTRODUCTION

Bacterial and fungal skin infections are common both in humans and animals, especially in companion animals such as cats and dogs. Use of systemic antimicrobial drugs has resulted in increased antimicrobial resistance (AMR). Under “One Health” approach, among the strategies to overcome AMR is topical delivery of combination of antimicrobials, which allows enhanced efficacy at lower concentrations of antimicrobials. Chlorhexidine digluconate (CHX) and miconazole nitrate (MN) are the most commonly used drugs for topical treatment [1]. In this study, we have used chitosan, which is a bioadhesive biopolymer exerting antimicrobial activity itself [2] to prepare the gels for delivery of combined antimicrobials, MN and CHX. Antimicrobial activity of the formulations was investigated against *S. pseudintermedius* and *M. pachydermatis*.

2. MATERIALS AND METHODS

2.1. Materials

MN was generously provided by IE Ulagay-Menarini Group (Turkey) and chitosan was generously provided by Koyo Co., LTD Japan. CHX, Tris base, EDTA and Tween 80® were purchased from Sigma-Aldrich (Germany). Tween 20® was purchased from BDH Laboratory Supplies Poole, England and propylene glycol from Merck Millipore (Germany). Mueller-Hinton broth was purchased from Merck (USA). All chemicals used were analytical grade unless otherwise stated.

2.2. Methods

Preparation of formulations

Gel formulations were prepared using base chitosan (degree of deacetylation: 85%, Molecular weight: 235 kDa) at 3% (w/v)

concentration in 2% v/v acetic acid. 2% w/v CHX and 2% w/v MN was incorporated into the gel. 4% Tween 20® and 1% Tween 80® were used as surfactants and 1% propylene glycol, 4% ethanol were added as co-solvents. Tris-EDTA (TE) at 16:1 (w:w) ratio was incorporated into the gels in order to enhance the antimicrobial activity.

Cell viability studies

MTT assay was performed on L929 mouse fibroblast cells to determine cell viability.

Antimicrobial activity

Antimicrobial activity of the gel formulations against *S. pseudintermedius* and *M. pachydermatis* were evaluated using broth microdilution assay according to Clinical and Laboratory Standards Institute (CLSI) guidelines [3,4]. Inoculum for *S. pseudintermedius* was adjusted to 2×10^8 CFU/mL, broth dilution was performed with Mueller-Hinton Broth and incubated at 35°C for 24 h. Inoculum for *M. pachydermatis* was adjusted to 7.5×10^6 CFU/mL and broth dilution was performed with Saboraud dextrose broth (SBD) containing 1% Tween 80, and incubated at 35°C for 72 h.

3. RESULTS AND DISCUSSION

White, homogenous opaque gels were prepared with suitable adhesivity, spreadability and viscosity for topical application on skin as described previously (5). The release profiles of the drugs were also shown to be different, due to the different solubility properties of the drugs, with high released amount of CHX, whilst a lower release with MN, which has low solubility, however it was shown that the drug was accumulated on the surface [5].

3.1. Cell viability

The results obtained for cell viability are shown in Fig. 1. The developed formulation has been

shown to be biocompatible without causing any decrease in cell viability at all concentrations. The viability obtained with the formulation was higher than the CHX which has cytotoxic effect on cells and the CHX-MN combination.

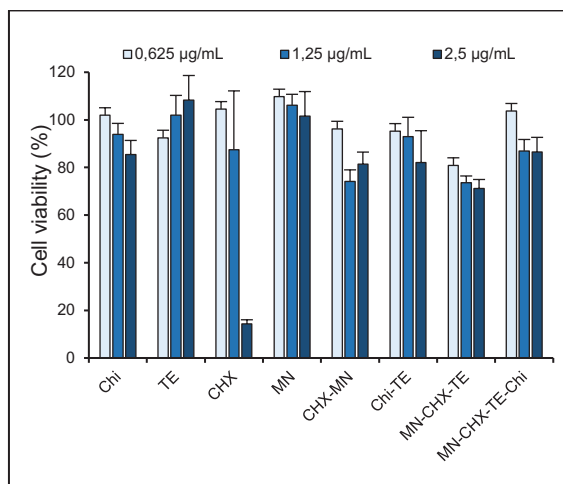


Figure 1. Cell viability of the formulations after 24h (n=5) (CHX and MN at a concentrations of 2.5, 1.25 and 0.625 µg/mL).

3.2. Antimicrobial Activity

MIC values obtained against *S. pseudintermedius* and *M. pachydermatis* are given in Table 1. Combination of CHX and MN was shown to increase the antimicrobial activity against *S. pseudintermedius*. The antimicrobial activity of the formulation was found to be similar to that obtained with the combination of CHX and MN. Antimicrobial activity against *M. pachydermatis* was found to be enhanced significantly with the developed formulation when compared to that obtained with combination of CHX and MN. Further enhancement in microbial activity was observed with incorporation of Tris-EDTA (p<0.05).

Table 1. MIC values against *S.pseudintermedius* and *M. pachydermatis*

	MIC (µg/mL)	
	<i>S. pseudintermedius</i>	<i>M. pachydermatis</i>
CHX	0.33	9.77
MN	0.33	2.44
CHX-MN	0.20	2.44
TE	1000: 62.5	>1000:62.5*
CHX-MN-TE	0.39	0.31
Chi (3%)	7.32	14.65
Chi-CHX	0.24	4.89
Chi-CHX-MN	0.20	2.44
Chi-MN-TE	0.98	2.03
Chi-CHX-MN-TE	0.20	1.02

* no inhibition was observed

4. CONCLUSION

In this study, we have demonstrated that the developed bioadhesive gel formulation is biocompatible and provides enhanced antimicrobial activity against *S. pseudintermedius* and *M. pachydermatis*, in addition to other pathogens tested previously, *S. aureus* and *M. canis* [5] and can be used safely for the topical treatment of skin infections in humans and animals. Besides its safety and enhanced activity, due to its bioadhesive and drug release properties, providing slow release as well as accumulation on the skin, it will be possible to decrease the frequency of application, thereby reduce the amount of the antimicrobials used for treatment, thereby resulting in a significant contribution to the combat against AMR.

5. REFERENCES

1. Mueller, R., S., et al. Vet Dermatol. 2012;23(4):330-e62.
2. Şenel S. React Funct Polymers, 2020;147:104452.
3. CLSI. Reference Method for Broth Dilution Antifungal Susceptibility Testing of Yeasts; Approved Standard, CLSI Document M27-A3, 3rd ed. 2008:PA, USA.
4. CLSI, Reference Method for Broth Dilution Antifungal Susceptibility Testing Filamentous Fungi, Approved Standard, CLSI document M38-A2. 2nd ed. 2008:PA, USA.
5. Türkmen, E., et al., *Development of a bioadhesive system for combined antimicrobial delivery for topical treatment of skin infections*. 20th IPTS, 21-23 February 2022, Ankara-Turkey.

ACKNOWLEDGEMENT

This study was supported by Hacettepe University Scientific Research Coordination Unit (Project number: THD-2020-18516). Authors are also thankful to Prof. Dr. Barış Sareyyüpoğlu, Veterinary Faculty, Ankara University for clinical isolate of *S. pseudintermedius* and Assoc. Prof. Dr. Kemal Metiner, Veterinary Faculty of Istanbul University for clinical isolate of *M. pachydermatis*.

TRANSCRIPTOME ANALYSIS REVEALS INVOLVEMENT OF THIOPURINE S-METHYLTRANSFERASE IN OXIDATION-REDUCTION PROCESSES

Alenka Šmid¹, Miha Štajdohar², Dunja Urbančič¹, Nataša Karas Kuželički¹, Riin Tamm³, Andres Metspalu³, Irena Mlinarič-Raščan¹

¹*Department of Clinical Biochemistry, University of Ljubljana, Faculty of Pharmacy, Slovenia,*

²*Genialis d.o.o., Slovenia,*

³*Estonian Genome Center, University of Tartu, Estonia*

1. INTRODUCTION

Thiopurine S-methyltransferase (TPMT) is involved in deactivation of thiopurine drugs which are used in the treatment of acute lymphoblastic leukemia, inflammatory bowel disease, and some other autoimmune disorders and represents a major determinant of thiopurine-related toxicities. Despite its well-known importance in thiopurine metabolism, the understanding of its endogenous role is lacking. The aim of the present study was to gain insight into the molecular processes involving TPMT by applying a matrix factorization-based data fusion approach to analyse blood-based whole-genome expression data from healthy volunteers combined with gene ontologies and protein-protein interactions databases.

2. MATERIALS AND METHODS

2.1. Subjects and sample collection

In this study, which was approved by the Research Ethics Committee of the University of Tartu, Estonia, we analysed blood samples of 1017 volunteers, donors to the Estonian Biobank. Three aliquots of blood were used: one for DNA extraction, one which was drawn into Tempus Blood RNA Tube for RNA extraction, and one for hemolysate preparation in which TPMT activity was measured. The demographic data of the donors (including age, and gender) were extracted from the Biobank database. The cohort consisted of 50.2% males and 49.8% females, with a mean age of 37.8 years.

2.2. TPMT genotyping, RNA analysis and TPMT activity measurement

Genotyping of the TPMT activity-deficient TPMT*3B (rs1800460), *3C (rs1142345) and *2 (rs1800462) alleles was carried out by TaqMan Genotyping Assays. Ambion

TotalPrep RNA Amplification Kit was used to transcribe 200 ng RNA which was then hybridized to the Illumina HT12v3 arrays according to the manufactures protocols. TPMT activity was measured in RBC hemolysates using the HPLC method as previously described (1).

2.3. Data collections and data fusion

We modelled gene associations with 6 data sets that describe the involvement of TPMT in intracellular processes by using a data fusion approach with penalized matrix tri-factorization (2). The model considered 3 types of objects: genes, GO terms, and subjects, on which six data sets (matrices) were built, each relating a pair of object types. Protein-protein interactions were included as constraints between corresponding genes. Proteins from the STRING database were used to build the constraint matrix Θ_2 . Degrees of interactions were normalized to values between 0 and -1. In case of no known interaction, the value was 0. Hierarchical structure of GO (Θ_3) was included by reasoning over *has_part*, *part_of* and *is_a* relations in the GO graph. A constraint between a pair of GO terms was set to $-0.2 \times \text{hops}$, where hops was the length of the shortest path between the two GO terms.

3. RESULTS AND DISCUSSION

3.1. TPMT gene association network built by data fusion approach

The model of TPMT gene association network was built for all subjects independently of their TPMT genotype-phenotype status. The network includes genes in the nodes that are connected based on the distance function, defined as the average Euclidean distance between genes in the reconstructed relation matrices $\hat{R}_{1,3}$ and $\hat{R}_{3,9}$. The part of the gene association network closest to TPMT is presented in Figure 1.

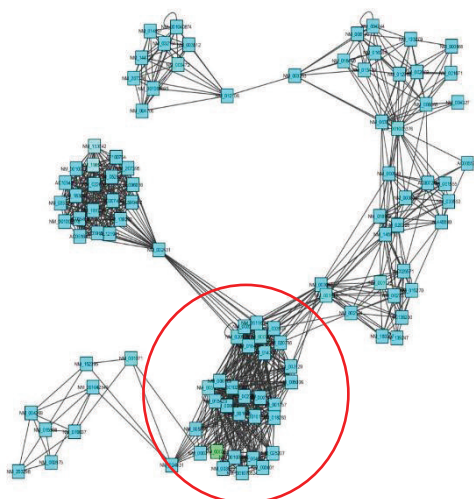


Figure 1. Part of a gene network showing genes clustered around TPMT constructed from the model for all subjects. Nodes represent genes and arches relations between genes. TPMT is represented by a green node. The genes in the red circle were analysed by DAVID functional annotation tool.

3.2. Analysis of the gene network suggests that TPMT is closely related to oxidation-reduction processes

Genes most similar to TPMT based on calculated distances (Figure 1, encircled red)—which among others contained PAICS, PPAT, GMPS and MTHFR—were analysed with DAVID’s functional annotation clustering tool.

Table 1. Functional Annotation Clustering of TPMT gene network using DAVID tools (the first top cluster).

Cluster 1	Enrichment Score: 3.8923084803846 044			
Category	Term	#	P	B
SP_PIR_KEYW ORDS	oxidoreductase	9	1.26 E-06	1.30 E-04
GOTERM_BP_F AT	GO:0055114~oxi dation reduction	9	8.90 E-06	5.11 E-04
SP_PIR_KEYW ORDS	nadp	5	8.44 E-05	0.00 1738
GOTERM_CC_F AT	GO:0000267~cell fraction	4	0.28 4677	0.66 3387
<i>Ndufb4, Cbr1, Mthfr, Gmpr2, Cyp51a1, Sqlc, Idh1, Cyp26a1, Ndufs1</i>				

Several enriched annotation clusters were identified, among which the most prominent one is related to oxidation-reduction processes (presented in Table 1). The cluster contains genes that 1) form the part of the mitochondrial

membrane respiratory chain NADH dehydrogenase (NDUFS1 and NDUFB4), 2) have a significant role in cytoplasmic NADPH production (IDH1), or 3) utilise NADPH as the cofactor in their enzymatic reactions (other genes). NADPH is a critical molecule for the maintenance of antioxidant cell capacity through the regeneration of reduced pools of glutathione in the transsulfuration pathway. This pathway is tightly connected with and dependant on one-carbon metabolism and methylation reactions. TPMT as methyltransferase utilizes SAM as a methyl donor and directly determines the methylation capacity of cells, which could in turn influence the redox capacity modulated by transsulfuration pathway.

4. CONCLUSION

In this study we used a matrix factorization-based data fusion approach in which we integrated whole genome gene expression data, gene ontology and protein–protein interaction data and applied it to investigate TPMT-related gene network and gain new insight into its biological role. The constructed model of TPMT-related gene network revealed that TPMT is closely related to genes involved in oxidation reduction processes and may thus play an important role in regulating cell redox capacity.

5. REFERENCES

1. Milek, M., et al. *Post-translational stabilization of thiopurine S-methyltransferase by S-adenosyl-L-methionine reveals regulation of TPMT*1 and *3C allozymes.* Biochemical Pharmacology, 2012. 83, 969-76
2. Zitnik, M. & Zupan, B. *Matrix factorization-based data fusion for gene function prediction in baker's yeast and slime mold.* Pacific Symposium on Biocomputing, 2014. 400-11.

ACKNOWLEDGMENT

This work was supported by the Slovenian Research Agency grant no. J3-3615 and by the Estonian Research Council (Grant IUT20-60) and Estonian Science Foundation (ETF9293).

MICRODIALYSIS AND NANOFILTRATION ALLOW TO DISTINGUISH MOLECULARLY DISSOLVED FROM COLLOID-ASSOCIATED DRUG CONCENTRATIONS DURING BIOMIMETIC DISSOLUTION TESTING OF SUPERSATURATING FORMULATIONS

Florentin Lukas Holzem ^a, Jeannine Petrig Schaffland ^c, Martin Brandl ^a, Annette Bauer- Brandl ^a, Cordula Stillhart ^b

^a Department of Physics, Chemistry & Pharmacy, University of Southern Denmark, Campusvej 55, 5230 Odense, Denmark

^b Pharmaceutical R&D, Formulation & Process Sciences, F. Hoffmann-La Roche Ltd., 4070 Basel, Switzerland

^c Roche Pharmaceutical Research & Early Development, Pre-Clinical CMC, Roche Innovation Center Basel, F. Hoffmann-La Roche Ltd., 4070 Basel, Switzerland

1. INTRODUCTION

Many new drug entities are poorly water-soluble and thus require solubility-enhancing formulations to ensure sufficient bioavailability. On the other hand, it is more and more accepted that not all “dissolved” states of a drug contribute equally to enhanced absorption, i.e. an increase in apparent solubility does not necessarily go in parallel with an increase in molecularly dissolved drug, the latter being regarded as the key driving force for absorption.

Our study aimed to provide time-resolved information on the dissolution, supersaturation, and precipitation behavior of molecularly dissolved drug as released from an amorphous solid dispersion and a surfactant-containing crystalline suspension of Posaconazole (PCZ), a weakly basic and poorly water-soluble drug. Thereby, we aimed to gain a deeper mechanistic understanding of enabling formulation principles and possibly establish a dynamic biopharmaceutical assessment tool for molecularly dissolved drug released from enabling formulations.

2. MATERIALS AND METHODS

2.1. Materials

For details on chemicals and media, pls check the published article

2.2. Methods

A two-staged dissolution test, with media transition from simulated gastric fluid (SGF) to fasted state simulated intestinal fluid (FaSSIF),

was performed with three alternative sampling approaches in parallel: the classical bench centrifugation approach was used to assess total dissolved concentrations, while a nanofiltration method and a microdialysis setup were tested for their ability to discriminate molecularly and colloid-associated drug concentrations over time. For comparison, a single-stage dissolution setup was performed, where a marketed PCZ suspension was dispersed in biomimetic media with increasing amounts of solubilizing agents to understand their effect on the concentration of molecularly dissolved drug.

3. RESULTS AND DISCUSSION

It was demonstrated that the microdialysis setup allowed to follow the molecularly dissolved drug concentration in a time-resolved manner during the single- and two-stage dissolution tests with marginal delays.

Interestingly, the PCZ concentrations measured by the nanofiltration approach differed from both, the molecularly dissolved (assessed by microdialysis) and apparently dissolved (assessed by centrifuge) PCZ concentrations, indicating that nanofiltration may allow to differentiate between different colloid-associated (apparently) dissolved drug species.

Moreover, it was shown that the release of the molecularly dissolved drug from an amorphous solid dispersion did not correlate at all with the results obtained by the centrifugation method:

While this conventional sampling revealed a classical spring and parachute concentration /

OP30

time-profile with a high degree of (apparent) supersaturation, the concentration of molecularly dissolved drug (assessed by the microdialysis setup) indicated an initial short decline of PCZ concentration, followed by a prolonged (moderate) molecular supersaturation. This observation may give rise to a re-thinking of the current mechanistic understanding of how amorphous solid dispersions enhance oral bioavailability.

4. CONCLUSION

In essence, the current study provides data which indicate a benefit of both the microdialysis sampling and nanofiltration approaches for the in vitro biopharmaceutical assessment of enabling drug formulations.

5. REFERENCES

The abstract is taken from the following publication:

Holzem, F.L., et al., *Microdialysis and nanofiltration allow to distinguish molecularly dissolved from colloid-associated drug concentrations during biomimetic dissolution testing of supersaturating formulations* European Journal of Pharmaceutical Sciences, 2022. 174: article 106166

For further references pls check the published article's reference list.

ACKNOWLEDGMENT

This project has received funding from the European Union's Horizon 2020 research and innovation program under the Marie Skłodowska-Curie grant agreement No 955756 ITN InPharma).

Furthermore, the authors are grateful for fruitful discussions enabled by funding from European Union's Horizon 2020 framework program (COST action UNGAP CA162050) and Nordforsk program Nordic University Hub (project #85352).

MEMANTINE LOADED PLGA NANOPARTICLES FOR ALZHEIMER'S DISEASE

Gizem Tezel^{1,2}, Tuba Reçber³, Sıla Ulutürk⁴, Selin Seda Timur¹, Emirhan Nemitlu³, Sıla Gülbağ Pınar² Güneş Esendağlı⁴, Hakan Eroğlu¹

¹ Department of Pharmaceutical Technology, Faculty of Pharmacy, Hacettepe University, Turkey

² Department of Pharmaceutical Technology, Faculty of Pharmacy, Süleyman Demirel University, Turkey

³ Department of Analytical Chemistry, Faculty of Pharmacy, Hacettepe University, Turkey

⁴ Department of Basic Oncology, Hacettepe University Cancer Institute, Turkey

1. INTRODUCTION

Alzheimer disease (AD) is one of the most common neurodegenerative diseases in the world. It is a neurodegenerative disease of the central nervous system and is classified under dementia. According to a predictive statistics 6.2 million Americans having age of 65 and older are living with AD today [1]. The major boundary for the treatment of AD is the Blood Brain Barrier. Tight junctions of the BBB, limit the passage of active pharmaceutical ingredients from systemic circulation to the brain. Nanotechnology brings new insights for access to the BBB with localized and active drug delivery.

Memantine HCl (Mem HCl) is a N-methyl D-aspartate (NMDA) receptor antagonist which is used for the non-competitive inhibition of NMDA receptors and used to provide neuroprotection [2]. Chemical structure of Memantine does not contain chromophore group. For this reason, analytical method development for quantification of Mem HCl by UV detection is quite difficult [3].

In the present study Mem HCl loaded PLGA nanoparticles were prepared and characterized. LC-MS method for Mem HCl quantization developed and validated.

2. MATERIALS AND METHODS

2.1. Materials

PLGA (50:50, 24.000-38.000MA) and TPGS (D- α -Tocopheryl polyethylene glycol succinate) were purchased from Sigma Aldrich. Mem HCl obtained as a generous gift from Ali Raif Pharmaceuticals (Turkey) and all the other chemicals used were analytical grade.

2.2. Preparation of the Mem HCl loaded Nanoparticles

Double emulsion method was used for the preparation of Mem HCl loaded PLGA nanoparticles. For the formation of organic phase (o) a predetermined amount of PLGA was dissolved in ethyl acetate. For the formation of aqueous phase (w₁) Mem HCl was dissolved in deionised water containing PVA or TPGS in different concentrations. w₁ phase was poured into oil phase dropwise under magnetic stirring and for primary emulsion (w₁/o) formation and sonication energy was applied. For the second emulsification step deionised water containing PVA or TPGS (w₂) was dispersed in w₁/o emulsion and sonication was applied again to form w₁/o/w₂ secondary emulsion. After solvent evaporation NPs were centrifugated at 13.750 RCF for 30 minutes.

2.3. In-Vitro Drug Release

In-vitro drug release of Mem HCl loaded NPs was studied in a dialysis bag technique under sink conditions for 72 h. Firstly, a volume of 5 ml of formulation was placed directly into a dialysis bag (cellulose membrane, 12–14 kDa, size 25mm 100ft 16 mm diameter, Spectra por/4) and each bag was placed in 100 ml of isotonic phosphate-buffered saline (PBS), pH 7.4, at 37 °C. The samples were analysed by LC-MS.

2.4. LC-ESI-MS/MS Method

The LC-ESI-MS/MS system (Shimadzu, Japan) consists of an LC system (Shimadzu LC-20AXR) combined with a triple quadrupole tandem mass spectrometer (Shimadzu 8030 MS/MS). Chromatographic analysis parameters were as follows: At 40°C, C18 column (GL Sciences, 50 x 3.0 mm, 2.1 μ m), gradient elution method used which has two phases %0.1 Formic acid in water (phase A) and %0.1 Formic acid in Methanol (phase B). 0.4 ml/min flow rate was used, injection volume was set as 1 μ L. Total analysis time was 5 minutes. MRM mode was used for MS analysis.

OP31

2.5. In-vitro Cell Culture Studies

Cytotoxicity test of Mem HCl carried out with MTT test in HEK293T cells. After that Mem HCl loaded nanosystems and empty nanosystems applied to same cells. Mem HCl applied in 300 μ M, 150 μ M, 75 μ M, 37,5 μ M, 18,75 μ M, 9,3 μ M concentrations to HEK213T.

3. RESULTS AND DISCUSSION

3.1. Optimization of NP Parameters

Mean average particle size (Z-AVE) and polydispersity index (PI) of NPs were determined by photon correlation spectroscopy (PCS) using a Zeta Sizer Nano ZS (Malvern). Studies showed that the particle size increased with increasing polymer concentration. But this increase can be controlled with optimizing sonication parameters. Particle size decreased with increasing surfactant concentration. Lastly with the use of %0.2 TPGS, encapsulation efficacy (EE) was increased. F11 showed highest EE which was %55. Formulation parameters of Mem HCl loaded PLGA nanoparticles shown in Table 1.

Table 1. Formulation parameters of Mem HCl loaded PLGA nanoparticles

	Memantine HCl (C)	Polymer (C)	Phase ratios (w/o/w)	PVA (%)	Particle Size (nm)	PDI	Zeta Pot.
F1	9 mg/ml	10mg/ml	1/0,2/1	0.75	322.2	0.314	-1.16
F2	9 mg/ml	10mg/ml	1/0,2/1	1	341.8	0.334	-1.68
F3	9 mg/ml	10mg/ml	1/0,2/1	2	325.6	0.175	-1.22
F4	9 mg/ml	10mg/ml	1/0,2/2,4	2	596.4	0.369	-1.13
F5	9 mg/ml	10mg/ml	1/0,3/1	2	1052	0.930	-1.54
F6	3 mg/ml	10mg/ml	2/1/2	2	196.4	0.310	-0.47
F6.2	3 mg/ml	10mg/ml	3/1/2	2	100.0	0.135	-1.07
F6.3	3 mg/ml	10mg/ml	4/1/2	2	102.0	0.115	-1.21
F6.4	3 mg/ml	15mg/ml	2/1/2	2	185.8	0.274	-1.48
F6.5	3 mg/ml	5 mg/ml	2/1/2	2	221.2	0.254	-1.09
F6.6	3 mg/ml	5 mg/ml	2/1/2	1	544.8	0.736	-1.62
F6.7	3 mg/ml	10mg/ml	2/1/2	1	244.0	0.291	-1.22
F6.8	3 mg/ml	15mg/ml	2/1/2	1	199.0	0.240	-1.07
F7	3 mg/ml	15mg/ml	2/1/2	1	170.7	0.217	-1.36
F8	3 mg/ml	15mg/ml	2/1/2	1	202.5	0.254	-1.34
F9	10 mg/ml	15mg/ml	0.5/1/2	1	200.6	0.260	-1.23
F10	10 mg/ml	15mg/ml	1/1/2	1	211.6	0.260	-1.28
F11	10 mg/ml	15mg/ml	2/1/2	TPGS	206.6	0.243	-2.93
F12	10 mg/ml	15mg/ml (acid term.)	2/1/2	1 (w) 2(w)	203.9	0.234	-1.04

3.2. In vitro Drug Release

The release profile of the Mem HCl loaded NP (F11) was presented in Figure 1.

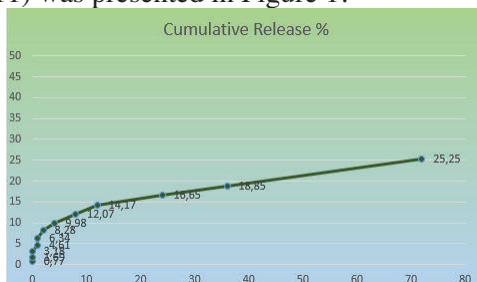


Figure 1. In vitro release profile of Mem HCl loaded NP (F11)

3.3. Analytical Method Validation

Analytical resolution of Mem HCl peak was presented in Figure 2.

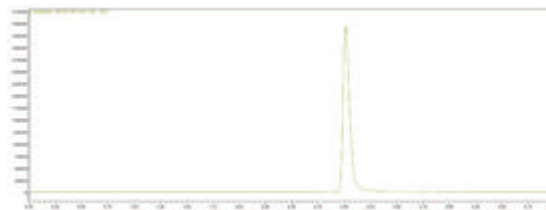


Figure 2. Memantine HCl resolution in LC-MS

3.4. In-vitro Cell Culture Studies

Mem HCl MTT test results in HEK293 were showed in Figure 2.

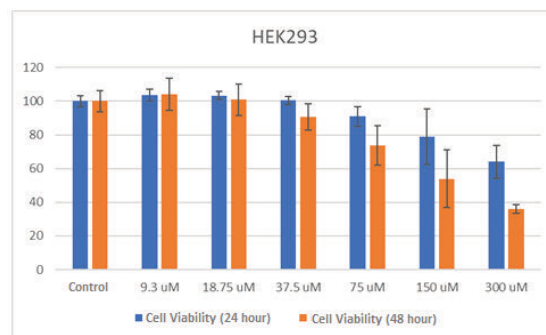


Figure 3. Mem HCl MTT test results in HEK293

4. CONCLUSION

In this study sustained release of encapsulated Mem HCl was demonstrated by the in-vitro release study as a new drug delivery system for AD cytotoxicity of Mem HCl controlled with MTT test. Also new analytical method was successfully validated for Mem HCl.

5. REFERENCES

- 2021 Alzheimer's disease facts and figures. The Journal of Alzheimer's Association, 2021. 17:327-406.
- Tezel G., Timur S.S., et.al., A Snapshot on the Current Status of Alzheimer's Disease, Treatment Perspectives, in-Vitro and in-Vivo Research Studies and Future Opportunities. Chemical Pharmaceutical Bulletin, 2019. 67, 1030-1041
- Sulochana P.S., Sharma K., et.al., Review of the validated HPLC and LC-MS/MS methods for determination of drugs used in clinical practice for Alzheimer's disease. Biomedical Chromatography ,2014. 28: 1431-1490.

AN ASSESSMENTS OF TITANATE NANOTUBES PERFORMANCE AS PROTEIN CARRIERS

Tamás Sovány¹, Yasmin Ranjous¹, Natalie Deiringer², Zoltán Kónya¹, Géza Regdon jr.¹, Wolfgang Friess²

¹*Institute of Pharmaceutical Technology and Regulatory Affairs, University of Szeged, Hungary*

²*Chair of Pharmaceutical Technology and Biopharmaceutics, Ludwig Maximilians University, Germany*

1. INTRODUCTION

Biopharmaceuticals are of emerging interest for the treatment of various diseases such as cancer or autoimmune diseases due to their potent therapeutic ability. However, proteins have certain limitations such as poor pharmacokinetics, potential immunogenicity, lack of stability, short circulation half-life, which necessitates the use of proper delivery systems. Knowledge on potential protein-carrier interactions and their effect on protein conformation is necessary for the selection of suitable systems [1].

Titanate nanotubes (TNTs) usually have been utilized in immobilized form to modify the surface of titanium implants to improve biocompatibility, but it is also possible to use them as drug-delivery systems [19, 20]. TNTs may enhance the wettability and surface area of titanium, leading to a higher protein adsorption [21], which indicates their potential as possible delivery system for biopharmaceuticals. The aim of present study was to test the suitability of hydrothermally synthesized free TNTs as possible carriers by evaluating their protein binding capacity. The adsorption of proteins on naïve H-TNTs and Magnesium stearate (MgSt) functionalized TNTs under different experimental conditions was investigated.

2. MATERIALS AND METHODS

2.1. Materials

H-TNTs and MgSt-TNTs were prepared at the Department of Applied and Environmental Chemistry, University of Szeged following the method of Ranjous et al [23], where the currently tested samples are referred as H-TNT and MgSt-TNT 47, respectively. Lysozyme (Ovobest Eiprodukte GmbH & Co. KG, Neuenkirchen-Vörden, Germany), served as model protein during adsorption studies.

2.2. Methods

Zeta potential of H-TNTs and MgSt-TNTs was measured with Nano ZS Zetasizer (Malvern Instruments, Herrenberg, Germany), using a 4 mW He-Ne laser at 633 nm, in a filtered aqueous solution of 10 mM NaCl at 25°C. The pH was adjusted using NaOH or HCl.

Autosorb 1 (Quantachrome, Odelzhausen, Germany) apparatus was used to measure the specific surface area of H-TNTs and MgSt-TNTs using nitrogen gas adsorption and Brunauer-Emmet-Teller isotherm analysis.

To study the protein adsorption TNTs were dispersed in respective formulation buffer in an ultrasonic bath for 15 mins. After that, lysozyme stock solution was added to the Eppendorf tube which was placed in an overhead shaker for 120 min. The samples were then centrifuged for 10 min at 10,000 rpm to separate the free lysozyme in the supernatant from the TNT-Lysozyme complex in the sediment.

Lysozyme in the supernatant was quantified to derive the amount of adsorbed protein on TNTs (Calbiochem non-interfering CA protein assay; Merck, Darmstadt, Germany).

The protein conformation was analysed by FT-IR (Bruker Optik GmbH, Ettlingen, Germany), using transmission mode, 4 cm⁻¹ spatial resolution and scan number of 256.

Lysozyme activity was measured by the enzymatic assay from Sigma-Aldrich. *Micrococcus lysodeikticus* bacterial suspension was prepared by using 10 mM pH=6.24 potassium phosphate buffer. 100 µl of TNT-bonded lysozyme sample prepared under different conditions was added to 2500 µl bacterial suspension and decrease in absorbance was measured against blank of buffer by UV-

VIS spectrophotometry. TNT-free lysozyme stock solution was used as control.

3. RESULTS AND DISCUSSION

Despite of the near identical size, a substantially different was detected with 217 m²/g vs. 100 m²/g surface area in case of H-TNTs and MgSt-TNTs, respectively. Interestingly, despite of the lower surface area the MgSt functionalized samples bound almost double the amount of lysozyme per m² as compared to H-TNTs (4,8 mg vs. 2.2 mg, respectively) (Fig. 1), which may be due to the increased surface hydrophobicity of the functionalized samples which enables stronger binding and offers proper binding sites for both polar and apolar regions of the protein The absorbed protein is generally stable despite the low pH or high salt concentrations necessary to facilitate protein-carrier interactions and increase the adsorbed amounts.

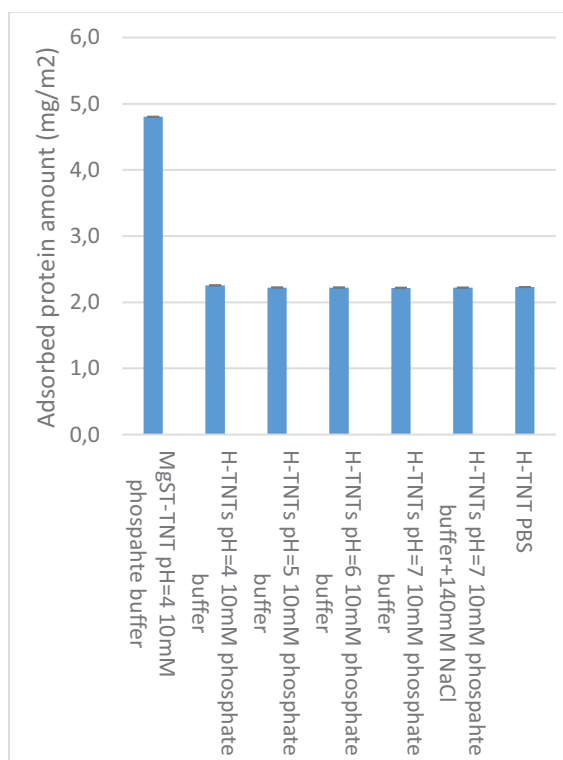


Figure 1. Amount of absorbed lysozyme per m² TNT from different buffers

FT-IR results confirmed that binding may induce moderate, but reversible changes in protein structure, while activity assays revealed that activity was better preserved in case of higher bonded amounts.

Table 1. Remaining enzymatic activity of various samples

HTNTs pH=4	64.00%
HTNTs pH=5	52.25%
HTNTs pH=6	57.85%
HTNTs pH=7	67.49%
HTNTs pH=7 +140mm NaCl	84.21%
HTNTs/ PBS	78.42%
MgSt-TNTs/ PBS	87.13%

4. CONCLUSION

It may be concluded that TNTs may effectively bind proteins and may stabilize their conformation even under highly denaturing conditions and therefore may help to preserve the activity of biopharmaceuticals.

5. REFERENCES

- Dimitrov, D.S., *Therapeutic proteins*. Therapeutic Proteins, 2012. 899: 1-26.
- Liu, W., et al. *Synthesis of TiO₂ nanotubes with ZnO nanoparticles to achieve antibacterial properties and stem cell compatibility*. Nanoscale, 2014. 6(15): 9050-9062.
- Peng, L., et al. *Long-term small molecule and protein elution from TiO₂ nanotubes*. Nano Letters, 2009. 9(5): 1932-1936.
- Kulkarni, M., et al. *Binding of plasma proteins to titanium dioxide nanotubes with different diameters*. International Journal of Nanomedicine, 2015. 10: 1359.
- Ranjous, Y., et al. *Evaluation of the permeability and in vitro cytotoxicity of functionalized titanate nanotubes on Caco-2 cell line*. Acta Pharmaceutica Hungarica, 2021. 91(1): 31-39.

ACKNOWLEDGMENT

Project no. TKP2021-EGA-32 has been implemented with the support provided by the Ministry of Innovation and Technology of Hungary from the National Research, Development and Innovation Fund, financed under the TKP2021-EGA funding scheme.

IMMUNOMODULATORY PROPERTIES OF SIMVASTATIN EMBEDDED IN LIPOSOMES AND ELECTROSPUN NANOFIBERS FOR WOUND HEALING

Anže Zidar¹, Luca Casula², Julijana Kristl¹, Matjaž Jeras¹, Špela Zupancič¹

¹University of Ljubljana, Faculty of Pharmacy, Aškerčeva cesta 7, 1000 Ljubljana, Slovenia

²Department of Life and Environmental Sciences, University of Cagliari, Via Ospedale 72, 09124 Cagliari, Italy

1. INTRODUCTION

Wound can be described as a discontinuity of the normal anatomic structure of the tissue due to an exogenous laceration. Although the skin exhibits rapid self-regenerative capacity, healing might fail, due to repeated infection, dysfunctional immune function and other factors, which lead to formation of chronic wounds [1].

Recent studies have shown the remarkable effects of simvastatin (SIM) as immunomodulatory and antibacterial agent in chronic wound treatment. Its immunomodulatory activity is mostly linked to interference with the recruitment and activation of peripheral blood mononuclear cells (PBMC) through suppression of their markers and cytokine expression. SIM, due to its antimicrobial activity also contributes to successful treatment of infected skin wounds [2].

For efficient delivery of APIs to wounds many delivery systems have been studied and nano delivery systems showed great promise, especially electrospun polymeric nanofibers with intrinsic wound healing and skin regeneration stimulating capacities. Nanofibers mimic morphology of the extracellular matrix, which combined with their mechanical performance, physical properties, and flexibility, enables structural support, promotes cell growth, and proliferation [3].

Due to low aqueous solubility and stability of SIM, the drug was first incorporated in liposomes with butylated hydroxyanisole (BHA) to increase its stability. We expected that the combination of two nanocarrier technologies would provide excellent biocompatibility, controlled release, and mechanical properties of delivery systems.

Therefore, the aim of this work was to design and evaluate the safety and immunomodulatory efficacy of SIM-loaded liposomes embedded in

a nanofibrous scaffold as a delivery system for wound healing.

2. EXPERIMENTAL METHODS

2.1. Delivery system preparation

Firstly, phosphatidylcholine, SIM and BHA were hydrated in water and immediately sonicated using a high intensity ultrasonic processor (Cole-Parmer, USA) to obtain liposomes. Then the polymeric solutions were prepared by dissolving sodium alginate and polyethylene oxide (PEO) in water or liposomal dispersions. After 10 h these solutions were transferred in a plastic syringe and fixed into the electrospinning device (Fluidnatek LE100; BioInicia SL, Valencia, Spain). The electrospinning was carried out in a climatic chamber enabling controlled process parameters.

2.3. In vitro cellular tests

Different formulations without and with SIM were tested on cells to determine the effect of components and formulations.

The cytotoxicity of formulations was tested on human NCTC 2544 keratinocyte cell line cells. Keratinocytes were seeded in a 96-well flat bottom tissue culture plate in DMEM medium and incubated for 12 h. After that, tested formulations were added with 0,1 % of dimethyl sulfoxide (DMSO) to increase the solubility of SIM and 20 % of fetal bovine serum (FBS) for keratinocyte growth. Formulations contained different SIM concentrations, i.e. 0, 0.4, 4, 40 and 400 $\mu\text{g/ml}$. Cultures were incubated for 72 h and then MTS assay was performed, with absorbances being measured at 490 nm, using a microplate reader (Agilent BioTek Synergy H4, CA, USA).

Immunomodulatory effects were assessed as T lymphocyte (main cells in PBMCs) proliferation inhibition in a homeostatic and simulated hyper-inflamed microenvironments, following the addition of phytohemagglutinin L (PHA-L). PBMCs were suspended in

OP33

BioTarget® medium and transferred in 96 - U well microtiter plates, treated with different formulations and cultured for 72 h at 37 °C in a 5% CO₂ incubator. Then the MTS assay was performed as described above.

3. RESULTS AND DISCUSSION

3.1. Effect of formulations on NCTC 2544 keratinocyte cell line cells viability

We tested three groups of formulations: placebo, liposomal SIM and nanofiber formulations with liposomes and SIM. Figure 1. presents the dependence of keratinocyte viability on SIM concentration in each formulation tested. We found that nanofiber formulations had a slower release of liposomes and SIM in comparison to liposomes with SIM. As seen in Fig. 1. liposomal formulations showed no cytotoxicity up to 4 µg/ml of SIM, whereas nanofiber formulations were not cytotoxic up to 40 µg/ml.

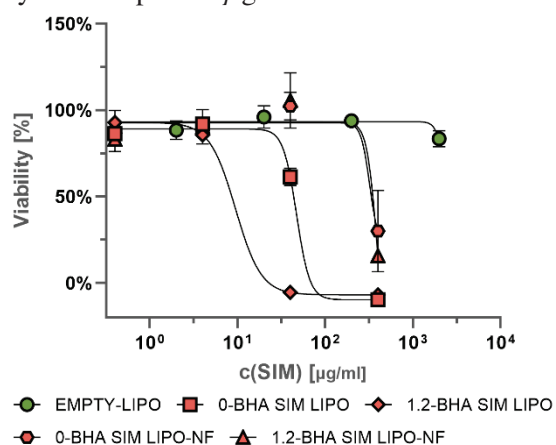


Figure 1. Effect of different formulations on NCTC 2544 cells viability. LIPO – liposomes, NF – nanofibers.

3.2. Immunomodulation of formulations

Immunomodulation of SIM containing formulations was quantified by proliferation inhibition of lymphocytes T compared to controls (without SIM). SIM concentration of 0.4 µg/ml was tested on lymphocytes. We show in Figure 2 that the liposomal formulations inhibited homeostatic PBMC proliferation, while nanofibers did not. This is better for the safety profile, as the inhibition of basal cell functions can lead to adverse effects. On the other hand, all formulations containing SIM significantly inhibited PHA-L induced proliferation of T cells (results not shown), thereby confirming their immunomodulatory properties. The immunomodulation in inflamed environment is especially important for

reducing the harmful effects of over-activated immune system.

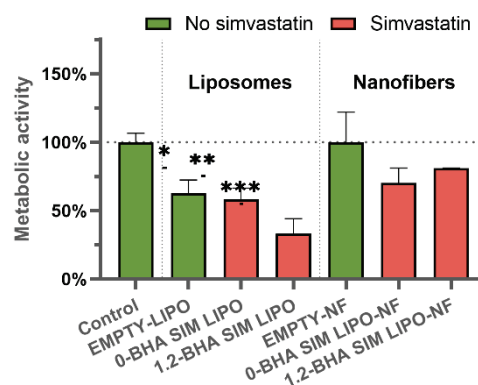


Figure 2. PBMC metabolic activity assessed by MTS test in a non-inflammatory environment.

4. CONCLUSION

Nanofiber formulations have superior safety and efficacy properties in comparison to liposomal formulations containing SIM. They exert lower cytotoxicity on NCTC 2544 cells, do not significantly influence PBMC functions in a non-inflammatory environment and still hamper inflammation in a PHA-L induced inflammatory environment. The difference between liposomal and nanofiber formulations can be ascribed to multiple reasons: slower release of liposomes from nanofibers, different size and size distribution of liposomes after resuspension of nanofibers and/or the effect of nanofibers and polymers on the cells.

Considering the results of all performed tests, nanofiber formulations proved to be an excellent option for incorporating SIM for wound healing applications.

5. REFERENCES

1. Raziyeva K, et al. Immunology of Acute and Chronic Wound Healing. *Biomolecules*. 2021 May 8;11(5).
2. Rego AC, et al. Simvastatin improves the healing of infected skin wounds of rats. *Acta Cir Bras*. 2007 Mar-Apr;22 Suppl 1:57-63.
3. Zidar A, et al. Treatment challenges and delivery systems in immunomodulation and probiotic therapies for periodontitis. *Expert Opinion on Drug Delivery*. 2021 2021/09/02;18(9):1229-1244.

THE EFFECT OF THE STRUCTURE – THE EVALUATION OF THE DISINTEGRATION AND THE DISSOLUTION PROCESSES OF 3D PRINTED ORODISPERSIBLE TABLETS

**Jolanta Pyteraf¹, Witold Jamróz¹, Mateusz Kurek¹, Adam Paclawski¹, Urszula Bąk¹,
and Renata Jachowicz¹**

¹ *Department of Pharmaceutical Technology and Biopharmaceutics, Jagiellonian University Medical College,
Medyczna 9, 30-688 Krakow, Poland; jolanta.pyteraf@uj.edu.pl (J.P.)*

1. INTRODUCTION

3D printing technologies are considered as a potential way for the production of small batches of customized dosage forms [1]. Printlets' structure can be precisely designed and accurately reproduced during printing, which creates a great opportunity to fabricate a dosage form characterized by the targeted quality profile.

The aim of the presented research was to analyze the process of disintegration and drug dissolution from orodispersible tablets (ODTs) printed with the fused deposition modeling (FDM) method.

2. MATERIALS AND METHODS

2.1. Materials

Fluconazole (99.5%, Henan Tianfu Chemical Co. Ltd., China) served as a model active ingredient (API), while poly(vinyl alcohol) (Parateck[®] MXP, Merck KGaA, Germany) was used as a filament-forming polymer.

2.2. Hot-Melt Extrusion

Filament composed of 40% of FLU and 60% of PVA was prepared using a 12-mm corotating twin-screw, hot-melt extruder (RES-2P/12A Explorer, Zamak Mercator[®], Poland) equipped with a 1.75 mm nozzle at 147°C.

2.3. 3D printing of ODTs

The tablets were designed using Blender[®] 2.90 software (Blender Foundation, The Netherlands) and sliced using Voxelize[®] (version 1.4.18, Zmorph S.A., Poland).



Figure 1. Tablets designs.

Structures of tablets, presented in Fig. 1 were selected based on the results of our previous studies [2]. Printlets containing 50 mg of FLU were manufactured by FDM ZMorph[®] 2.0 S (Poland) equipped with a 0.2 mm nozzle at 192°C and 10 mm/s of printing speed.

2.4. Evaluation of tablets' disintegration process and drug dissolution characteristics.

To evaluate the disintegration properties of printed ODTs the pharmacopoeial disintegration test was performed in SAPO ED-2 apparatus (Electrolab, India) in 700 mL of purified heated water. Additionally, the tablets' height changes caused by disintegration were registered using BJKS-13 apparatus [3].

Surface dissolution imaging apparatus SDi2 (Pion-Inc, UK) was applied to determine the disintegration and drug dissolution processes. Tablets were placed in a custom-made holder and analyzed at $\lambda_1 = 255$ nm and $\lambda_2 = 280$ nm. The drug dissolution profiles were analyzed in USP 4 apparatus at water (Erweka DFZ60, Germany). For both above-mentioned tests, the amount of API released was assessed in-line with UV-VIS Shimadzu 1800 spectrophotometer (Japan) at $\lambda = 261$ nm.

3. RESULTS AND DISCUSSION

3.1. 3D printed tablets

Filament was characterized by very good printability which resulted in small weight variations (Tab. 1).

Table 1. Tablets' attributes.

	Basic	Crown	Infill 15%
Average mass (mg \pm SD)	118.8 \pm 2.1	118.9 \pm 1.5	121.1 \pm 2.2
Dose (mg \pm SD)	49.5 \pm 0.9	49.6 \pm 0.6	50.5 \pm 0.9
Disintegration time (s \pm SD)	186 \pm 11	112 \pm 8	88 \pm 3

OP34

3.2. Disintegration and dissolution characteristics.

The basic-shaped tablets had a full outline and a porous infill, and their disintegration time slightly exceeded the limit of three minutes (Tab. 1). In the case of crown and infill 15% tablets, the porous structure facilitated the penetration of water, which resulted in a shorter disintegration time. The differences in the disintegration process are also visible in Fig. 2: in the case of basic-shaped tablets the gradual disintegration of the tablet's outline is clearly marked.

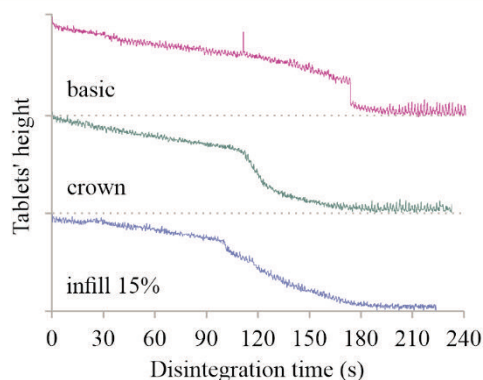


Figure 2. The disintegration profiles of 3D printed tablets obtained by BJKS-13 apparatus.

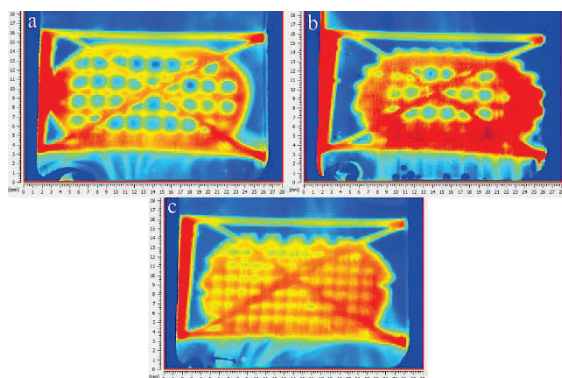


Figure 3. UV views of the tablets in the initial phase of the study in SDi2 (time = 0 min, $\lambda = 255$ nm): basic (a), crown (b), and infill 15% (c).

Based on the surface dissolution imaging analysis (Fig. 3), the outline of basic tablets started to deform after 5 min. of the study. This effect was similar in the case of crown-shaped tablets, characterized by a porous outline. The disintegration of the infill 15% tablets was uniform throughout the entire tablet volume. The disintegration of the infill 15% tablets was faster compared to the basic and crown printlets, resulting in a rapid release of API. However, regardless of the tablet shape, the release profiles of the FLU presented at Fig. 4 were similar –

over 80% of API was released within 15 minutes of testing.

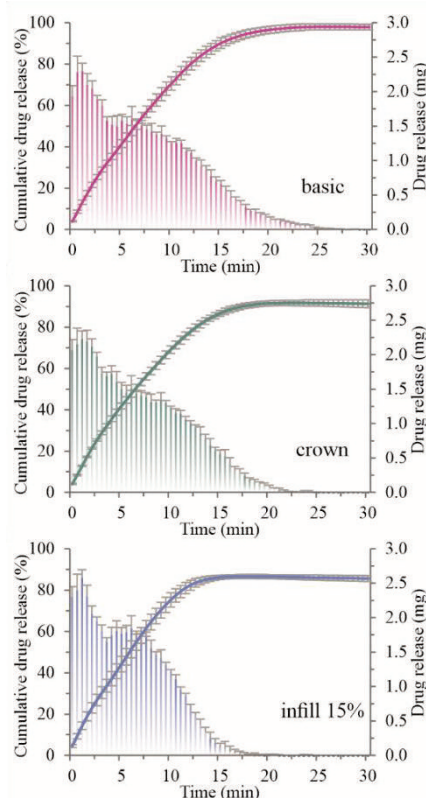


Figure 4. Drug dissolution profiles from 3DP tablets.

4. CONCLUSION

The FDM technology allows for the production of tablets with a complicated internal structure, facilitating the penetration of water into the tablet, which results in its rapid disintegration. The applied methods allowed the analysis of the mechanisms of the tablets' disintegration process and the release of the API.

5. REFERENCES

1. Zema, L., et al., *Three-Dimensional Printing of Medicinal Products and the Challenge of Personalized Therapy*. J. Pharm. Sci. 2017, 106: 1697–1705.
2. Tranová, T., et al., *Fused Deposition Modeling as a Possible Approach for the Preparation of Orodispersible Tablets*. Pharmaceuticals 2022, 15, 69.
3. Brniak, W., et al., *The Practical Approach to the Evaluation of Methods Used to Determine the Disintegration Time of Orally Disintegrating Tablets (ODTs)*. Saudi Pharm. J. 2015, 23: 437–443.

ACKNOWLEDGMENT

The authors acknowledge the National Science Centre, Poland for financial support (grant OPUS 16 no 2018/31/B/ST8/01327).

EXPLORING THE POTENTIAL OF NEW BULKING AGENTS FOR LYOPHILISED BIOPHARMACEUTICAL FORMULATIONS INTENDED FOR SUBCUTANEOUS ADMINISTRATION

Maja Bjelošević, Pegi Ahlin Grabnar

University of Ljubljana, Faculty of Pharmacy, Chair of Pharmaceutical Technology, Aškerčeva c. 7, 1000 Ljubljana, Slovenia

1. INTRODUCTION

To date, intravenous (IV) injections and infusions are the most common dosage forms for administering biopharmaceuticals, although the current trend is oriented towards subcutaneous (SC) administration, which provides many advantages compared to the IV route. On the negative side, the most limiting factor in SC application is the relatively small injection volume, i.e., ≤ 2 mL, and therefore highly concentrated (above 100 mg/mL) protein formulations are required. The development of such formulations is associated with many challenges, with ensuring protein stability and formulation injectability being the most demanding. Proteins are generally susceptible to chemical and physical instability. Stabilisers are essential to prevent protein aggregation, and the lyophilised form of such a drug is often preferred. In addition, the increased viscosity in highly concentrated formulations is an obstacle as it limits their development and administration [1, 2].

The research aims were to test the effects of monoclonal antibody (mAb) concentration (30, 60, 90, 120 mg/mL) on viscosity, reconstitution time, cake appearance and mAb stability. In addition, the potential of amino acids (phenylalanine, isoleucine, lysine, proline, arginine, methionine) as bulking agents on the critical quality attributes of lyophilisate formulations was investigated at low and high mAb concentrations compared to mannitol.

2. MATERIALS AND METHODS

2.1. Materials

The model IgG mAb was obtained from Lek d.d. (Slovenia). All amino acids and mannitol were from Merck (Germany). Polysorbate 20 was from J.T. Baker (USA). Ultra-pure water was from a Milli-Q purification system (Bedford, MA, USA).

2.2. Methods:

Sample preparation

The starting lyophilised formulations were reconstituted with ultra-pure water to obtain the target mAb concentrations and the appropriate amounts of mannitol or selected amino acid at the different ratios to sucrose, were added. In all formulations, the molar ratio between mAb and sucrose was 1:450. At the end, polysorbate 20 was added (0.02% (w/v)) and 2.0 mL of the filtered solution was filled into vials.

Viscosity

Viscosity was measured on a viscometer (RheoSense, USA) using microfluidic technology, at 25 °C. A chip with a 2 mm × 13 mm rectangular slit and a 50- μ m-deep microfluidic channel was used.

Reconstitution time and visual appearance

The reconstitution time was determined by dissolution of the lyophilised products and visual evaluation was carried out after each lyophilisation cycle.

Dynamic light scattering (DLS)

The particle sizes were measured before and after lyophilisation, to reveal any aggregates.

Size exclusion chromatography (SEC)

Measurements were performed at 210 nm, at a flow rate of 0.4 mL/min, and a column

OP35

temperature of 40 °C. The relative levels of aggregation products and monomers were calculated.

3. RESULTS AND DISCUSSION

3.1. Effects of mAb concentration on viscosity, stability, and reconstitution time

As hypothesized, the trend of increasing viscosity with increasing mAb concentration was confirmed, as none of the formulations exceeded the threshold of 50 mPa·s. However, during preparation of the formulation with 120 mg/mL mAb, there were some problems with filtration and filling. Because the amounts of sucrose in all samples were high enough to stabilise the mAb and the lyophilisation conditions were safe enough, neither the stability of the mAb nor the appearance of lyophilisates were compromised. In contrast, reconstitution times were greatly prolonged by the increased mAb concentrations and were acceptable (<5 min) for formulations containing 30 mg/mL and 60 mg/mL mAb, whereas they were >30 min for 120 mg/mL mAb (Table 1).

Table 1. Viscosity and reconstitution time for formulations with no bulking agents.

mAb concentration (mg/mL)	Viscosity (mPa·s)	Reconstitution time (s)
30	1.3	70
60	2.6	170
90	6.5	360
120	21.5	2070

3.2. Impact of new bulking agents

Among all the amino acids tested, the most appropriate appearance was found for lyophilisates with isoleucine or phenylalanine in a sucrose ratio of 1:4, while for the other amino acids shrunken cakes were obtained. It was also found that both amino acids can preserve the stability of mAb and thus represent a potential for the replacement of mannitol and glycine. However, we demonstrated that this applies just for formulations with low mAb concentration, while for highly concentrated mAb formulations, the addition of both amino

acids resulted in prolonged reconstitution times (Figure 1).

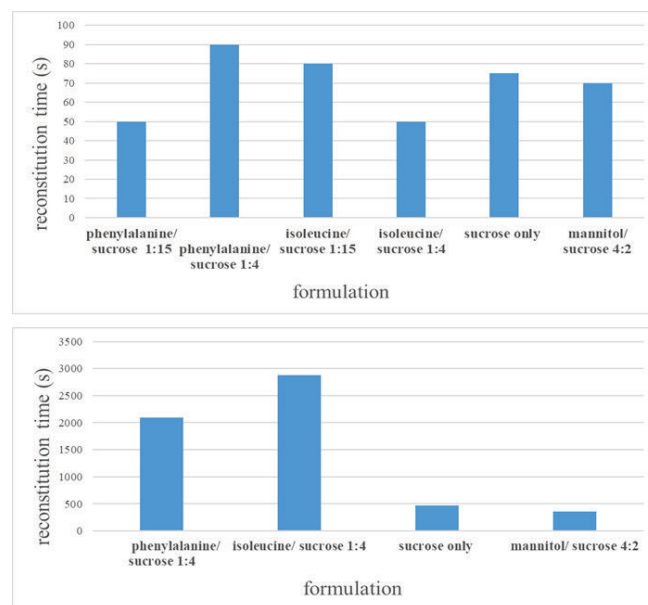


Figure 1. Reconstitution times of formulations with 30 mg/mL (up) and 90 mg/mL (down) mAb.

4. CONCLUSION

The development of protein therapeutics for SC administration raises several issues, some of which remain unresolved. The main conclusion is that isoleucine for low mAb concentrations is a promising candidate to replace mannitol because it provides suitable reconstitution time, cake appearance, and mAb stability, whereas further strategies to shorten reconstitution times of highly concentrated mAb formulations should be discovered.

5. REFERENCES

1. Bjelošević, M., et al., Effects of monoclonal antibody concentration and type of bulking agent on critical quality attributes of lyophilisates. *Drug Delivery Science and Technology*, 2021. 63:102510.
2. Bjelošević, M., et al., Excipients in freeze-dried biopharmaceuticals: Contributions toward formulation stability and lyophilisation cycle optimization. *International Journal of Pharmaceutics*, 2020. 576:119029.

ACKNOWLEDGMENT

The authors acknowledge financial support from the Slovenian Research Agency (Research Core Funding, No. P1-0189), and analytical support from company Lek d.d.

CYCLODEXTRIN POLYMER-BASED siRNA DELIVERY SYSTEMS

Ágnes Rusznyák^{1,2}, Milo Malanga³, Judit Váradi¹, Ildikó Bácskay^{1,2}, Miklós Vecsernyés¹, Ferenc Fenyvesi¹

¹Department of Pharmaceutical Technology, University of Debrecen, Debrecen, Hungary

²Institute of Healthcare Industry, University of Debrecen, Debrecen, Hungary

³CycloLab Ltd, Budapest, Hungary

1. INTRODUCTION

Cyclodextrin polymers are widely used excipients mainly in the pharmaceutical industry, but are also increasingly used in the cosmetics and food industry today [1]. Cyclodextrin polymers, as well as monomeric cyclodextrin molecules, are popular for increasing the water solubility of lipophilic drugs and stabilization. siRNA is a double-stranded, non-coding RNA molecule containing 20 to 27 base pairs and used for gene silencing.

Cyclodextrin-based systems are also used as siRNA delivery agents [2], so we aimed to investigate the siRNA carrying capacity of two cyclodextrin polymers, quaternary amino beta-cyclodextrin polymer (QABCDP) and amino beta-cyclodextrin polymer (NHBCDP). Polyethyleneimine (PEI) was used as a control vehicle. Our aim was to investigate the properties and the cellular internalization on Caco-2 cell line.

2. MATERIALS AND METHODS

The different polymer solutions effects on Caco-2 cell proliferation were measured by RTCA method. The properties of the formulated polyplexes were investigated by dynamic light scattering technology (DLS) and zeta potential measurements. The cellular uptake of the polyplexes was investigated by confocal microscopy and flow cytometry.

3. RESULTS AND DISCUSSION

Based on our RTCA studies, it can be stated that 50 and 100 nM polymer solutions did not affect cell proliferation. The complexation was successful, as the size and zeta-potential of both siRNA and polymer changed after complexation. Confocal microscopy and flow cytometry experiments revealed, that QABCDP polyplexes are taken up by cells and localized in the cytoplasm. Complexes formed with PEI

were found along the cell membrane, even polyplexes formulated with NHBCD polymer were not taken up.

4. CONCLUSION

In summary, we have successfully formulated siRNA-cyclodextrin polymer polyplexes, which did not affect cell proliferation and QABCDP polyplex was taken up by cells.

5. REFERENCES

1. Crini, G.; Fourmentin, S.; Fenyvesi, É.; Torri, G.; Fourmentin, M.; Morin-Crini, N. Cyclodextrins, from molecules to applications. *Environ. Chem. Lett.* **2018**, *16*, 1361–1375, doi:10.1007/s10311-018-0763-2.
2. Liu, J.; Ding, X.; Fu, Y.; Xiang, C.; Yuan, Y.; Zhang, Y.; Yu, P. Cyclodextrins based delivery systems for macro biomolecules. *Eur. J. Med. Chem.* **2021**, *212*, 113105, doi:10.1016/j.ejmech.2020.113105.

ACKNOWLEDGMENT

The work/publication is supported by the EFOP-3.6.1-16-2016-00022 and FK17 (124634). Project no. TKP2021-EGA-18 has been implemented with the support provided from the National Research, Development and Innovation Fund of Hungary, financed under the TKP2021-EGA funding scheme.

OPEN LIQUID-SURFACE ULTRASOUND-ENHANCED ELECTROSPINNING FOR GENERATING MULTILAYERED NANOFIBER STRUCTURES

Arle Kõrkjas¹, Kaarel Laar¹, Ari Salmi², Joni Mäkinen², Edward Hægström², Karin Kogermann¹, Jyrki Heinämäki¹, Ivo Laidmäe^{1,3,*}

¹*Institute of Pharmacy, University of Tartu, Estonia*

²*Electronics Research Laboratory, Department of Physics, University of Helsinki, Finland*

³*Department of Immunology, Institute of Biomedicine and Translational Medicine, University of Tartu, Estonia*

1. INTRODUCTION

Chronic wounds are major challenge for the health care system [1]. There's a lack of chronic wound specific dressings [2] and advanced wound dressings could help with this issue [3]. Conventional wound dressings face many challenges [3]. Advanced nanofiber dressings hold great potential in addressing these challenges [4]. In this study we take a closer look at specific process parameters of the Ultrasound-Enhanced electrospinning (USES, **Figure 1**) system and utilize them for creating multi-layered nanofiber structures which could be used for better chronic wound therapy [5].

2. MATERIALS AND METHODS

2.1. Materials

Polyethylene oxide, PEO (an average molecular weight of 900,000 Da) (Sigma-Aldrich Inc., U.S.A) was used as a mat forming polymer as a safe and established water-soluble synthetic polymer enabling the use of aqueous solution in an electrospinning process. Purified water was used as a solvent for preparing the aqueous PEO solutions (4% w/v and 3.5% w/v) applied in the USES experiments.

2.2. Fabrication of nanofibers

An in-house USES method was used to generate nanofibers and multilayered nanofiber mats, describe in detail in previous paper (Nieminen et al. 2018). Three types of tests were conducted – 1) increase of burst rate (BR), 2) increase of burst count (BC) and 3) increase of total relative acoustic power (APrel) over multiple layers of nanofibers.

2.3. Characterization of nanofibers

Scanning electron microscopy (SEM) was applied to study the size and morphology of the nanofibers with approximately 50 randomized

measurements taken from a single sample, using ImageJ software.

The presence of potential process induced transformations (PITs) of PEO in a needleless USES process were studied by Fourier transform infrared (FTIR) spectroscopy (IRPrestige 21, Shimadzu corporation) with a single reflection attenuated total reflection (ATR) crystal.

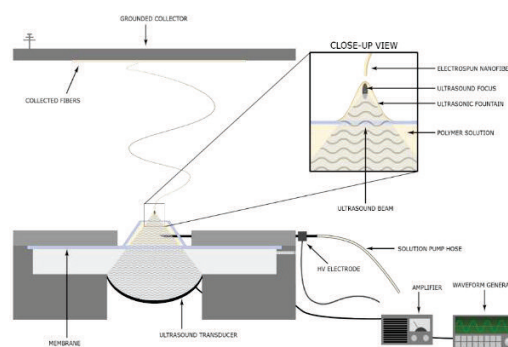


Figure 1. Schematic of the USES system setup for electrospinning multi-layered nanofiber structures

3. RESULTS AND DISCUSSION

3.1. Study on USES parameters

We investigated the impact of a stepwise change in two independent USES process parameters (ultrasound BR and BC) on the fiber diameter in the multilayered nanofibrous mats. The BR was increased for every subsequent fiber layer that was generated, and the total number of nanofiber layers generated was eight. The magnitude of other process parameters were kept constant. Results from BR test are shown on Figure 2.

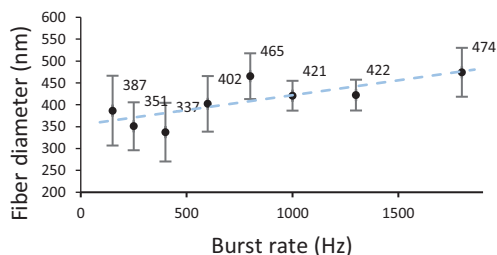


Figure 2. USES electrospun nanofiber diameters at different BR values over eight separate layers.

Similar investigation was conducted with BC where parameter was increased over 11 subsequent layers. BC test results are shown on Figure 3.

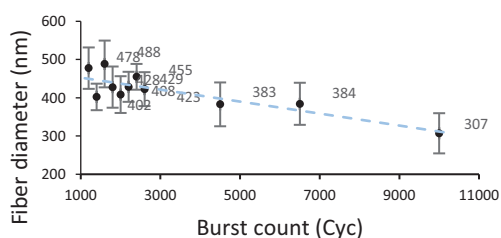


Figure 3. USES electrospun nanofiber diameters at different BC values over 11 separate layers.

3.3. Discussion

As BR was increased stepwise from 150 Hz to 1800 Hz, the average fiber size increased from 387 nm to 474 nm, respectively. In the present study, we used duty cycle (DC) levels in the range of 2.2% and 26.2%, suggesting that there is still room to increase the BR for generating the nanofibers with higher fiber diameter, if the ultrasonic fountain is stable enough.

Increasing BC reduced the average diameter of nanofibers in the fiber layers generated by USES. As BC was increased from 1200 cycles to 10000 cycles, the average diameter of nanofibers decreased by 170 nm. Applying BC above 4500 cycles resulted in the average diameter of nanofibers (fiber layers) ranging from 300 nm to 400 nm. Even though, there was a downward trend in the fiber thickness with increasing BC, trend was not monotoneus.

Minor changes in other USES parameters were necessary per test to stabilize the ultrasonic cone on top of the solution in the vessel. Electrospinning was not possible with unstable ultrasonic cone.

4. CONCLUSION

The fabrication of the multilayered nanofibrous mats was further developed by stepwise altering the critical process parameters in the USES system to modify the nanofiber size in the different fiber layers. In two sets of experiments we showed great potential in modifying nanofiber thickness on fly to produce advanced nanofiber structures. Based on the results obtained, we believe that USES could hold promise in fabricating multilayered (gradient) nanofibrous structures for wound healing applications.

5. REFERENCES

1. Landén, N. X., Li, D. and Ståhle, M. ‘Transition from inflammation to proliferation: a critical step during wound healing’, Cellular and Molecular Life Sciences 2016 73:20, 73(20), pp. 3861–3885.
2. Gupta, S. et al. ‘Chronic wounds-Magnitude, Socioeconomic Burden and Consequences’. Wounds Asia 2021, Vol 4 Issue 1
3. Zahedi, P. et al. ‘A review on wound dressings with an emphasis on electrospun nanofibrous polymeric bandages’, Polymers for Advanced Technologies, 2021(2), pp. 77–95.
4. Chen, S. et al. ‘Recent advances in electrospun nanofibers for wound healing’, Nanomedicine (Lond). 2017 Jun;12(11):1335-1352.
5. Ansari, S., Khorshidi, S. and Karkhaneh, A. ‘Engineering of gradient osteochondral tissue: From nature to lab’, Acta Biomaterialia, 2019 87, pp. 41–54.

ACKNOWLEDGMENT

This work is supported by the Estonian Research Council projects IUT 34-18, PRG1507 and PRG712. The Estonian Ministry of Education and Research is acknowledged for a financial support. The present study was also supported by the “Acouspin - Accelerated wound healing” project funded by the Business Finland. This presentation is funded by the Doctoral School of Cinical Medicine, supported by the European Union, European Regional Development Fund (University of Tartu’s ASTRA project PER ASPERA).

DEVELOPMENT OF PEPTIDES AS AFFINITY LIGANDS FOR HUMAN ANTIBODY PURIFICATION

Tomaž Bratkovič¹, Krištof Bozovičar¹, Anže Meden², Barbara Jenko Bizjan³

¹*Department of Pharmaceutical Biology, Faculty of Pharmacy, University of Ljubljana, Slovenia*

²*Department of Pharmaceutical Chemistry, Faculty of Pharmacy, University of Ljubljana, Slovenia*

³*Division of Paediatrics, University Medical Centre Ljubljana, Slovenia*

1. INTRODUCTION

Peptides theoretically overcome many shortcomings of larger proteins as ligands for affinity purification of biological molecules [1,2]. Firstly, they interact with cognate targets with moderate affinity, allowing mild elution, thus preserving the target's structural and functional integrity. Secondly, lacking a higher-order structure, peptides are resistant to harsh conditions of sanitization, thereby extending the lifetime of the affinity column. Thirdly, they can be reproducibly and cost-efficiently synthesized at large scale. Here, we report the development of selective peptide ligands binding all 4 subclasses of human immunoglobulin G and an affinity matrix for antibody purification.

2. MATERIALS AND METHODS

2.1. Materials

PhD-12 random peptide phage display library kit was procured from New England Biolabs (Ipswich, MA, USA). Phagemid pIT2, helper phage KM13, and *E. coli* strain TG1 were obtained from Source BioScience (Nottingham, UK). Human Fc fragment was procured from Athens Research & Technology (Athens, GA, USA). Leftover therapeutic polyspecific (Octagam) and monoclonal antibodies from multidose vials were kindly donated by Profs. Samo Zver and David Drobne (University Medical Centre Ljubljana).

2.2. Screening of random peptide library

PhD-12 phage library was screened in solution against a pool of biotinylated human IgG Fc regions [3]. Three selection rounds were performed and affinities of peptide hits were comparatively assessed by phage ELISA assay.

2.3. Structure-activity relationship (SAR) analysis

The lead peptide was subjected to on-phage N- and C-terminal trimming and alanine scanning to identify residues involved in Fc binding [3].

2.4. Design and screening of focused peptide library

A phagemid-displayed focused library was constructed based on the minimal peptide sequence that retained Fc binding, in which the non-essential residues were randomized. The library was screened against immobilized human polyspecific IgG and eluted phagemid virions were subjected to NGS sequencing [4].

2.5. Affinity matrix production and characterization

The peptide ligand exhibiting the highest affinity to human IgG was synthesized with a C-terminal cysteine and coupled to bromohydrin-activated Workbeads resin (Bio-Works, Uppsala, Sweden) via tris(2-aminoethyl)amine and bromoacetic acid [5]. Affinity matrix was characterized with regard to selectivity, specificity, and dynamic binding capacity.

3. RESULTS AND DISCUSSION

3.1. Identification of lead peptide and SAR analysis

We identified 6 unique low-homology peptides as selective Fc binders by screening a random dodecapeptide phage library. The peptide displaying the highest affinity (AGNGSYWYQVWF) was chosen as a lead for further characterization. SAR analysis identified the minimal sequence GSYWYQVWF required for binding with all 5 aromatic residues seemingly making essential contacts to IgG Fc region.

3.2. Development of improved peptide ligand

We designed a focused peptide library based on the minimized affinity peptide by combining

soft and hard randomization of residues. Peptides GX(Y/F)W(Y/F)XXW(Y/F) (where X denotes any amino acid) were displayed on phagemid virions at one copy per phage to prevent avidity effects. A single panning round was performed and the entire eluted phagemid pool was sequenced. Enrichment was monitored by comparing clone frequency against that found in the pre-screened library. The highest affinity peptide was also most highly enriched and was termed peptide A (GSYWYNVWF).

3.3. Functionality demonstration of affinity matrix

We coupled synthetic peptide A to cross-linked agarose beads via a short branched linker to increase ligand density and prevent its steric hindrance. The affinity matrix bound all 4 human IgG subclasses. The determined dynamic binding capacity (DBC) for infliximab (a chimeric IgG1) was ~44 mg/mL (Fig. 1), on par with that of a commercial protein A-based affinity column. Furthermore, our affinity matrix displayed high selectivity, enabling enrichment of IgG from a mixture with bovine serum albumin (BSA) (Fig. 2).

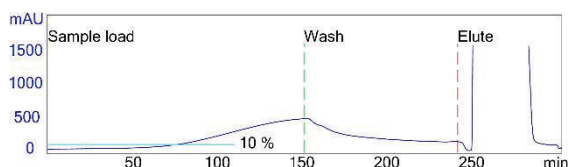


Figure 1. A representative chromatogram of DBC determination for 1 mL peptide A affinity column.



Figure 2. SDS-PAGE analysis of eluted fractions for assessment of binding specificity. A 1:4 mixture (mass ratio) of infliximab and BSA was loaded on the column and eluted with 20 mM glycine-HCl buffer (pH 3.0). E1-E4 – sequential eluted fractions; FT – flow-through.

3.4. Outlook

In addition to affinity chromatography, our peptides might find use as selective ligands for homogenous non-covalent antibody immobilization on immunoprecipitation beads and/or biosensor surfaces. We are currently developing cyclized analogues of peptide A with still improved affinity towards the Fc region.

4. CONCLUSION

We have developed selective peptide binders of human IgG Fc region and demonstrated their use as ligands for affinity purification of antibodies. The peptide-based affinity matrix displayed excellent chemical stability and dynamic binding capacity, and afforded high purity antibodies.

5. REFERENCES

1. Barredo-Vacchelli, G.R., et al., *Peptide Affinity Chromatography Applied to Therapeutic Antibodies Purification. International Journal of Peptide Research and Therapeutics*, 2021. 27(4): 2905-2921.
2. Kruljec, N. & Bratkovič, T., *Alternative Affinity Ligands for Immunoglobulins. Bioconjugate Chemistry*, 2017. 28(8): 2009-2030.
3. Kruljec, N., et al., *Development and Characterization of Peptide Ligands of Immunoglobulin G Fc Region. Bioconjugate Chemistry*, 2018. 29(8): 2763-2775
4. Bozovičar, K., et al., *Focused Peptide Library Screening as a Route to a Superior Affinity Ligand for Antibody Purification. Scientific Reports*, 2021. 11(1): 11650.
5. Islam, T., et al., *Optimization of Sequence, Display, and Mode of Operation of IgG-Binding Peptide Ligands to Develop Robust, High-Capacity Affinity Adsorbents That Afford High IgG Product Quality. International Journal of Molecular Sciences*, 2019. 20(1): 161.

ACKNOWLEDGMENT

We are grateful to former lab members Peter Molek, PhD and Nika Kruljec, PhD for invaluable discussions and help with screening phage libraries. This work was supported by the Slovenian Research Agency (program P4-0127) and the University of Ljubljana Innovation Fund (Grant 820-1/2020-33).

ENGINEERING IL-6-BINDING LACTIC ACID BACTERIA FOR ALLEVIATION OF INFLAMMATORY BOWEL DISEASE

Abida Zahirović¹, Aleš Berlec^{1,2}

¹ Department of Biotechnology, Jožef Stefan Institute, Slovenia

² Faculty of Pharmacy, University of Ljubljana, Slovenia

1. INTRODUCTION

Inflammatory bowel disease (IBD) is associated with increased levels of interleukin (IL)-6 in serum and intestinal mucosa [1]. Its removal from the intestine can help reduce the inflammation in IBD patients. Systemic administration of anti-cytokine agents can cause side effects, including severe opportunistic infections and malignancies.

This can be avoided by local administration of cytokine-binding proteins into the gastrointestinal tract using bacteria as an oral delivery system. Food-grade lactic acid bacteria (LAB), such as *Lactococcus lactis* (*L. lactis*), represent a suitable host for that purpose.

This species is relatively resistant to gastric acid and bile salts, thrives in the intestinal environment, but does not colonize the gastrointestinal tract and therefore has a low potential to negatively affect the gut microbiota. Microbial imbalance (dysbiosis) plays a crucial role in the pathology of IBD. LAB have been shown to possess immunostimulatory and probiotic properties, which represents an important advantage for IBD treatment. Probiotic administration has been shown to correct dysbiosis in IBD.

Harnessing these beneficial properties of LAB, we set out to develop *L. lactis* as a live carrier of the anti-IL-6 affibody that will be able to decrease the content of free IL-6 in the intestine and thus block its detrimental effects in IBD. In this study, we displayed IL-6-binding affibody on the surface of *L. lactis* and demonstrated a high degree of IL-6 removal by the engineered bacteria *in vitro*.

2. MATERIALS AND METHODS

IL-6-binding affibody was previously selected by Yu et al. [2]. For *L. lactis* surface display, the expression cassette consisted of Usp45 secretion signal, IL-6-binding affibody (denoted ZIL), and AcmA protein anchor. The presence of affibody in the lysate of engineered bacteria was evaluated by Western blotting. The extent of affibody surface display and its functionality was assessed by confocal microscopy and flow cytometry. Removal of IL-6 from the surrounding medium by the engineered *L. lactis* was evaluated using enzyme-linked immunosorbent assay (ELISA). To determine the half-maximal effective concentration (EC₅₀), the percentage of IL-6 removal was plotted against various bacterial concentrations and fitted to a four-parameter sigmoidal curve.

3. RESULTS AND DISCUSSION

Anti-IL-6 affibody was expressed in *L. lactis* in fusion with lactococcal secretion peptide and anchoring protein. A high amount of affibody was detected on bacterial surface (Fig. 1a) and its functionality was validated by confirmation of interaction with the target i.e. biotinylated human IL-6 (Fig. 1b).

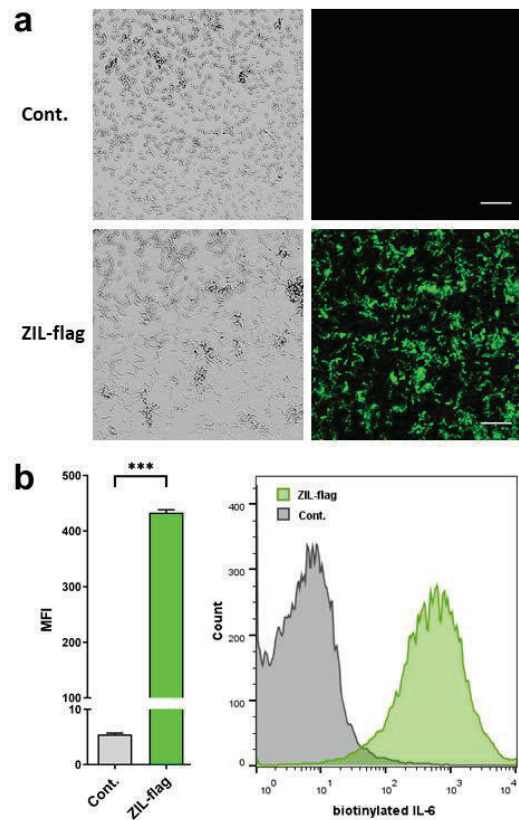


Figure 1. (a) Representative confocal microscopy images visualizing ZIL-flag at the bacterial surface. (b) Flow cytometric analysis showing binding of ZIL-flag-displaying *L. lactis* to human biotin-conjugated IL-6 demonstrating that surface-displayed IL-6-binding affibody is functional. ZIL-flag, *L. lactis* harbouring pSD-ZIL-flag plasmid. Cont., *L. lactis* harbouring empty plasmid pNZ8148.

Affibody-displaying *L. lactis* sequestered recombinant human IL-6 from the solution in a concentration-dependent manner by up to 99%. The removal was equally efficient across different IL-6 levels (150-1200 pg/mL) that were found to be clinically relevant in IBD patients, indicating high binding capacity. Engineered bacteria showed no binding to mouse IL-6 or other pro-inflammatory cytokines, thus proving to be highly species- and antigen-specific. The ability of engineered bacteria to capture IL-6 from cell culture supernatant was assessed using immunostimulated human monocytic cell lines (THP-1 and U-937) differentiated into macrophage-like cells. This model was established to mimic the inflammatory conditions in inflamed submucosa of IBD

patients. Affibody-displaying *L. lactis* reduced the content of IL-6 in the supernatants of both cell lines in a concentration-dependent manner by up to 94% (Fig. 2).

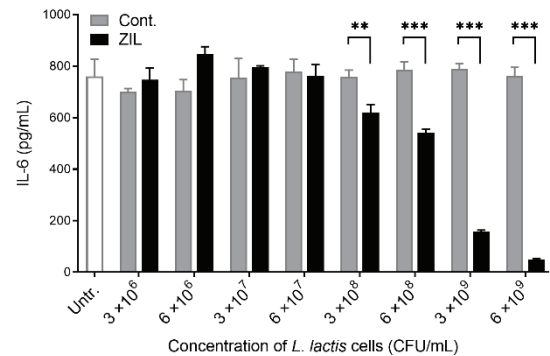


Figure 2. Representative ELISA experiment showing concentrations of IL-6 that remained in the supernatant of differentiated THP-1 cells following incubation with affibody-displaying *L. lactis* (ZIL). Cont., *L. lactis* control cells containing empty plasmid pNZ8148. Untr., untreated supernatant.

Dose response analysis showed that bacterial cell concentrations of 10⁷ and 10⁹ CFU/mL were required for half-maximal removal of recombinant and macrophage-derived IL-6, respectively.

4. CONCLUSION

Taken together, we developed *Lactococcus lactis* with potent and selective IL-6 binding activity by displaying IL-6-specific affibody on its surface. Developed strain is suitable for further development as an alternative IBD treatment, which combines local neutralization of IL-6 with beneficial effects of oral probiotics.

5. REFERENCES

1. Neurath, MF. *Cytokines in inflammatory bowel disease*. Nature Reviews Immunology, 2014. 14:329-342.
2. Yu, F., et al., *An affibody-adalimumab hybrid blocks combined IL-6 and TNF-triggered serum amyloid A secretion in vivo*. MAbs, 2014. 6:1598-1607.

EXPRESSION, PURIFICATION, AND NMR INVESTIGATION OF HUMAN KHSRP DNA BINDING PROTEIN USING *E. COLI* SYSTEM**Pasquale Russomanno¹, Diego Brancaccio¹, Jussara Amato¹, Antonio Randazzo¹, Bruno Pagano¹**¹ *Department of Pharmacy, University of Naples Federico II, Via D. Montesano 49, 80131 Naples, Italy***1. INTRODUCTION**

Proteins that bind nucleic acids regulate many cellular processes, including transcription, translation, gene silencing, microRNA biogenesis and telomere maintenance. RNA-binding proteins are typically considered functionally distinct from DNA-binding proteins and studied independently, but some of these proteins, known as DNA- and RNA-binding proteins (DRBPs), have domains able to bind both DNA and RNA with different specificity and manner. One of the known bivalent domains present in DRBPs is the K homology (KH) domain [1,2].

KHSRP (also known as KSRP or FBP2) is a multifunctional nucleic acid binding protein, present in the nucleus and cytoplasm [3]. It regulates transcription, mRNA translation, miRNA biogenesis, and modulates diverse cellular functions, including cell differentiation/proliferation and innate immunity, playing a key role in immune cell function and tumor progression [4-6]. Particularly, the over-expression of KHSRP has been shown to promote *c-myc* transcription, a well-known proto-oncogene involved in a broad spectrum of human cancers [6,7].

KHSRP (1-711) is composed of a structured central nucleic acid binding region that includes four KH domains (130-503) and two N- (1-129) and C-terminal (504-711) unfolded regions [3,8]. This particular structure and its ability to bind to nucleic acids have made its biochemical, biophysical, and structural studies very difficult. To date, KHSRP expression and purification have shown several limitations.

Here, we present a new approach to express and purify human KHSRP using the *Escherichia Coli* system. In addition, 1D ¹H-NMR experiments have been performed to detect its interaction with a G-quadruplex (G4) forming DNA sequence from the promoter region of *c-myc* gene.

2. MATERIALS AND METHODS**2.1. Materials**

The plasmids encoding KHSRP full length and KHSRP₁₃₀₋₅₀₃ were cloned into pGEX-6P-1 vector and all recombinant proteins were overexpressed in *E. Coli* BL21(DE3). The *c-myc* gene promoter DNA sequence was chemically synthesized at a 1- μ mol scale on an ABI 394 DNA/RNA synthesizer (Applied Biosystem, CA, USA).

For 1D ¹H-NMR assay, 200 μ L of 20 μ M KHSRP or KHSRP₁₃₀₋₅₀₃ and 20 μ M *c-myc* in 25 mM Tris-HCl buffer (pH 7.4) supplemented with 150 mM NaCl and 10% D₂O, were used. All spectra were acquired on a BRUKER AVANCE NEO 600 MHz spectrometer equipped with a Z-gradient cryoprobe four-channel equipped with a refrigerated SampleJet autosampler at 298 K, using 256 scans per spectrum with a recovery delay of 1.5 sec.

2.2. Protein expression and purification

Cells cultured in LB media were initially grown at 37 °C and subsequently cooled to 18 °C to obtain the soluble protein. Then, after lysis by sonication, the solution was cyclically loaded onto a GST-column. Several elution steps, using different buffers with increasing pH and NaCl concentration, were performed to break the bond between KHSRP and the bacterial

OP40

DNA. Finally, GST-tag was removed, and the protein purified by size exclusion chromatography. Similar methodology was used to obtain KHSRP₁₃₀₋₅₀₃ composed of only the central nucleic acid binding region.

2.3. NMR experiments

1D ¹H-NMR spectra confirmed the correct folding of KHSRP full length and KHSRP₁₃₀₋₅₀₃. 1D ¹H-spectra of KHSRP₁₃₀₋₅₀₃ were recorded before and after the addition of increasing amounts of *c-myc* gene promoter sequence to the solution containing the free protein. The same macromolecule-based 1D ¹H-NMR spectra were performed on *c-myc* gene promoter sequence before and after the addition of increasing amounts of KHSRP₁₃₀₋₅₀₃.

3. RESULTS AND DISCUSSION

Analysis of 1D ¹H-NMR spectra of KHSRP full length and KHSRP₁₃₀₋₅₀₃ indicates that both proteins obtained with the expression and purification procedure described above are correctly folded: the methyl signal under 0 ppm indicates the presence of a hydrophobic region, while the good dispersion of NH signals at 9 ppm indicates the presence of tertiary and secondary structures of the protein.

In the first NMR experiment, when *c-myc* G4 is added to KHSRP₁₃₀₋₅₀₃, a decrease in the intensity of the signals in the aliphatic and aromatic regions of the free protein, as well as the appearance of new signals, are observed. This confirms unequivocally the formation of a DNA-protein complex.

Comparable results were obtained upon the addition of increasing amounts of KHSRP₁₃₀₋₅₀₃ to the solution of containing the free *c-myc* DNA. During the NMR titration specific aromatic signals of the free DNA decrease in intensity upon the addition of increasing concentrations of the protein. This indicates a specific binding between *c-myc* G4 and KHSRP₁₃₀₋₅₀₃.

4. CONCLUSION

KHSRP is a promising therapeutic target for the prevention and treatment of cancer, but its in

vitro studies are very difficult due to complicated protein expression and purification. Our results describe, for the first time, a new approach to express and purify human KHSRP, using *Escherichia Coli* system and a different purification method without precipitation and refolding, to obtain the protein in its native folding. Moreover, using 1D ¹H-NMR spectra we confirmed the correct folding of KHSRP and thus validated our expression and purification method. Finally, macromolecule-based 1D ¹H-NMR experiments were performed on KHSRP₁₃₀₋₅₀₃ to detect and characterize its interaction with a G4-forming sequence from *c-myc* promoter.

5. REFERENCES

- [1] Hudson WH, Ortlund EA. Nat Rev Mol Cell Biol. 2014, 15, 749-60.
- [2] García-Mauriño SM, Rivero-Rodríguez F, Velázquez-Cruz A, Hernández-Vellisca M, Díaz-Quintana A, De la Rosa MA, Díaz-Moreno I. Front Mol Biosci. 2017, 4, 71.
- [3] Duncan R, Bazar L, Michelotti G, Tomonaga T, Krutzsch H, Avigan M, Levens D. Genes Dev. 1994, 8, 465-80.
- [4] Briata P, Chen CY, Ramos A, Gherzi R. Biochim Biophys Acta. 2013, 1829, 689-94.
- [5] Briata P, Bordo D, Puppo M, Gorlero F, Rossi M, Perrone-Bizzozero N, Gherzi R. Wiley Interdiscip Rev RNA. 2016, 7, 227-40.
- [6] Palzer KA, Bolduan V, Käfer R, Kleinert H, Bros M, Pautz A. Cells. 2022, 11, 1482.
- [7] Ramdzan M, Zubaidah, Gek San Tan, Sandra B. E. Tan, Seng Gee Lim, Qingsong Lin and Maxey C. M. Chung. Proteomics 2008, 8, 5086–5096
- [8] Gherzi R, Chen CY, Ramos A, Briata P. Semin Cell Dev Biol. 2014, 34, 2-8.

ACKNOWLEDGMENT

This work was supported by an AIRC grant (ID. 24590 to B.P.)

Poster Presentations

P01	Maja Bjelošević, Odon Planinšek, Pegi Ahlin Grabnar* ORAL LYOPHILISATES: A TYPE OF PATIENT-FRIENDLY DOSAGE FORM
P02	Ivana Aleksić*, Slobodanka Ćirin-Varađan, Teodora Glišić, Mihal Đuriš, Jelena Đuriš, Jelena Parojčić EVALUATION OF DILUTION CAPACITY AND COMPACTION BEHAVIOUR OF THE EXCIPIENTS CO-PROCESSED BY IN SITU FLUIDIZED BED MELT GRANULATION
P03	Fatima K. Al-Sulaiti, Fatma Kır, Selma Sahin* CRUSHING EFFECT ON DISSOLUTION PROFILES OF METOPROLOL SUCCINATE MODIFIED RELEASE TABLETS
P04	Petra Arany*, Pálma Fehér, Zoltán Ujhelyi, Miklós Vecsernyés, Renátó Kovács, Mariann Zichar, Ildikó Papp, Géza Regdon, Jr., Mónika Béres, Melinda Szalóki, Ildikó Bácskay MANUFACTURING AND EXAMINATION OF 3D PRINTED VAGINAL DRUG DELIVERY SYSTEMS
P05	Grega Bajc*, Gregor Ratek, Franc Vrečer, Klemen Korasa DEVELOPMENT OF A COLOURANT SELECTION MODEL IN FILM COATING FOR ACHIEVING TARGETED COLOUR OF FILM-COATED TABLETS
P06	Hilke Lösing, Jonas Borregaard Eriksen, Regina Scherließ, Annette Bauer-Brandl* INTRINSIC DISSOLUTION RATE: MEASUREMENT USING AN INEXPENSIVE ALTERNATIVE TO THE PHARMACOPOEIAL DIE HOLDER
P07	Ana Baumgartner*, Odon Planinšek EFFECT OF PROCESS PARAMETERS IN HIGH SHEAR GRANULATION ON PARTICLE SIZE, COMPRESSIBILITY AND COMPACTIBILITY OF GRANULATED MESOPOROUS SILICA
P08	Nevin Celebi*, Ayse Nur Oktay, Sibel Ilbasmis-Tamer, Sevtap Han, Orhan Uludag EVALUATION OF ANALGESIC AND ANTI-INFLAMMATORY EFFECTS OF CYCLODEXTRIN-BASED FLURBIPROFEN NANOGELS FOR DERMAL APPLICATION
P09	Jeppe J. Christiansen*, Jonas B. Eriksen, Jarkko Rautio, Marika Ruponen, Annette Bauer-Brandl, Martin Brandl COMBINED IN-VITRO DISSOLUTION-/ ENZYMATIC CONVERSION-/ PERMEATION-STUDIES OF THE PRODRUG FOSAMPRENAVIR
P10	Mikolaj Czajkowski*, Paulina Skupin-Mrugalska, Bartłomiej Milanowski, Annette Bauer-Brandl, Martin Brandl THE INFLUENCE OF PHOSPHATIDYLCHOLINE CONTENT IN HYDROGENATED PHOSPHOLIPID/POLYMER-BASED SOLID DISPERSIONS ON THE DISSOLUTION PROFILE OF A POORLY SOLUBLE DRUG
P11	Davide D'Angelo*, Eride Quarta, Stefania Glieca, Veronica Chierici, Giada Varacca, Martina Brandolini, Lisa Flammini, Simona Bertoni, Vittorio Sambri, Fabio Sonvico, Ruggero Bettini, Francesca Buttini DRY POWDER FORMULATION OF CYCLOSPORINE A FOR IMMUNOSUPPRESSIVE TREATMENT
P12	Mine DİRİL*, K. Volkan Ozdokur, Yeliz Yıldırım, H. Yeşim Karasulu DEVELOPMENT AND IN VITRO-IN VIVO EVALUATION OF GLYCYRRETTIC ACID ACTIVE TARGETED PROLIPOSOMAL DRUG DELIVERY SYSTEMS FOR TREATMENT LIVER CANCER
P13	Jelena Đoković*, Sanela Savić, Nebojša Cekić, Snežana Savić A PROPOSAL OF INNOVATIVE INJECTABILITY ASSESMENT METHOD FOR INTRAVENIOUS FORMULATIONS – CASE STUDY ON PEGYLATED NANOEMULSIONS
P14	Črt Dragar, Sebastjan Nemeč, Slavko Kralj, Petra Kocbek ELECTROSPINNING AS A DRYING METHOD FOR MAGNETIC NANOPARTICLE DISPERSIONS
P15	Fanni Falusi*, Szilvia Berkó, Mária Budai-Szűcs, Anita Kovács

	FORMULATION AND INVESTIGATION OF THE EFFECT OF POLYMERS ON DERMAL FOAM PROPERTIES USING THE QUALITY BY DESIGN (QbD) APPROACH
P16	Pálma Fehér*, Marc Le Borgne, Florent Perret, Christelle Marminon, Zoltán Ujhelyi, Ágota Pető, Liza Józsa, Miklós Vecsernyés, Ildikó Bácskay FORMULATION OF NANOPARTICLES CONTAINING CASEIN KINASE 2 INHIBITOR FOR THE THERAPY OF GLIOBLASTOMA
P17	Felicijan Tjaša*, Rede Katarina, Cof Greta, Bogataj Marija THE INFLUENCE OF SIMULATED WATER GASTRIC EMPTYING PROFILES ON DISSOLUTION OF MODEL DRUGS
P18	Merve Geyik, Burcu Nacak, Melek Nur Bilal, Tugba Gulsun, Selma Sahin*, Levent Oner, Yagmur Akdag DRY POWDER INHALER FORMULATIONS CONTAINING GEFITINIB NANOPARTICLES
P19	Teodora Glišić*, Ilija German Ilić, Jelena Parojčić, Ivana Aleksić COMPARATIVE COMPRESSION CHARACTERIZATION OF LIQUISOLID SYSTEMS PREPARED WITH MESOPOROUS CARRIERS
P20	Filip Gorachinov*, Fatima Mraiche, Diala Alhaj Moustafa, Ola Hisari, Damjan Georgievski, Jensa Joseph, Katerina Goracinova DESIGN AND EVALUATION OF HYALURONIC ACID DECORATED MULTIFUNCTIONAL PCL-b-PEI NANOPARTICLES
P21	Mirjam Gosenca Matjaž*, Katarina Bolko Seljak NANOCELLULOSE-BASED FILM-FORMING HYDROGELS CONTAINING BETAMETHASONE DIPROPIONATE: DEVELOPMENT AND PHYSICAL EVALUATION
P22	Blaž Grilc*, Tjaša Felicijan, Timeja Planinšek Parfant, Odon Planinšek VALSARTAN BUCCAL FILMS FORMULATION DEVELOPMENT WITH THE IMAGE ANALYSIS
P23	Adam Haimhoffer*, Licia Dossi, Ildikó Bácskai, Ferenc Fenyvesi NEW HIGHLIGHTS OF THE DRUG CARRIER PEG-B-CYCLODEXTRIN POLYMER
P24	Hana Hořavová*, Jan Gajdziok PREPARATION AND EVALUATION OF SPRAY-DRIED MICROPARTICLES CONTAINING N-ACETYLCYSTEINE FOR LUNG APPLICATION
P25	Witold Jamróz*, Jolanta Pyteraf, Mateusz Kurek, Thao Tranová, Jan Loskot, Jitka Mužíková, Renata Jachowicz THE EFFECT OF THE HIGH DRUG LOAD – THE EVALUATION OF THE PROPERTIES OF 3D PRINTED ORODISPERSIBLE TABLETS (ODTS) WITH 70% OF DRUG CONTENT
P26	Bisera Jurišić Dukovski*, Josip Ljubica, Petra Kocbek, Luka Bočkor, Jasmina Lovrić HCE-T CELL-BASED CORNEAL EPITHELIAL MODEL: SCALE-DOWN TO 96-WELL INSERT PLATES
P27	Mohammed Kalayi*, Berna Uzun, Arkan Barbar, Buket Aksu FORMULATION AND CHARACTERIZATION OF MUCO-ADHESIVE ORAL FILMS CONTAINING LIDOCAINE HYDROCHLORIDE USING QUALITY BY DESIGN APPROACHES
P28	Mateusz Kurek*, Jolanta Pyteraf, Witold Jamroz, Justyna Knapik-Kowalczyk, Marian Paluch, Renata Jachowicz STABILITY EVALUATION OF FLUCONAZOLE-LOADED FILAMENTS AND 3D PRINTED ORODISPERSIBLE TABLETS
P29	Jakob T. Lynnerup*, Jonas B Eriksen, Ann Mari Holsæter, Martin Brandl THE EFFECT OF NANO-MILLING ON DISSOLUTION/PERMEATION OF POORLY SOLUBLE DRUG COMPOUNDS
P30	Jelena Mitrović*, Maja Bjelošević, Daniel E. Knutson, Aleksandar Kremenović, Dominique Lunter, Pegi Ahlin Grabnar, James M. Cook, Miroslav M. Savić, Snežana D. Savić

	FREEZE-DRIED NANOCRYSTAL DISPERSION OF NOVEL DEUTERATED PYRAZOLOQUINOLINONE LIGAND (DK-I-56-1): PROCESS PARAMETERS AND CRYOPROTECTANT SELECTION THROUGH STABILITY STUDY
P31	Sebastjan Nemeč*, Tanja Potrč, Petra Kocbek, Slavko Kralj PREPARATION OF ANISOTROPIC HOLLOW SILICA NANOSTRUCTURES
P32	Zeliha Duygu Özdal*, Sevgi Takka PREPARATION AND IN VITRO CHARACTERIZATION OF ONDANSETRON HYDROCHLORIDE LOADED LIPOSOME FORMULATIONS
P33	Petra Party*, Rita Ambrus DEVELOPMENT OF COMBINED INHALABLE FORMULATION OF IBUPROFEN AND MANNITOL FOR THE TREATMENT OF CYSTIC FIBROSIS
P34	Nikola Pešić*, Mirjana Krkobabić, Ivana Adamov, Svetlana Ibrić, Branka Ivković, Đorđe Medarević ORAL DOSAGE FORMS WITH CARVEDILOL FABRICATED BY SELECTIVE LASER SINTERING (SLS) 3D PRINTING TECHNIQUE
P35	Vladimir Petkov*, Zahari Vinarov, Slavka Tcholakova DISSOLUTION KINETICS OF GLIBENCLAMIDE AMORPHOUS SOLID DISPERSIONS IN BIORELEVANT MEDIA
P36	Ágota Pető*, Dóra Kósa, Ádám Haimhoffer, Dániel Nemes, Pálma Fehér, Zoltán Ujhelyi, Judit Váradi, Ferenc Fenyvesi, Miklós Vecsernyés, Zoltán Tóth, Annamária Pallag, Tünde Jurca, Ildikó Bácskay TOPICAL FORMULATION OF LYOPHILIZED P. CORONARIUS FLOWER AND LEAF EXTRACTS, ANTIMICROBIAL ASSESSMENT OF THE PLANT
P37	Odon Planinšek*, Ana Baumgartner, Blaž Grilc FENOFIBRATE ORODISPERSIBLE TABLET MADE WITH GRANULATED MESOPOROUS SILICA
P38	Kaisa Põhako*, Kairi Lorenz, Marta Putrinš, Külli Kingo, Tanel Tenson, Karin Kogermann EX VIVO BIOFILM MODEL ON PIG SKIN TO TEST THE EFFICACY OF ELECTROSPUN ANTIMICROBIAL DRUG-LOADED FIBER MATERIALS AS WOUND DRESSING
P39	Mitja Pohlen*, Jurij Aguiar Zdovc, Jurij Trontelj, Janez Mravljak, Mirjam Gosenca Matjaž, Iztok Grabnar, Tomaž Snoj, Rok Dreu RELATIVE BIOAVAILABILITY ENHANCEMENT OF SIMVASTATIN VIA DRY EMULSION SYSTEMS: COMPARISON OF SPRAY DRYING AND FLUID BED LAYERING TECHNOLOGY
P40	Chrystalla Protopapa*, Marilena Vlachou, Angeliki Siamidi, Evi Christodoulou, Nikolaos D. Bikiaris COMPARISON OF THE RELEASE PROFILES OF MELATONIN FROM MATRIX TABLETS CONTAINING POLY(ϵ -CAPROLACTONE) AND COPOLYMERS
P41	Zrinka Rajić*, Goran Poje, Lais Pessanha de Carvalho, Jana Held, Ivana Perković, Tana Tandarić, Robert Vianello HARMIQUINS, NOVEL POTENT ANTIPLASMODIAL HITS
P42	Dávid Sinka*, Enikő Doma, Mercédesz Varga, Pálma Fehér, Liza Józsa, Zoltán Ujhelyi, Ildikó Bácskay FORMULATION AND PERMEABILITY STUDIES OF FENUGREEK (TRIGONELLA FOENUM-GRAECUM) CONTAINING SEDDS
P43	Bence Sipos*, Ildikó Csóka, Piroska Szabó-Révész, Gábor Katona SOLUBILITY ENHANCEMENT OF MEGESTROL-ACETATE VIA MICELLE AND POLYMERIC MICELLE FORMULATION
P44	Barbara Sterle Zorec*, Hana Kokot, Stane Pajk, Janez Štrancar, Rok Dreu VISUALISATION OF SIMVASTATIN CORE-SHELL PARTICLES PREPARED BY ELECTROSPRAYING METHOD USING STIMULATED EMISSION DEPLETION MICROSCOPY
P45	Spase Stojanov*, Tina Vida Plavec, Julijana Kristl, Špela Zupančič, Aleš Berlec ELECTROSPUN NANOFIBERS AS A DELIVERY SYSTEM FOR VAGINAL PROBIOTICS

P46	Boglárka Szalai*, Mária Budai-Szücs, Orsolya Jójárt-Laczkovich EVALUATION OF DEXAMETHASONE CONTAINING IN SITU GELLING MUCOADHESIVE EYE DROPS
P47	Eva Tavčar* SOLUBILITY ASSESSMENT OF CANNABIDIOL IN DIFFERENT SOLVENTS
P48	Biljana Temova*, Betka Krampelj, Petra Kocbek DEVELOPMENT OF CHITOSAN AND ALGINATE BASED NANOFIBERS FOR WOUND HEALING APPLICATION
P49	Erna Turković*, Ivana Vasiljević, Dragana Vasiljević, Svetlana Ibrić, Jelena Parojčić APPLICATION OF SUPPORT VECTOR MACHINE LEARNING FOR ORODISPERSIBLE FILMS DISINTEGRATION TIME PREDICTION
P50	Luca Éva Uhljar*, Balázs Kürtösi, Rita Ambrus DEVELOPMENT OF A PREPARATION METHOD FOR NANOCAPSULES USING FACTORIAL DESIGN
P51	Zoltán Ujhelyi*, Dóra Kósa, Ágota Pető, Thinh To Quoc, Ildikó Bácskay DEVELOPMENT AND EVALUATION OF FDM PRINTED NASAL DEVICE FOR SOLID NANOPARTICLES
P52	Judit Váradi*, Lóránd Erdélyi, Ferenc Fenyvesi, Gábor Vasvári, Ádám Haimhoffer, Ilona Bereczki, György Vámosi, Miklós Vecsernyés, Ildikó Bácskay, Renátó Kovács INVESTIGATION OF THE EFFECTIVENESS OF CHITOSAN COATING ON PROBIOTIC MICROCAPSULES AND INTERACTION WITH LACTOBACILLUS PLANTARUM
P53	Patrícia Varga*, Csilla Bartos, Rita Ambrus INVESTIGATION OF MELOXICAM POTASSIUM CONTAINING NANOPARTICLES FOR INTRANASAL ADMINISTRATION
P54	Ivana Vasiljević*, Erna Turković, Jelena Parojčić HOW FORMULATION PARAMETERS AFFECT COMPRESSION BEHAVIOUR OF MULTIPARTICULATE UNITS PREPARED BY SELECTIVE LASER SINTERING?
P55	Mercedes Vitek*, Alenka Zvonar Pobirk, Žiga Medoš, Mirjam Gosenca Matjaž FLAXSEED-OIL BASED LYOTROPIC LIQUID CRYSTALS: INFLUENCE OF MICROSTRUCTURE ON BETAMETHASONE DIPROPIONATE RELEASE PROFILE
P56	Lamija Hindija, Jasmina Hadžiabdić, Merima Sirbubalo, Amina Tucak-Smajić, Ognjenka Rahić, Stanko Srčić, Edina Vranić* SOLUBILITY ENHANCEMENT OF DIMENHYDINATE BY INCLUSION COMPLEXATION WITH SULFOBUTYL ETHER β -CYCLODEXTRIN
P57	Alenka Zvonar Pobirk*, Mila Kovačević, Ilja German Ilić, Mirjana Gašperlin THE INFLUENCE OF POLYMERIC PRECIPITATION INHIBITORS ON SOLUBILITY CHARACTERISTICS OF CARVEDILOL-LOADED SMEDDS
P58	Timeja Planinšek Parfant*, Anja Hrovat, Robert Roškar SIMULTANEOUS DETERMINATION OF FIVE NITROSAMINES IN SARTAN DRUG PRODUCTS BY A LC-MS/MS METHOD
P60	Tin Takač*, Milena Jadrijević-Mladar Takač, Tomislav Jednačak PREDICTION OF ENVIRONMENTAL MICROBIAL DEGRADATION OF AZITHROMYCIN IN SOIL AND WATER AND METABOLISM IN HUMANS
P61	Žane Temova Rakuša*, Robert Roškar A FAST HPLC-DAD METHOD FOR THE SIMULTANEOUS DETERMINATION OF ALL MAIN WATER-SOLUBLE VITAMINS IN FOODS AND SUPPLEMENTS
P62	Ilona Bereczki*, Henrietta Papp, Veronika Nagy, Attila Agócs, Ferenc Jakab, Pál Herczegh, Anikó Borbás NATURAL APOCAROTENOIDS AND THEIR SEMISYNTHETIC GLYCOPEPTIDE CONJUGATES AGAINST SARS-COV-2
P63	Svit Ferjančič Benetik*, Boris Markoj, Matic Proj, Damijan Knez, Stanislav Gobec, Aleš Obreza, Urban Košak DESIGN, SYNTHESIS AND EVALUATION OF NOVEL BChE/p38 α MAPK DUAL INHIBITORS FOR THE TREATMENT OF ALZHEIMER'S DISEASE

P64	Yavana Ganesh*, Jonathan E. Forman, Kabrena E. Rodda, John R. Cort, Ellen M. Wynkoop COUNTERING DIVERSION OF PHARMACEUTICAL-BASED COMPOUNDS ALONG THE CHEMICAL SUPPLY CHAIN: A WORKSHOP
P65	Špela Gubič*, Louise Antonia Hendrickx , Xiaoyi Shi, Žan Toplak, Kenny M. Van Theemsche , Ernesto Lopes Pinheiro-Junior, Steve Peigneur, Alain J. Labro, Luis A. Pardo, Jan Tytgat, Tihomir Tomašič, Lucija Peterlin Mašič DESIGN OF NEW POTENT AND SELECTIVE THIOPHENE-BASED KV1.3 INHIBITORS AND THEIR POTENTIAL FOR ANTICANCER ACTIVITY
P66	Bálint Lőrinczi*, Zsófia Sánta, István Szatmári SYNTHESIS AND TRANSFORMATION OF AZA KYNURENIC ACID DERIVATIVES
P67	Marina Marinović, Zrinka Rajić SYNTHESIS OF NEW CARBAMATE-TYPE HARMICINES
P68	Martina Piga*, Zoltán Varga, Ádám Fehér, Ferenc Papp, Eva Korpos Pintye-Gyuri, Tihomir Tomašič, Nace Zidar DISCOVERY OF INHIBITORS OF Hv1 PROTON CHANNELS AS POTENTIAL ANTICANCER DRUGS
P69	Žan Toplak*, Louise Antonia Hendrickx, Špela Gubič, Jan Tytgat, Luis A. Pardo, Lucija Peterlin Mašič, Tihomir Tomašič IN SILICO DISCOVERY AND OPTIMISATION OF VOLTAGE-GATED POTASSIUM CHANNEL KV10.1 INHIBITORS WITH ANTIPROLIFERATIVE ACTIVITY
P70	Selena Pavšič*, Janko Kos, Anja Pišlar DIFFERENTIATION OF SH-SY5Y CELLS INTO SPECIFIC NEURONAL PHENOTYPES: IN VITRO MODEL OF NEURODEGENERATION
P71	Tina Vida Plavec*, Aleš Berlec ENGINEERING LACTOCOCCUS LACTIS TO INHIBIT INTESTINAL INFLAMMATION THROUGH SMALL PROTEIN BLOCKERS OF IL-23/IL-17 AXIS USING NOVEL BGLBRICK ASSEMBLY METHOD
P72	Luka Hiti*, Tijana Markovič, Irena Mlinarič-Raščan UTILISATION OF LYMPHOBLASTOID CELL LINES AS IN VITRO MODELS OF OVER-ACTIVATED IMMUNE RESPONSE FOR DRUG REPURPOSING
P73	Nataša Karas Kuželički*, Alenka Šmid, Tina Kek, Eberlinc Andreja, Irena Mlinarič-Raščan, Ksenija Geršak HIGHER INCIDENCE OF COMMON POLYMORPHISMS IN THE GENES OF FOLATE AND METHIONINE CYCLES IN CHILDREN WITH OROFACIAL CLEFTS
P74	Tijana Markovič*, Alenka Šmid, Helena Podgornik, Matevž Škerget, Irena Mlinarič-Raščan FACTORS INFLUENCING INTER-INDIVIDUAL DIFFERENCES IN RESPONSE TO PROSTAGLANDIN EP4 RECEPTOR AGONIST IN CHRONIC LYMPHOCYTIC LEUKEMIA CELLS
P75	Panagiotis-Dimitrios Mingas*, Jurij Zdovc, Iztok Grabnar, David Drobne, Tomaž Vovk DEVELOPMENT OF A METHOD FOR THE THERAPEUTIC DRUG MONITORING OF USTEKINUMAB IN DRIED BLOOD SPOTS
P76	Armando Tratenšek*, Jurij Zdovc, Igor Locatelli, Iztok Grabnar, David Drobne, Tomaž Vovk ASSOCIATION OF OXIDATIVE STRESS-RELATED BIOMARKERS WITH DISEASE ACTIVITY IN PATIENTS WITH INFLAMMATORY BOWEL DISEASE

ORAL LYOPHILISATES: A TYPE OF PATIENT-FRIENDLY DOSAGE FORM

Maja Bjelošević, Odon Planinšek, Pegi Ahlin Grabnar

University of Ljubljana, Faculty of Pharmacy, Department of Pharmaceutical Technology, Aškerčeva
c. 7, 1000 Ljubljana, Slovenia

1. INTRODUCTION

Orodispersible drug formulations represent one of the current trends in the pharmaceutical field, mostly with the purposes for pediatric and geriatric patients. The main advantage of orodispersible dosage forms is that they are appropriate for patients with swallowing problems, leading to improvements in patients' compliance. Oral lyophilisates are solid forms, obtained by lyophilisation, intended either to be placed in the mouth or to be dispersed (or dissolved) in water before administration. Typically, oral lyophilisates are composed of binders and fillers, taste modifiers, colorants, sweeteners, and preservatives. Binders, such as gelatin, sodium alginate, polyvinylpyrrolidone, form an amorphous matrix of lyophilisate and provide appropriate mechanical strength. As fillers, sugars, and sugar alcohols, such as sucrose, mannitol or sorbitol are used [1, 2].

The objectives of the present work were: (i) to develop and evaluate an optimised formulation for preparation of oral lyophilisates, based on mannitol, gelatin, and polyvinylpyrrolidone K25; and (ii) to examine the influence of glycine, and croscarmellose on quality attributes of lyophilisates.

2. MATERIALS AND METHODS

2.1. Materials

Gelatin, polyvinylpyrrolidone (PVP) K25 were from Sigma-Aldrich, Germany, while glycine, mannitol, and croscarmellose were purchased from Merck, Germany

2.2. Methods

Sample preparation

First, the half amount of water was weighted in beaker, and during constant mixing excipients were added. At the end, the full amount of water was added, and 2 mL of samples were aliquoted

in 10 mL beakers and kept at -20 °C for 24 hours.

Lyophilisation process

Lyophilisation was conducted in a laboratory freeze-dryer (Epsilon 2-6D; Christ, Osterode am Harz, Germany). In freezing step, the shelf temperature was -45 °C. During primary drying, the shelf temperature was raised to 20 °C at 0.5 °C/min, with chamber pressure of 0.10 mbar, while in secondary drying temperature was set to 40 °C.

Product appearance

Oral lyophilisates were visually evaluated after the completion of each lyophilisation cycle.

Disintegration time

Oral lyophilisates were placed in 200 mL of water (22 °C), and time needed to complete disintegration was determined. According to European Pharmacopoeia oral lyophilisates have to disintegrate within 3 min.

3. RESULTS AND DISCUSSION

3.1. The effect of ratio between gelatin, PVP K25, and mannitol

At the beginning, formulations with fixed gelatin to mannitol mass ratio 1:5 were tested, while their total concentration in liquid formulations varied from 6 to 30 % (w/w). The obtained results showed that all these oral lyophilisates with mannitol and gelatin express disintegration time above 3 min, indicating that gelatin formed rugged cake structure with no pores. On the contrary, lyophilisates which contain PVP K25 instead of gelatin, were friable and cracked. Therefore three-component lyophilisates formed from liquid formulations with 6 % (w/w) excipients (gelatin, PVP K25, mannitol) were tested. Results in Table 1 indicate that higher content of gelatin resulted in longer disintegration time, while lower gelatin content results in inappropriate appearance of lyophilisates (Figure 1). By

P01

increasing PVP K25 content, the disintegration times were not significantly different. Considering disintegration time and visual appearance, we determined gelatin: PVP K25: mannitol (1: 2: 5) formulation as the most suitable.

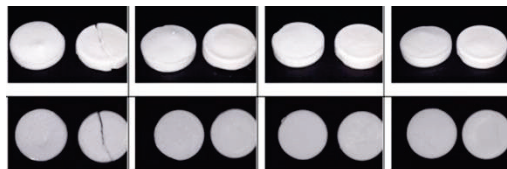


Figure 1. Appearance of oral lyophilisates with ratio gelatin: PVP K25: mannitol = 0.5 : 1 : 5; 0.5: 2: 5; 1: 1: 5 and 1: 2: 5. (from left to right).

3.2. The effect of glycine and croscarmellose

Four-component formulations were prepared from gelatin, mannitol, PVP K25, and glycine or croscarmellose. As can be seen in Table 1, the disintegration time of the lyophilisates with either glycine or croscarmellose depended on the gelatin concentration. While croscarmellose provided lyophilisates with shorter disintegration time and also appropriate visual appearance, glycine only had a positive effect on the elegant appearance of lyophilisate cake (Figure 2).



Figure 2. Appearance of lyophilisates with ratio gelatin: PVP K25: glycine/ croscarmellose: mannitol = 0.5: 2: 0.5: 4.5 (glycine left, croscarmellose right).

Table 1. The composition of tested formulations and their disintegration times and evaluated visual appearance.

ratio of excipients		disintegration time (s)		appearance	
gelatin	PVP K25	glycine	croscarmellose	mannitol	
0.5	1	0	0	5 12	X
0.5	2	0	0	5 9	X
1	1	0	0	5 42	✓
1	2	0	0	5 45	✓
0	2	0.5	0	4.5 22	✓
0.5	2	0.5	0	4.5 50	✓
0	2	0	0.5	4.5 10	✓
0.5	2	0	0.5	4.5 12	✓

1 2 0 0.5 4.5 15



4. CONCLUSION

The present study demonstrates that the selection of excipients has a great importance in obtaining oral lyophilisates with acceptable quality attributes, among which disintegration time is one of the most important. To summarize, the most suitable formulations for further drug incorporation are liquid formulations containing 6 % (w/w) excipients in the ratio 1: 2: 5 for gelatin: PVP K25: mannitol, and 0.5: 2: 0.5: 4.5 for gelatin: PVP K25: glycine/ croscarmellose: mannitol.

5. REFERENCES

1. Casian, T., et al., QbD for pediatric oral lyophilisates development: risk assessment followed by screening and optimization. Drug Development and Industrial Pharmacy, 2017. 43(12):1932-1944.
2. Slavkova, M., et al., Orodispersible drug formulations for children and elderly. European Journal of Pharmaceutical Sciences, 2015. 75:2-9.

ACKNOWLEDGMENT

The authors acknowledge financial support from the Slovenian Research Agency (Research Core Funding, No. P1-0189) and all colleagues contributed to the present research work.

EVALUATION OF DILUTION CAPACITY AND COMPACTION BEHAVIOUR OF THE EXCIPIENTS CO-PROCESSED BY IN SITU FLUIDIZED BED MELT GRANULATION

Ivana Aleksić¹, Slobodanka Ćirin-Varađan¹, Teodora Glišić¹, Mihal Đuriš², Jelena Đuriš¹, Jelena Parojčić¹

¹*Department of Pharmaceutical Technology and Cosmetology, University of Belgrade – Faculty of Pharmacy, Serbia*

²*Department of Catalysis and Chemical Engineering, Institute of Chemistry, Technology and Metallurgy—National Institute of the Republic of Serbia, Serbia*

1. INTRODUCTION

Co-processing has emerged as a suitable approach to meet the increasing demands for excipients with improved tableting performance. Apart from the most commonly used energy-consuming co-processing methods (e.g. spray-drying and wet granulation), melt granulation as a solvent-free and more environmentally friendly technique has recently gained more attention [1].

The aim of the present study was to investigate the influence of meltable binder particle size and compaction parameters on dilution capacity and compaction behaviour of lactose-based co-processed excipients.

2. MATERIALS AND METHODS

2.1. Materials

Paracetamol (Acros Organics, Belgium) was used as the model drug. Lactose monohydrate (Carlo Erba Reagents, Italy) was used as filler and glyceryl palmitostearate (Precirol[®] ATO 5 Gattefossé S.A.S, France) as meltable binder.

2.2. Preparation of co-processed excipients

Co-processed excipients were prepared by in situ melt granulation in Mycrolab fluid bed processor (OYSTAR Hüttlin, Germany). Precirol[®] particles (15%) from the 125–180 μm ($\approx 150 \mu\text{m}$) or 600–710 μm sieve fraction ($\approx 655 \mu\text{m}$) were used for granulation of lactose (85%). The inlet air flow rate was 30 m^3/h , and product temperature during agglomeration was 65 $^\circ\text{C}$.

2.3. Particle size and shape analysis

Granule size distribution was evaluated by sieve analysis, and median particle diameter (d_{50}) was calculated by linear interpolation of the cumulative percentage frequency curve. Granule shape was examined by 2D scanned image (4800 dpi resolution) analysis using ImageJ software. The aspect ratio (AR) and

circularity (C) were calculated for granule shape evaluation.

2.3. Determination of the Carr index

The bulk and tapped (1250 taps) densities of co-processed excipients and their mixtures with 30, 40 or 50% paracetamol were determined using tap density tester STAV 2003 (J. Engelsmann AG, Germany), and Carr index was calculated.

2.4. Dynamic compaction analysis

Co-processed excipients and their mixtures with paracetamol were compressed on a single punch instrumented tablet press (GTP D series, Gamlen Tableting Ltd, UK). Compacts (100 mg) were compressed under compression load of 200 kg ($\approx 70 \text{ MPa}$) or 500 kg ($\approx 173 \text{ MPa}$), and compression speed of 60 or 120 mm/min. 6 mm flat faced punches were used. The obtained force-displacement curves were used to calculate: net work of compression (NW), detachment stress (DS), ejection stress (ES). Tablet crushing force was determined using tablet hardness tester Erweka TBH 125D (Erweka GmbH, Germany), and the values obtained were used to calculate tensile strength (TS). Elastic recovery (24 h after compression) was calculated, as well.

2.4. Experimental Design

In order to investigate the influence of binder particle size, paracetamol content and compression speed on the abovementioned compaction properties, compacts were prepared, at compression load of 500 kg, according to 2³ full factorial design.

3. RESULTS AND DISCUSSION

3.1. Particle size and shape

Larger initial binder particle size led to formation of larger and more spherical granules (Table 1).

Table 1. The size and shape of the co-processed excipients' particles.

Binder PS (μm)	d_{50}	AR	C
150	564.9	1.33	0.81
655	846.2	1.14	0.86

3.2. Flowability

The Carr index values obtained indicated considerably better flowability of the co-processed excipient prepared by using larger binder particles (P655) in comparison with the excipient prepared with smaller binder particles (P150). This might be ascribed to more spherical and larger particles of P655. However, the addition of paracetamol led to an increase in Carr index values and less pronounced differences between two excipients (Fig. 1).

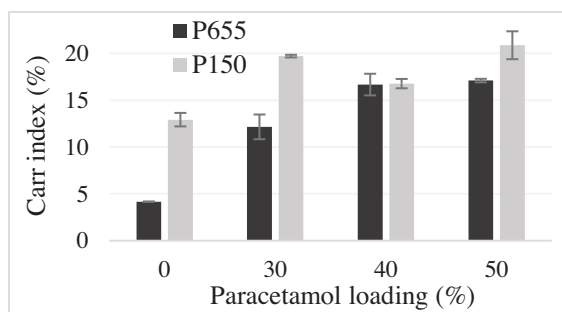


Figure 1. The influence of paracetamol loading on flowability of co-processed excipients.

3.3. Compaction behaviour

The results obtained revealed better mechanical properties of P150 in comparison with P655 compacts, irrespective of the compression pressure applied. The addition of paracetamol, as the model API with poor compaction properties, led to decrease in tensile strength of the compacts prepared with both excipients, and paracetamol content showed statistically significant influence on TS ($p < 0.0001$). Acceptable tensile strength (> 1 MPa) could be achieved for compacts with 30% paracetamol compressed at higher compression pressure (≈ 173 MPa).

Paracetamol content, compression speed and interaction between binder particle size and paracetamol content were found to significantly affect NW. The influence of binder particle size was more pronounced at higher paracetamol content, with lower NW observed in the case of P655. Higher compression speed led to higher NW.

Relatively low values of detachment and ejection stress (< 3.5 MPa) indicate good antiadhesive and lubricating properties of the investigated excipients. Lower values of both parameters were observed in the case of P655 which could be related to different agglomeration mechanisms involved. Besides binder particle size, compression speed and paracetamol content were found to significantly influence these properties.

Elastic recovery values of the investigated samples ranged between 12 and 28%. In the case of both excipients, higher elastic recovery values were obtained at higher compression pressure. ER values of the compacts prepared at higher compression pressure were significantly affected by compression speed and interactions of the investigated variables.

4. CONCLUSION

The results obtained show that meltable binder particle size affects granule size and shape, and consequently may influence flowability and compaction behaviour of the co-processed excipients. Interactions between binder particle size and compaction variables were also found to affect compaction properties of the investigated excipients.

5. REFERENCES

- Ćirin-Varadan, S., et al., *Comparative evaluation of mechanical properties of lactose-based excipients co-processed with lipophilic glycerides as meltable binders*. Journal of Drug Delivery Science and Technology, 2022. 67: 102981.

ACKNOWLEDGMENT

This research was funded by the Ministry of Education, Science and Technological Development, Republic of Serbia through Grant Agreement with University of Belgrade-Faculty of Pharmacy No: 451-03-68/2022-14/200161.

CRUSHING EFFECT ON DISSOLUTION PROFILES OF METOPROLOL SUCCINATE MODIFIED RELEASE TABLETS

Fatima K. Al-Sulaiti¹; Fatma Kır¹; Selma Sahin¹

¹*Department of Pharmaceutical Technology, Hacettepe University Faculty of Pharmacy, Ankara, Turkey*
Correspondence: sahin.selma@gmail.com

1. INTRODUCTION

Oral dosage forms are one of the most used formulations in clinical practice, due to easy and practical administration and lower costs. For patients with swallowing difficulties or enteral feeding tubes, solid dosage forms are modified to facilitate the administration by crushing. According to the dosage form specifications and clinical condition of the patient, immediate release (IR) tablets can be crushed and dispersed in water. However, other oral dosage forms (i.e. modified-release (MR), enteric-coated tablets, film-coated tablets) should not be crushed due to potentially unpredictable release properties, which may result in supratherapeutic or subtherapeutic in vivo drug concentrations.

On the other hand, the absence of an IR-alternative makes it sometimes necessary for clinicians to apply this practice, although the evidence based-guidelines clearly state that non-IR oral solid dosage forms cannot be crushed. Therefore, in the real clinical practice, many non-IR dosage forms are crushed and administered to patients with swallowing difficulties or feeding tubes (i.e. dysphagia, enteral-feeding tubes) [1, 2].

The effect of crushing on dissolution profiles of commercially available metoprolol succinate MR (MS-MR) tablets available in Turkish market was evaluated in this study.

2. MATERIALS AND METHODS

2.1. Materials

MS-MR (100 mg, AstraZeneca) tablets were purchased from a community pharmacy in Turkey. Monobasic potassium phosphate ($\geq 99\%$; Sigma-Aldrich, St. Louis, MO USA), and sodium hydroxide ($\geq 97\%$; Merck, Germany) were used as received.

2.2. Method for Tablet Crushing Technique

Whole MS-MR tablets were manually crushed to powder state using mortar and pestle technique to mimic the hospital practices.

2.3. Dissolution Studies

Dissolution studies were conducted in compliance with USP monograph (USP30) conditions (Table 1) using Sotax dissolution testing instrument (Basel, Switzerland). Each sample (5 mL) was withdrawn and then replaced with an equal volume of fresh medium. Samples were filtered through a 0.45- μm membrane filter and then analysed (Shimadzu UV-1800) at 227 nm using UV-Spectrophotometer.

Table 1. Conditions of dissolution studies.

Apparatus	Apparatus 2 (paddle)
Speed	50 rpm
Medium	pH 6.8 phosphate buffer
Medium Volume	500 mL
Temperature	37 \pm 0.5°C
Sampling Time	1, 4, 8, 20, 24 h

3. RESULTS AND DISCUSSION

No standard tablet-crushing protocol exists to date. Hospital practices include the use of a mortar and pestle or pill crusher device, mixing with food or thickened fluid vehicles, or flushing the powder through the enteral feeding tubes with water. In our study, we crushed MS-MR tablets using a mortar and pestle to mimic the crushing process of tablets applied in hospitals.

The sampling time continued for up to 24 hours as it was stated in the medication package insert that MS-MR tablets maintain stable concentration in blood for 24 hours.

P03

The dissolution profiles of MS whole tablets and crushed tablets in pH 6.8 phosphate buffer are shown in Figure 1.

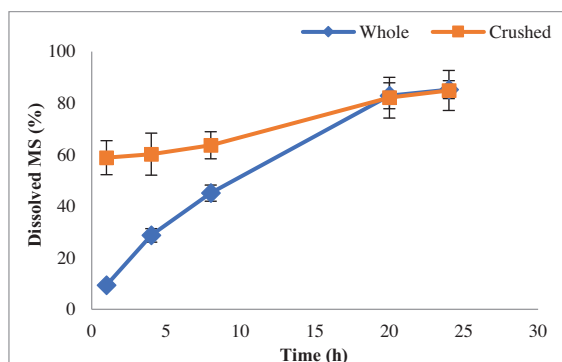


Figure 1. Dissolution profiles of whole and crushed MS-MR tablets (mean \pm standard deviation; n=6).

The dissolution profile obtained for the whole tablet is in accordance with the reference values in the USP (not more than 25% in 1 hour, between 20 and 40% in 4 hours, between 40 and 60% in 8 hours, not less than 80% in 20 hours). According to the dissolution profile of crushed tablets, dissolution was greater than 50% within 1 hour but then approached approximately 80% within 24 hours. Therefore, the results for the crushed tablet were not found to meet the USP criteria.

The f2 similarity factor used to compare the similarities of the two dissolution profiles was calculated as 28.02 (<50) indicating that the two dissolution profiles were not similar. The f1 difference factor was calculated as 40.02 (≥ 15) conforming the difference between the dissolution profiles.

The results suggest the possibility that release profile has changed as a result of the deformation of the polymeric membrane structure that controls the drug release rate from microencapsulated cores containing MS. Since the deformation of polymeric membrane structures after tablets were crushed could be heterogeneous, the standard deviation of six replicates was found higher than the whole tablets.

4. CONCLUSION

In Turkey, MS-MR tablets are crushed in critically ill patients using feeding tubes. Our study demonstrated that crushing changes the dissolution profile of MS-MR tablets. This suggests the clinical impact on blood-

concentration profiles in the feeding tube patient population. Therefore, future research is needed to determine specific dosing recommendations, achieve therapeutic efficacy and prevent possible toxicity when crushing MS-MR tablets.

5. REFERENCES

1. Demirkan, K., et al., *Assessment of drug administration via feeding tube and the knowledge of health-care professionals in a university hospital*. *European Journal of Clinical Nutrition*, 2017. 71(2): 164-8.
2. Wasylewicz, ATM., et al., *Clinical decision support system-assisted pharmacy intervention reduces feeding tube-related medication errors in hospitalized patients: A focus on medication suitable for feeding-tube administration*. *Journal of Parenteral and Enteral Nutrition*, 2021. 45(3): 625-32.

ACKNOWLEDGMENT

This study was supported by Hacettepe University Scientific Research Projects Coordination Unit with TSA-2022-19747 fund.

MANUFACTURING AND EXAMINATION OF 3D PRINTED VAGINAL DRUG DELIVERY SYSTEMS

Petra Arany¹, Pálma Fehér¹; Zoltán Ujhelyi¹; Miklós Vecsernyés¹; Renátó Kovács²; Mariann Zichar³; Ildikó Papp³, Géza Regdon, Jr. ⁴, Mónika Béres ⁵, Melinda Szalóki ⁶, Ildikó Bácskay^{*1}

¹Department of Pharmaceutical Technology, Faculty of Pharmacy, University of Debrecen, Hungary

²Department of Medical Microbiology, Faculty of Medicine and Faculty of Pharmacy, University of Debrecen, Hungary

³Department of Computer Graphics and Image Processing, Faculty of Informatics, University of Debrecen, Hungary

⁴Institute of Pharmaceutical Technology and Regulatory Affairs, University of Szeged, Hungary

⁵Department of Medical Imaging, Faculty of Medicine, University of Debrecen, Debrecen, Hungary

⁶Department of Biomaterials and Prosthetic Dentistry, Faculty of Dentistry, University of Debrecen, Hungary

1. INTRODUCTION

Vaginal drug delivery systems can provide a long-term and constant liberation of the active pharmaceutical ingredient even for months. [1] For our experiment, FDM 3D printing was used to manufacture the vaginal ring samples from thermoplastic polyurethane filament, which enables fast manufacturing of complex, personalized medications. 3D printing can be an excellent alternative instead of industrial manufacturing, which is complicated and time-consuming. [2] In our work, the 3D printed vaginal rings were filled manually with jellified metronidazole or chloramphenicol for the treatment of bacterial vaginosis. The samples material structure and biocompatibility properties were determined. [3]

2. MATERIALS AND METHODS

2.1. Materials

For the 3D printing process, polylactic acid (PLA), PLA Gypsum, PLA Foam and thermoplastic polyurethane (TPU) was used. As a jellifying agent Carbopol 934, medium molecular weight chitosan, hydroxyl ethyl cellulose and agar-agar was used. As an active pharmaceutical ingredient metronidazole and chloramphenicol were used.

2.2. Method – Sample manufacturing

The digital design of the samples were designed using SolidWorks. The shape was based on a commercially available vaginal ring but the edges were chamfered. Each sample was 5 mm tall and printed in two different diameters (39.19 and 41.19 mm) to provide the perfect fitting. Four different formulations were prepared based on the jellifying agent and all four formulation was homogenized with

metronidazole and chloramphenicol separately. This gels were manually filled to the pre-printed vaginal rings.

2.3. Method – Material structure

Sample characterisation by thermogravimetric (TG) and heatflow (DSC) analysis, contact angle measurement and microcomputed tomography (MicroCT).

2.4. Method – Dissolution test

The dissolution test was carried out by a USP Type I Erweka DT 800 dissolution apparatus. Dissolution medium of 200 ml of simulated vaginal fluid at pH 4.2 was used at 37°C.

2.5. Method – Biocompatibility test

A long-term MTT cell viability assay was performed to determine if any kind of xenobiotic is dissolved from the samples. Microbiological test was performed to determine the effectiveness of the samples.

3. RESULTS AND DISCUSSION

3.1. Sample manufacturing

Our research group had successfully printed the TPU based vaginal rings by FDM 3D printing with the adequate printing parameters. Successfully manufactured API containing gels in three different formulations and successfully filled the samples manually.

3.2. Material structure

The TG/DSC curves confirmed that the API's should be filled manually to eliminate the degradation due to high printing temperature. (Fig. 1)

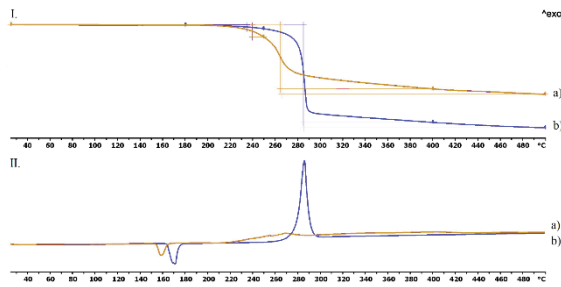


Figure 1. Thermogravimetric (I) and heatflow (II) analysis of the chloramphenicol (a) and the metronidazole (b).

3.3. Dissolution test

Based on the dissolution test results and the f1-f2 analysis all samples can be described with different dissolution test results. (Fig. 2)

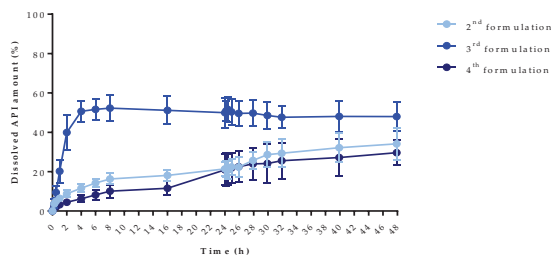


Figure 2. Dissolved API amount (%) versus time (h) for samples jellified with metronidazole.

3.4. Biocompatibility test

The vaginal ring showed no cytotoxicity based on the ISO 10993-5:2009(E) A.2.4 standard. Based on the microbiological experiment the metronidazole and chitosan containing sample showed bactericidal effect within 24 hour against the just metronidazole or just chitosan containing samples. (Fig. 3)

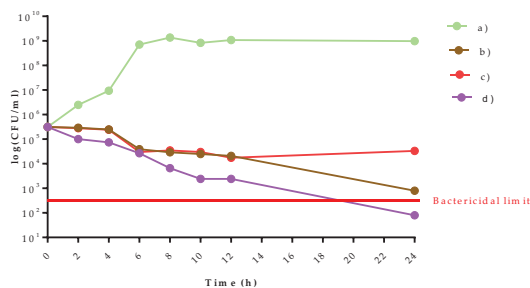


Figure 3. The logarithmical colony-forming unit (CFU)/mL in case of E. coli versus time (h) where (a) empty; (b) metronidazole containing (c) 3 w/w% chitosan and 4 w/w% hydroxyethyl cellulose-containing; (d) 3 w/w% chitosan and metronidazole containing vaginal ring.

4. CONCLUSION

In conclusion, vaginal rings from thermoplastic polyurethane were successfully 3D printed by FDM technology. The pre-printed samples were filled with chloramphenicol or metronidazole and jellified with chitosan/HEC or agar-agar. Based on the dissolution curves, the used API and jellifying agent can modify the dissolved API amount. Based on the MTT assay results, TPU polymer can be considered cytocompatible.

The microbiological evaluation confirmed that metronidazole and chitosan have a synergistic effect against E. coli. Based on the overall project, TPU polymer filled with metronidazole was suggested for further investigations.

5. REFERENCES

1. Pelle P. et al., Preparation and clinical use of combined broad spectrum vaginal suppositories. *ORV Hetil*, 1980, 17: 1015-7.
2. Chia H. N. et al., Recent advances in 3D printing of biomaterials. *J. Biol. Eng.*, 2015, 9: 1–14
3. Arany et al., Manufacturing and examination of vaginal drug delivery system by FDM 3D printing. *Pharmaceutics*, 2021, 13, 1714

ACKNOWLEDGMENT

Supported by the ÚNKP-20-3 New National Excellence Program of the Ministry for Innovation and Technology from the source of the National Research, Development and Innovation Fund. The project was supported by the Gedeon Richter’s Talentum Foundation (1103 Budapest, Gyömrői út 19-21, Hungary). This work was supported by the European Union and the European Regional Development Fund [GINOP-2.3.2.-15-2016-00011]. The publication is supported by the GINOP-2.3.4-15-2020-00008 project. The project is co-financed by the European Union and the European Regional Development Fund. The research was supported by the Thematic Excellence Programme (TKP2020-IKA-04) of the Ministry for Innovation and Technology in Hungary”.

DEVELOPMENT OF A COLOURANT SELECTION MODEL IN FILM COATING FOR ACHIEVING TARGETED COLOUR OF FILM-COATED TABLETS

Grega Bajc¹, Gregor Ratek¹, Franc Vrečer^{1,2}, Klemen Korasa¹

¹R&D, Krka d.d., Šmarješka cesta 6, 8501 Novo mesto, Slovenia

²University of Ljubljana, Faculty of Pharmacy, Aškerčeva 7, 1000 Ljubljana, Slovenia

1. INTRODUCTION

Colour is a very important characteristic of film-coated tablets. It ensures easier recognition, harder forgery and it often leads to better patient compliance. The desired colouring of a film-coated tablet is achieved by using an abundance of pigments [1]. In recent years, though, this is becoming increasingly more difficult due to new toxicological studies suggesting some of those pigments are unsafe [2]. New EMA recommendations in a reflection paper on the pharmaceutical development of medicines for use in older population are suggesting innovator and generic products should have the same key visual appearance (i.e. colour, size etc.) to the degree (legally) possible [3]. When developing a product, the obstacle how to reproduce reliably the desired shade of colour is often encountered.

In the present study, a model was created that converts the L^* , a^* , and b^* colour coordinates/values of a reference film-coated tablet into the colourant composition, resulting in the targeted colour.

2. MATERIALS AND METHODS

2.1. Materials

Film coatings of different colours, using red and yellow pigments were prepared. The materials needed were placebo tablet cores and components of film coating including yellow or/and red iron oxide pigment (Venator Pigments S.p.A., Italy) and commercially available mixture Opadry[®] (Colorcon, USA) consisting of HPMC polymer, plasticizer (PEG), lubricant (talcum) and titanium dioxide.

2.2. Method

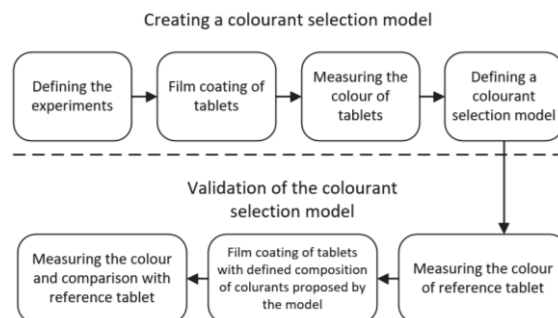


Figure 1. Model development plan

Experiments were planned using the Design of experiments method (Design Expert software, version 12 (StatEase, USA)). The quantitative limits of components included were set based on previous experiences and are described in Table 1.

Table 1. Design space limits

Parameter	Lower limit	Upper limit
Opadry [®]	97.0 %	100.0 %
Red iron oxide	0.0 %	3.0 %
Yellow iron oxide	0.0 %	3.0 %

Based on the proposed limits, an experimental space with 19 experiments was created. Two experiments had the same composition as the test of colour reproducibility.

Tablets were coated in GCII coating machine (Glatt, Germany). Colours of tablets were measured with HunterLabUltraScan VIS colour measurement spectrophotometer (Hunter Lab, USA), which defines the colour in CIEL*a*b* colour space with L^* , a^* and b^* colour values on the basis of which the model was set.

It was used to predict colourants for film coating of the independent test batches, which were later compared with reference products.

3. RESULTS AND DISCUSSION

3.1. L^* , a^* and b^* models

Colours were defined with L^* , a^* and b^* values. L^* value describes the brightness on a scale between 0 and 100. a^* value indicates how green to red the colour is on scale between -127 and +127 and b^* indicates how blue to yellow it is on scale between -128 and +127.

With the tested film coatings we achieved colour coordinates in the range: L* between 68.24 and 103.33, a* between -0.18 and 28.25 and b* between 4.87 and 41.94. For designing the experimental space, special quartic design model was used. From results we gained polynomial (regression) equations for L*, a*, and b* which enable calculation of colour values out of colourants selection, and, in reverse colourant selection, out of colour values. The following contour graphs show the best visualization of those three equations.

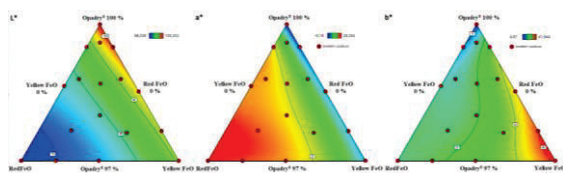


Figure 2. Contour graphs for L*, a* and b*. In the left corners of graphs is 3% of red FeO, in the right corners is 3% of yellow FeO and in the upper corners is 100% of Opadry®. Red shows the highest value, while blue shows the lowest value of L*, a* and b*.

The first graph shows that the highest value of L* is reached in an area with the highest amount of Opadry® and the lowest in the area with the highest amount of red iron oxide. The a* graph shows that the highest a* is achieved in the area with the highest amount of red iron oxide. The b* graph shows the highest b* is within the area of the highest yellow oxide amount.

The suitability of the model can be assessed with the value of adjusted R². It represents the proportion of variability in our results explained by our model. The adjusted R² values of all three models are presented in Table 2. These values indicate a good fit of the results.

Table 2. Adjusted coefficient of determination of L*, a*, and b* models

	L*model	a*model	b*model
adjusted R ²	0.9915	0.9787	0.9797

3.2. Validation of a colour selection model

The best comparison between the reference tablets and test tablets is made by ΔE value (i.e. colour difference). The human eye does not perceive the difference between two colours when ΔE is below 2.

$$\Delta E_{ab}^* = \sqrt{(\Delta L^*)^2 + (\Delta a^*)^2 + (\Delta b^*)^2}$$

ΔE reveals the largest colour difference for the brightest tablets and the lowest for the light pink. Even though the ΔE was more than 2, there was only a slight difference in colour observed by visual inspection. However, for inexperienced observers all the test tablets are virtually identical to the reference tablets.

Table 3. Comparison of reference film-coated tablet and test film-coated tablet based on proposed colourant selection.

	1	2	3
Reference film-coated tablet			
Test film-coated tablet			
Colour difference (ΔE)	7.32	3.50	1.81

4. CONCLUSIONS

In our study, a colourant selection model was developed by applying DoE principle and colourimeter. The colours of reference tablets were measured, and a designed model was used to predict the optimal selection of two pigments needed to achieve the desired colour of film-coated tablets. The model successfully predicted the optimal colourant composition. Further research is necessary to improve accuracy and expand the measuring range of similar predictive models.

5. REFERENCES

1. M. Mishar, P. Biswal, Bhadouriya Anupam, and Yadav Vivek, “An updated review on colorants as the pharmaceutical excipients,” *International journal of pharmaceutical, chemical and biological sciences*, vol. 5(4), pp. 1004–1017, 2015.
2. F. Aguilar *et al.*, “Scientific Opinion of the Panel on Food Additives, Flavourings, Processing Aids and Food Contact Materials (AFC) PANEL MEMBERS *,” 2008.
3. E. Medicines Agency, “Reflection paper on the pharmaceutical development of medicines for use in the older population,” 2020.

ACKNOWLEDGMENT

Authors would like to thank Krka, d. d., Novo mesto for providing support for the study.

INTRINSIC DISSOLUTION RATE: MEASUREMENT USING AN INEXPENSIVE ALTERNATIVE TO THE PHARMACOPOEIAL DIE HOLDER

Hilke Lösing^{1,2}, Jonas Borregaard Eriksen¹, Regina Scherließ², Annette Bauer-Brandl¹

¹*Department of Physics Chemistry and Pharmacy, University of Southern Denmark, Odense M, Denmark*

²*Department of Pharmaceutics and Biopharmaceutics, Kiel University, Grasweg 9a, 24118 Kiel, Germany*

1. INTRODUCTION

The dissolution rate is in many cases rate-determining for absorption of poorly water-soluble active pharmaceutical ingredients. Intrinsic dissolution rate (IDR) is dissolution rate normalized to the surface area and is measured of compacted substances with minimal porosity in a special die holder to keep the surface area constant.

Monograph 2.9.29 in the European Pharmacopoeia (Ph. Eur.) describes testing the IDR of a substance in the dissolution apparatus, either top-down or at the bottom with the paddle rotating above [European Pharmacopoeia, 2021]. The standard apparatus needs 150 - 700 mg, which is not always available in drug development [Teleki et al., 2020; Tseng et al., 2014]. It appears to be a common problem that APIs may not attach to the holders [Bartolomei et al., 2006].

Removable adhesive gum (RAG) used in households and offices consists of the polymer polyisobutylene with inorganic fillers such as titanium-(IV)-oxide and contains no added organic solvents. In the present study we tested whether removable adhesive gum (RAG) can replace the die holder when evaluating the IDR. Co-crystals of acyclovir and glutaric acid were used as a model substance of tricky properties in terms of sitting in the die holder.

2. MATERIALS AND METHODS

2.1. Materials

Acyclovir and co-crystals of acyclovir and glutaric acid in a molar ratio of 1:1 were used as model compounds. Acyclovir was from Aber GmbH (Karlsruhe, Germany) and glutaric acid from Sigma Aldrich (Brøndby, Denmark). A 0.1 M phosphate buffer pH 7.4 was prepared as described in Ph. Eur. monograph 4.1.3. [European Pharmacopoeia, 2021]. The removable adhesive gum RAG named "Linex

Tack-ALL" was purchased from Hamelin (Denmark).

2.2. Preparation of substance and tablet

Co-crystals were prepared in a ball mill model Retsch MM2000 in a molar ratio of 1:1. were ball milled for 4 h at an amplitude of 20 mm. Flat faced tablets (approx. 60 mg of substance) were compressed on a EK0 tablet press by hand and kept under full pressure for 30 sec.

2.3. Preparation of the device

The device was made by kneading approx. 1.5 g of RAG thoroughly and shaping it into a ball, placing the ball on a coin, and then pushing a tablet of the compound of interest into the RAG. The RAG was then shaped around the tablet by hand to ensure a constant surface area. We confirmed no visible grooves in the RAG. Wearing gloves proved best to ensure that the RAG did not get contaminated. The coin ensured that the tablet was heavy enough to sink to the bottom, and the stirring motion did not move it from its position. If the coin did not sink to the centre of the vessel, it was carefully pushed in place with a bar. We used a € 10-cent coin, but any other coin or disc would do the same.

2.4. Intrinsic dissolution testing

900 ml of degassed 0.1 M phosphate buffer pH 7.4 were utilized as the medium at 37 °C, and the stirring speed was 50 rpm. Each tablet had a mass of approx. 60 mg and approx. 1.5 g of the RAG were utilized. the exposed area was 0.22 cm². Every five minutes, a sample of 5 ml was taken with a syringe and filtered with a 0.45 µm filter. In total, the intrinsic dissolution was determined for half an hour, and HPLC was used for quantification. The IDR of acyclovir in mg/h/cm² was calculated from the slope of the regression line. At each time point, the mean and standard deviations were calculated (n = 3).

3. RESULTS AND DISCUSSION

3.1. Validation of the use of RAG

The RAG did not release any detectable substances into the media. No adsorption nor permeation of the tested substances through the RAG was detected.

3.2. Intrinsic Dissolution Rates

For both Acyclovir and the co-crystal, the dissolution process of the substance was followed and plotted cumulative vs. time (Figure 1).

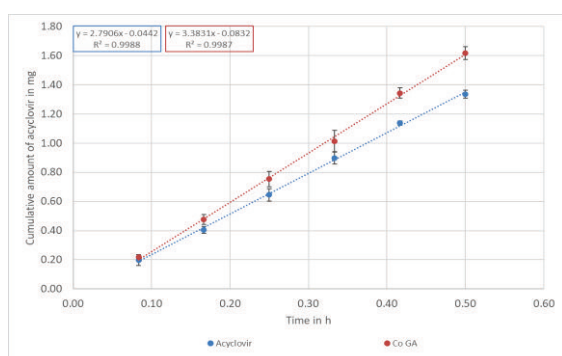


Figure 1. Cumulative amount of acyclovir in mg against the time in hours, for acyclovir and Co GA (from intrinsic dissolution testing). Data are represented as mean \pm SD (n = 3)..

Plotting the cumulative amount of acyclovir in mg vs. time (5, 10, 15, 20, 25, 30 min time points) produced a linear relation with correlation coefficients larger than 0.998. The coefficient of variation (% CV) (n = 6) of the IDR was less than 3.5 %, indicating good reproducibility.

Figure 2 shows the intrinsic dissolution rate values:

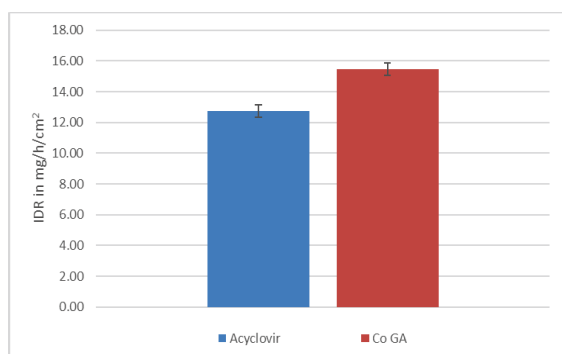


Figure 2. Intrinsic dissolution values f in mg/h/cm² of acyclovir and Co GA. Data are represented as mean \pm SD (n = 3).

The IDR was found to be 12.76 mg/h/cm² for acyclovir, and 15.46 mg/h/cm² for Co GA. This means that the co-crystals had a 1.2-fold higher IDR.

4. CONCLUSION

These values confirm that the RAG may be a good alternative for investigating the IDR.

RAG does not interfere with the media or substances tested. Linear and reproducible values for the IDR were obtained with the model substances acyclovir and acyclovir: glutaric acid co-crystals. It can therefore be argued that the RAG is a good alternative for determining the IDR of these substances. The RAG is widely available and not expensive. It is easy to shape and can therefore be used for different tablet sizes including minitables.

5. REFERENCES

1. European Pharmacopoeia, 2.9.29. Intrinsic dissolution, 10th edition, Council of Europe, Strasbourg, 2021.

ACKNOWLEDGMENT

The authors are grateful for a mobility grant to HL, and collaborative work between the two institutions enabled by funding from Nordforsk Program Nordic University Hub (Project number 85352 “Nordic PoP”).

EFFECT OF PROCESS PARAMETERS IN HIGH SHEAR GRANULATION ON PARTICLE SIZE, COMPRESSIBILITY AND COMPACTIBILITY OF GRANULATED MESOPOROUS SILICA

Ana Baumgartner¹, Odon Planinšek¹

¹*Department of Pharmaceutical Technology, Faculty of Pharmacy, University of Ljubljana, Slovenia*

1. INTRODUCTION

Mesoporous silica is investigated as a promising carrier for amorphous solid dispersions, but its major limitations are poor flow and compression properties, which are related to small particle size [1]. Hence, a novel co-processed material was developed consisting of mesoporous silica and a sugar alcohol isomalt acting as a binder which connects small silica particles into granules. Besides bigger particle size, such material should have better flow and compression properties as well as high enough specific surface area for impregnation with poorly water-soluble drug. The purpose of this study was to examine the effect of process parameters in high shear granulation on particle size in relation to compressibility and compactibility of such material by Design of Experiments (DoE) study.

2. MATERIALS AND METHODS

2.1. Materials

Isomalt (GalenIQ 800) was kindly donated by Beneo (Germany). Mesoporous silica (Syloid 244 FP) was obtained from Grace Davison, Grace GmbH & Co. KG (Worms, Germany). Water was purified by reverse osmosis.

2.2. Preparation of granulates

Co-processed excipients were made by wet granulation in a high-shear mixer (ProCept 4M8-TriX, 1L vessel, Belgium). Distilled water was added as granulation liquid to the blend of isomalt and silica dropwise at a specific flow rate. Wet granulate was sieved through a 2 mm sieve and dried on trays at 60 °C until moisture content was below 2%. Dried granulate was sieved through 710 μm sieve, and particles that passed 80 μm sieve were discharged.

2.3. Experimental design

A central composite orthogonal design was used for DoE study. Experimental design and analysis were performed by Modde Software (Sartorius, Germany). Independent variables

were isomalt amount and water amount, water addition rate and granulator impeller speed. For statistical analysis and model setting, $\alpha=0.10$ was chosen to determine significant variables for the following observed responses: particle size parameters (d10, d50, d90, span) and compressibility and compactibility parameters (Heckel constant and compactibility slope [c_p ; tensile strength vs. compression pressure]).

2.4. Particle size determination

Particle size parameters d10, d50 and d90 were measured by laser diffraction method with a dry powder feeder (Mastersizer 3000, Malvern, UK). Span as a measure of particle size distribution was calculated according to the following equation: $span = (d90 - d10)/d50$.

2.5. Compactibility and compressibility evaluation

For each granulate, 10–15 500 mg tablets were compressed at different compaction pressures using single-punch tablet press (Kilian SP300, IMA, Germany) with round flat-faced punches. The following tablet characteristics were evaluated: tablet mass (Mettler Toledo, Switzerland), thickness and diameter (micrometer, Mitutoyo, Japan), crushing force (hardness tester VK200, Varian Inc., USA), true density (helium pycnometer AccuPyc 1330, Micromeritics, USA). Heckel constant and c_p were determined by linear regression.

3. RESULTS AND DISCUSSION

3.1. Effect of process parameters on particle size

Out of 27 performed experiments, 7 ended in an over-wet granulate and were therefore not further evaluated. After eliminating insignificant factors, good models for d10, d50, d90 and span were obtained (Table 1).

Table 1. Model characteristics for d10, d50 and d90

	d10	d50	d90	span
R ²	0.92	0.88	0.93	0.88

P07

R² (adj)	0.88	0.86	0.82	0.82
Q²	0.78	0.78	0.57	0.66
Model validity	0.79	0.78	0.85	0.44
Reproducibility	0.93	0.92	0.89	0.98

It was observed that amount of added water and impeller speed have a positive effect on particle size, meaning that the higher those values are, the larger particles are formed (Figure 1). This can be explained by the fact that increasing these factors contributes to higher liquid saturation of the granulate during the process,

which means more liquid on the surface and thus granule growth by coalescence [2]. However, if both factors are set on high levels, there are high chances of overgranulation, as was the case in the experiments that were discarded. On the other hand, water addition rate has a negative effect on particle size. The reason for this could be that slower addition rate means longer process time and thus more time for the granules to form. Slower water addition rate also results in narrower particle size distribution, which is a desired characteristic as well.

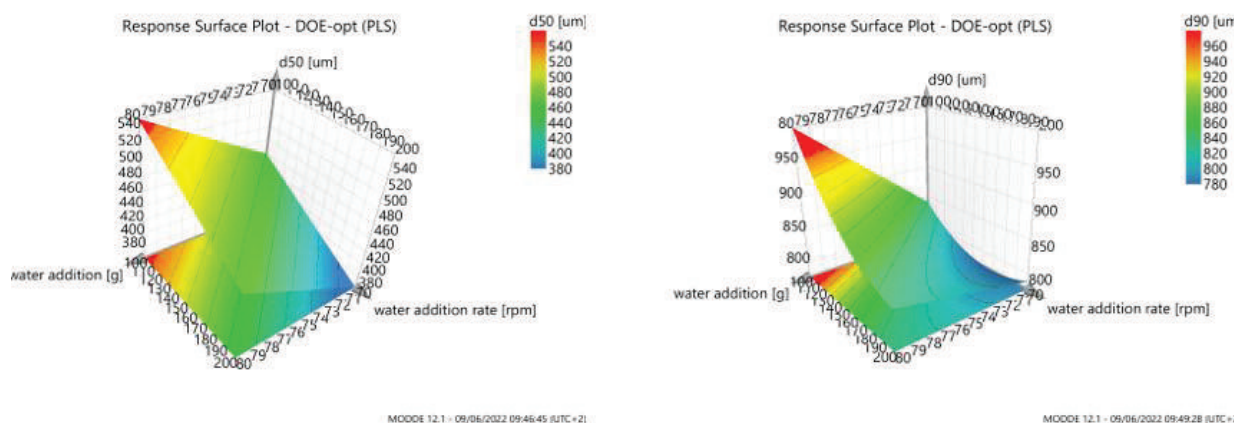


Figure 1. Visualisation of effect of water amount and addition rate on d50 and d90. Impeller speed was 200 rpm and isomalt amount was 17.5 g in both cases.

3.2. Effect of process parameters on compressibility and compactibility

The models acquired to explain the effects of process parameters on compressibility (Heckel constant) and compactibility (c_p) were less good (R^2 (adj) = 0.57 and 0.66, respectively; Q^2 = 0.49 and 0.49, respectively). However, it is still possible to distinguish the main effects. Water addition rate has a positive effect in both cases, meaning that faster rate results in more compressible and compact granulate. This is in contrast to its effect on particle size, which is somewhat surprising. Also, higher amount of binder seems to increase granule compressibility.

4. CONCLUSION

High shear granulation of mesoporous silica with isomalt is a complex process with many process parameters in interplay that govern product characteristics. Although some trends can be seen from the models acquired by a DoE study, more detailed studies are needed to predict the characteristics studied in this research.

5. REFERENCES

1. Baumgartner A, Planinšek O. *Application of commercially available mesoporous silica for drug dissolution enhancement in oral drug delivery.* EJPS, 2021. 167:106015.
2. Badawy SI, et al. *Effect of process parameters on compressibility of granulation manufactured in a high-shear mixer.* International Journal of Pharmaceutics, 2000. 198(1):51-61.

ACKNOWLEDGMENT

The authors acknowledge the financial support provided by the Slovenian Research Agency (Program Code P1-0189).

EVALUATION OF ANALGESIC AND ANTI-INFLAMMATORY EFFECTS OF CYCLODEXTRIN-BASED FLURBIPROFEN NANOGELS FOR DERMAL APPLICATION

Nevin Celebi^{1,2}, Ayse Nur Oktay^{1,3}, Sibel Ilbasemis-Tamer¹, Sevtap Han⁴, Orhan Uludag⁴

¹Department of Pharmaceutical Technology, Gazi University-Faculty of Pharmacy, Ankara, Türkiye,

²Department of Pharmaceutical Technology, Başkent University-Faculty of Pharmacy, Ankara, Türkiye

³Department of Pharmaceutical Technology, University of Health Sciences- Gulhane Faculty of Pharmacy, Ankara, Türkiye

⁴Department of Pharmacology, Gazi University-Faculty of Pharmacy, Ankara, Türkiye

1. INTRODUCTION

Flurbiprofen (FB) is an effective nonsteroidal anti-inflammatory drug utilized in the treatments of chronic and acute inflammatory diseases such as soft tissue injuries, osteoarthritis, rheumatic arthritis and sunburn. But its poor water solubility limits its absorption, thus its dermal bioavailability [1]. Cyclodextrin-based nanogels could be promising for the dermal application of drugs with low water solubility. The main aim of this study was to investigate the in vivo analgesic and anti-inflammatory effects of the optimized flurbiprofen cyclodextrin-based nanogel formulation in rats.

2. MATERIALS AND METHODS

2.1. Materials

Flurbiprofen (FB) was kindly provided by Sanovel Drug Company (Istanbul, Turkey). Hydroxypropyl beta cyclodextrin (HPβCD) and Span 80 were purchased from Sigma- Aldrich®. All the other chemicals were analytical grade.

2.2. Preparation of FB-loaded cyclodextrin-based nanogel formulation

FB-loaded cyclodextrin-based nanogel formulations were prepared via emulsification/solvent evaporation process and optimized with Design of Experiment(DoE) with factorial design. To prepare the FB-loaded cyclodextrin based nanogels, the FB: HPβCD ratio was determined as 1:1 molar ratio with phase solubility studies [2]. The FB content in nanogel formulation was adjusted 4% w/w.

2.3. Preparation of HPMC gel containing cyclodextrin-based nanogel

The weighed HPMC K100 LV powder (5% w/v) was dispersed in the CD-based nanogel

(FB-free or FB-loaded) and then stirred at 500 rpm under a magnetic stirrer (IKA® Eurostar 20) for 60 min at room temperature until a homogeneous gel was obtained.

2.4. Evaluation of Analgesic and Anti-inflammatory Effects of FB-loaded Cyclodextrin Based Nanogels

All the animal protocols were approved by the ethical committee of Gazi University (148677). Formulations were applied at the dosage of 20 mg/kg (FB) to all animal groups (Table 1).

Table 1. Animal groups

ANIMAL GROUPS (Albino male rats (230±10 g))	n ¹	n ²
1.Group (A1, B1) : Control Group	6	6
2.Group (A2, B2): FB-free nanogel in HPMC gel	6	6
3.Group (A3, B3): FB loaded nanogel in HPMC gel	6	6
4. Group (A4, B4): Reference Group (FB in HPMC gel)	6	6
	24	24

n¹: Number of rats used to evaluate the anti-inflammatory effect

n²: Number of rats used to evaluate the analgesic effect

A1-A4: Groups for evaluations of anti-inflammatory effect

B1-B4: Groups for evaluation of analgesic effect

2.4.1. Evaluation of the anti-inflammatory effect

Carrageenan induced rat hind paw edema method was used to examine anti-inflammatory effect. All formulations were applied topically to the plantar surface of the hind paw of rats, and 100 µl of 1% w/v carrageenan was injected into the right hind paw of each rat, 30 min after administration. Physiologic saline (100 µl/paw) was injected into the subplantar tissue of the left hind paw of each rat. Paw volumes were measured by a plethysmograph at 0, 60, 180, 240, 360 and 480. minutes and 24 hours after carrageenan injection. The percentage inhibition of edema was calculated by the following formula:

$$\text{Inhibition of edema \%} = [1 (Vt/Vc)] \times 100$$

Vt: Rat paw edema volume of the treated groups

Vc: Mean edema volume of the control group

2.4.2. Evaluation of the analgesic effect

The tail flick method was used to determine of analgesic effect. The time between placing the rat’s tail on the radiant heat source (IR intensity: 75, Cut off time: 10 s) and sharp withdrawal of the tail was noted as reaction time. Tail-flick test was performed before, and at 30, 60 and 180 minutes after drug administration. The percentage analgesic effect was calculated according to the following formula:

$$\% \text{ Analgesic activity} = \frac{(\text{Observed} - \text{Basal reaction time}) \times 100}{\text{Cut off} - \text{Basal reaction time}}$$

3. RESULTS AND DISCUSSION

PS, PDI and ZP values of optimum nanogel formulation were found 295.5±7.5 nm, 0.336±0.128, -31.9±0.5 mV; respectively. All characterization studies of gel formulations (visual examination, pH, drug content analysis, viscosity measurement, dynamic rheological properties, stability and permeability studies) showed the FB-loaded nanogel in HPMC gel was found better than coarse FB in HPMC gel (Fig.1).

Anti-inflammatory effect studies showed the lower paw volume was observed in the groups applied with FB-loaded nanogel in HPMC gel than those of the coarse powder of FB in HPMC gel. FB-loaded nanogel in HPMC gel (20 mg/kg) inhibited the development of edema from the 1st hour and its effect proceeded during the 24 hours with the lowest paw edema volume.

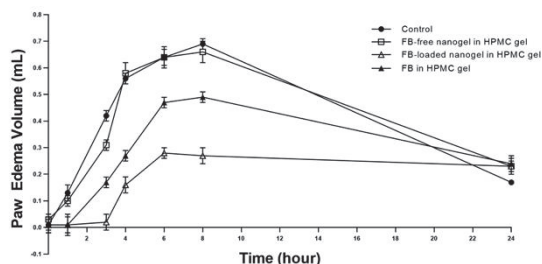


Figure 1. Effect of different formulations on paw volume in carrageenan-induced paw edema in rats. Values were expressed as mean±SEM (n=6).

As results of analgesic effect studies; latency times in the all groups were similar before and 30 min after gel administrations. In the 60 min and 180. min of FB-loaded nanogel in HPMC gel treatment, latency time was found to be significantly prolonged compared to the control group (p<0.05) (Fig.2).

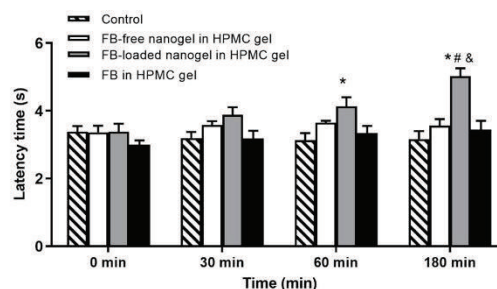


Figure 2. Latency time in the tail-flick test in the rats. *p<0.05 different from control. Values were expressed as Mean±SEM (n=6).

4. CONCLUSION

This study demonstrated that the anti-inflammatory and analgesic effects of flurbiprofen were increased by FB nanogel in HPMC gel formulation compare with FB in HPMC gel.

5. REFERENCES

1. Oktay, A.N., Karakucuk, A., Ilbasemis-Tamer, S., Celebi, N. Dermal flurbiprofen nanosuspensions: Optimization with design of experiment approach and in vitro evaluation. *European Journal of Pharmaceutical Sciences*, 2018. 122: 254-263.
2. Oktay A.N. Insights to the phase solubility diagrams of flurbiprofen with inclusion complex, *Journal of Research in Pharmacy*, 2021. 25(2): 196-208.

ACKNOWLEDGMENT

This study was supported by Tubitak (Project No:117S149).

COMBINED IN-VITRO DISSOLUTION-/ ENZYMATIC CONVERSION-/ PERMEATION-STUDIES OF THE PRODRUG FOSAMPRENAVIR

**Jeppe J. Christiansen¹, Jonas B. Eriksen¹, Jarkko Rautio², Marika Ruponen²,
Annette Bauer-Brandl¹, Martin Brandl¹**

¹Department of Physics, Chemistry & Pharmacy, University of Southern Denmark, Odense, Denmark

²School of Pharmacy, University of Eastern Finland, Kuopio, Finland

1. INTRODUCTION

Prodrugs are pharmacologically inactive substances that are converted in the body (e.g. by enzymatic action) into a pharmacologically active drugs.

In recent years a tendency towards more lipophilic, but poorly water-soluble new drug molecules has been observed. Various candidate-enabling strategies have been tested in order to overcome this challenge. A probate strategy used to overcome poor water solubility is to make a phosphate ester prodrug. Phosphate esters are charged moieties of enhanced solubility. They are hypothesized to be readily absorbed upon cleavage by alkaline phosphatase found in the intestine.

The current study aimed to conduct combined *in vitro* dissolution / enzymatic conversion / permeability studies of the prodrug fosamprenavir, which by cleavage, turns into the parent drug amprenavir, a potent HIV protease inhibitor.

2. MATERIALS AND METHODS

2.1. MDCK II permeability study

The Permeability studies with amprenavir and fosamprenavir were conducted with MDCK II cells that naturally express the alkaline phosphatase.

2.3. PermeaPad[®] permeability study

The permeability studies were made on an artificial set-up in side-by-side cells with added bovine alkaline phosphatase. In the artificial set-up, the donor and acceptor compartment was separated by the biomimetic barrier PermeaPad[®]. A microdialysis probe was added to the donor to follow the conversion of fosamprenavir to amprenavir.

3. RESULTS AND DISCUSSION

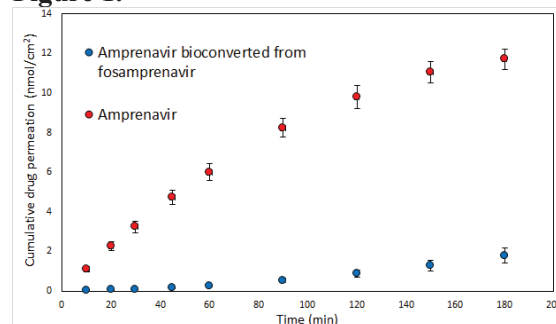
3.1. MDCK II permeability study

The more water-soluble prodrug fosamprenavir has the potential of causing a supersaturation of amprenavir, when enzymatically cleaved by alkaline phosphatase. The bioconversion of fosamprenavir to amprenavir in the MDCK II cells was poor, and a supersaturation of amprenavir was not achieved. This resulted in amprenavir solutions permeating more than the bioconverted amprenavir from the concentrated fosamprenavir solutions (Figure 1). Another issue was the loss of sink conditions during the experiments, likely due to too leaky MDCK II cells.

3.2. PermeaPad[®] permeability study

The permeability experiments with artificial set-up showed great potential to follow the bioconversion rate combined with the permeability study. The system was modulated by the amount of alkaline phosphatase added to the donor side. A supersaturation of amprenavir was observed in all experiments and caused an increased flux compared to an amprenavir suspension. A human dose dissolution permeation experiment was performed with fosamprenavir, where the microdialysis showed two replicates, where the supersaturation remained stable over 3 hours, and one collapsed after 2 hours (Figure 2).

Figure 1.



P09

Figure 1. Permeability experiments of amprenavir and fosamprenavir converted to amprenavir over MDCK II cells (n=6).

Figure 2.

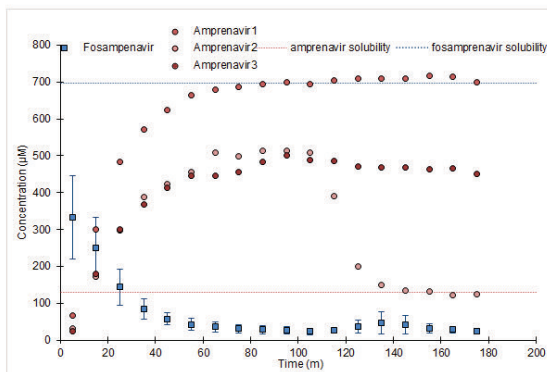


Figure 2. Human dose *in vitro* dissolution / enzymatic conversion / permeability study of fosamprenavir with 30 U/mL alkaline phosphatase. The measurements were done with a microdialysis setup. Three replicates are individually plotted.

Figure 3.

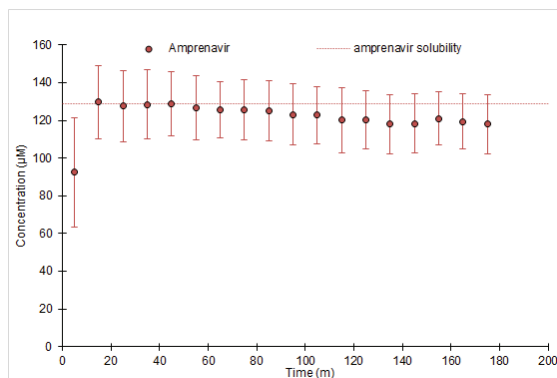


Figure 3. Amprenavir suspension measured with a microdialysis setup (n=3).

4. CONCLUSION

The side-by-side cell set-up with microdialysis and PermeaPad[®] showed great potential for permeability studies on prodrugs. The microdialysis system made it easy to follow the bioconversion rate during the permeability studies. The MDCK II permeability studies were not as optimal as the bioconversion rate of fosamprenavir was slower than expected.

5. REFERENCES

1. Stella VJ, Nti-addae KW. Prodrug strategies to overcome poor water solubility. *Advanced drug delivery reviews*. 2007;59(7): 677–94.

2. Brouwers J, Tack J, Augustijns Patrick. In vitro behavior of a phosphate ester prodrug of amprenavir in human intestinal fluids and in the caco-2 system: Illustration of intraluminal supersaturation. *Int j pharm*. 2007;336: 302–9

ACKNOWLEDGMENT

The authors are grateful for a mobility grant to JJC and collaborative work between the two institutions enabled by funding from Nordforsk program Nordic University Hub (project #85352) “NordicPOP”.

THE INFLUENCE OF PHOSPHATIDYLCHOLINE CONTENT IN HYDROGENATED PHOSPHOLIPID/POLYMER-BASED SOLID DISPERSIONS ON THE DISSOLUTION PROFILE OF A POORLY SOLUBLE DRUG

Mikolaj Czajkowski¹, Paulina Skupin-Mrugalska¹, Bartłomiej Milanowski², Annette Bauer-Brandl³, Martin Brandl³

¹*Department of Inorganic and Analytical Chemistry, Poznan University of Medical Sciences, Poland*

²*Department of Pharmaceutical Technology, Poznan University of Medical Sciences, Poland*

³*Department of Physics, Chemistry and Pharmacy, University of Southern Denmark, Denmark*

1. INTRODUCTION

Oral formulations remain the preferable way of administering drugs due to patient compliance, non-invasiveness, ease of use and safety. Currently, more than 90% of novel drug entities are poorly soluble [1]. One strategy employed to overcome this problem is using amorphous solid dispersions (ASD), usually polymer-based formulations. Novel excipients are still needed to improve the stability and performance of ASD. Due to their potential solubilizing ability and stabilizing effect in ASD, phospholipids (PLs) seem valuable materials as co-formers of ASD. Hydrogenated PLs are of interest to be applied.

The aim of this study was to establish the content of saturated PL in ternary solid dispersions of fenofibrate (FEN) in mixed PL/polymer matrices. Additionally, we evaluated whether phosphatidylcholine content in the saturated PL may affect the dissolution rate of FEN.

2. MATERIALS AND METHODS

2.1. Materials

Reagents used in this study were of analytical grade unless stated otherwise. Kollidon VA64 (VA64) was kindly donated by BASF SE (Ludwigshafen, Germany). FEN, trifluoroacetic acid (TFA), sodium hydroxide, sodium chloride, sodium phosphate monobasic monohydrate, sodium phosphate dibasic dihydrate, and *tert*-butanol were purchased from Sigma-Aldrich (St. Louis, MI, USA). Hydrogenated soybean phosphatidylcholine, i.e., PHOSPHOLIPON P90H (containing >90% hydrogenated soybean phosphatidyl-choline) and LIPOID P 75-3 (P75-3) (with 70% phosphatidylcholine) were kindly donated by Lipoid GmbH (Ludwigshafen, Germany).

2.2. Freeze-drying of binary and ternary dispersions

Solid dispersions were prepared by freeze-drying from water/alcohol solutions. Formulations were frozen overnight at -82°C and placed on a pre-cooled (-60°C) freeze-dryer shelf. The freeze-drying cycle comprised the main drying (+25°C, 0.1 mbar) for 24 h and final drying (+50°C, 0.01 mbar) for 3 h.

2.3. Powder X-ray diffraction (PXRD)

PXRD (D2 PHASER, Bruker, Billerica, MA, USA) was performed to characterize the solid-state of obtained binary and ternary dispersions. Samples were exposed to Cu K α radiation and measured within the angular range of 5°-45° with 0.02 step size mode and scanning speed of 10°/min.

2.4. Dissolution test in USP 4 apparatus (flow-through cell)

Dissolution testing was performed in a closed-loop configuration of a semi-automated flow-through cell dissolution system comprising a SOTAX CE 7 smart unit with a set of seven cells with 12 mm diameter, a SOTAX CP 7-35 piston pump and a SOTAX C-613 7 channel fraction collector. Each cell was prepared by placing a 5-mm ruby bead in the cone's apex, and the cone was filled with 1-mm glass beads. The cell was closed with a prepared insert and filter head containing a microfibre glass filter and a hydrophilic PTFE membrane with a pore size of 2.7 and 0.2 μ m (Munktell-Munskjö, Helsinki, Finland and Omnipore, Sigma-Aldrich, St. Louis, MI), respectively. The Phosphate Saline Buffer pH 7.4 was used as dissolution medium, pumped at the rate of 16 mL/min. Samples were withdrawn at 5, 10, 15, 30, 60, 120, 240, 480, 720, and 1440 min. with diluted with a twofold volume of methanol, and FEN was quantified by HPLC.

3. RESULTS AND DISCUSSION

3.1. PXRD

All binary and ternary formulations obtained by the freeze-drying method were amorphous, with no Bragg peaks present at the X-ray diffractograms.

3.2. Dissolution testing

The dissolution profiles of FEN in various formulations were determined in phosphate buffer saline pH 7.4 are presented in Figure 1. A fixed drug loading of 20% (w/w) was used, and the saturated PL (P90H or P75-3) was applied at variable content ranging from 0.5 to 20% (w/w). The dissolution testing showed a synergistic effect of polymer and saturated PL when ternary PL/polymer/FEN dispersions were compared to binary PL/FEN or polymer/FEN dispersions. Also, it was demonstrated that the phosphatidylcholine content in the saturated PLs influences the ability to induce supersaturation. The higher supersaturation concentrations were observed when saturated PL with lower phosphatidylcholine content was used. Noteworthy, supersaturation increased up to a critical amount of saturated PL of 2.5% (P75-3) and 1% (P90H) and subsequently dropped down with the increasing PL content (Figure 1). We assumed that at higher PL content, polymer and PL molecules form large multilamellar micelles that precipitate and entrap FEN. While at lower PL content, upon hydration in the dissolution media, VA64/PL creates smaller colloidal species that can pass through the applied filter and be observed as a supersaturation.

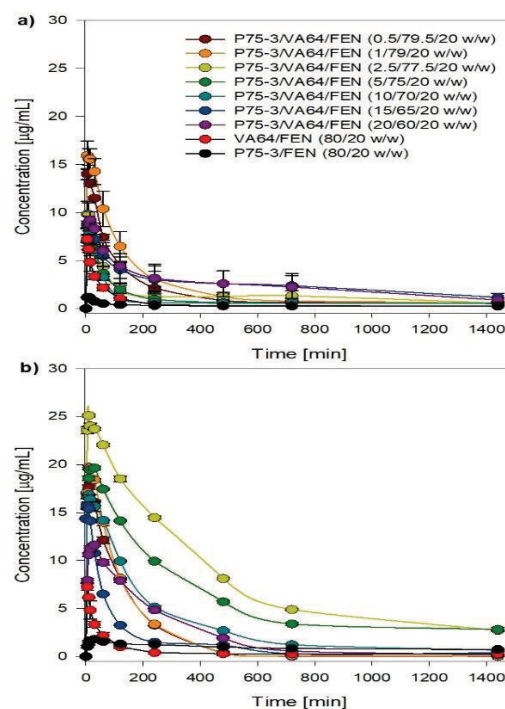


Figure 1. Phospholipid dissolution profiles of FEN from PL/VA64/FEN, VA64/FEN and PL/FEN dispersions with a) P75-3 and b) P90H, obtained using the USP 4 apparatus.

4. CONCLUSION

FEN's amorphous solid dispersions can be obtained by freeze-drying. Ternary matrices composed of PL/polymer/FEN have a higher ability to induce and maintain supersaturation than binary ones. The ability to generate and sustain supersaturation increases up to the critical content of saturated PL (2.5% for P75-3, 1% for P90H). The content of phosphatidylcholine in hydrogenated PL influences the supersaturation maintenance ability.

5. REFERENCES

1. Gigliobianco M. R. *et al.* *Pharmaceutics* (2018), 10(3), 134

ACKNOWLEDGMENT

The authors acknowledge the financial support from the Phospholipid Research Center under grant PSM-2020-085/1-1.

DRY POWDER FORMULATION OF CYCLOSPORINE A FOR IMMUNOSUPPRESSIVE TREATMENT

Davide D'Angelo¹, Eride Quarta¹, Stefania Glieca¹, Veronica Chierici¹, Giada Varacca¹, Martina Brandolini², Lisa Flammini¹, Simona Bertoni¹, Vittorio Sambri², Fabio Sonvico¹, Ruggero Bettini¹, Francesca Buttini¹

¹*Department of Pharmacy, University of Parma, Parco Area delle Scienze 27/A, 43124 Parma, Italy*

²*Microbiology Unit, The Great Romagna Area Hub Laboratory, 47522 Pievesestina, Cesena, Italy*

1. INTRODUCTION

Cyclosporine A (CsA) is a calcineurin inhibitor drug, widely used in the treatment of autoimmune conditions and in the immunosuppressive treatment after organ transplantation [1]. This requires the use of high dosages between 5 and 15 mg/kg/day which can lead to nephrotoxicity and hepatotoxicity. Moreover, it is reported that the drug bioavailability upon oral administration is only about 40%.

The aim of this work was the formulation of a dry powder for inhalation containing cyclosporine. This formulation was designed for the prevention of rejection after lung transplantation and potentially to treat the viral infection Covid-19 [2]. The advantage of this formulation is the possibility of reducing the dose currently administered orally, and the achievement of a greater local concentration of drug in the lung.

2. MATERIALS AND METHODS**2.1. Materials**

CsA (CAS Number 59865-13-3) was purchased from Metapharmaceutical (Barcelona, Spain). HPMC extra-dry capsules for use in dry powder inhalers, Quali-V[®]-I size #3, were provided by Qualicaps (Madrid, ES) and a single dose dry powder inhaler RS01 high resistant was gifted by Plastiap (Lecco, IT).

Mannitol was purchased from Roquette (Lestrem, France), glycine was purchased from Sigma Aldrich (St Louis, MO, USA). All other chemicals used were obtained from commercial suppliers and were of analytical grade. The human lung adenocarcinoma cell line A549, monocytic cell line THP-1 and VERO E6 cells were purchased from the American Type Culture Collection.

2.2. Methods

The inhalation powder was produced by spray drying a solution of water and ethanol at 45% v/v with 1% w/v of solids concentration. The dissolution of the powder was studied by using a vertical diffusion cell apparatus called Respicell[®]. Respirability was studied using NGI. Each HPMC capsule was filled with 20 mg of CsA and loaded into a dry powder inhaler RS01 activated at a flow rate of 60 L/min. Cell viability on A549 and THP-1 was assessed. The anti-inflammatory effect as reduction of IL-6 expression on A549 and THP-1 in co-culture was evaluated through the IL-6 ELISA test. The antiviral effect was studied on Vero E6 cells infected with SARS-CoV-2 variant omicron BA.1 at a concentration of 0.005 m.o.i. Cells were treated with CsA one hour before infection, two hours post-infection or simultaneously with a viral infection.

3. RESULTS AND DISCUSSION**3.1. Results and Discussion**

The powder containing 80% CsA and 20% mannitol was efficiently produced through the spray-drying method and this powder has been shown to have a higher dissolution rate than raw material. Moreover, this powder presented a FPF of 83.28± 0.69 and an MMAD of 2.5 μm. No significant cytotoxic effect was observed from in vitro studies, moreover, a powerful anti-inflammatory effect was observed on cell co-culture. In this study, it was also demonstrated a significant antiviral effect against the omicron BA-1 variant of SARS-

P11

CoV-2, in particular, during pretreatment and simultaneous treatment to infection (Figure 1).

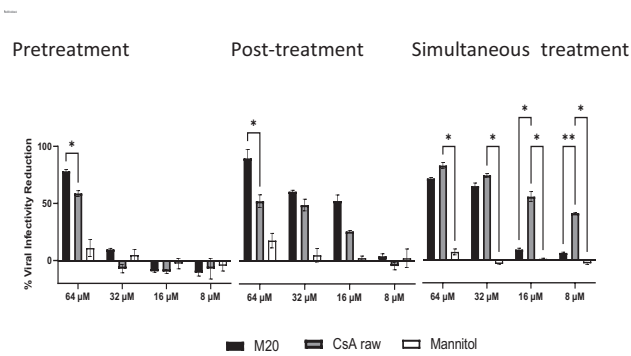


Figure 1. Viral concentration 0.005 m.o.i.; Cell line: Vero E6; Pretreatment: one hour before infection; Post-treatment: two hours post infection; Samples suspended in PBS. *P <0.05 vs CsA raw.

4. CONCLUSION

Due to its technological characteristics and encouraging in vitro results, this new inhalable CsA dry powder formulation could represent an innovative strategy, not only in the prevention of transplant rejection but potentially also in the treatment of patients with covid-19.

5. REFERENCES

1. Fahr A Cyclosporin Clinical Pharmacokinetics. Clinical Pharmacokinet 1993. 24:472–495
2. Molyvdas A, Matalon S, Cyclosporine: an old weapon in the fight against coronaviruses. European Respiratory Journal 2020. 56:2002484

DEVELOPMENT AND IN VITRO-IN VIVO EVALUATION OF GLYCYRRETTINIC ACID ACTIVE TARGETED PROLIPOSOMAL DRUG DELIVERY SYSTEMS FOR TREATMENT LIVER CANCER

Mine DİRİL¹, K. Volkan Ozdokur², Yeliz Yıldırım³, H. Yeşim Karasulu¹

¹*Department of Pharmaceutical Technology, Faculty of Pharmacy, Ege University, Izmir, TURKEY*

²*Department of Chemistry, Faculty of Science and Art, Erzincan Binali Yıldırım University ,Erzincan, TURKEY*

³*Department of Physicochemistry, Faculty of Science, Ege University, Izmir, TURKEY*

1. INTRODUCTION

Liver cancer is the fifth most common cancer in men and the ninth most common cancer in women, and the survival rate in the last five years has been reported to be less than 9% (1). Doxorubicin Hydrochloride (Dox-HCl), one of the active ingredients used in cancer treatment, is an anthracycline antibiotic that acts on the cell by interfering between DNA base pairs and it has many side effects (2). For this reason, it is very important to develop a drug delivery system that can eliminate these side effects. Studies have shown that Glycyrrhetic acid (GA), which is an active targeting molecule, stops cell cycle against hepatocellular carcinoma (3). The primary goal of this study is to reduce the toxic effect of Dox-HCl in healthy tissues by providing active targeting by conjugation of glycyrrhetic acid to the PEG molecule. Liposomal drug delivery systems are composed of phospholipids, which are the main components of the body, however, it is relatively unstable colloidal systems(4). Another goal of this study is to prevent the stability problems of lipids in liposomal drug delivery systems. For this reason develop proliposomal drug delivery systems by lyophilizing liposomal formulation.

2. MATERIALS AND METHODS

2.1. Materials

Doxorubicin Hydrochloride supplied by Deva İlaç. All other excipients are pharm grade. Caelyx® pegylated solution for infusion (Schering plough /ABD) was used as the reference drug.

2.2. HPLC validation of Doxorubicin

The following system was used for the validation of Dox-HCl; Detector: UV; Mobile phase: Acetonitrile- 0.01 M (sodium lauryl sulfate pH adjusted to 2.5) (50:50); Column: Eclipse Plus C18, 4.6 x 250mm, 5µm; Flow

rate: 1 mL/min; Colon temperature: 25°C; Wavelength: 254 nm.

2.3. DSPE-PEG 2000- Glycerretinic acid Synthesis

GA and DSPE-PEG2,000-NHS at a molar ratio of 3:1 was dissolved in dimethyl sulfoxide in the presence of 1-Ethyl-3-(3-dimethylaminopropyl) carbodiimide (1.58 mg) and 20 µL triethylamine was added to the reaction system to regulate pH.

2.4. Development Pegylated Active-Targeted Proliposome Formulation

Lipid hydration method was used for liposome formulation. Different drug:lipid ratio was tried for develop liposomal drug delivery systems. For proliposome formulation, different amounts of mannitol was used lyophilization step.

2.5. In vitro Studies of Pegylated Active-Targeted Proliposome Formulation

In vitro characterization studies (pH, particle size, zeta potential, viscosity, encapsulation, drug loading, humidity, time to disperse), in vitro release studies, cytotoxicity studies, stability studies, drug permeability studies were performed.

2.6. In vivo studies

Liver cancer was developed on CD-1 nude mice with Hep G2 cell lines for the efficiency studies. Comparative IVIS images were taken in the negative control group, Caelyx-administered group and pegylated active targeted proliposome formulation-administered group.

3. RESULTS AND DISCUSSION

3.1 HPLC validation of Doxorubicin

All results were found to comply with the criteria given in the ICH guide.

3.2. DSPE-PEG 2000- Glycerretinic acid Synthesis

GA and DSPE-PEG2,000-NHS conjugation was carried out successfully.

P12

3.3. Development Pegylated Active-Targeted Proliposome Formulation

The highest encapsulation capacity was found in the formulation with a drug:lipid ratio of 0.4. The use of 7% mannitol was provided effective drying and cake formation.

3.4. In vitro Studies of Pegylated Active-Targeted Proliposome Formulation

Pegylated active-targeted proliposome formulation characterisation results were shown

. In vitro release studies were shown **Figure 4**. IC50 values of Hep G2, Mahlavu and Huh 7 cell lines, Dox-HCl and pegylated active-targeted proliposome formulation were found 6.5 μ M.

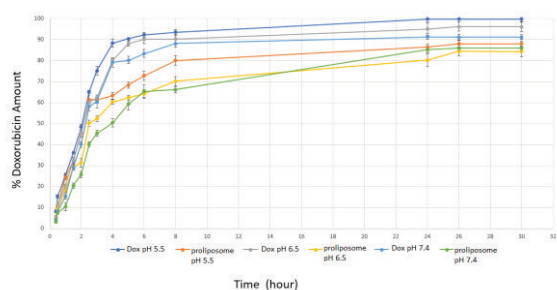


Figure 4. In vitro release studies

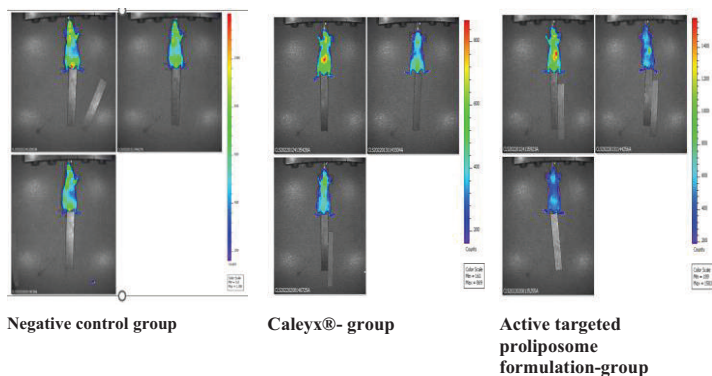


Figure 5. Efficiency studies-IVIS

Table 1. In vitro characterisation results

	Pegylated active-targeted, proliposome formulation
pH	6.5
Particle size (nm)	120
Zeta potential (mV)	9.57
Polydispersity index	0.36
Viscosity (cp)	11.3
Encapsulation (%)	90.0
Drug Loading(%)	100.0
Humidity (%)	0.0019
Time to disperse (sec)	10

3.5. In vivo studies

Liver cancer model has been successfully developed. Efficiency studies were shown Error! Reference source not found.. IVIS images were taken at the beginning, after the first dose treatment and after the second dose treatment. After the first dose treatment of pegylated active-targeted proliposome formulation, a significant reduction in tumor was observed.

4. CONCLUSION

Obtained results indicated that; pegylated active-targeted proliposome formulation containing Dox-HCl has been shown to be promising in the treatment of liver cancer in future studies.

5. REFERENCES

- Schlachterman, A., Craft, W., et al. World J Gastroenterol, 2015, 21 (28): 8478-8491
- Hanna, A., Lam, A., at all. Adverse Effects of Doxorubicin and Its Metabolic Product on Cardiac RyR2 and SERCA2A, 2014, Mol Pharmacol 86: 438–449.
- Cao, M., Gao, Y., et all. Glycyrrhizin Acid and Glycyrrhetic Acid Modified Polyethyleneimine for Targeted DNA Delivery to Hepatocellular Carcinoma, 2019, Int. J. Mol. Sci, 20, 5074.
- Hiral, M., Bijal, P., Rakesh, P. Review of Proliposomes as novel drug delivery system. 2015, Pha In J, 4(3), 61-67.

A PROPOSAL OF INNOVATIVE INJECTABILITY ASSESMENT METHOD FOR INTRAVENIOUS FORMULATIONS – CASE STUDY ON PEGYLATED NANOEMULSIONS

Jelena Đoković¹, Sanela Savić², Nebojša Cekić^{2,3}, Snežana Savić¹

¹*Department of Pharmaceutical Technology and Cosmetology, Faculty of pharmacy, University of Belgrade, Serbia*

²*DCP Hemigal, Serbia*

³*Department of Pharmaceutical Technology and Cosmetology, Faculty of Technology, University of Niš, Serbia*

1. INTRODUCTION

Syringeability and injectability are recognised as fundamental performance parameters / critical quality attributes of any parenteral dosage form. Syringeability refers to the ability of an injectable preparation to transfer from a vial through a hypodermic needle prior an injection, while injectability is defined as the force, or pressure, required to inject the formulation from a syringe-needle system into the tissue [1]. When developing drug delivery systems, the priority is usually the release kinetics, biocompatibility or other factors that may come in conflict with the optimal parameters for the applicability of those systems [2]. The aim of this research was to develop a method that could be used for injectability assessment of the intravenous formulations and the application of this method on curcumin-loaded PEGylated nanoemulsions (NEs) in order to gage the impact of PEGylation on NEs injectability.

2. MATERIALS AND METHODS

2.1. Nanoemulsion preparation

Nanoemulsions were prepared using high pressure homogenization method. The aqueous phase (glycerol, polysorbate 80, sodium oleate and highly purified water) was added into the oil phase (soybean oil, soybean lecithin, medium chain triglycerides, butylhydroxytoluene, benzyl alcohol, curcumin and PEGylated phospholipid – PEG2000-DSPE in 0.1 %, 0.3 % or 0.6 % concentrations) and mixed using rotor-stator homogenizer (IKA Ultra-Turrax® T25 digital, IKA®-Werke GmbH and Co. KG, Staufen, Germany), and further processed on high pressure homogenizer (EmulsiFlex-C3, Avestin Inc., Canada) at 800 bar for 10 discontinued cycles. The non PEGylated formulation was marked as CS, and

the PEGylated ones were marked S1, S3 and S6, referring to the PEG2000-DSPE concentration.

2.2. Physicochemical characterization

The NEs droplet size (Z-Ave) and droplet size distribution (PDI) were determined with Zetasizer Nano ZS90 (Malvern Instruments Ltd., Worcestershire). Rheological analysis was performed using MCR 302 air-bearing rheometer (Anton Paar, Graz, Austria) equipped with coaxial cylinders system (CC27 measuring bob with C-PTD 180/Air) with sheer rate range of 0.1-100 s⁻¹ at 20°C.

2.3. Injectability assesment

The injectability of the NEs was expressed as force (N) needed to extrude the NE in the function of the extruded volume (ml). About 10 ml of the NE was loaded into the 10 ml syringe and extruded through the 25 G scalp vein infusion set (Romed, Wilnis, Netherlands) into the blood mimicking solution, circulating through pump at 4 ml/min, in order to assess the NEs' performance in the prospective intravenous administration. The NEs were extruded at 1 mm/s croshead speed of the loading cell of the texture analyzer (EZ-LX Compact Table-Top Testing Machine, Shimadzu, Japan) with the Trapezium software version 1.5 used for data collection and analysis

3. RESULTS AND DISCUSSION

3.1. Physicochemical characterization

The NEs have average size of about 100 nm, with the PDI values below 0.20, indicating suitability for intravenous application. It could be observed from Fig. 1 that the addition of PEGylated phospholipids caused an increase in NE viscosity, as could be expected given that the polyethylene glycols are used in parenteral suspensions as stabilizing - rheology modifying agents [3].

P13

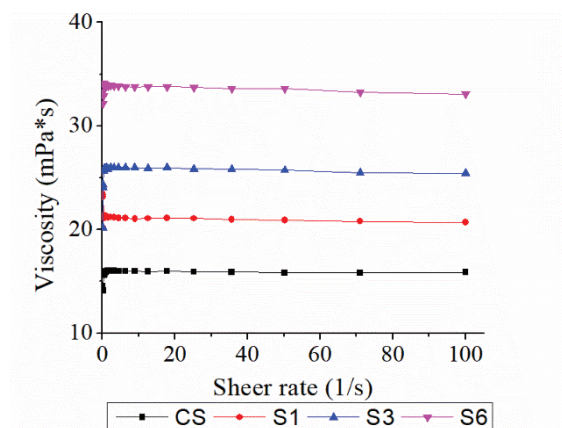


Figure 1. NE viscosity

3.2. Injectability assessment

The injectability assessment was performed with syringe-needle system used in our laboratory for intravenous administration in *in vivo* animal studies. As blood-mimicking solution, 36.6 %, v/v, glycerol solution was used [4]. It could be observed from Fig. 2 that the injectability of NEs depended on their viscosity, with the higher pressure needed to extrude the formulations with the higher PEG2000-DSPE concentration. Even though, to the best of our knowledge, there are no studies investigating the injectability of the intravenous preparations, based on some previous research on subcutaneous model [5], it is recommended the maximum force used to inject the formulations should be kept about 20 N, which would eliminate S3 and S6 from further investigation (Fig. 2).

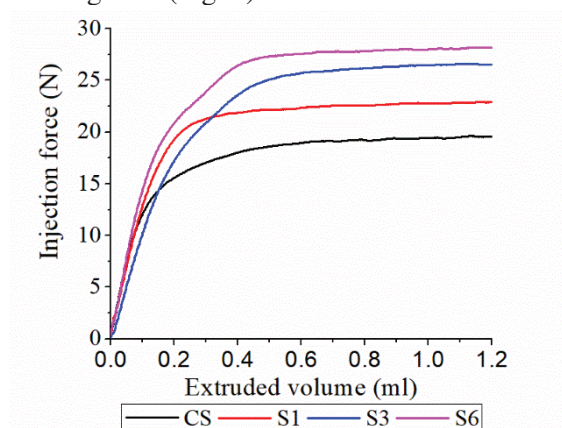


Figure 2. NE injectability

4. CONCLUSION

The injectability method used in this research proved as a useful tool in screening formulations adequate for prospective intravenous use.

5. REFERENCES

1. Cilurzo, F., et al. *Injectability Evaluation: An Open Issue*. AAPS PharmSciTech, 2011. 12(2): 604-609.
2. Sarmadi, M., et al. *Modeling, design, and machine learning-based framework for optimal injectability of microparticle-based drug formulations*. Science advances, 2020. 6: eabb6594.
3. Gullapalli, R. P., Mazzitelli, C. L. *Polyethylene glycols in oral and parenteral formulations—A critical review*. International Journal of Pharmaceutics, 2015. 496(2): 219-239.
4. Yousif, M. Y., et al. *Deriving a blood-mimicking fluid for particle image velocimetry in Sylgard-184 vascular models*. In Annual International Conference of the IEEE Engineering in Medicine and Biology Society, 2009 (pp. 1412-1415).
5. Watt, R. P., et al. (2019). *Injectability as a function of viscosity and dosing materials for subcutaneous administration*. International Journal of Pharmaceutics, 2019:554, 376-386.

ACKNOWLEDGMENT

This research was funded by the MESDT, Republic of Serbia through Grant Agreement with University of Belgrade-Faculty of Pharmacy No: 451-03-68/2022-14/200161 and supported by the Science Fund of the Republic of Serbia, GRANT No 7749108, *Neuroimmune aspects of mood, anxiety and cognitive effects of leads/drug candidates acting at GABAA and/or sigma-2 receptors: In vitro/in vivo delineation by nano- and hiPSC-based platform - NanoCellEmoCog*.

ELECTROSPINNING AS A DRYING METHOD FOR MAGNETIC NANOPARTICLE DISPERSIONS

Črt Dragar¹, Sebastjan Nemec^{1,2}, Slavko Kralj^{1,2,3}, Petra Kocbek¹

¹University of Ljubljana, Faculty of Pharmacy, Department of Pharmaceutical Technology, Slovenia

²Jožef Stefan Institute, Department for Materials Synthesis, Slovenia

³Nanos SCI, Nanos Scientifica d.o.o., Slovenia

1. INTRODUCTION

With their unique chemical, physical, and biological properties iron-oxide-based magnetic nanoparticles (MNPs) are believed to be one of the most promising novel drug delivery systems [1]. However, their long-term physical stability in dispersions still represents an important technological challenge [2]. To improve the physical stability of nanoparticulate dispersions, the particle surface modifications or the addition of stabilizers have been investigated, but it was shown that such approaches may strongly affect the properties of MNPs [2]. Therefore, the methods for the transformation of MNP dispersions into stable, redispersible dry products have been intensively investigated in the last two decades. However, the currently available methods usually require relatively large amounts of excipients to preserve MNP size and result in fluffy powdered products, which can provoke adverse health effects in humans, if inhaled unintentionally [3]. The aim of our study was thus to adopt the electrospinning method for the transformation of MNP dispersions into a dry non-powdered product, which would enable the rapid and simple reconstitution of MNPs.

2. MATERIALS AND METHODS

2.1. Materials

All materials used were of reagent grade and from commercial sources. The initial ethanol-based MNP dispersions (iNANOvative™) were kindly provided by Nanos Scientifica Ltd. (Nanos SCI, Ljubljana, Slovenia).

2.2. Drying of Magnetic Nanoparticle Dispersions by Electrospinning

MNP dispersions with different amounts of MNPs (Table 1) were dried using the electrospinning device in the horizontal setting (temperature, 25 °C; relative humidity, ≤ 35%; voltage, 15 kV; flow rate, 1.77 mL/h; collector-needle distance, 15 cm). The MNP dispersions for drying were prepared by dissolution of

polymers, namely poloxamer 188 and polyethylene oxide in weight ratio 1:1, in the initial ethanol-based MNP dispersion.

Table 1. Composition of MNP dispersions for drying.

Formulation	MNP s [mg]	Polymer s [mg]	Ethanol * [g]
F0	0	240	8
F1	60	240	8
F2	120	240	8
F3	180	240	8
F4	240	240	8
F5	300	240	8
F6	360	240	8

*The ethanol used was 96% (v/v).

2.3. Characterization of Electrospun Products

The electrospun products were characterized regarding the morphology (scanning electron microscopy, SEM), the internal structure (transmission electron microscopy, TEM), and MNP content (thermogravimetric analysis, TGA). The electrospun products were reconstituted in 0.9% (w/v) NaCl (~1 mg/mL) by vortex mixing for 3 min. The MNP hydrodynamic size and particle size distribution were measured by photon correlation spectroscopy, whereas MNP zeta potential was measured by laser Doppler anemometry.

3. RESULTS AND DISCUSSION

MNPs used in our study were composed of self-assembled multiple 10 nm superparamagnetic iron oxide nanocrystals. The nanocrystal clusters were coated with a 10 nm thick silica shell as previously reported [4]. Their mean hydrodynamic size in the initial dispersion was (356 ± 9) nm.

The electrospinning enabled the formation of the dry products with the nanofiber morphology as revealed by the SEM analyses (Fig. 1). The TEM analyses confirmed that MNPs have been

P14

successfully incorporated into the polymer matrix of nanofibers (Fig. 2).

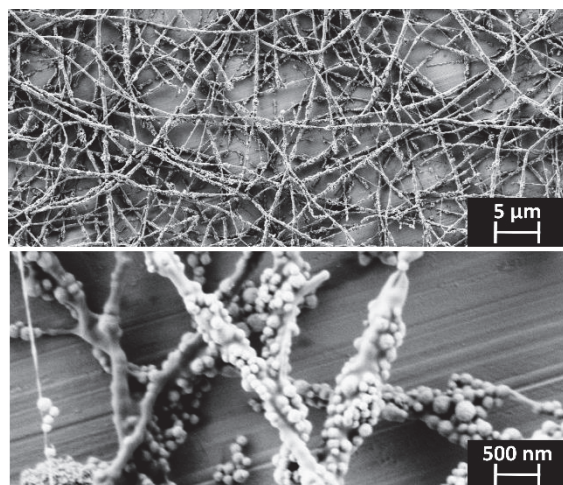


Figure 1. Representative SEM images of the electrospun product with 50% (w/w) of MNPs (formulation F4) at lower (top) and higher (bottom) magnification.

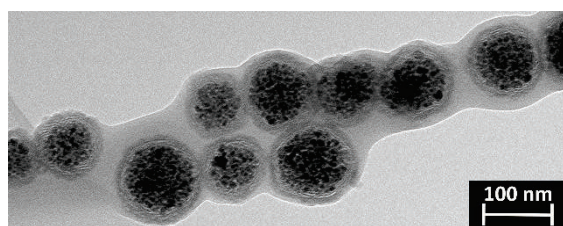


Figure 2. Representative TEM image of the electrospun product with 50% (w/w) of MNPs (formulation F4).

Additionally, the TGA revealed no losses of MNPs during electrospinning and homogenous distribution of MNPs in the electrospun products. Based on the hydrodynamic size of MNPs after the reconstitution, we can conclude that the maximal MNP loading in the electrospun product, which still enables efficient reconstitution and preserved size of MNPs, is 50% (w/w) (Fig. 3, formulation F4). The hydrodynamic size of MNPs after the reconstitution from formulations F1-F4 in 0.9% (w/v) NaCl changed only slightly compared to the MNPs in the initial dispersion (MNPs/e), indicating the suitability of the technological procedure to preserve the particle size also in the presence of salts in the dispersion medium.

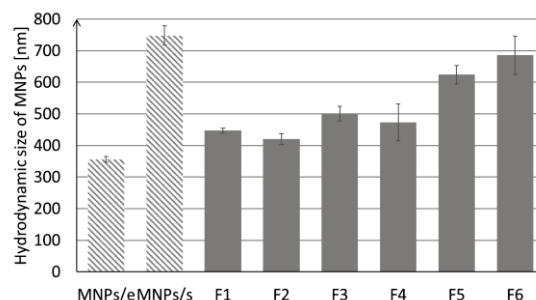


Figure 3. Hydrodynamic size of MNPs after the reconstitution in 0.9% (w/v) NaCl from formulations F1-F6 and the hydrodynamic size of MNPs in the initial dispersion (MNPs/e) and initial dispersion diluted with 0.9% (w/v) NaCl (MNPs/s).

4. CONCLUSION

We have established electrospinning as an efficient method for the transformation of MNP dispersions into redispersible dry products, which can contain up to 50% (w/w) of MNPs. The electrospun product in a form of a nanofiber mat prevents unintentional MNP aerosolization and thus ambient exposure to MNPs. The excipients used in the formulation, i.e., hydrophilic polymers, enable simple and rapid reconstitution of MNPs just prior to application, insignificantly contribute to the tonicity of the obtained dispersion, and improve MNP stability in 0.9% (w/v) NaCl.

5. REFERENCES

1. Dragar, Č., et al., *Bioevaluation methods for iron-oxide-based magnetic nanoparticles*. International Journal of Pharmaceutics, 2021. 597: 120348.
2. Ong, H.T., et al., *Fatty acid coated iron oxide nanoparticle: Effect on stability, particle size and magnetic properties*. Colloids and Surfaces A: Physicochemical and Engineering Aspects, 2020. 606: 125371.
3. Valdiglesias, V., et al., *Are iron oxide nanoparticles safe? Current knowledge and future perspectives*. Journal of Trace Elements in Medicine and Biology, 2016. 38: 52-63.
4. Kralj, S., Makovec, D., *Magnetic assembly of superparamagnetic iron oxide nanoparticle clusters into nanochains and nanobundles*. ACS Nano, 2015. 9: 9700-9707.

ACKNOWLEDGMENT

The authors gratefully acknowledge the financial support provided by the Slovenian Research Agency (Program Codes P1-0189, P1-0420, and P2-0089 and Projects J2-3043, J2-3040, J2-3046, J3-3079, and J1-7302).

FORMULATION AND INVESTIGATION OF THE EFFECT OF POLYMERS ON DERMAL FOAM PROPERTIES USING THE QUALITY BY DESIGN (QbD) APPROACH

Fanni Falusi¹, Szilvia Berkó¹, Mária Budai-Szűcs¹, Anita Kovács¹

¹*University of Szeged, Institute of Pharmaceutical Technology and Regulatory Affairs, Hungary*

1. INTRODUCTION

Dermal foams are promising drug delivery systems due to their advantages and ease of application. In particular, they are beneficial for the treatment of skin conditions when patients have highly inflamed and sensitive skin, as the application of the foam minimizes the need for skin contact [1].

Foams provide an innovative, easy to apply, novel alternative for creams and ointments, hence there are still few test methods in the literature. For this reason, our research aimed to develop stable foam formulations containing different types of polymers, determine the proper methods to investigate their physicochemical and structural properties and compare the results of different methods. To ensure quality-based development, the QbD approach was applied. The QbD concept involves identifying the quality target product profile (QTTP), the critical material attributes (CMAs), and critical process parameters (CPPs) into the critical quality attributes (CQAs) of dermal foam at the beginning of the development [2].

2. MATERIALS AND METHODS

2.1. Materials

Kolliphor RH 40 was obtained from BASF SE Chemtrade GmbH (Ludwigshafen, Germany). Labrasol ALF was from Gattefossé (Saint-Priest Cedex, France), Xantural® 180 was provided by CP Kelco A Huber Company (Atlanta, GA, USA). Verstatil PC was purchased from Biesterfeld GmbH (Hamburg, Germany). Hydroxyethylcellulose (Ph. Eur. 9.) was supplied by Molar Chemicals Ltd. (Budapest, Hungary). Purified and deionized water was used (Milli-Q system, Millipore, Milford, MA, USA). HyaCare50, HyaCare Filler CL and HyaCare Tremella were product samples from Evonik Industries AG (Essen, North Rhine-Westphalia, Germany).

2.2. The QbD methodology

The QbD is a science-based and risk-managed approach to drug development that starts with pre-defined goals. The CQAs were defined with the consideration of the attributes of the liquid system and the foam system. After the determination of CQAs, the following step is to determine the critical material attributes and the critical process parameters of the foams with risk assessment.

2.3. Preparation of foams

Based on the results of the initial risk assessment, the polymer concentration and type were critical material attributes. Therefore, the effect of five different polymers on the foam structure has been investigated. The formulations contain 2 different concentrations of xanthan gum, hydroxyethyl cellulose (HEC), low molecular weight hyaluronic acid (LMW-HA), high molecular weight hyaluronic acid (HMW-HA), and cross-linked hyaluronic acid (CL-(Phase B)). The foaming agents are mainly surfactants (Phase A). All formulations contain the same amount of surfactants (Phase B). Phase C contains the microbiological preservative. The bulk liquid is prepared by mixing Phase A, B, and C. To produce the foam, the bulk liquid is stirred at 2000 rpm for 5 minutes.

2.4 Investigation of foam properties

Through the determination of macroscopic properties, information on the stability of foam formulations can be acquired. With a light microscope, the stability of foams, as well as the kinetics of the destabilization mechanism was analyzed. Rheological measurements could detect deformations in the structure of the foam due to different forces. The dermal application of foam could be modeled with a texture analyzer.

3. RESULTS AND DISCUSSION

3.1. Initial risk assessment

The QTPP of the foams includes the route of administration, dosage form, site of action, the appearance of the drug delivery system, stability of the liquid system and the foam system, appearance of the liquid and the foam system, and the polymer content of the foam for stability. The CQAs were defined with the consideration of the attributes of the liquid system and the foam formed, too. In the case of risk assessment quality management tools have been used (e.g. Ishikawa diagram, Pareto analysis, risk estimate matrix, etc.).

3.2. Investigation of foam properties

Macroscopic properties

The following parameters can be determined through the macroscopic investigations: foam expansion (FE, %), foam volume stability (FVS, %), relative foam density (RFD). In the tested formulations, foams containing xanthan gum and HMW-HA had the highest stability but the lowest foam expansion values. Among the tested formulations, the well-foaming composition were foams with an FE-value above 100 % and the most stable formulations were the formulations with FVS-value above 70 %.

Microscopic properties

All foam systems were polydisperse. The kinetics of foam destabilization was also observed with microscopic examinations (Fig. 1.). The microscopic pictures showed that the increasing size of the bubbles leads to the destabilization of the foam over time. Foams with an initial bubble count above 100 were microscopically stable.

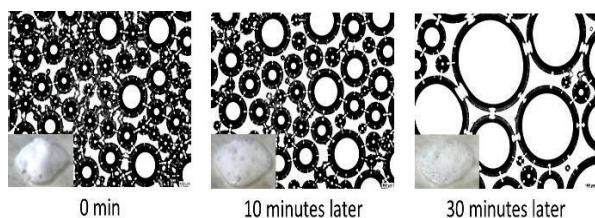


Figure 1. The analysis of foam kinetics through microscopic images.

Rheology

Two typical amplitude sweep curves can be distinguished: one which represents a wider linear viscoelastic envelope, the elastic modulus

is higher than the viscous one, and the moduli are constant up to higher strain values, indicating a more stable coherent structure. The other type of rheological behavior of the foam is when G'' dominates over G' in the entire strain range, and a crossover point cannot be detected. These preparations did not form a real coherent foam structure.

Spreadability

On the basis of the results, in general, the polymer content improved the firmness of the foam, which would prevent the formulation from flowing off the skin. Our results indicate that xanthan gum-containing and HMW-HA-containing foams met the pre-established requirement and correlated with the results of the macroscopic investigations.

4. CONCLUSION

In summary, the polymer content has a great effect on the properties of the foams. The chosen methods reinforce each other and help to select a formula for dermal application. Based on our results, formulations containing xanthan gum and HMW-HA had good foam properties and will be appropriate delivery systems for an active pharmaceutical ingredient. The results of the different methods showed good correlation and can be used in preformulation studies to select the optimal formulation.

5. REFERENCES

1. Parsa et al., *Foam in pharmaceutical and medical applications*, Current Opinion in Colloid&Interface Science 44 (2019)
2. F.Falusi, et al., *Investigation of the effect of polymers on dermal foam properties using the QbD approach*. European Journal of Pharmaceutical Sciences 173 (2022).

ACKNOWLEDGMENT

The research was supported by the Gedeon Richter Plc. Centennial Foundation (Gyömrői 19-21, Budapest, H-1103, HU). Project no. TKP2021-EGA-32 has been implemented with the support provided by the Ministry of Innovation and Technology of Hungary from the National Research, Development and Innovation Fund, financed under the TKP2021-EGA funding scheme.

FORMULATION OF NANOPARTICLES CONTAINING CASEIN KINASE 2 INHIBITOR FOR THE THERAPY OF GLIOBLASTOMA

Pálma Fehér¹, Marc Le Borgne², Florent Perret², Christelle Marminon², Zoltán Ujhelyi¹, Ágota Petó¹, Liza Józsa¹, Miklós Vecsernyés¹, Ildikó Bácskay^{1,3}

¹*Department of Pharmaceutical Technology, Faculty of Pharmacy, University of Debrecen*

²*Chemistry Department, Faculty of Pharmacy, University of Claude Bernard Lyon*

³*Institute of Healthcare Industry, University of Debrecen*

1. INTRODUCTION

Glioblastoma (GBM) is the most common primary central nervous system tumour in adults, represents about 15% of all primary brain tumours. The limited and less-effective treatment options for these highly aggressive GBMs call for the development of new techniques and the improvement of existing technologies [1,2]. Casein kinase 2 (CK2) is overexpressed in GBM samples. Recent evidence suggests CK2 inhibitor is a promising therapeutic target for GBM. CK2 inhibition was shown to decrease cell migration and adhesion, increase cellular apoptosis and inhibit tumour growth in GBM cells [3].

The aim of research was the formulation and investigation of microcapsules containing a CK 2 inhibitor.

2. MATERIALS AND METHODS

2.1. Materials

CK 2 inhibitor was synthesized by the Faculty of Pharmacy, University of Claude Bernard Lyon. Sodium alginate was obtained from BÜCHI Labortechnik AG (Flawil, Switzerland). Calcium chloride dehydrate, ninety-six-well cell plates was purchased from VWR International (Debrecen, Hungary). Caco-2 cell line was originated from the European Collection of Cell Cultures (ECACC, Public Health England, Salisbury, UK).

2.2. Preparation of CK2 inhibitor- loaded alginate beads

The CK2 inhibitor-loaded alginate nanobeads were prepared by a controlled polymerization

method using a Büchi Encapsulator B-395 Pro apparatus. CK 2 inhibitor was finely distributed in 40 mL of 1.50% sodium-alginate solution. The polymer-pharmakon mixture was forced into the pulsation chamber by a syringe pump at speed 5.00 mL/min. The alginate beads were left to harden for 15 min in calcium-chloride solution. The finely divided particles were washed with distilled water and filtered on a 0.4 μm pore size membrane by a vacuum pump and freeze dried for 24 h at $-110\text{ }^{\circ}\text{C}$ [4].

2.3. Encapsulation efficiency

To determine the encapsulated drug content in the beads, a 1 mL sample was measured from 100 mM of the calcium-chloride hardening solution right after formulation. Drug concentration was determined by spectrophotometer.

2.4. Determination of Mean particle size and Zeta potential

The nanoparticle size and Zeta potential of the formulations were determined by Malvern Zetasizer Nano S instrument.

2.5. In vitro dissolution test

Erweka DT800 equipment was used for the experiment. Rotating paddle method was chosen, (75 rpm and 900 ml dissolution media) Samples were taken at predetermined intervals. Duration: 24 h. Absorbance of dissolved CK2-inhibitor was measured at 420 nm (UV-VIS, Shimadzu UV-1601).

2.6. Cell Viability Assay

Caco-2 cell viability was evaluated using the MTT method. Cells were harvested and seeded

P16

at a density of 10^4 Cells/well on flat-bottom 96-well tissue culture plates. Cells were allowed to grow for 7 days. Mitochondrial activity of the cells was determined after 3 h incubation with MTT at the concentration of 0.50 mg/ml. Dark blue formazan crystals were dissolved in acidic isopropanol. Absorbance was measured with a FLUOstar OPTIMA micro-plate reader at 570 nm against a 690 nm reference.

3. RESULTS AND DISCUSSION

3.1. Encapsulation efficiency

The encapsulation efficiency measurements resulted in at least 64 ± 0.72 %.

3.2. Mean Particle Size and Zeta potential

Table 1. Particle size and zeta potential of CK2 inhibitor beads

Mean Particle size (\pm SD) nm	345.8 ± 6.02
Zeta potential	-23.6 ± 5.04 mV

3.3. Results of in vitro dissolution test

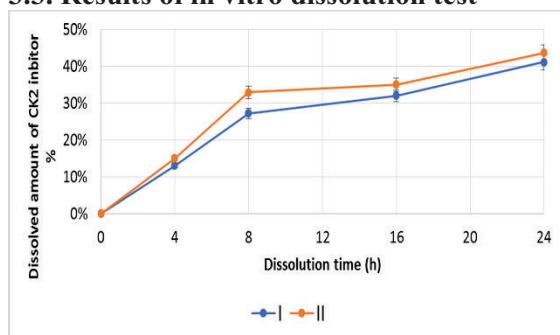


Figure 1. In vitro dissolution profile of CK2 inhibitor beads

3.4. MTT test

According to the results of MTT test the samples were safe in the applied concentrations. Cell viability is demonstrated as the percentage of the untreated control.

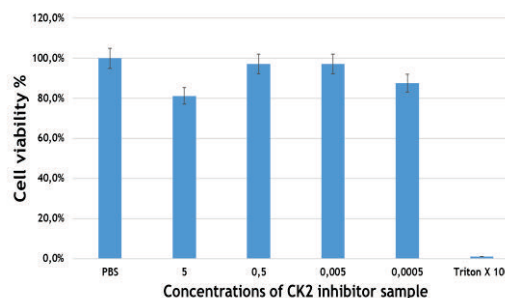


Figure 2. Results of MTT test

4. CONCLUSION

Microencapsulation of CK2 inhibitor offers the possibility of releasing therapeutic agents to targeted areas of the brain, which could provide new directions for the treatment of neurological diseases such as GBM.

5. REFERENCES

1. Marc Fakhoury, *Drug delivery approaches for the treatment of glioblastoma multiforme* Artificial Cells, Nanomedicine, and Biotechnology, 2016, 44(6):1365 –1373.
2. Justin S. Michael Et Al, *Nanotechnology for treatment of glioblastoma multiforme*, Journal Of Translational Internal Medicine, 2018, 6 (3):128-133.
3. Haitao Ji et al, *The Role of Protein Kinase CK2 in Glioblastoma Development*, 2013, 19(23):6335-6337
4. Yu-Tsai Yang et al., *Preparation of alginate beads containing a prodrug of Diethylenetriaminepentaacetic Acid*, Carbohydrate Polymers, 2013, 92(2):1915-1920

ACKNOWLEDGMENT

2019-2.1.11-TÉT-2020-00098 „Formulation of Casein Kinase 2 inhibitor nanoparticles in glioblastoma brain tumor therapy”
“Project no. TKP2021-EGA-18 has been implemented with the support provided from the National Research, Development and Innovation Fund of Hungary, financed under the TKP2021-EGA funding scheme.”

THE INFLUENCE OF SIMULATED WATER GASTRIC EMPTYING PROFILES ON DISSOLUTION OF MODEL DRUGS

Felician Tjaša¹, Rede Katarina¹, Cof Greta¹, Bogataj Marija¹

¹Department of Biopharmaceutics and Pharmacokinetics, Faculty of Pharmacy, University of Ljubljana, Slovenia

1. INTRODUCTION

Different and highly variable physiological factors can affect formulation / drug performance in the gastrointestinal tract and influence drug absorption in the small intestine. Especially of great importance are properties of the fluids throughout the GI tract: their composition (buffer species and concentrations, presence of solubilizing components), buffer capacity, volumes, pH values, viscosity, and hydrodynamics, especially gastric emptying (GE) [1].

The study aimed to simulate different fasted water GE profiles in an *in vitro* dissolution system and assess their influence on dissolution of three model drugs.

2. MATERIALS AND METHODS

2.1. Selection of the GE profiles

Two distinct individual *in vivo* GE profiles after ingestion of 240 mL of water were selected from the literature [2], that represented slow GE (subject 8) and fast GE kinetics (subject 13).

2.2 Simulation of GE profiles using the glass-bead flow-through system

Using the *in vitro* glass-bead flow-through system [3], the selected *in vivo* GE profiles were simulated. In the beginning, 35 mL of 0.001 M HCl and 240 mL of water were combined and added to the working vessel. Fresh 0.001 M HCl was constantly delivered into the vessel with a flow rate of 2 mL/min. 25 g of glass beads (diameter 1 mm) and a magnetic stirring bar were added to the vessel. The medium in the working vessel was heated to 36.5 °C and stirred at 50 rpm. The volume of the medium in the working vessel was changing throughout the experiment to resemble the *in vivo* gastric volumes. The flow rates through the tube, that pumped the medium out of the vessel, were accordingly altered to cause suitable change in the medium volume in the working vessel. Simulation of GE profiles proceeded until a

basal medium volume in the working vessel (i.e. 35 mL) was reached.

2.2. Tablet manufacture

400 mg tablets were manually compressed at the University of Ljubljana, Faculty of Pharmacy, using 12 mm flat-faced punches and were composed of: drug (25 %; paracetamol (PAR) or diclofenac sodium (DF-Na) or dipyridamole (DPL)), lactose monohydrate (66.5 %), HPMC SB-4 (7.5 %) and Mg-stearate (1 %).

2.3. Dissolution experiments

Dissolution experiments were performed using the glass-bead flow-through dissolution system under the conditions of the selected simulated GE profiles. The experiments began by placing a weighed tablet into the working vessel containing a mixture of HCl and water. Samples, pumped out of the vessel, were collected in different time intervals, filtered through 0.45 µm RC filters, diluted and the concentration of dissolved drug was measured using the UV-Vis spectrophotometer.

2.4. pH measurements in the vessel

In separate experiments, pH in the working vessel during simulation of GE profiles with and without tablet addition was also measured.

3. RESULTS AND DISCUSSION

3.1. *In vitro* simulation of the selected GE profiles

With some adjustments compared to *in vivo* values of gastric volumes, both GE profiles were successfully and reproducibly simulated in the *in vitro* flow-through system. *In vivo* and *in vitro* simulated fast and slow GE profiles are presented in Figure 1.

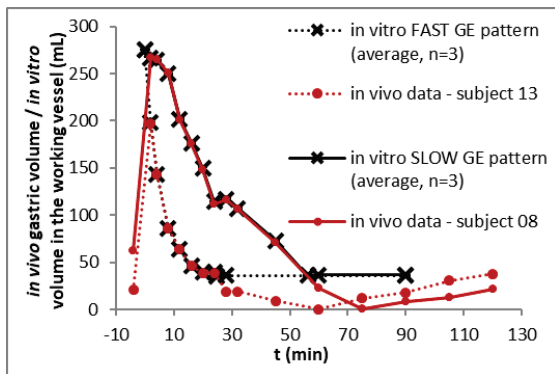


Figure 1. The individual *in vivo* gastric fluid volumes after ingestion of 240 mL of water (red lines, [2]) and simulated *in vitro* GE profiles in the flow-through dissolution system (black lines).

3.2. Dissolution results

Dissolution experiments were performed with tablets containing PAR, DF-Na or DPL. Differences in the amount of dissolved drug can be seen for tablets containing DF-Na or PAR when two different GE profiles were simulated (Figure 2).

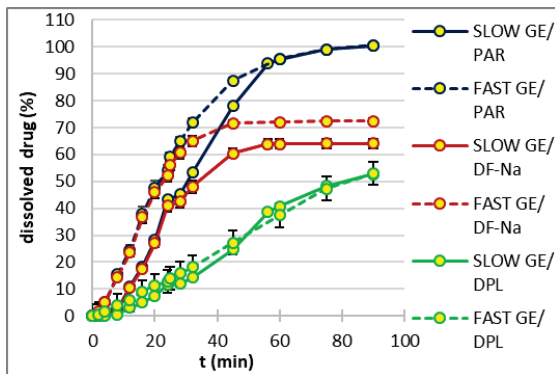


Figure 2. Dissolved drug (%) from tablets containing PAR (blue lines), DF-Na (red lines) or DPL (green lines) in experiments with simulated slow GE profile (full lines) or fast GE profile (dashed lines).

The simulation of a fast GE profile resulted in a faster dissolution and/or higher percent of the dissolved drug for DF-Na and PAR tablets compared to a slow GE profile. For tablets containing DPL, the GE profile did not affect the amount of dissolved drug, probably due to the drug's poor solubility and low dissolution rate in 0.001 M HCl, additionally diluted by water. In Figure 3, pH profiles during experiments with or without tablet are presented. The pH of the medium at the beginning of the experiment was approximately 3.9 and it gradually decreased back to pH 3 due to the delivery of fresh 0.001 M HCl into the vessel. The decrease in pH was faster when fast GE profile was simulated. PAR dissolution did

not alter pH in the vessel. Both, DPL and DF-Na dissolution increased medium pH for a certain time.

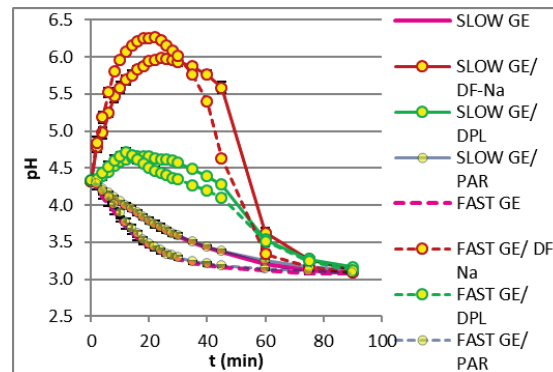


Figure 3. pH profiles during simulation of slow (full lines) and fast (dashed lines) GE profiles without or with tablets (PAR, DF-Na or DPL).

pH changes were the greatest in the case of DF-Na and affected its dissolution. High pH value at the beginning increased dissolution, whereas decreasing the pH back to pH 3 prevented the dissolution of the whole dose due to lower solubility of diclofenac at pH 3.

4. CONCLUSION

Simulation of GE profiles after ingestion of 240 mL of water was performed in the *in vitro* glass-bead flow-through system. The effect of different GE rates on dissolution was observed for tablets with PAR and DF-Na, but not for DPL. The results show, that the effect of water ingestion and its GE on dissolution could depend on drug physico-chemical properties, especially its solubility and dissolution rate.

5. REFERENCES

1. Mudie D.M., et al., Physiological parameters for oral delivery and *in vitro* testing. *Molecular Pharmaceutics*, 2010. 7(5): 1388-1405
2. Mudie D.M., et al., Quantification of gastrointestinal liquid volumes and distribution following a 240 mL dose of water in the fasted state. *Molecular Pharmaceutics*, 2014. 11(9): 3039-3047
3. Bogataj M., et al., Development of a glass-bead device for dissolution testing. *Dissolution Technologies*, 2015. 22(3): 18-24

ACKNOWLEDGMENT

The authors acknowledge dr. Luca Marciani (University of Nottingham) for providing raw data of individual *in vivo* GE profiles and Slovenian Research Agency for the financial support (grant number P1-0189).

DRY POWDER INHALER FORMULATIONS CONTAINING GEFITINIB NANOPARTICLES

Merve Geyik¹, Burcu Nacak², Melek Nur Bilal², Tugba Gulsun¹, Selma Sahin¹,
Levent Oner¹, Yagmur Akdag¹

¹Department of Pharmaceutical Technology, Faculty of Pharmacy, Hacettepe University, Ankara, Turkey

²Faculty of Pharmacy, Hacettepe University, Ankara, Turkey

1. INTRODUCTION

Lung cancer is one of the deadliest types of cancer, and chemotherapy treatment is at the forefront of treatment methods. However, severe side effects resulting from conventional chemotherapeutic applications have led researchers to search for new drug delivery systems in chemotherapy. Nanoparticulate systems enable to accumulate at the tumor site at lower doses thanks to active and passive targeting methods.

Inhalation therapy is a method that has been used for years and can provide a local effect on the lung, and at the same time, a systemic effect can be easily achieved thanks to the capillaries in the alveoli. Dry-powder inhalers (DPIs) are advantageous inhaler products due to their good formulation stability, environment friendliness, easy storage conditions and least requirement on actuation-inhalation coordination [1]. In this study a nanoparticulate system which contains human serum albumin (HSA)-gefitinib is covered with different carriers to produce a dry powder inhaler with suitable aerodynamic parameters for pulmonary delivery.

2. MATERIALS AND METHODS

2.1. Materials

Gefitinib was kindly provided by Nobel (Istanbul, Turkey). HSA solution of Grifols (1 mL of the aqueous solution containing 0.2 g human albumin, 0.016 mmol sodium caprylate, 0.016 mmol sodium N-acetyltryptophanate) was used as an HSA source. D-Mannitol and trehalose were purchased from Merck and Goldbio, respectively. Sucrose was purchased from Isolab, lactose monohydrate was supplied by BASF Pharma. RS01 device was donated by Plastiapa SpA (Italy). All other chemicals were of analytical grade.

2.2. Preparation of HSA-gefitinib nanoparticles

HSA-gefitinib nanoparticles are prepared with the NAB™ technology method with minor modification [2]. The gefitinib solution slowly injected to aqueous solution (0.2% HSA(w/v)) under 11,000 rpm. Then, the crude emulsion was homogenized in high pressure homogenizer (20,000 psi, 20 cycles). Afterward, the nanoemulsion was rotary evaporated to remove the organic solvent.

2.3. Preparation of dry powder inhaler formulations

Gefitinib-HSA nanoparticle suspensions (220 nm) are covered by %50 (w/w) with four different carriers (mannitol, lactose, sucrose, and trehalose) and frozen at -20°C for 24 hours. Then, they were lyophilized for 72 hours at a pressure of 0.01 mmHg at -80°C. Obtained powders were weighed into size 3 HPMC capsules and were placed in RS01 devices.

2.4. Andersen Cascade Impactor analysis

The aerodynamic parameters of the formulations were calculated using the Andersen Cascade Impactor (ACI) taking into account the criteria of European and American Pharmacopoeias. ACI plates were coated with a 2% (w/v) solution of Tween 20 in ethanol to ensure that the particles adhere to the plates at each stage of the device. The device was activated for 4 seconds, with an air flow rate of 60 L/min, to provide 4 L of air flow from the inhaler. Inhaler device, capsule, mouthpiece, induction port, stages and filter were washed separately with acetonitrile.

The emitted fraction (EF %) is calculated by dividing the emitted dose by the recovered active substance from the ACI system. Mass-median aerodynamic diameter (MMAD) is obtained from the cumulative percent graph of active substance content (log-probability graph)

P18

as a function of aerodynamic diameter. Fine particle dose (FPD) was calculated as the amount of active substance in the formulation with an aerodynamic diameter of less than 5 μm . The fine particle fraction (FPF) was calculated by dividing the FPD by ED.

2.5. HPLC method

Active substance at every stage of ACI device was quantified by a HPLC method. The mobile phase was acetonitrile:130 mM ammonium acetate buffer pH 5; 37: 63 (v/v %). Active substance was observed at 30°C column temperature at 260 nm [3].

2.6. Measurement of particle size distributions

The particle size distributions and zeta potential of obtained nanoparticle suspension were measured with Malvern Zetasizer Nano ZS (Malvern Instruments, UK).

3. RESULTS AND DISCUSSION

3.1. Redispersibility in water after lyophilization

Redispersibility can be explained as ability of nanoaggregates, nanocomposites or microcarrier systems to release nanoparticles in similar characteristics to the primary nanoparticles upon exposure to humidity in vitro or to lung fluids in vivo [4]. Obtained dry powder inhaler formulations with no carrier (DPI-1), with lactose (DPI-2), with sucrose (DPI-3), with trehalose (DPI-4) and with mannitol (DPI-5) were dispersed in distilled water and particle size distributions and zeta potential were measured (Table 1).

DPI-1 showed that lyophilization process did not cause growth of particles, but rather reduced the size of them. Also, all the carriers except lactose caused a decrease in particle size. The high positive charge may prevent the particles from aggregation during the lyophilization process.

Table 1. Particle size distribution and zeta potential of nanosuspensions and DPIs (n=3, mean \pm SD)

Formulation	Nanoparticle suspension (before lyophilization)			Lyophilized powder		
	Particle size (nm)	PDI	Zeta potential (mV)	Particle size (nm)	PDI	Zeta potential (mV)
DP I-1	256.3 \pm 13.12	0.368 \pm 0.020	33.3 \pm 0.02	233.5 \pm 11.40	0.432 \pm 0.017	28.1 \pm 0.551

DP I-2	219.9 \pm 3.758	0.358 \pm 0.019	34.0 \pm 1.510	252.5 \pm 3.332	0.448 \pm 0.008	24.6 \pm 0.265
DP I-3	219.9 \pm 3.758	0.358 \pm 0.019	34.0 \pm 1.510	195.2 \pm 5.62	0.452 \pm 0.017	26.0 \pm 0.600
DP I-4	219.9 \pm 3.758	0.358 \pm 0.019	34.0 \pm 1.510	167.9 \pm 5.052	0.372 \pm 0.018	26.2 \pm 0.404
DP I-5	219.9 \pm 3.758	0.358 \pm 0.019	34.0 \pm 1.510	160.1 \pm 343.897	0.361 \pm 0.027	20.9 \pm 2.370

3.3. Aerodynamic parameters

The aerodynamic parameters of the listed formulations have shown in Table 2. DPI-2 and DPI-5 have the most desired MMAD values which are smaller than 5 μm . All the formulations have a high EF % shows that the formulations have good emitting capacity. The FPF % higher than 40 % has been achieved with the mannitol as a carrier.

Table 2. Aerodynamic parameters of DPI formulations.

Formulation	EF %	MMAD (μm)	FPD (μg)	FPF %
DPI-1	99.6	5.11	89.1	36.1
DPI-2	97.9	4.34	13.0	38.3
DPI-3	99.9	5.75	15.9	13.5
DPI-4	98.8	5.18	41.5	36.5
DPI-5	98.9	4.27	27.2	41.4

4. CONCLUSION

DPI formulations, which contain positively charged nanoparticles of approximately 220 nm size combined with different carriers, have good water redispersion. Formulations that have FPF % of more than 35 % show that they can penetrate deep enough into the lungs for drug delivery.

5. REFERENCES

- Zhong, Q, *Co-Spray Dried Mannitol/Poly(amidoamine)-Doxorubicin Dry-Powder Inhaler Formulations for Lung Adenocarcinoma: Morphology, In Vitro Evaluation, and Aerodynamic Performance*, AAPS PharmSciTech, 2018. 19(2): 531-540
- Desai et al., (2010). US20100226996.
- Chandrashekar, K.A., et al., *Separation and estimation of process-related impurities of gefitinib by reverse-phase high-performance liquid chromatography*. Journal of Chromatography Science, 2014. 52(8): 799-805.
- Al -Hallak, M. K., et al. *Pulmonary delivery of inhalable nanoparticles: drypowder inhalers*. Therapeutic Delivery, 2011. 2(10): 1313-1324.

ACKNOWLEDGMENT

This study was supported by a grant from the Scientific and Technological Research Council of Turkey (TÜBİTAK; SBAG-120S895).

COMPARATIVE COMPRESSION CHARACTERIZATION OF LIQUISOLID SYSTEMS PREPARED WITH MESOPOROUS CARRIERS

Teodora Glišić¹, Ilija German Ilić², Jelena Parojčić¹, Ivana Aleksić¹

¹*Department of Pharmaceutical Technology and Cosmetology, University of Belgrade, Faculty of Pharmacy, Serbia*

²*Department of Pharmaceutical Technology, Faculty of Pharmacy, University of Ljubljana, Slovenia*

1. INTRODUCTION

Maintaining good compaction properties of liquid systems (LSS) is particularly challenging in the case of high-dose drugs [1]. High amount of liquid phase within LSS, required to dissolve/suspend higher amount of drug substance, while necessary for improvement of bioavailability, can cause difficulties during the tableting process, resulting in low tablet hardness or even inability of admixtures to be directly compressed. This has led to the development of new highly porous carriers, specifically designed for LSS, that can adsorb/absorb very high amount of liquid phase. The aim of this study was to investigate the compaction properties of LSS, prepared with three types of novel silica-based mesoporous carriers, using dynamic compaction analysis as a tool, with the focus on compressibility, compactibility and tableting of these systems [2].

2. MATERIALS AND METHODS

2.1. Materials

Amorphous magnesium aluminometasilicate (Neusilin[®] US2, Fuji Chemical Industry Co, Ltd., Japan) and two types of amorphous mesoporous silicon dioxide (Syloid[®] XDP 3050 and Syloid[®] XDP 3150, Grace GmbH, Germany) were used as carriers. Colloidal silicon dioxide (Aerosil 200, Evonik Industries AG, Germany) was used as coating material and polyethylene glycol 400 (PEG 400, Fagron, Netherlands) was used as liquid phase.

2.2. Liquid Admixture Preparation

LS admixtures (Table 1) were prepared using Mycrolab fluid bed processor (OYSTAR Hüttlin, Germany), with the operating temperature of 30°C, inlet air flow rate of 20 m³/h, and liquid feed rate of 12 g/min.

Table 1. Composition of prepared LS admixtures

Liquisolid admixtures ^a	R ^b	Liquid load	PEG 400 (%)
S1	10	0.7	38.9
S2	30	0.7	40.4
S3	10	0.6	35.3
S4	30	0.6	36.7
N1	10	1.1	49.8
N2	30	1.2	54.7

^a type of carrier used: S1, S2 - Syloid[®] XDP 3050, S3, S4 - Syloid[®] XDP 3150, N1, N2 - Neusilin[®] US2; ^bcarrier to coating material ratio

2.3. Powder density

LS admixtures' true densities were determined by helium pycnometer (AccuPyc 1330, Micromeritics, GA) while bulk and tapped densities were measured using a graduated cylinder and a volumeter (STAV 2003, J. Engelsmann AG, Germany).

2.4. Powder morphology

The morphology of LS particles was examined using a scanning electron microscope (SEM, Supra 35VP, Carl Zeiss, Germany).

2.5. Dynamic compaction analysis

Dynamic compaction analysis was performed on an instrumented tablet press (GTP D series, Gamlen Tableting Ltd, UK). 6 mm flat faced punches were used at a compaction speed of 60 mm/min, with compression load ranging from 250 to 500 kg, with a 50 kg increment.

3. RESULTS AND DISCUSSION

3.1. Compressibility of LS admixtures

Regardless of the compaction pressure applied and differences in liquid load, very high values of solid fraction were observed in LS compacts with Neusilin[®] US2 (0.90-0.94). On the other hand, LS compacts with both Syloid[®] XDP carriers exhibited lower relative density (0.59-0.89) that was affected by changes in the

P19

applied compaction pressure. Compressibility profiles suggest that carrier particle size and the amount of coating material used, had an effect on relative density. An increase in the amount of coating material used had a negative impact on compressibility and lower values of solid fraction were achieved.

3.2. Compactibility of LS admixtures

Admixtures N1 and N2 could be considered as having good compactibility [3]. Compacts with Neusilin® US2 achieved higher tensile strength values compared to compacts with Syloid® XDP, even at low compaction pressures. Particle geometry and shape (Fig. 1) can affect the way particles interact during tableting and therefore may affect their mechanical characteristics. Differences in particle size could be a reason for lower values of solid fraction and tensile strength observed in compacts prepared with Syloid® XDP 3150 compared to compacts with Syloid® XDP 3050 as carrier.

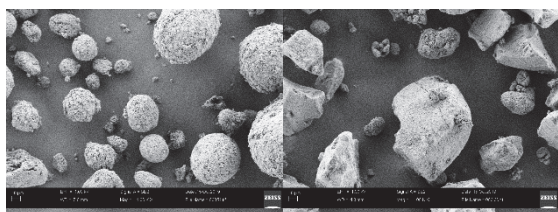


Figure 1. SEM micrographies of LS particles: admixture N1 (left) and S1 (right)

3.3. Tableability of LS admixtures

Despite the significantly higher liquid load, better tableability was observed in LSS with Neusilin® US2 as carrier with tensile strength ranging from 1,68 to 2,55 and 1,61 to 2,11 for formulations N1 and N2, respectively. Although relatively similar values of tensile strength were achieved, tableability profiles indicate that there are differences in compaction behavior between formulations N1 and N2. Higher values of tensile strength observed at the same compression pressure indicate better tableability of LS admixtures with Syloid® XDP 3050 compared to those with Syloid® XDP 3150 as carrier. Interestingly, formulations with Syloid® XDP 3050 had higher liquid load which implies that this formulation factor had lesser influence on tableability compared to the properties of the carrier itself (such as particle size and specific surface area). The lowest tableability was observed in LS admixtures S3 and S4 with

compact tensile strength lower than 1 MPa at all but highest compaction pressure applied.

4. CONCLUSION

Out of the three investigated carriers, Neusilin® US2 showed the best compaction properties despite its high liquid load. LS admixtures with this carrier exhibited the highest values of tensile strength and solid fraction at relatively low compression pressures. Pronounced differences have been noticed between the two Syloid carriers, which indicates the effect of carrier particle size on compaction properties of LS admixtures.

5. REFERENCES

1. Lu, M., et al., *Liquisolid technique and its applications in pharmaceuticals*. Asian Journal of Pharmaceutical Sciences, 2017.12(2):115-123.
2. *United States Pharmacopeia and National Formulary (USP 44 - NF 39)*. United States Pharmacopeial Convention; 2021.
3. Pitt, KG., et al., *Compression prediction accuracy from small scale compaction studies to production presses*. Powder Technology, 2015, 270: 490-493.

ACKNOWLEDGMENT

This research was funded by the Ministry of Education, Science and Technological Development, Republic of Serbia through Grant Agreement with University of Belgrade Faculty of Pharmacy No: 451-03-68/2022-14/200161.

DESIGN AND EVALUATION OF HYALURONIC ACID DECORATED MULTIFUNCTIONAL PCL-b-PEI NANOPARTICLES

Filip Gorachinov¹, Fatima Mraiche^{2,3}, Diala Alhaj Moustafa^{2,3}, Ola Hisari^{2,3}, Damjan Georgievski¹, Jensa Joseph^{2,3}, Katerina Goracinova¹

¹Faculty of Pharmacy, Ss. Cyril and Methodius University in Skopje, Skopje, N.Macedonia

²College of Pharmacy, Qatar University, ³Biomedical and Pharmaceutical Research Unit, QU Health Doha, Qatar University, Doha, Qatar

1. INTRODUCTION

Paclitaxel (PTX) loaded hyaluronic acid (HA) decorated polycaprolactone-b-polyethyleneimine (PCL-b-PEI) multifunctional nanocarriers were developed with the goal of increasing payload delivery in NSCLC cells positive for CD 44. Hyaluronic acid forms a bioresponsive shell with a dual role, improving tumor localization by the EPR effect and targeting the overexpressed CD 44 receptor. Further, in the tumor microenvironment, hyaluronidase overexpression may catalyze the degradation of hyaluronic acid, expose polyethyleneimine chains and reverse the nanoparticle (NP) charge which will further influence cellular trafficking and endosomal escape of the nanoparticles (1). The aim of this study was to develop a reproducible technological approach for preparation of HA decorated PCL-b-PEI nanoparticles using D-optimal experimental design and to evaluate NPs properties.

2. MATERIALS AND METHODS

2.1. Materials

Poly- ϵ -caprolactone-branched-polyethyleneimine (PCL-b-PEI, Mw ~ 40.000-800 Da) was purchased from Akina, Inc. IN, USA and poly(ethyleneoxide)-b-poly(propyleneoxide)-b-poly(ethyleneoxide) (PEO-PPO-PEO, Lutrol® F127) was purchased from BASF, Germany. N-Hydroxysulfosuccinimide sodium salt and N-(3-Dimethyl-aminopropyl)-N'-ethylcarbodiimide hydrochloride were acquired from Sigma-Aldrich, USA. Low molecular hyaluronic acid sodium salt HA5K (Mw less than 10.000 Da) was purchased from Lifecore Biomedical; and all other chemicals were analytical grade purchased from Sigma-Aldrich, USA.

2.2. Experimental design, preparation and physicochemical evaluation of NPs
D-optimal design matrix (19 experiments,

quadratic regression model) where each factor was varied at five different levels in the D-optimal design algorithm was developed (MODDE experimental design software, Umetrics, Sartorius, Stedim Biotech) and used to evaluate the influence of copolymer, Lutrol®F127, and drug concentration upon the particle size (PS), drug content (DC) and efficacy of encapsulation (EE). Optimization procedure was carried out using the desirability function. The goal was set to minimize the particle size, maximize the efficacy of loading and drug content. Ultrasound assisted nanoprecipitation was used for preparation of the PCL-b-PEI NPs (Ultrasound homogenizer 300VT, Biologics Inc) according to the D-optimal design matrix. PCL-PEI-HA conjugation was performed by amidation of HA carboxylates with amino-groups from PEI using EDC as a coupling agent. PCL-b-PEI-HA conjugates were further subjected to polyelectrolyte complexation of unreacted amino groups from PEI with HA.

PS, size distribution and zeta potential of the polymeric NPs were determined by Zetasizer Nano ZS (Malvern Instruments, UK). Previously validated HPLC method was used for quantification of encapsulated Paclitaxel as well as calculation of the EE and DC (Waters HPLC system, mobile phase ammonium acetate pH=5.0/ acetonitrile/ methanol; 50:40:10; column Symmetry® C18, 4.6x100mm, 3.5 μ m (Waters, USA), flow rate 1.4 ml/min; Agilent 1100 DAD detector at a wavelength of 230 nm). In-vitro drug release studies of optimized formulation, FTIR analysis, SEM studies as well as cytotoxicity and efficacy evaluation using MTT and LDH assay on H322 and A549 cell lines were also performed. Results from the D-optimal design study and characterization of design matrix samples will be presented further.

3. RESULTS AND DISCUSSION

3.1.D-optimal design results

The design was fitted with multiple regression analysis and the statistical results pointed to high correlation (R^2) among the formulation parameters and the factors as well as high predictivity (Q^2) of the values for the evaluated parameters (PS $R^2 = 0.9502$ and $Q^2 = 0.6218$; EE $R^2 = 0.9481$ and $Q^2 = 0.5710$, DC $R^2 = 0.9845$ and $Q^2 = 0.9020$).

The factors influencing the particle size, efficacy of encapsulation and the drug content are presented in Fig 1.

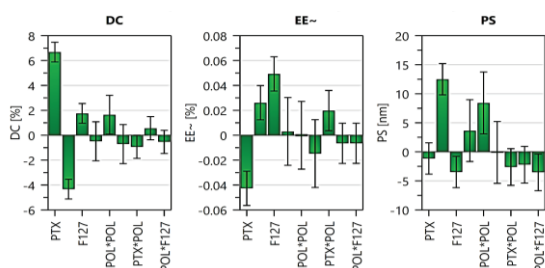


Figure 1. Factors and factor coefficients influencing PS, EE and DC

The influence of polymer and drug concentration on the drug content, efficacy of encapsulation and particle size at fixed value of Pluronic F127 is presented in Fig. 2.

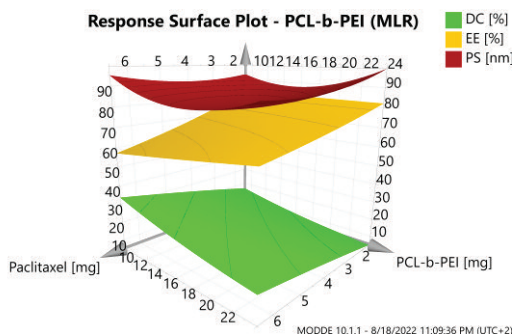


Figure 2. Response surface plot for EE, DC, PS (Pluronic F125 value 5 mg)

The desirability function gave several optimized formulations. The design space for DCmax, EEmax and PSmin is presented in Figure 3.

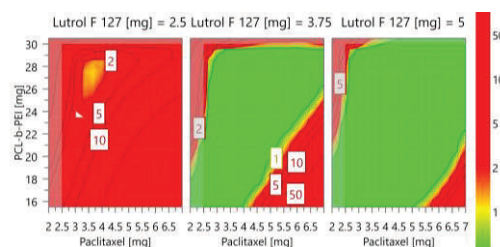


Figure 3. Design space and % of failure

3.2.Characterization of the design matrix samples and HA decorated NPs

PCL-b-PEI self-assembled into nanoparticles with size in a range of $80 \pm 1.2 - 120 \pm 2.1$ nm and displayed zeta-potential of $+36.2 \pm 1.4$ mV (average value, $n=19$, nonsignificant difference among matrix samples). Conjugated PTX(PCL-PEI-HA) NPs showed zeta potential of -1.2 ± 0.4 mV and particle size of 103 ± 2.2 nm ($PDI = 0.11 \pm 0.02$). After additional HA electrostatic adsorption, the NPs showed -15 ± 0.56 mV zeta potential and the average size of 111.3 ± 1.4 nm ($PDI = 0.18 \pm 0.02$). Conjugation of HA and the presence of stable HA layer was confirmed using FTIR and DSC studies. MTT and LDH test of the blank HA decorated NPs pointed to high viability of treated A549 and H322 cells (24 and 48 h).

4. CONCLUSION

D-optimal design was successfully used to optimize the PS, EE and DC of the PCL-b-PEI NPs. HA decoration improved biocompatibility and EPR effect by reversing the positive PEI charge to almost neutral charge or negative charge. HA is specific for overexpressed CD44 receptor but may also enable multimodality feature leading to exposure of PEI chains in tumor microenvironment due to enzyme hydrolysis leading to improved internalization and endosomal escape.

5. REFERENCES

1. Maiolino S., et al., *Biodegradable nanoparticles sequentially decorated with Polyethyleneimine and Hyaluronan for the targeted delivery of docetaxel to airway cancer cells.*, Journal of Nanobiotechnology (2015) 13:29

ACKNOWLEDGMENT

This project has received support from UREP24-057-3-022 award from the Qatar National Research Fund. The statements made herein are solely the responsibility of the author[s].

NANOCELLULOSE-BASED FILM-FORMING HYDROGELS CONTAINING BETAMETHASONE DIPROPIONATE: DEVELOPMENT AND PHYSICAL EVALUATION

Mirjam Gosenca Matjaz^{1*} and Katarina Bolko Seljak¹

*mirjam.gosenca.matjaz@ffa.uni-lj.si

¹Department of Pharmaceutical Technology, Faculty of Pharmacy, University of Ljubljana, Slovenia

1. INTRODUCTION

Atopic dermatitis (AD) is a chronic inflammatory skin disease with the lifetime prevalence of up to 30 % in children and 10 % in adults. Dysfunction of skin barrier, typical for AD, results in characteristic features of atopic skin being dry, sensitive, accompanied by intense itch. Daily skin care routine has an important role in AD management, whereas treatment options span from local anti-inflammatory therapy to systemic therapy in cases of severe AD [1].

Various dermal formulations are being investigated for AD treatment. One of advanced approaches is use of hydrogels as film forming systems upon dermal application. Namely, hydrogel is applied directly to the skin forming a thin, transparent film *in situ* upon solvent evaporation [2]. While primarily suggested for prolonged delivery, in the case of AD treatment the additional value of film-forming hydrogels is providing a physical barrier on the skin surface that is lacking in atopic skin.

In drug delivery, biocompatible and biodegradable polymers are used. One such polymer, nanocrystalline cellulose (NCC), is gaining interest due to its excellent and attractive mechanical and chemical characteristics in addition to renewability, although its properties may differ based on source and manufacturing procedure [3].

In this study, novel film-forming hydrogels based on two different NCCs, combined with one of the natural polymers (alginate or pectin) plus glycerol were developed for incorporation of betamethasone dipropionate (BDP) and evaluated as innovative delivery system for AD treatment.

2. MATERIALS AND METHODS

2.1. Materials

For preparation of film-forming hydrogels gel NCC ((gNCC) Nanocrystacell, Slovenia) or powder NCC ((pNCC) Cellulforce, Canada), sodium alginate ((ALG) Protanal[®] LF 10/60, FMC BioPolymer, USA), pectin ((PEC) Sigma-Aldrich, USA), glycerol (Pharmachem, Slovenia) and purified water were used. Capryol[™] 90 (Gattefosse, France) and Cremophor[®] EL (BASF, Germany) were used for formation of self-microemulsifying drug delivery system (SMEDDS) for dissolving BDP (Sicor, Italy).

2.2. Hydrogel preparation and DSC analysis

For NCC-ALG or NCC-PEC hydrogels, BDP-loaded or unloaded SMEDDS diluted with water was added to NCC, followed by alginate or pectin plus glycerol. The NCC/natural polymer ratio was 1/2, while SMEDDS and glycerol content was 3 and 5 %, respectively. Drug content in BDP-loaded hydrogels was 0,64 mg/1 g.

For DSC measurements (Mettler Toledo, Switzerland) samples were heated from 25 to 250 °C with heating rate 10 K/min at nitrogen flow of 50 ml/min.

2.3. Film preparation and evaluation

Hydrogels were evenly distributed across glass plate using ZUA applicator and dried at 32 °C to form films that were cut into even pieces. Films were evaluated for residual moisture content and thickness. *In vitro* ability to retain water evaporation was evaluated using Tewameter[®]TM 300 (Courage&Khazaka GmbH, Germany) with films placed in Franz diffusion cells.

3. RESULTS AND DISCUSSION

3.1. Hydrogel preparation and evaluation

BDP is practically insoluble in water, therefore a challenge to prepare BDP-loaded hydrogels was resolved by prior dissolution in SMEDDS. The mixture of Cremophor® EL/Capryol™ 90 in 8/2 ratio was chosen on the merit of its high BDP saturated solubility and ability to form microemulsions upon water dilution without BDP precipitation (data not shown).

Regarding DSC analysis, broad endothermic peak can be seen for all hydrogels, ranging between 104–108 °C representing water evaporation. No additional endothermic peak was observed in case of BDP-loaded hydrogels, confirming that BDP remains dissolved upon incorporation into hydrogels (example of NCC-ALG hydrogels in Fig. 1).

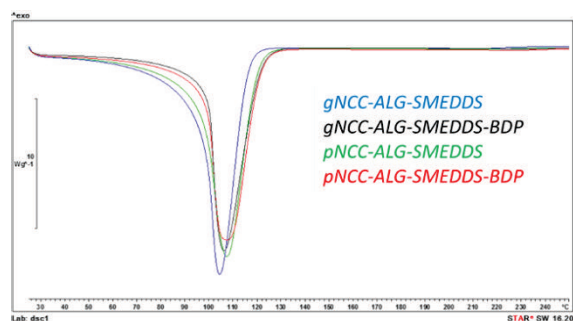


Figure 1. DSC heating curves of BDP-loaded and unloaded NCC-ALG hydrogels.

3.3. Film preparation and evaluation

Films were prepared from hydrogels using solvent evaporation method at 32 °C, i.e. skin surface temperature. The prepared films showed a low residual moisture content (up to 2,15 % for NCC-PEC films and up to 1,5 % for NCC-ALG films, being higher in case of gNCC or/and incorporated BDP). Incorporation of BDP had also an impact on film thickness, being the maximum in case of BDP-loaded pNCC-ALG films, i.e. $0,078 \pm 0,008$ mm.

Increased transepidermal water loss due to impaired skin barrier function is distinctive for atopic skin [4], therefore formulations that enable water retention in skin are especially beneficial in AD treatment. Prepared films decreased *in vitro* water evaporation (Fig. 2) with statistically significant difference ($p < 0,05$) compared to cellulose acetate membrane that was used as carrier for films between donor and acceptor compartment of Franz diffusion cells.

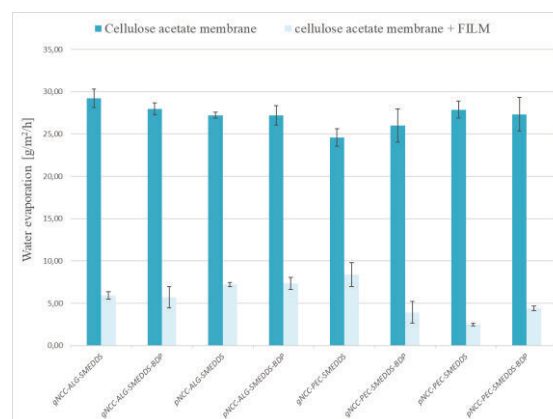


Figure 2. Water evaporation ($\text{g}/\text{m}^2/\text{h}$) for cellulose acetate membrane (basal value) compared to cellulose acetate membrane with film (the water evaporation was measured prior wetting of films). Data are expressed as mean \pm S.D. ($n = 3$).

4. CONCLUSION

Both types of NCC were proven to be suitable for formation of film-forming hydrogels in combination with alginate or pectin. BDP was successfully incorporated and remained dissolved using SMEDDS. Using solvent evaporation method flexible films were formed at 32 °C and significantly reduced *in vitro* water evaporation was observed.

NCC-based film forming hydrogels therefore present novel and perspective delivery system for AD treatment.

5. REFERENCES

1. Weidinger S., et al., *Atopic dermatitis*. Nature Reviews Disease Primers, 2018. 4(1): 1.
2. Kathe K., et al., *Film forming systems for topical and transdermal drug delivery*. Asian Journal of Pharmaceutical Sciences, 2017. 12(6): 487-497.
3. Trache D, et. al. *Nanocellulose: From Fundamentals to Advanced Applications*. Frontiers in Chemistry, 2020. 8: 392.
4. Montero-Vilchez T., et al., *Skin Barrier Function in Psoriasis and Atopic Dermatitis: Transepidermal Water Loss and Temperature as Useful Tools to Assess Disease Severity*. Journal of Clinical Medicine, 2021. 10(2): 359.

ACKNOWLEDGMENT

The authors acknowledge financial support from the Slovenian Research Agency (research core funding, No. P1-0189).

VALSARTAN BUCCAL FILMS FORMULATION DEVELOPMENT WITH THE IMAGE ANALYSIS

Blaž Grilc¹, Tjaša Felicijan², Timeja Planinšek Parfant², Odon Planinšek¹

¹*Department of Pharmaceutical Technology,*

²*Department of Biopharmaceutics and Pharmacokinetics, University of Ljubljana, Faculty of Pharmacy, Slovenia*

1. INTRODUCTION

Buccal administration of drugs is a promising alternative for patients who are less responsive to conventional oral administration, such as pediatric patients. Buccal films for pediatric use have already been proposed by several research groups [1,2]. The incidence and prevalence of hypertension in pediatrics have increased over the past 30 years, largely due to lifestyle changes in children and adolescents [3]. The recommended starting dose of valsartan in children is 1.3 mg/kg once daily (maximum dose 40 mg), which should be adjusted according to blood pressure response [4]. Some unique challenges arise in the development of buccal films, such as breaking of the film, entrapment of bubbles, and inhomogeneous distribution of the drug. All of these effects are undesirable and difficult to evaluate. Observation of the film provides information on the homogeneity, presence of crystals, bubbles, and mechanical properties of the films. With the introduction of image analysis, unbiased comparison is possible without the risk of subjective evaluation and with repeatable results. The use of multilayer convolutional neural networks (CNN) has been introduced in the field of image analysis. The trained neural network behaves like the human visual cortex and can adapt its discrimination capabilities to a new challenge. Using this approach, images of buccal films were compared and classified by quality using a pre-trained CNN. The aim was to compare results with the drug release from different films and evaluate their capability of films performance prediction.

2. MATERIALS AND METHODS

2.1. Materials

Na-alginate (Protanal LF 10/60, Dupont, USA), xylitol (Xylisorb 100DC, Roquette, France), isomalt (Beneo-Palatinit, Germany), valsartan

(Matrix Fine Chemicals, Switzerland), ethanol (Merck, Germany).

2.2. Preparation of films

Films were prepared by applying the wet film solution to the glass plate at a height of 1500 μm using the applicator. The film solution was prepared by carefully mixing Na-alginate with water and plasticizer. During mixing with a propeller stirrer at 800 rpm, an ethanol solution of valsartan was introduced into the polymer. A reduced combinatorial design was used to study the effects of six factors. The amounts of valsartan, Na-alginate, isomalt, xylitol, EtOH and water were varied and their effects on visual appearance, dissolution properties and crystallinity were studied.

a. Image analytics

Images of finally produced films were embedded using a pre-trained CNN "Inception v3". The distances between the image data were evaluated by comparing the cosine distance and the results were displayed in the dendrogram. The clusters were connected using Ward's linkage method.

b. Other methods

All films were also tested with Raman microscopy mapping (Xplora Plus Horiba, Japan), moisture content KF titration (Titroline[®] 7500, Germany), TGA and DSC (Mettler Toledo TGA/DSC1), particle size distribution (Mastersizer 3000) and dynamic contact angle evaluation (KRÜSS DSA 100). The release rate of valsartan from the films was evaluated using four different methods (USP I, USP II, modified USP IV and innovative cell for film release (ICRF)).

3. RESULTS AND DISCUSSION

3.1. Image analytics

The distances between the obtained data sets were compared and the results were presented in the form of a dendrogram (Figure 1). The data were hierarchically clustered and four main clusters were identified at a height ratio of 45%.

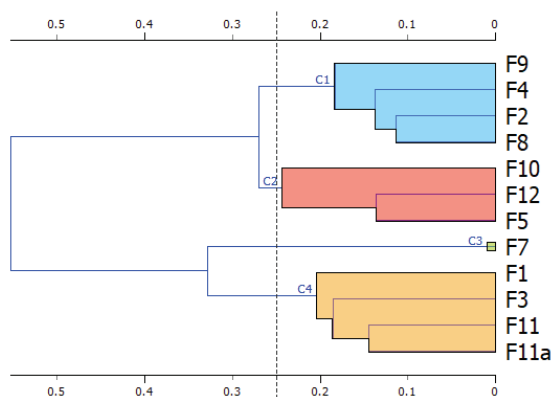


Figure 6: Dendrogram of image data distances.

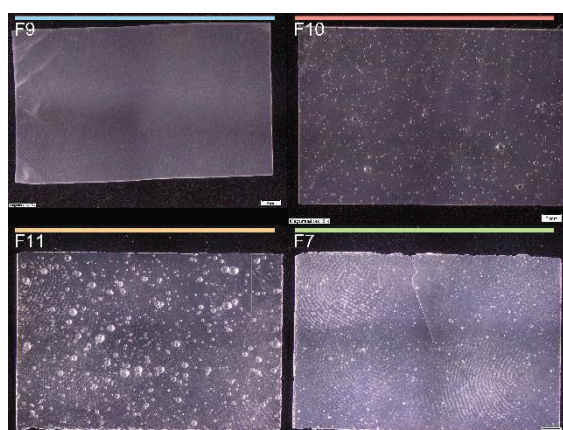


Figure 2: A representative from each cluster.

Figure 2 shows a single representative film from each cluster. Films with trapped bubbles and broken edges were found in the C4 (orange) cluster. Broken edges formed during cutting indicate that the film has poor mechanical properties and therefore tears easily during handling. Trapped bubbles affect the homogeneity of the drug distribution in the film and have a poor esthetic appearance. Films with a smaller and less dense distribution of bubbles and sharp cut edges were located in cluster C2 (red). Cluster C3 (green) contained a film with a white sheen, which could be due to light scattering by crystals on the film surface. Films with a smooth surface, homogeneity, sharp edges, no bubbles, and no crystals were in cluster C1 (blue). The result shows that the design space of cluster C1 offers the greatest

potential for future optimization. Image analysis provided a complementary approach to visual inspection. Hierarchical clustering allowed characterization and grouping of the films by an independent observer. This approach helps identify films or groups of films with visually similar characteristics, assisting the researcher in decision making.

3.2. Dissolution testing

The evaluation of the dissolution of the films revealed differences between the dissolution methods. In addition, some of the methods showed greater differences between formulations than others. The ICRF method was found to be superior than the modified USP IV method in terms of discriminability and repeatability.

4. CONCLUSION

Image analysis proved to be a supportive technique in visual evaluation of film quality. Visual observation with the naked eye is usually sufficient, but at the same time it is difficult to rank a large number of images by quality without a proper ranking tool. Even more important than ranking is finding the regions of the design space where the quality is within the desired parameters. Identifying these clusters of images that contain films of similar quality can help researchers choose the right path for further formulation development.

5. REFERENCES

1. Khan S., et al., *Formulation, Characterisation and Stabilisation of Buccal Films for Paediatric Drug Delivery of Omeprazole*. AAPS PharmSciTech. 2015 Aug 1;16(4):800–10.
2. Friedrichsdorf S, et al., *Management of breakthrough pain in children with cancer*. JPR. 2014 Mar;117.
3. Ashraf M, et al., *Pediatric hypertension: an updated review*. Clin Hypertens. 2020 Dec;26(1):22.
4. Kapur G., *Clinical utility of valsartan in the treatment of hypertension in children and adolescents*. PPA. 2011 Mar;149.

ACKNOWLEDGMENT

This research was funded by Slovenian Research Agency (ARRS), grant number [P1 0189].

NEW HIGHLIGHTS OF THE DRUG CARRIER PEG-B-CYCLODEXTRIN POLYMER

Adam Haimhoffer^{1,2}, Licia Dossi³, Ildikó Bácskai^{1,2}, Ferenc Fenyvesi¹

¹*Department of Pharmaceutical Technology, University of Debrecen, Hungary*

²*Institute of Healthcare Industry, University of Debrecen, Hungary*

³*Cranfield Defence and Security, Cranfield University, United Kingdom*

1. INTRODUCTION

Cyclodextrin and polymer binary systems are used to improve the solubilization of poorly soluble drugs when high amount of CD is needed for complexation. To achieve higher degrees of drug solubilization, the synergistic solubilizing effect of a cyclodextrin and a water-soluble polymer was used.

To take advantage of ternary complexes, high molecular weight crosslinking agents are now used for many cyclodextrin polymerizations [1]. The resulting polymers have more advantageous properties than the native CDs or binary systems.

Our aim was to test the water-soluble polyethylene glycol cross-linked β -CD polymer (fig 1.), which offers a combination of β -CD and PEG properties [2]. Estradiol was chosen as a model drug, which can be solubilized by cyclodextrin, cyclodextrin polymers and PEG 400 too.

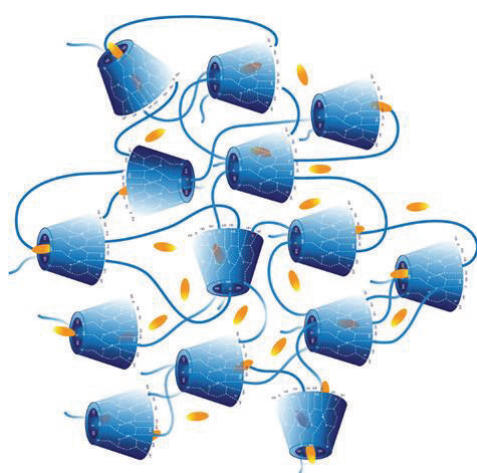


Figure 1. Schematic structure of PEG- β -cyclodextrin polymer and API complex. The yellow colored API molecules are entrapped in the β CD cavity and in the 3D cross-linked area.

2. MATERIALS AND METHODS

2.1. Materials

The β -cyclodextrin polymer cross-linked with polyethylene glycol diglycidyl ether (β CPGD) was synthesized at Cranfield University in the UK as previously described. Estradiol, cell culture and other reagents were from Sigma-Aldrich Ltd. (Budapest, Hungary).

2.2. Cytotoxicity test

The cytotoxic effects of the cyclodextrin polymers were evaluated using the MTT test. The Caco-2 cell line and NIH/3T3 fibroblast cell line were obtained from the European Collection of Authenticated Cell Cultures (ECACC, UK). Cells were maintained in Dulbecco's modified Eagle's medium at 37 °C in an incubator containing 5 % CO₂. 10,000 cells/well were seeded on 96-well plates. After 3 days, the medium was removed, and the cells were incubated for 30 min with the solutions of cyclodextrin polymers at 37 °C. Then the samples were removed, and a 0.5 mg/ml MTT solution was added to each well. The plates were incubated for 3 h, then the MTT solution was removed and 0.1 ml of isopropanol – 1 M hydrochloride acid (25:1) was added to each well to dissolve the formed formazan crystals. The absorbance of formazan was measured at 570 nm and the background was measured at 690 nm by Thermo-Fisher Multiskan Go (Thermo-Fisher, USA) microplate reader.

2.3. Phase-Solubility Test

The phase-solubility test was performed by adding a fixed excess amount of β -estradiol powder (20 mg) to 2.0 ml aqueous solutions containing β CD, PEG, β CD and PEG mixture, and PEG- β -cyclodextrin polymer at increasing concentrations (0.05 – 1.0 m/m %). The vials were vortexed for 30 seconds to achieve well-mixed dispersions. They were rotated at room temperature at 50 rpm and protected from light. After 72 h, each vial was centrifuged at 11000 rpm for 20 min. The samples were taken from

the clear supernatant, and the estradiol content of the samples was analysed by UV spectrophotometer (Shimadzu UV-1900) at 280 nm.

2.4. Dynamic light scattering (DLS) measurements of complexes

The effect of complexation on the average particle size and particle size distribution of 0.5 m/m % solution of complexes was measured by DSL. The cyclodextrin polymer solutions and complex solutions were measured using a Malvern Nano-ZS Zetasizer (Malvern Instruments, UK) in purified water.

3. RESULTS AND DISCUSSION

3.1. Cytotoxicity test

The cyclodextrin polymers were not cytotoxic on Caco-2 cells after 30 min of incubation up to 10.0 m/m % concentration. The cell viability did not decrease below 60% compared to the control. In the case of NIH/3T3 fibroblast cell, the cell viability changed as expected.

3.2. Phase-Solubility Test

Based on the phase solubility curves, PEG cannot be used to increase the solubility of estradiol. When using β CD, a A_N -type curve is observed, the curve flattens, and the precipitation of the formed complex is observed to form an over-saturated solution. There is no significant improvement with the concomitant use of PEG and β CD. In case of PEG- β -cyclodextrin polymer the line is A_L -type, the solubility of estradiol increased with increasing polymer concentration. Significantly better solubility was obtained, although the CD content of the polymer was only around 50%. Thus, to focus to β CD component, it can be said to have increased solubility of estradiol by more than 2-fold, as if ternary complexation had been used.

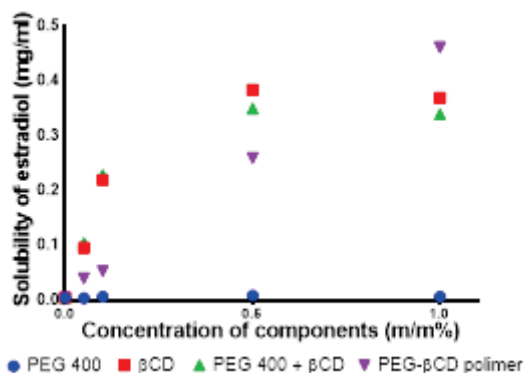


Figure 2. Phase-solubility curve presents the solubility of estradiol (mg/ml) in water versus the m/m % concentration of the β CD (red), PEG (blue), β CD and PEG mixture (green), and PEG- β -cyclodextrin polymer (purple)

3.3. Dynamic light scattering (DLS) measurements of complexes

The size of the complexes formed (270.70 ± 10.10 nm) after complexation is several times bigger than the polymer size (49.76 ± 0.43 nm). During complex formation, the estradiol is able to connect to polymer chains and form a coherent colloidal solution.

4. CONCLUSION

In terms of results, it can be said that the polymer did not cause cell death in either the Caco-2 or fibroblast cell line. Estradiol has better complexing properties with PEG- β -cyclodextrin polymer, than the β CD or binary system. Furthermore, the formed matrix system provides an opportunity to develop drug delivery systems. Our other goals include the development and tests of a subcutaneous formulation.

5. REFERENCES

1. Haimhoffer, A. et al.; Cyclodextrins in drug delivery systems and their effects on biological barriers. *Sci. Pharm.* 2019, 87,
2. Haimhoffer, Á. et al.; Preformulation Studies and Bioavailability Enhancement of Curcumin with a 'Two in One' PEG- β -Cyclodextrin Polymer. *Pharmaceutics* 2021, 13,

ACKNOWLEDGMENT

Project no. TKP2021-EGA-18 has been implemented with the support provided from the National Research, Development and Innovation Fund of Hungary, financed under the TKP2021-EGA funding scheme.

PREPARATION AND EVALUATION OF SPRAY-DRIED MICROPARTICLES CONTAINING N-ACETYLCYSTEINE FOR LUNG APPLICATION

Hana Hořavová¹, Jan Gajdziok¹

¹*Department of Pharmaceutical Technology, Faculty of Pharmacy, Masaryk University, Czech Republic*

1. INTRODUCTION

Inhalation is the preferred administration route of active substances for lung diseases (e.g., cystic fibrosis). The basic therapeutic approach to this disease is the administration of mucolytics. One of the commonly used is N-acetylcysteine. Its administration in dry microparticles can bring advantages like higher physical and chemical stability, better control of particles' size and deposition, and a reduced risk of bronchoconstriction after inhalation compared to a liquid aerosol [1]. Spray drying of N-acetylcysteine (NAC) was proved to be problematic due to its high hygroscopicity [2] and low glass transition temperature ($T_g \approx 10^\circ\text{C}$) [3]. This work optimized the process by applying different drying conditions and additives to obtain solid microparticles suitable for inhalation.

2. MATERIALS AND METHODS

2.1. Materials

Active agent N-acetylcysteine (NAC; Myproteine) is a mucolytic disrupting disulfide bonds in the mucus structure. Mannitol (MAN; Penta) was used as a carrier material to dilute mucus by its high osmotic activity. Leucine (LEU; Myproteine) was used as an anti-adherent improving aerodynamic properties and reducing hygroscopicity. Sodium hydroxide (Dr. Kulich Pharma) solution was added to form a salt of NAC and thus reduce its hygroscopicity. Dextran 10 (DEX; Carl Roth), maltodextrins (MD) with different dextrose equivalents (DE = 2, 6, or 9; Roquette), and low-molecular chitosan (CHIT; Sigma Aldrich) were used to increase the T_g . The composition of prepared batches is listed in Table 1.

2.3. Method

A 10% (w/w) aqueous solution was prepared for all the materials in each batch ahead of drying. Subsequently, the solution underwent a spray-drying process using a LabPlant SD06. The parameters used were: inlet temperature 100 –

180 °C, feed rate 10 – 20 device units, airflow rate 35 device units, atomization pressure 2 bars. Dry powders were evaluated by SEM Tescan MIRA 3. Size distribution and median size were determined using laser diffraction (HORIBA Partica LA-960). Aerodynamic properties (MMAD = mass median aerodynamic diameter, FPF = fine particle fraction) were determined using Small-Scale Powder disperser TSI 3433 and Aerodynamic Particle Sizer TSI 3321.

3. RESULTS AND DISCUSSION

In neutralized batches, particle median size increased with increasing drying temperature, while MMAD decreased after the initial increase (Fig. 2). That corresponds with the increasing porosity of the particles observed in SEM images. Decreasing the feed rate led to more spherical and smaller particles.

A higher dextran concentration caused decreasing in both median size and MMAD with increased FPF. These particles were better separated with a smoother surface and fewer aggregates. However, the dextran concentration seemed not sufficient to increase the T_g enough. Imamura et al. described a more significant increase in T_g from 40% dextran content [4].

Dextrose equivalent of maltodextrin has a nonlinear effect on the particles' median size, but increased MMAD and FPF were observed with higher DE. That means smaller particles creating larger aggregates or particles with different densities were formed. The more wrinkled surface also influenced the results.

In chitosan batches, the same dependencies as in dextran batches were observed. On the other hand, chitosan did not show a good ability to encapsulate NAC as its crystals were seen on the SEM images.

All the described excipients showed a positive effect on the formation of spherical

P24

microparticles compared to previous excipient-free products (not published). Nevertheless, the particles were stuck to aggregates. The only approach leading to separated individual particles was increasing the leucine content up to 30%. With increasing leucine content, both median size and MMAD decrease, and FPF increase with best results with 20 or 25% of leucine (Fig. 1). The further increase did not bring better aerodynamic properties, and a higher number of collapsed particles was obtained.

Table 1. Composition of prepared batches.

Sample name	MAN [g]	NAC [g]	LEU [g]	DEX [g]	MD [g]	CHIT [g]
NAC 1-5	30	15 neutr.	5	-	-	-
ND 1	22,5	15	5	7,5	-	-
ND 2	15	15	5	15	-	-
NM 1	15	15	5	-	15 (2)	-
NM 2	15	15	5	-	15 (6)	-
NM 3	15	15	5	-	15 (9)	-
NCH 1	27,5	15	5	-	-	2,5
NCH 2	25	15	5	-	-	5
NL 10%	30	15	5	-	-	-
NL 15%	27,5	15	7,5	-	-	-
NL 20%	25	15	10	-	-	-
NL 25%	22,5	15	12,5	-	-	-
NL 30%	20	15	15	-	-	-

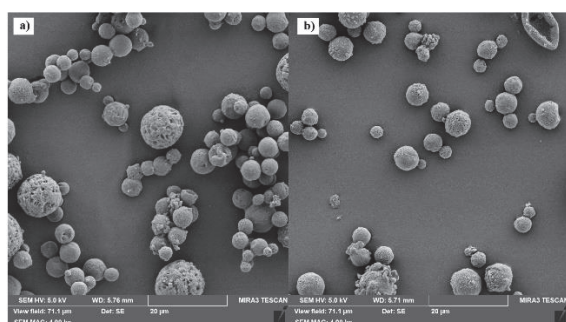


Figure 1. SEM images (magnification 5000x) of batches a) NL 20%, b) NL 25%.

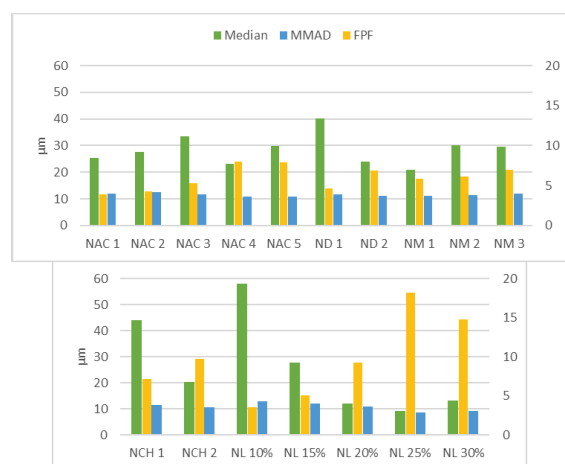


Figure 2. Results of median size, MMAD, and FPF.

4. CONCLUSION

Although the addition of the excipients resulted in spherical primary particles, the particles were present in aggregates and exceeded the recommended size. Best results were found with an increase in the leucine content. Batches with a concentration of 20 and 25% met the requirements for inhalation particles best. These batches showed the largest fine particle fractions and the smallest particle sizes, including narrow size distribution and appropriate morphology and shape. However, further research is needed to achieve even smaller particle sizes.

5. REFERENCES

1. Henke, M. O., et al., *Mucolytics in cystic fibrosis*. Paediatric Respiratory Reviews, 2007. 8(1): 24-29.
2. Lababidi, N., et al., *Spray-drying of inhalable, multifunctional formulations for the treatment of biofilms formed in cystic fibrosis*. Journal of Controlled Release, 2019. 314: 62-71.
3. Odziomek, M., et al., *Conception, preparation and properties of functional carrier particles for pulmonary drug delivery*. International Journal of Pharmaceutics, 2012. 433(1-2): 51-59.
4. Imamura, K., et al., *Water sorption and glass transition behaviors of freeze-dried sucrose-dextran mixtures*. Journal of Pharmaceutical Sciences, 2002. 91(10): 2175-2181.

ACKNOWLEDGMENT

This work was supported by the project MUNI/A/1213/2020.

Aerodynamic measurements were performed at the Faculty of Mechanical Engineering, University of Technology, Brno.

THE EFFECT OF THE HIGH DRUG LOAD – THE EVALUATION OF THE PROPERTIES OF 3D PRINTED ORODISPERSIBLE TABLETS (ODTs) WITH 70% OF DRUG CONTENT

Witold Jamróz¹, Jolanta Pyteraf¹, Mateusz Kurek¹, Thao Tranová², Jan Loskot³, Jitka Mužíková², and Renata Jachowicz¹

¹*Department of Pharmaceutical Technology and Biopharmaceutics, Jagiellonian University Medical College, Krakow, Poland; witold.jamroz@uj.edu.pl (W.J.)*

²*Department of Pharmaceutical Technology, Faculty of Pharmacy in Hradec Králové, Charles University, Czech Republic;*

³*Department of Physics, Faculty of Science, University of Hradec Králové, Czech Republic*

1. INTRODUCTION

Fused deposition modeling (FDM) is a 3D printing (3DP) method that is considered as a potential tool for the preparation of personalized dosage forms [1]. In this method filaments containing API (active pharmaceutical ingredient) are utilized in dosage form preparation. The high drug content in the filaments allows for the preparation of tablets with a variety of drug doses [2]. However, the stability and printability of the high drug-loaded filaments after storage are questionable.

The aim of the studies was to verify the possibility of ODF tablets preparation by means of the 3DP FDM method with the extremely high (70%) API content filaments, which were freshly prepared (F) or after one-year storage (O) in the room conditions.

2. MATERIALS AND METHODS

2.1. Materials

Fluconazole (FLU, China) served as a model drug, while poly(vinyl alcohol) (PVA, Pardeck[®] MXP, Merck KGaA, Germany) was used as a filament-forming polymer.

2.2. Hot-Melt Extrusion

Filament composed of 70% of FLU and 30% of PVA was prepared using a 12-mm corotating twin-screw, hot-melt extruder (RES-2P/12A Explorer, Zamak Mercator[®], Poland) equipped with a 1.75 mm nozzle at 137°C.

2.3. Evaluation of filaments' properties

Mechanical properties were evaluated with an EZ-SX tensile tester (Shimadzu) while the microstructure was examined using a scanning electron microscope FlexSEM 1000 (Hitachi).

2.4. 3D printing of ODTs

The ODTs projects were designed using Blender[®] 2.90 software and prepared for the printing in Voxelizer[®] slicing software. The layer height was set at 0.1 mm with 10% of infill density and one outline. Tablets containing 50 mg of FLU were manufactured by ZMorph[®] 2.0 S (Poland), equipped with a 0.2 mm nozzle at 182°C and 10 mm/s of printing speed. Glass build plate temperature was 60°C.

2.5. Tablets disintegration

Disintegration time of the tablets were evaluated by means of Pharmacopoeial (PhEur 10) method (2.9.1) in SAPO ED-2 apparatus (Electrolab, India) in 700 mL of purified water. Additionally, changes in the tablet's height during disintegration were recorded using in-house developed apparatus (BJKSN-13) [3].

2.6. Dissolution study

Surface dissolution imaging apparatus SDi2 (Pion-Inc, UK) was applied to determine the dissolution processes of API from printed tablets. Tablets were analysed at $\lambda = 255$ or 280 nm. Additionally, a real-time disintegration process was observed by the UV camera. The amount of released FLU was assessed in-line with UV-VIS Shimadzu 1800 spectrophotometer (Japan) at $\lambda = 261$ nm.

3. RESULTS AND DISCUSSION

3.1. 3D printed tablets

Filaments were characterized by good printability which resulted in small weight variations (Tab. 1). During printing process the tension between filament driving rollers were reduced to avoid filaments fracture.

Table 1. Tablets' attributes.

	F	O
--	----------	----------

Average mass (mg \pm SD)	64.92 \pm 3.79	71.07 \pm 3.99
Dose (mg \pm SD)	48.35 \pm 2.82	50.03 \pm 2.81
Disintegration time (s \pm SD)	128 \pm 7.81	139 \pm 36.94

3.2. Disintegration and dissolution characteristics.

In both cases: freshly prepared filament or after one-year storage, the disintegration time of tablets was under 3 min (Tab. 1) which meets the Pharmacopoeial requirements for ODTs. Changes in the tablet' height during the disintegration process were also similar Fig. 1.

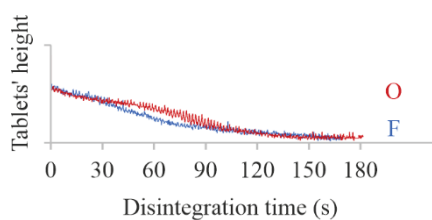


Figure 1. The disintegration profiles of 3D printed tablets obtained by BJKS-13 apparatus.

Based on the surface dissolution imaging analysis (Fig. 2), the infill of **O** tablets was almost completely dissolved after 3 min. After 10 min, in both cases, only outline is visible.

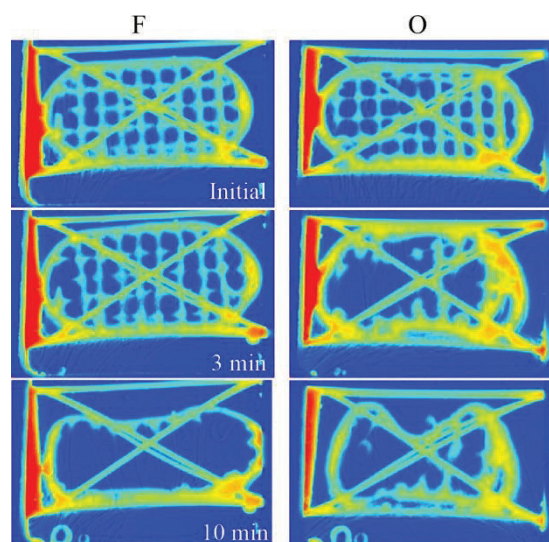


Figure 2. UV views of the tablets in the initial phase, after 3, and 10 min of the study in SDi2, $\lambda_2 = 280$ nm.

This differences in disintegration behaviour were observed in dissolution profiles. From **O** tablets over 80% of API was released after 15 min whereas from **F** tablets 68%. However, over 95 % of FLU was released within 30 minutes of testing (Fig. 3).

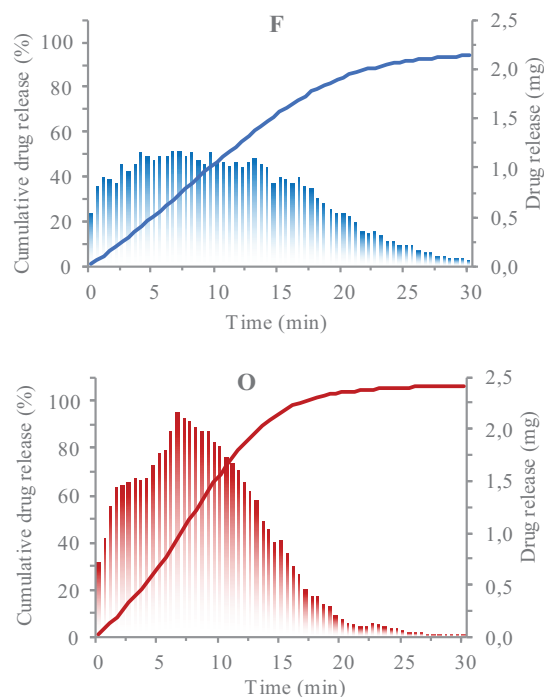


Figure 3. Drug dissolution profiles from 3DP tablets.

4. CONCLUSION

The FDM technology allows for the fabrication of high drug-loaded ODTs. The printability of the filament containing 70% of FLU after one year of storage is sufficient, and the tablets' properties are comparable with tablets prepared with fresh filament.

5. REFERENCES

1. Zema, L., et al., *Three-Dimensional Printing of Medicinal Products and the Challenge of Personalized Therapy*. J. Pharm. Sci. 2017, 106: 1697–1705.
2. Pyteraf, J. et al., *How to Obtain the Maximum Properties Flexibility of 3D Printed Ketoprofen Tablets Using Only One Drug-Loaded Filament?* Molecules 2021, 26, 3106
3. Brniak, W., et al., *The Practical Approach to the Evaluation of Methods Used to Determine the Disintegration Time of Orally Disintegrating Tablets (ODTs)*. Saudi Pharm. J. 2015, 23: 437–443.

ACKNOWLEDGMENT

The authors acknowledge the National Science Centre, Poland for financial support (grant OPUS 16 no 2018/31/B/ST8/01327).

HCE-T CELL-BASED CORNEAL EPITHELIAL MODEL: SCALE-DOWN TO 96-WELL INSERT PLATES

Bisera Jurišić Dukovski¹, Josip Ljubica¹, Petra Kocbek², Luka Bočkor³, Jasmina Lovrić¹

¹*Department of Pharmaceutical Technology, Faculty of Pharmacy and Biochemistry, University of Zagreb, Croatia*

²*Department of Pharmaceutical Technology, Faculty of Pharmacy, University of Ljubljana, Slovenia*

³*Institute for Anthropological Research, Croatia*

1. INTRODUCTION

HCE-T cell line is the most extensively characterized human-derived cell line of corneal epithelium. 3D HCE-T models are commonly cultured on 12-well insert plates and are widely used for permeability and biocompatibility testing of eye preparations [1, 2]. The aim of this research was transfer of a 3D HCE-T model from 12 to 96-well insert plate, in order to develop a high-throughput screening (HTS) model of human corneal epithelium.

2. MATERIALS AND METHODS

2.1. Materials

The cells were stained using 4',6-diamidino-2-phenylindole (DAPI, Invitrogen, USA). Fluoroshield™ mounting medium with DAPI was purchased from Sigma-Aldrich (Germany) and 3-[4,5-dimethylthiazol-2-yl]-2,5-diphenyl tetrazolium bromide (MTT) was purchased from Carbosynth (UK). For nanoemulsion (NE) preparation the following substances were used: ibuprofen (Hubei Biocause Pharmaceutical, China), Miglyol® 812 (Kemig, Croatia), lecithin S45 (Lipoid, Germany), LMW chitosan (Sigma-Aldrich), Kolliphor® EL (BASF, Germany), glycerol (T.T.T., Croatia) and purified water (SG, Germany).

2.2. Cell culture conditions

HCE-T cells (RIKEN Cell Bank, Japan) were cultivated in DMEM/F12 medium (Sigma-Aldrich) supplemented with FBS (5%, Capricorn, Germany), insulin (5 µg/mL, Sigma-Aldrich), dimethyl sulfoxide (0.5%, Applichem, Germany), epidermal growth factor (10 ng/mL, Sigma-Aldrich) and antibiotic-antimycotic solution (Sigma-Aldrich) at 37°C in a humidified atmosphere with 5% CO₂.

2.3. Cultivation of a 3D HTS HCE-T model

The cells were seeded (1×10⁴ cells per well) on polycarbonate membranes of a 96-well insert

plate (PSHT004S5, Merck, Germany) pre-coated with rat tail type I collagen (Sigma-Aldrich) and human fibronectin (Sigma-Aldrich). The cells were cultivated submerged in the medium (75 µL apical and 250 µL basolateral volume) during 7 days and were subsequently exposed to the air-liquid interface (ALI) for 3 days.

2.4. Histomorphological characterization

The cells were fixed with 4% paraformaldehyde (Sigma-Aldrich) at different time points after seeding and the cell nuclei were stained with DAPI. The membranes with cells were mounted onto glass slides with mounting medium and the cover slips were sealed with a nail polish. The cell nuclei were imaged using confocal fluorescence microscope (ImageXpress® Micro Confocal, Molecular Devices, USA) at 60× magnification.

2.5. Biocompatibility assay

Ophthalmic NEs were produced using microfluidizer (Microfluidics LM20, USA) at 1000 bar and 5 cycles and their composition is shown in table 1. The NEs were diluted 10 times in HBSS buffer (pH 6) and the HTS model was exposed to the diluted formulations for 30 min at 37°C. The viability of the cells was determined with MTT assay and the results were compared with the results obtained previously on a 12-well plate HCE-T model.

3. RESULTS AND DISCUSSION

3.1. Histomorphological features of HTS HCE-T model

The HCE-T model was successfully cultivated on a 96-well insert plate. After a 7-day cultivation period in submerged conditions a confluent monolayer was formed and 3 days after ALI exposure multiple layers were observed (Figure 1a). However, HTS HCE-T

P26

model was characterized with fewer cell layers (3-5) and uneven thickness compared to the 12-well plate model [1].

3.2. HTS HCE-T model viability

The viability of cells in the HTS HCE-T model after treatment with ophthalmic NEs was high (about 80%). However, it was lower than the viability of cells in a 12-well plate model treated with the same formulations, under the same conditions (Figure 1b) [2].

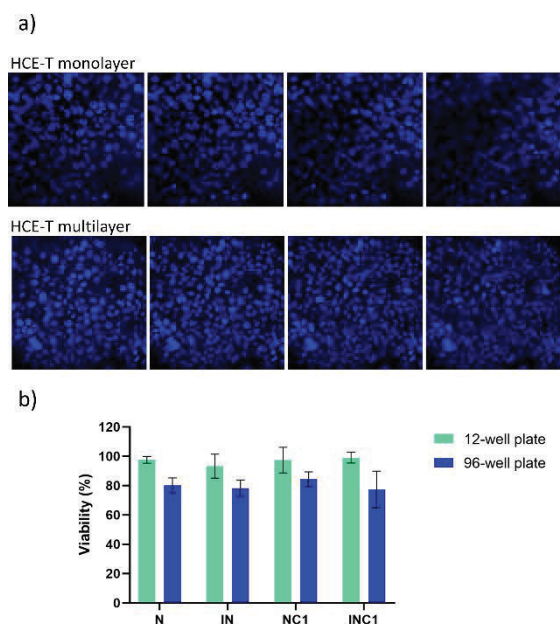


Figure 1. Z-stack images of HTS HCE-T model captured with confocal fluorescence microscope prior ALI exposure (monolayer) and 3 days after ALI exposure (multilayer) (a); the viability of cells treated with ophthalmic NEs on 12-well and 96-well insert plates (b).

Table 1. The ophthalmic NE composition. The abbreviations in the brackets refer to the controls, i.e. drug-free formulations.

Formulation	Water phase (%, w/w)	Oil phase (%, w/w)
IN (N)	Kolliphor® EL 0.25 Glycerol 2.5 Water up to 100	Ibuprofen 0.2 Miglyol 812 2.5 Lecithin 0.05
INC1 (NC1)	Chitosan 0.05 Kolliphor® EL 0.25 Glycerol 2.5 Water up to 100	Ibuprofen 0.2 Miglyol 812 2.5 Lecithin 0.05

4. CONCLUSION

A HTS 3D HCE-T model of human corneal epithelium can be cultivated on 96-well insert plates. However, slower cell proliferation and greater sensitivity to the ophthalmic NEs was observed in comparison to the standard 12-well plate HCE-T model. Thus, further optimisation of cultivation conditions is necessary to achieve higher similarity with the standard 12-well plate HCE-T model.

5. REFERENCES

1. M. Juretić *et al.*, HCE-T cell-based permeability model: A well-maintained or a highly variable barrier phenotype?, *Eur. J. Pharm. Sci.*, 2017. vol. 104, pp. 23–30
2. B. Jurišić Dukovski *et al.*, Functional ibuprofen-loaded cationic nanoemulsion: Development and optimization for dry eye disease treatment, *Int. J. Pharm.*, 2020. vol. 576, 118979.

ACKNOWLEDGMENT

This work was supported by the project BeatDED (IP-2019-04-2174) funded by the Croatian Science Foundation and 2 projects funded by the European Regional Development Fund, namely FarmInova (KK.01.1.1.02.0021) and BIOANT (KK.01.1.1.02.0002).

Josip Ljubica is recipient of a PhD fellowship from the Croatian Science Foundation (programme Young researchers' career development project – training of new doctoral students).

FORMULATION AND CHARACTERIZATION OF MUCO-ADHESIVE ORAL FILMS CONTAINING LIDOCAINE HYDROCHLORIDE USING QUALITY BY DESIGN APPROACHES

Mohammed Kalayi¹, Berna Uzun¹, Arkan Barbar¹, Buket Aksu¹

¹*Department of Pharmaceutical Technology, Altınbaş University, Türkiye*

1. INTRODUCTION

Mucoadhesive systems are the systems which exist in a close connection with mucous membrane, absorption tissue and site of action. Mucoadhesive films are the oral dosage forms which adheres to the mucosa and delivers the drug though it with a purpose of improvement in local effects as well as systematic effects [1]. Mucoadhesive drug delivery systems prolong the residence time of the dosage form at the site of application or absorption. They provide rapid absorption considering the surface area they reach and high blood flow, so that they provide effective treatment. QbD approach which provides a strategic process in product development used for this study. QbD guarantees that, quality is offered by manufacturing instead of product testing. So that, QbD ensures manufacturing of higher quality drugs within a shorter period and low costs [2]. Lidocaine, which is the API of this study, is a local anesthetic, cardiac depressant, and a pre-operation material for dental use. The aim of the study was to ensure that the muco-adhesive films containing lidocaine HCl for dental usage has demanded quality attributes during the product development with implementation of QbD approach.

2. MATERIALS AND METHODS

2.1. Materials

Lidocaine HCl (Doğa İlaç, Istanbul, Turkey), HPMC (Sigma Aldrich, Switzerland), CMC (Aklar Kimya Ankara, Türkiye), Glycerol (Tekkim Kimya, Bursa, Türkiye), Texture Analyzer (Stablemicrosystems, United Kingdom), Dry Heat Sterilizer (Nüve, Turkey), Moisture Analyzer (Shimadzu, Japan), Orbital Shaker (Ika, Germany).

2.2. Preparation of muco-adhesive film formulations

Lidocaine loaded oral film were prepared by solvent casting method, using HPMC and NaCMC sodium carboxymethyl cellulose as muco-adhesive polymer. After dissolving lidocaine HCl in distilled water, the polymers were allowed to swell in 20 mL of distilled water and stirred until completely dissolved. Glycerol was used as plasticizer. After all of the solutions were fully dissolved, beakers were left in a refrigerator for a full day to remove the air bubbles. The bubble-free solutions were carefully casted onto petri dishes. Films were dried at 45 °C for 48 hours to evaporate the solvent in a dry heat sterilizer. The dried films were packed in aluminum foil and stored in desiccator at room temperature to keep their integrity.

2.3. Optimization of muco-adhesive oralfilm of lidocaine hcl

After pre-formulation studies, optimization of the films was performed by Box Behnken design using MODDE Pro version 12.1 software. Concentration of HPMC (X1), Na CMC (X2) both as muco-adhesive polymers and concentration of glycerol (X3) as plasticizer were chosen as independent variable. Dependent variable pH (Y1), disintegration time (Y2), tensile strength (Y3), and percentage elongation (Y4). Total of 12 film formulations (F1- F12) shown in the Table 1 were taken and each film formulation was characterized in triplicate.

3. RESULTS AND DISCUSSION

3.1. Results and discussion of muco-adhesive lidocaine hcl film formulations

3.1.1. Mechanical Properties

Tensile strength and elongation at break (mechanical properties) are vital for packing, handling procedures, dissolution behavior as well as stability of the film [3]. Tensile strength of the oral films which prepared with high amount of polymer are showed high results compared with low concentrations. Using NaCMC and HPMC in combinations showed higher tensile strength compared to using them alone. Using 1% of NaCMC and 2% HPMC showed higher tensile strength and using 0.5% NaCMC alone showed the lowest tensile strength. Almost all of the results showed that, increasing the amount of plasticizer led to decrease in tensile strength. The percentage elongation of oral films was found between 10.554-99.402% (F1-F12). Increasing the amount of plasticizer are leading to increased amount of percentage elongation as showed in most of the formulations. The reason of increase in elongation occurs since plasticizers decrease the inter-molecular bonds of polymer matrix and change them with hydrogen bonds formed between polymer and plasticizer molecules. Formulation F3, F4, F10 and F11 showed good elongation and tensile strength compared to other formulations.

Table 1. Composition of film formulations

Content (g)	HPMC	CMC	Glycerol	Lidocaine HCl
F1	0.2	0	0.08	17.76
F2	0.2	0	0.2	17.64
F3	0.2	0.2	0.08	17.56
F4	0.2	0.2	0.2	17.44
F5	0	0.1	0.08	17.86

F6	0	0.1	0.2	17.74
F7	0.4	0.1	0.08	17.46
F8	0.4	0.1	0.2	17.34
F9	0	0.2	0.14	17.7
F10	0.4	0	0.14	17.5
F11	0.4	0.2	0.14	17.3
F12	0.2	0.1	0.14	17.6

4. CONCLUSION

By using QbD approaches different types of polymer and concentrations for polymers and plasticizer are used as independent variable and pH, disintegration time and mechanical properties including tensile strength and percentage elongation are used as dependent variable to develop optimized formulation. MODDE Pro version 12.1 software was used for the optimization process and according to the results, design space was obtained. By using MODDE Pro version 12.1 software and linking it with QbD approaches, we understood the effect of polymer type and concentrations as well as plasticizer concentration on the disintegration time, pH, tensile strength, and percentage elongation. The results showed that our optimum films exhibited good mechanical properties including tensile strength and percentage elongation

5. REFERENCES

1. Silva, B. M., et al., *Mucoadhesive oral films: The potential for unmet needs*. International journal of pharmaceutics, 2015. 494(1), 537-551.
2. Aksu, B., et al., *Quality by design (QbD) for pharmaceutical area*. İstanbul Ecz. Fak. Derg. / J. Fac. Pharm. İstanbul, 2015.45(2), 233-251
3. Özcan Bülbül, E., et al., *Product transfer from lab-scale to pilot-scale of quetiapine fumarate orodispersible films using quality by design approach*. Journal of Drug Delivery Science and Technology, 2019. 54.

STABILITY EVALUATION OF FLUCONAZOLE-LOADED FILAMENTS AND 3D PRINTED ORODISPERSIBLE TABLETS

Mateusz Kurek¹, Jolanta Pyteraf¹, Witold Jamroz¹, Justyna Knapik-Kowalczyk², Marian Paluch², and Renata Jachowicz¹

¹*Department of Pharmaceutical Technology and Biopharmaceutics, Jagiellonian University Medical College, Medyczna 9, 30-688 Krakow, Poland; mateusz.kurek@uj.edu.pl*

²*A. Chelkowski Institute of Physics, University of Silesia in Katowice, ul. 75 Pulku Piechoty 1, 41-500 Chorzow, Poland*

1. INTRODUCTION

Fused deposition modeling (FDM) is considered as 3D printing method which has the potential to be introduced as a preparation method for personalized medicines. This technology utilizes filaments as a semi-product which should maintain its properties, i.e. mechanical and physicochemical properties, for a long time. 3D printed dosage forms should also be stable, but as the on-demand prepared drugs, their stability can be significantly shorter e.g. two weeks.

The purpose of the presented study was to analyze the impact of long-term storage on fluconazole-loaded filaments and short-term storage of tablets printed with the fused deposition modeling method.

2. MATERIALS AND METHODS

2.1. Materials

Fluconazole (FLU, 99.5%, Henan Tianfu Chemical Co. Ltd., China) was used as the model active pharmaceutical ingredient (API) and poly(vinyl alcohol) (Pardeck[®] MXP, Merck KGaA, Germany) as a filament-forming polymer.

2.2. Hot-Melt Extrusion

Filaments with 20%, 40% and 70% of fluconazole were successfully extruded using a 12-mm corotating twin-screw hot-melt extruder (RES-2P/12A Explorer, Zamak Mercator[®], Poland) equipped with a 1.75 mm nozzle at 160°C, 147°C, and 137°C respectively. The filament was collected on an air-cooled conveyor belt and cut into approx. 2 m pieces.

2.3. 3D printing

The tablets were designed with Blender[®] 2.90 software (Blender Foundation, The Netherlands) and sliced using Voxelize[®] (version 1.4.18, Zmorph S.A., Poland). Printlets

containing 50 mg of FLU were manufactured by FDM ZMorph[®] 2.0 S (Poland) equipped with a 0.2 mm nozzle at 190 °C (20%, 40%) and 170 °C (70%) with 10 mm/s printing speed.

2.4. Evaluation of mechanical properties.

The uniformity of the filament was evaluated using a two-dimensional laser diameter gauge (LDM25XY, Mercury-Tech Co., Ltd., China). Mechanical properties were measured in a stretching test for six randomly taken filament pieces (n=6) carried out with an EZ-SX tensile tester (Shimadzu, Japan).

2.5. Differential scanning calorimetry

The thermal properties of the raw materials and the extrudates and tablets were examined using a DSC 1 STAR^e system (Mettler-Toledo, Switzerland).

2.6. Disintegration time

Pharmacopeial disintegration test was performed in SAPO ED-2 apparatus (Electrolab, India) in 700 mL of purified water maintained at 37 °C.

2.6. Stability tests

All filaments were stored in string bags for 8 months, while tablets were kept in tablet dispenser for 14 days under ambient conditions (temp. 20-25 °C). After that, samples were reevaluated and the results were compared to the freshly prepared filaments and tablets.

3. RESULTS AND DISCUSSION

Freshly prepared filaments were characterized by good mechanical properties, which resulted in their good printability. After eight months of storage, the breaking force decreased significantly, while the elasticity specified by the Young modulus was a little higher than for freshly prepared filaments. The loss of strength and increase in elasticity may be caused by water absorption during storage. The

mechanical characteristic is presented in Table 1.

Table 2. Mechanical properties of the filaments.

Filament	Force (N)	SD	Young modulus (MPa)	SD
20% fresh	212.4	41.3	2070.9	117.9
20% aged	91.2	23.0	2219.9	141.4
40% fresh	152.1	22.5	1877.9	91.0
40% aged	68.6	20.7	2281.5	168.8
70% fresh	52.6	15.8	1341.3	185.2
70% aged	12.9	4.3	1634.3	247.7

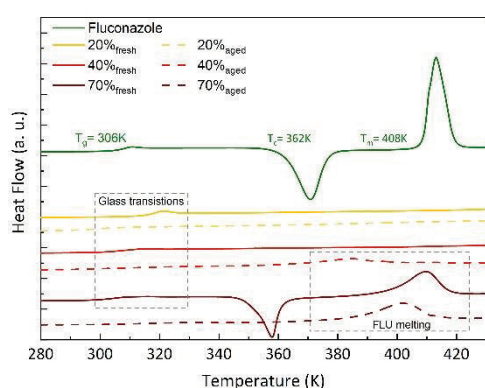


Figure 7. Comparison of thermograms of freshly prepared and aged filaments.

The DSC analysis revealed that fluconazole crystallization occurs even in freshly prepared filaments with 70% fluconazole. After the storage time, an endothermic peak can be observed in the thermogram of the 40% fluconazole loaded filament while no sign of crystallinity was found for aged filaments with 20% API. Despite the changes in filaments mechanical properties and molecular order their printability was maintained. In Table 2 the comparison of the tablets properties produced with fresh and aged filaments is presented. The appearance of tablets produced with freshly extruded and aged filaments was comparable as all the physicochemical changes in the polymer matrix were reversed in the melting stage during the 3D printing process.

Table 2. Comparison of properties of selected tablets.

Used filament	Avg. mass (mg)	SD	Disintegr. time (s)	SD
20% fresh	243.6	6.1	126	12
20% aged	239.5	1.8	134	1
40% fresh	121.1	2.2	88	3

40% aged	126.2	5.6	113	24
70% fresh	64.9	3.8	128	8
70% aged	71.1	4.0	136	37

The results of the disintegration time measurement showed that tablets with slightly longer disintegration times are produced with aged filaments. It was possible to produce tablets within mass variation pharmacopeial limit using either fresh or aged filament.

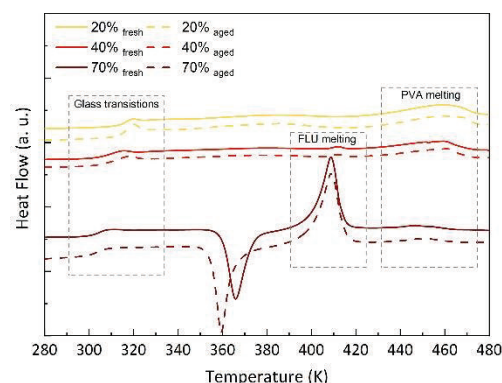


Figure 8. Thermograms of fresh and 14-day-old tablets prepared from freshly extruded filaments.

There were no significant differences in the thermal properties prepared from the freshly extruded and aged filaments. The 3D printed tablets after 14 days of storage under ambient conditions remained almost unchanged in terms of crystallinity as the DSC curves were comparable.

5. CONCLUSION

The drug loading in the filaments and 3D printed tablets has influenced its properties. However, the storage did not affect the printability of the filaments and had only a slight impact on the 3D printed tablet attributes, such as disintegration time.

ACKNOWLEDGMENT

The authors acknowledge the National Science Centre, Poland for financial support (grant OPUS 16 no 2018/31/B/ST8/01327).

THE EFFECT OF NANO-MILLING ON DISSOLUTION/PERMEATION OF POORLY SOLUBLE DRUG COMPOUNDS

Jakob T. Lynnerup^{1,2}, **Jonas B Eriksen**¹, **Ann Mari Holsæter**², **Martin Brandl**¹

¹Department of Physics, Chemistry & Pharmacy, University of Southern Denmark (SDU), Denmark

²Drug Transport and Delivery Research Group, Department of Pharmacy, UiT The Arctic University of Norway

1. INTRODUCTION AND AIM

Many new drug entities arising are categorised as class II compounds by the Biopharmaceutical Classification System, indicating low solubility and fair permeability. These poorly soluble drug compounds show poor oral bioavailability due to the low solubility. Different “candidate-enabling” formulation principles are under investigation to either increase the solubility or the dissolution rate of these compounds or both. One of these is particle size reduction, such as micronization and nano-milling [1].

The aim of this study was to produce nanoparticles of the poorly soluble model drug compounds Fenofibrate (FNB) and Cinnarizine (CNZ), further examining the combined dissolution and permeation behaviour of these compounds upon nano-milling.

2. MATERIALS AND METHODS

2.1 Nano-milling

Wet bead milling using dual asymmetric centrifugation was explored, using SpeedMixer™ DAC 150.1 FVZ-K (Synergy Devices Ltd, High Wycombe, U.K.).

2.4 Combined dissolution/permeation- study dissolution/permeation setup was utilised: Firstly, 10 mg of raw API was added to the bottom chamber of jacketed Franz cells and stirred by a magnetic stirrer V6A (PermeGear Inc). Cellophane was used as the permeation barrier. The bottom chamber was filled with PBS and the top chamber was filled with 1 mL of acceptor medium.

2.5 API quantification

by reverse phase high HPLC: FNB was quantified with a XSelect CSH C18 column (Waters Corp, Milford, MA, U.S.) with a mobile phase consisting of 80 % (v/v) of acetonitrile (ACN) and 20 % (v/v) of 0.1 %

(v/v) trifluoroacetic acid in purified water at a flowrate of 1.0 mL min⁻¹ and a column temperature of 40 °C.

3. RESULTS AND DISCUSSION

3.1. Nano-milling

nanoparticles were produced fast obtaining nanoparticles after only 5 minutes (figure 1). Increasing the milling time led to smaller particle sizes and a bigger partition of particles in the nanosized range (figure 1 & 2).

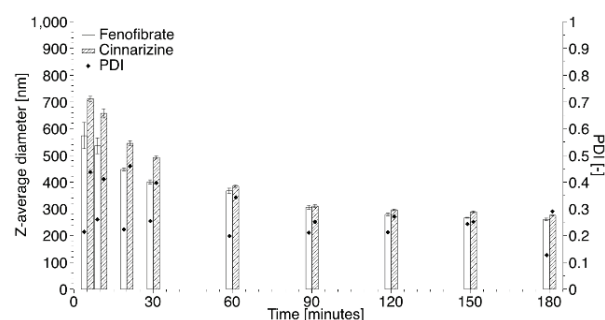


Figure 1. PSD as z-average diameter of FNB (open bars) and CNZ (crossed bars) as well as PDI (closed diamonds) of nanoparticle suspensions milled at 1500 rpm, measured at different timepoints, reported as mean ± SD (n = 3). A milling time of 90 minutes was identified as optimum and used for further experiments.

3.2. Physical characterisation

The produced nanoparticles were crystalline with regards to DSC and XRPD (data not shown here).

No obvious phase changes can be determined based on these results, but further investigation is needed.

3.3. Combined dissolution and permeation

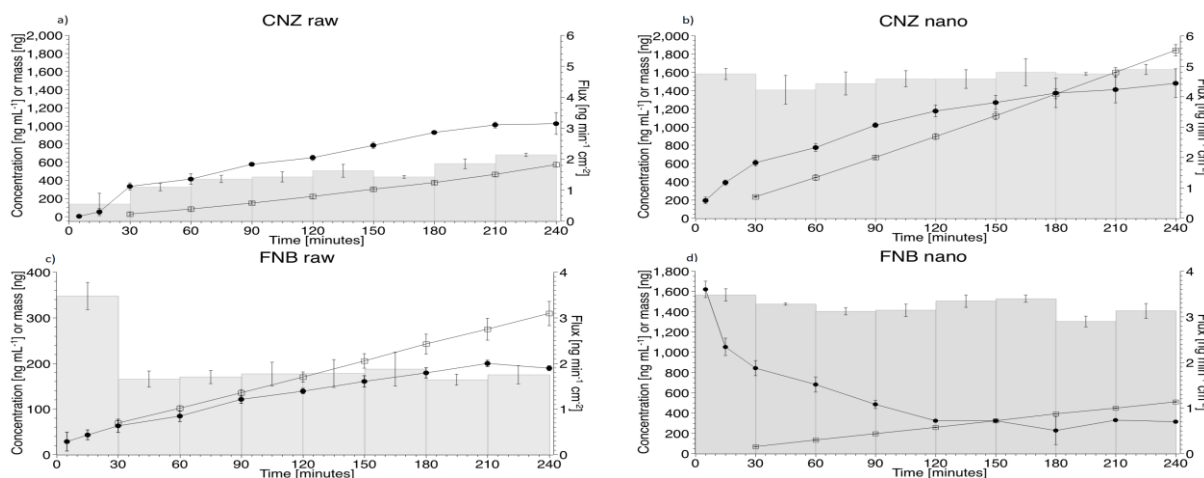


Fig. 2. Dissolution in PBS and permeation profiles shown as the concentration of dissolved API in the donor compartment (closed circles), cumulative mass of permeated drug (open squares), and flux values (grey bars) of raw CNZ (a), CNZ nanoparticles (b), raw FNB (c), and FNB nanoparticles (d) at 37 °C, reported as mean \pm SD (n = 3).

Before conducting the combined dissolution and permeation experiments, the solubility of the produced nanoparticles was investigated. No apparent difference in solubility could be observed after equilibration over 72 hours.

The nanoparticles obtained showed an increase in dissolution and permeation when compared to the pure compounds. FNB nanoparticles induced a transient supersaturated state. The amount of dissolved drug rapidly fell to the drug solubility over 120 minutes. This behaviour of nanoparticles is similar to that found for the commercial product Lipidil 145 ONE® found by Sironi *et al.* (2017) [2]. CNZ nanoparticles instead showed a faster dissolution rate. This increase in dissolved drug, when compared to the pure compound, resulted in a higher permeation and flux for both FNB and CNZ. The faster dissolution rate could also be attributed from the addition of solubilizers during the production of the nanoparticles. As the contribution of release of drug from particles in suspension and solubilised drug is not differentiated in these experiments.

4. CONCLUSION

Nanoparticles of the poorly soluble drug compounds Fenofibrate and Cinnarizine could be produced using the SpeedMixer™ DAC

150.1 FVZ-K. The produced nanoparticles were crystalline and no phase changes could be observed, however further investigation of the physical characteristics are needed.

The nanoparticles of Fenofibrate induced a transient supersaturated state, thereby increasing the permeation. Cinnarizine nanoparticles increased the dissolution rate and thereby increased the permeation. Further experiments are needed to determine the partition of solubilizers on the dissolution and permeation behaviour.

5. REFERENCES

1. Buckley, S. T. et al., *Biopharmaceutical classification of poorly soluble drugs with respect to "enabling formulations"*. European Journal of Pharmaceutical Sciences, 2013, 50.
2. Sironi, D. et al., *Dynamic dissolution/permeation-testing of nano- and microparticle formulations of fenofibrate*. European Journal of Pharmaceutical Sciences, 2017, 96.

ACKNOWLEDGMENT

The authors are grateful for a mobility grant to JTL and collaborative work between the two institutions enabled by funding from Nordforsk program Nordic University Hub (project #85352) "NordicPOP". Excellent lab-support by Kirill Jefimov is gratefully acknowledged.

FREEZE-DRIED NANOCRYSTAL DISPERSION OF NOVEL DEUTERATED PYRAZOLOQUINOLINONE LIGAND (DK-I-56-1): PROCESS PARAMETERS AND CRYOPROTECTANT SELECTION THROUGH STABILITY STUDY

Jelena Mitrović¹, Maja Bjelošević², Daniel E. Knutson³, Aleksandar Kremenović⁴, Dominique Lunter⁵, Pegi Ahlin Grabnar², James M. Cook³, Miroslav M. Savić⁶, Snežana D. Savić¹

¹*Department of Pharmaceutical Technology and Cosmetology, University of Belgrade–Faculty of Pharmacy, Serbia*

²*Department of Pharmaceutical Technology, University of Ljubljana, Faculty of Pharmacy, Slovenia*

³*Department of Chemistry and Biochemistry, University of Wisconsin–Milwaukee, United States*

⁴*Laboratory of Crystallography, University of Belgrade–Faculty of Mining and Geology, Serbia*

⁵*Institut für Pharmazeutische Technologie, Eberhard-Karls Universität Tübingen, Germany*

⁶*Department of Pharmacology, University of Belgrade – Faculty of Pharmacy, Serbia*

1. INTRODUCTION

Nanocrystal dispersions are considered as the universal formulation strategy for brick dust substances. However, the stability of these systems to aggregation represents a big issue. To overcome this, nanocrystal dispersions are usually solidified by freeze-drying (lyophilization). During this process the risk of aggregation is considered to be high, due to ice formation and/or water loss. To prevent the aggregation, for the particle size preservation, therefore, it is necessary to add cryoprotectants/lyoprotectants, among which sugars are most commonly used. To ensure good structure of the cake, bulking agents are often included in formulations, as well [1,2], although in nanocrystalline dispersions the combination of cryoprotectants and bulking agents is not frequent nor much investigated.

Nanocrystals of DK-I-56-1 (7-methoxy-2-(4-methoxy-d3-phenyl)-2,5-dihydro-3H-pyrazolo[4,3-c]quinolin-3-one), patent protected pyrazoloquinolinone ligand, have been developed recently, and characterized in terms of physicochemical properties and pharmacokinetics after intraperitoneal administration in mice. These formulations were stable for three weeks [3]. Our aim in this study was to improve the stability by freeze-drying, and investigate the influence of different concentrations and physical form of cryoprotectants (sucrose, trehalose) and bulking agent (mannitol) as well as different primary drying conditions on the aggregation prevention.

2. MATERIALS AND METHODS

2.1. Materials

DK-I-56-1 was synthesized at the Department of Chemistry and Biochemistry, University of Wisconsin—Milwaukee, USA. The following other materials were used: polysorbate 80, poloxamer 407, sucrose, mannitol (Sigma-Aldrich Laborchemikalien GmbH, Germany) and trehalose (Carl Roth GmbH, Germany).

2.2. Lyophilization

Nanocrystal dispersions stabilized by polysorbate 80 and poloxamer 407 were prepared by wet ball milling [3]. After addition of mannitol (M), sucrose (S), or trehalose (T) alone or in combination samples were freeze-dried. Two processes were applied: (1) freezing at -80 °C (3 h), primary drying at -10 °C, 0.340 mbar, secondary drying at 25 °C (24 h) or (2) freezing at -50 °C (3 h), primary drying at -45 °C, 0.2 mbar (21 h), secondary drying at 20 °C (30 h). Samples were stored in crimped vials at 25 °C (lyophilization 1) or 2-8 °C (lyophilization 2) for three months.

2.3. Physicochemical characterization

Particle size (z-ave) was measured by Zetasizer Nano ZS (Malvern Instruments, UK) and Mastersizer (Malvern Mastersizer 2000 Malvern, UK). Redispersibility index (RDI) was calculated as z-ave (before)/z-ave (after) and expressed in percentages. Physical state of samples was determined by differential scanning calorimetry (DSC1; Mettler Toledo, Switzerland), powder X-ray diffraction (Rigaku Smartlab X-ray Diffractometer) and polarized light microscopy (PLM) (Carl Zeiss ApoTome Imager Z1 microscope Zeiss, Germany).

3. RESULTS AND DISCUSSION

Right after preparation, nanocrystal dispersions were with submicron particle size around 160 nm, and PDI below 0.2, suggesting narrow size distribution. In the cryoprotectant screening phase, sucrose and/or mannitol were added in different concentrations. It was shown that 10% of the total stabilizer concentration was needed for the particle size preservation: the achieved RDI was above 95%, while cakes with sucrose alone or in combination with mannitol in ratio 1:1 or 3:2 were also with satisfied appearance (Figure 1).

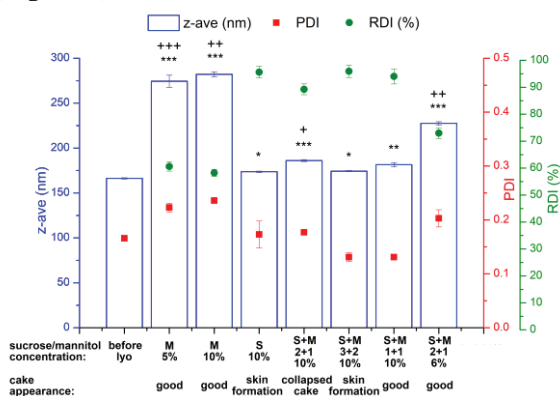


Figure 1. Particle size (z-ave), polydispersity index (PDI), redispersibility index (RDI) and cake appearance after lyophilization.

Lyophilization was conducted above or below the glass transition temperature of the maximally freeze-concentrated solution (T_g') (around $-39\text{ }^{\circ}\text{C}$). When primary drying was performed at $-10\text{ }^{\circ}\text{C}$, no aggregation was noticed right after lyophilization, but particle size increased significantly, lowering down the RDI to $< 50\%$, after one month storage at $25\text{ }^{\circ}\text{C}$. This was confirmed by laser diffraction. In lyophilization 2, with primary drying at temperature below T_g' , trehalose was also used in the same concentration as sucrose and in combination with mannitol. Interestingly, in this process parameters setup, sucrose or trehalose alone did not prevent aggregation during freeze-drying. Particle size remained almost unchanged in formulation S+M 3+2 (RDI 95%) or slightly higher in T+M 3+2 (RDI 90%), after three months storage, suggesting it was most probably the optimal combination for the stabilization.

Physical state analysis revealed that sucrose and mannitol in samples lyophilized by process 1 were in crystalline state, as well as sucrose when used alone in lyophilization 2. Trehalose, on the other hand was amorphous in all samples

containing it. Amorphous state of lyoprotectants allows maximal hydrogen bonding due to higher molecule flexibility and availability of hydroxyl groups [3]. Surprisingly, mannitol as a substance with high crystallization tendency was with low crystallinity in lyophilizates. These observations were confirmed by PLM. It is possible that it formed interactions with sucrose or nanocrystal stabilizers [4].

4. CONCLUSION

Results from this study demonstrated freeze-drying as an important technique for the improvement of nanocrystals stability. However, the selection of cryoprotectant and bulking agent ratio beside process parameters (primary drying at $-45\text{ }^{\circ}\text{C}$) was crucial to get freeze-dried samples with good stability. Sucrose or trehalose in combination with mannitol (ratio 3+2) in total concentration 10% successfully hindered aggregation, thus prolonging the stability to 3 months at $2\text{-}8\text{ }^{\circ}\text{C}$.

5. REFERENCES

1. Van Eerdenbrugh, B., et al. *Top-down production of drug nanocrystals: nanosuspension stabilization, miniaturization and transformation into solid products*. International journal of pharmaceutics, 2008. 364(1): 64-75.
2. Trenkenschuh, E., and Friess, W. *Freeze-drying of nanoparticles: How to overcome colloidal instability by formulation and process optimization*. European Journal of Pharmaceutics and Biopharmaceutics, 2021.165: 345-360.
3. Mitrović, J.R., et al. *Overcoming the low oral bioavailability of deuterated pyrazoloquinolinone ligand DK-I-60-3 by nanonization: A knowledge-based approach*. Pharmaceutics, 2021. 13(8): 1188.
4. Kumar, S., et al. *Sugars as bulking agents to prevent nano-crystal aggregation during spray or freeze-drying*. International journal of pharmaceutics, 2014. 471(1-2): 303-311.

ACKNOWLEDGMENT

This research was supported by the Science Fund of the Republic of Serbia, grant No. 7749108, project Neuroimmune aspects of mood, anxiety and cognitive effects of leads/drug candidates acting at GABAA and/or sigma-2 receptors: In vitro/in vivo delineation by nano- and hiPSC-based platforms-NanoCellEemoCog.

PREPARATION OF ANISOTROPIC HOLLOW SILICA NANOSTRUCTURES

Sebastjan Nemec^{1,2}, Tanja Potrč², Petra Kocbek², Slavko Kralj^{1,2,3}

¹*Department for Materials Synthesis, Jožef Stefan Institute, Jamova 39, 1000 Ljubljana, Slovenia,*

²*Faculty of Pharmacy, University of Ljubljana, Aškerčeva cesta 7, 1000 Ljubljana, Slovenia,*

³*Nanos SCI, Nanos Scientifica d.o.o., Teslova 30, 1000 Ljubljana, Slovenia*

1. INTRODUCTION

Nanostructures with hollow compartments are a particular class of nanomaterials [1]. The internal void offers a space for the incorporation of various functional cargo(s), such as drugs and catalysts. However, the available synthetic procedures to prepare such complex nanostructures are scarce and not well elucidated. So far, various approaches have been studied to prepare hollow nanostructures. The most widely used etching methods rely on selective removal of sacrificial core from pre-synthesized nanoparticles while retaining the outer shell intact. If the sacrificial core is not removed completely, partially hollow nanostructures are obtained which may offer combined functionalities of the shell and the remaining core [2]. However, the procedures for the preparation of partially hollow nanostructures are generally even more challenging than obtaining completely hollow nanostructures, as the core removal process needs to be precisely controlled and should offer the possibility for rapid termination of the core removal procedure. Core-shell nanoparticles provide an elegant way to control the core removal process. The shell that surrounds the core provides a degree of protection to the core and may regulate the rate of core removal process. By changing the thickness and porosity of the shell, the core removal rate can be effectively controlled.

Therefore, in our work we focused on the preparation of (partially) hollow nanostructures, i.e. nanochains, based on core-shell superparamagnetic nanoparticles and investigation, how the thickness and porosity of the silica shell affect the removal of magnetic core.

2. MATERIALS AND METHODS

2.1. Materials

Three different types of silica coated nanochains were used for the preparation of the partially hollow nanostructures. Commercially available 1 μm long nanochains coated with a thin 3 – 5 nm layer of low-porous silica (Fig. 1A) were provided by

Nanos SCI (Slovenia) [4]. Additional coating of porous silica was deposited on the surface of nanochains either by using the standard Stöber silica synthesis procedure [3] or our own soft-templating procedure [5].

2.2. Methods

The acid etching procedures were carried out using 3 M or 12 M hydrochloric acid (HCl). Suspensions of nanochains with different silica coatings were mixed with either 3 M or 12 M HCl to prepare partially hollow or completely hollow silica nanostructures, respectively. To terminate the core removal process, the formed (partially) hollow nanostructures were centrifuged and quickly washed several times with water, freed in liquid nitrogen and dried using lyophilization.

2.3. Characterization

All types of nanochains, either treated with HCl or not, were characterised using transmission electron microscopy (TEM) and nitrogen sorption analysis.

3. RESULTS AND DISCUSSION

We chose thin-silica-coated iron oxide-based nanochains as starting nanomaterial for the preparation of (partially) hollow nanostructures. To study the effect of different silica shells on the removal rate of the iron oxide cores, we coated the commercial nanochains with an additional ~30 nm thick low-porous silica shell or a ~60 nm thick mesoporous silica shell with pore diameter of ~15 nm.

The combination of iron oxide core and silica shell is suitable for the preparation of (partially) hollow nanostructures using HCl etching method due to the differences in solubility of both materials in HCl. In contrast to silica, iron oxide is well soluble in HCl. This enabled us to use HCl etching to selectively (partially) remove the iron oxide cores and retain the outer silica shells intact. Complete iron oxide core removal was achieved using concentrated 12 M HCl in all three different nanochain samples. The etching was conducted until we achieved a

complete removal of the core, which was confirmed by TEM (Fig. 1B-D). On the other hand, partially hollow nanostructures were prepared using 3 M HCl and precisely controlled etching times, that were determined experimentally.

Nitrogen sorption analyses showed increased specific surface areas and pore volumes of the hollow nanostructures, compared to their corresponding starting non-etched nanochains. The highest specific surface area and pore volume increase were determined for the complete core removal of commercial nanochains, with an increase from 223 m²/g to 537 m²/g and 0.6 mL/g to 2.9 mL/g, respectively. The time needed to achieve complete core removal was the longest (2 h) for the thick low-porous silica-coated nanochains, whereas the etching times for the thin low-porous and mesoporous silica coated nanochains were in both cases shorter, i.e., less than 1 min. Such time difference indicates the increased dissolution-protecting ability of the thick low-porous silica coating of nanochains towards HCl etching. Even though the mesoporous silica coated nanochains had the thickest silica shell, the large number of centro-radial pores diminished the shell's protecting ability.

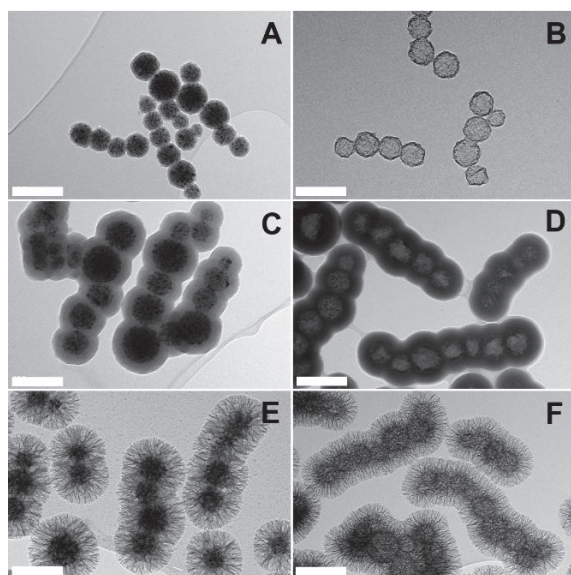


Figure 1. TEM micrographs of non-etched thin-silica (A), thick low-porous silica (C), and mesoporous silica (E) coated nanochains and their (partially) hollow counterparts: thin-silica (B), thick low-porous silica (D), and mesoporous silica (F) nanostructures. Scale bars: 500 nm.

4. CONCLUSION

We successfully prepared (partially) hollow silica nanostructures using HCl etching from silica-coated iron oxide-based nanochains. By synthesizing an additional coating, we prepared thicker and/or mesoporous silica shells on the commercial nanochains. Furthermore, we examined how different thicknesses and morphologies of the silica shell affect the removal rate of the iron oxide cores. By applying silica shells which provide larger degree of protection of the iron oxide against acid dissolution, we are able to control the core removal process in order to obtain partially hollow nanostructures. The prepared partially hollow nanostructures will be investigated in future as magneto responsive delivery systems for different types of drug molecules.

5. REFERENCES

1. Sharma, J., et al., *Hollow silica particles: recent progress and future perspectives*, *Nanomaterials*, 2020, 10(8).
2. Priebe, M., et al., *Nanorattles or yolk-shell nanoparticles – What are they, how are they made, and what are they good for?*, *Chemistry – A European Journal*, 2015, 21(10): 3854-3874.
3. Stober, W., et al., *Controlled growth of monodisperse silica spheres in the micron size range*, 1968, 26(01): 1599.
4. Kralj, S., et al., *Magnetic Assembly of Superparamagnetic Iron Oxide Nanoparticle Clusters into Nanochains and Nanobundles*, *ACS Nano*, 2015, 9(10): 9700-9707.
5. Nemeč, S., et al., *A Versatile Interfacial Coassembly Method for Fabrication of Tunable Silica Shells with Radially Aligned Dual Mesopores on Diverse Magnetic Core Nanoparticles*, *ACS Applied Materials & Interfaces*, 2021, 13(1): 1883-1894.

ACKNOWLEDGMENT

The authors acknowledge the financial support from the Slovenian Research Agency (ARRS; Young Researcher Scheme 1000-18-0106, ARRS projects: J2-3043, J2-3040, J2-3046, J3-3079 and Core Funding program P2-0089) and the CENN Nanocenter for use of electron microscopes.

PREPARATION AND IN VITRO CHARACTERIZATION OF ONDANSETRON HYDROCHLORIDE LOADED LIPOSOME FORMULATIONS

Zeliha Duygu Özdal^{1,2}, Sevgi Takka¹

¹Gazi University, Department of Pharmaceutical Technology, Faculty of Pharmacy, Ankara, Turkey,

²Erzincan Binali Yıldırım University, Department of Pharmaceutical Technology, Faculty of Pharmacy, Erzincan, Turkey

1. INTRODUCTION

Ondansetron hydrochloride (OND) is a hydrophilic drug used for management of chemotherapy, radiotherapy, and surgery induced nausea and vomiting. OND has low oral bioavailability and short half-life therefore it needs to administrate several times in a day [1]. OND has a pH-dependent solubility. The solubility decreases as the pH of the aqueous phase increases [2]. OND-loaded liposome (LPs) formulations have been prepared to reduce dosing frequency by prolonging the drug's residence time in circulation. This study was aimed to improve the encapsulation efficiency by utilizing the pH-dependent solubility of OND.

2. MATERIALS AND METHODS

2.1. Materials

1,2-dipalmitoyl-sn-glycero-3-phosphocholine, 16:0 PC (DPPC), hydrogenated soy phosphatidylcholine (HSPC), and cholesterol were purchased from Avanti Polar Inc USA. Chloroform was purchased from Sigma. OND was a gift from Adeka Pharmaceutical (Istanbul, Turkey).

2.2. Preparation of Liposomes

OND loaded LPs were prepared by film hydration method. Briefly, different molar ratio of phospholipid (PL) and cholesterol were dissolved in chloroform (2 mL) as shown in Table 1. Chloroform was evaporated to obtain the thin film. The film was hydrated using 5 mL ultrapure water containing 4 mg OND. For LP5 formulation, drug was mixed with lipids and dissolved in chloroform. After evaporation the film was hydrated using 5 mL phosphate buffer solution (pH 7.4) to increase the encapsulation efficiency by reducing the drug leakage. In order to reduce particle size, the liposomal suspension was first sonicated with a probe-

type sonicator at 20% amplitude for 15 minutes at 2 s on and 3 s off intervals, then extruded. LPs were recovered by centrifugation at 18000 rpm for 45 min, and lyophilized.

Table 1. Composition of OND loaded LPs

Formulation	PL:CHOL(molar ratio)	PL
LP1	2:1	DPPC
LP2	4:1	DPPC
LP3	6:1	DPPC
LP4	2:1	HSPC
LP5	6:1	DPPC

2.3. Characterization of Liposomes

The mean particle size (PS), size distribution (PDI) and zeta potential (ZP) of LPs were analysed by Zetasizer Nano ZS (Malvern Instruments Malvern, UK).

Encapsulation efficiency (EE%) was determined by lyophilized LPs formulations dissolving in methanol. OND amount in this solution was determined by HPLC analysis at 310 nm.

The possible interactions between drug and the components of LPs were examined by Differential scanning calorimetry (DSC) and Fourier-Transform Infrared Spectroscopy (FTIR).

The in vitro release profile of OND loaded LPs formulations and free OND were compared using Franz cell with a dialysis membrane with a molecular weight cut-off of 14 kDa at pH 7.4. The samples were withdrawn from receptor phase at the determined time points of 0.5, 1, 2, 3, 4, 6, 8, 12, 24 h and replaced with the fresh buffer. The samples were analysed by HPLC.

3. RESULTS AND DISCUSSION

OND loaded sustained release LPs formulations were prepared successfully by film hydration

P32

method. The effect of type and molar ratio of phospholipid and pH of hydration media on formulation characteristic of the LPs were evaluated and presented in Table 2. The particle size of the formulations from LP1 to LP4 was measured between 178-217 nm and PDI values below 0.15. However, the particle size of LP5 formulation was 368 nm, PDI value was around 0.5.

The EE% of the LP1 and LP4 formulations prepared using different PL types were determined to be similar. Although the encapsulation efficiency increased as the amount of PL increased, it was still low. The pH of the aqueous phase was altered to reduce drug leakage and enhance the EE%. The EE% increased from 16 % to 38 % at pH7.4, where the solubility of OND is low.

Table 2. Physicochemical properties of LPs formulations

	PS	PDI	ZP	%EE
LP1	178,2± 2,6	0,072± 0,004	-15,2± 6,2	3,89± 0,25
LP2	217,0± 6,3	0,148± 0,047	-11,4± 3,0	8,43± 0,13
LP3	212,3± 5,5	0,138± 0,022	-7,38± 1,9	16,98± 0,36
LP4	187,3± 4,8	0,082± 0,015	-28,8± 0,3	3,50± 0,14
LP5	368,6± 26,7	0,495± 0,059	-17,1± 4,0	38,16± 5,63

As a result of DSC and FTIR analysis, no interaction was observed between the drug and excipients.

Free OND was almost completely released in 8 h while all LPs formulations were exhibited sustained release profiles (Fig 1). It was observed that increasing the molar ratio of phospholipid decreased the cumulative release amount of drug in the LPs prepared with DPPC. On the other hand, HSPC LPs had a slower release profile. The phase transition temperature (T_g) of DPPC and HSPC are 41 and 55°C, respectively. The lipid membranes with higher T_g demonstrate lower fluidity compared to membranes with lower T_g [3]. Therefore, lower drug released was obtained from HSPC LPs. There was no significant difference between the release profiles of the LP3 and LP5 formulations (p>0.05).

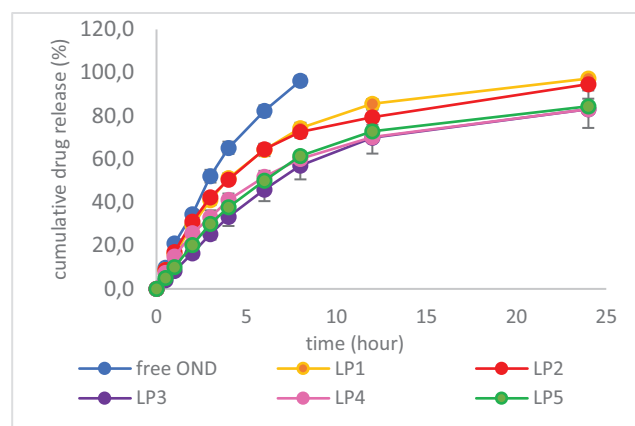


Figure 1. Release profile of OND loaded LPs and free OND

4. CONCLUSION

Results indicate that the molar ratio, type, and T_g of phospholipids affect the physicochemical properties of LPs. Moreover, higher EE% was obtained by altering the pH of the aqueous phase. All formulations were exhibited a sustained-release characteristic profile.

5. REFERENCES

1. Ye J.H., et al., Ondansetron: A Selective 5-HT₃ Receptor Antagonist and Its Applications in CNS-Related Disorders. *CNS Drug Reviews*, 2001. 7:199-213.
2. Duong, V. A., et al., Preparation of ondansetron hydrochloride-loaded nanostructured lipid carriers using solvent injection method for enhancement of pharmacokinetic properties. *Pharmaceutical research*, 36(10), 1-12
3. Chen J., et al., Influence of lipid composition on the phase transition temperature of liposomes composed of both DPPC and HSPC. *Drug Development and Industrial Pharmacy*, 2013; 39(2): 197–204.

ACKNOWLEDGMENT

This work has been supported by Gazi University Scientific Research Projects Coordination Unit under grant number TCD-2021-6957.

DEVELOPMENT OF COMBINED INHALABLE FORMULATION OF IBUPROFEN AND MANNITOL FOR THE TREATMENT OF CYSTIC FIBROSIS

Petra Party¹, Rita Ambrus¹

¹*Institute of Pharmaceutical Technology and Regulatory Affairs, University of Szeged, Hungary*

1. INTRODUCTION

Ibuprofen (IBU) is a nonsteroidal anti-inflammatory drug (NSAID), and inflammation is a hallmark of cystic fibrosis (CF), which contributes to lung destruction. IBU has a significant effect on slowing the disease progression and it is well tolerated. [1] Mannitol (MAN) helps to dilute the thick, viscous mucus, which is the main problem of CF.[2] Both of the mentioned drugs should be applied in high dose. Therefore, the preparation of inhalable IBU and MAN particles could be efficient for targeted lung delivery, therefore the applied dose could be reduced. We aimed to combine IBU and MAN in a dry powder formulation to help patients, who suffer from CF.

2. MATERIALS AND METHODS

2.1. Materials

The active ingredient (API) was ibuprofen (*Egis Pharmaceuticals PLC., Budapest, Hungary*). Poloxamer-188 (POL) (*Sigma-Aldrich, Darmstadt, Germany*) D-mannitol (MAN), (*Molar Chemicals Kft, Halásztelek, Hungary*) and L-leucine (LEU), (*AppliChem GmbH, Darmstadt, Germany*) were the excipients.

2.2. Preparation of the samples

Firstly, a presuspension was made, which contained 2.00 g of pure IBU and 18.0 g of 1 % POL solution. The milling medium was 20.00 g of ZrO₂ beads in a high performance mill (*Planetary Micro Mill Pulverisette 7, Fritsch, Idar-Oberstein, Germany Retsch Planetary Ball Mill PM 100 MA, Retsch GmbH, Haan, Germany*). Rotation speed (800 rpm), milling duration (4 cycles) was applied, each milling cycle comprised 15 min rotation followed by 10 min pause. Different compositions were prepared by adding MAN and LEU. Secondly, inhalable microparticles were produced by spray-drying (*Büchi Mini Spray Dryer B-191, Büchi, Flawil, Switzerland*). The spray-drying properties were the following: inlet temperature: 70 °C, outlet temperature: 40 °C,

aspirator capacity: 85%, airflow rate: 500 L/h, and feed pump rate: 10%. [3]

2.3. Investigation methods

The investigation protocol of the dry powder inhalers was followed during the characterization of our products. [4] Laser diffraction was used to determine the particle size and the particle size distribution of the microsuspension and the spray-dried samples (*Malvern Mastersizer Scirocco 2000, Malvern Instruments Ltd., Worcestershire, UK*). The active ingredient content and the solubility of the spray-dried samples was determined spectrophotometrically (*ATI-UNICAM UV/VIS Spectrophotometer, Cambridge, UK*). To establish the crystalline character of the samples X-ray powder diffraction (XRPD) spectra were recorded (*BRUKER D8 Advance X-ray diffractometer, Bruker AXS GmbH, Karlsruhe, Germany*). The bulk and tapped densities of the formulations were measured using a tap density tester (*ETD-1020x, Electrolab, Mumbai, India*). The in vitro aerodynamic properties were investigated with Andersen Cascade Impactor (*Apparatus D, Copley Scientific LTD., 250 Nottingham, UK*).

3. RESULTS AND DISCUSSION

As a result of wet milling IBU was micronized (Table 1.). The particle size of the spray-dried formulations was in the required pulmonary size range in the case of LEU containing samples (Table 1.). LEU also had an increasing effect on the yield of spray-drying. The content of API was correlated with the theoretical numbers. The solubility of the IBU was improved thanks to the micronization. The compressibility index increased by adding more LEU (Table 2.): According to the XRPD spectra, IBU became amorphous after the preparation process (Figure 1.). The best formulation (IBU1_POL_MAN2_LEU1) was chosen for the in vitro aerodynamic measurements, which were implemented using Ezeeflo™ hydroxypropyl methylcellulose

capsules (*ACG-Associated Capsules Pvt. Ltd., Mumbai, India*) and gelatine capsules (*Capsugel, Bornem, Belgium*). The MMAD (mass median aerodynamic diameter and FPF (fine particle fraction) were convenient for pulmonary application (Table 3.).

Table 1. Particle size of the raw API, the suspension and the spray-dried samples. Data are means ± SD (n = 3 independent measurements).

Samples	D [0.5] (µm)	Span	SSA (m ² /g)
IBU_POL_suspension	4.234±0.51	3.922±0.33	1.630±0.09
IBU1_POL	7.174±1.06	4.212±0.28	1.022±0.13
IBU1_POL_MAN2	8.071±1.99	2.04±0.71	0.994±0.05
IBU1_POL_MAN2_LEU0.5	3.380±0.13	3.513±1.44	2.105±0.13
IBU1_POL_MAN2_LEU1	3.275±0.10	1.657±0.30	2.175±0.05

Table 2. Density measurements of the spray-dried compositions. Data are means ± SD (n = 3 independent measurements).

Samples	Bulk density (g/cm ³)	Tappe d density (g/cm ³)	Carr index
IBU1_POL	0.13	0.16	20.00
IBU1_POL_MAN2	0.17	0.25	33.33
IBU1_POL_MAN2_LEU0.5	0.22	0.35	37.14
IBU1_POL_MAN2_LEU1	0.17±	0.28±	38.00±

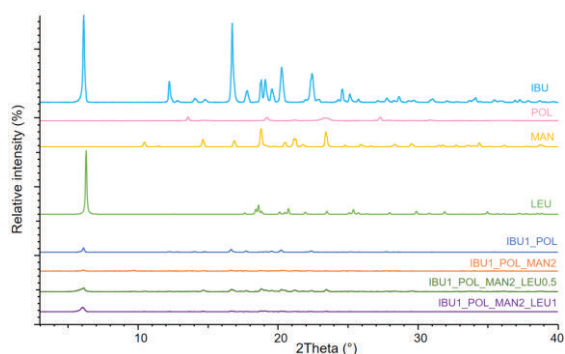


Figure 1. XRPD results of the raw materials and the spray-dried samples.

Table 3. In vitro aerodynamic properties of the spray-dried sample (IBU1_POL_MAN2_LEU1). Data are means ± SD (n = 3 independent measurements).

Samples	FPF (%)	MMAD (µm)
Cellulose capsule	60.72±0.39	2.58±0.29
Gelatine capsule	55.92±0.80	3.30±0.71

4. CONCLUSION

We successfully formulated IBU and MAN containing inhalable powders. We managed to micronize the API and improve its solubility. We observed the effect of LEU on the yield of spray-drying, the particle size and the density. Based on the proper aerodynamic diameter and fine particle fraction, the formulations are promising for further characterization. In the future, we can provide a combined, innovative treatment for CF.

5. REFERENCES

1. Sheikh, Z., et al., *Is there a role for inhaled anti-inflammatory drugs in cystic fibrosis treatment?* Expert Opin. Orphan Drugs 2018, 6, 69–84.
2. Bilton, D., et al. *Inhaled dry powder mannitol in cystic fibrosis: An efficacy and safety study.* Eur. Respir. J. 2011, 38, 1071–1080.
3. Party, P., et al. *Formulation and In Vitro and In Silico Characterization of “ Nano-in-Micro ” Dry Powder Inhalers Containing Meloxicam.* Pharmaceutics 2021, 13, 1–18.
4. Pallagi, E., et al. *New aspects of developing a dry powder inhalation formulation applying the quality-by-design approach.* Int. J. Pharm. 2016, 511, 151–160.

ACKNOWLEDGMENT

The work was supported by Gedeon Richter’s Talentum Foundation, and Gedeon Richter Plc. Centennial Foundation (Gyömrői 19-21, Budapest, H-1103, HU), and Project no. TKP2021-EGA-32 implemented with support provided by the Ministry of Innovation and Technology of Hungary from the National Research, Development, and Innovation Fund, financed under the TKP2021-EGA funding scheme, and Hungarian-Slovenian Bilateral Project 2019-2.1.11-TÉT-2020-00147.

ORAL DOSAGE FORMS WITH CARVEDILOL FABRICATED BY SELECTIVE LASER SINTERING (SLS) 3D PRINTING TECHNIQUE

Nikola Pešić¹, Mirjana Krkobabić², Ivana Adamov¹, Svetlana Ibrić¹, Branka Ivković³, Đorđe Medarević¹

¹Department of Pharmaceutical Technology and Cosmetology, Faculty of Pharmacy, Belgrade, Serbia

²Pharmaceutical and Chemical Industry, Zdravlje AD, Leskovac, Serbia

³Department of Pharmaceutical Chemistry, Faculty of Pharmacy, Belgrade, Serbia

1. INTRODUCTION

When it comes to pharmacy, 3D printing has gained immense popularity in recent years due to its revolutionary use in printing drugs tailored to individual patient needs [1,2]. Selective laser sintering (SLS) is an industrial 3D printing technique which uses a powder bed to build up the 3D object thanks to a laser which binds the powder particles together. Advantages of SLS technique include the fact that it is a solvent-free process and offers relatively fast production. Until today, a limited number of studies investigating the production of drug dosage forms using SLS have been reported [2,3].

2. MATERIALS AND METHODS

2.1. Materials

Carvedilol (CRV) was used as a model substance in this study and it was donated by Hemofarm (Vršac, Serbia). The following excipients used to obtain 3D printing tablets: polyvinyl alcohol (PVA, Merck), mannitol (Parteck® M, Merck), Ludipress® (coprocessed excipient consisting of 93% lactose monohydrate, 3.5% crospovidone (Kollidon® CL) and 3.5% povidone K30 (Kollidon® 30), BASF), talc (Merck) and candurin (Candurin® Gold Sheen, Merck).

2.2. Preparation of formulations

The compositions of the formulations are shown in Table 1.

Table 1. Composition of the formulations

Material	Formulation 1	Formulation 2
CRV	10%	10%
PVA	55%	55%
Parteck® M	30%	/
Ludipress®	/	30%
Talc	2%	2%
Candurin® Gold Sheen	3%	3%

Powder for 3D printing was obtained by mixing all the components of the formulation and sifting through a sieve with a diameter of 180 μm .

2.3. 3D printing of oral dosage forms

A cylindrical 3D models of the printed tablets (8.00 mm diameter and 2.00 mm thickness) were designed with Autodesk Fusion 360 software version 2.0.8809 (Autodesk Inc, San Rafael, CA, USA), exported as a stereolithography file (.stl) and printed with Sintratec Kit 3D printer (Sintratec AG, Switzerland). The printing parameters were controlled using Sintratec 3D printer software. After a series of variations in temperature and laser speed, the optimal values of these parameters used in the 3D printing process were established and shown in Table 2.

Table 2. SLS 3D printing process parameters

Surface Temperature (°C)	Chamber Temperature (°C)	Laser speed (mm/s)	Hatch space
80 °C	70 °C	60	250 μm

2.4. Mechanical properties of 3D tablets

Tablets (n = 10) were weighed on a Sartorius BP 210 D analytical balance (Sartorius, Goettingen, Germany) and measured (diameter and thickness) using a digital caliper (Vogel, Kevelaer, Germany).

2.5. Powder X-ray diffraction analysis (PXRD)

PXRD analysis was performed to assess whether the laser induced amorphization of any of the compounds, especially amorphization of poorly soluble CRV. Samples were collected using a Philips PW-1050 (Philips, The Netherlands) diffractometer, operated at 40 kV and 30 mA, using Ni-filtered Cu K α radiation.

P34

2.6. Dissolution and Drug Release Analysis

Dissolution testing was performed under non-sink conditions using mini paddle apparatus (Erweka DT 600, Germany) with a paddle rotation speed of 50 rpm for 8 h, in 100 ml of phosphate buffer (pH 6.8). The amount of dissolved CRV was determined by HPLC method using Dionex Ultimate 3000 (Thermo Scientific, USA) HPLC system.

3. RESULTS AND DISCUSSION

3.1. 3D printing process

It was shown that SLS printer was able to fabricate 3D tablets with CRV, as well as that success of the printing process depended on the used printing parameters.

3.2. Mechanical properties of 3D tablets

The dimensions of the obtained 3D tablets were in accordance with the defined values of the created 3D models (F1: 8.10 ± 0.08 mm diameter and 2.10 ± 0.13 mm thickness, F2: 8.13 ± 0.09 mm diameter and 2.10 ± 0.12 mm thickness). Significant variations in tablet weight between formulations were not observed ($m_1=0.146 \pm 0.04$; $m_2=0.136 \pm 0.03$).

3.3. Powder X-ray diffraction analysis (PXRD)

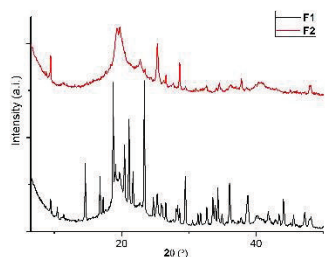


Figure 1. The X-ray powder diffraction of F1 and F2.

3.4. Dissolution and Drug Release Analysis

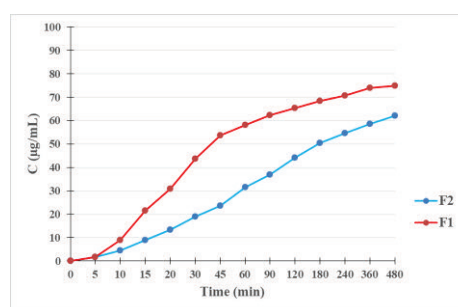


Figure 2. Dissolution profiles of 3D printing tablets

4. CONCLUSION

SLA represents a new chapter in 3D printing of solid oral dosage forms and in individualized therapy in particular. By adjusting the formulation and process parameters, it was possible to produce SLS tablets with co-amorphous CRV and PVA as a main polymer. Complete drug release was achieved under non sink conditions after 8 hours in phosphate buffer. The tailoring of drug release might be achieved by varying formulation factors as well as process parameters, although it could be governed by the composition of the whole formulation.

5. REFERENCES

1. Goynez, A., et al., 3D Printing of Medicines: Engineering Novel Oral Devices with Unique Design and Drug Release Characteristics. *Molecular pharmaceutics*, 2015. 12(11): 4077-4084.
2. Fina, F., et al.,
3. Goyanez, A., et al., Effect of geometry on drug release from 3D printed tablets. *International Journal of Pharmaceutics*, 2015(494):657-663.

DISSOLUTION KINETICS OF GLIBENCLAMIDE AMORPHOUS SOLID DISPERSIONS IN BIORELEVANT MEDIA

Vladimir Petkov, Zahari Vinarov, Slavka Tcholakova

Department of chemical and pharmaceutical engineering, Sofia university „Saint Kliment Ohridski “Bulgaria”

1. INTRODUCTION

A substantial part of modern drugs exhibit poor aqueous solubility, which leads to low or highly variable oral bioavailability. One of the approaches to overcome this issue is the preparation of amorphous solid dispersions, which can form supersaturated solutions that drive liquid-liquid phase separation.

The aim of the current study was to investigate the supersaturation propensity and liquid-liquid phase separation of glibenclamide ASDs prepared by spray-drying with hydroxypropylcellulose with low (HPC-SSL) or high molecular weight (HPC-L) and hydroxypropylmethylcellulose acetate succinate (HPMCAS-HG).

2. MATERIALS AND METHODS

2.1. Materials

Glibenclamide (99 %, Alfa Aesar), HPC-SSL and HPC-L (NISSO Chemical Europe GmbH), HPMCAS-HG (Shin-Etsu), NaCl (Sigma-Aldrich), KCl (Sigma-Aldrich), NaHCO₃ (Sigma-Aldrich), Hydrochloric acid 37% (Honeywell), bovine bile 50% (Sigma-Aldrich)

2.2. Methods

Glibenclamide ASDs were prepared by dissolving drug and polymer (at 1:3 drug to polymer ratio) in a mixture of dichloromethane and methanol at a total concentration of 5 wt %. All solutions were spray dried by using Buchi mini spray drier B-290. The samples were spray dried at 10ml/min flow rate, 70% aspiration and 50 °C inlet temperature. Differential scanning calorimetry, polarized light microscopy (PLM) and wide-angle X-ray scattering (WAXS) were used to characterize the solid state of the obtained formulations. High performance liquid chromatography (HPLC), was used to obtain the dissolution kinetics in biorelevant media. UV-Vis spectroscopy was used to determine the amorphous solubility of the drug and dynamic light scattering (DLS) was used to study the colloids in the supersaturated solutions.

3. RESULTS AND DISCUSSION

3.1. Solid state analysis

The spray-dried formulations were characterized by polarized light microscopy, WAXS and differential scanning calorimetry. The results showed that the drug was in an amorphous state in all studied systems. The used polymers ensured stability for > 90 days.

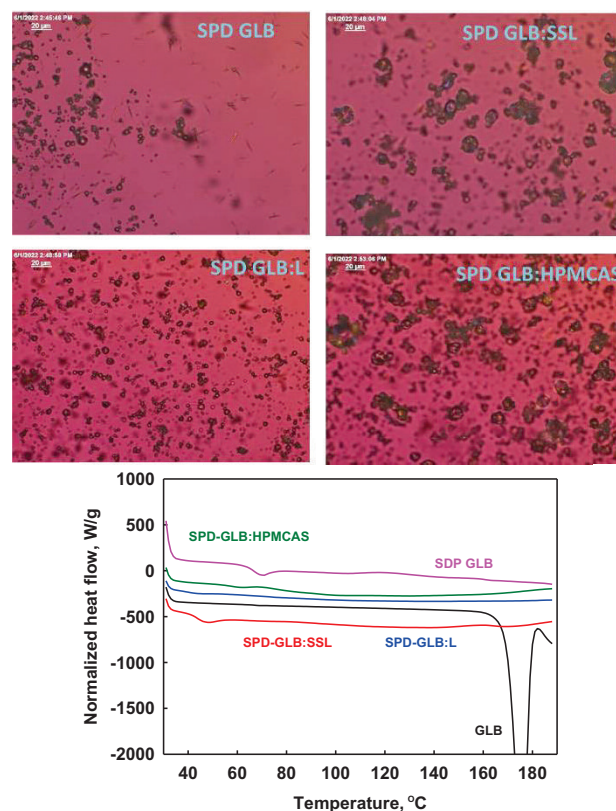


Figure 1. PLM images and DSC analysis of the spray-dried formulations.

3.3. Amorphous solubility determination

The amorphous solubility of glibenclamide in different media was evaluated using a solvent shift method. The results showed that the amorphous solubility is highly affected by the presence of bile salts and polymers in the solution. When present, bile salts increase the amorphous solubility to around 500 µg/ml compared to a simple phosphate buffered with

pH-7 in which phase separation occurs at around $250\mu\text{g/ml}$. Polymers can also have an impact on the amorphous solubility of the drug. In presence of bile salts, HPC SSL raises the amorphous solubility to around $575\mu\text{g/ml}$ and HPMCAS lowers the amorphous solubility to $440\mu\text{g/ml}$.

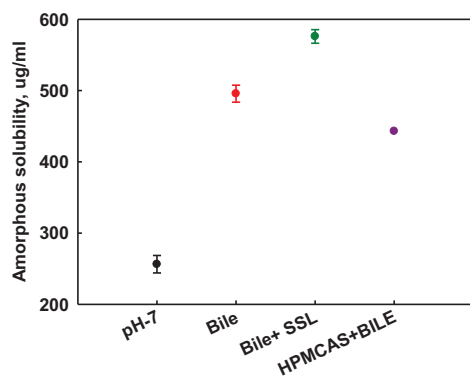


Figure 2. Effect of media on amorphous solubility.

3.2. Drug release kinetics in biorelevant media.

The spray dried formulations showed dramatic increase in the dissolved drug concentrations compared to the crystalline compound at the single-stage intestinal conditions model (Figure 3A) and also in the gastro-intestinal transfer model (Figure 3B). Interestingly, the neat amorphous glibenclamide (obtained after spray drying) showed very high drug concentrations, similar to polymer-based formulations, in the single-stage model. In contrast, very low drug concentrations, similar to the crystalline drug were measured in the gastrointestinal transfer model, indicating crystallization of the amorphous glibenclamide in the gastric phase.

In respect to the effect of the polymer type, the low molecular weight HPC-SSL showed superior performance compared to HPMCAS-HG in both models. The high-molecular weight HPC-L showed similar drug release kinetics to HPC-SSL in the single-stage model (intestinal conditions only), whereas slightly slower drug release was measured in the gastrointestinal transfer model. All formulations were stable during dissolution, showing no sign of precipitation.

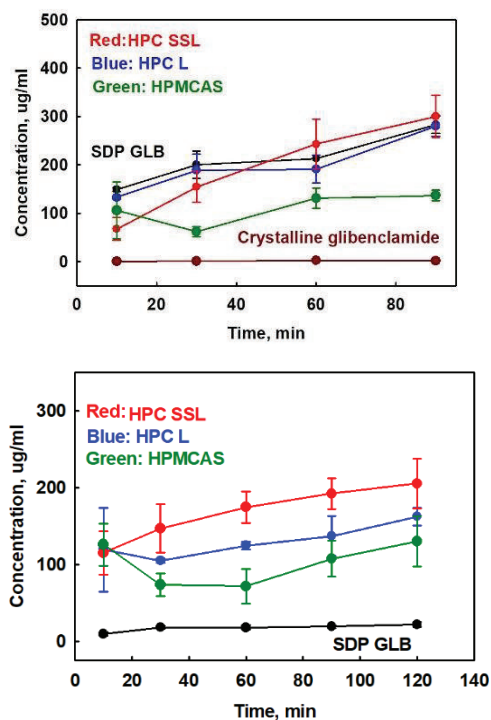


Figure 3. Dissolution kinetics of glibenclamide formulations in (A) single stage intestinal model and (B) gastrointestinal transfer model

4. CONCLUSION

Spray-drying was successfully used to prepare amorphous glibenclamide formulations with excellent storage stability. The ASDs enhanced the drug release by several orders of magnitude, compared to the crystalline drug. The studied polymers (HPC-SSL, HPC-L and HPMCAS-HG) stabilized the amorphous state of the drug during storage, but also during dissolution in the stomach compartment. Best performance was observed for the low molecular weight HPC-L, where concentrations up to $300\mu\text{g/mL}$ were measured. The measured amorphous solubilities in biorelevant media (which exceed the drug concentrations measured during ASD dissolution) and the DLS results suggest that liquid-liquid phase separation does not occur in these systems and the drug is molecularly dissolved.

ACKNOWLEDGMENT

Part of the research is done using equipment bought for project bg05m2op001-1.002-0012 financed by op neig sufinanced by the European union via european structural and investment funds.

TOPICAL FORMULATION OF LYOPHILIZED *P. CORONARIUS* FLOWER AND LEAF EXTRACTS, ANTIMICROBIAL ASSESSMENT OF THE PLANT

Ágota Pető^{1,2}, Dóra Kósa^{1,2}, Ádám Haimhoffer¹, Dániel Nemes¹, Pálma Fehér¹, Zoltán Ujhelyi¹, Judit Váradi¹, Ferenc Fenyvesi¹, Miklós Vecsernyés¹, Zoltán Tóth³, Annamária Pallag⁴, Tünde Jurca⁴, Ildikó Bácskay^{1,2}

¹Department of Pharmaceutical Technology, Faculty of Pharmacy, University of Debrecen, Hungary

²Institute of Healthcare Industry, University of Debrecen, Hungary

³Department of Medical Microbiology, Faculty of Medicine, University of Debrecen, Hungary

⁴Department of Pharmacy, Faculty of Medicine and Pharmacy, University of Oradea, Romania

1. INTRODUCTION

The medicinal use of herbs is very popular, and there is a high demand for herbal preparations among patients because of their beneficial effects [1]. *P. coronarius* is widely used in folk medicine for the treatment of various diseases, its antimicrobial effects are well known, but scientifically less investigated and no external preparation is available of the herb yet [2]. The objective of our work was to formulate O/W emulsion ointments using lyophilized *P. coronarius* flower or leaf extracts with the addition of different penetration enhancers [3,4].

2. MATERIALS AND METHODS

2.1. Materials

SP70 sucrose ester was kindly gifted by Sisterna (Roosendaal, The Netherlands). **Cetostearyl alcohol**, propylene glycol, stearic acid, isopropyl myristate, conservant solution were obtained from Hungaropharma Ltd. (Budapest, Hungary). HaCaT cells were supplied from Cell Lines Service (CLS, Heidelberg, Germany). Transcutol, Tefose 63, Sedefos 75 was a kind gift from Gattefossé (Lyon, France).

2.2. Method

After the preparations were formulated *in vitro* release studies and texture analysis of the ointments were formulated. In addition, antimicrobial testing of the lyophilized extracts and biocompatibility investigation of the selected excipients were carried out. Bioactive compound content had been determined by HPLC method.

3. RESULTS AND DISCUSSION

3.1. Texture analysis

Texture analysis revealed that the compositions have adequate consistency, those formulations, which contain Tefose 63 have slightly harder consistency.

3.2. *In vitro* release

The results of *in vitro* release studies by Franz diffusion chamber apparatus revealed, that the best release profile was achieved by that preparation, which contained SP70 sucrose ester, closely followed by those ones, which were prepared with Tefose 63.

3.3. Antimicrobial testing

P. coronarius flower was not able to inhibit or delay the growth of bacteria or fungi, but the leaf was able to delay the growth of *C. albicans* and *S. aureus* compared to the control.

3.4. MTT test

The results of MTT experiments demonstrated that the selected excipients and the preparations are safe under *in vitro* conditions.

3.5. Bioactive compound content

The leaf of *P. coronarius* contains a high amount of delphinidin 3-rutinoside chloride (0.3354 mg/100 mg), as well as luteolin 7-glucoside (0.2528 mg/ 100 mg) and 7-methoxycoumarin (0.2061 mg/100 mg) compared to the other components. The flower contains bergapten in a high amount (2.8370 mg/100 mg), as well as caffeic acid (1.8407 mg/100 mg), delphinidin 3-rutinoside chloride (1.7928 mg/100 mg), 7-methoxycoumarin (1.6725 mg/100 mg). The flower contains delphinidin 3-rutinoside chloride and 7-methoxycoumarin in a much higher amount, than the leaf.

4. CONCLUSION

According to the results the composition and the selected excipients of the ointments have a great impact on the drug release, texture and bioavailability of the preparation. During microbiological testing, *P. coronarius* leaf was effective against *E. coli* and *S. aureus*. *P. coronarius* is a promising herb, and its topical application in antimicrobial therapy can be a useful addition to modern medical therapy.

5. REFERENCES

1. Klecáková, J.; Chobot, V.; Jahodár, L.; Laakso, I.; Víchová, P. Antiradical Activity of Petals of *Philadelphus Coronarius* L. *Cent. Eur. J. Public Health* **2004**, *12 Suppl*, S39-40.
2. Valko, V.; Fickova, M.; Pravdova, E.; Nagy, M.; Grancai, D.; Czigle, S. Cytotoxicity of Water Extracts from Leaves and Branches of *Philadelphus Coronarius* L. *Biomed. Pap. Med. Fac. Univ. Palacky. Olomouc. Czech. Repub.* **2006**, *150*, 71–73, doi:10.5507/bp.2006.007.
3. Nagy, M.; Grancai, D.; Jantova, S.; Ruzekova, L. Antibacterial Activity of Plant Extracts from the Families Fabaceae, Oleaceae, Philadelphaceae, Rosaceae and Staphyleaceae. *Phyther. Res.* **2000**, *14*, 601–603.
4. Hano, C.; Tungmunnithum, D. Plant Polyphenols, More than Just Simple Natural Antioxidants: Oxidative Stress, Aging and Age-Related Diseases. *Medicines* **2020**, *7*, 26, doi:10.3390/medicines7050026.

ACKNOWLEDGMENT

Project no. TKP2021-EGA-18 has been implemented with the support provided from the National Research, Development and Innovation Fund of Hungary, financed under the TKP2021-EGA funding scheme. The research was carried out under the project Debrecen Venture Table S Catapult (EFOP-3.6.1-16-2016-0002). The project was supported by the European Union and co-funded by the European Social Fund. The work is supported by the GINOP-2.3.4-15-2020-00008 project. The project is co-financed by the European Union and the European Regional Development Fund. The present work was supported by grant from The Ministry of Hungary Domus Hungarica 2019. The research was co-financed by the Richter Gedeon Talent Foundation.

FENOFIBRATE ORODISPERSIBLE TABLET MADE WITH GRANULATED MESOPOROUS SILICA

Odon Planinšek, Ana Baumgartner, Blaž Grilc

¹Department for Pharmaceutical Technology, Faculty of Pharmacy, University of Ljubljana, Slovenia

1. INTRODUCTION

The fabrication of amorphous solid dispersions is an approach to improve the dissolution of sparingly soluble active substances in water. Among hydrophilic water insoluble excipients for the production of solid dispersions, mesoporous silicon dioxide is the most promising [1]. Many research works have shown the feasibility of incorporating sparingly soluble active ingredients into mesoporous materials, with the main disadvantage of obtained amorphous solid dispersions having poor flowability and compressibility. In our study, we solved this problem by granulating of mesoporous silicon dioxide with erythritol and subsequent impregnation with the poorly water-soluble active ingredient, fenofibrate.

2. MATERIALS AND METHODS

2.1. Materials

- a) Model active pharmaceutical ingredient: Fenofibrate-Biosynth, Carbosynth, Great Britain.
- b) Mesoporous silicon dioxide: Syloid 244FP, Grace, Germany.
- c) Silicon dioxide binder: Erythrytol, Instantina, Austria.
- d) 2-propanol: Merck, Germany.
- e) Croscarmellose Sodium, Ac-Di-Sol®, Dupont, USA.

2.2. Syloid 244FP granulation

Syloid 244FP was granulated with Erythrytol and water as a granulating liquid in high shear granulator ProCept 4M8-TriX (Belgium). Syloid to Erythritol proportion in dry granules was 2:1.

2.3. Granules and Syloid244FP impregnation

Granules were impregnated with 20% of 26,7% of fenofibrate from 2-propanol solution in rotavapor (Büchi R-114, Switzerland). Pure Syloid 244FP particles were impregnated with fenofibrate in the same way as erythritol granules.

2.4. Orodispersible tablet formulation

3% of AcDiSol was added to impregnates granules and compressed into tablets containing 140 mg of fenofibrate using 12 mm flat punches at 25 kN compression force.

2.5. Granules and solid dispersions evaluation

- a) Specific surface area of nonimpregnated Syloid and of fenofibrate impregnated granules was determined with BET Surface area analyzer Nova 2000, Quantachrome, Germany.
- b) Particle size analysis of powder samples was performed by laser diffraction method, Mastersizer 3000, Malvern, UK using Aero S dry powder disperser.
- c) Thermal properties of produced solid dispersion were determined with Differential scanning calorimeter DSC1, Mettler Toledo, Switzerland.
- d) Orodispersible tablet disintegration time determination was determined in water using Erweka ZT320 disintegration tester (Germany) at 37°C.
- e) Dissolution of pure fenofibrate, of fenofibrate physical mixtures with Syloid 244FP and erythritol and from solid dispersions containing the same proportion of active ingredient as physical mixtures was determined in water phosphate buffer at pH 6,8. Concentrations at six time points from 5 to 60 min were determined with Hewlett Packard 8453 UV-VIS spectrophotometer (USA) ($\lambda=250$ nm)

3. RESULTS AND DISCUSSION

3.1. Specific surface area

Syloid has large specific surface area (SSA) 377 m²/g (Table 1) which can adsorb significant amount of active pharmaceutical ingredient. Granulation of silica decreased this property to 217 m²/g. Theoretically SSA should be of 248 m²/g. Difference between these two values can be attributed to the portion of erythritol that

P37

impregnated pores. As expected, impregnation of silica pores with fenofibrate decreased SSA of granules. Higher the amount of fenofibrate, lower the SSA of the product (Table 1). However, for all the solid dispersions (granulated and non-granulated) specific surface area is much larger than for pure fenofibrate (0.5 m²/g).

3.2. Particle size

Granulation of silica increased particle size from 4 μm to 65 μm. This property of granules enabled their tableting which could not be performed with pure silica particles or with fenofibrate impregnated silica particles.

Table 1. BET specific surface area and average particle size.

Sample	BET area (m ² /g)	Average size (μm)
Syloid 244FP	377	3,8
Fenofibrate	0.5	41.5
Granulated Syloid FP244+Erythritol 2:1	217	65
20% solid dispersion	121	4,0
30% solid dispersion	80	3,7
20% Tableted gran. solid dispersion	125	85,9
26,7% Tableted gran. solid dispersion	82	42,6

3.2. Thermal properties

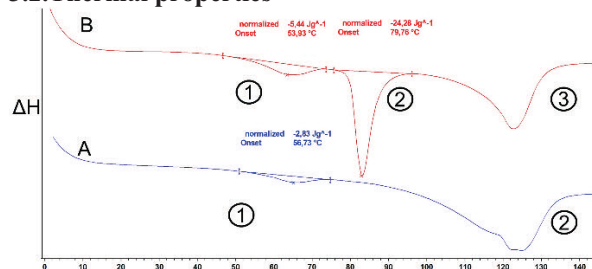


Figure 1. DSC curves of impregnated granules composed of Syloid 244FP and erythritol with fenofibrate. A -20% fenofibrate content, B-26,7 % fenofibrate content.

DSC curve for impregnated granules with 20 % of fenofibrate shows three peaks:

1-melting of fenofibrate nanoparticles located in mesopores.

2-melting of fenofibrate crystals at 80 °C.

3-melting of erythritol crystals at about 110 °C.

DSC curve for impregnated granules with 26,7

% of fenofibrate shows two main peaks:

1-melting of fenofibrate nanoparticles located in mesopores.

2-melting of erythritol crystals at about 110 °C.

3.3. Tablet disintegration time

Disintegration time of tablets was less than a minute.

3.4. Dissolution of fenofibrate from solid dispersions

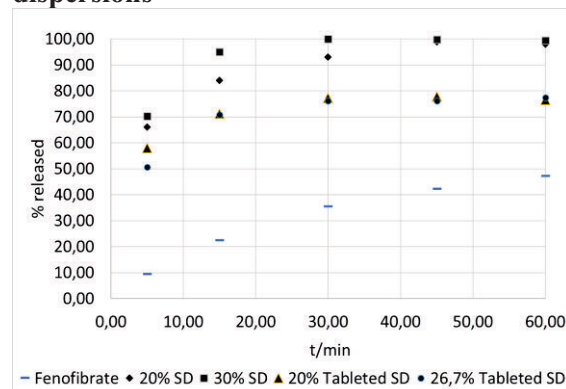


Figure 2: Dissolution profiles of pure fenofibrate, solid dispersions and tableted granulated solid dispersions

Formulation of solid dispersions significantly improved the dissolution of fenofibrate (Figure 2). Although the orodispersible tablet formulation shows inferior dissolution compared to the pure solid dispersions, it is reasonable to develop a patient friendly dosage form which still perform much better than pure fenofibrate.

4. CONCLUSION

Co-processing of Syloid 244 FP with erythritol enables formation of a solid dispersion of sparingly soluble fenofibrate with improved dissolution and can be easily compressed into anorodispersible tablet.

5. REFERENCES

1. Baumgartner A., Planinšek O. Application of commercially available mesoporous silica for drug dissolution enhancement in oral drug delivery. *European Journal of Pharmaceutical Science* 2021, 167, 1-13.

ACKNOWLEDGMENT

The authors acknowledge financial support from the Slovenian Research Agency (Research Core Funding, No. P1-0189).

EX VIVO BIOFILM MODEL ON PIG SKIN TO TEST THE EFFICACY OF ELECTROSPUN ANTIMICROBIAL DRUG-LOADED FIBER MATERIALS AS WOUND DRESSING

Kaisa Põhako¹, Kairi Lorenz¹, Marta Putrinš^{1,2}, Külli Kingo³, Tanel Tenson², Karin Kogermann¹

¹ Institute of Pharmacy, University of Tartu, Estonia,

² Institute of Technology, University of Tartu, Estonia,

³ Dermatology Clinic of Tartu University Hospital

1. INTRODUCTION

Chronic wounds are a growing problem to healthcare systems all over the world. Often chronic wounds may become infected with bacteria. The presence of bacterial biofilms in combination with the lack of suitable topical antimicrobial treatments makes the wound care even more challenging.¹

In the last decades, scientists are searching for novel wound care approaches. One possible solution could be antimicrobial electrospun fiber dressings for the local treatment of wounds. Electrospinning is a fiber production method, which enables to incorporate different drugs and antimicrobial agents into the fiber structure. This feature makes electrospun fibers a desirable material to be used as a wound dressing.²

With new potential medical devices (e.g. wound dressings), it is very important to test their safety, efficacy and biocompatibility. Variety of skin and wound infection models are developed and used to test novel wound dressing materials. Such novel materials require more biorelevant testing methods in order to understand their quality and real potential for the treatment of infected wounds.³

The aim of this work was to develop *ex vivo* infected wound model on pig skin to test the antimicrobial efficacy of electrospun fiber dressings.

2. MATERIALS AND METHODS

2.1. Preparation of electrospun dressings

Monoaxial electrospinning was used to create four different fiber matrices - two antimicrobial model drug loaded matrices and two of their respective controls. Exact compositions of the fibers together with fiber diameters are presented in Table 1.

2.2. *Ex vivo* pig skin wound infection model development

Ex vivo wound infection models were developed on pig skin using pathogenic wound bacteria (Fig 1.). A wound was created using a biopsy punch needle and infected with bacteria (*E. coli*, *S. aureus*, *S. epidermidis*). Electrospun fiber matrices were placed over the infected wound and the whole construct was incubated up to 72 h at 37°C.

2.3. Colony forming unit (CFU) determination

To indicate the inhibitory effect of the electrospun fiber materials on bacterial growth, CFU detection was carried out. A pig skin and electrospun fibers from wound model were washed with 1xPBS and formed biofilm was disrupted by sonification and vortexing. Samples containing disrupted biofilm were plated on LB plates, incubated at 37°C for 24 h and counted.

2.4. Microscopy

The biofilm formed in the model and the efficacy of antimicrobial fiber matrices were visualized using scanning electron microscopy (SEM). Firstly, samples were fixed with formaldehyde and dried with ethanol, then SEM imaging was carried out.

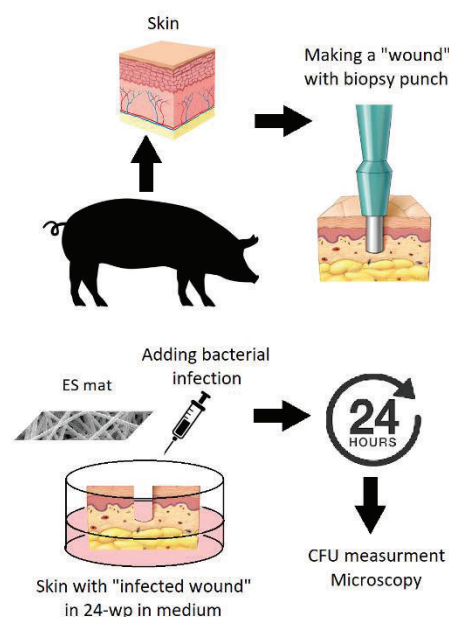
3. RESULTS AND DISCUSSION

An antibiotic (Ab) loaded and antimicrobial peptide (AMP) loaded fiber matrices and their respective pristine polymeric fiber matrices were successfully produced by monoaxial electrospinning. The measured fiber diameters (n=100) were all above 1 micrometer (Table 1).

Table 1. Description of electrospun fiber materials used.

Sample name	Composition	Diameter size (μm)
Mat A	mixture of hydrophilic and hydrophobic polymers	2.2 ± 5.7
Mat A+Ab	mixture of hydrophilic and hydrophobic polymers and antibiotic (Ab)	2.9 ± 1.1
Mat B	hydrophobic polymer	3.6 ± 0.5
Mat B+AMP	hydrophobic polymer and antimicrobial peptide (AMP)	1.3 ± 0.2

The *ex vivo* wound infection model enabled to mimic the biorelevant conditions of infected wound and the formation of bacterial biofilm was detected (**Figure 1**). The model results revealed, that pristine fiber matrices were suitable surfaces for bacteria to grow on and form a biofilm. The latter is important to keep in mind while designing novel wound dressings. Fibrous matrices with antimicrobial agents prevented the biofilm formation and significantly inhibited the bacterial growth in the wound model due to the release of drugs from electrospun fibers and antibiofilm properties of the dressings. CFU counting and microscopy enabled to understand the biofilm formation and effect of antimicrobial fiber matrices.

**Figure 1.** Experimental set up of infected *ex vivo* wound model on pig skin.

4. CONCLUSION

In conclusion, developed *ex vivo* wound infection model on the pig skin is suitable for testing the antimicrobial effect of electrospun fiber matrices. Both tested antimicrobial fiber matrices hold potential to be used as antimicrobial wound dressings for the treatment of wound infections. Further studies will reveal their *in vitro* safety and *in vivo* efficacy and biocompatibility.

ACKNOWLEDGMENT

The study was funded by the Estonian Research Council project PRG 1507.

REFERENCES

1. Percival, S. L., McCarty, S. M. & Lipsky, B. Biofilms and Wounds: An Overview of the Evidence. *Adv. Wound Care* **4**, 373–381 (2015).
2. Cui, W., Zhou, Y. & Chang, J. Electrospun nanofibrous materials for tissue engineering and drug delivery. *Sci. Technol. Adv. Mater.* **11**, 014108 (2010).
3. Ud-Din, S. & Bayat, A. Non-animal models of wound healing in cutaneous repair: In silico, in vitro, ex vivo, and in vivo models of wounds and scars in human skin. *Wound Repair Regen.* **25**, 164–176 (2017).

RELATIVE BIOAVAILABILITY ENHANCEMENT OF SIMVASTATIN VIA DRY EMULSION SYSTEMS: COMPARISON OF SPRAY DRYING AND FLUID BED LAYERING TECHNOLOGY

Mitja Pohlen¹; Jurij Aguiar Zdovc¹, Jurij Trontelj¹, Janez Mravljak¹, Mirjam Gosenca Matjaž¹, Iztok Grabnar¹, Tomaž Snoj², Rok Dreu¹,

¹Faculty of Pharmacy, University of Ljubljana, Aškerčeva cesta 7, SI-1000 Ljubljana, Slovenia

²Veterinary Faculty, University of Ljubljana, Gerbičeva 60, SI-1000 Ljubljana, Slovenia

1. INTRODUCTION

In recent decades more and more newly discovered drugs are active pharmaceutical ingredients (APIs) exhibiting poor biopharmaceutical characteristics, especially low water solubility [1].

The aim of this study was to compare two dry emulsion forming techniques, i.e. spray drying (SPD) and fluid bed layering (FBD) in terms of process, physicochemical product characteristics and bioavailability enhancement of the model drug, simvastatin (SV). The critical quality attributes (CQAs) were compared based on two previously conducted Design of Experiment studies (DoE) [2, 3]. A final pharmacokinetic (PK) study was conducted in rats to evaluate the *in vivo* performance of optimised products from each technique and compared with a SMEDDS formulation, a spray dried formulation with SV glyceride mimetic and a physical powder mixture resembling a generic SV tablet.

2. MATERIALS AND METHODS

2.1. Materials

Simvastatin (pharmaceutical grade, Krka d.d.), 1-oleoyl-rac-glycerol (technical grade ~40% (TLC)), Tween® 20 (Merck, Germany), Pharmcoat 603 (ShinEtsu, Japan), Miglyol® 812 (Sasol, Germany), mannitol (Roquette, France), Cellets 200 (Harke Pharma GmbH, Germany), Avicel® PH 101, lactose mesh 200 (Lek d.d., Slovenia), Magnesium stearate (Merck KGaA, Darmstadt), SV-D6 standard and Simvastatin hydroxy acid (SVA)-D6 (Toronto Research Chemicals, Canada). All solvents for UPLC analysis were of HPLC grade. All other reagents used were of analytical grade.

2.2.1. Process and formulation development

For a comprehensive description of the process and formulation parameters, the reader is directed to two studies [2, 3].

Briefly, coating experiments were performed using the GPCG-1 process equipment (Glatt® GmbH, Germany) utilising a modified Wurster-type process chamber equipped with swirl generator design. For the SPD process a Mini spray dryer B-290 (Büchi, Switzerland) was employed.

Emulsion component limits, where the formulations were processable, were set for both technologies and were used as the experimental space for the DoE study (Table 1).

Table 1. Excipients weight proportion limits for DoE study.

Formulation	Weight proportion limits (%)			
	FBD		SPD	
	Low	High	Low	High
Oil	27.86	33.17	27.00	40.00
Mannitol	52.00	65.15	49.04	61.84
HPMC	5.42	14.21	8.46	10.66
Tween® 20	0.50	2.50	0.50	2.50

2.2.2. Physicochemical characterization and *in vivo* evaluation

Dry emulsions were compared according to process yield (PY), drug content, stability, encapsulation efficiency (EE), particle size, morphology, redispersibility and dissolution performance. For the *in vivo* evaluation, Wistar female rats were divided into 5 groups of 12 animals and administered orally by gavage (1 mg of SV per 100 g of body weight).

3. RESULTS AND DISCUSSION

3.1. Process and product comparison

The comparison of EE, PY, drug content and 1 month stability is shown in Table 2. In SPD, a much higher inlet/product temperature was

needed to successfully perform the process, compared to FBD, which can degrade API, thus lowering the EE. Additionally, FBD, which produced bigger particles provided significantly ($\alpha = 0.05$) higher one month relative drug content stability.

Table 2. Process yield, drug content and one month stability of dry emulsion products (average values).

	SPD	FBD
Encapsulation efficiency (%)	68.4	80.0
Process yield (%)	71.5	83.3
Drug content (mg/g)	22.2	9.34
One month stability (%)	85.5	93.8

The individual particles of the spray dried dry emulsion powder were round in shape (Fig. 1. a), but they were physically bound and combined into fractal agglomerates (median particle size $d_{50} = 56 \mu\text{m}$), which makes them less suitable for further processing, compared to round shaped (Fig. 1. b) and bigger (median size of $d_{50} = 336 \mu\text{m}$) dry emulsion layered pellets.

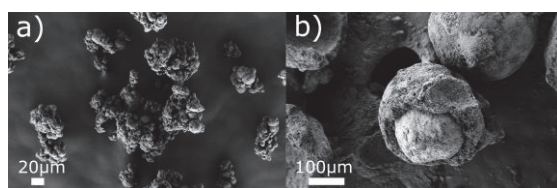


Figure 1: Dry emulsion products: a) spray dried dry emulsion powder; b) dry emulsion layered pellets.

Regardless of the reconstitution parameter used, differences between optimised products of both technologies are marginal. Dissolution tests showed a more than 18- and 20- fold increase (compared to crystalline SV) in drug dissolution for fluid bed layered dry emulsion pellets and spray dried dry emulsion powders, respectively.

3.2. In vivo study

A one-compartment model with two parallel first order absorption processes for SV, and additional absorption process for SVA, was chosen to describe the distribution of both SV and SVA. Fluid bed dry emulsion layered pellets provided the highest increase in relative bioavailability (215%) within the group of five formulations.

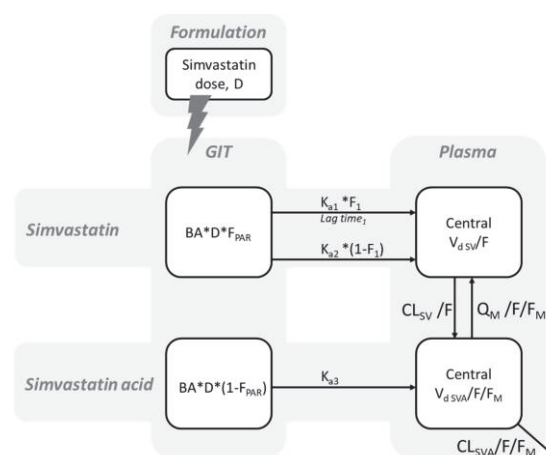


Figure 2: The schematic representation of the final population PK model for SV and SVA.

4. CONCLUSION

Two dry emulsion production techniques, i.e. FBD technology and SPD technology were compared. FBD showed significantly better process yield, encapsulation efficiency, improved stability and better morphology for further processing into a final dosage form. SPD allowed us to broaden the limits of formulation component variables, resulting in a higher drug content. Fluid bed layered dry emulsion pellets provided the highest increase in relative bioavailability within the group of five formulations, confirming the superiority of FBD over SPD for potent/low dose APIs formulated as dry emulsion systems.

5. REFERENCES

1. Buckley S.T., et al., *Biopharmaceutical classification of poorly soluble drugs with respect to 'enabling formulations*. EJPS, 2013. 50: 8–16.
2. Pohlen M., et al., *Preparation, Physicochemical Characterisation and DoE Optimisation of a Spray-Dried Dry Emulsion Platform for Delivery of a Poorly Soluble Drug, Simvastatin*. AAPS PharmSciTech. 2020. 21: 119.
3. Pohlen M., et al., *A redispersible dry emulsion system with simvastatin prepared via fluid bed layering as a means of dissolution enhancement of a lipophilic drug*. International Journal of Pharmaceutics, 2018. 549: 325-334.

ACKNOWLEDGMENT

The authors thank Krka, d.d. Novo Mesto, Slovenia and the Faculty of Pharmacy, University of Ljubljana, Slovenia (Slovenian Research Agency under contract number P1-0189), for supporting this study.

COMPARISON OF THE RELEASE PROFILES OF MELATONIN FROM MATRIX TABLETS CONTAINING POLY(ϵ -CAPROLACTONE) AND COPOLYMERS

Chrystalla Protopapa¹, Marilena Vlachou¹, Angeliki Siamidi¹, Evi Christodoulou², Nikolaos D. Bikiaris²

¹*Division of Pharmaceutical Technology, Department of Pharmacy, National and Kapodistrian University of Athens, Greece*

²*Department of Chemistry, Laboratory of Polymer Chemistry and Technology, Aristotle University of Thessaloniki, Greece*

1. INTRODUCTION

The pineal hormone that regulates the circadian rhythm is melatonin (MLT, Fig. 1). In the elderly, though, its excretion is significantly lowered, and exogenous administration of the hormone is needed to compensate for its diminished concentration. However, due to MLT's poor bioavailability and short biological half-life, modified release formulations are needed [1]. Our research group has been studying a plethora of biopolymers with diverse chemical structures, as excipients in per os administered solid dosage forms [2-5]. In the context of this study, MLT matrix tablets, containing polycaprolactone (PCL) and its copolymer, methoxy poly(ethylene glycol)-co-PCL (mPEG-PCL) (Fig. 1), have been developed and evaluated with respect to their dissolution profile, aiming at dealing with sleep onset and/or maintenance dysfunctions, caused by low MLT concentrations in the body

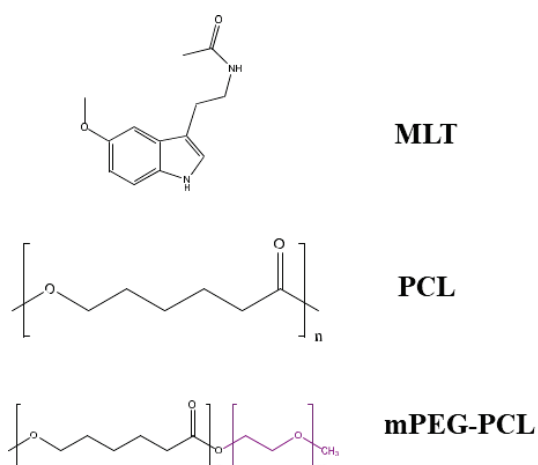


Figure 1. Chemical structures of MLT, PCL and mPEG-PCL.

2.1. Materials

The polymeric materials (neat PCL, mPEG-PCL [1:3] and mPEG-PCL [1:1]) were newly synthesized (by ring-opening polymerization of ϵ -caprolactone) and kindly donated by Professor Dimitrios Bikiaris's group, Laboratory of Chemistry and Technology of Polymers and Dyes, in the Department of Chemistry of the Aristotle University of Thessaloniki. Other excipients used for the tablets' production included lactose monohydrate, Avicel PH102, and magnesium stearate. The commercially available drug Circadin® was purchased from a local pharmacy.

2.2. Methods

The tablets were prepared using the excipients, shown in Table 1, by direct compression. A USP apparatus II was used for the dissolution experiments, which were carried out in aqueous media, A: pH 1.2, for 2 h, and B: pH 6.8, for 6 h, in order to simulate the conditions in the gastrointestinal track. The samples were analysed using a UV spectrophotometer (λ_{max} = 278), and dissolution curves were constructed.

Table 1. Formulations (F1-F3) of MLT

Ingredients	F1 (mg)	F2 (mg)	F3 (mg)
Melatonin	2	2	2
Neat PCL	150		
mPEG-PCL [1:3]		150	
mPEG-PCL [1:1]			150
Lactose Monohydrate	10	10	10
Avicel PH 102	36	36	36

2. MATERIALS AND METHODS

3. RESULTS AND DISCUSSION

The aqueous dissolution test results obtained for MLT from the developed formulations and MLT from the commercially available drug Circadin® are presented in Figure 1.

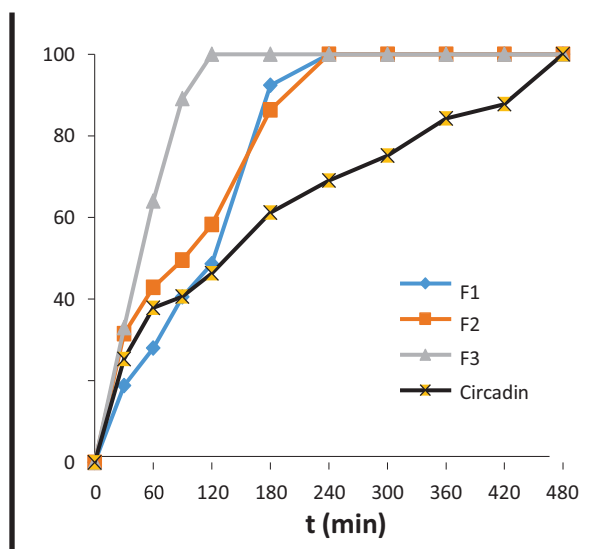


Figure 1. In vitro % release of MLT from Circadin® vs. time, at pH 1.2 (0-120 min) and at pH 6.8 (120-480 min) (SD<2) (n= 3).

From the release curves seen in Fig. 1, it can be assumed that the MLT release from formulation F1, containing neat PCL, resembles the MLT release from the commercially available drug Circadin®, during the first 2 hours at pH 1.2. Also, it was observed that the release of MLT from formulation F2, containing mPEG-PCL [1:3], resembles the release profile of formulation F1 that contains neat PCL through the whole dissolution process (8 hours). On the other hand, the hormone's release from the formulation F3, that contains mPEG-PCL [1:1], was particularly high (100% at 2 hours), indicating that the larger the amount of the hydrophilic mPEG-segment onto the PCL backbone, the more enhanced the MLT's release.

4. CONCLUSION

We have shown that the formulations developed for the MLT's effective release lead to its 100% release during the first 2 hours (F1 and 4 hours F2 and F3). These formulations are considered appropriate for treating sleep onset dysfunctions, in contrast to the commercially available drug Circadin®, which is suitable for treating combined sleep onset/sleep maintenance problems.

5. REFERENCES

1. Arendt J, Melatonin and human rhythms, *Chronobiol. Int.*, 2006, 23, (1-2), 21-37
2. Vlachou M, Stavrou G, Siamidi A, et al. N-Acetylserotonin vs Melatonin: In vitro controlled release from hydrophilic matrix tablets LDDD, 2019, 16(3): 347-352.
3. Vlachou M, Siamidi A, Anagnostopoulou D, et al. Modified release of the pineal hormone melatonin from matrix tablets containing poly(L-lactic acid) and its copolymers. *Polymers*, 2022, 14(8), 1504.
4. Vlachou M, Kikionis S, Siamidi A, et al.. Modified in vitro release of melatonin loaded in nanofibrous electrospun mats incorporated into mono-layered and three-layered tablets. *J Pharm Sci*, 2019, 108(2):970-976.
5. Vlachou M, Tragou K, Siamidi A, et al. Modified in vitro release of the chronobiotic hormone melatonin from matrix tablets based on the marine sulfated polysaccharide ulvan. *J DDST*, 2018, 44:41-48.

HARMIQUINS, NOVEL POTENT ANTIPLASMODIAL HITS

Zrinka Rajić¹, Goran Poje¹, Lais Pessanha de Carvalho², Jana Held², Ivana Perković¹, Tana Tandarić³, Robert Vianello³

¹Department of Medicinal Chemistry, University of Zagreb Faculty of Pharmacy and Biochemistry, Croatia

²Institute of Tropical Medicine, University of Tübingen, Germany

³Ruđer Bošković Institute, Croatia

1. INTRODUCTION

Malaria is the deadliest protozoan infectious disease widely spread in the tropical and subtropical areas [1]. As existing antimalarials are losing their efficacy due to the emergence of resistant *Plasmodium* strains, there is an urgent need for novel agents. Molecular hybridization, fusion of at least two pharmacophores with individual activity, represents a popular approach to obtain dual-acting antimalarial agents [2]. We decided to employ that strategy and to combine two scaffolds with known antimalarial activity, harmine and chloroquine, to produce hybrid agents, harmiquins.

2. MATERIALS AND METHODS

2.1. General synthetic procedures

Triazole-type (TT) harmiquins **18-25**: A suspension of harmine-/7-chloroquinoline-based alkyne (0.230 mmol), the corresponding 7-chloroquinoline-/harmine-based azide (0.253 mmol), catalytic amount of Cu(OAc)₂ in MeOH (5 mL) was stirred at rt for 24 h, and solvent evaporated. Amide-type (AT) harmiquins **26, 27**: A solution of a harmine-based carboxylic acid (0.176 mmol), DIEA (0.352 mmol), HATU (0.176 mmol) and 7-chloroquinoline-based amine (0.160 mmol) in DCM (4 mL) was stirred at rt for 18 h, and solvent evaporated. AT harmiquins **28-32**: A suspension of 7-chloroquinoline-based carboxylic acid (0.211 mmol), harmine-based amine (0.192 mmol), TEA (0.422 mmol) and T3P (0.211 mmol) in DMF (2 mL) was stirred at rt for 18 h, followed by dropwise addition of 5% NaOH. The formed precipitate was filtered off.

Crude products were purified by column chromatography, followed by trituration with diethyl ether.

2.2. *In vitro* drug sensitivity assay against erythrocytic stages of *P. falciparum*

Antiplasmodial activity was evaluated against four laboratory *P. falciparum* strains (3D7, CQ-sensitive; 7G8, CQ-resistant; Dd2 and K1, multidrug-resistant,) using the histidine-rich protein 2 assay [3].

2.3. *In vitro* cytotoxicity assay

Cytotoxicity against a human cell line (HepG2) was evaluated using the neutral red assay [3].

2.4. Inhibition of heme polymerisation

The inhibition assay of heme polymerisation was performed as previously described [4].

2.5. Computational details

The starting point of our molecular dynamics simulations was a *P. falciparum* heat shock protein 90 (PfHsp90) N-terminal domain structure obtained from the Protein Data Bank (accession code 3K60). The analysis was performed as previously described [3].

3. RESULTS AND DISCUSSION

3.1. Chemistry

A library consisting of TT and AT harmiquins was prepared. Structural diversity was achieved by derivatizing harmine's α -carboline core at 5 different positions, namely C-1, C-3, O-6, O-7 and N-9. TT harmiquins were prepared by Cu(I)-catalysed azide-alkyne cycloaddition, using the Cu(II) acetate precatalyst in methanol. On the other hand, AT harmiquins were synthesized by a simple and straightforward coupling reaction, using either HATU/DIEA or T3P/TEA.

3.2. *In vitro* evaluation of antiplasmodial activities

Harmiquins exhibited remarkable activity against the erythrocytic stage of *P. falciparum* life cycle, in nanomolar range. The results have

P41

shown that AT harmiquins and most TT harmiquins were significantly more active than the parent compound harmine and that the optimal position for the substitution of the \square -carboline ring is N-9. In general, AT harmiquins were more active than TT harmiquins against all strains of *P. falciparum* tested. Although Pf3D7 strain was the most sensitive (9/15 compounds showed activity less than 100 nM), 10/15 harmiquins exhibited higher activity than CQ against PfDd2 and 7/15 against PfK1 and Pf7G8.

3.3. *In vitro* evaluation of cytotoxicity

Screening of the cytotoxic activity of harmiquins against HepG2 was performed with the aim of evaluating their selectivity against *Plasmodium* over mammalian cells. The cytotoxicity of all compounds tested was similar, and the majority of harmiquins exhibited IC₅₀ values in the 5-20 μ M range. Since most compounds showed antimalarial activity in the nanomolar range, we concluded that harmiquins have significant selectivity against *Plasmodium*.

3.4. Possible mechanism of action

The ability of harmiquins to inhibit heme polymerization was examined *in vitro*. The results have shown that TT harmiquins significantly inhibited heme polymerisation (6/8), whereas AT harmiquins were not as effective (2/7). On the other hand, computational analysis was utilized to provide an insight into the binding of a representative set of derivatives towards PfHsp90. Calculated ΔG_{BIND} values were all exergonic, thereby indicating a favourable binding of all derivatives towards PfHsp90, which agrees with their demonstrated biological activities. Our analysis confirmed the highest activity of compound **32**, with the calculated affinity of $-38.2 \text{ kcal mol}^{-1}$, thereby demonstrating its optimal positioning within the PfHsp90 interior.

4. CONCLUSION

Here we present design and synthesis of AT and TT harmiquins, evaluation of their biological activity and possible mechanism of action. Harmiquins displayed remarkable activity against the erythrocytic life stage of CQ-sensitive, as well as CQ-resistant *Plasmodium* strains. The most active compound, AT harmiquine **32**, displayed a 5.5-fold higher activity against Pf3D7 than CQ (IC₅₀ = 2 ± 0.3

nM), at least 15.9-fold higher activity than CQ against *P. falciparum* CQ-resistant strains and had a very high selectivity index (4450). Two possible mechanisms of action, inhibition of heme polymerisation and binding to PfHsp90, might play a role in the inhibition of *Plasmodium* intraerythrocytic development.

5. REFERENCES

1. World Malaria Report 2021, World Health Organisation 2021.
2. Agrawal, S., et al., Association of a novel mutation in the *Plasmodium falciparum* chloroquine resistance transporter with decreased piperazine sensitivity, *Journal of Infectious Diseases* 2017. 216: 468–476.
3. Perković, I., et al., *Harmicines - harmine and cinnamic acid hybrids as novel antiplasmodial hits*, *European Journal of Medicinal Chemistry* 2020. 187:111927.
4. Olafson, K. N., et al., *Mechanisms of hematin crystallization and inhibition by the antimalarial drug chloroquine*, *Proceedings of the National Academy of Sciences* 2015. 112: 4946-4951.

ACKNOWLEDGMENT

The authors acknowledge the financial support by the Croatian Science Foundation (research project UIP-2017-05-5160), University of Zagreb (support for 2020), and Fundação para a Ciência e Tecnologia, Portugal (FCT) (grant 02/SAICT/2017/29550).

FORMULATION AND PERMEABILITY STUDIES OF FENUGREEK (TRIGONELLA FOENUM-GRAECUM) CONTAINING SEDDS

Dávid Sinka¹, Enikő Doma¹, Mercédesz Varga¹, Pálma Fehér¹, Liza Józsa¹, Zoltán Ujhelyi¹, Ildikó Bácskay¹

¹*Department of Pharmaceutical Technology, University of Debrecen, Hungary*

1. INTRODUCTION

Fenugreek is used as a spice and a traditional herbal medicine for a variety of purposes, given its antidiabetic and antioxidant effects. Self-emulsifying drug delivery systems (SEDDS) of herbal drugs are targets of extensive research aiming to increase bioavailability and stability. [1,2]

The study's objective was to formulate SEDDS containing *Trigonella foenum-graecum* extract to improve the stability of herbal extract and to increase their permeability through a Caco-2 monolayer.

2. MATERIALS AND METHODS

A characterized fenugreek dry extract was used for the formulations, while the SEDDS properties were examined by particle size analysis and zeta potential measurements. Permeability assays were carried out on Caco-2 cell monolayers, the integrity of which was monitored by follow-up trans-epithelial electric resistance measurements (TEER). Cytocompatibility was tested by the MTT method, and an indirect dissolution test was performed, using DPPH antioxidant reagent..

3. RESULTS AND DISCUSSION

Two different SEDDS compositions were formulated from a standardized fenugreek dry extract at either the micro- or the nanoemulsion scale with sufficient stability, enhanced bioavailability of the compounds, and sustained release from HPMC capsules.

4. CONCLUSION

Based on our results, a modern, non-toxic, cytocompatible fenugreek SEDDS formulation with high antioxidant capacity was developed in order to improve the permeability and bioavailability of all components.

5. REFERENCES

1. Snehlata, H.S.; Payal, D.R. Fenugreek (*Trigonella foenum-graecum* L.): An overview. *Int. J. Curr. Pharm. Rev. Res.* 2011, 2, 169–187.
2. Pavoni, L.; Perinelli, D.R.; Bonacucina, G.; Cespi, M.; Palmieri, G.F. An Overview of Micro- and Nanoemulsions as Vehicles for Essential Oils: Formulation, Preparation and Stability. *Nanomaterials* 2020, 10, 135.

ACKNOWLEDGMENT

Project no. TKP2021-EGA-18 has been implemented with the support provided from the National Research, Development and Innovation Fund of Hungary, financed under the TKP2021-EGA funding scheme.

SOLUBILITY ENHANCEMENT OF MEGESTROL-ACETATE VIA MICELLE AND POLYMERIC MICELLE FORMULATION

Bence Sipos¹, Ildikó Csóka¹, Piroska Szabó-Révész¹, Gábor Katona¹

¹*University of Szeged, Faculty of Pharmacy, Institute of Pharmaceutical Technology and Regulatory Affairs, Hungary*

1. INTRODUCTION

Oral drug administration faces a number of challenges, especially for drugs with poor water solubility and/or permeability. Megestrol-acetate (MGA) is characterized by these factors leading to high required dosages with lower patient adherence. By utilizing surfactant type excipients, these parameters can be optimized for the better, however choosing the proper solubilizing agent is of paramount importance. A comparison study was conducted in order to (i) investigate the processability of the micelle-forming Cremophor® RH 40 and the polymeric micelle former Soluplus® via melt technology; (ii) differentiate the structure characteristics of these two surfactant-based granules and (iii) to determine the colloidal and in vitro gastric behaviour of the micelle carrier systems [1].

2. MATERIALS AND METHODS

2.1. Materials

The carrier forming materials D-xylitol (XYL), β-D-mannitol (MAN) and polyethylene glycol 6000 (PEG 6000) were purchased from Sigma-Aldrich (Budapest, Hungary). The solubilizing agents Cremophor® RH 40 (CR 40) and Soluplus® (SP) were obtained from BASF GmbH (Ludwigshafen, Germany). Megestrol-acetate (Farmabios S. p. A., Pavia, Italy) was chosen as the model material for this experimental work. Powders for the biorelevant gastric fluids were purchased from Biorelevant.com Ltd. (London, UK).

2.2. Development of the carrier

For the preparation of the carrier, melt granulation was applied. XYL, MAN and PEG 6000 were melted together on a sand bath at 112

°C. The solubilizers were dispersed individually at this temperature. Each sample was cooled down at 80 °C and MGA was dispersed in them. Before the total solidification of the melt at 33 °C, the mass was dispersed through a sieve with a mesh size of 1.2 mm.

2.3. Solid state characterization

The thermal behaviour was investigated via differential scanning calorimetry and thermogravimetry. Crystallinity was determined by X-ray powder diffraction and granule size and distribution was measured with laser diffraction.

2.4. Micelle characterization

Micelle size and distribution was measured by dynamic light scattering. The thermodynamic solubility was determined by the oversaturation method and the solubility related parameters were calculated. Surface free energy and polarity was measured by contact angle determination.

2.5. In vitro gastric drug release study

The modified paddle method was used to examine the rate of drug release from the surfactant-free and the surfactant-containing MGA granules. Two separate dissolution media were used: fasted and fed state simulated gastric fluid. Six mathematical drug release models were fitted with the obtained cumulative drug release vs. time curves to describe the kinetics.

3. RESULTS AND DISCUSSION

3.1. Characterization of MGA in the carrier

On the DSC thermogram of crystalline MGA, the characteristic melting point at 217.95 °C can be observed, which cannot be found on the other thermograms of the granule formulations. This

supports the successful melting and dispersing of MGA in the molten carrier system. The peak around 60 °C is assigned to the melting point of PEG 6000 and the peak around 91 °C is the eutectic melt of XYL-MAN (Figure 1.)

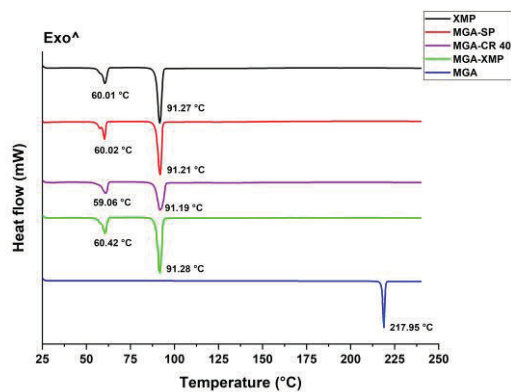


Figure 1. DSC thermograms of MGA and the granules. XMP, the carrier system; MGA – SP and MGA – CR 40, the surfactant-loaded systems; MGA – XMP, surfactant-free granule.

The diffractograms of the granules support this result, as the characteristic crystalline peak of MGA cannot be found in the granule systems (Figure 2.).

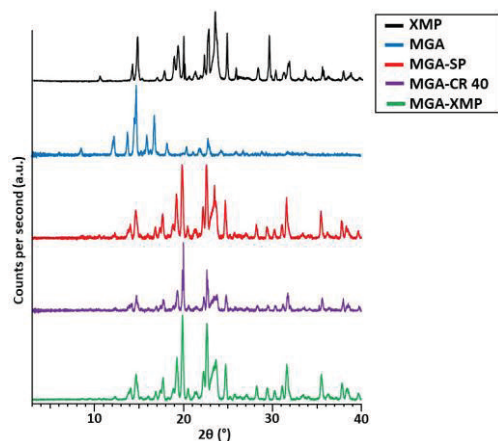


Figure 2. XRPD diffractograms of MGA and the granule systems

3.2. Micelle characterization

The MGA-SP formulation prevailed in case of successful micelle preparation with optimal nanocharacteristics. The average hydrodynamic diameter was 102.27 nm, with a distribution expressed as polydispersity index of 0.259. The monodisperse polymeric micelles had a zeta potential of -12.99 mV.

3.3. In vitro gastric release study

The proper nanoparticle characteristics contributed to higher dissolution rate both in fasted and fed state drug release media (Figure 3.). The formulation followed Higuchi kinetics which is typical for a rapid drug release system and for polymeric micelles.

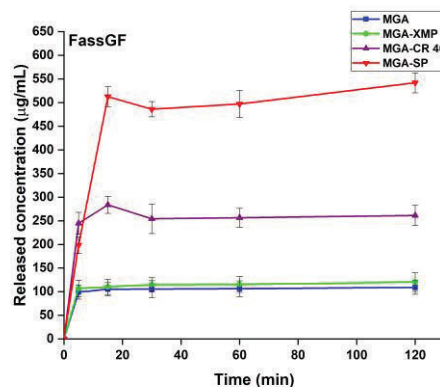


Figure 3. Example drug release curve of MGA and the granule systems in fasted state gastric drug release media. Data are presented as means \pm SD.

4. CONCLUSION

All in all, it can be concluded that the polymeric micelle forming Soluplus[®] has better potential in the enhanced drug release and delivery of MGA over classic micelle forming surfactants.

5. REFERENCES

1. G, K., et al., *Characterizing the Drug-Release Enhancement Effect of Surfactants on Megestrol-Acetate-Loaded Granules*. Pharmaceuticals, 2022. 15(2): 113

ACKNOWLEDGMENT

The work was supported the Gedeon Richter Plc. Centennial Foundation (Gyömrői 19-21, Budapest, H-1103, HU) and Project no TKP 2021 EGA 32 implemented with support provided by the Ministry of Innovation and Technology of Hungary from the National Research, Development, and Innovation Fund, financed under the TKP 2021 EGA funding scheme.

VISUALISATION OF SIMVASTATIN CORE-SHELL PARTICLES PREPARED BY ELECTROSPRAYING METHOD USING STIMULATED EMISSION DEPLETION MICROSCOPY

Barbara Sterle Zorec¹, Hana Kokot², Stane Pajk³, Janez Štrancar², Rok Dreu¹

¹*Department of Pharmaceutical Technology, Faculty of Pharmacy, University of Ljubljana, Slovenia*

²*Department of Condensed Matter Physics, Jožef Stefan Institute, Ljubljana, Slovenia*

³*Department of Pharmaceutical Chemistry, Faculty of Pharmacy, University of Ljubljana, Slovenia*

1. INTRODUCTION

In recent decades, biodegradable drug-loaded polymeric nano/microparticles have gained considerable attention in the field of drug delivery and are constantly being investigated for their efficacy in modifying drug release, improving drug solubility and/or stability [1]. The preparation of core-shell particles can further improve the above properties, making them an attractive carrier for drug loading. Various methods have been presented for the preparation of core-shell particles, but electrospraying seems to be the most promising with its numerous advantages. Electrospraying can be used to generate size-controlled, nearly monodisperse core-shell particles by optimising the process parameters and solution properties [2]. However, visualisation of such core-shell particles remains a major challenge. Scientists mainly use scanning electron microscopy (SEM) and transmission electron microscopy (TEM) to visualise core-shell particles. In contrast, stimulated emission depletion microscopy (STED) has not been used so far. STED produces images with resolution down to 20 nm by selectively deactivating fluorophores, which minimises the illumination area at the focal point and thus increases the achievable resolution for a given system, enabling the observation of structures smaller than the diffraction light limit. However, only photostable fluorescent molecules with appropriate spectral characteristics can be used for this purpose. The present study was devoted to STED visualisation of core-shell particles containing simvastatin as a poorly soluble drug prepared by the coaxial electrospraying method. For this purpose, an efficient fluorescent probe was synthesised and introduced into the shell polymer solution for subsequent STED visualisation.

2. MATERIALS AND METHODS

2.1. Materials

Polyvinylpyrrolidone (PVP, pharmaceutical grade, donation by Lek d.d.) of 50,000 daltons (PVP K30), polycaprolactone of 14000 daltons (PCL, Sigma Aldrich, USA), simvastatin (SIM, pharmaceutical grade, donation by Krka d.d.), 2-propanol (Merck KGaA, Germany), chloroform (Merck KGaA, Germany), Prolong Gold Antifade mountant (ThermoFisher Scientific), and #1.5H cover glasses (Paul Marienfeld) were used in this work. All solvents and other reagents used for UPLC analysis were of HPLC grade.

2.2. Particle preparation

Nanoparticles were fabricated by electrospraying using vertically positioned core-shell nozzle setup (Fluidnatek LE-100 apparatus; Bioinicia, Spain) at temperature of 25 ± 2 °C and relative humidity of 35 ± 2 %. Positive high voltage (8.8–13.4 kV) was applied to the nozzle while the collector was charged negatively with -3.0 kV. Drug and polymer formulation included core (PVP of 4.5% (w/V) and SIM of 7.5% (w/V) dissolved in 2-propanol) and shell (PCL of 2% (w/v) and fluorescent probe SAG38 of 0.02 mM) solution. The process parameters involved different core (0.3 – 0.6 mL/h) and shell solution flow rates (1.0 – 1.5 mL/h), while the distance of the nozzle to collector remained the same throughout all the experiments (20 cm). The particles were sprayed directly onto #1.5H cover glasses and mounted with Prolong Gold Antifade after drying.

2.5. STED microscopy

The high-resolution STED micrographs of the fluorescent core-shell particles were measured on a custom-built STED microscope (Abberior Instruments) [3] with 80 MHz pulsed lasers and a 60x water immersion objective (NA 1.2). The

fluorophores were excited at 561 nm and their emission was depleted by a STED laser at 775 nm, shaped to obtain the best possible 3D resolution. After passing through a pinhole (1.1 A.U), the emitted photons with wavelengths in the range of 580–625 nm were detected on an APD (filters by Semrock). The pixel size was 30 nm, and the dwell time and laser powers were optimised for each sample. Image Acquisition and basic analysis were performed with Inspector Software (v16.3, Abberior Instruments).

3. RESULTS AND DISCUSSION

3.1. Fluorescent probe

Fluorescent probe SAG38 (Fig. 1) is a derivative of coumarin 6. Compared to the latter, SAG38 is more lipophilic and has significantly red-shifted excitation and emission spectra with their respective maxima at 547 nm and 625 nm. Importantly the emission of SAG38 at 775 nm is large enough to be successfully depleted by the 775 nm STED laser, and the probe is very photostable, making it ideal for STED microscopy.

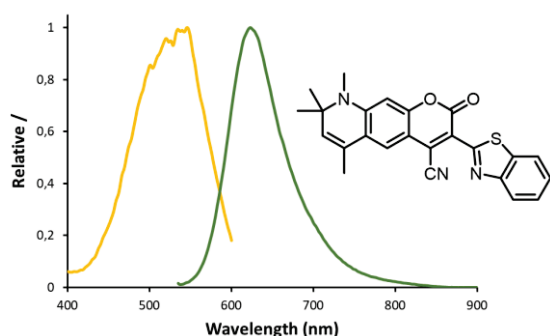


Figure 1. Left: excitation (yellow) and emission (green) spectra of SAG38. Right: structure of SAG38.

3.2. Particle visualisation and morphology

The concentration of the fluorescent probe in the shell solution was very important and influenced the intensity of the final microscopic images. The probe concentration varied, with 0.02 mM being the most optimal.

Core-shell particles were prepared, varying the flow ratio between core and shell solution to obtain particles whose core components are completely encased in shell polymer. At the same time, the flow rates were also varied according to the process stability to get a nicely stable Taylor cone. A look at Figure 2 shows that the particle shell is not complete when the

shell flow rate is too low (Fig. 2a). However, if the shell flow rate is increased sufficiently, a completed shell can be observed that completely encases the core components (Fig. 2b). Further increasing the flow rate of the shell solution resulted in shrinkage of the core (Fig. 2c) and numerous particles containing only the shell polymer (Fig. 2d). The flow rate that proved to be optimal was 0.3 ml/h for the core and 1.2 ml/h for the shell.

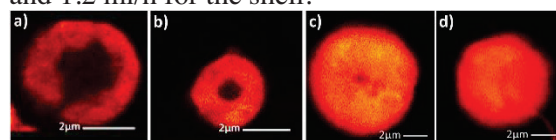


Figure 2. Typical super-resolution STED micrographs of core-shell particles containing fluorescent probe in shell solution. The flow ratio between the core and shell solution decreases from left to right.

4. CONCLUSION

The results presented show that STED microscopy is an important alternative for visualisation of core-shell particles, where the addition of a suitable fluorescent probe in the shell at the right concentration is crucial. To achieve that the shell completely envelops the core of the particle, the flow rate between the two is of great importance.

5. REFERENCES

2. Kumar, B., et al., *Recent advance in nanoparticles-mediated drug delivery*. Journal of drug delivery science and technology, 2017. Volume 41: p. 260-268.
3. Sterle Zorec, B. et. al., *Particle properties and drug metastable solubility of simvastatin containing PVP matrix particles prepared by electrospraying technique*. European Journal of Pharmaceutical Sciences, 2021. Vol.158:p.1-10.
4. Kokot, H. et. al., *Prediction of Chronic Inflammation for Inhaled Particles: the Impact of Material Cycling and Quarantining in the Lung Epithelium*. Adv. Mater. 2020, 32.

ACKNOWLEDGMENT

The authors gratefully acknowledge the financial support provided by the Slovenian Research Agency (Program P1-0189).

ELECTROSPUN NANOFIBERS AS A DELIVERY SYSTEM FOR VAGINAL PROBIOTICS

Spase Stojanov^{1,2}, Tina Vida Plavec^{1,2}, Julijana Kristl², Špela Zupančič², Aleš Berlec^{1,2}

¹Department of Biotechnology, Jožef Stefan Institute, Slovenia

²Faculty of Pharmacy, University of Ljubljana, Slovenia

1. INTRODUCTION

The female vagina is dominated by species of the genus *Lactobacillus*. A decrease in their numbers allows overgrowth of opportunistic pathogens, leading to vaginal infections. The use of vaginal lactobacilli as probiotics can restore the disturbed vaginal microbiota and stop the development of the infections. The lack of a proper delivery system and techniques to study the functionality of lactobacilli hinders their use as probiotics. Nanofibers, produced by electrospinning, are a promising delivery system for biological drugs [1] and vaginal lactobacilli [2, 3]. Electrospinning is a technique in which a high voltage is applied to a polymer solution, resulting in elongation of the polymer and evaporation of the solvent [4]. The aim of our study was to address two major limitations of vaginal probiotics, namely, development of a solid nanofiber delivery system for local administration, and techniques for the studies of probiotic release and distribution. We studied three vaginal lactobacilli (*L. crispatus*, *L. gasseri* and *L. jensenii*) and *L. plantarum* as a control. For the first part of our research we genetically engineered the four species to express fluorescent proteins with different spectral properties (IRFP, GFP, mCherry and mTagBFP2) and incorporated them into polyethylene oxide (PEO) nanofibers [2]. In the second part, we tested the stability of non-transformed vaginal lactobacilli in three different polymer solutions: PEO, PEO/alginate and PEO/alginate/sucrose. The three formulations were used to prepare nanofibers with incorporated lactobacilli. Viability tests

were performed immediately after electrospinning and after 56 days of storage.

2. MATERIALS AND METHODS

2.1. Electrospinning of lactobacilli

Lactobacilli (10^{10} - 10^{14} CFU/ml) were mixed with different polymer solution (PEO, PEO/alginate and PEO/alginate/sucrose) and filled into 5 mL syringe attached to an electrospinning machine. The flow rate of the polymer dispersion was 150-250 μ l/h and the applied voltage was 10-13 kV. The nanofibers were collected on aluminium foil.

2.2. Genetic engineering of lactobacilli

Four genes encoding fluorescent proteins with different spectral properties, e.g. IRFP, GFP, mCherry and mTagBFP2, were cloned under the control of the *ldh* promoter and inserted into the pNZ8418 plasmid. The four plasmids were then loaded into lactobacilli using cell wall weakening agents and different electroporation protocols [2].

2.3. Viability assays

The viability of lactobacilli was analysed in polymer solutions, in nanofibers immediately after electrospinning and after storage (56 days). Series of ten-fold dilutions of bacteria-polymer dispersions and dissolved nanofibers loaded with bacteria were prepared. Bacterial viability was tested using the drop plate method [5], whereby 10 μ L drops of each dilution were pipetted onto MRS agar plates and incubated anaerobically at 37 °C for 2-3 days.

3. RESULTS AND DISCUSSION

3.1. Nanofiber morphology

Incorporation of lactobacilli into nanofibers was confirmed by scanning electron (Fig. 1) and confocal microscope. Incorporation was observed with specific thickenings in the nanofibers. Incorporated lactobacilli and addition of excipients changed the mean diameter of the nanofibers.

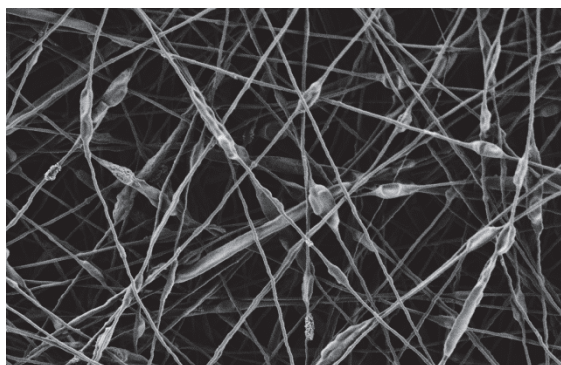


Figure 1. Scanning electron microscope of a mixture of four lactobacilli incorporated into PEO nanofibers.

3.2. Fluorescent detection of lactobacilli after their release from nanofibers

Lactobacilli retained their fluorescence after release from the nanofibers. Fluorescence signals depended on species, with *L. plantarum* demonstrating the highest fluorescence and *L. crispatus* the lowest. Fluorescent proteins were used to distinguish lactobacilli in a mixture and for studying individual lactobacilli distribution.

3.3. Viability of lactobacilli in different polymer and nanofiber formulations

Lower temperatures (4 °C) and the addition of sucrose to the polymers improved the viability of the lactobacilli. Bacterial viability in polymer solution reflected the stability of bacteria during electrospinning. Sucrose also protected *L. crispatus* and *L. jensenii* during electrospinning and *L. gasseri* and *L. jensenii* during storage. The protective effect of sucrose might be related to its interaction with the bacterial proteins, as we showed using DSC and FTIR methods. All lactobacilli species in all formulations showed

some viability after 56 days. *L. gasseri* showed the highest viability, followed by *L. jensenii* and *L. crispatus*.

4. CONCLUSION

In this research, we provide two solutions for higher applicability of vaginal probiotics. We have shown that electrospun nanofibers are a suitable delivery system for vaginal probiotics that can preserve bacterial viability. Fluorescent proteins enable easy and real-time tracking of bacteria after their release. With this study we contribute to the development of novel medicine against vaginal infections.

5. REFERENCES

1. Stojanov, S., et al., *Electrospun nanofibers as carriers of microorganisms, stem cells, proteins, and nucleic acids in therapeutic and other applications*. *Frontiers in bioengineering and biotechnology*, 2020. 8: 130.
2. Stojanov, S., et al., *Engineering of vaginal lactobacilli to express fluorescent proteins enables the analysis of their mixture in nanofibers*. *International journal of molecular sciences*, 2021. 22(24): 13631.
3. Silva, J.A., et al., *Immobilization of vaginal Lactobacillus in polymeric nanofibers for its incorporation in vaginal probiotic products*. *European journal of pharmaceutical sciences*, 2021. 105563.
4. Pelipenko, J., et al., *Critical attributes of nanofibers: preparation, drug loading, and tissue regeneration*. *International journal of pharmaceutics*, 2015. 484 (1): 57-74.
5. Herigstad, B., et al., *How to optimize the drop plate method for enumerating bacteria*. *Journal of microbiological methods*, 2001.44(2):121-129.

ACKNOWLEDGMENT

Slovenian Research Agency (grants N3-0184, P1-0189 and P4-0127) and Public Scholarship, Development, Disability and Maintenance Fund of the Republic of Slovenia – Ad Futura for S.S.

EVALUATION OF DEXAMETHASONE CONTAINING *IN SITU* GELLING MUCOADHESIVE EYE DROPS

Boglárika Szalai¹, Mária Budai-Szűcs¹, Orsolya Jójárt-Laczkovich¹

¹*Institute of Pharmaceutical Technology and Regulatory Affairs, University of Szeged, Hungary*

1. INTRODUCTION

Eye drops are commonly used for the treatment of ocular diseases. The complex elimination mechanisms of the eye cause poor bioavailability of this route of administration. Dexamethasone (DXM) is frequently used to treat non-infectious inflammatory ocular diseases. The low water-solubility and penetration ability of dexamethasone decrease its biological effectiveness. This work aims to formulate *in situ* gel-forming mucoadhesive eye drops containing dexamethasone-cyclodextrin inclusion complex to improve the residence time and the solubility of the active pharmaceutical ingredient (API).

2. MATERIALS AND METHODS

2.1. Materials

For the complexation of DXM (2 - hydroxypropyl)- β -cyclodextrin (DS~4.5; HPBCD) was chosen. The lowest necessary amount of HPBCD was applied to solubilize the therapeutic concentration of DXM. Poloxamer 407 (P407) was used to form thermosensitive *in situ* gelling eye drops, and 2 mucoadhesive polymers were combined with it. The concentration of the 3 polymers was investigated on 3 levels.

2.2. Rheological studies

Rheological studies were carried out to investigate the gelling properties of the gels: gelling temperature and gelling time were measured.

2.3. Tensile test

Mucoadhesivity of the eye drops were examined with a texture analyzer applying a mucoadhesion test rig. A mucin covered surface was used to imitate the surface of the eye.

Adhesive force and work of adhesion were determined based on the force-distance curves.

2.4. *In vitro* drug release study

The dialysis sac method [1] was used to investigate the *in vitro* drug release of the formulations. The studies were carried out at 35°C, the release medium was simulated tear fluid. The released amount of DXM was measured by HPLC method. DXM suspension and DXM-HPBCD solution were used as reference preparations.

3. RESULTS AND DISCUSSION

3.1. Rheological studies

The gelling temperature and the gelling time of the samples ranged from 23 to 37°C and from 0 to 7 min., respectively. Both parameters were determined by the concentration of P407: increasing the P407 concentration decreased the gelling temperature and the gelling time. Formulations with a gelling temperature above room temperature but under body temperature and with rapid gelation are desired.

3.2. Tensile test

Depending on the composition of the formulations the adhesive force and work of adhesion values were between 800 and 2100 mN and 40 and 130 mN.mm, respectively. Most of the formulations exhibited adequate mucoadhesive properties.

3.3. *In vitro* drug release study

During the investigation, DXM was completely released from the DXM-HPBCD solution while only about 51% of the API was released from the suspension. Regarding the *in situ* gels, the released amount of DXM was higher compared to the suspension; moreover, the dissolution wasn't complete after 6 h. The dissolution

P46

curves suggested that more API might have dissolved over a longer period.

4. CONCLUSION

We managed to formulate *in situ* gelling mucoadhesive eye drops containing DXM-HPBCD inclusion complex. The complexation ensured the dissolution of the therapeutic concentration of DXM in the formulations. The eye drops had proper gelling properties: the gelling temperature was neither too low nor too high, also the sol-gel transition was rapid enough not to be washed away easily. Satisfying mucoadhesivity was achieved by adding mucoadhesive polymers to the formulations. The gels displayed better *in vitro* drug release properties than the DXM suspension while providing prolonged dissolution.

These results may be promising in formulating ocular *in situ* gels with prolonged residence time due to their mucoadhesive properties, thus increasing the bioavailability of eye drops.

5. REFERENCES

1. Kiss, E. L., et al., *Development and Characterization of Potential Ocular Mucoadhesive Nano Lipid Carriers Using Full Factorial Design*. *Pharmaceutics*, 2020. 12(7): 682.

ACKNOWLEDGMENT

Project no. TKP2021-EGA-32 has been implemented with the support provided by the Ministry of Innovation and Technology of Hungary from the National Research, Development and Innovation Fund, financed under the TKP2021-EGA funding scheme.

SOLUBILITY ASSESSMENT OF CANNABIDIOL IN DIFFERENT SOLVENTS

Eva Tavčar¹¹The Department of Pharmaceutical Biology, University of Ljubljana, Faculty for Pharmacy, Slovenia

1. INTRODUCTION

Cannabidiol (CBD) is a cannabinoid, naturally occurring in cannabis (*Cannabis sativa*, L.). It exhibits pharmacological effects on vertebrates by acting on cannabinoid receptors, without causing mental impairment [1]. Over the last ten years, the use and recognition of CBD have increased significantly among the general public. Apart from being an active pharmaceutical ingredient in medicines, such as Epidyolex[®], Sativex[®], and magistral preparations, CBD is being increasingly used in food supplements and cosmetic products [2]. Nevertheless, there is little data in the literature describing its technological properties. Therefore, we researched the solubility of CBD in the solvents that are most important for its pharmaceutical use.

2. MATERIALS AND METHODS

2.1. Materials

Cannabidiol isolate of 98,62 % purity (Dr. Ehrenstorfer, Germany).

Solvents of p.a. purity: Propylene glycol, triethyl citrate, PEG 400, triacetin, ethanol, methanol, isooctane, acetone, isopropanol, DMSO, 1-butanol, dimethylformamide, cyclohexane, dichloromethane, diethyl ether. Oils, purchased as food products: Medium-chain triglycerides, hemp seed oil, olive oil, and chia seed oil.

Solvents for HPLC analysis of HPLC purity: acetonitrile, water, and trifluoroacetic acid.

2.2. Solubility

Solubility was determined by using the shake-flask method. Firstly, CBD suspensions were prepared (at room temperature), then shaken for 48 h on a shaker, filtered, and diluted.

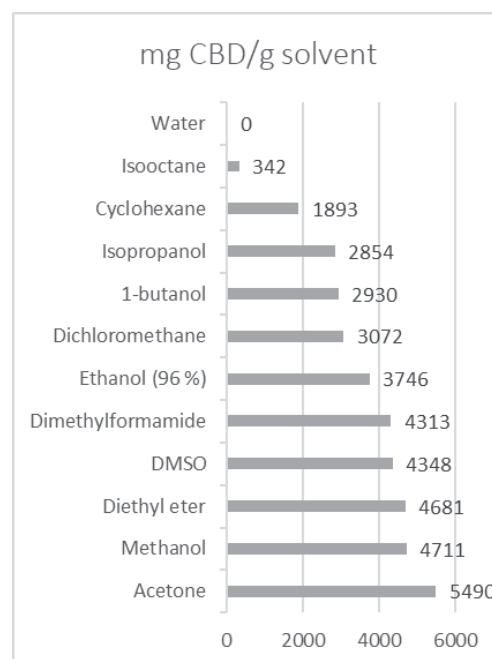
2.3. HPLC analysis

CBD concentration was determined by the HPLC method, using the Phenomenex Kinetex C18 column (100 mm/4,6 mm/2.7 μ m) and HPLC system Shimadzu, Kyoto, Japan (DGU-20As, LC-20AD XR, SIL-20AC XR, CTO-20AC, SPD-M20A). Mobile phase A was water with 2 % acetonitrile and 0.1 % trifluoroacetic acid. Mobile phase B consisted of acetonitrile with 2 % water and 0.1 % trifluoroacetic acid. The gradient started with 44 % B, rising to 100 % during the following 10 minutes with a flow rate of 2 mL/min at 40 °C. The injection volume was 5 μ L. The analytes were detected at 220 nm.

3. RESULTS AND DISCUSSION

3.1. Solubility of CBD in laboratory solvents

Measured solubility was highest in acetone, methanol, and diethyl ether, followed by other laboratory solvents. Solubility in water was not observed within the limits of detection (Fig. 1).



P47

Figure 1. Solubility of CBD in laboratory solvents.

3.2. Solubility of CBD in pharmaceutical solvents

CBD was also very soluble in the solvents that are often used for the production of CBD products. Among them, solubility was highest in triacetin, PEG 400, and triethyl citrate. It was slightly worse in propylene glycol. By adding water to propylene glycol, we discovered that even a small addition of water greatly reduces the solubility of CBD (Fig. 2).

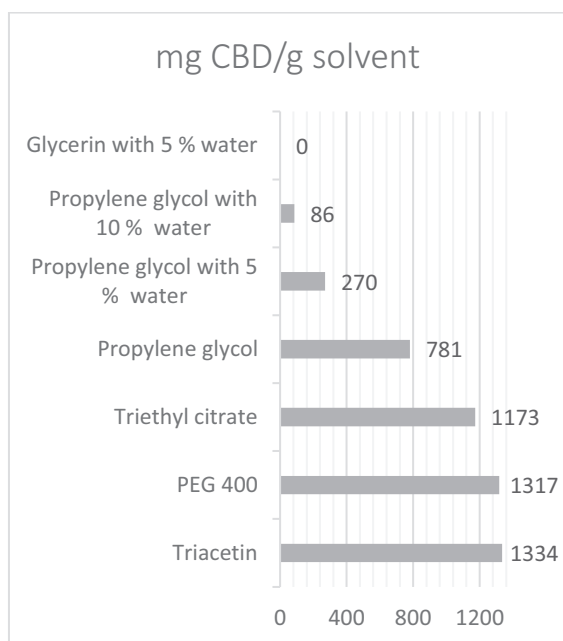


Figure 2. Solubility of CBD in pharmaceutical solvents.

3.3. Solubility in vegetable oils

Among vegetable oils, CBD was most soluble in MCT oil and least soluble in olive oil. This indicates that the longer the triglyceride chain of the oil, the poorer is CBD solubility (Fig. 3).

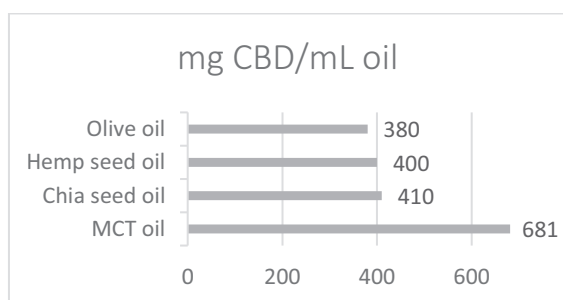


Figure 3. Solubility of CBD in vegetable oils.

4. CONCLUSION

The best laboratory solvent for CBD is acetone, following methanol. Among edible pharmaceutical solvents, CBD is well soluble in triacetin, PEG 400, triethyl citrate, and propylene glycol, following edible oils. CBD is not soluble in water and even small addition of water has a great impact on its solubility in other solvents.

5. REFERENCES

1. Bonini S. A. et al.: *Cannabis sativa: A comprehensive ethnopharmacological review of a medicinal plant with a long history*. Journal of Ethnopharmacology 2018; 227: 300-315.
2. Francke N. M. et al.: *Formulation of Cannabidiol in Colloidal Lipid Carriers*, Molecules 2021, 26.

DEVELOPMENT OF CHITOSAN AND ALGINATE BASED NANOFIBERS FOR WOUND HEALING APPLICATION

Biljana Temova^{1,2}, Betka Krampelj², Petra Kocbek²

¹Agency for Medicinal Products and Medical Devices of the Republic of Slovenia (JAZMP), Ljubljana, Slovenia

²Department of Pharmaceutical Technology, Faculty of Pharmacy, University of Ljubljana, Slovenia

1. INTRODUCTION

The primary goal of innovative wound healing is to create conditions that enable a fast formation of healthy tissue by stimulation of the normal restoration processes. Novel approaches are thus evolving in the field of advanced therapeutical medicinal products. The preparation of such medicines involves isolation of allogeneic or autologous cells, their proliferation *in vitro* and seeding on/in a biocompatible three-dimensional matrix, which provides physical support to cells. Nanofibers have attracted significant interest in the preparation of such scaffolds, since they can serve as a drug delivery system for different bioactive molecules [1], mimic the structural building blocks of the natural extracellular matrix and provide a suitable microenvironment for cell adhesion, growth, and proliferation [2]. To achieve this nanofiber morphology should be stable in wet tissue environment. Thus, the aim of our study was development of such nanofibers. Chitosan (CS) and alginate (ALG) were selected as polymer matrix formers, since they are biocompatible, non-toxic, natural polymers with adequate water absorption and poly(ethylene oxide) (PEO) was added to improve the spinnability of polymer solutions. To increase the water stability of nanofibers calcium ions were added to the ALG/PEO, which have cross-linked ALG polymer chains.

2. MATERIALS AND METHODS

2.2. Preparation of polymer solutions

The polymer solutions (Table I) were prepared just prior electrospinning. CS and PEO were dissolved in 3% (v/v) acetic acid and Triton X-100 (0.3%, w/v) was added. ALG and PEO were dissolved in purified water and Triton X-100 (0.3%, w/v) or CaCl₂ (0.5-2.0%, w/w_{ALG}) was added before electrospinning.

Table 1: The composition of polymer solutions: CS/PEO 400 kDa (A), CS/PEO 900 kDa (B),

CS/PEO 2000 kDa (C), ALG/PEO 2000 kDa (D), and ALG/PEO 2000 kDa with CaCl₂ (E)

Weight ratio % (w/v)	90/10	80/20	70/30	60/40	50/50	40/60	30/70
2.0					E*		
2.5		C	C	A, B, C, E**			
3.0			C	B, C	B, C	A, B, C	B
3.2					D, E***		
3.5					B, C	A, B, C	
4.0	D	D	D	D	B, D	A, C	
4.5				D	D		

* with 0.7% and 2.0% (w/w) CaCl₂; **with 0.5%, 1.2% and 1.5% (w/w) CaCl₂; ***with 0.5%, 0.9%, 1.2% and 1.5% (w/w) CaCl₂

2.3. Electrospinning

Fluidnatek LE-100 (Bioinicia, Valencia, Spain) was used for nanofiber preparation. A 10 mL syringe was fitted with a metal needle 0.7 mm in diameter. The distance to the collector was fixed to 15 cm for CS/PEO and to 20 cm for ALG/PEO solutions. The pump rate was set to 100-800 μ L/h. A voltage was varied from 10 kV to 25 kV. All nanofibers were electrospun at 37 \pm 2 $^{\circ}$ C and RH of 16 \pm 2 %.

2.4. Characterization of nanofibers

The morphology of the electrospun products was analyzed using scanning electron microscopy (SEM) (Supra35 VP; Carl Zeiss, Oberkochen, Germany). The mean diameters of selected nanofibers were determined based on a representative SEM images using the ImageJ 1.53k software (NIH, USA).

The nanofibers were electrospun onto glass coverslips for evaluation of their stability in water. The coverslips with nanofibers were then soaked in 20 mL of purified water. Changes in their morphology were examined under an inverted light microscope 1 h, 24 h and 48 h since the beginning of the experiment.

3. RESULTS AND DISCUSSION

The focus of our work was to develop hydrophilic nanofibers, stable in aqueous environment, as a novel drug delivery system

for bioactive molecules for wound healing. A variety of polymer solutions based on CS and ALG was thus prepared and electrospun to investigate their spinnability and formation of nanofibrillar product.

3.1. Chitosan/PEO nanofibers

CS/PEO nanofibers were prepared from polymer solutions containing polymers in weight ratios 60/40, 50/50, 40/60 and 30/70, respectively. The total polymer concentration was 3.0%-4.0% (w/v) in the case of PEO 400 kDa and PEO 900 kDa and 3.0%-3.5% (w/v) in the case of PEO 2000 kDa. The diameters of the selected electrospun nanofibers are presented in Table 2. SEM image of nanofibers prepared from 3.0% (w/v) CS/PEO 2000 kDa (40/60) solution with Triton X-100 shows smooth nanofibrillar morphology, without any beads (Figure 1A). The persistence of nanofibers morphology in water correlated with the amount of CS in the polymer solution. The fibrillar morphology of CS/PEO 2000 kDa (40/60) nanofibers was preserved during 48 h incubation in water, indicating their potential for wound healing application.

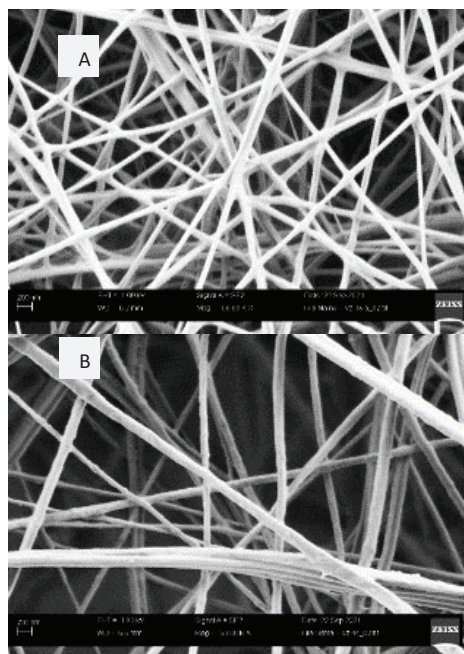


Figure 1. Representative SEM image of (A) CS/PEO and (B) ALG/PEO nanofibers.

3.2. Alginate/PEO nanofibers

ALG/PEO 2000 kDa nanofibers were prepared from polymer solutions containing polymer in weight ratios 80/20, 70/30, 60/40 and 50/50, respectively. The total polymer concentration was 2.0-4.5% (w/v). The diameters of selected nanofibers are presented in Table 2. The

morphology of nanofibers prepared from 4.0% (w/v) ALG/PEO (70/30) solution with Triton X-100 is shown in Figure 1B. The crosslinked ALG/PEO nanofibers were more stable in water than ALG/PEO nanofibers, however their morphology was not preserved during 24 h incubation. This indicates that 2.0% (w/w) CaCl₂ in polymer solution did not enable formation of nanofibers sufficiently resistant to aqueous environment and further research with higher concentrations of CaCl₂ is thus needed.

Table 2: Average diameters of CS/PEO and ALG/PEO nanofibers.

% (w/v)	Composition	Weight ratio	Diameter (nm)
3.0	CS/PEO (900 kDa) + Triton X-100	60/40	111
3.0	CS/PEO (900 kDa)	30/70	81
3.0	CS/PEO (2000 kDa) + Triton X-100	40/60	111
4.0	ALG/PEO (2000 kDa)	70/30	192
4.0	ALG/PEO (2000 kDa) + Triton X-100	70/30	147
4.0	ALG/PEO (2000 kDa)	50/50	281
4.5	ALG/PEO (2000 kDa)	50/50	235
4.5	ALG/PEO (2000 kDa) + Triton X-100	50/50	193

4. CONCLUSION

CS/PEO and ALG/PEO nanofibers were successfully electrospun. CS/PEO 2000 kDa (40/60) nanofibers showed preserved morphology (48 h) in aqueous environment, but morphology of ALG/PEO nanofibers with CaCl₂ was not preserved, thus their composition should be further optimized for potential application in wound healing.

5. REFERENCES

- Bertoncelj V., et. al., *Development and bioevaluation of nanofibers with blood-derived growth factors for dermal wound healing*. European Journal of Pharmaceutics and Biopharmaceutics, 2014. 88 (1): 64-74.
- Lee V. K., et. al., *Design and fabrication of human skin by three-dimensional bioprinting*. Tissue Engineering. Part C, Methods, 2014. 20 (6): 473-84.

ACKNOWLEDGMENT

The authors gratefully acknowledge the financial support provided by the Slovenian Research Agency (Program Codes P1-0420 and P1-0189) and JAZMP.

APPLICATION OF SUPPORT VECTOR MACHINE LEARNING FOR ORODISPERSIBLE FILMS DISINTEGRATION TIME PREDICTION

Erna Turković, Ivana Vasiljević, Dragana Vasiljević, Svetlana Ibrić, Jelena Parojčić

Department of Pharmaceutical Technology and Cosmetology, University of Belgrade – Faculty of Pharmacy, Serbia

1. INTRODUCTION

Orodispersible films (ODF) have emerged as innovative dosage forms that provide wide variety of advantages for patients and manufacturers over conventional dosage forms. The prominent characteristic of ODFs is fast disintegration followed by good patients acceptability [1]. Therefore, relevant disintegration time (DT) is usually considered as ODF critical quality attribute. Extensive research on ODFs is generating a lot of data, but lack of standardization is the main obstacle that limits their comparative evaluation. The following work aims to explore literature data on ODFs characteristics using the predictive data-classification algorithm Support vector machine (SVM) and assess its applicability in pharmaceutical development based on the set of experimentally obtained data.

2. MATERIALS AND METHODS

2.1. Materials

Hydroxypropyl cellulose (Klucel GF, Ashland, USA), ethanol ($\geq 99.8\%$, Honeywell, Charlotte, NC, USA) and glycerol, 85% (w/w) (Ph. Eur.) were used for preparation of printing and casting dispersion.

2.2. Data pre-processing

Comprehensive data exploration has been conducted in the PubMed database using most common synonyms for ODFs with fifteen synonyms in singular and plural. Built database had following attributes: manufacturing approach, polymer selection, polymer molecular weight (KDa), polymer load (%), mechanical properties (tensile strength (MPa), Young's modulus (MPa), elongation at break (%)), disintegration method and disintegration time (DT) (s).

2.3. ODF preparation and characterisation

Polymer dispersions for solvent casting and semi-solid extrusion 3D printing were prepared

by dispersing HPC in ethanol:glycerol solution followed by continuous stirring on the magnetic stirrer. Prepared dispersions were: (i) casted on a unit-dose plexiglas plates, or (ii) printed using Ultimaker 2+ (Ultimaker, , Netherlands). ODFs were characterized in terms of mechanical properties using Z-LX Table-Top Testing Machine (Shimadzu, Japan) and DT using adapted compendial tester (Erweka ZT52, Germany) with a weight.

3. RESULTS AND DISCUSSION

3.1. Data pre-processing

274 papers (without reviews) were identified via search, of which 112 were included in the database.

Table 1. Classification of disintegration testing and manufacturing methods

Disintegration testing methods	Manufacturing methods
Compendial method for solid dosage forms – 1	Solvent casting – 1
Adapted compendial method (with clamp/frame) – 2	Inkjet printing – 2
Adapted compendial method (with clamp/frame and weight) – 3	3D printing – 3
Drop method / Slide frame method (without weight) – 4	Electrospinning – 4
Drop method / Slide frame method (with weight) – 5	Hot-melt extrusion – 5
Petri dish / Beaker / Glass vial method (with agitation) – 6	
Petri dish / Beaker / Glass vial method (without agitation) – 7	
Other – 8	

Nominal data from literature was transformed into numerical, using coding operator so that each nominal data had corresponding numerical value. Critical attributes for films fast disintegration were derived. 18 polymers were included as categorical data and were further differentiated on the basis of molecular weight. Values for most commonly evaluated mechanical properties were included as

numerical data. Different DT methods were classified in seven classes (Table 1), while the manufacturing methods were classified in five classes. RapidMiner Studio 9.10 (RapidMiner, Dortmund, Germany) was used to transform data and employ SMV algorithm.

3.2. SVM model prediction

Attributes with the highest weight were polymer load and DT method employed (Figure 1). The polymer type and characteristic did have conclusive effects on DT as their weight varied during data mining. This can be attributed to inconclusive data provided in papers and lot of missing values for those attributes. Mechanical properties had low weight, which can be explained with the broad value range for those attributes. Different research groups had different approach to disintegration testing, which lowered model precision as it was reported that SVM does not have high accuracy when data is imbalanced [3]. Relative error value was 20%, which can be considered as high, but, having in mind great diversity in presented data and methodology, obtained value is still acceptable for the pilot study.

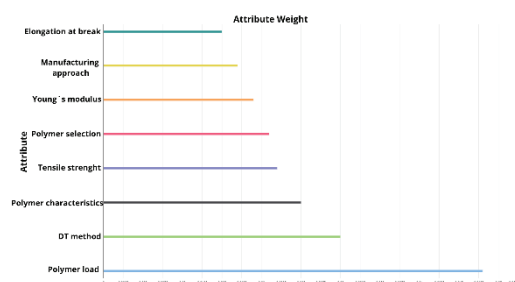


Figure 1. Attribute weight in predicting model

3.3. Experimental validation

HPC-based films prepared by 3D printing had tensile strength, elongation at break and Young's modulus of 3.5 MPa, 137% and 5 MPa, respectively. Average DT was 69 s. For casted films, relevant values were 3.4 MPa, 105% and 3 MPa, and DT was 27 s. Experimentally obtained results were entered into model simulator (Figure 2) to simulate situation reflecting the experimental set up in which HPC-based films were prepared by 3D printing and solvent casting, and relevant attribute values obtained by samples characterization. In the case were manufacturing method was set to be 3D printing (coded as 1) predicted DT value was close to experimentally obtained value, i.e. 71.7 and 69 s, respectively.

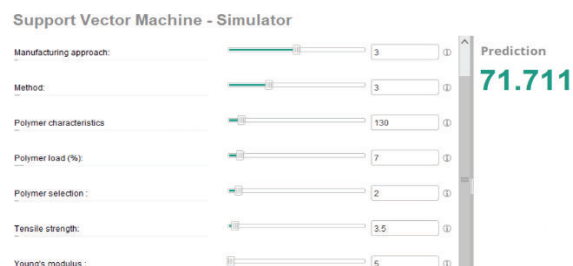


Figure 2. Model simulator used to predict DT of 3D printed HPC-based films

When solvent casting method was considered, predicted DT value was remarkably higher than the experimentally obtained one, indicating bad predictability. It might be assumed that good predictability obtained in the case of 3D printed films is associated with lower data variability due to more simple sample composition and robust preparation method. In the case of casted films, data was much more complex due to a higher number of research papers and approaches to characterisation.

4. CONCLUSION

The obtained results indicate that SVM algorithm can be employed to predict ODF DT value based on the dataset created using literature data. However, in order to obtain meaningful predictions, larger dataset, with fewer inconsistencies and less missing values would be advantageous.

5. REFERENCES

1. Scarpa, M., et al., *Key acceptability attributes of orodispersible films*. European Journal of Pharmaceutics and Biopharmaceutics, 2018, 125: 131-140.
2. Preis, M., et al., *Comparative study on novel test systems to determine disintegration time of orodispersible films*. Journal of Pharmacy and Pharmacology, 2014, 66: 1102-1111.
3. Wu, G and Chang, E.Y. *Adaptive feature-space conformal transformation for imbalanced-data learning*. Proceedings of the 20th ICML, Washington DC, 2003. 816-823.

ACKNOWLEDGMENT

This work was financially supported by the Ministry of Education, Science and Technological Development of the Republic of Serbia (project 451-03-68/2022-14/200161).

DEVELOPMENT OF A PREPARATION METHOD FOR NANOCAPSULES USING FACTORIAL DESIGN

Luca Éva Uhljar¹, Balázs Kürtösi¹, Rita Ambrus¹

¹*Institute of Pharmaceutical Technology and Regulatory Affairs, University of Szeged, Hungary*

1. INTRODUCTION

In the production of medicines, particular attention should be paid to the quality of the product. For this reason, FDA proposes the use of Quality by design (QbD), a process that allows quality to be built into medicines [1]. As part of the QbD, the Critical Quality Attributes and Critical Process Parameters are determined in order to define the Design Space of the production. Factorial design is a research methodology, also used in QbD, that allows us to obtain reliable results and correlations from a smaller number of experiments.

Nowadays, nano-drug delivery systems have become prominent. Polymer nanocapsules (NCs) are innovative drug delivery systems that are composed of an oil-filled core and a biodegradable polymer shell. NCs have several advantages, such as increased drug stability, solubility and permeability, and reduced toxicity, as well as tailored therapy through controllable drug release. NCs can be formulated mainly for alternative administration routes, e.g., topical, parenteral, nasal and pulmonary.

NCs can be produced in several ways, of which solvent displacement method is a simple three-step process. In the first step, a nanoemulsion of the oil and aqueous phases is formed by continuous mixing. In the second step, the nanoemulsion droplets are coated with the shell-forming polymer, also by dripping and continuous mixing. The third step is the purification of the NCs by ultracentrifuge. The properties of the NCs (e.g., size, size distribution, stability) can be controlled by varying the preparation parameters. By choosing the appropriate parameters, NCs with optimal properties can be produced.

The aim of the present research was to prepare NCs incorporating diverse active pharmaceutical ingredients (API) by solvent displacement method while specifying the optimal ranges of preparation parameters, thus facilitating the creation of a future Design Space.

2. MATERIALS AND METHODS

2.1. Materials

The drugs tested were lamotrigine, ciprofloxacin, and propranolol. The adjuvants forming the core of the NCs were PEG-stearate-40, Transcutol, and oleic acid, while the shell was made up of chitosan. The aqueous phase was ultra-purified water.

2.3. Preparation of the nanocapsules

One of the criteria for factorial experiment design is to have measurable and controllable production parameters. For this purpose, continuous mixing was ensured by a magnet stirrer with digital display. The oil phase and after the polymer solution were dripped through a needle into the aqueous phase via a peristaltic pump with adjustable flow rate.

2.2. Setting up a factorial design

As part of the QbD, the Critical Quality Attributes and Critical Process Parameters that determine the quality of NCs have been collected and systematized in an Ishikawa-diagram during a previous work of our research group [2]. In this work, the process parameters affecting product quality were the mixing rate (rpm), the flow rate (mL/min) of the oil phase, and the diameter of the needle (G). For the factorial design, we chose these parameters as independent variables and then varied them at three levels, setting up an 3^{3-1} factorial design (Table 1).

P50

The most important characteristics of NCs are particle size and size distribution (PdI), which can be measured by dynamic light scattering (DLS), and stability, which can be determined from the surface charge (Zeta potential). Therefore, these properties were chosen as the dependent variables in the factorial design.

Table 1. Independent variables of the 3³⁻¹ factorial design

mixing speed (rpm)	flow rate (mL/min)	diameter of the needle (G)
200	0.35	18
200	1.06	23
200	1.76	20
850	0.35	18
850	1.06	20
850	1.76	23
1500	0.35	20
1500	1.06	18
1500	1.76	23

3. RESULTS AND DISCUSSION

NCs containing lamotrigine, ciprofloxacin and propranolol were prepared and examined according to the 3³⁻¹ factorial design. To ensure that the concentration of the API would not influence the results, NCs were prepared using 2 mg/mL solutions of all three APIs.

For critical properties, the acceptance criteria were set to a maximum of 400 nm for size, 0.2 for PdI, and a minimum of 5 mV for Zeta potential (Fig.1).

The encapsulation of lamotrigine and ciprofloxacin resulted in a product with satisfactory properties over almost the entire range of the chosen adjustment parameters. Overall, a higher mixing rate is recommended. This is also recommended for propranolol, but even so, a homogeneous particle size distribution cannot be ensured.

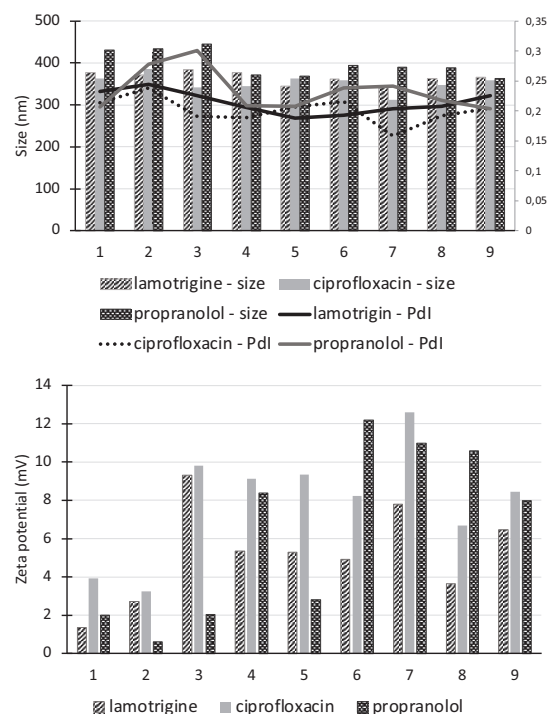


Figure 1. Investigated properties of the NC samples

4. CONCLUSION

NCs containing lamotrigine, ciprofloxacin and propranolol were prepared. Most of the samples meet the criteria, therefore the investigated method was considered robust. Among the preparation parameters, the mixing speed was found to be the most relevant factor. It is recommended to keep it high during the production of NCs by solvent displacement method.

5. REFERENCES

1. Yu, L. X., et al., *Understanding Pharmaceutical Quality by Design*. The AAPS Journal, 2014. 16(4): 771-783.
2. Gieszinger, P., et al., *Preparation and characterization of lamotrigine containing nanocapsules for nasal administration*. European Journal of Pharmaceutics and Biopharmaceutics, 2020. 153(2020): 177-186.

ACKNOWLEDGMENT

This work was supported by the UNKP-21-3-II. New National Excellence Program of the Ministry for Innovation and Technology. Also, 2019-2.1.11-TÉT-2020-00147 and Gedeon Richter Plc. Centenial Foundation are acknowledged.

DEVELOPMENT AND EVALUATION OF FDM PRINTED NASAL DEVICE FOR SOLID NANOPARTICLES

Zoltán Ujhelyi^{1,2}, Dóra Kósa^{1,2,3}, Ágota Pető^{1,2,3}, Thinh To Quoc², Ildikó Bácskay^{1,2,3}

¹*Department of Pharmaceutical Technology, University of Debrecen, Hungary*

²*Doctoral School of Pharmaceutical Sciences, University of Debrecen, Hungary*

³*Healthcare Industry Institute, University of Debrecen, Hungary*

1. INTRODUCTION

Nasal drug administration has been in the focus of scientific interest for decades. A number of drug delivery systems and devices have been already on the market. Their advantageous properties are not questionable. Most nasal preparations are liquids that can cause discomfort to patients during the application. The aim of the research was to develop and characterise novel nanoparticles that provide improved bioavailability of incorporated pharmaceutical compounds. Finely divided nanoparticles were formed by Büchi B90 Nano Spray dryer. A major step in the development of the drug carrier was the selection of the appropriate inert carrier compounds. Besides the selection of suitable carriers physical and biocompatibility parameters had been evaluated as well. Moreover, in connection with the project, an individual drug delivery device and a protective nasal filter were also developed with FDM 3D technology.

2. MATERIALS AND METHODS

2.1. Materials

Chlorpromazine Lauroglycol FCC, KolliphorEL, Transcutol HP, Miglyol 840, DMSO, Labrafil 1944, Glycerolum 85%, Labrasol, Propylene glycol, PVA, Mannitolum, Maltodextrin, BSA, RPMI 2650 nasal epithelial cell line, MTT cell viability assay kit, PLA filaments.

2.2. Formulation of SNEDD systems

The formation of self-assembling emulsion systems was performed by titrometric dilution of the appropriate combination of surfactants (Fig. 1). Biocompatibility assays of selected compounds and performed systems had been

performed on RPMI 2650 immortalised nasal epithelial cell line by MTT viability assay.

2.3. Formulation of solid nano carriers

Solid phase nanoparticles were formed by BUCH B 90 Nano Spray dryer apparatus. The physical properties of the formed systems were examined by two methods. The particle size distribution of the formed nanoparticles was investigated in dispersion state using Malven ZSPNano Zetasizer. SEM images were taken to examine the morphology of the formed nanoparticles.

2.3. Preparation of nasal filters and nasal drug delivery devices

The devices were manufactured using FDM 3D printing technology after 3D computer design, upon the anatomical features. Performed devices had been refined upon the kind suggestions of our volunteers

3. RESULTS AND DISCUSSION

3.1. Formulation of SNEDD systems

In our experiments, five surfactant combinations were created by titration with self-assembling ability. All compositions were stable after two week standing at RT.

Smix A	Lauroglycol Cremophor Transcutol HP	FCC EL
SmixB	Miglyol 840 Cremophor (DMSO:glicerin, 1:3)	EL

P51

SmixC	Labrafil 1944 Labrasol Cremophor Propylene glycol	EL
SmixD	Labrasol Transcutol Cremophor (DMSO glicern, 1:3)	EL
SmixE	Lauroglycol Cremophor Transcutol HP	90 EL

Table 1. Compositons of performed SNEDDS.

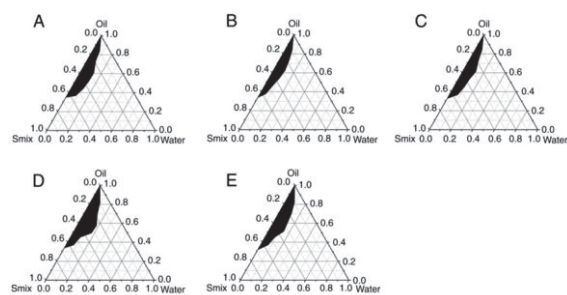


Figure 1. Pseudoternary diagrams of performed SNEDDS.

3.2. Formulation of solid nano carriers

PVA based chlorpromazine solid nano carriers had been formulated. SEM investigations confirmed the appropriate morphology of the particles. Size distribution measurements confirmed that the size of the performed particals is between 30 and 300 nm in case of different compositions.

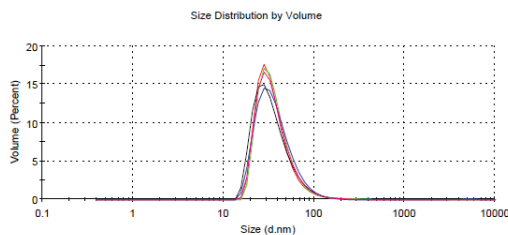


Figure 2. Size distribution of composition B combined PVA particles

3.3. Preparation of nasal filters and nasal drug delivery devices

PLA base nasal filter devices and individual nasal delivery device had been developed by 3D FDM technique.



Figure 3. Computer draft and FDM printed model of nasal device

4. CONCLUSION

Our result might ensure useful data for further development strategies in nasal drug delivery system development

5. REFERENCES

1. Flavia Laffleur et al. Progress in nasal drug delivery systems, International Journal of Pharmaceutics, Volume 607, 2021, 120994
2. Patrícia Henriques et al. Spray Dried Powders For Nasal Delivery: Process And Formulation Considerations, European Journal Of Pharmaceutics And Biopharmaceutics, Volume 176, 2022, Pages 1-20,
3. Niklas Sandler Salmela et al. Towards fabrication of 3D printed medical devices to prevent biofilm formation, International Journal of Pharmaceutics, Volume 459, Issues 1–2, 2014, Pages 62-64.

ACKNOWLEDGMENT

Research was supported by GINOP-2.3.4-15-2016-00002 and project no. TKP2021-EGA-18 Has been implemented with the support provided from the National Research, Development And Innovation Fund of Hungary, financed under the TKP2021-EGA funding scheme.

INVESTIGATION OF THE EFFECTIVENESS OF CHITOSAN COATING ON PROBIOTIC MICROCAPSULES AND INTERACTION WITH LACTOBACILLUS PLANTARUM

Judit Váradi¹, Lóránd Erdélyi¹, Ferenc Fenyvesi¹, Gábor Vasvári¹, Ádám Haimhoffer¹ Ilona Bereczki², György Vámosi³, Miklós Vecsernyés¹, Ildikó Bácskay¹, Renátó Kovács⁴

¹Department of Pharmaceutical Technology, University of Debrecen, Hungary

²Department of Pharmaceutical Chemistry, University of Debrecen, Hungary

³Department of Biophysics and Cell Biology, University of Debrecen, Hungary

⁴Department of Medical Microbiology, University of Debrecen, Hungary

1. INTRODUCTION

Chitosan is a mucoadhesive polymer, a commonly used gelling agent. However, it has antibiotic activity, which is used as an adjuvant in addition to antifungal and antibiotic agents in topical formulations. In the present study chitosan-coated and Eudragit L100-55 coated alginate microspheres were produced to encapsulate *Lactobacillus plantarum* probiotic bacteria.

According to our previous results, the chitosan used as a coating significantly reduced the number of germs, which may result in reduced efficacy of the probiotic preparation. Concentration-dependent interactions with *Lactobacillus plantarum* and the resulting bacteriostatic/bactericidal effect were investigated.

2. MATERIALS AND METHODS

2.1. Materials

Lactobacillus plantarum subsp. *plantarum* (ATCC 14917) was bought from ATCC (USA). Low (50-190 kDa, LMW), medium (MMW) and high (310-375 kDa, HMW) molecular weight chitosan were purchased from Sigma-Aldrich (Budapest, Hungary).

2.2. Preparation and Coating of Alginate Microcapsules

Probiotic bacterium-loaded alginate microcapsules were prepared by gelation method. Planktonic bacterium suspension was added to sterile sodium alginate solution. The vibration nozzle technology was used by Buchi 390-Pro equipment. Microcapsules were allowed to harden in calcium chloride solution. The chitosan coating of wet microcapsules was

performed by adding 0.4 w/w% LMW chitosan solution. Wet alginate and chitosan coated microcapsules were lyophilized to increase their shelf life. A portion of the dried alginate microcapsules was coated with Eudragit L100-55 in Mini-Glatt fluid bed system.

2.3. Dissolution Test in Simulated Gastrointestinal Fluids

The dissolution test was performed in simulated gastric (pH 2.0) than intestinal fluids (pH 7.4). Samples were collected every hour, and the microcapsules were dissolved in simulated gastric juice for 60 minutes and in simulated intestinal fluid for an additional 180 minutes.

2.4. Live/Dead Cell Determination Dissolved from Coated and Uncoated Microcapsules

All dissolution samples were centrifuged, and the bacterial cells were stained with SYTOX Green reagent. Samples were analyzed with Guava Easy Cyte 6HT-2L flow cytometer (Merck Ltd., Darmstadt, Germany). Released cell numbers and live /dead ratios were evaluated (1).

2.5. Determination of Dissolved Chitosan Coat

FITC-labeled LMW chitosan was used to quantify the chitosan coating of the microcapsule. The preparation of the microcapsules, coating and dissolution test were same as previously described. However, ¼ partially FITC-labelled chitosan was used for coating. The fluorescence of the samples was examined by microplate reader (1).

2.6. Determination of Minimum Inhibitory Concentration (MIC)

Chitosan MICs were determined using the CLSI standard broth microdilution method. MICs

P52

were read after 24 h using the partial inhibition criterion as outlined in the guidelines (at least 50 % growth reduction as compared to the growth control) (2).

2.7. Time-Kill Assay

In time-kill assays the effect of LMW, MMW, HMW chitosan was investigated on *Lactobacillus plantarum*. The starting inoculum was 10^6 CFU/mL, the chitosan concentrations were 0,003-0,125 %. All tubes were plated at 0, 4, 8, 12, and 24 h and CFU were determined (2).

3. RESULTS AND DISCUSSION

3.1. Live/Dead Cell Determination Dissolved from Coated and Uncoated Microcapsules

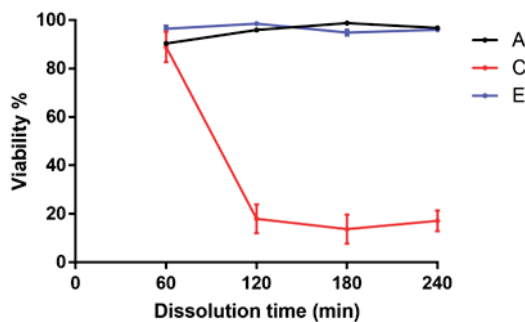


Figure 1. Viability of released *L. plantarum*. Uncoated alginate (A), chitosan-coated (C), and Eudragit-coated (E) microcapsules were investigated in triplet. Data are presented as means \pm SDs, $n = 3$ (1)

3.2. Determination of Dissolved Chitosan Coat

In view of the labeling efficiency and the labeled chitosan ratio in the coating solution, the concentration of chitosan in the dissolution medium was 0.043% (1).

3.3. Determination of Minimum Inhibitory Concentration (MIC)

The low molecular weight chitosan (LMW) MIC value were determined: 0,015%. The inhibitory concentration of chitosan decreases with increasing molecular weight.

3.4. Time-Kill Assay

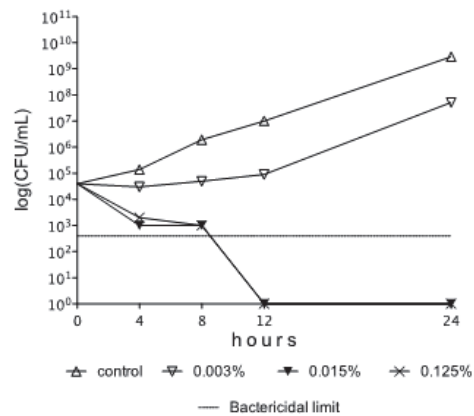


Figure 2. Representative time-kill curve of LMW chitosan.

The time-kill assay was performed with all three chitosan samples. Based on our results, with increasing molecular weight, we observed a decrease in CFU at earlier time points at the same concentrations. This assay samples were investigated parallel by flow cytometry (method described in 2.4. section). The results of the time-kill assay were confirmed by the flow cytometric results.

4. CONCLUSION

The antimicrobial activity of chitosan has not been studied in the probiotic formulations in which it is a disadvantage. In our studies, we revealed that chitosan used as a coating can form concentrations above the MIC concentration in the dissolution medium. In our latest studies, we confirmed the interaction of chitosan with *L. plantarum*, which resulted a bacteriostatic and bactericidal effect depending on the concentration. In addition to the time-killing assay, the interaction was also confirmed by confocal microscopy.

5. REFERENCES

1. Erdélyi, L., et al., *Investigation of the Role and Effectiveness of Chitosan Coating on Probiotic Microcapsules*. Polymers, 2022. 14(9):1664.
2. Papp Z., et al., *Unpredictable In Vitro Killing Activity of Amphotericin B against Four Candida auris Clades*. Pathogens, 2021 10(8):990.

ACKNOWLEDGMENT

Project no. TKP2021-EGA-18 has been implemented with the support provided from the National Research, Development and Innovation Fund of Hungary, financed under the TKP2021-EGA funding scheme.

INVESTIGATION OF MELOXICAM POTASSIUM CONTAINING NANOPARTICLES FOR INTRANASAL ADMINISTRATION

Patrícia Varga¹, Csilla Bartos¹, Rita Ambrus¹

¹Faculty of Pharmacy, Institute of Pharmaceutical Technology and Regulatory Affairs, University of Szeged, 6720 Szeged, Hungary

1. INTRODUCTION

Nose is a potential route to deliver active pharmaceutical ingredients (APIs) to the systemic circulation or the central nervous system. The absorbed drugs avoid the first pass hepatic metabolism and rapid onset of action may occur [1,2]. However, the excipients and the dosage form need to be carefully chosen because of the hindering effect of the mucociliary clearance and the limited absorption of certain molecules on the bioavailability [3,4]. Mucoadhesive polymers can increase the contact time of the APIs with the mucosa, and permeability enhancers can improve the absorption of the drugs so that higher bioavailability can be achieved [5,6]. Among nasal dosage forms, nasal powders appear to be a better choice than drops, sprays or ointments, because their residence time is higher on the mucosal surface, and their stability is higher because of their low moisture content. Also, there is no need to use preservatives during their preparation process which are often irritating for the sensitive nasal mucosa [7].

In our work, we aimed to produce nasally applicable meloxicam potassium containing cyclodextrin nanospheres by spray drying to induce rapid analgesic effect.

2. MATERIALS AND METHODS

2.1. Materials

Meloxicam potassium monohydrate (MEL-P) was used as the API. (2-Hydroxy)-propyl- β -cyclodextrin, (HP β CD) α -cyclodextrin (α CD), poly(vinylalcohol) (PVA) and hyaluronic acid (HA) were used as permeability enhancing and mucoadhesive excipients.

2.2. Preparation of the formulations

The formulations (HP β CD_MEL-P; HP β CD_MEL-P_PVA; α CD_MEL-P; α CD_MEL-P_PVA) were prepared by nano spray drying using a BÜCHI Nano Spray Dryer B-90 HP (BÜCHI Labortechnik AG, Flawil, Switzerland) applying 80 °C of inlet air temperature.

2.3. Characterization of the formulations

The size, shape and surface characteristics of the prepared particles were observed with scanning electron microscopy (SEM).

The crystallinity of the products and the physical mixtures (PMs) as controls was investigated with X-ray powder diffractometry (XRPD).

The thermal properties of the prepared samples and the physical mixtures (PMs) as controls were determined by differential scanning calorimetry (DSC).

The determination of secondary interactions between MEL-P and the excipients was carried out with Fourier-transformed infrared spectroscopy (FTIR).

The *in vitro* diffusion of MEL-P was investigated using a modified horizontal diffusion cell which modelled the nasal conditions. An artificial membrane soaked in isopropyl myristate was applied to illustrate the lipophilic mucosa.

The *ex vivo* permeation studies were performed using human nasal mucosa as the membrane in the modified horizontal diffusion cell. The test was carried out on the formulations that showed the best *in vivo* results.

3. RESULTS AND DISCUSSION

As a result of spray drying, smooth surfaced, round shaped, nanosized particles were successfully prepared (Figure 1).

On the XRPD diffractograms of the spray dried samples, the disappearance of the diffraction peaks assigned to crystalline MEL-P and α CD indicated their amorphization and the formation of the inclusion complexes.

According to the DSC measurements, the endothermic peaks of crystalline MEL-P on the curves disappeared in all of the spray dried samples compared to the PMs. This suggests the amorphization of the drug and the formation of inclusion complexes with the cyclodextrins.

Besides, on the FTIR spectra, the shifting of the peaks assigned to the stretching and the bending vibration of H-O in the samples could indicate the formation of hydrogen bonds between the MEL-P and the cyclodextrins.

Based on the results of *in vitro* and *ex vivo* permeation studies, the presence of HA resulted in the decrease of MEL-P permeation, while PVA seemed to affect beneficially the diffusion of MEL-P under nasal conditions. The highest amount of MEL-P permeated from the α CD_MEL-P_PVA sample both *in vitro* and *ex vivo* (Figure 2).

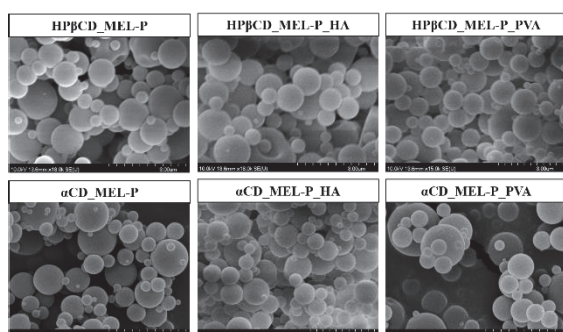


Figure 1. SEM images of the spray dried samples

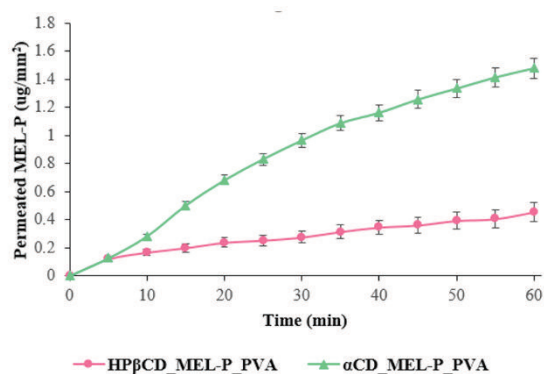


Figure 2. *Ex vivo* diffusion of MEL-P

4. CONCLUSION

Spherical nanoparticles containing amorphous MEL-P were successfully prepared and the formation of API-cyclodextrin complexes were confirmed. Based on the results of *in vitro* and *ex vivo* permeation studies, the highest amount of MEL-P diffused from the α CD_MEL-P_PVA sample. The prepared formulations may be suitable for delivering MEL-P to the systemic circulation through the nasal route and relieve pain rapidly after further optimization.

5. REFERENCES

1. Ugwoke, Michael I., et al. *Nasal mucoadhesive drug delivery: background, applications, trends and future perspectives*. Advanced drug delivery reviews, 2005. 57(11): 1640-1665.
2. Mathias, NR.; Hussain, MA. *Non-invasive systemic drug delivery: developability considerations for alternate routes of administration*. Journal of pharmaceutical sciences, 2010, 99(1): 1-20.
3. Illum, L.. *Nasal drug delivery—possibilities, problems and solutions*. Journal of controlled release, 2003. 87(1-3), 187-198.
4. Inoue, D., et al. *The relationship between in vivo nasal drug clearance and in vitro nasal mucociliary clearance: Application to the prediction of nasal drug absorption*. European Journal of Pharmaceutical Sciences, 2018. 117, 21-26.
5. Jiang, L., et al. *The application of mucoadhesive polymers in nasal drug delivery*. Drug development and industrial pharmacy, 2010. 36(3): 323-336.
6. Davis, S. S., & Illum, L. *Absorption enhancers for nasal drug delivery*. Clinical pharmacokinetics, 2003. 42(13), 1107-1128..
7. Kublik, H., & Vidgren, M. T. *Nasal delivery systems and their effect on deposition and absorption*. Advanced drug delivery reviews, 1998. 29(1-2), 157-177.

ACKNOWLEDGMENT

This work was supported by the Ministry of Human Capacities, Hungary grant TKP2021-EGA-32 and GINOP 2.2.1-15-2016-00007 Projects.

HOW FORMULATION PARAMETERS AFFECT COMPRESSION BEHAVIOUR OF MULTIPARTICULATE UNITS PREPARED BY SELECTIVE LASER SINTERING?

Ivana Vasiljević, Erna Turković, Jelena Parojčić

Department of Pharmaceutical Technology and Cosmetology, University of Belgrade – Faculty of Pharmacy, Serbia

1. INTRODUCTION

Selective laser sintering (SLS) represents novel 3D printing technology recently introduced in drug fabrication. It is applicable in different dosage forms preparation, including multiparticulate units (MPUs) (1). The characteristics of the obtained MPUs remain to be described, particularly their compression behaviour and mechanical properties of the obtained compacts.

The aim of this work was to investigate compaction suitability of MPUs prepared by SLS printing and investigate the effect of model drug type, polymer type and MPU size as well as compression pressure on the compression-related parameters (detachment and ejection stress, nett work of compression) and the obtained compacts characteristics (out-of-die elastic recovery, solid fraction and tensile strength).

2. MATERIALS AND METHODS

2.1. Materials

The MPUs were prepared using either ethyl cellulose (EC, Ethocel, Fluka, Switzerland) or methacrylic acid-ethyl acrylate copolymer (1:1) (MA-EA, Eudragit L 100-55, Evonik, Germany) as polymer forming matrices. Ibuprofen (IBU) and caffeine (CAF) were used as model drugs and Candurin® Gold Sheen (CGS, Merck KGaA, Germany) was added as pharmaceutical grade colorant.

2.2. Multiparticulate units preparation

Spherical 3D models were designed and imported as print job file (.stec) to desktop SLS printer Sintratec Kit (Sintratec AG, Switzerland). Samples composition is presented in Table 1 (C-samples contain CAF, while I-samples contain IBU).

Sample	Model drug (10%)	Polymer (87%)	Colorant (3%)	Size (mm)
C1/I1	CAF / IBU	EC	CGS	1
C2/I2				2
C3/I3		MA-EA		1
C4/I4				2

Table 1. Multiparticulate units composition

2.3. Multiparticulate units compression

MPU compacts (100 mg) were prepared on an instrumented tablet press GTP series D (Gamlen Tableting Ltd, UK) in the single compression mode, under the compression loads of 250 and 500 kg, using 6 mm diameter flat punch, at the compaction speed 30 mm/min. The supporting software enabled complete visualization of the upper punch position and force in real time. The measured force-displacement curves were used to calculate nett work of compression, friction force between lower punch and tablet during detachment phase (detachment stress) and friction force between die and tablet in the ejection phase (ejection stress).

Compact dimensions were determined 24 hours after compression. Caliper was used to measure the out-of-die compact thickness (t), while compact diameter (R) and hardness (F) were measured using the hardness tester Erweka TBH 125D (Erweka GmbH, Germany). The obtained values were used to calculate compact tensile strength, solid fraction and out-of-die elastic recovery.

In order to statistically investigate the input parameter effects (polymer type, model drug type and MPU size), experimental design was applied, using software Design-Expert v.7.0 (Stat-Ease Inc, USA).

3. RESULTS AND DISCUSSION

3.1. Multiparticulate units compression

The prepared compact tensile strength was generally higher than 1 MPa and acceptable (2), as represented in Fig. 1, while solid fraction ranged from 67.67 (C4) to 89.46% (C1 and I1). MPUs containing CAF and MPUs with MA-EA exhibited higher increase in solid fraction and tensile strength when compression load was increased, in comparison to samples prepared with IBU or EC, respectively. This indicates better tableability and compressibility. MPU samples with MA-EA or 1 mm size exhibited higher nett work of compression, but also higher values of elastic recovery. Higher energy input corresponds to higher compressibility and susceptibility to particle consolidation. Ejection stress values did not exceed 3 MPa, which is associated with compact defect propensity (3), while detachment stress was lower than 4 MPa. This indicates that the prepared samples do not stick to punch and die and may be easily detached.

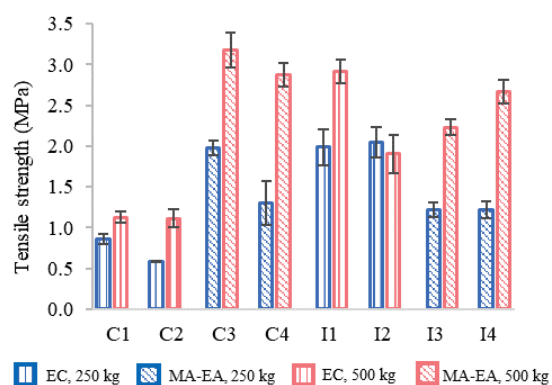


Figure 1. The obtained MPU tensile strength values

All of the investigated factors (model drug type, polymer type, MPU size and compression pressure), as well as model drug-polymer type and model drug-compression pressure interaction significantly affected compact tensile strength ($p < 0.0001$). In the case of MPUs containing CAF as model drug and EC as polymer, higher compression pressure increased tensile strength more notably. In the case of detachment stress, model drug type, polymer type and compression pressure were found as relevant factors ($p = 0.0013$), while ejection stress was affected by polymer type, compression pressure and their interaction ($p = 0.0097$). Elastic recovery was impacted by all the investigated parameters, as well as model

drug type-polymer type and model drug type-compression pressure interaction ($p < 0.0001$). Higher compression pressure increased the elastic recovery values more notably in the case of IBU or EC samples. Model drug type, polymer type and compression pressure affected nett work ($p < 0.001$), as well as model drug-compression pressure and polymer type-compression pressure interaction. Based on the investigated MPU samples, software-aided prediction recognized IBU, MA-EA and 1 mm-MPUs size as desirable for obtaining compacts with high tensile strength, but also low elastic recovery, low detachment and ejection stress and high nett work values.

4. CONCLUSION

The multiparticulate units were successfully compressed into compacts with good tensile strength values (higher than 1 MPa, generally), low detachment and ejection stress (lower than 3 and 4 MPa, respectively). MPUs containing CAF and MPUs with MA-EA exhibited higher tableability and compressibility in comparison to samples prepared with IBU or EC, respectively.

Polymer type and compression pressure affected all the investigated compact characteristics (tensile strength, detachment and ejection stress, out-of-die elastic recovery and nett work of compression), while MPU size impact on the observed parameters was the lowest. MPUs containing IBU and MA-EA, with 1 mm size were recognized as preferable for obtaining compacts with favourable characteristics.

5. REFERENCES

1. Awad, A., et al. *3D printed pellets (miniprintlets): A novel, multi-drug, controlled release platform technology*. *Pharmaceutics*, 2019. 11(4): 148.
2. Hancock, B.C., *Identifying Candidates for Direct Compression Using Material-Sparing Formulation Tools*, presented at AAPS, 2004.
3. Pitt, K.G., et al., *Compression prediction accuracy from small scale compaction studies to production presses*. *Powder Technology*, 2015. 270: 490-493.

ACKNOWLEDGMENT

This work was financially supported by the Ministry of Education, Science and Technological Development of the Republic of Serbia (project 451-03-68/2022-14/200161).

FLAXSEED-OIL BASED LYOTROPIC LIQUID CRYSTALS: INFLUENCE OF MICROSTRUCTURE ON BETAMETHASONE DIPROPIONATE RELEASE PROFILE

Mercedes Vitek¹, Alenka Zvonar Pobirk¹, Žiga Medoš², Mirjam Gosenca Matjaž¹

¹Department of Pharmaceutical Technology, Faculty of Pharmacy, University of Ljubljana, Slovenia

²Department of Chemistry and Biochemistry, Faculty of Chemistry and Chemical Technology, University of Ljubljana, Slovenia

1. INTRODUCTION

In recent years lyotropic liquid crystals (LLCs) have attracted great interest as an outstanding drug delivery platform. They can form a well-defined and complex microstructure. LLCs with lamellar structure are especially suitable for dermal drug delivery due to similarity with intercellular lipids of *stratum corneum*. Thus, they can provide improved bioavailability, target the site of action, and hence limit the secondary effects of the incorporated drug. In addition, when composed of ingredients with skin supportive properties, they can restore skin barrier function [1, 2, 3].

Considering all the advantages, which improve patient adherence, lamellar LLCs are especially suitable for the treatment of chronic skin diseases, which represent a particularly heavy burden for the patients. In that regards, atopic dermatitis (AD) is one of the most common chronic skin diseases that greatly impairs a patient's life [4].

The aim of this study was to evaluate and compare flaxseed oil-based LLCs loaded with betamethasone dipropionate (BD). Flaxseed oil is known for its anti-inflammatory activity and BD represents the mainstay drug for mild to moderate AD treatment. The studied LLCs varied in type of surfactants and water content. Microstructure of the systems was investigated by small-angle X-ray scattering (SAXS) method and linked with the interpretation of the BD release profile using Franz diffusion cells.

2. MATERIALS AND METHODS

2.1. Materials

LLCs consisted of flaxseed oil (A.C.E.F. s.p.a., Italy), mixture of Lipoid S-100[®] (Lipoid GmbH, Germany) and Tween 80[®] (Merck KGaA, Germany) or Montanov[™] 68 (Factory

Organica, Slovenia), and bidistilled water. BD was from ACA Pharma NV, Belgium. Beloderm[®] (reference medicinal product) was from Belupo d.o.o., Slovenia.

2.2. Sample preparation

LCCs (Table 1) were prepared from homogeneous mixtures of lipid-surfactant phase and BD (0,64 mg/g) that were adequately diluted with bidistilled water.

Table 1. Composition [w/w %] of the studied LLCs.

LCC	Flaxseed oil	Lecithin + Tween 80	Lecithin + Montanov 68	Water
1	28	42	/	30
2	20	30	/	50
3	16	/	24	60
4	8	/	12	80

2.3. SAXS analysis

Analysis was performed at 25, 32, and 37 °C by Kratky camera system (Anton Paar, Austria), attached to a conventional X-ray generator (Bruker AXS, Karlsruhe, Germany), equipped with a sealed X-ray tube (Cu-anode target type).

2.4. *In vitro* release study

BD release through Strat-M[®] membranes was evaluated using Franz diffusion cells (n=6) with a diffusion area of 0.785 cm² for 24 hours at 32 °C by HPLC (Agilent 1100 Series, USA).

3. RESULTS AND DISCUSSION

3.1. SAXS analysis

Structural evaluation by SAXS (Fig. 1 and Fig. 2) showed that temperature did not have a significant effect on the microstructure of the studied LLCs therefore being preserved following skin application (i.e., 32 °C). Further, the microstructure was not altered by incorporation of BD. As regards LCC1 and LLC2, values of the scattering vector q showed

the ratio $q_1:q_2=1:2$, indicative for lamellar mesophases. For the LCC3 and LCC4, the ratio was $q_1:q_2:q_3=1:2:3$ and $q_1:q_2:q_3:q_4=1:2:3:4$, respectively. The ratio is also representative for lamellar LCCs, however, the terminal part of the scattering curves indicated presence of micelle structures as well [3, 5].

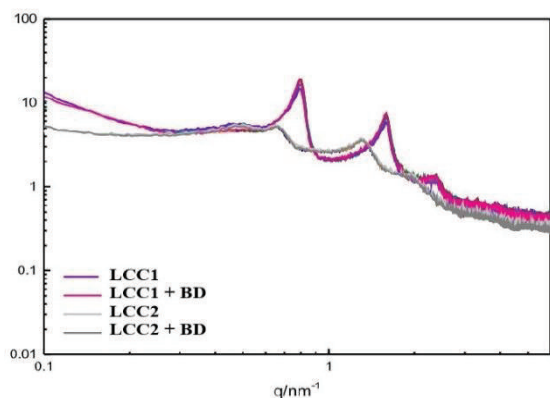


Figure 1. SAXS curves of LCC1 and LCC2.

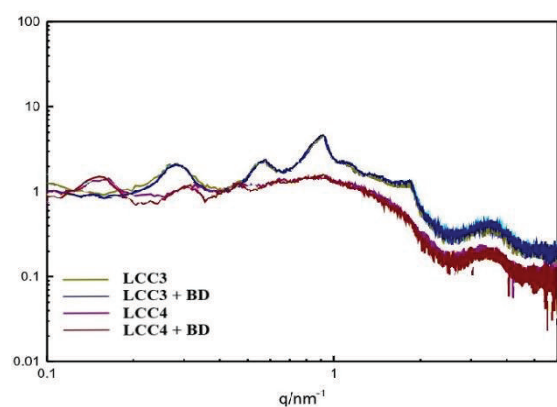


Figure 2. SAXS curves of LCC2 and LCC4.

3.2. *In vitro* release study

BD was released from all studied LCCs in greater extent compared to Beloderm® (with the same BD content) (Fig. 3.).

The drug release was significantly influenced by microstructure of the individual systems. The release of BD was the fastest and the highest after 24 hours in case of LCC4 with the most numerous and pronounced presence of micelles in coexistence with lamellar mesophases as confirmed by SAXS analysis.

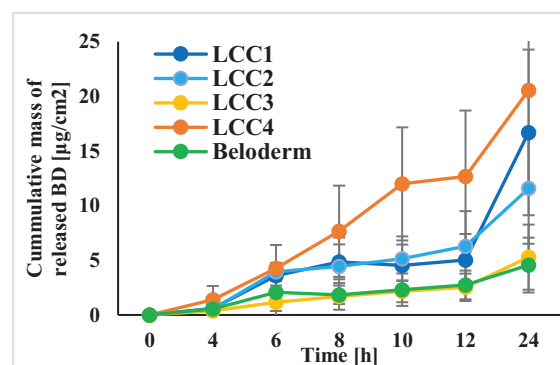


Figure 3. Release profile of BD from studied LCCs.

4. CONCLUSION

In the present work, release profile of BD was evaluated for LCCs with different type of surfactants and water content in relationship to their microstructure determined by SAXS. Obtained data show great potential for further *in vitro* evaluation on keratinocyte cell line and prospective therapeutic efficacy of these systems.

5. REFERENCES

1. Silvestrini, AVP., et al., *Advances in lyotropic liquid crystal systems for skin drug delivery*. Expert Opinion on Drug Delivery, 2020. 17(12): 1781-1805.
2. Vitek, M., et al., *A comparative study of lipid-based drug delivery systems with different microstructure for combined dermal administration of antioxidant vitamins*. Journal of Dispersion Science and Technology, 2022. Ahead-Of-Print: 1-14.
3. Gosenca, M., et al., *Lecithin based lamellar liquid crystals as a physiologically acceptable dermal delivery system for ascorbyl palmitate*. European Journal of Pharmaceutical Sciences, 2013. 50(1): 114-22.
4. Weidinger, S., et al., *Atopic dermatitis*. Nature Reviews Disease Primers. 4(1): 1.
5. Lombardo, D., et al., *Evidence of premicellar aggregates in aqueous solution of amphiphilic PDMS-PEO block copolymer*. Physical Chemistry Chemical Physics. 21(22): 11983-91.

ACKNOWLEDGMENT

This work was supported by the Slovenian Research Agency under Grant P1-0189.

BY INCLUSION COMPLEXATION WITH SULFOBUTYL ETHER β -CYCLODEXTRIN

Lamija Hindija¹, Jasmina Hadžiabdić¹, Merima Sirbubalo¹, Amina Tucak-Smajić¹, Ognjenka Rahić¹, Stanko Srčić², Edina Vranić¹

¹*Department of Pharmaceutical Technology, University of Sarajevo – Faculty of Pharmacy, Bosnia and Herzegovina*

²*Department of Pharmaceutical Technology, Faculty of Pharmacy, University of Ljubljana, Slovenia*

1. INTRODUCTION

Dimenhydrinate (DMH) is an antiemetic drug made of diphenhydramine and 8-chlorotheophylline. It's a slightly soluble drug with water solubility of 3 mg/mL [1]. Cyclodextrins (CDs), amphiphilic oligosaccharides, make inclusion complexes with poorly water-soluble drugs. Host-guest interaction occurs by expelling water molecules from inner hydrophobic CD cavity and creating non-covalent bonds with guest molecules. Complexation provides solubility and stability improvement, physical separation of incompatible drugs and taste masking. Limited solubility of natural β -cyclodextrin can be exceeded by substitution of reactive hydroxyl groups and using sulfobutyl ether β -cyclodextrin (SBE- β -CD) to increase hydrophilicity and inclusion ability [2, 3].

2. MATERIALS AND METHODS

2.1. Materials

DMH was kindly supplied by Bosnalijek, d. d., B&H and Dexolve™ (SBE- β -CD) was generously gifted from CycloLab, Hungary.

2.2. Phase solubility study

Phase solubility study was conducted to determine stability constant (K_s) and complexation efficacy (CE), important for assessing the binding characteristics of DMH and SBE- β -CD. An excess amount of DMH was mixed in aqueous solutions containing increasing amounts of SBE- β -CD (4.62 - 231.12 mmol/L) using a magnetic stirrer (Witeg, WiseStir MSH-20D) at 25°C for 24h. The aliquot was filtered and DMH concentration was determined at 277 nm (Shimadzu UV-VIS spectrophotometer-1601). Measurements were made in triplicates.

2.3. Attenuated Total Reflectance - Fourier Transform Infrared Spectroscopy (ATR/FTIR)

ATR/FTIR spectra of pure DMH, SBE- β -CD, their physical mixture and inclusion complexes prepared by kneading and solvent evaporation methods were recorded (Cary 360 FTIR (ATR) spectrophotometer, Agilent). The spectra were collected from 32 scans, in 4000-650 cm^{-1} scanning range, at 4 cm^{-1} resolution.

3. RESULTS AND DISCUSSION

3.1. Phase solubility study

Phase solubility diagram shows linear increment of DMH solubility in solutions of SBE- β -CD, indicating an A_L -type isotherm. The slope was less than unity, suggesting a formation of a 1:1 complex (Fig. 1).

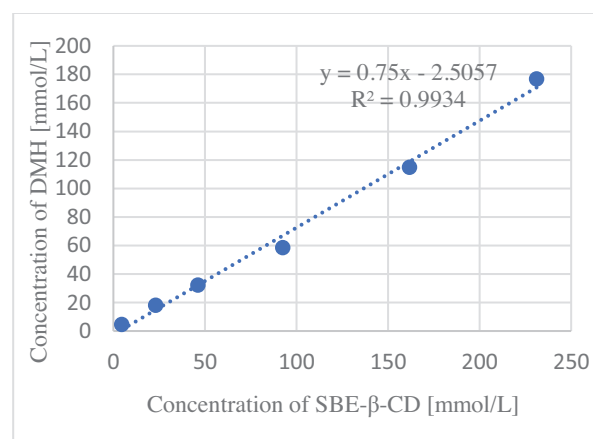


Figure 1. Phase solubility diagram of DMH and SBE- β -CD in distilled water

The value of K_s was 148.88 M^{-1} and calculated from the equation:

$$K = \frac{\text{slope}}{S_0(1 - \text{slope})}$$

Complexes with K_s between 100 - 5000 M^{-1} are suitable for practical applications. Values below 100 M^{-1} indicate very labile complexes with premature release of the guest and insignificant improvement in solubility. Values of K_s over

5000 are specific for very stable complexes where the release of the guest from the CD cavity is incomplete or obstructed.

To avoid inaccuracy in interpretation of the results due to dependence of K_s on small changes in S_0 (intrinsic drug solubility) and possible self-association of lipophilic drug molecules in aqueous media, CE was determined from the equation:

$$CE = S_0 K_{1:1} = \frac{\text{slope}}{1 - \text{slope}}$$

The value of CE was 3 which implies formation of a relatively stable complex.

3.2. FTIR analysis

Changes of characteristic bands in FTIR spectra of DMH and SBE- β -CD in 1:1 complexes prepared by kneading and solvent evaporation method were analyzed concerning pure substances and their physical mixture.

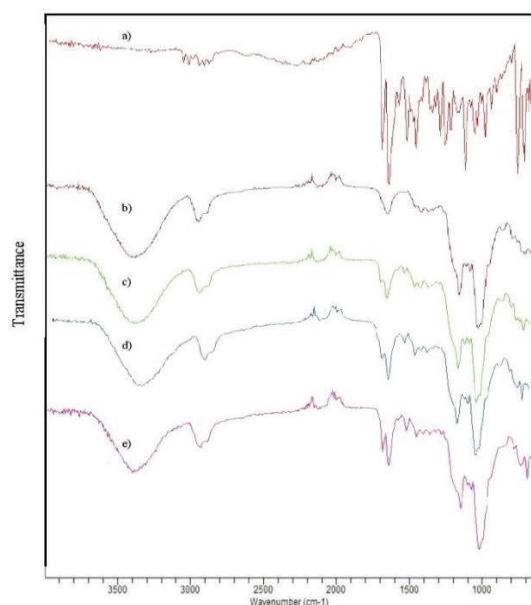


Figure 2. FTIR spectra of a) pure DMH; b) pure SBE- β -CD; c) physical mixture; d) inclusion complex prepared by solvent evaporation method; e) inclusion complex prepared by kneading method

Specific bands of pure DMH (Fig. 2 a) are at 3059.6 cm^{-1} (stretching of amino groups), 1644.3 cm^{-1} (C=O stretching), 1112.9 cm^{-1} (C=C stretching of the aromatic rings) and 749.3 cm^{-1} (C-Cl stretching of carbonyl chloride). Specific bands of pure SBE- β -CD (Fig. 2 b) are at 3384.4 cm^{-1} (O-H stretching vibrations), 2931.6 cm^{-1} (asymmetric and symmetric vibrations of -CH and -CH₂), 1640.0 cm^{-1} (d-HOH bending of water molecules attached to CD), 1153.0 cm^{-1} (C-H and C-O vibrations) and 1025.0 cm^{-1} (S=O

vibrations). Spectra of physical mixture (Fig. 2 c) showed slight shiftment of some bands to different wavelengths implying partial embedding of DMH into CD cavity. More significant changes in position, intensity and shape of the band at 1645 cm^{-1} were recorded in spectra of inclusion complexes (Fig. 2 d and e), pointing to possible displacement of water molecules with DMH molecules in the central cavity of SBE- β -CD. Absence of DMH specific bands in spectra of physical mixture and complex suggests possible interaction with SBE- β -CD just by blending and also confirms complex formation.

4. CONCLUSION

Inclusion complexation with SBE- β -CD may overcome poor solubility of DMH. The results of phase solubility study indicate the formation of a 1:1 complex and FTIR analysis showed that both solvent evaporation and kneading methods provide successful complexation.

5. REFERENCES

1. Khan, Q., Shah, S. N. H., Arshad, M. S., Usman, F., Khalil, R., et al., *Formulation and optimization of dimenhydrinate emulgels for topical delivery using response surface methodology*. Pakistan Journal of Pharmaceutical Sciences, 2021. 34(1): 245-255
2. Aiassa, V., Garnero, C., Longhi, M., Zoppi, A. *Cyclodextrin Multicomponent Complexes: Pharmaceutical Applications*. Pharmaceutics, 2021. 13: 1099
3. Sadaquat, H., Akhtar, M. *Comparative effects of β -cyclodextrin, HP- β -cyclodextrin and SBE- β -cyclodextrin on the solubility and dissolution of docetaxel via inclusion complexation*. Journal of Inclusion Phenomena and Macrocyclic Chemistry, 2020. 96: 333-351

THE INFLUENCE OF POLYMERIC PRECIPITATION INHIBITORS ON SOLUBILITY CHARACTERISTICS OF CARVEDILOL-LOADED SMEDDS

Alenka Zvonar Pobirk¹, Mila Kovačević¹, Ilja German Ilič¹, Mirjana Gašperlin¹

¹University of Ljubljana, Faculty of Pharmacy, Department of Pharmaceutical Technology, Slovenia

1. INTRODUCTION

In the last decade, researchers are extensively investigating the self-microemulsifying drug delivery systems (SMEDDS), a lipid-based formulation developed to improve the solubility of poorly water-soluble drugs, such as carvedilol [1]. In some cases, by formulating SMEDDS it might not be possible to preserve sufficient solubilization capacity upon their dispersion, which increases the risk for drug precipitation in the gastro-intestine. Since the positive pharmacological effect is in correlation with the amount of drug absorbed, the addition of polymeric precipitation inhibitors (PPIs) found to be valuable to prevent the drug precipitation [2]. Thus, the aim of this study was to investigate whether the presence of PPI shows effectiveness in inhibition of carvedilol precipitation from SMEDDS, and to identify the optimal type and concentration of PPI.

2. MATERIALS AND METHODS

2.1. Materials

Carvedilol was used as a model drug. Liquid SMEDDS was composed of mixture of Capmul[®] MCM EP/NF (mono-diglyceride of medium chain fatty acids), refined castor oil, Kollisolv[®] PEG E 400 and Kolliphor[®] RH 40 (polyoxy 40 hydrogenated castor oil).

Different polymers (added to liquid SMEDDS) were used as precipitation inhibitors: povidone K30 (PVP K30), hypromellose (Pharmacoat[®] 606) and Soluplus[®].

2.2. Preparation and characterization of liquid SMEDDS containing PPIs

Liquid SMEDDS was prepared by heating the components (40 % w/w Kolliphor[®] RH, 10 % w/w Capmul[®] MCM EP/NF, 10 % w/w castor oil and 40 % w/w PEG 400) at 40°C and stirring

until homogenous mixture was obtained. Subsequently, carvedilol was added (in content of 120 mg per 1 g of SMEDDS), as well as PPI (in concentration range 0-5 % w/w).

Carvedilol precipitation from prepared SMEDDS was further investigated for *in vitro* dissolution properties under non-sink conditions at pH 6,8.

3. RESULTS AND DISCUSSION

3.1. Determination of supersaturation for *in vitro* carvedilol dissolution testing

Drug precipitation typically occurs during supersaturation state formed upon dilution (and digestion) of formulation in the gastro-intestine. Thus, it was necessary to mimic this condition in order to study the influence of PPI on carvedilol precipitation from liquid SMEDDS. Different degrees of carvedilol supersaturation were tested to identify the one, at which its precipitation is the most pronounced and therefore the effect of PPI is the most visible. Testing conditions in which carvedilol concentration exceeds saturated solubility in dissolution medium for about 3-times, was found as optimal to study the influence of PPI on precipitation of carvedilol from drug loaded SMEDDS.

3.2. The influence of PPI type and concentration on carvedilol precipitation from liquid SMEDDS

All three PPIs tested delayed the precipitation of carvedilol after dispersion of SMEDDS in aqueous media. Soluplus[®] turned out to be the most effective, as the supersaturation was maintained for the entire testing period (8 h) when added in 5 % w/w concentration. When SMEDDS was admixed with the same amount of Pharmacoat[®] 606, carvedilol concentration remained above 95 % even after 7 h. The worse

carvedilol dissolution performance was observed for SMEDDS with addition of 3 % w/w PVP K30, that postponed drug precipitation only for 60 min. Additionally, the drug concentration dropped below 50 % after 4 h (Fig. 1.). This was to some extent in contrary to our expectations, as PVP K30 showed good drug solubilization ability in our previous research, focusing of solidification of carvedilol loaded SMEDDS with swirling fluidized bed pellet coating (3).

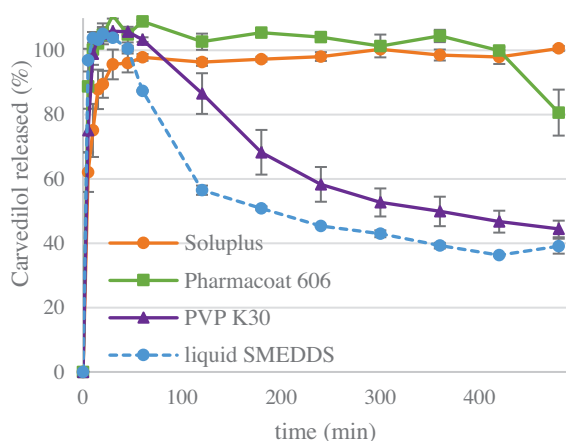


Figure 1. *In vitro* carvedilol dissolution profile of liquid SMEDDS containing different PPIs.

In addition to the type of PPI, its concentration in the SMEDDS must also be considered in order to develop drug loaded SMEDDS with optimal solubility characteristics. Indeed, concentration of PPI was found to considerably correlate with time during which carvedilol was in supersaturated state. Higher Soluplus® concentrations demonstrated longer supersaturation periods, as shown in Fig. 2.

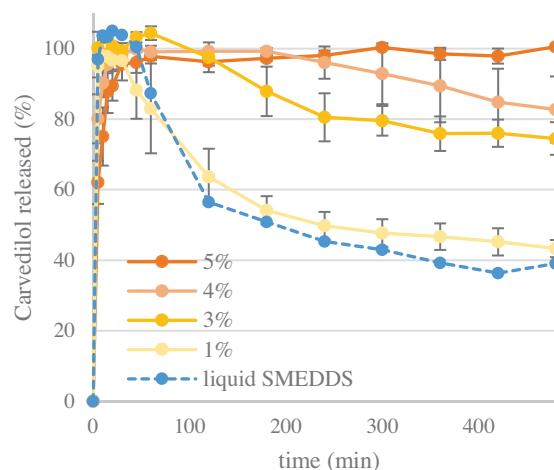


Figure 2. *In vitro* carvedilol dissolution profiles of liquid SMEDDS containing different concentrations of Soluplus®.

4. CONCLUSION

By incorporating PPI into SMEDDS formulation, it was possible to produce high-drug load SMEDDS, with low risk for carvedilol precipitation upon dispersion in aqueous media. With the addition of Soluplus® and Pharmacoat® 606 (5 % w/w), carvedilol concentration was maintained in supersaturated state for 8 h, in that way preventing the untimely precipitation, that would most probably lead to incomplete carvedilol absorption and inadequate therapeutic effect.

5. REFERENCES

1. Čerpnjak K. et al. Lipid-based systems as a promising approach for enhancing the bioavailability of poorly water-soluble drugs. *Acta Pharmaceutica*. 2013 63(4): 427–45.
2. Warren D.B. et al. Using polymeric precipitation inhibitors to improve the absorption of poorly water-soluble drugs: A mechanistic basis for utility. *Journal of Drug Targeting*. 2010 18(10): 704–31.
3. Mandić J. et al. Solidification of carvedilol loaded SMEDDS by swirling fluidized bed pellet coating. *International Journal of Pharmaceutics*, 2019, 566: 89-100.

SIMULTANEOUS DETERMINATION OF FIVE NITROSAMINES IN SARTAN DRUG PRODUCTS BY A LC-MS/MS METHOD

Timeja Planinšek Parfant¹, Anja Hrovat¹, Robert Roškar¹

¹ *Department of Biopharmaceutics and Pharmacokinetics, University of Ljubljana, Faculty of Pharmacy, Slovenia*

1. INTRODUCTION

Since 2018, interest in N-nitrosamines (NAs) increased dramatically among pharmaceutical regulatory authorities, industry and researchers when they were first detected in angiotensin II receptor antagonists' medicines which caused global recalls [1]. NAs are a group of N-nitroso compounds and are potent carcinogens in several animal species and some are classified as probable or possible human carcinogens based on International Agency for Research on Cancer (IARC) classification system [2]. Therefore, European Medicines Agency (EMA) and Food and Drug Administration (FDA) have established acceptable daily intake limits (8-1300 ng/day) for 18 and 9 NAs, respectively [1,3]. Due to the lack of analytical methods for the simultaneous determination of NAs in pharmaceuticals, our main objective was to develop a sufficiently sensitive and selective analytical method for the simultaneous quantification of five NAs in sartan drug products (DPs).

2. MATERIALS AND METHODS

2.1. Reagents and chemicals

Reference standards of N-Nitrosodiethylamine (NDEA) and N-Nitrosodimethylamine (NDMA) were obtained from Sigma-Aldrich, N-nitroso-N-methyl-aminobutyric acid (NMBA) and N-Nitrosodiisopropylamine (NDIPA) were obtained from Carbosynth and N-Nitrosoethylisopropylamine (NEIPA) was obtained from LGC. DPs were purchased from local pharmacy. Methanol, acetonitrile and isopropanol were purchased from Honeywell, ethanol absolute and formic acid were purchased from Merck. For LC-MS/MS analysis, LC-MS-grade methanol (Honeywell)

was used. All sample solutions and mobile phase were prepared using the Milli-Q water obtained through a Milli-Q A10 Advantage water purification system.

2.2. LC-MS/MS method

A Kinetex F5 100 × 2.1 mm, 2.6 μm particle size column (Phenomenex, USA) with gradient elution at 0.3 mL/min using 0.05% formic acid and methanol were used for the optimal separation on a UHPLC 1290 Infinity coupled to 6460 Triple Quadrupole mass spectrometer. To determine the effect of ionization and sample injection volume on the matrix effect, two methods utilizing both ESI and APCI ion source were developed which operated in MRM mode (Agilent Technologies, USA), and different sample injection volumes were used.

2.3. Sample preparation

For the evaluation of optimal NA extraction from DPs different solvents were added to defined amounts of ground tablets. To reduce the matrix effect, selected solvent was added to various amounts of ground tablets. Samples were then vortexed for 5 minutes, sonicated for 30 minutes and centrifuged for 10 minutes at 16100 g at 25 °C. Prior to LC-MS/MS analysis, the samples were filtered through 0.22 μm RC syringe filters. The developed analytical method was validated according to ICH guidelines and was successfully applied to real samples [4].

3. RESULTS AND DISCUSSION

The lowest matrix effect and good chromatographic peak shape was obtained using methanol in MilliQ (1:1, v/v) among other used solvents for extraction (acetonitrile, isopropanol or ethanol in MilliQ (1:1, v/v),

methanol or mixture of acetonitrile and methanol 1:1, v/v). Among solvents with different methanol contents in MilliQ, the best results were obtained using 20% methanol in MilliQ. The addition of formic acid to solvent for extraction did not affect matrix effect or recovery. The sample amount and sample injection volume had a significant influence on the matrix effect when using the ESI ion source compared to the APCI (Fig. 1).

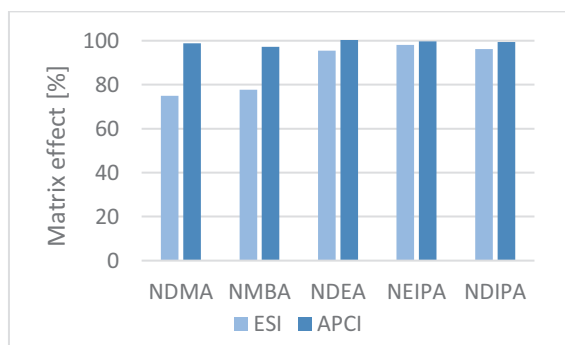


Figure 1. The influence of ion source on matrix effect.

Also, the sensitivity for all analytes (except for NMBA) increased when the APCI ion source was used. The most significant improvement in sensitivity (20-fold) was observed for NDMA. The method was validated according to ICH guidelines and was proved to be linear in the concentration range 0.25-200 $\mu\text{g/L}$. Accuracy and precision were within acceptable limits (< 5%) and suitable selectivity was achieved. The method was successfully applied to real samples and tested for the presence of NAs impurities in six selected sartan-containing DPs. The NA content in all analyzed DPs was below the detection limit. The developed analytical method is suitable for the detection of all five NAs in selected DPs at the regulatory levels. The limit of quantification is achieved in all selected DPs, except for NDEA and NEIPA in some samples (Table 1). The required LOQs for NDEA and NEIPA in this samples could be reached by further method optimization (e.g. increasing the amount of ground tablets).

Table 1. Limit of detection (LOD) and limit of quantification (LOQ) according to regulatory levels for the NAs in DP. Green (+) - the NA

content can be detected (> LOD) or quantified (> LOQ), red (-) - the NAs content cannot be quantified.

	NDMA		NMBA		NDEA		NEIPA		NDIPA	
	LOD	LOQ	LOD	LOQ	LOD	LOQ	LOD	LOQ	LOD	LOQ
DP1	+	+	+	+	+	-	+	-	+	+
DP2	+	+	+	+	+	+	+	+	+	+
DP3	+	+	+	+	+	-	+	-	+	+
DP4	+	+	+	+	+	-	+	-	+	+
DP5	+	+	+	+	+	+	+	+	+	+
DP6	+	+	+	+	+	-	+	-	+	+

4. CONCLUSION

A highly sensitive and selective analytical method for the determination of five regulated NAs (NDMA, NMBA, NDEA, NDIPA and NEIPA) in sartan DPs was developed. It was found out that ion source has a significant effect on matrix effect and sensitivity of all analytes. The method was fully validated and was successfully applied to real samples, where all met the regulatory requirements for nitrosamine content. The results demonstrated that the proposed analytical method is suitable for routine analysis of selected NA in sartans with the LOQ within regulatory levels.

5. REFERENCES

1. EMA, *Questions and answers for marketing authorisation holders/applicants on the CHMP Opinion for the Article 5(3) of Regulation (EC) No 726/2004 referral on nitrosamine impurities in human medicinal products*, EMA/409815/2020, 2022.
2. List of Classifications – IARC Monographs on the Identification of Carcinogenic Hazards to Humans. <https://monographs.iarc.fr/list-of-classifications> (accessed 09 Jun 2022).
3. FDA, *Guidance for Industry. Control of Nitrosamine Impurities in Human Drugs*, FDA-2020-D-1530, 2021.
4. ICH Q2 (R1), 2005.

ACKNOWLEDGMENT

This research was funded by Slovenian Research Agency (ARRS), grant number [P1-0189].

PREDICTION OF ENVIRONMENTAL MICROBIAL DEGRADATION OF AZITHROMYCIN IN SOIL AND WATER AND METABOLISM IN HUMANS

Tin Takač¹, Milena Jadrijević-Mladar Takač², Tomislav Jednačak³

¹University of Zagreb, Faculty of Science, Doctoral Study in Chemistry, Zagreb, Croatia;

²University of Zagreb, Zagreb, Croatia;

³University of Zagreb, Faculty of Science, Zagreb, Croatia

1. INTRODUCTION

Several contaminants of emerging concern (CECs), including macrolide antibiotics, enter aquatic compartments, such as surface water, groundwater and even drinking water at concentrations ranging from a few ng L⁻¹ to several µg L⁻¹ [1]. As conventional wastewater treatment plants are not designed to remove complex organic compounds, such as pharmaceuticals, their metabolites, and potential transformation products, CECs enter the environment and can have adverse effects on living organisms and plants. Among the different classes of pharmaceuticals found in the environment, special attention has been paid to macrolide antibiotics, such as azithromycin, clarithromycin, and erythromycin, which are the most discussed because of their potential to contribute to the development of antimicrobial resistance (AMR) [2]. To date most studies have focused on the parent compounds, and little attention has been paid to the intermediates/metabolites they produce. Drugs excreted by humans and/or animals may be present in wastewater treatment plant effluents at higher concentrations than in their respective influents, because they are excreted as conjugates, which are broken down in wastewater treatment plants and generally metabolized during biological treatment, increasing the concentration of the parent compound at the output of the treatment plants. Since there is a lack of data on the chronic toxicity of such compounds, and ecotoxicological data for mixtures of drugs, their metabolites, and transformation products,

it is of great importance to study their potential degradation pathways.

2. MATERIALS AND METHODS

2.1. Materials

The macrolide antibiotic azithromycin was used in this study.

2.2. Methods

Using BioTransformer 3, a web server software available at www.biotransformer.ca [3] the aerobic and anaerobic microbial degradation of azithromycin in the environment in soil and water was performed and the predicted biotransformation metabolites were compared with the predicted metabolites of azithromycin in humans.

3. RESULTS AND DISCUSSION

3.1. Predicted aerobic and anaerobic microbial degradation of azithromycin in the environment.

Several aerobic and anaerobic intermediates/metabolites were predicted for the azithromycin molecule (Table 1, Figure 1) most of which are formed by oxidation of the hydroxyl group at positions C2' (1), C11 (2), C4'' (3), or after hydrolysis of the glycoside bonds and removal of the sugar moieties, by oxidation of the formed hydroxyl groups to ketone moieties, C3 (8), C5 (7), C1' (4) and C1'' (11) or by reduction of formed ketones to the secondary hydroxyl group at positions C3 (10), C5 (5), C1' (6) and C1'' (9). In addition to the oxidation/reduction reactions, hydrolysis of the

P60

lactone bond was also observed, **13**: C1(=O)–OH and C13–OH, as well as the formation of C3'' (**12**) metabolites after *O*-dealkylation.

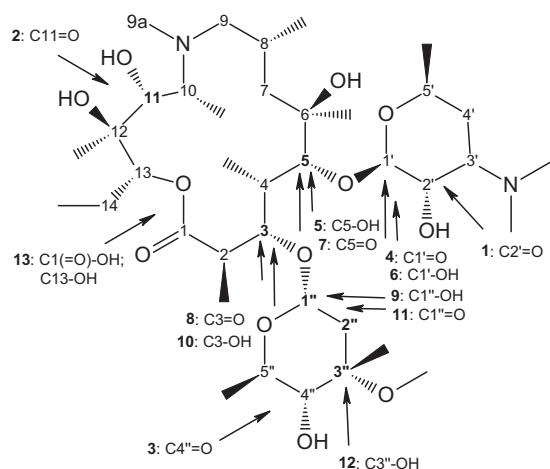


Figure 1. Predicted environmental aerobic and anaerobic microbial degradation of azithromycin in soil and water (www.biotransformer.ca) [3]

Table 1. List of predicted microbial aerobic and anaerobic metabolites of azithromycin in the environment.

No	MF	MW	AlogP
1	C ₃₈ H ₇₀ N ₂ O ₁₂	746.49	2.33
2	C ₃₈ H ₇₀ N ₂ O ₁₂	746.49	2.33
3	C ₃₈ H ₇₀ N ₂ O ₁₂	746.49	2.33
4	C ₈ H ₁₅ NO ₃	173.11	0.02
5	C ₃₀ H ₅₇ NO ₁₀	591.40	1.69
6	C ₈ H ₁₇ NO ₃	175.12	-0.37
7	C ₃₀ H ₅₅ NO ₁₀	589.38	1.92
8	C ₃₀ H ₅₆ N ₂ O ₉	588.40	1.79
9	C ₈ H ₁₆ O ₄	176.11	0.25
10	C ₃₀ H ₅₈ N ₂ O ₉	590.41	1.56
11	C ₈ H ₁₄ O ₄	174.09	0.08
12	C ₃₇ H ₇₀ N ₂ O ₁₂	734.49	1.67
13	[C ₃₈ H ₇₃ N ₂ O ₁₃] ⁻	765.51	0.79

MF –molecular formula of formed metabolite;
MW - molecular weight; AlogP - lipophilicity

3.2. Predicted metabolism of azithromycin in humans

The predicted metabolites formed by CYP enzymes in humans are similar to the predicted oxidative/reductive degradation products in the environment, but also include *N*-dealkylated metabolites. In human metabolism, the degradation of the lactone ring was not predicted. Conjugation with glucuronic acid at positions C2' (**1**), C6 (**2**) C11 (**3**), C12 (**4**), C4''

(**5**) and the charged glucuronide R–N⁺(CH₃)₂–Gluc (**6**) were predicted (Figure 2).

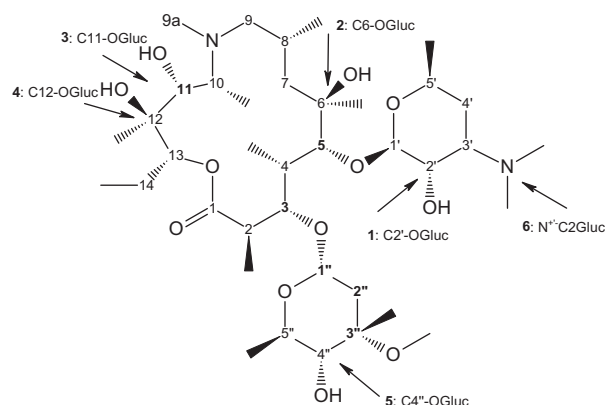


Figure 2. Predicted conjugation metabolites of azithromycin with glucuronic acid (www.biotransformer.ca) [3]

4. CONCLUSION

The predicted biotransformation of azithromycin either by microbial degradation in the environment or by metabolism in humans by CYP enzymes or glucuronic acid conjugation generates many metabolites that may increase the environmental toxicity of this antibiotic and its contribution to antimicrobial resistance (AMR).

5. REFERENCES

- Barbosa, M. O., et al., *Occurrence and removal of organic micropollutants: An overview of the watch list of EU Decision 2015/495*. Water Research, 2016, 94: 257–279.
- Kümmerer, K., *Antibiotics in the aquatic environment — A review — Part I*. Chemosphere 2009, 75(4): 417–434.
- Djombou-Feunang, Y., et al., *BioTransformer: A comprehensive computational tool for small molecule metabolism prediction and metabolite identification*. Journal Cheminformatics 2019, 11(2): 1–25.

A FAST HPLC-DAD METHOD FOR THE SIMULTANEOUS DETERMINATION OF ALL MAIN WATER-SOLUBLE VITAMINS IN FOODS AND SUPPLEMENTS

Žane Temova Rakuša, Robert Rožkar

Department of Biopharmaceutics and Pharmacokinetics, Faculty of Pharmacy, University of Ljubljana, Slovenia

1. INTRODUCTION

Water-soluble vitamins (WSV) are essential nutrients and common ingredients in fortified foods (FF), food supplements (FS), and medicines. One of the main issues in the formulation, production, and quality assurance of WSV products is their general instability, leading to degradation under various production and storage conditions, which manufacturers typically conceal with overages [1]. Aware of this, the European Commission published guidance on the acceptable overages and tolerances for vitamin contents in relation to the labeled values: 80-150% for FS and 65-150% for FF [2]. Despite the wide acceptance limits, a growing number of studies reveal WSV contents outside these intervals and even above their tolerable upper intake levels in FF and FS [1,3]. Thus, quality control of these loosely regulated products (FF and FS) using proper analytical methodology is crucial in ensuring their quality, safety, and efficacy. Though, their analytics is complicated due to different WSV amounts in FF and FS (e.g., up to 20,000 fold differences between C and B12), lack of chromophores (B5 and B7), limited stability (C and B9), and water solubility (B2, B9) [1]. Despite the recent progress in WSV analytics, enabling the simultaneous analysis of the main WSV in a single run [1], with the development of the food and pharmaceuticals industry, the new finding and use of new vitamin forms (e.g., 5-methyl-tetrahydrofolic acid (MTHFA), there is scope for improvement of the current WSV analytics. Thus, we aimed to develop a fast and simple method for the simultaneous analysis of WSV in their most common forms, including the active folate form MTHFA and the WSV, typically determined individually because of their low concentrations (B7 and B12).

2. MATERIALS AND METHODS

2.1. Chemicals and reagents

WSV standards: L-ascorbic acid (C, 99.4%), thiamin hydrochloride (B1, 99.9%), riboflavin (B2, 100.0%), nicotinamide (B3, 99.9%), calcium-D-pantothenate (B5, 99.0%), pyridoxine hydrochloride (B6, 100.0%), and cyanocobalamin (B12, 99.8%) were purchased from Sigma-Aldrich (Germany). D-biotin (B7, 100.6%), MTHFA (98.1%), and folic acid (B9, 97.8%) were purchased from Carbosynth (UK). HPLC grade methanol was purchased from Sigma-Aldrich (Germany) and sodium dihydrogen phosphate monohydrate from Merck (Germany). Ultra-pure water was obtained through a Milli-Q purification system A10 Advantage (Millipore Corporation, USA).

2.2. HPLC-DAD analysis

A chromatographic system Infinity 1290 (Agilent Technologies, USA), equipped with a diode array detector (DAD) and EZChrom acquisition system was used for the analysis. An XSelect CSH C18 150×4.6 mm, 3.5 μm column (Waters Corporation, USA) at 40°C and a mobile phase consisting of solvent A: 25 mM NaH₂PO₄×H₂O, pH = 4.0, and solvent B: methanol were used. Initial isocratic elution (99% A and 1% B), followed by gradient elution (up to 35% B) at a flow rate of 1 mL/min was utilized for the separation of all evaluated WSV in a total run time of 15 min. The injection volume was 5 μL during validation and was adjusted according to WSV contents in FF and FS (from 0.2 to 20 μL). Detection was carried out at different characteristic wavelengths for the individual WSV (210, 245, 260, 287, 362, and 445 nm).

2.3. Method validation

The method was validated following the ICH guidelines Q2(R1) [4] in terms of specificity, linearity, accuracy, precision, limit of detection (LOD), limit of quantification (LOQ), sample stability, and recovery. The concentration ranges were adjusted to the WSV recommended

P61

daily amounts (RDA). Thus, 100% RDA represents the RDA dissolved in 200 mL, except for B7 and B12, where due to low RDAs higher concentrations were used. Seven calibration standards containing 5-400% RDA of the WSV, and three quality control samples (low, medium, and high) were prepared daily, on each of the three validation days. The samples were prepared in 0.1 mM EDTA (0.1 mM EDTA containing 1 mM NaOH for B2, B7, B9, and MTHFA).

2.3. Method application

The method was applied to assay WSV content in 10 commercial FF (vitamin waters) and 10 FS (capsules (FS1) and tablets (FS2-9)). The tested FF were directly injected into the UHPLC system. FS samples were prepared by a previously developed extraction procedure [1].

3. RESULTS AND DISCUSSION

3.1. Method development

Our main aim was to develop the first so far reported HPLC-DAD method for the simultaneous analysis of all main WSV, including the newer and active folate form MTHFA, as well as B7 and B12, which usually require individual analysis due to their low amounts in FF and FS. As WSV are typically found in combinations or all together in FF and FS, by the development of this method, we provided a tool for their fast and simple analysis using common systems (HPLC-DAD). The developed method resulted in symmetric and separated peaks (Fig.1) and significantly shorter run time compared to other similar published methods for the analysis of less WSV.

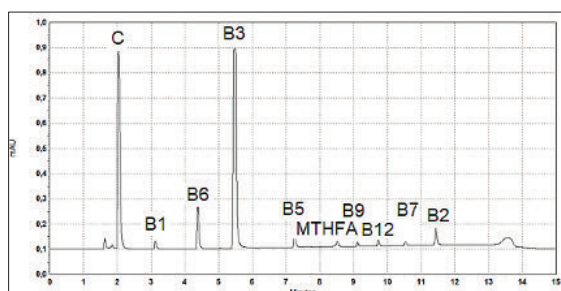


Figure 1. Chromatogram of a standard mixture of WSV at 210 nm, representing their chromatographic separation.

3.2. Method validation

The method was successfully validated according to ICH guidelines Q2(R1) [4] proving its selectivity, linearity over the

selected concentration ranges, precision, accuracy, recovery, and sample stability.

3.3. Method application

The obtained results for the WSV assay (Table 1) confirm the applicability of the method and emphasize the importance of the quality control of FF and FS, as all products, except FF5 contained an inappropriate amount of at least one WSV considering the European Commission acceptable tolerances.

Table 1. WSV assay in the tested FF and FS.

Product	C	B1	B2	B3	B5	B6	B7	B9	MTHFA	B12
FF 1										
FF 2										
FF 3										
FF 4										
FF 5										
FF 6										
FF 7										
FF 8										
FF 9										
FF 10										
FS 1										
FS 2										
FS 3										
FS 4										
FS 5										
FS 6										
FS 7										
FS 8										
FS 9										
FS 10										

Green – contents within, red – above, and orange, below the acceptable tolerances, blue – contents below the LOD.

4. CONCLUSION

The developed method represents a step forward in WSV analysis, enabling the analysis of all WSV with single sample preparation and chromatographic run in a favourable analysis time of 15 min.

5. REFERENCES

1. Temova Rakuša Ž., et. al., *Comprehensive Approach for the Simultaneous Analysis of All Main Water-Soluble Vitamins in Multivitamin Preparations by a Stability-Indicating HPLC-DAD Method*. Food Chemistry, 2021. 337: 127768.
2. European Commission Setting of Tolerances for Nutrient Values Declared on a Label Guidance For Food Supplements, 2014.
3. Andrews K.W., et al. *Analytical Ingredient Content and Variability of Adult Multivitamin/Mineral Products: National Estimates for the Dietary Supplement Ingredient Database*. The American Journal of Clinical Nutrition, 2017. 105:526–539.
4. ICH Harmonised Tripartite Guideline Validation of Analytical Procedures: Text and Methodology Q2(R1). 2005.

NATURAL APOCAROTENOIDS AND THEIR SEMISYNTHETIC GLYCOPEPTIDE CONJUGATES AGAINST SARS-COV-2

Ilona Berezki,^{1,2} **Henrietta Papp**,^{2,3} **Veronika Nagy**,⁴ **Attila Agócs**,⁴ **Ferenc Jakab**,^{2,3}
Pál Herczegh,¹ **Anikó Borbás**^{1,2}

¹Department of Pharmaceutical Chemistry, University of Debrecen, Egyetem tér 1, H-4032 Debrecen, Hungary

²National Laboratory of Virology, Szentágotthai Research Centre, Ifjúság útja 20, H-7624 Pécs, Hungary

³Institute of Biology, Faculty of Sciences, University of Pécs, Ifjúság útja 6, H-7624 Pécs, Hungary

⁴Department of Biochemistry and Medical Chemistry, Medical School, University of Pécs, Szigeti u. 12, H-7624 Pécs, Hungary

1. INTRODUCTION

The development of effective antiviral drugs against SARS-CoV-2 is one of the most important tasks today. The clinically used glycopeptide antibiotic, teicoplanin, emerged as a potential antiviral [1], and its efficacy can be improved with lipophilic modifications [2], but unfortunately their cytotoxicity is also elevated. Apocarotenoids are produced naturally in plants by oxidative cleavage of carotenoids. They are not toxic hydrophobic substances with beneficial biological effects. We planned to synthesize new types of lipophilic glycopeptide antibiotic derivatives equipped with different apocarotenoid side chains. All conjugates effectively inhibited SARS-CoV-2 replication and interestingly, bixin also exerted remarkable anti-SARS-CoV-2 activity on its own.

2. MATERIALS AND METHODS

2.1. Synthesis of glycopeptide derivatives

For the synthesis of glycopeptide conjugates, we used bixin (**1a**), crocetin monomethyl ester (**1b**) and β -apo-8'-carotenoic acid (**1c**) as

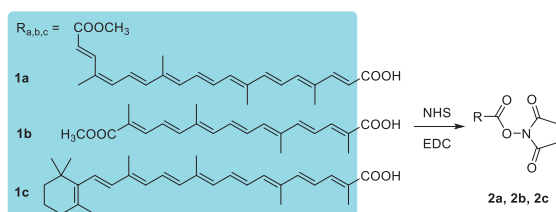


Figure 1. Preparation of the active esters from apocarotenoids.

apocarotenoids (Figure 1.) and teicoplanin, teicoplanin pseudoaglycone and ristocetin aglycone as glycopeptides.

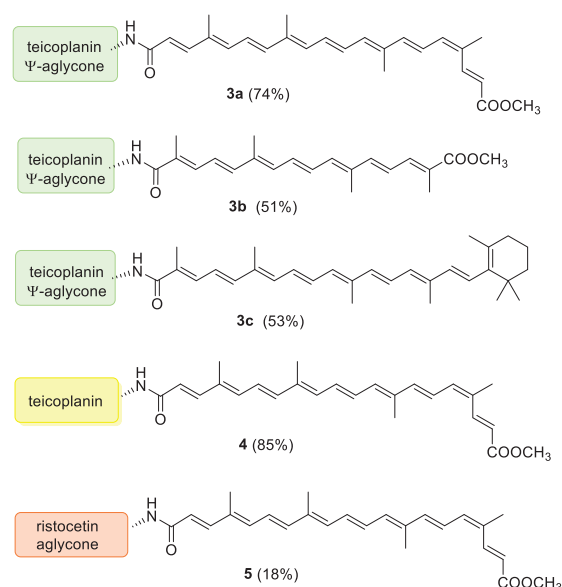


Figure 2. Apocarotenoid-glycopeptide conjugates.

From apocarotenoids (**1a**, **1b** and **1c**) active esters were prepared (**2a**, **2b** and **2c**) and the *N*-terminal primary amino groups of glycopeptide derivatives were acylated by these active esters to produce apocarotenoid derivatives.

2.2. Antiviral evaluations

Antiviral activity of the semisynthetic derivatives as well as the starting glycopeptides and apocarotenoids was evaluated in Vero E6 cells using three orthogonal assays. The one order of magnitude difference between the EC_{50} values can be explained by the four times lower multiplicity of infection and the removal of the viral inoculum after a half hour incubation in the RNA reduction assay.

To elucidate the mechanism of antiviral action of the active derivatives, human cathepsin L and B (required for the viral infection of SARS-

P62

CoV-2) and viral 3CLPro inhibitory assays were performed.

Table 1. Antiviral effects of the glycopeptide conjugates and apocarotenoids.

Compound	SARS-CoV-2 RNA reduction EC ₅₀ (μM)	SARS-CoV-2 CPE, EC ₅₀ (μM)	SARS-CoV-2 IFA, EC ₅₀ (μM)	CC ₅₀ (μM)
3a	5.9	91±88	74±20	>100
3b	5.2	19 ±1.8	8.8±1.4	>100
3c	4.4	56±10	24±5.3	>100
4	1.8	56 ±6.2	51±9.8	>100
5	6.7	n.d.	n.d.	n.d.
Teicoplanin ψglycone	not active at 50 μM	n.d.	n.d.	n.d.
Teicoplanin	5.6	16 ±1.7	18±5.4	>100
Ristocetin aglycone	not active at 50 μM	n.d.	n.d.	n.d.
1a	5.9	14±3.5	28±8.8	>100
1b	not active at 50 μM	n.d.	n.d.	n.d.
1c	15	14±2.2	31±7.9	>100

3. RESULTS AND DISCUSSION

The semisynthetic glycopeptides and native teicoplanin inhibited the viral reproduction with similarly high efficacy, the EC₅₀ values were in the low micromolar range in the RNA reduction assay and in the ten-micromolar range in the CPE-based and immunofluorescent assays. Although, the most interesting finding of this study is the remarkable, unexpected antiviral activity of two apocarotenoids, bixin (**1a**), and β-apo-8'-carotenoic acid (**1c**). The activity of bixin is based on cathepsin L inhibition while conjugates of teicoplanin pseudoaglycone with apocarotenoids have a combined mechanism of action based on cathepsin and 3CLPro inhibition.

4. CONCLUSION

The aim of this work was to study the effect of lipophilic carotenoid side chains on the anti-SARS-CoV-2 activity of the glycopeptide

antibiotic teicoplanin and ristocetin. Several derivatives have been synthesized, which showed remarkable antiviral activity and were completely devoid of cytotoxicity. However, the anti-SARS-CoV-2 activity of the natural food colorant bixin seems to be the most interesting and promising result.

5. REFERENCES

1. Zhou, N., et al., *Glycopeptide antibiotics potently inhibit cathepsin L in the late endosome/lysosome and block the entry of Ebola virus, Middle East respiratory syndrome coronavirus (MERS-CoV), and severe acute respiratory syndrome coronavirus (SARS-CoV)*. Journal of Biological Chemistry, 2016, 291(17), 9218–9232.
2. Szűcs, Z., et al., *Structure-activity relationship studies of lipophilic teicoplanin pseudoaglycon derivatives as new anti-influenza virus agents*. European Journal of Medicinal Chemistry, 2018, 157, 1017–1030.

ACKNOWLEDGMENT

This work was supported by the European Regional Development Fund under the projects GINOP-2.3.2-15-2016-00044, and GINOP-2.3.4-15-2020-00008. This research was also funded by the National Research, Development and Innovation Office of Hungary (K 131493). Viral RNA reduction assay was supported by the European Union, and co-financed by the European Social Fund: Comprehensive Development for Implementing Smart Specialization Strategies at the University of Pécs (EFOP-3.6.1.-16-2016-00004), and by the Ministry for Innovation and Technology of Hungary (TUDFO/47138/2019-ITM). Project no. TKP2021-NVA-07 and TKP2021-EGA-13 have been implemented with the support provided from the National Research, Development and Innovation Fund of Hungary, financed under the TKP2021-NVA and TKP2021-EGA funding schemes.

DESIGN, SYNTHESIS AND EVALUATION OF NOVEL BChE/p38 α MAPK DUAL INHIBITORS FOR THE TREATMENT OF ALZHEIMER'S DISEASE

Svit Ferjančič Benetik¹; Boris Markoja¹; Matic Proj¹; Damijan Knez¹; Stanislav Gobec¹; Aleš Obreza¹; Urban Košak¹

¹University of Ljubljana, Faculty of Pharmacy, Aškerčeva 7, 1000 rLjubljana, Slovenia
Correspondence: ales.obreza@ffa.uni-lj.si

1. INTRODUCTION

Alzheimer's disease (AD) is a progressive neurodegenerative disorder and represents a major cause of dementia leading to disability and death. It is estimated that around 50 million people worldwide suffer from AD or other dementias with the number expected to reach 75 million by 2030 [1].

There are only four marketed small-molecule drugs for the treatment of Alzheimer's disease – donepezil, galantamine, rivastigmine and memantine which only help to temporarily alleviate symptoms while the disease progresses. The recently approved monoclonal antibody aducanumab was designed to address the cause of AD by clearing off amyloid β ($A\beta$) aggregates but clinical trials showed no convincing evidence of reduced cognitive decline in patients. Design of novel effective disease-modifying drugs in this field therefore presents a major challenge in medicinal chemistry.

A multitude of hypotheses must be taken into account when explaining AD pathology - the most popular being the cholinergic, $A\beta$ toxicity, tau and inflammation hypothesis [2]. The cholinergic hypothesis states that forebrain cholinergic neuron loss is characteristic of AD, so by inhibiting the hydrolytic action of cholinesterases [acetylcholinesterase (AChE) and butyrylcholinesterase (BChE)], we may augment the activity of surviving cholinergic neurons [3]. This is the principle idea behind donepezil, galantamine and rivastigmine as well as the *in vivo* active piperidine-based selective BChE inhibitor developed previously by our research group [4].

Since cholinesterase inhibitors alone do not directly alter the pathophysiological processes in AD we aim to further exploit the possible drug targets in AD to halt disease progression by various mechanisms. According to one theory inflammation response is

the driving force in AD progression. $A\beta$ plaques stimulate microglial p38 α MAP kinase which then up-regulates proinflammatory cytokines such as TNF- α and IL-1 β . The latter then activates p38 α MAPK in astrocytes which leads to a chronic inflammatory state and excitotoxicity. Additionally, p38 α MAPK can phosphorylate the neurotoxic tau protein [5]. We intend to combine the cholinergic and inflammation hypothesis by developing dual BChE/p38 α MAPK inhibitors.

2. RESULTS AND DISCUSSION

First, a library of small molecules with confirmed activity against p38 α MAPK was prepared using ChEMBL and PDB (in ChEMBL activity threshold of $K_d/IC_{50} < 50 \mu\text{M}$ was accounted for). Of the 5490 compounds 172 were commercially available. These were further divided into 30 clusters according to molecular fingerprint and docked into the BChE active site gorge. According to docking results 8 best small molecules were purchased and evaluated *in vitro* against BChE by the method of Ellman.

Of the eight compounds, very promising activity against BChE was exhibited by ARRY-371797 (**Figure 1**) a p38 α MAPK inhibitor of Pfizer Inc. This molecule was then subjected to further optimization.

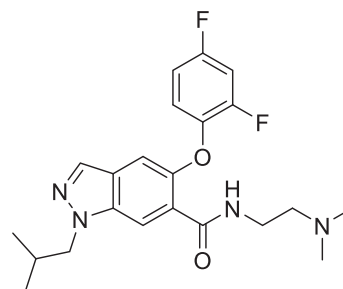


Figure 9. Structure of p38 α MAPK inhibitor ARRY-371797

3. CONCLUSION

We started the synthesis of analogues by substituting the indazole core with various azines, bicyclic nitrogen heterocycles and 4-phenyl azines. The analogues with switched positions of the amide and ether were also synthesized. All synthesized compounds were initially evaluated for their *in vitro* activity against p38 α MAPK and BChE with ADP-Glo kinase assay and Ellman's method respectively.

4. REFERENCES

1. Masters, CL., et al., *Alzheimer's disease*. Nature Reviews, Disease Primers, 2015. 1: 15056.
2. Kheiri, G., et al., *Role of p38/MAPKs in Alzheimer's disease implications for amyloid beta toxicity targeted therapy*. Reviews in the Neurosciences, 2019. 30(1): 9–30.
3. Darvesh, S., et al., *The biology of butyrylcholinesterase*. Nature reviews, Neuroscience, 2003. 4: 131–8.
4. Košak, U., et al., *Development of an in-vivo active reversible butyrylcholinesterase inhibitor*. Scientific Reports, 2016. 6(1): 39495.
5. Munoz, L., et al., *Targeting p38 MAPK pathway for the treatment of Alzheimer's disease*. Neuropharmacology, 2010. 58(3): 561–568.

ACKNOWLEDGMENT

The authors acknowledge the financial support from the Slovenian Research Agency.

COUNTERING DIVERSION OF PHARMACEUTICAL-BASED COMPOUNDS ALONG THE CHEMICAL SUPPLY CHAIN: A WORKSHOP

Yavana Ganesh¹, Jonathan E. Forman¹, Kabrena E. Rodda¹, John R. Cort², Ellen M. Wynkoop¹

¹National Security Directorate, Pacific Northwest National Laboratory, United States of America

²Earth and Biological Sciences Directorate, Pacific Northwest National Laboratory, United States of America

1. INTRODUCTION

Pharmaceuticals are chemical substances designed to act on physiological processes. Despite legitimate uses, there is potential to misuse pharmaceuticals for harmful purposes. State and non-State actors can exploit legitimate chemical supply chains to acquire pharmaceutical compounds, chemicals, and precursors. For example, in October 2002, Russian security forces used a pharmaceutical-based agent (PBA), suspected to be a fentanyl derivative, to end a hostage situation in the Dubrovka Theater Incident in Moscow, resulting in the death of 170 people and demonstrating the potential of weaponizing these substances. In 2021, to address the threat of pharmaceutical-based agents, Pacific Northwest National Laboratory developed a webinar series to raise awareness for international partners on Countering Diversion of Pharmaceutical Based Compounds Along the Chemical Supply Chain.

2. MATERIALS AND METHODS

2.1. Materials

Subject matter experts at Pacific Northwest National Laboratory developed a set of training modules covering the growing threat of pharmaceutical-based compounds, a Novichok agent case study, chemical weapons and Syria, and emerging threats in the pharmaceutical sector. These modules were delivered through the webinar series to government officials, chemical producers, distributors, academic researchers, and other stakeholders in pharmaceutical and chemical supply chains in

countries that play a role in the global trade of pharmaceutical chemicals.

2.2. Method

PNNL instructors used the Zoom and Mentimeter platforms to facilitate interactive presentations and discussions with webinar participants.

3. RESULTS AND DISCUSSION

3.1. Day one

The first day began with an interactive questionnaire to identify participants most pressing concerns with pharmaceutical-based agents and supply chain diversion. This was followed by presentations that discussed pharmaceutical-based agents with a focus on fentanyl as an archetypal PBA, legitimate uses of pharmaceuticals in health, medicine, and other sectors. The day concluded with presentations discussing the growing threat of PBAs as illicit drugs, fentanyl as an incapacitating agent, and PBAs as chemical weapons.

3.2. Day two

The second day began with an activity and discussion on identifying threats from PBAs in the participant country. This was followed by presentations discussing fentanyl and central-nervous system-acting agents within the context of the Chemical Weapons Convention, and a case study of Novichok poisoning. The day concluded with a presentation on improving supply chain security (Figure 1), where participants learned to recognize supply chain diversions through red-flag indicators and “know your customer” best practices.

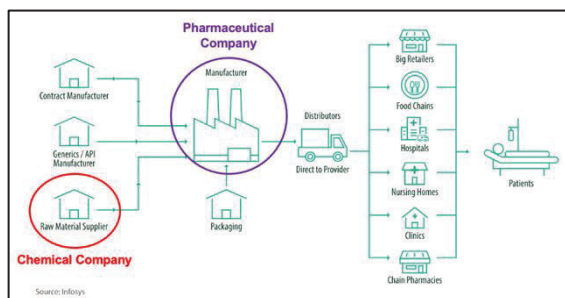


Figure 1. A generic pharmaceutical supply chain [1].

3.3. Day three

In the opening of day 3, participants applied knowledge from the first two days to identify supply chain security threats associated with a fictitious scenario. This was followed by presentations discussing emerging threats in the pharmaceutical sector, such as clandestine medicinal chemistry, custom synthesis, and novel countermeasures, and the roles of government regulators and industry in preventing the proliferation of PBAs. The day concluded with a roundtable discussion on identifying country-specific pharmaceutical supply chain security challenges.

3.4. Day four

The final day opens with a case study focused on the intersections of pharmaceutical-based production and chemical weapon-related activities. The day concludes with participants identifying actionable ways to address PBA-related challenges identified on day three.

4. CONCLUSION

The webinar series provided a forum for sharing perspectives and insights amongst stakeholders along the chemical supply chain. Participants were introduced to chemical security and through discussion identified specific challenges in their countries and mitigation tactics to counter diversion and proliferation.

5. REFERENCES

1. Gedan, M., Taylor, K, *Covid-19 and pharma supply chain resilience*. Infosys Knowledge Institute, 2020.

ACKNOWLEDGMENT

I want to thank Dr. Michael Jones for his support and encouragement of the webinar series and Dr. Kristin Omberg of Pacific Northwest National Laboratory for reviewing and providing constructive feedback in the development of this poster presentation.

DESIGN OF NEW POTENT AND SELECTIVE THIOPHENE-BASED K_v1.3 INHIBITORS AND THEIR POTENTIAL FOR ANTICANCER ACTIVITY

Špela Gubič¹, Louise Antonia Hendrickx², Xiaoyi Shi³, Žan Toplak¹, Kenny M. Van Theemsche^{4,5}, Ernesto Lopes Pinheiro-Junior², Steve Peigneur², Alain J. Labro^{4,5}, Luis A. Pardo³, Jan Tytgat², Tihomir Tomašič¹ and Lucija Peterlin Mašič^{1,*}

¹Faculty of Pharmacy, Aškerčeva 7, University of Ljubljana, 1000 Ljubljana, Slovenia;

²Campus Gasthuisberg, University of Leuven, Toxicology and Pharmacology, Onderwijs en Navorsing 2, Herestraat 49, 3000 Leuven, Belgium

³AG Oncophysiology, Max-Planck Institute for Multidisciplinary Sciences, Hermann-Rein-Str. 3, 37075 Göttingen, Germany

⁴Laboratory for Molecular, Cellular and Network Excitability, Department of Biomedical Sciences, University of Antwerp, 2610 Wilrijk, Belgium

⁵Department of Basic and Applied Medical Sciences, Ghent University, Corneel Heymanslaan 10 (Entrance 36), 9000 Ghent, Belgium

1. INTRODUCTION

The K_v1.3 channel has only recently emerged as a molecular target in cancer therapy. Cancer cells display mutations enabling extensive proliferation and resistance to apoptosis. K_v1.3 channel activity has been found to be involved in cell proliferation, migration, and invasion, which are among the most important processes in cancer progression. Moreover, overexpression of K_v1.3 enhances tumorigenic processes and promotes tumor progression [1–2]. The use of small-molecule K_v1.3 inhibitors could selectively suppress the proliferation of cancer cells, thus providing a new potential therapeutic approach [2]. Although K_v1.3 has been recognized as a tumor marker in cancer tissues with predominantly higher K_v1.3 expression, a clear pattern of altered K_v1.3 expression in cancer cells compared with healthy cells has not yet been found. The type and stage of disease also influence K_v1.3 expression. Up-regulated K_v1.3 expression was detected in breast, colon, and prostate tumors, in smooth muscle and skeletal muscle cancers, and in mature neoplastic B cells in chronic lymphocytic leukemia [3].

In previous work, we identified two new K_v1.3 inhibitors by virtual screening based on a 3D similarity search using the K_v1.3 inhibitor PAC as a query [4]. Hit compound (Figure 1) with an IC₅₀ of 17.4 μM (applied *ex vivo* in *Xenopus* oocytes expressing K_v1.3) was a weaker K_v1.3 inhibitor. However, it exhibited a good selectivity profile and did not affect other K_v1.x

family channels or more distantly related channels.

2. MATERIALS AND METHODS

2.1. Apoptosis and Proliferation Assays

For cell proliferation assays, cells were seeded at a density of 10,000 cells/well in 96-well flat bottom culture plates (Corning, Kaiserslautern, Germany) and proliferation was measured through culture confluency using an IncuCyte device (Sartorius, Göttingen, Germany). Every hour, two phase contrast images per well were acquired, and a confluency mask was generated by training the analysis algorithm using representative images. Every image was then analyzed using the obtained parameters to determine culture confluency. Treatments were then added when cells reached a confluency of ~30% (Panc-1) or ~55% (Colo-357), and proliferation was determined for the following 60 h. Proliferation is reported as confluency increase with respect to the start of the treatment.

Spheroids were cultured in round bottom ultra-low attachment 96-well plates (Corning). The optimal seeding densities were empirically determined (8000 cells/well for Colo-357 or 10,000 cells/well for Panc-1 spheroids). The cells were suspended in 2% Matrigel (Corning), centrifuged at 1000× g for 10 min and the spheroids were allowed to form in the incubator. Once the spheroids were formed, the treatments indicated together with 8.9 μM cycloheximide (as apoptosis sensitizer) were added and

apoptosis was determined by live imaging in the Incucyte system in real time for approximately 60 h using Caspase-3/7 green reagent (Sartorius) as a reporter of apoptosis, which crosses the cell membrane and is cleaved by the activated Caspase-3/7, resulting in the fluorescent staining of nuclear DNA. Apoptosis on Panc-1 tumor spheroids is presented as integrated green fluorescence in the whole spheroid.

3. RESULTS AND DISCUSSION

3.1. Design and Chemistry

Six different types of cyclopentane-, cyclohexane- and tetrahydropyran-based $K_v1.3$ inhibitors were designed and synthesized with the aim of increasing potency on $K_v1.3$, and selectivity against other members of K_v1 family of the hit compounds **4** (TVS-06) and **5** (TVS-12), and to investigate structure-activity relationships (SAR) important for $K_v1.3$ inhibition.

3.2. IC_{50} Determinations of the Most Potent $K_v1.3$ Inhibitors

The most potent compounds (**14**, **37**, **43** and **44**) and the reference compound PAP-1 were tested for $K_v1.3$ inhibition with an additional independent method of manual patch-clamp procedures on Ltk^- cells (Table 1). The aim was to demonstrate the inhibition of $K_v1.3$ in a mammalian cell line and to have a direct comparison with the positive control PAP-1, which was previously tested in L929 cells and human T-cells (IC_{50} of 2 nM). Interestingly, the reference compound PAP-1 had an IC_{50} value of 780 nM (manual voltage clamp on oocytes) and 370 nM (manual patch clamp on Ltk^- cells), which is a much lower potency compared to literature data (IC_{50} of 2 nM, L929 cells, manual whole-cell patch-clamp). The best compound of Types I- VI had comparable potency on oocytes (Table 1, manual voltage-clamp) and Ltk^- cells (manual patch-clamp) of 470 nM and 950 nM, respectively.

Table 1. Comparison of $K_v1.3$ IC_{50} values for compounds **14**, **37**, **43**, **44**, and PAP-1 obtained with HiClamp and manual voltage-clamp on *Xenopus laevis* oocytes and with manual patch-clamp on the Ltk^- cell-line.

Compound ID	IC_{50} (Manual Voltage-Clamp Oocytes) [μ M]	IC_{50} (HiClamp Oocytes) [μ M]	IC_{50} (Manual Patch-Clamp Ltk^-) [μ M]
-------------	---	--	--

PAP-1	0.78 ± 0.01	2.67 ± 0.30	0.37 ± 0.02
14	0.57 ± 0.36	1.03 ± 0.03	1.33 ± 0.20
37	3.96 ± 0.47	1.97 ± 0.14	1.35 ± 0.04
43	0.59 ± 0.15	1.20 ± 0.02	1.02 ± 0.07
44	0.47 ± 0.02	1.99 ± 0.61	0.95 ± 0.24

3.3. Effects on the Growth of Cell Lines in 2D and 3D Cell Cultures

$K_v1.3$ is associated with the control of cell proliferation in various cancer cell types. Therefore, we investigated the effects of compounds **14**, **37**, **43** and **44** on the proliferation of two pancreatic cancer cell lines, Panc-1 and Colo-357, which have been reported to overexpress $K_v1.3$. The compounds were tested at a concentration of 100 μ M, which is the maximal concentration we can achieve while maintaining a low concentration of vehicle (1% DMSO, which was also added to the control). Proliferation was determined as confluence of the culture using live cell imaging over a 72 h period. For Panc-1 cells (Fig. 1A,C), compound **44** caused moderate growth inhibition, whereas **14**, **43**, and especially **37** caused strong inhibition. However, the growth of Colo-357 cells (Fig. 1B,D) was not significantly affected by any of the compounds.

To test the ability of the compounds to inhibit tumour progression in a more predictive system, we performed experiments on tumour spheroids of the pancreatic cancer cell lines used for 2D culture. In Panc-1 spheroids (Fig. 1E), the compounds that effectively reduced proliferation in 2D culture (**14**, **37**, **43**, and **44**) did not induce detectable levels of apoptosis, whereas the reference compound PAP-1 did. In Colo-357 cell spheroids, significant induction of apoptosis was observed in the presence of the hit compound **4** (Fig. 6F). None of the other compounds tested differed significantly from the control. The degree of apoptosis induction was dose-dependent, although we could not use concentrations higher than 100 μ M and therefore cannot determine the IC_{50} for induction of apoptosis. The level of apoptosis achieved by 100 μ M of hit compound **4** was similar to that achieved by 50 μ M PAP-1 (**1**).

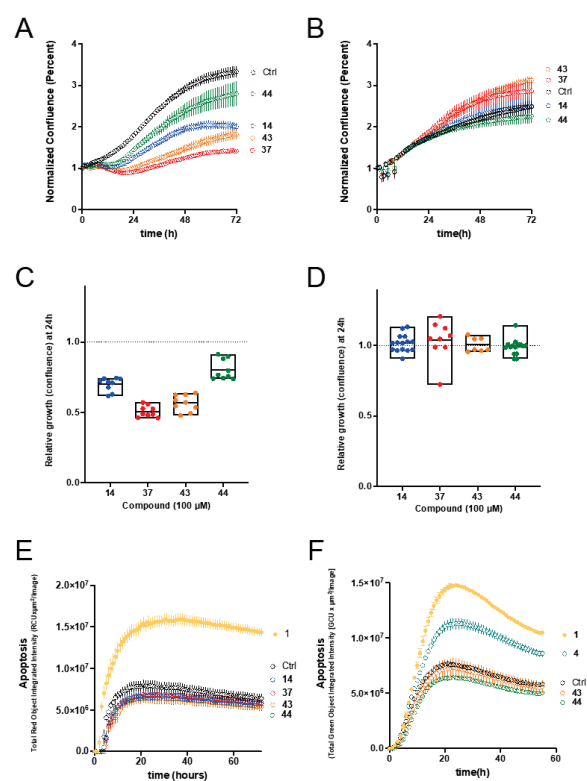


Figure 1. Effects on pancreatic cancer cell lines in 2D and 3D cell cultures. **(A)** Growth curves (culture confluence measured through phase contrast imaging) of Panc-1 cells in the presence of the indicated compounds (100 μM) or the vehicle (DMSO, black symbols). Mean \pm S.E.M, N = 9. **(B)** The equivalent experiment on Colo-357 cells revealed that the growth inhibition was cell-type specific. Mean \pm S.E.M, N = 15. The inhibition 24 h after the start of treatment is quantified in **(C,D)** for the data presented in **(A,B)** respectively. **(E)** Apoptosis measured as caspase 3/7 activity on Panc-1 tumor spheroids in the presence of the indicated compounds. **(F)** Apoptosis in Colo-357 tumor spheroids ($p < 0.001$, Mean \pm S.E.M, N = 4).

4. CONCLUSION

To discover a novel structural class of $\text{Kv}1.3$ inhibitors overexpressed in many different tumour types, we used a structural optimization approach and successfully prepared novel potent and selective thiophene-based $\text{Kv}1.3$ inhibitors [8]. We identified the potent and appropriately selective nanomolar $\text{Kv}1.3$ inhibitor **44** (Figure 1), which contains 3-thiophene and tetrahydropyran scaffolds. We demonstrated the inhibition of the Panc-1 cancer cell line proliferation by the new $\text{Kv}1.3$ inhibitors. Hit compound induced significant apoptosis in Colo-357 tumour spheroids, and

the extent of apoptosis achieved by 100 μM of hit compound was comparable to that achieved by 50 μM PAP-1. Based on the efficacy data in PDAC cell lines and Colo-357 tumour spheroids, we can assume that newly developed $\text{Kv}1.3$ inhibitors do not reach the mitochondrial $\text{Kv}1.3$ channels required for the induction of apoptosis. There is an opportunity to further develop the new structural class of potent and selective $\text{Kv}1.3$ inhibitors into mitochondrial $\text{Kv}1.3$ inhibitors by adding mitochondrial targeting moieties.

5. REFERENCES

1. Pérez-García, M.T.; Ciudad, P.; López-López, J.R. The Secret Life of Ion Channels: $\text{Kv}1.3$ Potassium Channels and Proliferation. *Am. J. Physiol.-Cell Physiol.* 2018, 314, C27–C42. <https://doi.org/10.1152/ajpcell.00136.2017>.
2. Teisseyre, A.; Palko-Labuz, A.; Sroda-Pomianek, K.; Michalak, K. Voltage-Gated Potassium Channel $\text{Kv}1.3$ as a Target in Therapy of Cancer. *Front. Oncol.* 2019, 9, 933. <https://doi.org/10.3389/fonc.2019.00933>.
3. Comes, N.; Bielanska, J.; Vallejo-Gracia, A.; Serrano-Albarrás, A.; Marruecos, L.; Gómez, D.; Soler, C.; Condom, E.; Ramón y Cajal, S.; Hernández-Losa, J.; et al. The Voltage-Dependent K^+ Channels $\text{Kv}1.3$ and $\text{Kv}1.5$ in Human Cancer. *Front. Physiol.* 2013, 4, 283. <https://doi.org/10.3389/fphys.2013.00283>.
4. Hendrickx, L.A.; Dobričić, V.; Toplak, Ž.; Peigneur, S.; Mašič, L.P.; Tomašič, T.; Tytgat, J. Design and Characterization of a Novel Structural Class of $\text{Kv}1.3$ Inhibitors. *Bioorganic Chem.* 2020, 98, 103746. <https://doi.org/10.1016/j.bioorg.2020.103746>.
5. Gubič, Š.; Hendrickx, L.A.; Shi, X.; Toplak, Ž.; Možina, Š.; Theemsche, K.M.V.; Pinheiro-Junior, E.L.; Peigneur, S.; Labro, A.J.; Pardo, L.A.; Tytgat, J.; Tomašič, T.; Mašič, L.P. Design of New Potent and Selective Thiophene-Based $\text{Kv}1.3$ Inhibitors and Their Potential for Anticancer Activity. *Cancers* 2022, 14, 2595. <https://doi.org/10.3390/cancers14112595>

SYNTHESIS AND TRANSFORMATION OF AZA-KYNURENIC ACID DERIVATIVES

Bálint Lőrinczi¹, Zsófia Sánta¹, István Szatmári¹

¹*Institute of Pharmaceutical Chemistry, Interdisciplinary Excellence Center, University of Szeged and MTA-SZTE Stereochemistry Research Group, Hungarian Academy of Sciences Eötvös u. 6, H-6720 Szeged, Hungary*

1. INTRODUCTION

Based on a 2019 report from WHO 55% of deaths worldwide are accounted for 10 diseases. The top two diseases are connected to ischaemic conditions and neurodegenerative diseases take number 7 on this list with lung cancer at number 6.

In the past few years the University of Szeged focused aimed toward the treatment of these conditions. In one of the still in progress research the main aim is on the derivatives of kynurenic acid (KYNA). In the last two decades it has been proven that loss of KYNA can be connected to neurodegenerative conditions such as Parkinson's or Huntington's disease. It has also been shown that it can also contribute to alleviate the symptoms of ischaemic conditions [1,2]. However, the direct medical usage of KYNA is inhibited because of its poor penetration through the blood-brain-barrier (BBB). There have already been several attempts trying to solve this problem, with the synthesis of derivatives through the alteration of the quinoline structure.

Derivatives of KYNA based on the functionalization of C-3 of the KYNA structure are getting abundant [3]; however, there has only been a few examples of derivatives bearing an additional nitrogen in position 3 (aza-kynurenic acid, aza-KYNA).

We aimed to create derivatives of this special aza-KYNA bearing a cationic center that is believed to promote the biological effect [4,5] of KYNA through better water solubility and blood-brain-barrier penetration.

2. MATERIALS AND METHODS

The ¹H-NMR spectra were recorded in DMSO-d₆ solutions in 5 mm tubes at room temperature (RT), on a Bruker DRX-500 spectrometer (Bruker Biospin, Karlsruhe, Baden Württemberg, Germany) at 500 (1H) MHz, with the deuterium signal of the solvent

as the lock and TMS as internal standard (1H). Melting points were determined on a Hinotek X-4 melting point apparatus. Merck Kieselgel 60F254 plates were used for TLC. CEM Discover SP microwave reactor was used for microwave treatment.

2.1. Materials

Starting materials in reagent grade were purchased from Sigma-Aldrich.

2.2. Methods

General procedure for the synthesis of 6- and 7-chloro-aza-KYNAs (3b,c)

In a 50 mL round bottom flask 5 mmol antranilic acid derivatives with 6 mmol of diethyl-oxalate was dissolved in 30 mL EtOH and refluxed for 8 hours. After evaporation of the solvent EtOAc was used for crystallization.

General procedure for the synthesis of 5- and 8-chloro-aza-KYNAs (6a,b)

In a 35 mL sized pressure-resistant vessel 0,25 mmol antranilic acid derivative and 5 mL of diethyl-oxalate was measured and treated at 110 °C for 3 h. The crystallized product was filtered and washed with 2 x 15 mL Et₂O.

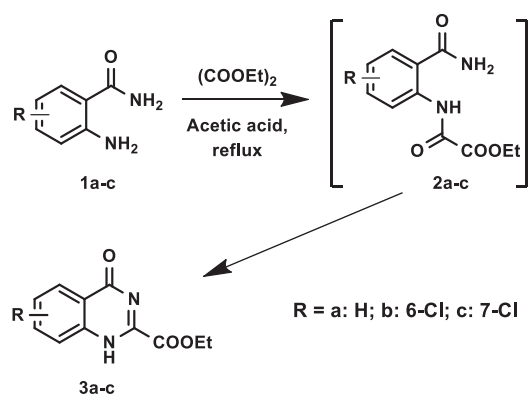
General procedure for the amidation of chloro-aza-KYNAs (7a-h)

In a round bottom flask 0,25 mmol from compounds **3a-c**, **6a** and 5 mmol from amines was dissolved in 20 mL EtOH and refluxed for 6 h. After evaporation of the solvent, the products were crystallized from 5 mL Et₂O.

3. RESULTS AND DISCUSSION

3.1. Aza-kynurenic acid and its 6- and 7-chloro derivatives

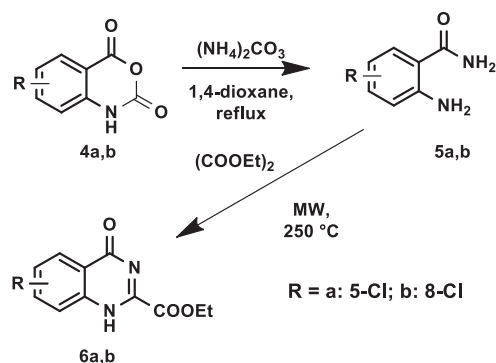
In case of the unsubstituted aza-KYNA (**3a**) and its 6- and 7-chloro derivatives (**3b,c**) the synthetic procedure described in literature yielded low amounts and was optimized using acid catalysis (Scheme 1).



Scheme 1. Synthesis of unsubstituted, 6- and 7-chloro-aza-KYNA derivatives.

3.2. 5- And 8-chloro-aza-KYNA derivatives

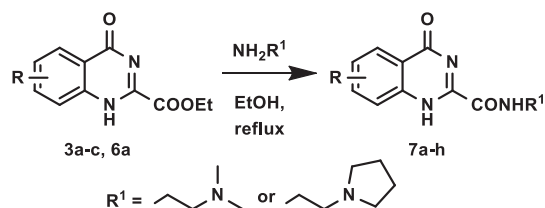
For the synthesis of 5- and 8-chloro-aza-KYNA derivatives (**6a,b**) the needed antranilic acid derivatives (**5a,b**) had to be synthesized. The best results were achieved starting from **4a,b**. However, the ring-closure had to be further altered and a microwave assisted procedure was developed (Scheme 2).



Scheme 2. Synthesis of 5- and 8-chloro-aza-KYNA derivatives.

3.2. Amidation of the aza-KYNA esters

After achieving the synthesis of the esters the amidation of the compounds was carried out utilizing direct amidation with the use of N^1, N^1 -dimethylethane-1,2-diamine and 2-(pyrrolidin-1-yl)ethanamine (Scheme 3). These amines contain the relevant cationic centers that are presumably needed for better biological activity.



Scheme 3. Direct amidation of the synthesized esters.

4. CONCLUSION

The synthesis of chloro-substituted aza-KYNA derivatives have successfully been optimized and in case of 5- and 8-chloro-aza-KYNA, a new procedure was developed for their synthesis. As a continuation of the previous KYNA based work, special amide derivatives of these compounds have also been synthesized with possible BBB penetrating and CNS effects.

5. REFERENCES

- Fülöp F., Szatmári I., Vámos E., Zádori D., Toldi J., Vécsei L. Syntheses, transformations and pharmaceutical applications of kynurenic acid derivatives *Curr. Med. Chem.* **2009**, *16* 4828.
- Gellért L.; Fuzik J.; Göblös A.; Sárközi K.; Marosi M.; Kis Z.; Farkas T.; Szatmári I.; Fülöp F.; Vécsei L.; Toldi J. Memantine and Kynurenic Acid: Current Neuropharmacological Aspects *Eur. J. Pharmacol.* **2011**, *667*, 182.
- Molnár, K.; Lőrinczi, B.; Fazakas, C.; Szatmári, I.; Fülöp, F.; Kmetykó, N.; Berkecz, R.; Ilisz, I.; Krizbai, A. I.; Wilhelm, I.; Vécsei, L. SZR-104, a novel kynurenic acid analogue with high permeability through the blood–brain barrier. *Pharmaceutics* **2021**, *13*, 61.
- Zádori D.; Veres G.; Szalárdy L.; Klivényi P.; Toldi J.; Vécsei L. Glutamatergic dysfunctioning in Alzheimer's disease and related therapeutic targets *J. Alzheimers Dis.* **2014**, *42*, 177.
- Greco R.; Demartini C.; Zanaboni A. M.; Redavide E.; Pampaloni S.; Toldi J.; Fülöp F.; Blandini F.; Nappi G.; Sandrini G.; Vécsei L.; Tassorelli C. Effects of kynurenic acid analogue 1 (KYNA-A1) in nitroglycerin-induced hyperalgesia: Targets and anti-migraine mechanisms *Cephalalgia* **2017**, *13*, 1272.

ACKNOWLEDGMENT

The authors' thanks are due to the Hungarian Research Foundation (OTKA No. K-138871) and the Ministry of Human Capacities, Hungary grant, TKP-2021-EGA-32. and to the Gedeon Richter Plc. Centennial Foundation.

SYNTHESIS OF NEW CARBAMATE-TYPE HARMICINES

Marina Marinović, Zrinka Rajić

Department of Medicinal Chemistry, University of Zagreb Faculty of Pharmacy and Biochemistry, Croatia

1. INTRODUCTION

Harmine is a naturally occurring β -carboline alkaloid that possesses a broad range of biological activities, including antitumor and antimalarial [1]. We designed and prepared several series of hybrid compounds in which harmine was covalently linked to other biologically active compounds: cinnamic acid derivatives (CADs, harmicines), quinolines (harmiquins), coumarins (harmirins) and ferrocene (harmicens), with the aim of improving its biological activities and overcoming the growing resistance to malaria and cancer chemotherapy [2,3]. The linker between the two moieties was either an amide bond or triazole ring. Our research showed that hybridization is a valuable strategy for obtaining compounds with enhanced activities. Encouraged by those results, we decided to prepare novel carbamate-type harmicines at the N-9 position of harmine's β -carboline core.

2. MATERIALS AND METHODS

The targeted carbamates **4a-g** were obtained by the reaction of amine **1** and cinnamyl alcohols **2a-g** under mild reaction conditions. Cinnamyl alcohols **2a-g** were prepared from the corresponding CADs, whereas amine **1** was prepared from harmine. To investigate the effect of substituents at the CADs benzene ring on harmicines biological activity, we chose seven CADs with different substitution pattern (*o*-Cl, *m*-Cl, *m*-OCF₃, *p*-Br, *p*-CH₃, *p*-CF₃, *p*-NO₂).

Reactions which require anhydrous conditions were performed under argon atmosphere in anhydrous solvents. All reagents and solvents were purchased from commercial sources. The title compounds **4a-g** were purified by column chromatography, triturated with diethyl ether

and fully characterized by standard methods (IR, ¹H- and ¹³C-NMR, and MS).

2.1. Synthesis of amine **1**

Alkylation of harmine at the N-9 position with 2-(Boc-amino)ethyl bromide in the presence of Cs₂CO₃ in anhydrous DMF followed by the removal of the Boc protecting group under acidic conditions (HCl/MeOH) resulted in the preparation of the primary amine **1**.

2.2. Synthesis of cinnamyl alcohols (**2a-g**)

Cinnamyl alcohols (**2a-g**) were prepared from the corresponding CADs. In the first step, CAD was converted to acyl chloride by the means of thionyl chloride and a catalytic amount of anhydrous DMF in anhydrous toluene. Acyl chloride was further reduced to the corresponding alcohol by sodium borohydride in anhydrous ether with the dropwise addition of anhydrous MeOH. This method enabled avoiding the use of stronger reductants, such as lithium aluminum hydride and partial reduction of the CAD double bond.

2.3. Synthesis of carbamate-type harmicines (**4a-g**)

Carbamate-type harmicines were synthesized by a straightforward two-step procedure. Firstly, the reaction of cinnamyl alcohols (**2a-g**) with 1,1'-carbonyldiimidazole (CDI) in anhydrous ether afforded alkoxy-carbonylimidazoles (**3a-g**) which consequently reacted with amine **1** in anhydrous DMF to yield carbamates **4a-g**.

3. RESULTS AND DISCUSSION

Here we present the synthesis of seven novel carbamate-type harmicines, harmine and CADs hybrids, synthesized at N-9 position of the harmine's β -carboline core.

3.1. Synthesis of amine 1

Primary amine **1** was obtained by the alkylation of harmine at the N-9 position and consequently the removal of the Boc protecting group. The synthetic route is depicted in Fig. 1.

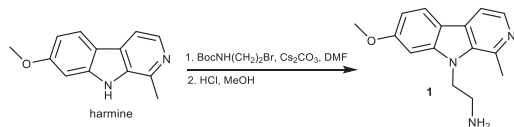


Figure 1. Synthetic pathway to amine **1**

3.2. Synthesis of cinnamyl alcohols (2a-g)

The synthetic route for the preparation of cinnamyl alcohols **2a-g** from acyl chlorides is depicted in Fig. 2.

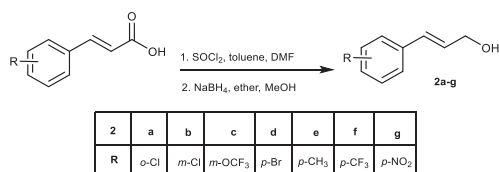


Figure 2. Synthetic pathway to cinnamyl alcohols **2a-g**

3.3. Synthesis of carbamate-type harmicines 4a-g

Carbamate-type harmicines were prepared by the reaction of amine **1** and cinnamyl alcohols **2a-g** in good to moderate yields (34–49%). The synthetic route and structures of novel harmicines **4a-g** are depicted in Fig. 3.

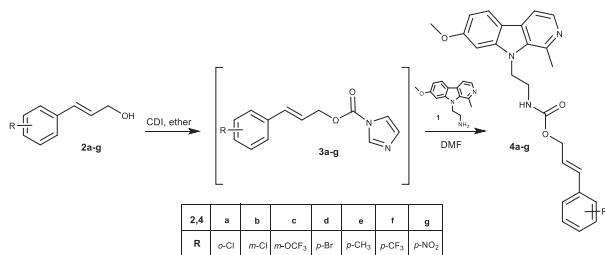


Figure 3. Synthetic pathway to carbamate-type harmicines **4a-g**

4. CONCLUSION

Seven novel carbamate-type harmicines **4a-g** were successfully synthesized and characterized. Evaluation of harmicines antimalarial activity, as well as cytotoxicity against human cell lines, is in progress.

5. REFERENCES

- Javeed, M., et al., *Harmine and its derivatives: Biological activities and therapeutic potential in human diseases*. Bangladesh Journal of Pharmacology, 2018. 13: 203-213.
- Marinović, M., et al., *Further investigation of harmicines as novel antiplasmodial agents: Synthesis, structure-activity relationship and insight into the mechanism of action*. European Journal of Medicinal Chemistry, 2021. 224: 113687.
- Pavić, K., et al., *Synthesis and Biological Evaluation of Harmirins, Novel Harmine–Coumarin Hybrids as Potential Anticancer Agents*. Molecules, 2021. 26: 6490.

ACKNOWLEDGMENT

This work was fully supported by the Croatian Science Foundation under the project number UIP-2017-05-5160 and by the Young researcher's career development project – training of doctoral students of the Croatian Science Foundation founded by the European Union from the European Social Fund. 

DISCOVERY OF INHIBITORS OF Hv1 PROTON CHANNELS AS POTENTIAL ANTICANCER DRUGS

Martina Piga¹; Zoltán Varga²; Ádám Fehér²; Ferenc Papp²; Eva Korpos Pintye-Gyuri²; Tihomir Tomašič¹; Nace Zidar¹

¹University of Ljubljana, Faculty of Pharmacy, Aškerčeva 7, 1000 Ljubljana, Slovenia

²University of Debrecen, Faculty of Medicine, Egyetem tér 1. H-4032 Debrecen, Hungary

Correspondence: nace.zidar@ffa.uni-lj.si

1. INTRODUCTION

Voltage-gated proton channels (Hv1) are proton-selective voltage-dependent channels that have been found in various mammalian cells as well as in cancer cells. They play an important role in many signaling pathways by regulating the intracellular pH and preventing intracellular acidification [1]. In physiological conditions, at the resting membrane potential, the channels are closed; however, when various pathological conditions occur, these channels can open even at the resting membrane potential. In this acidic microenvironment, tumor cells can adapt extremely well, while immune cells functions are impaired.

The aim of our work is to discover and evaluate a series of new Hv1 inhibitors. At present, there are no selective inhibitors specific for Hv1 proton channels. A selective Hv1 inhibitor would allow us to modulate the acidic tumor microenvironment and to study how this affects tumor cell functions and tumor growth. A neutral tumor microenvironment would support the tumor suppressive function of immune cells. Hv1 inhibitors could be used as therapeutics in the treatment of cancer or serve as adjuvants for other existing therapies.

2. MATERIALS AND METHODS

An open structure of the human Hv1 channel was used to perform virtual screening (VS) of an in-house library of compounds and selected known Hv1 inhibitors [2, 3]. Compounds were docked to the binding site of guanidine derivatives, such as 2-guanidinobenzimidazole

(2GBI), on the voltage-sensing domain [4]. A series of molecules was selected to be tested by patch-clamp electrophysiology on Hv1 channels. A small series of analogues was prepared by organic synthetic procedures and their identity and purity were evaluated by different spectroscopic and chromatographic techniques.

3. RESULTS AND DISCUSSION

Virtual screening results were evaluated, and a series of most promising hits were selected for biological evaluation on Hv1 channels. Four hits, NZ-10-2, NZ-49, NZ-58 and NZ-63-2 were found to have an effect on proton currents (more than 50% block at 50 μ M). The compound that showed the greatest effect, inhibiting the Hv1 current by more than 90% at 100 mV, was NZ-58 (Fig.1; Fig.2). Results obtained using the patch-clamp technique in the whole-cell configuration in Chinese Hamster Ovary (CHO) cells transfected with hHv1, show that binding of NZ-58 causes a rightward shift of the opening threshold potential, similar to that observed with the application of acidic extracellular solution. This suggests that NZ-58 binding modifies the opening of Hv1, most likely by hindering the movement of the voltage-sensing domain, allowing Hv1 to open only at more positive voltages. However, in a certain membrane potential range, binding of NZ-58 appears to have an inhibitory effect, but in a membrane potential-dependent manner. On the other hand, this compound has shown low selectivity because it also acts on voltage-gated sodium and potassium channels. For these

P68

molecules, dose-response tests, selectivity screening and viability assays would be the next steps and new molecules will be synthesized by systematically modifying key functional groups.

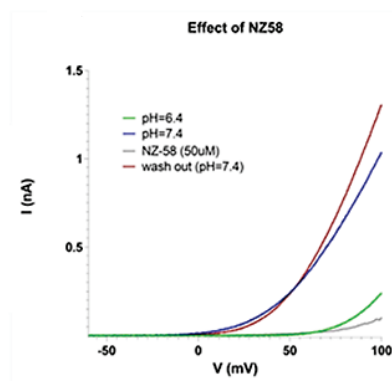


Figure 10. The effect of NZ-58 on Hv1 proton currents.

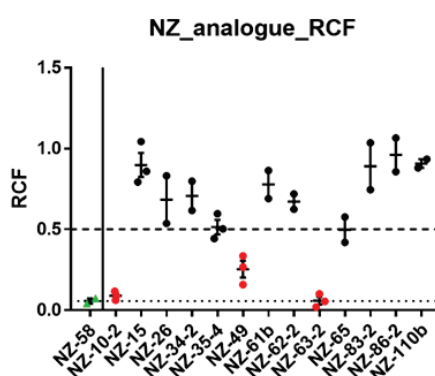


Figure 11. Effects of NZ analogues - remaining Hv1 current fraction measured at +100 mV in the presence of 50 μ M of the compounds.

In addition, three analogues of the recently discovered Hv1 inhibitors, so-called HIF (Hv1 Inhibitor Flexible) compounds were synthesized [3]. The general structure of these analogues comprises an aminoimidazole ring and an aromatic or aliphatic ring connected by flexible linkers (Fig.3). We wanted to investigate the effects of introducing an aromatic or aliphatic nitrogen-containing heterocycle on ligand-channel interactions. By introducing an amide bond and increasing the distance between the two cycles of the molecules, we wanted to better explore the 2GBI proposed binding-pocket.

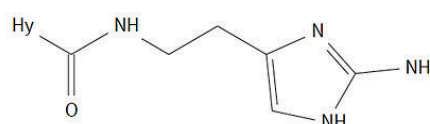


Figure 12. General structure of the new synthesized compounds - Hy=heterocycle.

4. CONCLUSION

By bringing together the knowledge and the results from ligand- and structure-based drug design, biophysical and pharmacological characterization, and medicinal chemistry methods, we have obtained a valid and solid starting point for the development of potential Hv1 inhibitors.

The selected promising hits will be used for further hit-to-lead optimization to obtain molecules with improved inhibitory potency, better hHv1 channel selectivity, and desired physicochemical properties.

5. REFERENCES

1. DeCoursey, T.E., *Voltage-gated proton channels: molecular biology, physiology, and pathophysiology of the H(V) family*. *Physiol Rev*, 2013. **93**(2): p. 599-652.
2. Geragotelis, A.D., et al., *Voltage-dependent structural models of the human Hv1 proton channel from long-timescale molecular dynamics simulations*. *Proc Natl Acad Sci U S A*, 2020. **117**(24): p. 13490-13498.
3. Zhao, C., et al., *HIFs: New arginine mimic inhibitors of the Hv1 channel with improved VSD-ligand interactions*. *J Gen Physiol*, 2021. **153**(9).
4. Hong, L., I.H. Kim, and F. Tombola, *Molecular determinants of Hv1 proton channel inhibition by guanidine derivatives*. *Proc Natl Acad Sci U S A*, 2014. **111**(27): p. 9971-6.

ACKNOWLEDGMENT

The authors acknowledge the financial support from the Slovenian Research agency.

IN SILICO DISCOVERY AND OPTIMISATION OF VOLTAGE-GATED POTASSIUM CHANNEL K_v10.1 INHIBITORS WITH ANTIPROLIFERATIVE ACTIVITY

Žan Toplak¹, Louise Antonia Hendrickx², Špela Gubič¹, Jan Tytgat², Luis A. Pardo³, Lucija Peterlin Mašič¹, Tihomir Tomašič¹

¹University of Ljubljana, Faculty of Pharmacy, Aškerčeva 7, 1000 Ljubljana; Slovenia

²University of Leuven, Toxicology and Pharmacology, Campus Gasthuisberg, Onderwijs en Navorsing 2, Herestraat 49, PO Box 922, 3000 Leuven, Belgium

³AG Oncophysiology, Max-Planck Institute for Experimental Medicine, Hermann-Rein-Str. 3, 37075 Göttingen, Germany

1. INTRODUCTION

The voltage-gated potassium channel K_v10.1 (Eag1) is a member of the ether-à-go-go family, which also includes the erg (eag-related gene, K_v11) subfamily. In healthy tissues, K_v10.1 is almost undetectable outside the central nervous system, although it is highly expressed in over 70% of human cancers, regardless of tumour type. On this basis, K_v10.1 is considered a nearly universal tumour marker and represents a promising new target for new anticancer drug discovery. The channel is involved in cell cycle control and cell proliferation, migration, angiogenesis, and resistance to hypoxia. However, to date, no K_v10.1-specific small-molecule inhibitors have been reported, as most of them also inhibit voltage-gated sodium channels or, most importantly, the cardiac hERG channel, thus posing the risk of cardiac side effects [1].

2. MATERIALS AND METHODS

2.1. *In silico* methods and organic synthesis

Homology modelling (Modeller9.21) was used to prepare open conformation of the channel used for virtual screening (LigandScout, OpenEye software) and molecular dynamics (NAMD). Structure and ligand-based pharmacophore modelling (LigandScout) were used for virtual screening and molecular dynamics.

2.3. *In vitro* methods

Electrophysiological recordings using whole-cell patch clamp method were performed to evaluate compound potency, selectivity, kinetics, and mode of inhibition.

Anticancer activity was determined using 2D and 3D cell based models. Antiproliferative activity and target selectivity were evaluated on MCF-7, Colo-357, and Panc1 cells lines.

3. RESULTS AND DISCUSSION

We utilized the ligand-based drug discovery methodology using 3D pharmacophore modelling (Fig. 1) and medicinal chemistry approaches to prepare a novel structural class of K_v10.1 inhibitors.

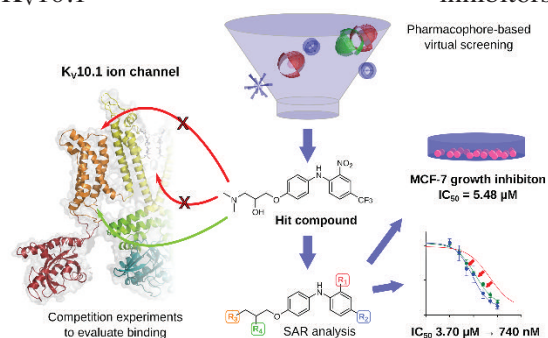


Figure 1. Pharmacophore-based virtual screening hit discovery and optimisation of novel voltage-gated potassium channel K_v10.1 inhibitors that have antiproliferative activity on cells.

Ligand-based pharmacophore was build based one the known purpurealidin series of compounds. This pharmacophore model was evaluated and used for virtual screening and identified 18 virtual screening hits. The virtual screening hit compound ZVS-08 (Fig. 1) exhibited an IC₅₀ value of 3.70 μM against K_v10.1 and inhibited the channel in a voltage-dependent manner consistent with the action of a gating modifier. Structural optimization resulted in the most potent K_v10.1 inhibitor of

the series with an IC_{50} value of 740 nM, which was potent on the MCF-7 cell line expressing high $K_v10.1$ levels and low hERG levels, induced significant apoptosis in tumour spheroids of Colo-357 cells, and was not mutagenic [2]. We have also developed a structure-based pharmacophore model from molecular dynamics simulations of $K_v10.1$ pore blockers (Fig. 2). Our data suggests that targeting the $K_v10.1$ channel pore is also likely to result in undesired hERG inhibition, and other potential binding sites should be explored to develop true $K_v10.1$ -selective inhibitors as new anticancer agents [3].

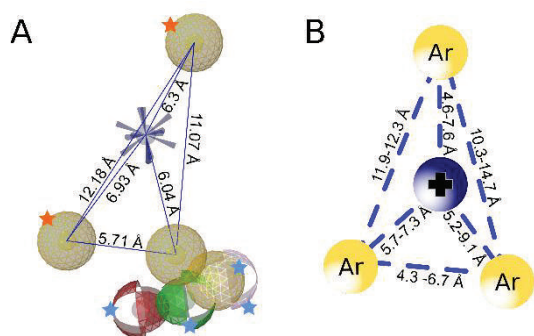


Figure 2. A) Structure-based pharmacophore model of $K_v10.1$ pore blockers, developed by molecular dynamics simulations. B) Similarity of our present model is seen by the hERG pharmacophore model described by Cavalli et al [4].

4. CONCLUSION

In this work, we used an innovative ligand-based pharmacophore modelling approach to create 3D pharmacophore models in combination with molecular dynamics to discover and evaluate hEAG1 inhibitors. The obtained results represent a good foundation for further development of hEAG1 inhibitors with antiproliferative activity and represents an original contribution to the science in the field of anticancer drug discovery.

5. REFERENCES

1) Toplak, Ž.; Hendrickx, L. A.; Abdelaziz, R.; Shi, X.; Peigneur, S.; Tomašič, T.; Tytgat, J.; Peterlin-Mašič, L.; Pardo, L. A. Overcoming Challenges of HERG Potassium Channel Liability through Rational Design: Eag1 Inhibitors for Cancer Treatment. *Medicinal Research Reviews*. 2022, 42 (1), 183–226.

2) Toplak, Ž.; Hendrickx, L. A.; Gubič, Š.; Možina, Š.; Žegura, B.; Štern, A.; Novak, M.; Shi, X.; Peigneur, S.; Tytgat, J.; Tomašič, T.; Pardo, L. A.; Mašič, L. P. 3D Pharmacophore-Based Discovery of Novel $K_v10.1$ Inhibitors with Antiproliferative Activity. *Cancers*. 2021, 13 (6), 1244.

3) Toplak, Ž.; Merzel, F.; Pardo, L. A.; Peterlin-Mašič, L.; Tomašič, T. Molecular Dynamics-Derived Pharmacophore Model Explaining the Nonselective Aspect of $K_v10.1$ Pore Blockers. *International Journal of Molecular Sciences*. 2021, 22 (16), 8999.

4) Cavalli, A.; Poluzzi, E.; De Ponti, F.; Recanatini, M. Toward a Pharmacophore for Drugs Inducing the Long QT Syndrome: Insights from a CoMFA Study of HERG K^+ Channel Blockers. *Journal of Medicinal Chemistry*. 2002, 45, 3844–3853.

ACKNOWLEDGMENT

We thank OpenEye Scientific Software, Santa Fe, NM, USA, for free academic licenses for the use of their software. Luis A. Pardo thanks the expert technical assistance of V. Díaz. Jan Tytgat was supported by grants G0E7120N, GOC2319N and GOA4919N (FWO-Vlaanderen), and grant CELSA/17/ 047 (KU Leuven). Steve Peigneur was supported by grant PDM/19/164 (KU Leuven). Lucija Peterlin-Mašič was supported by grants J1-9192, N1-0098, P1-0208 (ARRS), and grant CELSA 005-1/2017 (University of Ljubljana). Luis A. Pardo acknowledges the support of the Max-Planck Society, and the Göttingen Graduiertenschule für Neurowissenschaften, Biophysik und Molekulare Biowissenschaften (GGNB) (RA). This project has received funding from the from the Eur Union through Horizon 2020 research and innovation program under the Marie Skłodowska-Curie grant agreement No. 813834-PHIONIC-H2020-MSCA-ITN-2018. Open access funding enabled and organized by Projekt DEAL.

DIFFERENTIATION OF SH-SY5Y CELLS INTO SPECIFIC NEURONAL PHENOTYPES: *IN VITRO* MODEL OF NEURODEGENERATION

Selena Pavšič¹, Janko Kos^{1,2}, Anja Pišlar¹

¹*Department of Pharmaceutical Biology, Faculty of Pharmacy, University of Ljubljana, Slovenia*

²*Department of Biotechnology, Jožef Stefan Institute, Ljubljana, Slovenia*

1. INTRODUCTION

The human neuroblastoma SH-SY5Y cell line is the most frequently used *in vitro* cell model for neurodegeneration research. Retinoic acid (RA) in a combination with brain-derived neurotrophic factor (BDNF) induces differentiation toward a cholinergic neuronal phenotype, whereas treatment with RA followed by phorbol 12-myristate 13-acetate (PMA) results in dopaminergic neuronal phenotype - both the most affected neuron subsets in Alzheimer's and Parkinson's disease, respectively [1, 2]. Differentiated neuron-like cells could provide an effective tool for drug screening, which assesses sustainable therapies for neurodegenerative disorders [3, 4].

2. MATERIALS AND METHODS

2.1 Maintenance and Differentiation of SH-SY5Y Cells into Specific Neuronal Phenotype

Human SH-SY5Y cell line was cultured in DMEM/F12 containing 10% foetal bovine serum (FBS) and 1 % penicillin/streptomycin (P/S) in a humidified incubator at 37 °C with 5% CO₂. The cell medium was replaced every 3 days and cells were subcultured once they reached 80% confluence. After 24 h of plating the cells on a collagen-coated plate, differentiation was initiated by lowering FBS in the culture medium to 2% and 0,25 % P/S and supplementing with 10 µM RA for 7 days. This treatment was replaced every 3 days. To induce a specific neuronal phenotype, on the fourth day of differentiation RA was supplemented with 80 nM PMA or 50 ng/mL BDNF.

2.2 Morphological observation

The morphology of cells was visualized every day during differentiation protocol using a motorized inverted microscope EVOS Cell Imaging System.

2.3 Characterisation of Neuronal Phenotype

The flow cytometry method was used to define the SH-SY5Y cell differentiation into the individual neuronal phenotype by using general

markers (NeuN, GAP-43) and phenotypically characteristic, TH for dopaminergic neurons and ChAT for cholinergic neurons.

2.4 Cytotoxicity and Neuroprotective Assay in Differentiated Cells

The cytotoxic effect of 6-OHDA was tested on differentiated SH-SY5Y cells to determine the susceptibility of the different neuronal-like phenotypes to neuronal death. After a 7-day differentiation period and 24 h exposure to 100 µM 6-OHDA, cell viability was performed with 7AAD staining using flow cytometry. In the case of neuroprotection assay, on day 7, differentiated SH-SY5Y cells were pretreated with 10 µM rasagiline or safinamide for 1 h followed by 24 h treatment with 100 µM 6-OHDA and assessed by flow cytometry.

3. RESULTS AND DISCUSSION

3.1 Differentiation Protocol Increased Neurite Growth

The formation of a robust neuritic network is indicating a switch to a neuronal phenotype resembling a highly connected synaptic network. When compared to RA treatment, BDNF-treated cells exhibited longer neurites, while PMA-treated cells expressed more branched neurites (Fig 1).

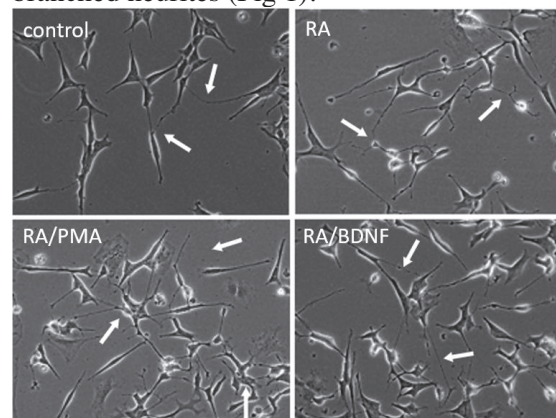


Figure 1. Morphology of SH-SY5Y cells on day 7 of the differentiation protocol. White arrows are indicating neurites.

3.2 Differentiation Protocol Induced a Shift into a Specific Neuronal Phenotype

We observed higher expression of dopaminergic marker (TH) in RA/PMA-treated cells and cholinergic marker (ChAT) in RA/BDNF-treated cells (Fig. 2). Differentiation towards the cholinergic phenotype using the ChAT marker cannot be confirmed in any other group of differentiated cells, while the expression level of TH is slightly increased in the treatment of RA and RA/BDNF cells.

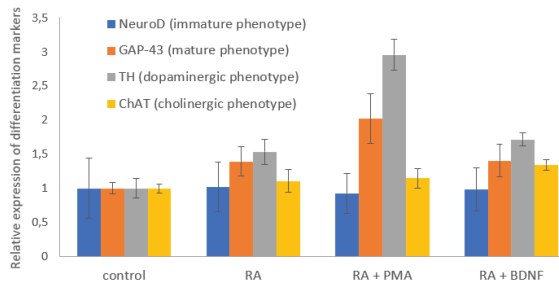


Figure 2. Relative expression of neuronal markers as the mean value of fluorescence intensity normalized to the control.

3.3 Neuroprotective Effect of 6-OHDA-Mediated Neurotoxicity by Rasagiline and Safinamide

The cytotoxic effect of 6-OHDA was significantly higher in RA/PMA and RA/BDNF differentiated cells, proposing SH-SY5Y cell differentiation as a suitable model for neurodegeneration (Fig. 3A). Moreover, the addition of inhibitors of monoamine oxidase, rasagiline, and safinamide, showed a significant positive effect on survivability in a neurotoxic environment induced by 6-OHDA compared to the control, indicating their neuroprotective effect (Fig. 3B).

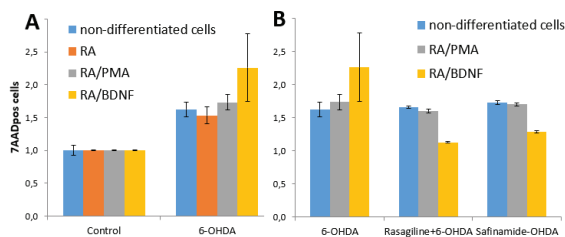


Figure 3. (A) 6-OHDA-induced toxicity in differentiated SH-SY5Y cells. (B) The effect of monoamine oxidase inhibitors on 6-OHDA-induced toxicity.

4. CONCLUSION

Our differentiation protocol revealed positive morphological and biochemical differentiation towards specific neuronal phenotype, indicating

the SH-SY5Y cell line as a useful *in vitro* model for neurodegenerative diseases. Moreover, the increased susceptibility to the neurotoxin 6-OHDA shows the formation of more neuron-like cells suitable for modelling PD and AD. The monoamine oxidase inhibitors showed promising neuroprotective effects, however, more biological replicates should be performed to confirm the applicability of the used *in vitro* model for drug discovery.

5. REFERENCES

- Hong-rong, X., et al. *SH-SY5Y human neuroblastoma cell line: in vitro cell model of dopaminergic neurons in Parkinson's disease.* Chinese Medical Journal, 2010. 123(8): 1086-1092.
- Kovalevich, J. and Langford, D., *Considerations for the Use of SH-SY5Y Neuroblastoma Cells in Neurobiology.* Neuronal Cell Culture, 2013. 1078: 9–21.
- Cetin, S., et al., *Cell-based models for Alzheimer's and Parkinson's disease: at the interface of biology and drug discovery.* Biomedicine & Pharmacotherapy, 2022. 149.
- [4] Slanzi, A. et al., *In vitro Models of Neurodegenerative Diseases.* Frontiers in Cell and Developmental Biology, 2020. 328.

ACKNOWLEDGMENT

We thank master's students Baldwin De Man and Nika Marin for their contribution to the research while completing their master's thesis.

ENGINEERING LACTOCOCCUS LACTIS TO INHIBIT INTESTINAL INFLAMMATION THROUGH SMALL PROTEIN BLOCKERS OF IL-23/IL-17 AXIS USING NOVEL BGLBRICK ASSEMBLY METHOD

Tina Vida Plavec^{1,2}, Aleš Berlec^{1,2}

¹Department of Biotechnology, Jožef Stefan Institute, Slovenia

²University of Ljubljana, Faculty of Pharmacy, Slovenia

1. INTRODUCTION

Lactococcus lactis is a food-grade model lactic acid bacterium (LAB), that is widely used as a cell factory for recombinant protein expression and is a promising vector for *in vivo* delivery of bioactive proteins. Genetically engineered LAB have already been proposed for the therapy of intestinal inflammation by interfering with pro-inflammatory cytokines and inhibiting the pro-inflammatory cascade [1,2]. Novel genetic engineering techniques offer the possibility of simultaneous multiple protein expression and the advantage of incorporating the desired modifications with good efficiency and using straightforward procedures. In this study, we constructed a new pNBBX plasmid based on the modified BglBrick system and used it to assemble multiple gene cassettes and achieve controlled simultaneous expression of multiple model proteins [3]. We demonstrated pNBBX to be a valuable tool for faster and more efficient genetic engineering in *L. lactis*. We used the pNBBX plasmid to engineer *L. lactis* to express proteins capable of inhibiting the IL-23/IL-17 pro-inflammatory axis, which has been shown to have a major impact on exacerbating intestinal inflammation. Our aim was to simultaneously target IL-23 and IL-17, as well as their receptors, to potentially achieve a synergistic effect. IL-23 is the first cytokine of the IL-23/Th17 axis. For its inhibition, we used previously prepared albumin binding domain (ABD)-derived antagonists of IL-23 receptor (REX-ligands) and ILP317 protein against the p19 subunit of IL-23, which inhibits binding of the IL-23 to its cognate cell-surface receptor. IL-23 stimulation of Th17 cells results in the production of IL-17. Therefore, to inhibit IL-17-mediated signaling, we made genetic

constructs and investigated the secretion of ABD-antagonists specific for human IL-17 receptor A (IL-17R) called ARS-ligands. We also displayed the IL-17 binding Fynomer on the surface of *L. lactis*. Similar to the co-expression of IL-23-neutralizing ILP/REX proteins, we simultaneously expressed the ARS-ligand of IL-17R and the IL-17 binding Fynomer to achieve potential synergy in preventing IL-17 signaling. The expression and function of each protein was evaluated and confirmed by western blotting, flow cytometry, fluorescent microscopy and ELISA assay. We established a cell model based on THP-1 cells for IL-23 secretion to study bacterial binding of secreted interleukins.

2. MATERIALS AND METHODS

2.1. Molecular cloning

Plasmid pNZ8148 was modified by inserting restriction enzyme recognition sites NheI and BglII upstream of the nisin promoter, and restriction enzyme recognition sites BclI and XhoI downstream of the transcription terminator (TT), resulting in plasmid pNBBX [3].

2.2. Flow cytometry

Flow cytometry was used to assess surface display and function of proteins interfering with IL-23/IL17 axis. Samples were analyzed with a flow cytometer (FACS Calibur; Becton Dickinson) using excitation at 488 nm and emission at 530 nm.

2.3. Cytokine binding assay

Fynomer-displaying *L. lactis* were resuspended in incubation buffer (PBS, 0.05% Tween and 0.1% BSA) containing IL-17A (300 pg/mL).

P71

Cells were removed after 2 h incubation and the concentrations of the remaining cytokines in the supernatant were determined according to the manufacturer's instructions (Human IL-17A ELISA development kit (HRP; Mabtech).

3. RESULTS AND DISCUSSION

3.1. BglBrick plasmid construction

We constructed the pNBBX plasmid (Fig. 1) by inserting four additional restriction sites into pNZ8148. For multiple gene cassette pNBBX, plasmids gene cassettes were inserted upstream of the first cassette using the restriction enzyme pairs *NheI/BglII* and *NheI/BclII*, or downstream using the restriction enzyme pairs *XhoI/BglII* and *XhoI/BclII*.

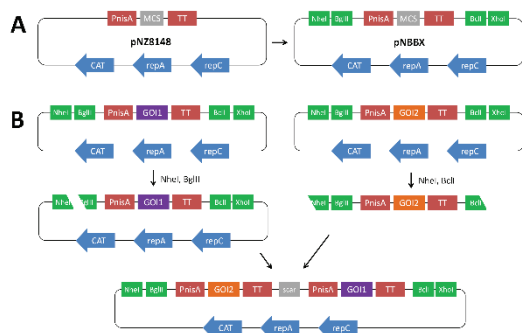


Figure 1. Preparation of BglBrick plasmid pNBBX (A). Example of upstream BglBrick cloning of a gene cassette using *NheI/BglII* for the backbone and *NheI/BclII* for the insert and exploiting *BglII/BclII* complementarity resulting in a scar (B). GOI, gene of interest, e.g. *REX009*, *REX125*, *ARS14*, *ARS19*, *ILP317*, *Fynomer*; PnisA, nisin promoter; TT, transcription terminator; MCS, multiple cloning site.

3.2. Concomitant expression and surface display

ILP and Fynomer binders were genetically labelled with Myc tag, and REX and ARS ligands with Flag tag to detect and monitor the expression level of an individual recombinant protein by western blotting, flow cytometry and fluorescence microscopy.

3.3. IL-17A binding assay

The binding of IL-17A by recombinant Fynomer-displaying *L. lactis* was evaluated by ELISA. 2×10^9 recombinant bacteria could remove up to 97 % of IL-17A from the solution (Fig. 3A). Binding depended on the cell number;

however, even 10-fold lower bacterial cell number could still remove up to 83 % of IL-17A (Fig. 3B).

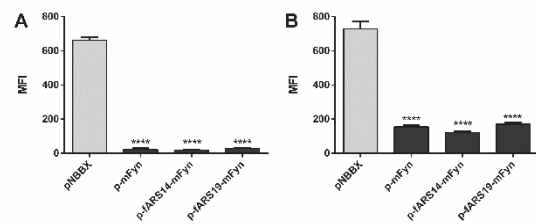


Figure 2. ELISA-determined IL-17A that remained in the solution after incubation of IL-17A with 2×10^9 CFU/mL (A) or 2×10^8 CFU/mL (B) recombinant *L. lactis* cells that displayed IL-17A-binding Fynomer (mFyn) on their surface in comparison to pNBBX empty plasmid control cells.

4. CONCLUSION

We used the recently constructed pNBBX plasmid to demonstrate its applicability and to interfere with the IL-23/IL-17 inflammatory pathway through simultaneous expression of IL-23 and IL-17 binders, as well as of their corresponding receptor antagonists in *L. lactis*. Finally, we tested the recombinant *L. lactis* in human cell culture model of inflammation.

5. REFERENCES

- Škrlec, K., et al., *p19-Targeting ILP protein blockers of IL-23/Th-17 pro-inflammatory axis displayed on engineered bacteria of food origin*. International journal of molecular sciences, 2018. 19(7):1933.
- Plavec, TV., et al., *Engineered Lactococcus lactis secreting IL-23 receptor-targeted REX protein blockers for modulation of IL-23/Th17-mediated inflammation*. Microorganisms, 2019. 7(5):152.
- Plavec, TV., et al., *Introduction of modified BglBrick system in Lactococcus lactis for straightforward assembly of multiple gene cassettes*. Frontiers in bioengineering and biotechnology, 2021. 9:797521.

ACKNOWLEDGMENT

This study was funded by the Slovenian Research Agency (grant numbers P4-0127, N3-0184, J4-9327).

UTILISATION OF LYMPHOBLASTOID CELL LINES AS *IN VITRO* MODELS OF OVER-ACTIVATED IMMUNE RESPONSE FOR DRUG REPURPOSING

Luka Hiti¹, Tijana Markovič¹, Irena Mlinarič-Raščan¹

¹*University of Ljubljana, Faculty of Pharmacy, Slovenia*

1. INTRODUCTION

Cytokine storm is a life-threatening systemic inflammatory syndrome involving the uncontrolled secretion of cytokines, which in severe cases leads to systemic organ dysfunction, and can end in death (1). Lymphoblastoid cell lines (LCLs) have proved to be a reliable *in vitro* model for evaluating the effect of compounds on cytokine production and secretion (2).

Many drugs not indicated for the modulation of an over-activated immune response have been used in clinical and preclinical trials since the onset of the Covid-19 pandemic (3). Among the more promising, in addition to corticosteroids, are proteasome inhibitors, Janus kinase inhibitors (JAKi), Bruton tyrosine kinase inhibitors (BTKi) (4). Serine protease inhibitors have also shown potential (5).

2. MATERIALS AND METHODS

2.1. Materials

Dexamethasone, cyclosporin A, ibrutinib, acalabrutinib, baricitinib, carfilzomib nafamostat mesylate, camostat mesylate, ibuprofen (all Sigma–Aldrich), and EP4 antagonist (Cayman Chemical) were dissolved in DMSO.

Human lymphoblastoid cell lines (LCLs) were obtained from the National Laboratory for the Genetics of Israeli Populations (NLGIP), a human diversity biobank at Tel-Aviv University, Tel Aviv, Israel.

2.2. Cytokine assay

The production of cytokines was analysed as described previously (2). Briefly, cells were pre-treated for 1 h with the non-cytotoxic

concentration of the compound of interest and activated by 0.5 mM ionomycin and 3.33 ng/ml PMA and incubated for 24 h. The resting, untreated cells and the ionomycin/PMA activated cells were used as controls. Cytokine production was assessed by BD Cytometric Bead Array (CBA) Human Inflammatory Cytokine kit (Contents: IL-8, IL-1b, IL-6, IL-10, TNF α and IL-12) using AttuneNext flow cytometer. Results are expressed in fold change against untreated activated controls.

3. RESULTS AND DISCUSSION

3.1. Selected compounds exhibit immunosuppressive effect

We evaluated the impact of 8 compounds on cytokine production (Fig. 1). Two known immunosuppressive drugs, dexamethasone and cyclosporin A, decreased the production of assessed cytokines. Six tested compounds displayed an immunosuppressive effect trend, evident from the decreased median fold change of pooled cytokine concentrations compared to untreated activated controls; conversely, increase in pooled cytokine production was detected with ibuprofen and EP4 antagonist.

3.2. Selected compounds has a specific cytokine-release signature

Next, we evaluated the impact of compounds on specific cytokine production. Dexamethasone and carfilzomib displayed the highest variation in cytokine production among the tested compounds (Fig. 2). Namely, proinflammatory cytokine levels (IL-8, IL-6, IL-12 and TNF α) were reduced, while immunoregulatory cytokine IL-10 was slightly elevated when LCLs were incubated with dexamethasone. This is in line with the previous studies. In contrast, all cytokines except IL-6 were

decreased when the cells were incubated with selective proteasome inhibitor carfilzomib. This indicates that immunomodulatory compounds have specific cytokine signature, which is likely also relevant for clinical use.

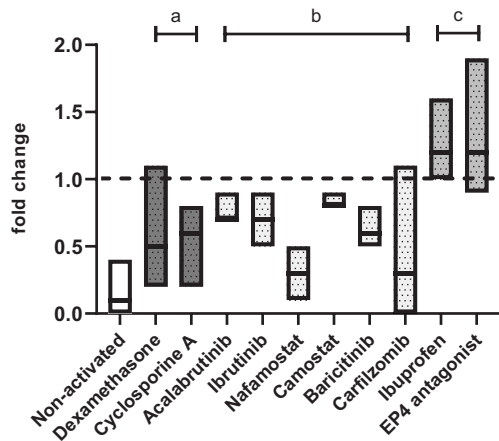


Figure 1. Pooled fold change in cytokine (IL-6, IL-8, IL-10, IL-12, and TNF α) concentration compared to ionomycin/PMA activated cells after 24h. Cytokine production was assessed in three LCLs. Boxes represent highest, lowest and median value for each compound. On the left are untreated and non-activated LCLs as starting point reference. (a) Known immunosuppressive effect; (b) observed immunosuppressive effect; (c) observed immunostimulatory effect.

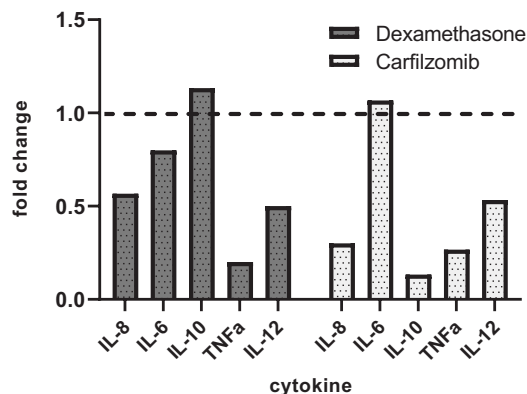


Figure 2. Average fold change of cytokine production as determined in three LCLs after 24h. The cells were pre-treated for 1h with dexamethasone and carfilzomib and activated by ionomycin/PMA.

4. CONCLUSION

Utilising LCLs, we evaluated several compounds with the potential for the treatment of Covid-19. Serine protease inhibitors, proteasome inhibitors, BTKi and JAKi were shown to display immunosuppressive effects and are as such interesting candidates for drug repurposing. However, special attention must be given to the specific cytokine-effect signature as different immunosuppressive compounds may not decrease the same cytokines (and to the same effect).

5. REFERENCES

1. Fajgenbaum, DC., et al., Cytokine Storm. *The New England Journal of Medicine*, 2020. 3;383(23):2255-2273.
2. Markovič, T., et al., Characterization of human lymphoblastoid cell lines as a novel in vitro test system to predict the immunotoxicity of xenobiotics. *Toxicology Letters*, 2015. 17;233(1):8-15.
3. Chakraborty, C., et al., The Drug Repurposing for COVID-19 Clinical Trials Provide Very Effective Therapeutic Combinations: Lessons Learned From Major Clinical Studies. *Frontiers in Pharmacology*, 2021. 18;12:704205.
4. Yang, L., et al., The signal pathways and treatment of cytokine storm in COVID-19. *Signal Transduction and Targeted Therapy*, 2021. 7;6(1):255.
5. Zhu, H., et al., Spontaneous binding of potential COVID-19 drugs (Camostat and Nafamostat) to human serine protease TMPRSS2. *Computational and Structural Biotechnology Journal*, 2020. 28;19:467-476.

ACKNOWLEDGMENT

This research was co-funded by the Slovenian Research Agency (Grant No. P1-0208 and NC-0004) and the European Regional Development Plan for EATRIS-TRISI, and by the European Union’s Horizon 2020 Research and Innovation programme (No. 871096).

HIGHER INCIDENCE OF COMMON POLYMORPHISMS IN THE GENES OF FOLATE AND METHIONINE CYCLES IN CHILDREN WITH OROFACIAL CLEFTS

Natasa Karas Kuzelicki¹, Alenka Smid¹, Tina Kek^{2,3}, Eberlinc Andreja⁴, Irena Mlinaric-Rascan¹, Ksenija Gersak^{2,3}

¹*Department of Clinical Biochemistry, Faculty of Pharmacy, University of Ljubljana, Slovenia*

²*Department of Obstetrics and Gynaecology, University Medical Centre Ljubljana, Slovenia*

³*Faculty of Medicine, University of Ljubljana, Slovenia*

⁴*Department of Maxillofacial and Oral Surgery, University Medical Center Ljubljana, Slovenia*

1. INTRODUCTION

Orofacial clefts (OFC) are one of the most common congenital malformations in humans, with the global incidence of 1 in 700 births. Although the etiopathogenesis of OFC was extensively researched, the environmental and genetic risk factors are unclear.

Recently, deficiency of folate intake and genetic aberrations of the folate and methionine cycles have been connected to several congenital malformations, including the OFC. Since then, many studies investigating the genetic variants in folate/methionine relevant genes have been performed, but their results have been ambiguous [1-4]. This might be due to the influence of several environmental and endogenous maternal risk factors during pregnancy that might mask the genetic influence of child's genome on the OFC formation.

To overcome this limitation, we performed the genetic analysis of selected genes involved in folate and methionine metabolism and transport in sibling pairs of OFC patients and their unaffected siblings. Since the siblings shared the prenatal environment we hypothesize that certain genetic influences might be discovered that might be confounded in classical case-control approach.

2. MATERIALS AND METHODS

2.1. Study subjects and study design

OFC cases consisted of children undergoing routine follow-up examinations before or after the corrective surgery of their OFC at the Department of Maxillofacial and Oral Surgery at University clinical center Ljubljana

(UKCLJ). Of 179 OFC patients fulfilling the inclusion criteria, 122 had a healthy sibling. Thus, 122 sibling pairs were included in the study. Of these, DNA sample was available for 45 sib pairs. All mothers completed questionnaires to evaluate demographic risk factors and the exposure to environmental OFC risk factors during pregnancy. All mothers and children older than 18 years signed the informed consent form and the study protocol was approved by the National Medical Ethics committee (No. 57/02/13).

2.2. DNA extraction and genotyping

DNA was extracted from buccal swabs by means of QIAamp DNA Mini Kit (Qiagen) according to the manufacturers' instructions.

Ten common polymorphisms (MAF \geq 25%) in nine genes involved in folate and methionine cycles were genotyped by means of TaqMan (Applied Biosystems) or LightSNiP (TIB MOLBIOL) probes: rs1544105 (FPGS), rs1677693 (DHFR), rs1801133 and rs1801131 (MTHFR), rs1801394 (MTRR), rs2236225 (MTHFD1), rs3733890 (BHMT), rs10948059 (GNMT) and rs2424913 (DNMT3B).

2.3. Statistical analysis

Paired samples t-test was used for Gaussian data and related-samples Wilcoxon signed rank test for non-Gaussian data. Related-samples McNemar test was used for the bi-categorical data, and related samples marginal homogeneity test for multi-categorical data. Holm-Sidak correction for multiple testing was applied.

3. RESULTS AND DISCUSSION

3.1. Demographic and environmental factors

Younger siblings in a sib pair were more often affected by OFC than older sibs, and advanced maternal age increased the risk of OFC. Furthermore, any medicine consumption or fever in the 1st trimester of pregnancy was associated with increased risk of OFC. However, after adjustment for multiple testing only the presence of a maternal fever during early pregnancy was associated with OFC in a child. 16,6% of mothers had fever during early pregnancy with the affected sibling, compared to 3,3% during a non-affected pregnancy ($p = 0,035$).

3.2. Genetic factors

Of 10 loci in nine investigated genes, four loci in three genes were associated with the increased risk of OFC: rs1801133 and rs1801131 (MTHFR), rs2236225 (MTHFD1) and rs10948059 (GNMT). However, after the adjustment for multiple testing, none of this associations stayed significant.

When taking into consideration all the investigated loci, we found a strong association between the total number of mutated alleles in nine genes associated with folate/methionine cycles and the OFC risk. Siblings who were affected with OFC had higher number of mutations (median (minimum-maximum): 12 (5-17)) in the abovementioned genes compared to their unaffected siblings (median (minimum-maximum): 9 (4-15)) ($p < 0,001$) (Figure 1).

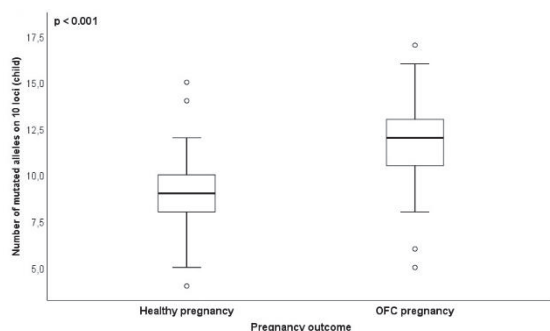


Figure 1. Total number of mutated alleles at 10 loci in a child. A comparison between healthy (median (minimum-maximum): 9 (4-15)) and OFC siblings (median (minimum-maximum): 12 (5-17)) ($p < 0,001$, Wilcoxon matched-pair

signed-rank test). Boxplots represent median and interquartile range.

These results are not unexpected, since in most families OFC is inherited as a complex multifactorial trait, where contribution of individual genes is relatively low, but additive contribution of several genes in a same metabolic pathway can have a profound impact on the disease occurrence.

4. CONCLUSION

To our knowledge, this is the first study to investigate OFC genetic risk factors of the folate/methionine metabolic pathways in OFC affected – unaffected sibling pairs.

The only environmental risk factor that differed between the affected and unaffected pregnancies was the increased body temperature of the mother in the 1st trimester of the pregnancy.

None of the investigated genetic loci in the genes of folate/methionine cycles was individually associated with OFC. However, when considering all of the investigated loci, a strong correlation between increased number of common polymorphisms in selected genes of folate/methionine cycles and OFC occurrence was detected. This is indicative of multifactorial inheritance pattern.

5. REFERENCES

1. Krapels IP, et al. Maternal nutritional status and the risk for orofacial cleft offspring in humans. *J Nutr.* 2004 Nov;134(11):3106-13
2. Johnson CY, et al. Folate intake, markers of folate status and oral clefts: is the evidence converging? *Int J Epidemiol.* 2008 Oct;37(5):1041-58.
3. Butali A, et al. Folic acid supplementation use and the MTHFR C677T polymorphism in orofacial clefts etiology: An individual participant data pooled-analysis. *Birth Defects Res A Clin Mol Teratol.* 2013 Aug;97(8):509-14.
4. De-Regil LM, et al. Effects and safety of periconceptional folate supplementation for preventing birth defects. *Cochrane Database Syst Rev.* 2010(10):CD007950.

ACKNOWLEDGMENT

The work was supported by Slovenian research agency grants no. J3-5507 and J3-8207.

FACTORS INFLUENCING INTER-INDIVIDUAL DIFFERENCES IN RESPONSE TO PROSTAGLANDIN EP4 RECEPTOR AGONIST IN CHRONIC LYMPHOCYTIC LEUKEMIA CELLS

Tijana Markovič¹, Alenka Šmid¹, Helena Podgornik^{1,2}, Matevž Škerget², Irena Mlinarič-Raščan¹

¹University of Ljubljana, Faculty of Pharmacy, Slovenia

²University Medical Centre Ljubljana, Department of Haematology, Ljubljana, Slovenia

1. INTRODUCTION

Chronic lymphocytic leukemia (CLL) is a very heterogenous disease, which is reflected in the development of the disease, prognosis and response to the therapy. *Ptger4* gene, encoding the EP4receptor was identified as a potential tumor suppressor and its expression was elevated on the malignantly transformed lymphocytes B (1). Our previous studies demonstrated that EP4 receptor agonists PgE1-OH and L-902,688 had selective cytotoxic effect on the primary CLL cells (2, 3). The aim of this study was to evaluate the impact of *Ptger4* expression levels and *Ptger4* expression-modulating polymorphisms as well as other clinical and prognostic factors on inter-individual variability in the response to PgE1-OH in CLL cells.

2. MATERIALS AND METHODS

2.1. Primary CLL cells

After obtaining informed consent in accordance with the ethical approval of the National Medical Ethics Committee of the Republic of Slovenia (Nr. 93/12/10), cells were collected from 151 patients with diagnosis of CLL at the University Medical centre, Ljubljana, Slovenia. Lymphocytes B were isolated using RosetteSep Ficol-Paque procedure.

2.2. Metabolic activity assay

The viability of cells treated with PgE1-OH (Cayman Chemical) was assessed using the resazurin based assay (PrestoBlue® Cell Viability Reagent).

2.3. Genotyping and expression of *Ptger4* gene

CLL samples were genotyped for the single nucleotide polymorphisms (SNPs) rs4495224 and rs7720838 (TaqMan genotyping assay). *Ptger4* mRNA expression was determined using TaqMan assay

3. RESULTS AND DISCUSSION

3.1. Inter-individual variability in the response to EP4 receptor agonist

PgE1-OH induced concentration-dependent decrease in cell viability (Fig. 1). The average EC50 values were 13.56 μ M after 24 h and 7.23 after 48 h. The EC50 values ranged from 0.97 μ M to 55.07 μ M after 24 h, revealing inter-individual variability in response to PgE1-OH, which is in agreement with the fact that CLL is very heterogeneous disease.

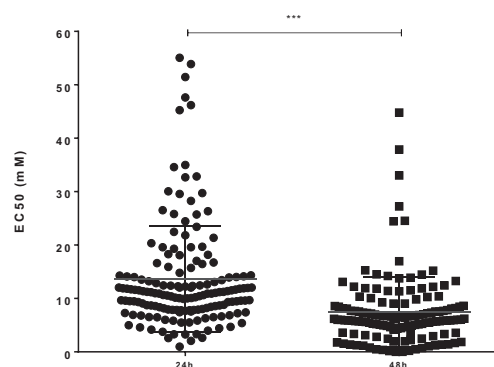


Figure 1. Inter-individual variability in the response to EP4 receptor agonist PgE1-OH. Each dot (24 h) or square (48 h) denotes EC50 value as determined on CLL cells from one patient. Unpaired t-test, *** p < 0.001

3.2. EP4 receptor agonist induces selective cytotoxicity in all subgroups of CLL cells

PgE1-OH was comparably cytotoxic in all subgroups of CLL cells (Fig. 2), which is of prime importance, especially for the patients with progressed disease with Binet stages B and C and with unfavourable prognostic factors, such as del11q and del17p, the latter leading to aberration of the tumor suppressor gene TP53 and predicting an aggressive disease course and refractoriness to chemoimmunotherapy. PgE1-OH may thus show potential also in patients with TP53 aberration.

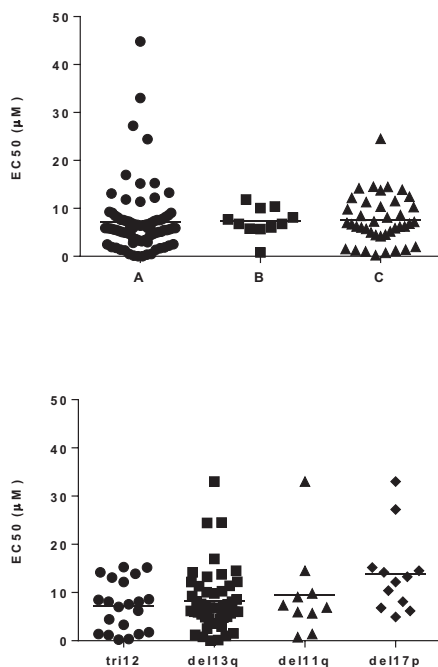


Figure 2. PgE1-OH is cytotoxic against all CLL cells including those from patients in (A) Binet stage C and (B) with dysfunctional TP53 (A) Each dot (Binet stage A), square (Binet stage B) and triangle (Binet stage C) denotes the EC50 value for PgE1-OH determined on cells obtained from one donor. (B) Each dot (tri12), square (del13q), triangle (del11q) and diamond (del17p) denotes the EC50 value for PgE1-OH determined on CLL cells obtained from one donor.

3.2. PgE1-OH is more cytotoxic towards the cells of male donors and carriers of variant rs4495224 A allele

The analysis revealed sex-dependent sensitivity of CLL cells to PgE1-OH, which was more cytotoxic to the cells of male compared to female donors (average EC50 values 14.2 μ M and 17.6 μ M, respectively; $p=0.02$). PgE1-OH was shown to be more cytotoxic towards the cells of the carriers of the variant rs4495224 A allele (average EC50 values 14.23 μ M in patients with rs4495224 AA/AC genotype and 18.59 μ M in patients with rs4495224 CC genotype; $p=0.03$). The analysis of *Ptger4* expression levels revealed that male patients had higher expression compared to female patients ($p=0.02$) as did the donors with the rs4495224 AA genotype compared to those with rs4495224 AC/CC genotype ($p=0.046$). A weak, but significant correlation between an increased expression of the *PTGER4* gene and lower EC50 values was also shown ($p=0.046$).

4. CONCLUSION

In conclusion, we identified EP4 receptor as promising therapeutic target and EP4 receptor agonist PgE1-OH as a promising drug candidate for the treatment of CLL.

5. REFERENCES

1. Markovič T et al. Structural features of subtype-selective EP receptor modulators. *Drug Discov Today*. 2017; 22(1):57-71.
2. Markovič T et al. The Enhanced Cytotoxic Effects in B-Cell Leukemia and Lymphoma Following Activation of Prostaglandin EP4 Receptor and Targeting of CD20 Antigen by Monoclonal Antibodies. *Int J Mol Sci*. 2022; Jan 29;23(3):159
3. Nabergoj S et al. EP4 receptor agonist L-902688 augments cytotoxic activities of ibrutinib, idelalisib, and venetoclax against chronic lymphocytic leukemia cells. *Biochem Pharmacol.*, 2021; 183:114352

ACKNOWLEDGMENT

This research was funded by the Slovenian Research Agency ARRS (Grant No. P1-0208 and NC-0004) and by the Ministry of Education, Science, and Sport (MIZŠ) and the European Regional Development Fund OP20.05187 RI-SI-EATRIS.

DEVELOPMENT OF A METHOD FOR THE THERAPEUTIC DRUG MONITORING OF USTEKINUMAB IN DRIED BLOOD SPOTS

Panagiotis-Dimitrios Mingas¹, Jurij Zdovc¹, Iztok Grabnar¹, David Drobne², Tomaž Vovk¹

¹*Faculty of Pharmacy, University of Ljubljana, Slovenia*

²*Department of Gastroenterology, University Medical Centre Ljubljana, Slovenia*

1. INTRODUCTION

Ustekinumab (UST) is a monoclonal antibody (mAb) indicated for the treatment of various autoimmune diseases, including the treatment of adult patients with active Crohn's disease [1]. Several studies associate higher serum concentration of mAbs, with higher chance of beneficial therapeutic outcomes. Therapeutic drug monitoring (TDM) can be a useful tool in decision-making for possible dose adjustment of mAbs and is routinely done, by collecting patients' venous blood samples via venipuncture [2]. However, a more patient-centric approach could be adopted without the need of regularly visiting healthcare institutions. Such is the method of dried blood spots (DBS), which can be performed by the patients at home. The aim of the study is to develop a method for the determination of UST concentrations in DBS.

2. MATERIALS AND METHODS

2.1. Materials

The DBS samples were collected on filter paper cards (Whatman™ 903 Protein Saver Cards, GE Healthcare, Dassel, Germany). Drug free venous blood was used for the preparation of DBS calibrators and quality control (QC) samples; it was obtained from healthy volunteers using lithium heparin (Li-heparin) vacutainer tubes (Becton and Dickinson, US). The enzyme-linked immunosorbent assay (ELISA) kits, as well as the UST stock solution used to spike blood, were purchased from ImmunoGuide® (AybayTech Biotechnology, Ankara, Turkey).

2.2. DBS method development

Drug free venous blood was collected in Li-heparin vacutainers, spiked with UST and spotted on the filter paper cards. The DBS were air dried for at least 3 h, avoiding direct sunlight. A punch of approximately 6 mm was taken from the central area of the DBS and it was transferred into an Eppendorf tube. 500 µL of extraction solution, prepared with phosphate-buffered saline (PBS) containing 0.05% Tween 20 and 0.05% NaN₃ (sodium azide) were added. The samples were then incubated for 4 h at 25 °C, while gently shaken (200 rpm, HeatMix Tehtnica, Domel). After the incubation, the ELISA assay was utilized to determine the concentration of UST.

2.3. DBS method validation

The analytical validation followed the latest guidelines of the International Association for Therapeutic Drug Monitoring and Clinical Toxicology [3]. The method was validated for selectivity, recovery, dilution integrity, linearity, accuracy, precision, lower and upper limit of quantification, and stability.

3. RESULTS AND DISCUSSION

3.1. Selectivity, recovery, and dilution integrity

For the selectivity, the drug free venous blood, obtained from five donors, was used to prepare blank DBS samples with specified Hct values (0.2, 0.3, 0.4, 0.5, 0.6). After the analysis, no significant differences were detected between blank DBS samples prepared from different donors. The mean recovery for the low (QC_L) and high (QC_H) quality control concentrations at two Hct levels (0.25 and 0.55), was 90 % and 82 %, respectively. The dilution integrity was

evaluated at two concentrations, 30 and 120 mg/L. After the additional dilution steps, the accuracy was 95 % and 96 %, respectively.

3.2. Calibration model, accuracy, precision, and limits of quantification

The developed method is linear from 3 to 12 mg/L, and it was evaluated by back-calculating the concentrations of the calibrators. The concentrations were within the limits described by the guidelines, ≤ 15 % of nominal value and ≤ 20 % for the lower limit of quantification (LLOQ). The slope and intercept values of the calibration curve are given in Table 1. The accuracy of LLOQ and QC were within the recommended limits, ≤ 20 % and ≤ 15%, respectively. The intra and inter-day precision of UST QC samples was below 19.9% and 11.2%, respectively. The intra- and inter-day accuracy of UST QC samples was between 84.2 – 101.1% and 90.1 – 106.4%, respectively. The LLOQ was 3 mg/L.

Linear response range (mg/L)		Intercept	Slope	r ²
Day 1	3-12 (mg/L)	0.2011	0.0955	0.9858
Day 2		0.3188	0.0969	0.9984
Day 3		0.1527	0.0892	0.9912

Table 1. Linear response range, intercept values, slope, and coefficient of determination (r²) for calibration curves of UST.

3.3. Stability

The stability of the UST DBS samples was determined at two concentration levels (QCL and QCH) and the cards were stored in airtight bags at RT and in a freezer at -20°C, for a period up to 5 months. Additionally, the DBS were also stored at 40°C, for 2 days. The above-mentioned storing conditions did not cause a significant change to the UST concentration, except QCL samples stored at -20°C for over 28 days, and QCH samples stored at -20°C for 152 days. The results of the stability studies can be seen in Figure 1.

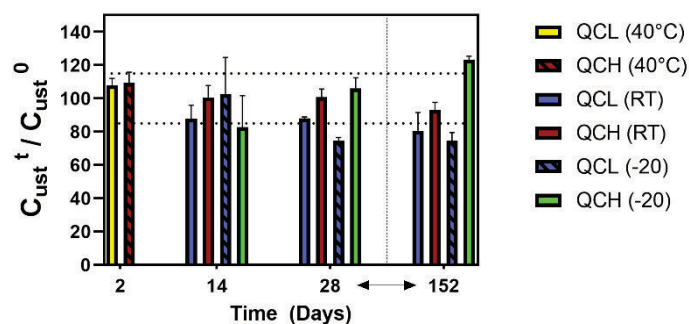


Figure 1. Stability of UST DBS at 3 different conditions (40°C, RT and -20°C) and two concentrations (QCL and QCH).

4. CONCLUSION

TDM is an important tool in dosage optimization of UST. We developed an alternative method, for the determination of concentration of UST in DBS. This method was validated in the range from 3 to 12 mg/L for UST. The long-term stability of DBS samples at room temperature could be advantageous, for the application of the method in clinical practice. With the ongoing clinical validation of the method we aim to demonstrate that DBS can serve as an alternative to venipuncture for the TDM of UST.

5. REFERENCES

1. Benson, JM., et al., Discovery and mechanism of ustekinumab: A human monoclonal antibody targeting interleukin-12 and interleukin-23 for treatment of immune-mediated disorders. Vol. 3, mAbs. 2011. p. 3–18.
2. Papamichael, K., et al., Therapeutic drug monitoring with biologic agents in immune mediated inflammatory diseases. Expert Rev Clin Immunol.2019;15(8):837–48.
3. Capiou, S., et al., Official International Association for Therapeutic Drug Monitoring and Clinical Toxicology Guideline: Development and Validation of Dried Blood Spot-Based Methods for Therapeutic Drug Monitoring. Ther Drug Monit. 2019;41(4):409–30.

ASSOCIATION OF OXIDATIVE STRESS-RELATED BIOMARKERS WITH DISEASE ACTIVITY IN PATIENTS WITH INFLAMMATORY BOWEL DISEASE

Armando Tratenšek¹, Jurij Zdovc¹, Igor Locatelli¹, Iztok Grabnar¹, David Drobne², Tomaž Vovk¹

¹*Faculty of Pharmacy, University of Ljubljana, Slovenia*

²*Department of Gastroenterology, University Medical Centre Ljubljana, Slovenia*

1. INTRODUCTION

There is emerging evidence that an imbalance between oxidants and antioxidant defence, commonly referred to as oxidative stress, plays a pivotal role in the pathogenesis of inflammatory bowel disease (IBD), namely Crohn's disease (CD) and ulcerative colitis (UC) [1,2]. Activated immune cells present in the inflamed intestinal mucosa excessively produce various reactive oxygen and nitrogen species which cause damage to biomacromolecules. To counteract the harmful processes, reactive species are neutralized by superoxide dismutase (SOD), catalase (CAT), glutathione peroxidase (GPx) and non-enzymatic antioxidants [1,2]. Oxidative stress-related biomarkers in patients with IBD have been detected in saliva, urine and blood. However, the relationship between these biomarkers and disease activity remains elusive and previously published studies yield contradictory results [3].

Patients in remission normally do not experience any clinical signs of the disease, hence we expect differences in the levels of oxidative stress-related biomarkers between patients with the active and inactive disease. Given the possibility that the clinically quiescent yet endoscopically active IBD patients are not recognized in time, these biomarkers could potentially serve as surrogate markers of underlying inflammation processes and help to better monitor the IBD itself without subjecting the patients to unpleasant endoscopic procedures [3].

The aim of our study was to conduct a meta-analysis to evaluate oxidative stress-related biomarkers in patients in remission, those in the

active phase of IBD, and healthy controls. Additionally, the most prominent markers were then further evaluated in plasma samples of patients with active and inactive CD.

2. MATERIALS AND METHODS

2.1. Systematic review and meta-analysis

The literature search was conducted in accordance with the Cochrane Handbook and PRISMA guidelines from various databases (PubMed, Embase, Web of Science). We included studies focusing on enzymatic (e.g. SOD, GPx, CAT) and non-enzymatic antioxidants (bilirubin, albumin, vitamins, free thiols) and on markers of oxidative damage to proteins (AOPP), DNA, and lipids (MDA) in both active and inactive IBD patients and healthy controls. Two reviewers independently extracted the markers of oxidative stress (marker name, mean and standard deviation) in each group.

The statistical analyses were performed in Review Manager 5.4. A mean difference in the levels of biomarkers between the investigated groups, divided by their respective standard deviation was used as a measure of effect size, i.e. standardized mean difference (SMD).

2.2. Patients

Frozen plasma samples from thirty-seven patients (eighteen females and nineteen males) diagnosed with CD and treated with ustekinumab were included in our study. Seventeen were defined as having active CD, and twenty patients were in remission.

2.3. Plasma malondialdehyde, free thiols advanced oxidation protein products

The concentration of malondialdehyde (MDA) was measured using high-performance liquid

P76

chromatography with an ultraviolet detector after prior derivatization with dinitrophenylhydrazine.

Free thiols (R-SH) were measured spectrophotometrically at 412 nm using a modified Ellman's method applicable for a microplate reader.

Advanced oxidation protein products (AOPP) were determined spectrophotometrically by measuring the absorbance at 340 nm.

3. RESULTS AND DISCUSSION

3.1. Systematic review and meta-analysis

Concentrations or activities were increased ($p < 0.05$) in IBD patients compared to healthy controls for the following markers (SMD): AOPP (1.81), MDA (0.87) and GPx (0.67). Concentrations or activities were decreased in IBD patients compared to healthy controls for GSH (-1.56), total antioxidant capacity and total antioxidant status (-1.32), albumin (-1.29), bilirubin (-1.09), vitamin A (-0.86), transferrin (-0.75), R-SH (-0.69), vitamin C (-0.66) and vitamin E (-0.41). Additionally, differences between the active and inactive group of patients were observed for bilirubin (active phase -3.10, inactive phase -0.78), catalase (active phase -0.68; inactive phase -0.10), transferrin (active phase -1.17, inactive phase -0.33) and AOPP (active (3.59) inactive IBD (0.89)).

3.2. Plasma malondialdehyde, free thiols and advanced oxidation protein products measurements

Results are depicted in Table 1. In accordance with meta-analysis results, MDA and AOPP concentrations were increased in patients with active CD, whereas R-SH levels did not differ between the two groups. Results were, however, not statistically significant, possibly due to a small sample size and poorly defined patient characteristics.

Table 1. Measurements of oxidative stress-related markers in plasma samples from active and inactive CD patients.

	Active disease (n = 17)	Remission (n = 20)
MDA [$\mu\text{mol/l}$]	4.89 \pm 0.91	4.39 \pm 1.23
	p=0.240*	
R-SH [$\mu\text{mol/l}$]	436.5 \pm 138.7	433.6 \pm 95.2
	p=0.856*	
AOPP [$\mu\text{mol/l}$]	229.2 \pm 101.3	215.5 \pm 94.8
	p=0.833*	

All values are given as the mean \pm SD; *independent samples t-test.

4. CONCLUSION

Based on meta-analysis results, measurements of concentrations or activities of bilirubin, CAT, transferrin and AOPP could serve as surrogate markers of underlying inflammation processes and help to better monitor the IBD. MDA and AOPP measurements in plasma samples were in agreement with meta-analysis results. The next step is to conduct a prospective study with homogenous, comparable and well-defined groups of patients.

5. REFERENCES

1. Tian T, Wang Z, Zhang J. Pathomechanisms of Oxidative Stress in Inflammatory Bowel Disease and Potential Antioxidant Therapies. *Oxid Med Cell Longev*. 2017;2017:4535194.
2. Maor I, Rainis T, Lanir A, Lavy A. Oxidative stress, inflammation and neutrophil superoxide release in patients with Crohn's disease: Distinction between active and non-active disease. *Digestive diseases and sciences*. 2008 Aug;53(8):2208–14.
3. Krzystek-Korpacka M, Kempinski R, Bromke MA, Neubauer K. Oxidative Stress Markers in Inflammatory Bowel Diseases: Systematic Review. *Diagnostics*. 2020 Aug 17;10(8):601.

SPONSORS

PLATINUM SPONSORS



KRKA

At Krka, our dedication lies in producing high quality products, and keeping people healthy is what motivates us. From start to finish, everything we do revolves around our patients and our attempts to help them preserve and improve their health. Each day, more than 50 million patients in 70 markets are treated with our medicines, which are marketed under our own brand names. This is possible because of our innovative products, investments, and market expansion. Stable sales growth, multiple research projects, and sound business performance have seen us grow into a multinational pharmaceutical business group with almost 13,000 employees.



član skupine Sandoz
a Sandoz company

LEK

Novartis is the leading provider of medicines in Slovenia operating through Lek, Novartis Pharma Services and Sandoz. We are delivering the Novartis strategy: to become focused medicines company powered by technology leadership in R&D, world-class commercialization, global access and data science. Together we build and maintain our reputation as a dynamic, ethical and trusted pharmaceutical company.

GOLD SPONSOR



BRINOX

Brinox is a company with almost forty years of experience offering complete turnkey process solutions and equipment for the biopharmaceutical, pharmaceutical, and food industries.

Brinox guides the customer along the entire path from a complex process challenge to an optimal solution, tailor-made to meet the customer's needs. With the aim of producing first-rate products and systems, we carry out all the steps necessary for success, from research and development, process engineering, design, manufacturing, automation, testing and qualification, installation and all after-sales services.

SILVER SPONSOR



ASAHI KASEI

We, the Asahi Kasei Group, contribute to life and living for people around the world. Asahi Kasei is the leading manufacturer and supplier of microcrystalline cellulose. We leveraged five decades of experience and our proprietary morphology design technology to create high-performance MCC products with unique properties. With their superior flowability and compactibility, our materials bring formulation design and tableting efficiency to a new level, particularly for high dose, small tablet, and low-compactibility drug formulations.

BRONZE SPONSORS

MERCK

MeltPrep

HARKE
Pharma

CHEMASS
MERILNI SISTEMI

TELEDYNE
HANSON RESEARCH
Everywhereyoulook™



ABL&E Group
Laboratory Equipment

Fluidnatek®
One Step Ahead
by Bioinicia

MUNIT
JETPHARMA • MICROCHEM
WE ARE MICRONIZATION

Labtim

SIMPLIVIA

METTLER TOLEDO

OTHER SPONSORS

SARTORIUS



Pfizer

MEDIS

avantor™
delivered by **VWR™**

Ljubljana
Ljubljana Tourism

mikrospolo
VAŠ PARTNER ZA LABORATORIJ